

AD-A049 767

RCA ELECTROMAGNETIC AND AVIATION SYSTEMS DIV VAN NUY--ETC F/G 1/2  
BEARING STUDY PROGRAM.(U)

APR 74 E JELLINEK, W KRAM, M LEVINSSEN

N62269-73-C-0906

UNCLASSIFIED

RCA-EASD-TP-2146

NL

1 OF 5

AD  
A049 767





AD A049767

AD No.

JDC FILE COPY

# RCA

Final Report

①  
50

## Bearing Study Program

Prepared for  
U.S. Naval Air Development Center  
Warminster, PA

Contract No. N62269-73-C-0906

mel

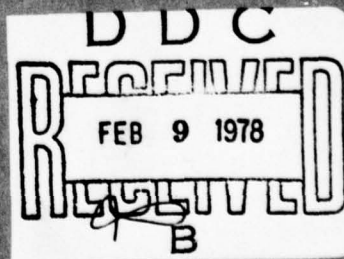
RCA

Prepared by

RCA Electronic and Aviation Systems Division | Van Nuys, CA

TP2146  
April 1974

405740



### DISTRIBUTION STATEMENT A

Approved for public release;  
Distribution Unlimited

# RCA

①

⑨ **Final Report.**

⑩ Ernest/Jellinek, Walter/Kram, M./Levinson,  
O.M./Woodward Bernard/Case

⑥ **Bearing Study Program.**

**Prepared for  
U.S. Naval Air Development Center  
Warminster, PA**

⑭ RCA-EASD-TP.2146

⑮  
**Contract No. N62269-73-C-0906**

DDC  
RECEIVED  
FEB 9 1978  
B

**Prepared by  
RCA | Government and Commercial Systems  
Electromagnetic and Aviation Systems Division | Van Nuys, CA**

⑪ TP2146  
April 1974

⑫ 447P.

**DISTRIBUTION STATEMENT A**  
Approved for public release;  
Distribution Unlimited

11 405740 503

## ABSTRACT

A study was conducted to assess the feasibility and define the system accuracy and equipment required to add a bearing measurement subsystem to the SECANT Collision Avoidance System (CAS). The results indicate the feasibility of achieving the accuracy required to serve useful functions. Equipment configurations required for Proximity Warning Indicator and CAS applications were evolved and are presented in detail in this study.

A design approach was developed and trade-off and accuracy analyses are presented.

The approach utilizes a ring array antenna consisting of vertical monopoles interconnected by stripline. It has a high accuracy outer ring of 16 monopoles, an inner ring of 4 monopoles for resolving ambiguities, and a central reference monopole. The array receives the signals transmitted by any of the equipment types in the SECANT family, and the relative bearing is determined by measuring the phase difference between the signals in the reference monopole and in the rings. Random errors are minimized by integration of the high pulse rate, frequency hopped signals. Predicted overall error is 1 degree, one sigma with a bias component of 0.8 degree and a random component of 0.5 degree.

An antenna array was constructed and tests in an anechoic chamber confirmed the validity of the design approach. Receiver and data processing configuration approaches were also developed for Proximity Warning Indicator and Collision Avoidance System applications. The general approach is also applicable to other system applications such as navigation, and electronic warfare.

|               |   |
|---------------|---|
| ACCESSION for |   |
| NTIS          | White Section <input checked="" type="checkbox"/> |
| DDC           | Bull Section <input type="checkbox"/>             |
| UNANNOUNCED   | <input type="checkbox"/>                          |
| JUSTIFICATION |   |

Preceding Page BLANK - F

|       |                       |
|-------|-----------------------|
| Dist. | AVAIL. and/or SPECIAL |
| A     |                       |



## TABLE OF CONTENTS

| Section |  | Page |
|---------|--|------|
|         | ABSTRACT .....   | iii  |
| 1.0     | INTRODUCTION .....   | 1-1  |
| 1.1     | GENERAL .....  | 1-1  |
| 1.2     | SUMMARY OF RESULTS .....                                     | 1-2  |
| 1.3     | CONCLUSIONS .....  | 1-9  |
| 1.4     | RECOMMENDATIONS .....  | 1-10 |
| 2.0     | ANALYSIS OF ACCURACY REQUIREMENTS (TASK 1) .....             | 2-1  |
| 2.1     | INTRODUCTION .....   | 2-1  |
| 2.2     | VISUAL BEARING INDICATOR .....                               | 2-2  |
| 2.3     | ACCURACY REQUIRED FOR UNNECESSARY<br>WARNING REDUCTION ..... | 2-2  |
| 2.3.1   | Introduction .....   | 2-2  |
| 2.3.2   | Threshold Setting vs. Bearing Error .....                    | 2-5  |
| 2.3.3   | Alarm Probabilities in Traffic<br>Environment .....          | 2-16 |
| 2.3.4   | Conclusions .....  | 2-26 |
| 2.4     | ACCURACY REQUIREMENTS FOR HORIZONTAL<br>MANEUVERING .....    | 2-27 |
| 2.4.1   | Results of SCI Study .....                                   | 2-27 |
| 2.4.2   | Erroneous Horizontal Maneuver Effects .....                  | 2-30 |
| 3.0     | CONFIGURATION ANALYSIS (TASK 2) .....                        | 3-1  |
| 3.1     | GENERAL .....  | 3-1  |
| 3.1.1   | General Description of System Concept .....                  | 3-3  |
| 3.1.1.1 | Dominant Concept Constraints .....                           | 3-3  |
| 3.1.1.2 | Basic System Concept .....                                   | 3-4  |
| 3.1.2   | Summary of Trade-Offs .....                                  | 3-10 |
| 3.1.2.1 | Trade-Off Approach .....                                     | 3-10 |
| 3.1.2.2 | Identification of Errors and Error<br>Control Methods .....  | 3-11 |
| 3.2     | ANTENNA CONFIGURATION ANALYSIS (TASK 2.1) .....              | 3-13 |
| 3.2.1   | Summary and Conclusions .....                                | 3-13 |
| 3.2.2   | Analysis of Interferometer Array .....                       | 3-15 |

# TABLE OF CONTENTS (Continued)

| Section   |  | Page |
|-----------|--|------|
| 3.2.3     | Analysis of Ring Arrays . . . . .  | 3-18 |
| 3.2.3.1   | Mode Definition and Geometry . . . . .   | 3-18 |
| 3.2.3.2   | Element Types . . . . .  | 3-23 |
| 3.2.3.3   | Trade-Offs Between Number of Elements and<br>Feed Circuitry; 3-Element - $H = 1$ . . . . . | 3-25 |
| 3.2.3.4   | 4-Element - $H = 1$ Array . . . . .  | 3-29 |
| 3.2.3.5   | Characteristics of 4-Element Array . . . . .   | 3-32 |
| 3.2.3.6   | Printed Circuit Design of 5-Element<br>Array - $H = 0$ and $H = 1$ . . . . .               | 3-44 |
| 3.2.3.7   | Higher Order Modes ( $H > 1$ ) . . . . .   | 3-48 |
| 3.2.3.8   | Feed Circuitry for the $H = 4$ Ring . . . . .  | 3-53 |
| 3.2.3.9   | Effect of Finite Ground Planes on<br>Radiation Characteristics . . . . .                   | 3-65 |
| 3.3       | SIGNAL PROCESSING CONFIGURATION ANALYSIS<br>(TASK 2.2) . . . . .                           | 3-70 |
| 3.3.1     | Local Multipath . . . . .  | 3-70 |
| 3.3.2     | Corange Target Interference . . . . .  | 3-71 |
| 3.3.3     | Aircraft Attitude Variations . . . . .   | 3-72 |
| 3.3.4     | Fruit Interference . . . . .   | 3-73 |
| 3.3.5     | Mutual Coupling Effects in Interferometer<br>Array . . . . .                               | 3-75 |
| 3.3.6     | Phase Nonlinearity in Ring Arrays . . . . .  | 3-75 |
| 3.3.7     | Thermal Noise Errors . . . . .   | 3-76 |
| 3.3.8     | Phase Comparator Resolution . . . . .  | 3-77 |
| 3.3.8.1   | Zero Crossover Phase Comparator . . . . .  | 3-77 |
| 3.3.8.1.1 | Clocked Crossover Method . . . . .   | 3-78 |
| 3.3.8.1.2 | Linear Ramp Function Method . . . . .  | 3-80 |
| 3.3.8.2   | Multiplier Phase Comparator . . . . .  | 3-82 |
| 3.3.8.3   | Comparison of Phase Detectors . . . . .  | 3-84 |
| 3.3.9     | Errors Encounterable with Pulsed Waves . . . . .   | 3-84 |
| 3.3.10    | Phase Variations in IF Limiter-Amplifiers . . . . .  | 3-88 |
| 3.3.11    | Effects of Interchannel Phase and Delay<br>Imbalances . . . . .                            | 3-91 |
| 3.3.11.1  | Phase Imbalance (Bias Error Generation) . . . . .  | 3-91 |
| 3.3.11.2  | Group Delay Differences (Random Error<br>Generation) . . . . .                             | 3-93 |

# TABLE OF CONTENTS (Continued)

| Section   |  | Page  |
|-----------|--|-------|
| 3.4       | DATA PROCESSING CONFIGURATION ANALYSIS<br>(TASK 2.3) . . . . .                         | 3-95  |
| 3.4.1     | Phase Measurement Data Processing . . . . .  | 3-95  |
| 3.4.1.1   | Purpose . . . . .  | 3-95  |
| 3.4.1.2   | Description . . . . .  | 3-95  |
| 3.4.1.3   | Comments on Algorithm Requirements . . . . .   | 3-100 |
| 3.4.1.4   | $\phi$ Computation in Block #17 . . . . .  | 3-100 |
| 3.4.2     | Miss Distance and Horizontal Bearing<br>Data Processing . . . . .                      | 3-103 |
| 3.5       | ACCURACY ANALYSIS (TASK 2.4) . . . . .   | 3-107 |
| 3.5.1     | Error Allocations . . . . .  | 3-108 |
| 3.5.1.1   | Estimates of Error Contributions . . . . .   | 3-108 |
| 3.5.1.2   | Estimate of Overall Error in Relative<br>Bearing . . . . .                             | 3-116 |
| 3.5.1.3   | Overall Error Estimate With Calibration<br>Corrections . . . . .                       | 3-117 |
| 3.5.2     | Major Error Contributors - Summary of<br>Analyses . . . . .                            | 3-118 |
| 3.5.2.1   | Ripple and Multipath Errors . . . . .  | 3-120 |
| 3.5.2.1.2 | Ripple Error Analysis . . . . .  | 3-120 |
| 3.5.2.1.3 | Multipath Error Effects (Mode 4) . . . . .   | 3-129 |
| 3.5.2.1.4 | Quantitative Results . . . . .   | 3-139 |
| 3.5.2.1.5 | Effect of Variability in Bearing and Swept<br>Bearing Probabilistic Analysis . . . . . | 3-145 |
| 3.5.2.2   | Addendum. Mode 1 Multipath Analysis . . . . .  | 3-164 |
| 3.5.2.2.1 | Ripple Error . . . . .   | 3-166 |
| 3.5.2.2.2 | Multipath Error . . . . .  | 3-171 |
| 3.5.2.2.3 | Quantitative Evaluation . . . . .  | 3-174 |
| 3.5.2.2.4 | Calibration Constant Compensation . . . . .  | 3-181 |
| 3.5.2.3   | Estimation of Fruit Errors in Bearing<br>Measurement . . . . .                         | 3-183 |
| 3.5.2.3.1 | Assumptions . . . . .  | 3-183 |
| 3.5.2.3.2 | Analysis . . . . .   | 3-183 |
| 3.5.2.3.3 | Conclusions . . . . .  | 3-186 |
| 3.5.2.4   | Attitude Errors . . . . .  | 3-188 |
| 3.5.2.4.1 | Abstract and Summary . . . . .   | 3-188 |
| 3.5.2.4.2 | Horizontal Bearing Error . . . . .   | 3-188 |
| 3.5.2.4.3 | Horizontal Miss Component Error . . . . .  | 3-189 |
| 3.5.2.4.4 | Quantitative Results . . . . .   | 3-196 |



# TABLE OF CONTENTS (Continued)

| Section    |  | Page |
|------------|--|------|
| 4.0        | BREADBOARD ANTENNA (TASK 3.1) . . . . .  | 4-1  |
| 4.1        | SUMMARY . . . . .  | 4-1  |
| 4.2        | CONCLUSIONS . . . . .  | 4-1  |
| 4.3        | ANTENNA MECHANICAL DESIGN . . . . .  | 4-2  |
| 4.4        | TEST PROCEDURES . . . . .  | 4-5  |
| 4.5        | RESULTS OF THE PATTERN MEASUREMENTS . . . . .  | 4-11 |
| 4.5.1      | H = 0 Mode . . . . .   | 4-11 |
| 4.5.2      | H = 4 Mode . . . . .   | 4-14 |
| 4.5.3      | Multipath Effects . . . . .  | 4-16 |
| 4.5.4      | Effect of Elevation Angle on Azimuth<br>Patterns . . . . .   | 4-22 |
| 5.0        | HARDWARE CHARACTERISTICS FOR RECEIVER, SIGNAL<br>PROCESSOR AND DATA PROCESSOR (TASKS 3.2,<br>3.3, 3.4) . . . . .       | 5-1  |
| 5.1        | GENERAL . . . . .  | 5-1  |
| 5.2        | RECEIVER CONFIGURATION . . . . .   | 5-4  |
| 5.3        | SIGNAL PROCESSING CONFIGURATION . . . . .  | 5-8  |
| 5.4        | DATA PROCESSING CONFIGURATION . . . . .  | 5-18 |
| 5.5        | PWI BEARING RECEIVER AND INFORMATION PRO-<br>CESSING CONFIGURATION . . . . .   | 5-20 |
| APPENDIX A | WORK STATEMENT . . . . .   | A-1  |
| APPENDIX B | PROBABILITY ANALYSIS . . . . .   | B-1  |
| APPENDIX C | ERROR ANALYSIS . . . . .   | C-1  |
| APPENDIX D | DETERMINATION OF THE MAXIMUM MISS DISTANCE<br>(M <sub>MAX</sub> ) OF THE TAU CRITERION . . . . .                       | D-1  |
| APPENDIX E | SIMULATION EQUATIONS . . . . .   | E-1  |
| APPENDIX F | PERFORMANCE SPECIFICATION FOR A SECANT<br>BEARING AND MISS-DISTANCE PROCESSING SUB-<br>SYSTEM OF A FULL CAS . . . . .  | F-1  |
| APPENDIX G | MUTUAL COUPLING EFFECTS IN CROSSED-AXIS<br>INTERFEROMETER . . . . .  | G-1  |
| APPENDIX H | BALUN FREQUENCY CHARACTERISTICS . . . . .  | H-1  |
| APPENDIX I | EXPRESSIONS FOR UNAMBIGUOUS RELATIVE BEARING<br>USING RING ARRAY ANTENNAS AND CROSSED-AXIS<br>INTERFEROMETER . . . . . | I-1  |
| APPENDIX J | PHASE TRANSIENTS IN DOUBLE-TUNED FILTERS . . . .   | J-1  |

## TABLE OF CONTENTS (Continued)

| Section  | Page |
|--|------|
| APPENDIX K   |      |
| SWEPT BEARING ERROR DUE TO INTERCHANNEL<br>PHASE IMBALANCE WHEN EMPLOYING THE<br>CROSSED-AXIS INTERFEROMETER . . . . . | K-1  |
| APPENDIX L   |      |
| DERIVATION OF ALGORITHM FOR MISS DISTANCE AND<br>HORIZONTAL BEARING DETERMINATION . . . . .                            | L-1  |
| APPENDIX M   |      |
| TWO-DIMENSIONAL BEARING SITING ERROR<br>DERIVATION . . . . .   | M-1  |
| APPENDIX N   |      |
| ESTIMATION OF REFLECTOR PARAMETER . . . . .  | N-1  |
| APPENDIX O   |      |
| ANALYTIC MODEL OF MULTIPATH TEST . . . . .   | O-1  |
| APPENDIX P   |      |
| REFERENCES . . . . .   | P-1  |
| APPENDIX Q   |      |
| BIBLIOGRAPHY . . . . .   | Q-1  |

## LIST OF ILLUSTRATIONS

| Figure |  | Page |
|--------|--|------|
| 1-1    | Breadboard Ring Array Antenna . . . . .  | 1-5  |
| 2-1    | Miss Distance (M) vs. Range (R) Locus of Tau Criterion . . . . .   | 2-4  |
| 2-2    | Missed Alarm Prob. - Single Conflict . . . . .   | 2-9  |
| 2-3    | Miss Threshold vs. Miss Sigma for Various Missed Alarm<br>Probabilities . . . . .  | 2-12 |
| 2-4    | Sigma of Swept Bearing, $\sigma(\Delta\beta) \sim \text{deg's.}$ vs. Miss Threshold<br>( $M_T \sim 1000$ 's of Feet) . . . . . | 2-13 |
| 2-5    | Sigma of Swept Bearing, $\sigma(\Delta\beta) \sim \text{deg's.}$ vs. Miss Threshold<br>( $M_T \sim 1000$ 's of Feet) . . . . . | 2-13 |
| 2-6    | Sigma of Swept Bearing, $\sigma(\Delta\beta) \sim \text{deg's.}$ Miss Threshold<br>( $M_T \sim 1000$ 's of Feet) . . . . .     | 2-14 |
| 2-7    | Sigma of Swept Bearing, $\sigma(\Delta\beta) \sim \text{deg's.}$ Miss Threshold<br>( $M_T \sim 1000$ 's of Feet) . . . . .     | 2-14 |
| 2-8    | Miss Alarm Threshold ( $M_T \sim 1000$ 's of Feet vs. False Alarm<br>Prob., $P_{fac}$ . . . . .                                | 2-15 |
| 2-9    | Miss Alarm Threshold ( $M_T \sim 1000$ 's of Feet vs. False Alarm<br>Prob., $P_{fac}$ . . . . .                                | 2-15 |
| 2-10   | Miss Alarm Threshold ( $M_T \sim 1000$ 's of Feet vs. $\eta = \% \text{ Re-}$<br>duction in $P_{fa}$ . . . . .                 | 2-17 |
| 2-11   | Miss Alarm Threshold ( $M_T \sim 1000$ 's of Feet vs. $\eta = \% \text{ Re-}$<br>duction in $P_{fa}$ . . . . .                 | 2-17 |

# LIST OF ILLUSTRATIONS (Continued)

| Figure |   | Page |
|--------|---|------|
| 2-12   | Relative Velocity ( $V_r$ ) ~ Knots vs. $\eta$ = % Reduction in $P_{fa}$ . . . . .              | 2-18 |
| 2-13   | Relative Velocity ( $V_r$ ) ~ Knots vs. $\eta$ = % Reduction in $P_{fa}$ . . . . .              | 2-18 |
| 2-14   | False Alarm Prob. vs. Missed Alarm Prob. - 1982 LAX<br>Traffic Model . . . . .                  | 2-22 |
| 2-15   | Tau 1 False Alarm and Missed Alarm Probabilities<br>(315 Knots) . . . . .                       | 2-23 |
| 2-16   | Tau 1 False Alarm and Missed Alarm Probabilities<br>(500 Knots) . . . . .                       | 2-23 |
| 2-17   | Tau 2 False Alarm and Missed Alarm Probabilities<br>(315 Knots) . . . . .                       | 2-24 |
| 2-18   | Tau 2 False Alarm and Missed Alarm Probabilities<br>(500 Knots) . . . . .                       | 2-24 |
| 2-19   | Erroneous Turn Command . . . . .  | 2-31 |
| 2-20   | Left Turn Command Probability . . . . .   | 2-31 |
| 2-21   | Probability of Erroneous Command vs. Sigma of Miss . . . . .                                    | 2-33 |
| 2-22   | Miss Threshold vs. Speed . . . . .  | 2-34 |
| 3-1    | Bearing Measurement Approach for Full CAS in SECANT . . . . .                                   | 3-5  |
| 3-2    | Noise Errors for Two Types of Phase Comparator . . . . .  | 3-8  |
| 3-3    | Pulse Sequences Used During VECAS Track . . . . .   | 3-9  |
| 3-4    | Analysis of Two-Element Interferometer Array . . . . .  | 3-16 |
| 3-5    | Analysis of Two-Element Interferometer Array (Cont'd) . . . . .                                 | 3-17 |
| 3-6    | Analysis of Two Element-Interferometer Array (Cont'd) . . . . .                                 | 3-19 |
| 3-7    | Analysis of Two Element Interferometer Array (Cont'd) . . . . .                                 | 3-20 |
| 3-8    | Analysis of Two Element Interferometer Array (Cont'd) . . . . .                                 | 3-21 |
| 3-9    | Geometry of Ring Elements . . . . .   | 3-24 |
| 3-10   | 3-Element Array - $H = 1$ . . . . .   | 3-26 |
| 3-11   | 3-Element Array - $H = 0$ and $H = 1$ . . . . .   | 3-28 |
| 3-12   | 3-Element Array - $H = 0$ and $H = 1$ . . . . .   | 3-30 |
| 3-13   | 4-Element Array - $H = 1$ . . . . .   | 3-31 |
| 3-14   | 4-Element Array - $H = 0$ and $H = 1$ . . . . .   | 3-33 |
| 3-15   | 5-Element Array - $H = 0$ and $H = +1$ . . . . .  | 3-34 |
| 3-16   | 4-Element Array - $H = 0$ . . . . .   | 3-35 |
| 3-17   | Four Element Array, $H = 1$ , Rosette Patterns Produced by<br>Subring A and Subring B . . . . . | 3-37 |
| 3-18   | 4-Element Array - $H = 1$ . . . . .   | 3-38 |
| 3-19   | 4-Element Array - $H = 1$ . . . . .   | 3-39 |
| 3-20   | 4-Element Array - $H = 0$ . . . . .   | 3-40 |
| 3-21   | 4-Element Array - $H = 1$ . . . . .   | 3-41 |
| 3-22   | 4-Element Array - $H = 1$ . . . . .   | 3-42 |
| 3-23   | 4-Element Array - $H = 1$ . . . . .   | 3-43 |
| 3-24   | Experimental Setup for $H = 1$ . . . . .  | 3-45 |
| 3-25   | 5-Element Array - $H = 0$ and $H = 1$ . . . . .   | 3-46 |



# LIST OF ILLUSTRATIONS (Continued)

| Figure |  | Page  |
|--------|--|-------|
| 3-26   | 5-Element Array - $H = 0$ and $H = 1$ . . . . .  | 3-49  |
| 3-27   | Far-Field Phase Variation for Higher Order Modes . . . . .                                     | 3-51  |
| 3-28   | Separation of Ring into Two Subrings and Mode Excitation<br>Circuitry . . . . .                | 3-52  |
| 3-29   | Rosette Patterns Produced by Subring A and Subring B . . . . .                                 | 3-54  |
| 3-30   | Azimuth Pattern of Single Subring for $H = 4$ . . . . .  | 3-55  |
| 3-31   | Theo. Elevation Patterns . . . . .   | 3-56  |
| 3-32   | Amplitude Difference Comparisons . . . . .   | 3-57  |
| 3-33   | $H = 4$ Feed Circuitry . . . . .   | 3-58  |
| 3-34   | Printed Circuitry for $H = 4$ Mode Subring . . . . .   | 3-60  |
| 3-35   | $H = 4$ Feed Circuitry . . . . .   | 3-61  |
| 3-36   | $H = 4$ Feed Circuitry (C) . . . . .   | 3-62  |
| 3-37   | Full Size Layout of Printed Circuitry for $1/4$ of the $H = 4$<br>Ring . . . . .               | 3-63  |
| 3-38   | Comparison of Rat Race and Square Hybrids . . . . .  | 3-64  |
| 3-39   | Theo. Elevation Pattern . . . . .  | 3-66  |
| 3-40   | Elev. Pattern With Small Ground Plane . . . . .  | 3-67  |
| 3-41   | Elevation Pattern of $\lambda/4$ Monopole Over a $6\lambda$ Diameter<br>Ground Plane . . . . . | 3-68  |
| 3-42   | Elev. Pattern Vs. Ground Plane Diameter . . . . .  | 3-69  |
| 3-43   | Basic Scheme of Quadrature Phase Comparator . . . . .  | 3-83  |
| 3-44   | Phase Transient Error of Double-Tuned Filter Section . . . . .                                 | 3-87  |
| 3-45   | Mean Phase Transient Error Over $0-360^\circ$ Phase Epoch<br>Range . . . . .                   | 3-89  |
| 3-46   | $\phi$ Meast. Data Processing Part 1 . . . . .   | 3-96  |
| 3-47   | $\phi$ Meast. Data Processing Part 2 . . . . .   | 3-97  |
| 3-48   | Mode 4 Ring Array . . . . .  | 3-121 |
| 3-49   | Ambiguity in $\phi$ . . . . .  | 3-121 |
| 3-50   | Interference Model . . . . .   | 3-130 |
| 3-51   | Reflector Limits . . . . .   | 3-130 |
| 3-52   | Multipath Model . . . . .  | 3-134 |
| 3-53   | Multipath Model for $X = 180^\circ$ . . . . .  | 3-134 |
| 3-54   | Reflection Limit . . . . .   | 3-140 |
| 3-55   | Run #2B Mean Error Vs. Bearing Angle . . . . .   | 3-146 |
| 3-56   | Run #5 Mean Error Vs. Bearing Angle . . . . .  | 3-147 |
| 3-57   | Run #15 Mean Error vs. Bearing Angle . . . . .   | 3-148 |
| 3-58   | Run #7 Mean Error vs. Bearing Angle . . . . .  | 3-149 |
| 3-59   | Run #4 Mean Error Vs. Bearing Angle . . . . .  | 3-150 |

# LIST OF ILLUSTRATIONS (Continued)

| Figure |   | Page  |
|--------|---|-------|
| 3-60   | Run #6 Mean Error vs. Bearing Angle . . . . .   | 3-151 |
| 3-61   | Run #16 Mean Error vs. Bearing Angle . . . . .  | 3-152 |
| 3-62   | Run #17 Mean Error vs. Bearing Angle . . . . .  | 3-153 |
| 3-63   | Run #8 Mean Error vs. Bearing Angle . . . . .   | 3-154 |
| 3-64   | Run #9 Mean Error vs. Bearing Angle . . . . .   | 3-155 |
| 3-65   | Reflection Limit . . . . .  | 3-140 |
| 3-66   | Swept Bearing at Threshold vs. Rel. Vel. . . . .  | 3-157 |
| 3-67   | Derivation of $F(\theta_1)$ . . . . .   | 3-140 |
| 3-68   | Regions of Validity of $F_1$ Function . . . . .   | 3-160 |
| 3-69   | Effect of Variable Amplitude of $d\hat{\theta}_T$ . . . . .                             | 3-160 |
| 3-70   | Acceptability Criterion . . . . .   | 3-165 |
| 3-71   | Mode 1 Array . . . . .  | 3-167 |
| 3-72   | Multipath Model . . . . .   | 3-167 |
| 3-73   | $d\hat{\theta}$ vs. $\theta$ . . . . .  | 3-176 |
| 3-74   | $d\hat{\theta}$ vs. $\theta$ . . . . .  | 3-177 |
| 3-75   | $d\hat{\theta}$ vs. $\theta$ . . . . .  | 3-178 |
| 3-76   | $d\hat{\theta}$ vs. $\theta$ . . . . .  | 3-179 |
| 3-77   | Orientation of Ring Arrays With Respect to Aircraft Axis . . . . .                      | 3-182 |
| 3-78   | Bearing Error Due to Fruit Interference . . . . .                                       | 3-187 |
| 3-79   | Horizontal Plane Conflict . . . . .   | 3-193 |
| 3-80   | $V_r$ Horizontal, Displaced $\Delta h$ . . . . .  | 3-193 |
| 3-81   | $V_r$ Horizontal, $M_H = 0$ . . . . .   | 3-193 |
| 3-82   | Range Alarm/Miss Threshold . . . . .  | 3-197 |
| 3-83   | Miss Sensitivity to Yaw Error . . . . .   | 3-197 |
| 3-84   | Miss Sensitivity to Yaw Error . . . . .   | 3-200 |
| 3-85   | Miss Sensitivities . . . . .  | 3-200 |
| 4-1    | Photo of Breadboard Antenna . . . . .   | 4-3   |
| 4-2    | Construction of Breadboard Antenna . . . . .  | 4-4   |
| 4-3    | Complete Antenna Assembly . . . . .   | 4-6   |
| 4-4    | Complete Antenna Assembly . . . . .   | 4-8   |
| 4-5    | Cross-Coupling Between Different Modes . . . . .  | 4-9   |
| 4-6    | Azimuth Bearing Vs. Phase Difference for $H = 0$ , $H = -1$ . . . . .                   | 4-13  |
| 4-7    | Bearing Vs. Phase Difference for $H = 0$ , $H = -4$ . . . . .                           | 4-15  |
| 4-8    | Bearing Vs. Phase Difference for $H = -4$ , $H = +4$ . . . . .                          | 4-17  |
| 4-9    | Bearing Vs. Phase for $H = 0$ , $H = -4$ , $H = +4$ at 1604 MHz,<br>With Cone . . . . . | 4-19  |
| 4-10   | Multipath and Ripple Error at 1604 MHz . . . . .  | 4-20  |
| 4-11   | Multipath Error at Various Frequencies . . . . .  | 4-21  |

# LIST OF ILLUSTRATIONS (Continued)

| Figure |   | Page |
|--------|---|------|
| 4-12   | Elev. Patt. - $\Phi$ Cus = $-67.5^\circ$ Comparison of Amp. & Phase<br>for Different Modes . . . . .            | 4-23 |
| 5-1    | SECANT Bearing Block Diagram . . . . .  | 5-2  |
| 5-2    | VECAS Track Format . . . . .  | 5-5  |
| 5-3    | Receiver Block Diagram . . . . .  | 5-6  |
| 5-4    | Signal Flow Diagram . . . . .   | 5-10 |
| 5-5    | Sampling Gate and Phase Interval Generation . . . . .   | 5-14 |
| 5-6    | Resolution, Digital, Pulse Width Detector Vernier . . . . .   | 5-15 |
| 5-7    | Phase Measurement Unit Block Diagram . . . . .  | 5-17 |
| 5-8    | Block Diagram of PWI Bearing Measurement System . . . . .   | 5-21 |
| 5-9    | 360° Discontinuity Corrector . . . . .  | 5-23 |
| B-1    | Gaussian Distribution of Error in Computed Miss . . . . .   | B-2  |
| C-1    | Conflict Triangle . . . . .   | C-2  |
| C-2    | Miss Error vs. $\sigma(\Delta\beta)$ . . . . .  | C-7  |
| C-3    | Miss Error vs. $\sigma(\Delta\beta)$ . . . . .  | C-8  |
| C-4    | Crossed Axis Interferometer . . . . .   | C-2  |
| D-1    | Tau Cardioid . . . . .  | D-2  |
| D-2    | Max. Miss on Range Alarm Cardioid . . . . .   | D-5  |
| E-1    | Relative Range Determination . . . . .  | E-2  |
| E-2    | Miss Component Determination . . . . .  | E-2  |
| E-3    | Frequency Histogram of Relative Range - A/C #710 . . . . .  | E-8  |
| E-4    | Frequency Histogram of Relative Range - A/C #49 . . . . .   | E-9  |
| E-5    | Frequency Histogram of Horizontal Miss - A/C #710 . . . . .   | E-10 |
| E-6    | Frequency Histogram of Horizontal Miss - A/C #49 . . . . .  | E-11 |
| F-1    | Basic Conceptual Scheme for Bearing Subsystem . . . . .   | F-6  |
| G-1    | Magnitude of Error in Crossed Axis Interometer Due to Mutual<br>Coupling Between Axial Monopole Pairs . . . . . | G-5  |
| H-1    | $\lambda/2$ Balun Frequency Characteristics (Magnitude) . . . . .   | H-2  |
| H-2    | $\lambda/2$ Balun Frequency Characteristics (Phase) . . . . .   | H-3  |
| H-3    | $\lambda/2$ Balun Frequency Characteristics . . . . .   | H-4  |
| I-1    | Geometry of Crossed-Axis Interferometer . . . . .   | I-3  |
| L-1    | Projected Miss . . . . .  | L-4  |
| L-2    | Three-Dimensional Miss Geometry . . . . .   | L-4  |
| L-3    | Attitude Angles . . . . .   | L-4  |
| L-4    | Horizontal Bearing Difference . . . . .   | L-8  |
| L-5    | Hazard Predictors . . . . .   | L-8  |
| L-6    | Conflict Geometry . . . . .   | L-8  |
| L-7    | Vertical Separation at Passing . . . . .  | L-18 |
| L-8    | Yaw Effect . . . . .  | L-18 |



# LIST OF ILLUSTRATIONS (Continued)

| Figure |   | Page |
|--------|---|------|
| L-9    | Case 1 Roll Change Only . . . . .               | L-18 |
| L-10   | Case 2 Pitch Change Only . . . . .              | L-24 |
| M-1    | Interference Model . . . . .                    | M-2  |
| N-1    | Radiation Patterns of Antenna Stubs . . . . .   | N-2  |
| N-2    | Enlargement of Figure 5 of Figure N-1 . . . . . | N-3  |
| O-1    | Test Configuration . . . . .                    | O-2  |
| O-2    | Near-Field vs. Far-Field Emission . . . . .     | O-2  |
| O-3    | Multipath Error (Test Simulation) . . . . .     | O-8  |

# LIST OF TABLES

| Table |  | Page  |
|-------|--|-------|
| 1-1   | Correlation Between Report Sections and SOW Tasks . . . . .                                      | 1-3   |
| 2-1   | $P_{mas}$ vs. $\sigma(\Delta\beta)$ , for $V_r = 315$ Knots, $\tau_2$ , $M_T = 2000$ ft. . . . . | 2-7   |
| 2-2   | $P_{mas}$ vs. $\sigma(\Delta\beta)$ for $V_r = 315$ Knots . . . . .                              | 2-8   |
| 2-3   | Values of $\sigma(\Delta\beta)$ for Various Values of $V_r$ and $(\delta M)$ . . . . .           | 2-10  |
| 2-4   | $M_T$ and $\sigma(\Delta\beta)$ Required for $P_{fac} = .5$ . . . . .                            | 2-19  |
| 2-5   | Cumulative Probabilities Based on Traffic Model . . . . .  | 2-20  |
| 2-6   | $\sigma(\Delta\beta)$ Requirement . . . . .  | 2-25  |
| 2-7   | Reduction of Unnecessary Alarms for $\sigma(\Delta\beta) = 0.8$ Degree . . . . .                 | 2-27  |
| 2-8   | Effect of Bearing Error on Horizontal Maneuvers . . . . .  | 2-29  |
| 2-9   | Summary of Accuracy Requirements . . . . .   | 2-36  |
| 3-1   | Identification of Bearing Measurement Errors . . . . .   | 3-12  |
| 3-2   | Comparison of DF Antenna Arrays . . . . .  | 3-22  |
| 3-3   | Error Analysis Results . . . . .   | 3-109 |
| 3-4   | Ripple Error at 1600 MHz . . . . .   | 3-126 |
| 3-5   | Direction of Arrival Reflection Limits . . . . .   | 3-139 |
| 3-6   | Transmission Sets . . . . .  | 3-141 |
| 3-7   | Ripple and Multipath Error . . . . .   | 3-142 |
| 3-8   | Summary, Mode 4 . . . . .  | 3-144 |
| 3-9   | Ripple Error Program Mode 1 . . . . .  | 3-170 |
| 3-10  | Mean Bearing Error (DTHT) as Function of Bearing<br>Angle (Theta) . . . . .                      | 3-175 |
| 3-11  | Summary, Mode 1 . . . . .  | 3-180 |
| 5-1   | Receiver Frequencies for Replies . . . . .   | 5-9   |
| 5-2   | Receiver Frequencies - Probes . . . . .  | 5-13  |
| C-1   | Kinematic and Error Sensitivity Parameters at $\tau$ Cardioid<br>Penetration . . . . .           | C-5   |

# LIST OF TABLES (Continued)

| Table |   | Page |
|-------|---|------|
| E-1   | Kinematic Quantities and Miss Components of Intruder Air-<br>craft in Traffic Environment . . . . . | E-7  |
| F-1   | Generic Types of Signal Inputs . . . . .  | F-4  |
| F-2   | Bearing Subsystem Bench Test Accuracy Requirements . . . . .  | F-17 |
| G-1   | Mutual Impedance Data . . . . .   | G-4  |
| L-1   | Miss Error for Roll (or Pitch) Change . . . . .   | L-22 |

## 1.0 INTRODUCTION

### 1.1 GENERAL

This is the Final Report of the Bearing Measurement Study Program performed for the Naval Air Development Center under contract N62269-73-C-0906. The work reported on herein is completely responsive to the contract *Statement of Work (SOW)* which is provided for reference as Appendix A.

The purpose of this study program was to investigate the feasibility of a relative bearing measurement subsystem which could provide useful functions in airborne anti-collision systems, such as:

- Visual indication of the relative position of conflicting aircraft

When incorporated in a range-altitude Proximity Warning Indicator (PWI), it could assist the pilot in visual acquisition of the alarm causing aircraft.

When incorporated in a Collision Avoidance System (CAS) using the Tau-Altitude criterion of ANTC-117, it could improve the control of the indicated threat and avoidance maneuver.

- Computation of the miss distance for conflicting aircraft

In a Tau-altitude CAS, it could eliminate alarms for conflicts that have sufficient miss distance.

In a Tau-altitude CAS (with additional computation and display capability) it could command a horizontal/vertical escape maneuver for situations where such a maneuver would be preferred over a vertical escape maneuver.

In Task 1, the bearing measurement accuracies required for the identified functions were analyzed. In Task 2.1 through 2.3, trade-off analyses were made to establish the preferred antenna, signal processing, and data processing configurations. Then in Task 2.4, the significant sources of error were evaluated and utilized to predict the bearing measurement accuracy. In Task 3.1, a breadboard antenna was built and tested; and in Task 3.2 through 3.4, the hardware characteristics were defined for the receiving, signal processing, and data processing portions of the system.

Each SOW task and the section of the report in which it is described is given in Table 1-1. The balance of this section provides a summary of the program and the conclusions derived.

## 1.2 SUMMARY OF RESULTS

### Task 1, Accuracy Requirements Analysis

- The Proximity Warning Indicator function has little influence on establishing the accuracy requirement for bearing measurement because of the large quantization needed in the display.
- A bearing measurement random error requirement of 0.56 degrees, one sigma, was established to provide the desired miss distance accuracy. The latter is independent of bias error over the region of interest. This miss distance accuracy could provide a significant reduction in the unnecessary alarms caused by the Tau-altitude criterion specified by ANTC-117.
- A bearing measurement accuracy requirement for commanding horizontal maneuvers was to be provided by a study being done by Systems Control, Inc. for the Transportation System Center. Their report indicates that 2.5 degrees (one sigma) is an acceptable value, but RCA believes that this value is excessive due to invalid assumptions in their study.



TABLE 1-1  
CORRELATION BETWEEN REPORT SECTIONS AND  
SOW TASKS

| REPORT<br>SECTION | WORK DESCRIPTION  | SOW TASK |
|-------------------|---|----------|
| 2.0               | Derivation of bearing measurement accuracy requirements | 1        |
| 3.0               | Configuration Analysis                                  | 2        |
| 3.2               | Antenna   | 2.1      |
| 3.3               | Signal Processing                                       | 2.2      |
| 3.4               | Data Processing   | 2.3      |
| 3.5               | Accuracy Analysis                                       | 2.4      |
| 4.0               | Build and test a breadboard antenna                     | 3.1      |
| 5.0               | Hardware Characteristics                                | 3        |
|                   | Receiver  | 3.2      |
|                   | Signal Processor  | 3.3      |
|                   | Data Processor  | 3.4      |

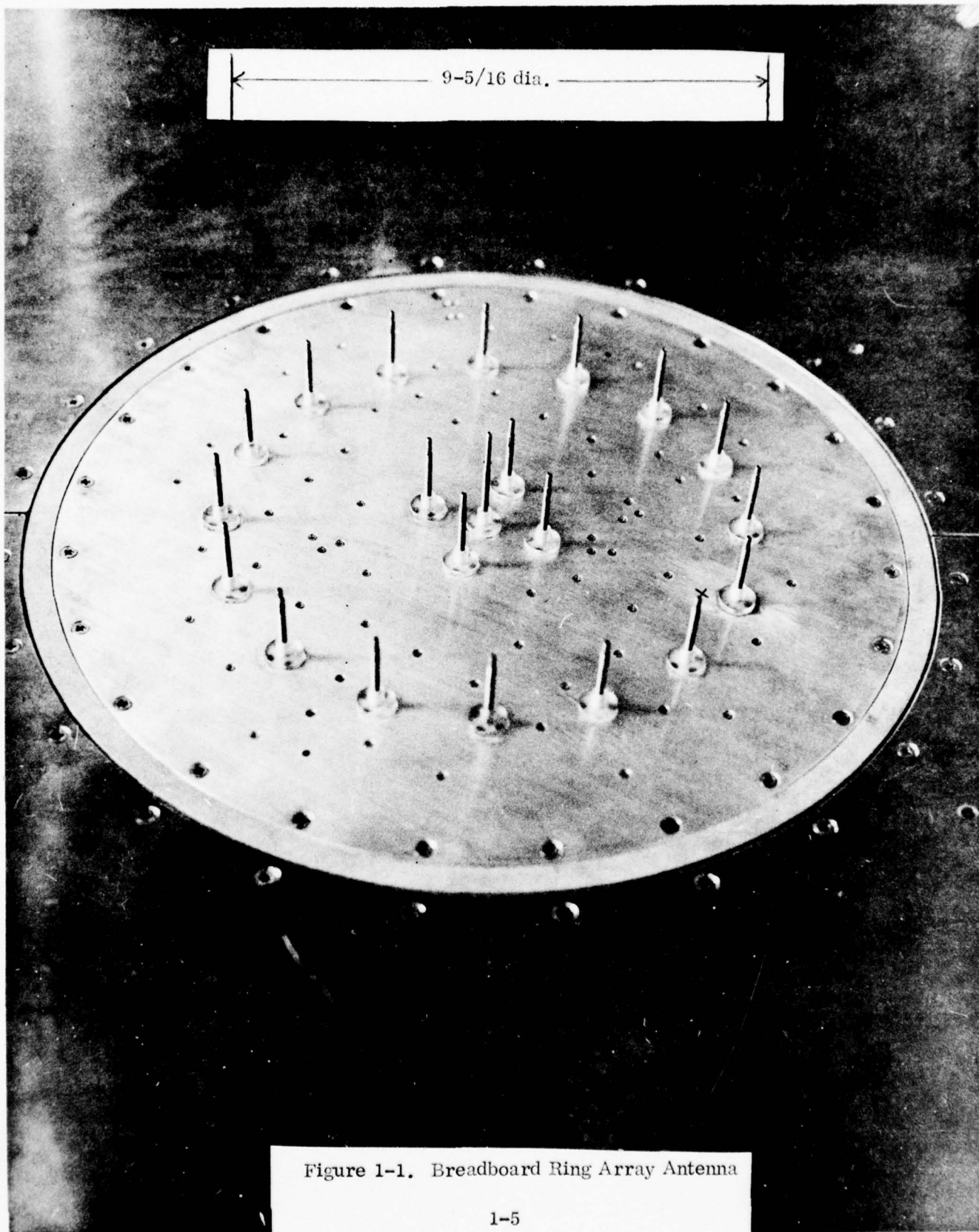
### Task 2.1, Antenna Configuration Analysis

- A ring array is preferred over the three element interferometer array originally proposed because it provides an output phase difference between two ports which is a linear function of target relative bearing, simplifying data processing requirements.
- For high accuracy applications, a four cycle ring array is preferred over a one cycle ring array because its azimuth sensitivity is four times as great. However, a one cycle array is also needed for determining the target's quadrant. The one cycle array alone will provide sufficient accuracy for the PWI application.
- The preferred antenna configuration for high accuracy applications is an array of 21 vertical monopoles, arranged in two rings around a central monopole (as shown in Figure 1-1). The four elements of the inner ring form the one cycle array whose output phase difference (relative to the center monopole) is a direct function of the target relative bearing. The sixteen elements of the outer ring form the four cycle array.
- Increasing the aperture of the antenna reduces the sensitivity to multipath but increases installation problems. A diameter of 9-5/16" was selected as most appropriate for the four cycle array.

### Task 2.2 and 2.3, Signal and Data Processing

- A double superheterodyne receiver will provide signals in its 2nd IF which preserve the phase of the RF signals received in the antenna and are suitable for phase measurement instrumentation. Two phase balanced receiver channels are needed to bring signals simultaneously from the reference monopole and either the one cycle or the four cycle array to the phase measurement instrumentation.





- Location of the front end of the receiver at the antenna site to provide 1st IF signals to the long cables between the antenna and the equipment unit will be required to reduce phase variations due to cable characteristic variations.
- Due to the accuracy requirements, it may be desirable to provide a means to check and correct the phase balance between the two channels periodically and automatically.
- An IF bandwidth of 6 MHz is required to limit phase transients sufficiently to permit accurate phase measurement. Time gating is also required for inhibiting phase measurement during the filter transients at the beginning and end of pulses.
- Sixty-two samples from the high accuracy four cycle antenna can be measured for each target during the last half of the SECANT track cycle. The measurements can be integrated and data processed to minimize random errors.
- Ten samples from the one cycle antenna can be measured for each target during the first half of the SECANT track cycle. The measurements can be integrated and data processed to remove bearing ambiguity from the four cycle antenna valuations.
- The continuous frequency hopping of the SECANT reply frequencies ( $P^+$ ,  $P^-$ ,  $Q^+$ ,  $Q^-$ ) provides frequency diversity which, through the integration process, tends to reduce multipath error. By increasing the spread of these frequencies to the maximum available in the 30 MHz CAS band, multipath error can be reduced significantly.
- Fruit effects can be minimized by range gating and data averaging. Furthermore, "wild" phase measurements caused by fruit interference on the reply being measured can be rejected.

- Bearing measurements must be corrected for aircraft attitude for accurate computation of miss distance. Because miss distance is computed from the difference in relative bearing measurements at two different times; the bearing measurements and aircraft attitude data must be stored, and the time difference must be known and utilized in the computation.
- The time difference will vary with traffic density. In order to have a large enough time difference for computation accuracy, the second bearing measurement should be inhibited until at least four seconds after the first measurement. Then the greatest time difference that may occur will be eight seconds, which is acceptable.

#### Task 2.4, Accuracy Analysis

- A detailed accuracy analysis, in which significant sources of error were analyzed, predicted the following measurement error characteristics.

| <u>Error Type</u>            | <u>Degrees (<math>1\sigma</math>)</u> |
|------------------------------|---------------------------------------|
| Relative Bearing ( $\beta$ ) |                                       |
| Overall                      | 1.0                                   |
| Bias                         | 0.8                                   |
| Random                       | 0.5                                   |

These results, however, are predicted upon assumptions which should be experimentally validated.

#### Task 3.1, Breadboard Antenna

- The 21 monopole, three ring array (shown in Figure 1-1), was built using stripline techniques. All transmission lines and hybrids for connecting the elements of each array to its connector were provided by appropriate etching of a copper clad dielectric sheet.



- Basic tests of the antenna in an anechoic chamber indicated good correspondence with expected performance. Some anomalies were found that are considered to be correctable by dimensional changes. The one cycle array had a high ripple (cyclic departure from linearity) which was found to be caused by reradiation from the four cycle array. This can be corrected by short circuiting the four cycle array when the one cycle array is being used.
- Patterns of phase difference versus azimuth angle indicated a bearing measurement accuracy close to the predicted value.
- The effect of multipath was explored by placing a cone reflector on the antenna table and observing the resulting change of azimuth pattern. The spacing of the reflector was not typical of aircraft surfaces due to the limited size of the turntable and the anechoic chamber. The result showed a peak error (maximum departure of indicated azimuth from actual azimuth) of 2 degrees. This value is slightly larger than the predicted value of 1.4 degrees.
- Frequency diversity reduced the multipath error to a peak value of 1.2 degrees. A reduction to 0.63 degrees is predicted for cases where the multipath reflector is at greater distances, which is more representative of aircraft structures.
- The variation of the azimuth characteristic with vertical angle was found to be suitably small.

#### Task 3.2, 3.3, 3.4, Hardware Characteristics

- A novel digital concept will permit phase measurements to be made with a quantization error of 0.04 degrees.
- The miss distance determination function can be omitted to reduce the complexity of the Bearing Measurement Subsystem for use with a PWI.

### 1.3 CONCLUSIONS

The following conclusions were reached as a result of this program:

- a. Based on the results of this analysis plus a limited antenna test, the ability to measure relative bearing of a cooperative target appears to be feasible.
- b. The model used in the analysis and tests of this program was based on data from typical aircraft antenna patterns. However, the degree of equivalence is not certain and should be confirmed by test.
- c. The indicated performance results from the combination of several unique techniques:
  - Four cycle ring antenna array
  - Frequency diversity
  - Time gating
  - Digital phase measurement
  - Integration and data processing of many independent measurements
  - Attitude compensation
- d. There are a number of potential applications for which a Bearing Measurement Subsystem of the type and capability described here can be useful. Further study of their usefulness and feasibility may be appropriate. Such applications include:
  - Proximity Warning System  
Similar to station-keeping but with less accuracy and resolution
  - Rendezvous Systems
  - Airborne Refueling
  - Sonobuoy Locating

- Carrier Homing
- Search and Rescue
- Navigation Systems
- Automatic Direction Finding (ADF)

#### 1.4 RECOMMENDATIONS

Because of the indication that the Bearing Measurement Subsystem is feasible, and because it is expected to be useful in a number of worthwhile applications, the following recommendations are made:

- a. The investigation of feasibility should be extended to field tests of the techniques and equipment proposed.
- b. The most useful of the potential applications should be identified and their feasibility determined by further studies. Such studies should include requirements definition and analysis, system concept design, equipment concept design, and cost projection.



## SECTION 2.0

### ANALYSIS OF ACCURACY REQUIREMENTS (TASK 1)

#### 2.1 INTRODUCTION

This section is responsive to Task 1 of the Statement of Work. The objective of the task is to define the accuracy requirement to be imposed on the bearing measurement subsystem for its three functional uses. These uses are:

a. Visual Bearing Indicator

A relative bearing indicator for use in conjunction with a Proximity Warning Indicator (PWI) or a Collision Avoidance System (CAS) to assist in pilot location of threatening aircraft.

b. Unnecessary Warning Elimination

Horizontal miss distance measurement for use in conjunction with a Vertical Escape CAS (VECAS) to eliminate some of the unnecessary warnings of the Tau criterion. Warnings are unnecessary when the miss distance is greater than a safe value but nevertheless exceeds the Tau criterion.

c. Horizontal Maneuvering

Miss distance measurement for use in conjunction with a CAS to determine when a horizontal maneuver should be initiated and the proper direction and duration of the maneuver.

The major effort on this task was specified to be on Function (b). The accuracy requirement for Function (a) was to be obtained from available FAA studies and for Function (c) from a study program being conducted by Systems Control, Inc. for the Transportation System Center.

The task results for each of these functions are described in Sections 2.2, 2.3, and 2.4 respectively. The overall conclusions are summarized in Section 2.5.

## 2.2 VISUAL BEARING INDICATOR

The accuracy requirement for bearing measurement when it is used as a visual indicator of threat relative bearing was determined from a study done by FAA contained in Report No. FAA-RD-71 entitled, "Reactions of Pilots to Warning Systems for Visual Collision Avoidance" dated December 1971. The conclusion was reached in that study that there was no value in using a warning sector of less than 30 degrees in azimuth. No specific investigation was made to determine the result of indicating the adjacent sector rather than the one in which the target is located. However, the study indicates that a minimum PWI without where-to-look information is of significant value in reducing undetected alarms. This implies that a wrong sector indication is relatively unimportant, and therefore, a one sigma error of as much as 15 degrees is acceptable.

These statements apply to the pilot display and indicate the quantization requirement. This would also specify the accuracy requirement for the bearing measurement subsystem. However, it is expected that the accuracy of a practical bearing measurement subsystem would be much better than required for this function. Therefore, the accuracy requirement used to set the design goal for this program will not be based on this function but on one of the more demanding functions to be discussed in the following subsections.

## 2.3 ACCURACY REQUIRED FOR UNNECESSARY WARNING REDUCTION

### 2.3.1 Introduction

This section investigates the accuracy required for swept bearing measurement when it is used to determine miss distance to reduce unnecessary alarms caused by the use of a Tau warning detector alone.

Taking a horizontal miss distance value of 1000 feet or less as unacceptable, then all Tau 1 or Tau 2 warnings on conflicts that have more than 1000 feet miss distance are considered unnecessary. A discriminator is postulated which determines miss distance prior to initiation of the Tau warning and, if greater than a threshold value  $M_T$ , will inhibit the Tau warning.

Previous work found that the least error sensitive approach for determining miss distance by measurements from one aircraft is to measure the relative range and the relative bearing at two successive times. Then

$$M \approx \frac{R_1 R_2 \Delta\beta}{\sqrt{(R_1 - R_2)^2 + R_1 R_2 (\Delta\beta)^2}}$$

where

$R_1$  = Relative range at time 1

$R_2$  = Relative range at time 2

$\Delta\beta$  = Swept bearing, the change in relative bearing from time 1 to time 2

The approximation is true for the small miss distances of concern to collision avoidance. This approach allows the miss distance to be measured as almost a direct function of swept bearing and is completely independent of a constant bias error in the bearing measurement.

The locus of the Tau-Range alarm  $R_T = R_O + T | - \dot{R} |$  plotted in a distance-to-go, miss coordinate system, is a cardioid (see Figure 2-1). If a critical miss  $M_C$ , corresponding to the hazardous near-miss condition (say 1000 ft.) is specified, then the region of the cardioid where the abscissa lies between  $M_C$  and  $M_{\max}$  (as well as between  $-M_C$  and  $-M_{\max}$ ) constitutes a region of unnecessary alarms. The probability of false



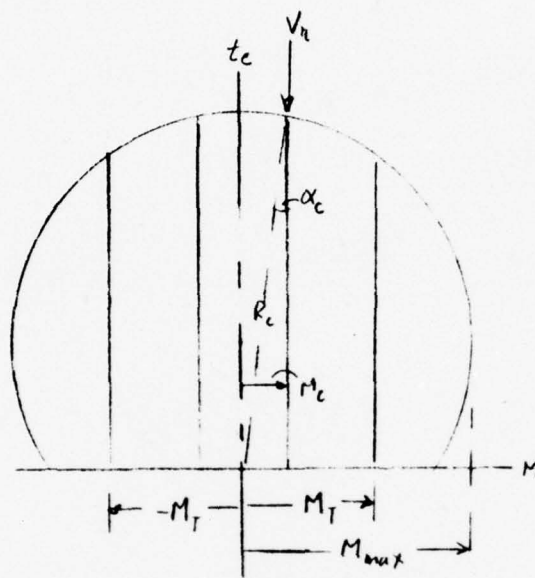


Figure 2-1. Miss Distance (M) vs. Range (R) Locus of Tau Criterion

alarms for the Tau ( $\tau$ ) system ( $P_{fa\tau}$ ) is then  $\frac{M_{\max} - M_C}{M_{\max}}$ . Ideally, then, if the miss distance sensor has a threshold  $M_T$  set equal to  $M_C$ , it would eliminate a wide region of alarms which would otherwise be generated by the Tau warning. Because of errors in measured range and bearing, there will be errors in computed miss distance. The errors incur a finite probability that the computed miss exceeds the alarm threshold, whence no alarm would be given when it should have been given. To reduce this probability of missed alarm, it is necessary to set the miss threshold to a value somewhat greater than the critical value, and to accept less than the ideal reduction in unnecessary alarms. The single conflict missed alarm probability ( $P_{mas}$ ) is computed as a function of miss threshold ( $M_T$ ) and of statistical error parameter in miss  $\sigma(\delta M)$ . The miss parameter being a function of relative velocity ( $V_R$ ) and of swept bearing error parameter  $\sigma(\Delta\beta)$ , it was then possible to plot  $M_T$  vs.  $\sigma(\Delta\beta)$  for specific values of  $P_{mas}$  and  $V_R$ . To definitize the selection of  $M_T$ , the false alarm probability ( $P_{fac}$ ) for the combined M- $\tau$  system is then  $M_T - M_C/M_{\max}$ , as leading to a factor ( $\eta$ ) to define the relative efficiency of improvement of the combined M- $\tau$  system.

$$\eta = \frac{M_{\max} - M_T}{M_{\max} - M_C} = \frac{P_{fa\tau} - P_{fac}}{P_{fa\tau}}$$

Evidently the smaller the threshold, the greater the effectiveness in eliminating false alarms. By specifying  $P_{fac} = 0.5$ , a region of acceptable values of  $M_T$  and  $\sigma(\Delta\beta)$  has been obtained for either  $\tau 1$  or  $\tau 2$  cardioid.

Finally, threshold values were tested under specified (simulated) traffic conditions. In the controlled environment of the 1982 LAX traffic model, the result is several orders of magnitude reduction in missed alarm probabilities. It appears then, that a specification of  $P_{mas} = .001$  for  $\tau 1$  cardioid, should be acceptable. Based on these values, an acceptable value of  $\sigma(\Delta\beta)$  has been determined, with suitable  $M_T$  being taken as function of relative velocity.

### 2.3.2 Threshold Setting vs. Bearing Error

For two aircraft in conflict, a missed alarm probability,  $P_{mas}$ , can be defined as the conditional probability; given that the intruder aircraft has penetrated a Tau cardioid

(either  $\tau_1$  or  $\tau_2$ ) and has a projected miss distance less than some critical value ( $M_C$ ), then  $P_{\text{mas}}$  is the probability that an alarm is not given; i.e., the indicated miss is greater than a specified miss alarm threshold. Thus,

$$\begin{aligned} P_{\text{mas}} &= -1 P(-M_T < \hat{M} < M_T) \\ &= 1 - 1/2 [\text{erf } x_2 + \text{erf } x_1] \end{aligned}$$

where (see App. B),

$$\begin{aligned} x_1 &= \frac{1}{\sqrt{2}} \left( \frac{M_T + M_C + \overline{\delta M}}{\sigma_M} \right) \\ x_2 &= \frac{1}{\sqrt{2}} \left( \frac{M_T - M_C - \overline{\delta M}}{\sigma_M} \right) \end{aligned}$$

and where  $\overline{\delta M}$  = bias error in miss estimate

$\sigma_M$  = std. deviation of error in miss estimate

The miss statistical parameters are functions of the error parameters in measured range and swept bearing, as discussed in App. C. They are evaluated at Tau cardioid penetration and at a critical miss distance taken as  $M_C = 1000$  feet (near-miss hazard criterion), see Figure 2-1. A standard 5 second interval is used for the measurement of swept bearing ( $\Delta\beta$ ). Tables 2-1 and 2-2 show sample printouts for  $P_{\text{mas}}$  as a function of  $\sigma(\Delta\beta)$  and for specified  $\tau$ ,  $V_r$ , and  $M_T$ .  $P_{\text{mas}}$  is shown plotted in Figure 2-2 as a function of  $\sigma_M$ , independent of  $\tau$  and  $V_r$ , and for zero bias error in  $\Delta\beta$ . (It is expected that systematic bearing errors will be predominantly a consequence of fruit interference and multipath effects; that is, the bias error may be nonstationary, time-dependent. The bias error is, therefore, neglected in the subsequent analysis, and it is to be understood that a sigma specification is inclusive of the bias effects, on an rss basis.) Table 2-3 provides a calibration table for converting  $\sigma(\delta M)$  to appropriate  $\sigma(\Delta\beta)$  at various speeds. Note that the required  $\sigma(\Delta\beta)$  decreases with increased



TABLE 2-1

Pmas vs  $\sigma(\Delta\beta)$ , for  $V_r = 315$  Knots,  $\tau_2$ ,  $M_T = 2000$  ft.

(Various Bias Error Ratios)

T= 2.00 MT= 2000.00 VR= 315.00

| SG(DB) | K(B)  | DEL(M)    | DEL(M)     | P <sub>4</sub> | I-PM   | PFA    | PMA    |
|--------|-------|-----------|------------|----------------|--------|--------|--------|
| 0.10   | -3.00 | 623.672   | -1864.367  | 0.9857         | 0.0342 | 0.9560 | 0.0003 |
| 0.10   | -1.00 | 623.672   | -617.127   | 0.9952         | 0.0043 | 0.9852 | 0.0000 |
| 0.10   | -0.50 | 623.672   | -305.317   | 0.9818         | 0.0182 | 0.9720 | 0.0002 |
| 0.10   | 0.00  | 623.672   | 6.493      | 0.9444         | 0.0556 | 0.9350 | 0.0006 |
| 0.10   | 0.50  | 623.672   | 318.303    | 0.8623         | 0.1372 | 0.8542 | 0.0014 |
| 0.10   | 1.00  | 623.672   | 630.113    | 0.7234         | 0.2766 | 0.7162 | 0.0028 |
| 0.10   | 3.00  | 623.672   | 1877.353   | 0.0799         | 0.9202 | 0.0790 | 0.0092 |
|        |       |           |            |                |        |        |        |
| 0.30   | -3.00 | 1870.877  | -5606.082  | 0.0816         | 0.9184 | 0.0808 | 0.0092 |
| 0.30   | -1.00 | 1870.877  | -1864.366  | 0.6652         | 0.3348 | 0.6585 | 0.0033 |
| 0.30   | -0.50 | 1870.877  | -928.937   | 0.7146         | 0.2854 | 0.7074 | 0.0029 |
| 0.30   | 0.00  | 1870.877  | 6.493      | 0.6483         | 0.3517 | 0.6418 | 0.0035 |
| 0.30   | 0.50  | 1870.877  | 941.923    | 0.4948         | 0.5052 | 0.4899 | 0.0051 |
| 0.30   | 1.00  | 1870.877  | 1877.353   | 0.3150         | 0.6850 | 0.3118 | 0.0069 |
| 0.30   | 3.00  | 1870.877  | 5619.070   | 0.0068         | 0.9932 | 0.0067 | 0.0099 |
|        |       |           |            |                |        |        |        |
| 0.50   | -3.00 | 3118.110  | -9347.801  | 0.0204         | 0.9796 | 0.0202 | 0.0098 |
| 0.50   | -1.00 | 3118.110  | -3111.606  | 0.3921         | 0.6079 | 0.3882 | 0.0061 |
| 0.50   | -0.50 | 3118.110  | -1552.557  | 0.4722         | 0.5278 | 0.4675 | 0.0053 |
| 0.50   | 0.00  | 3118.110  | 6.493      | 0.4575         | 0.5425 | 0.4529 | 0.0054 |
| 0.50   | 0.50  | 3118.110  | 1565.543   | 0.3565         | 0.6435 | 0.3529 | 0.0064 |
| 0.50   | 1.00  | 3118.110  | 3124.593   | 0.2231         | 0.7769 | 0.2208 | 0.0078 |
| 0.50   | 3.00  | 3118.110  | 9360.789   | 0.0036         | 0.9964 | 0.0036 | 0.0100 |
|        |       |           |            |                |        |        |        |
| 1.00   | -3.00 | 6236.203  | -18702.102 | 0.0051         | 0.9949 | 0.0051 | 0.0099 |
| 1.00   | -1.00 | 6236.203  | -6229.703  | 0.1791         | 0.8209 | 0.1773 | 0.0082 |
| 1.00   | -0.50 | 6236.203  | -3111.606  | 0.2380         | 0.7620 | 0.2356 | 0.0076 |
| 1.00   | 0.00  | 6236.203  | 6.493      | 0.2484         | 0.7516 | 0.2459 | 0.0075 |
| 1.00   | 0.50  | 6236.203  | 3124.593   | 0.2036         | 0.7964 | 0.2016 | 0.0080 |
| 1.00   | 1.00  | 6236.203  | 6242.691   | 0.1311         | 0.8689 | 0.1298 | 0.0087 |
| 1.00   | 3.00  | 6236.203  | 18715.090  | 0.0020         | 0.9980 | 0.0020 | 0.0100 |
|        |       |           |            |                |        |        |        |
| 1.30   | -3.00 | 8107.062  | -24314.684 | 0.0034         | 0.9966 | 0.0033 | 0.0100 |
| 1.30   | -1.00 | 8107.062  | -8100.562  | 0.1338         | 0.8662 | 0.1325 | 0.0087 |
| 1.30   | -0.50 | 8107.062  | -4047.037  | 0.1818         | 0.8182 | 0.1800 | 0.0082 |
| 1.30   | 0.00  | 8107.062  | 6.493      | 0.1934         | 0.8066 | 0.1915 | 0.0081 |
| 1.30   | 0.50  | 8107.062  | 4060.023   | 0.1610         | 0.8390 | 0.1594 | 0.0084 |
| 1.30   | 1.00  | 8107.062  | 8113.551   | 0.1049         | 0.8951 | 0.1039 | 0.0090 |
| 1.30   | 3.00  | 8107.062  | 24327.672  | 0.0016         | 0.9984 | 0.0016 | 0.0100 |
|        |       |           |            |                |        |        |        |
| 2.00   | -3.00 | 12472.402 | -37410.699 | 0.0019         | 0.9981 | 0.0018 | 0.0100 |
| 2.00   | -1.00 | 12472.402 | -12465.902 | 0.0838         | 0.9162 | 0.0830 | 0.0092 |
| 2.00   | -0.50 | 12472.402 | -6229.703  | 0.1168         | 0.8832 | 0.1156 | 0.0088 |
| 2.00   | 0.00  | 12472.402 | 6.493      | 0.1270         | 0.8730 | 0.1257 | 0.0087 |
| 2.00   | 0.50  | 12472.402 | 6242.691   | 0.1078         | 0.8922 | 0.1067 | 0.0089 |
| 2.00   | 1.00  | 12472.402 | 12478.891  | 0.0714         | 0.9286 | 0.0707 | 0.0093 |
| 2.00   | 3.00  | 12472.402 | 37423.687  | 0.0012         | 0.9988 | 0.0011 | 0.0100 |

TABLE 2-2

Pmas Vs.  $\sigma(\Delta\beta)$  for  $V_r = 315$  Knots( $\tau_2$ ,  $M_T = 11000$  ft.)

| $\tau_{AU} = 2.00$ $M_T = 11000.00$ $VR = 315.00$ |       |          |        |        |        |        |        |
|---|-------|----------|--------|--------|--------|--------|--------|
| SG(Db)  | K(Db) | SIS(M)   | DEL(M) | PM     | (1-PM) | PFA    | PHA    |
| 0.10  | 0.00  | 523.572  | 6.493  | 1.0000 | 0.0000 | 0.9900 | 0.0000 |
| 0.30  | 0.00  | 1270.877 | 6.493  | 1.0000 | 0.0000 | 0.9900 | 0.0000 |
| 0.50  | 0.00  | 3118.110 | 6.493  | 0.9993 | 0.0007 | 0.9893 | 0.0000 |
| 0.80  | 0.00  | 4998.366 | 6.493  | 0.9694 | 0.0306 | 0.9597 | 0.0003 |
| 1.00  | 0.00  | 6235.205 | 6.493  | 0.9184 | 0.0816 | 0.9092 | 0.0008 |
| 1.30  | 0.00  | 8107.064 | 6.493  | 0.8219 | 0.1781 | 0.8136 | 0.0018 |

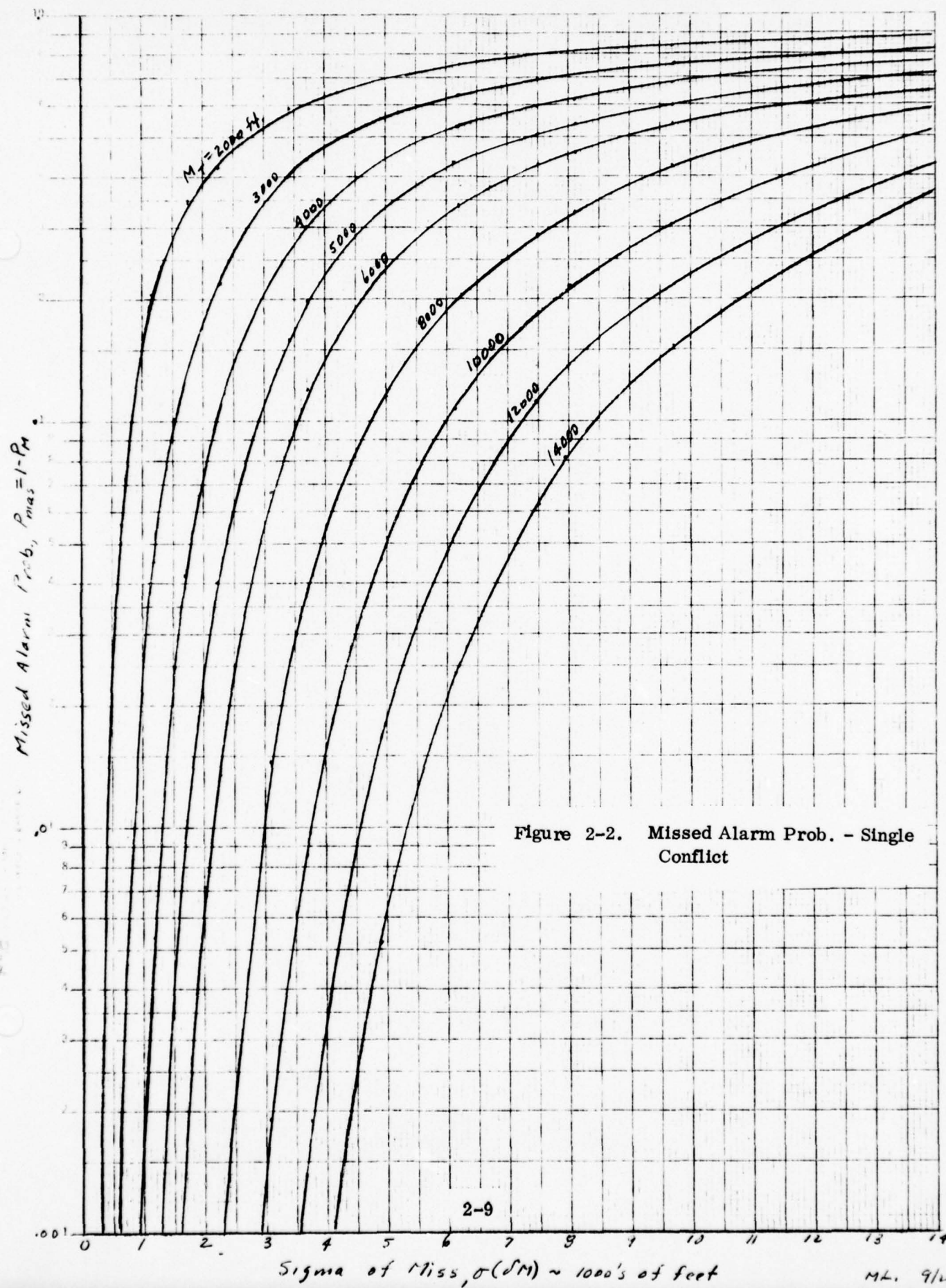


Figure 2-2. Missed Alarm Prob. - Single Conflict

2-9

ML 9/14/13



TABLE 2-3  
Values of  $\sigma(\Delta\delta)$  for Various Values of  $V_r$  and  $(\delta M)$   
 $\sigma(\delta M)$  to  $\sigma(\Delta\delta)$  CONVERSION

| $\tau$ | $V_r$<br>(Knots) | 1000 | 2000 | 3000 | 4000 | 5000 | 6000 | 7000 | 8000 | 9000 |
|--------|------------------|------|------|------|------|------|------|------|------|------|
| Tau 1  | 100              | 1.80 | 3.60 |      |      |      |      |      |      |      |
|        | 315              | .85  | 1.71 | 2.56 | 3.42 |      |      |      |      |      |
|        | 500              | .58  | 1.16 | 1.75 | 2.33 | 2.92 |      |      |      |      |
| Tau 2  | 100              | .17  | .33  | .50  | .66  | .82  | .98  | 1.14 | 1.31 | 1.48 |
|        | 315              | .16  | .32  | .48  | .64  | .80  | .96  | 1.12 | 1.28 | 1.44 |
|        | 500              | .13  | .27  | .40  | .54  | .67  | .80  | .94  | 1.07 | 1.21 |

Note:  $\sigma(\Delta\delta)$  given in degrees per five second interval

$V_r$  (relative velocity), for given  $\sigma(\delta M)$ . A different manner of presentation is given, Figure 2-3, where miss threshold  $M_T$  has been plotted against  $\sigma(\delta M)$  for specified values of  $P_{mas}$ . Given a value of  $\sigma(\delta M)$ , it is seen that the miss threshold must increase in order to decrease the missed alarm probability. Conversely, if the threshold is fixed, then  $\sigma(\delta M)$  must be reduced in order to reduce  $P_{mas}$ .

By employing Figure C-3, of Appendix C, the miss threshold required to achieve a specified  $P_{mas}$ , for specified  $\tau$  and  $V_r$ , can be displayed as a function of  $\sigma(\Delta\beta)$ . Figures 2-4 through 2-7 present this information. Evidently some additional criterion must be applied to definitize the  $M_T$  selection. This is taken to be the effectiveness in reducing the single conflict false alarm probability. In Figure 2-1, it is equally likely that  $M_T$  can have any value up to  $M_{max}$  (see Appendix D), then for the  $\tau$  only system, a measure of the expected number of false alarms is

$$P_{fa\tau} = \frac{M_{max} - M_C}{M_{max}}$$

since only for  $0 < M_t < M_C$  should an alarm be truly given. Evidently, in a combined  $\tau$ - $M$  system, we cannot make  $M_T = M_C$  because of measurement errors. As indicated in Figure 2-2, a sizeable threshold is desirable, for fixed  $\sigma(\Delta\beta)$ , in order to obtain a suitably low  $P_{mas}$ . On the other hand, lowering the threshold will decrease the false alarm probability. For the combined system,

$$P_{fac} = \frac{M_T - M_C}{M_{max}}$$

Figures 2-8 and 2-9 present  $P_{fac}$  as function of  $V_r$  and  $M_T$ .

A measure of effectiveness is the percent improvement (i.e., reduction in false alarm probability) of the combined  $M$ - $\tau$  from the  $\tau$  system.

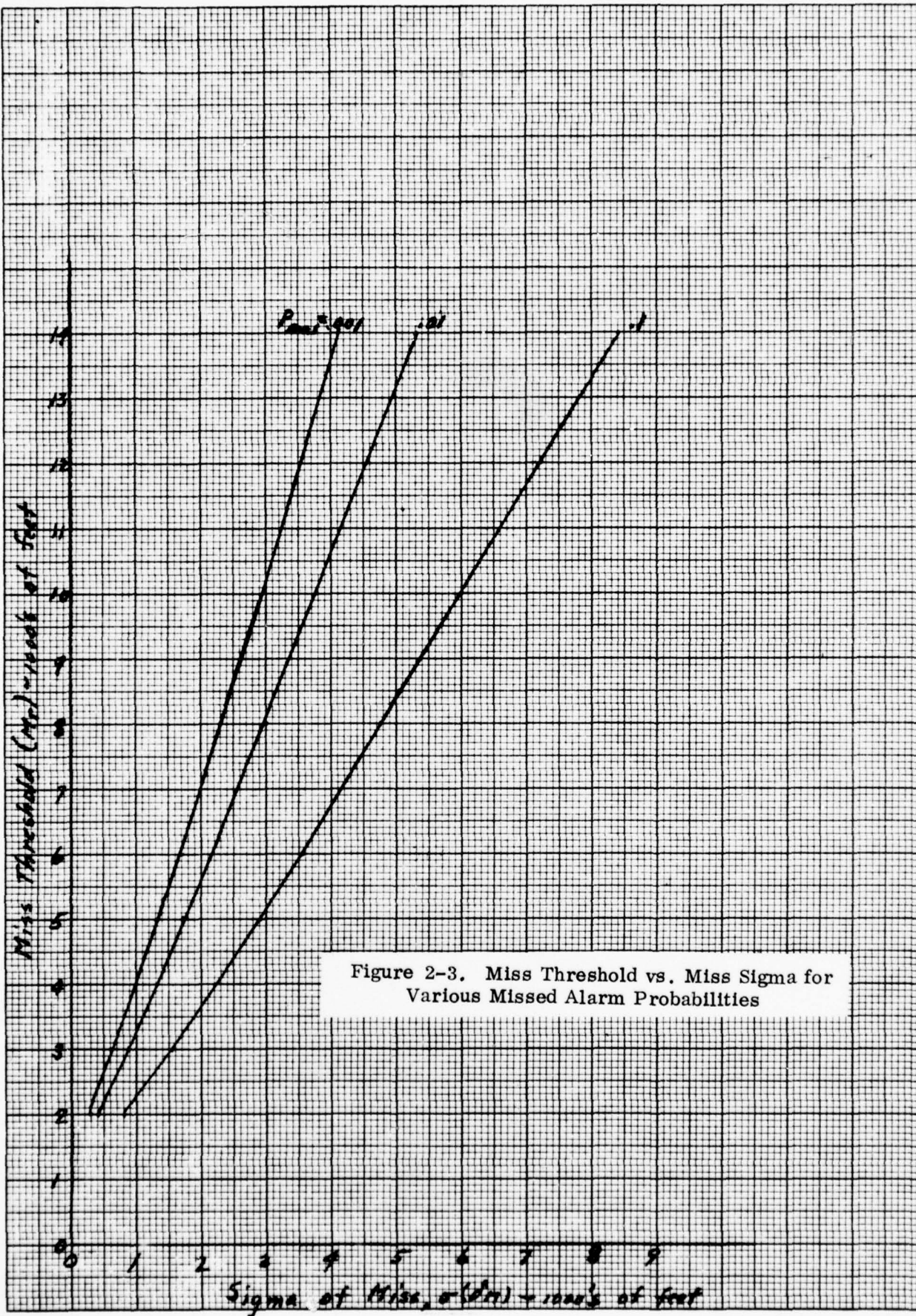
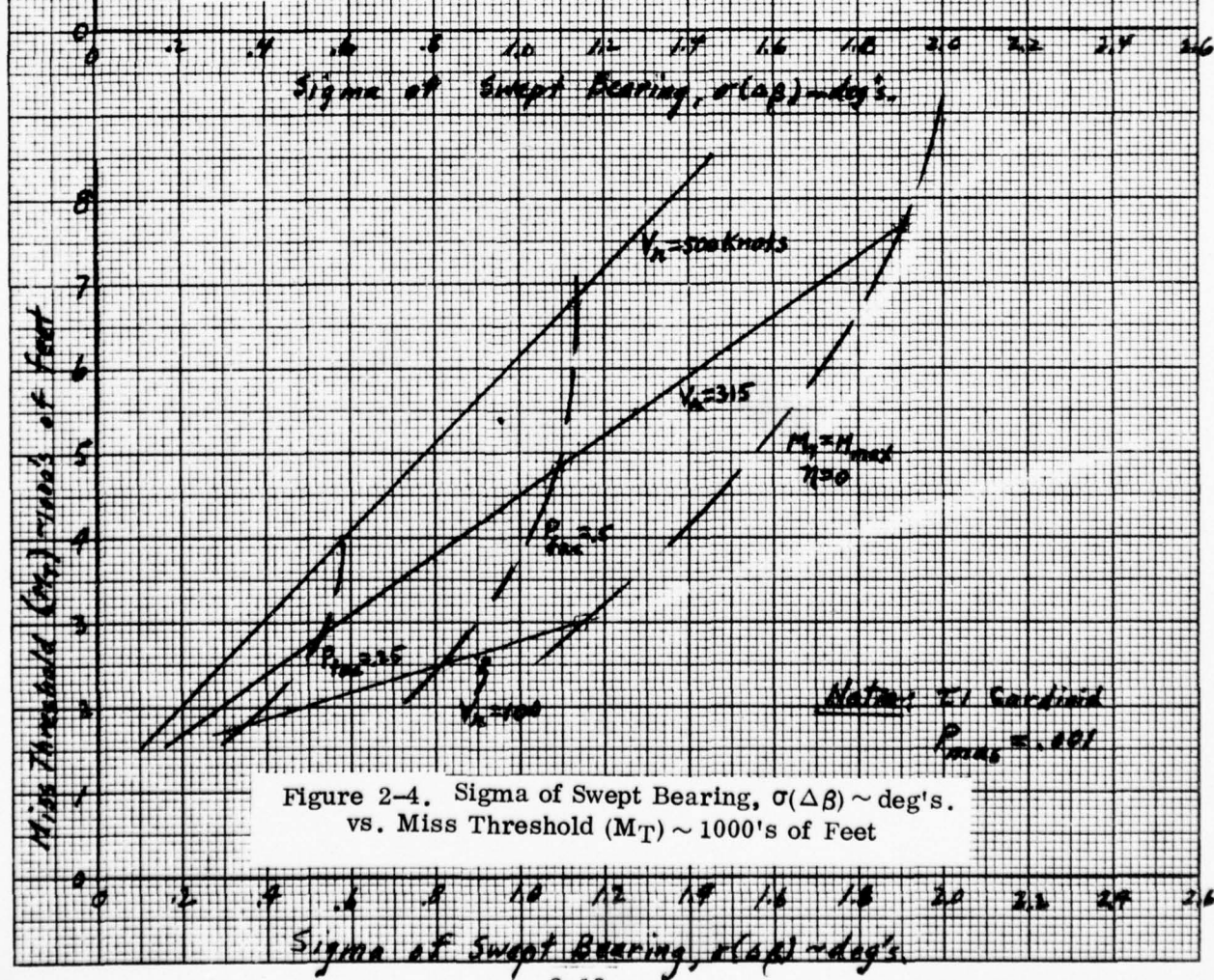
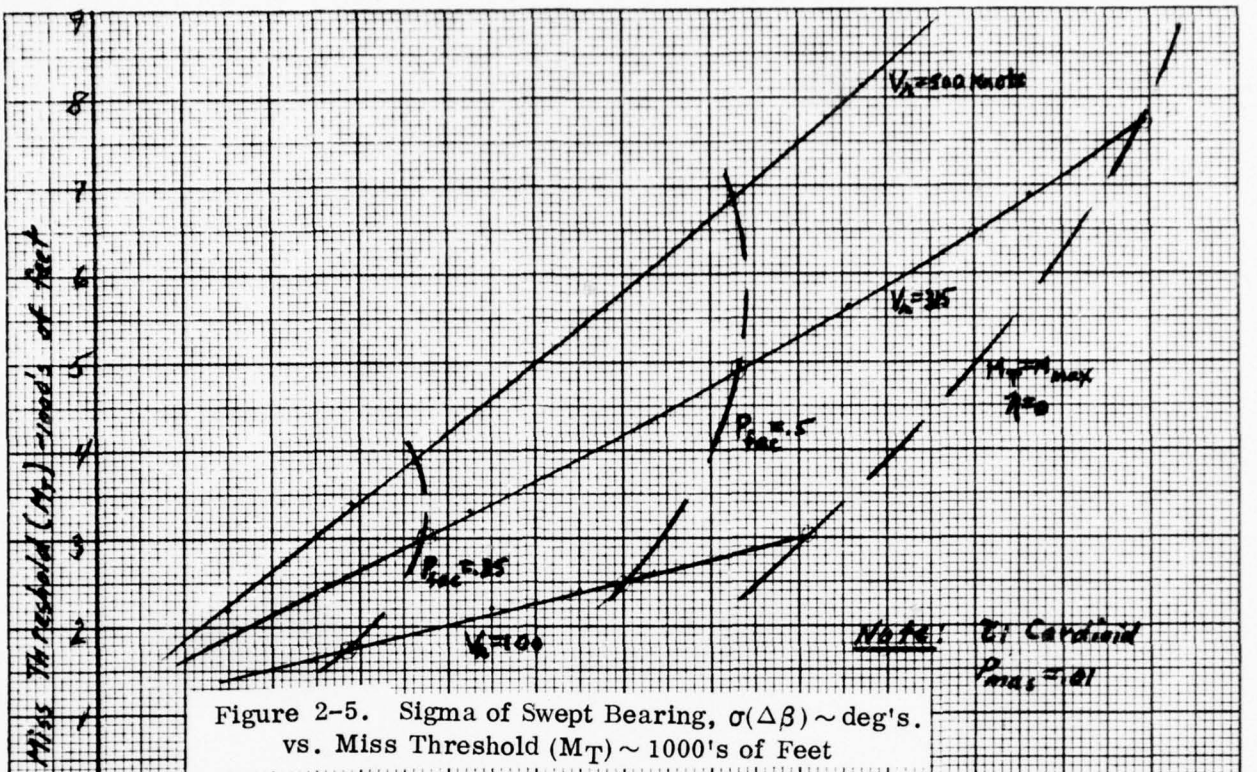
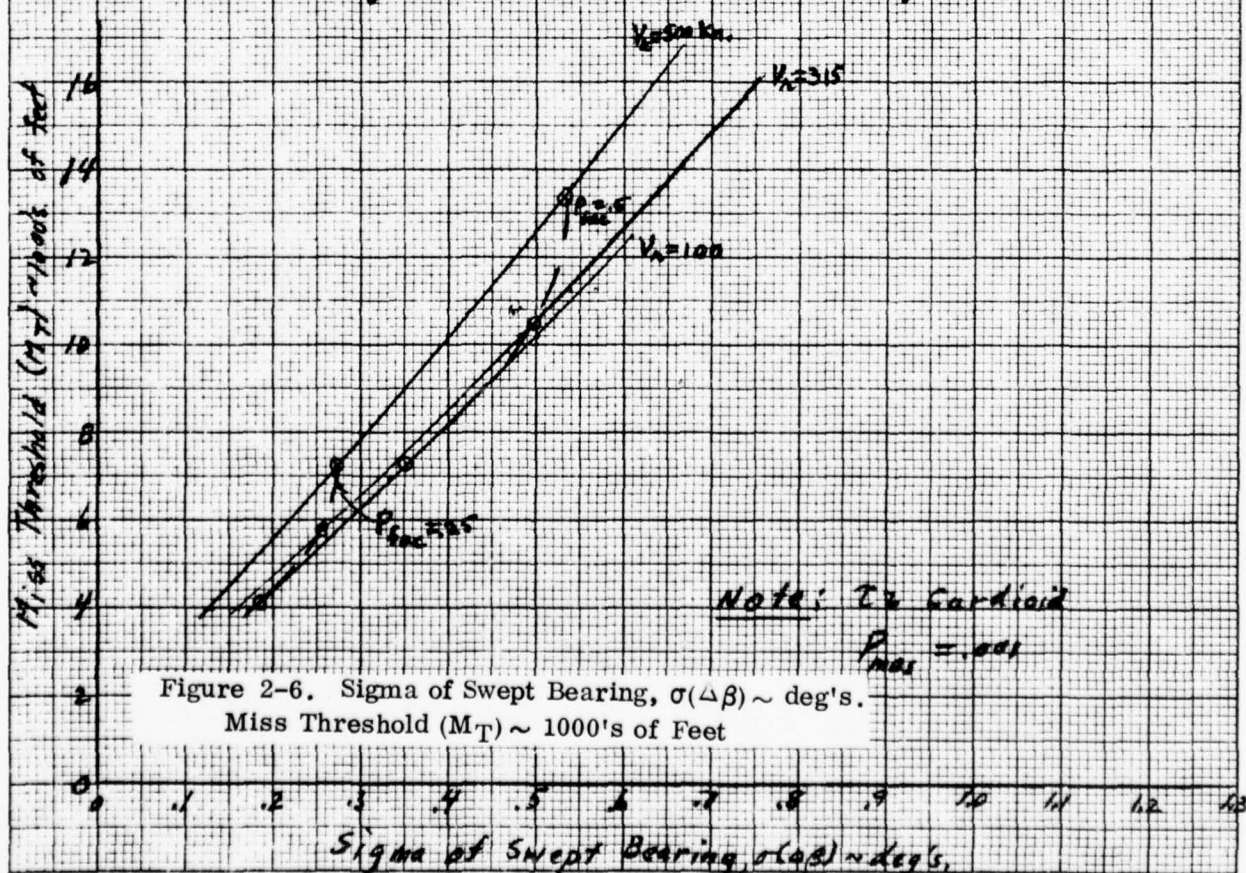
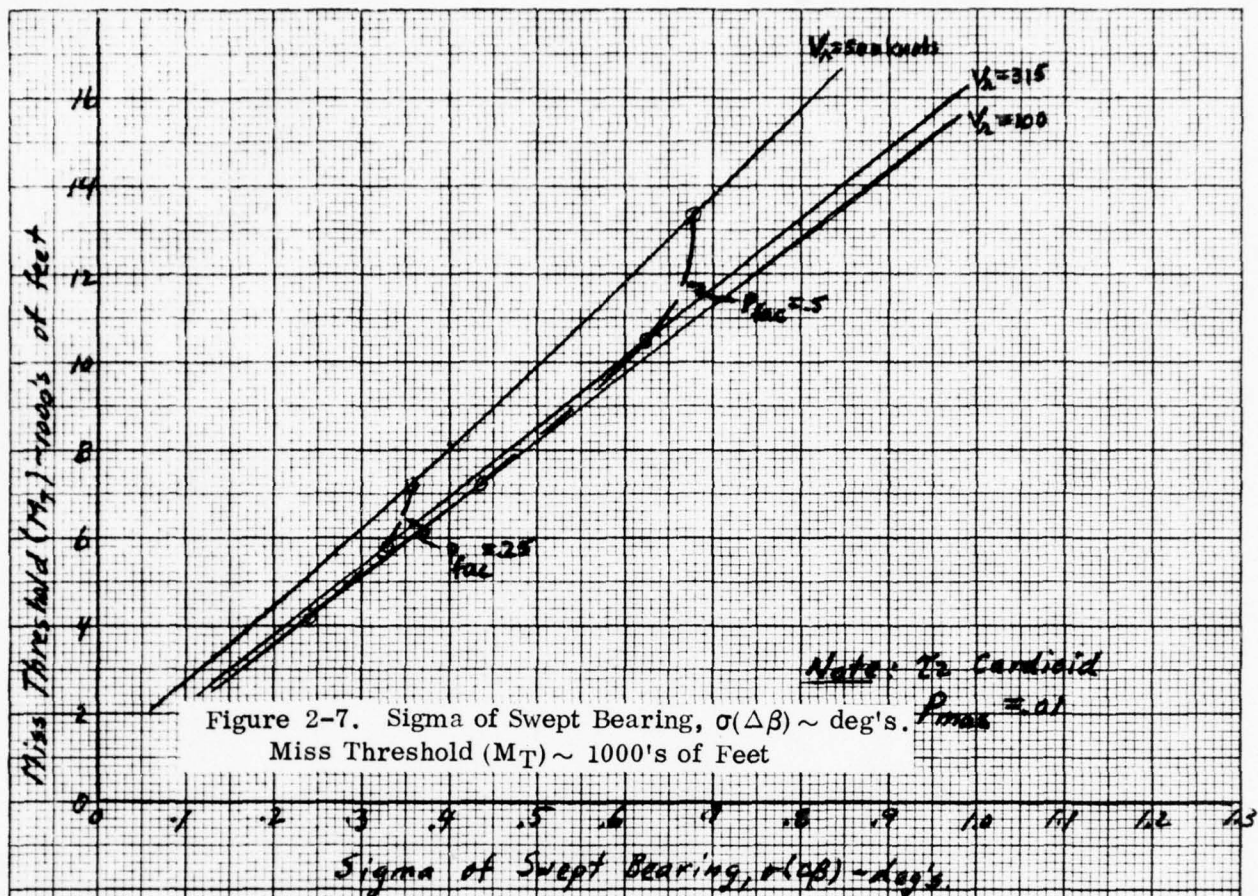


Figure 2-3. Miss Threshold vs. Miss Sigma for Various Missed Alarm Probabilities

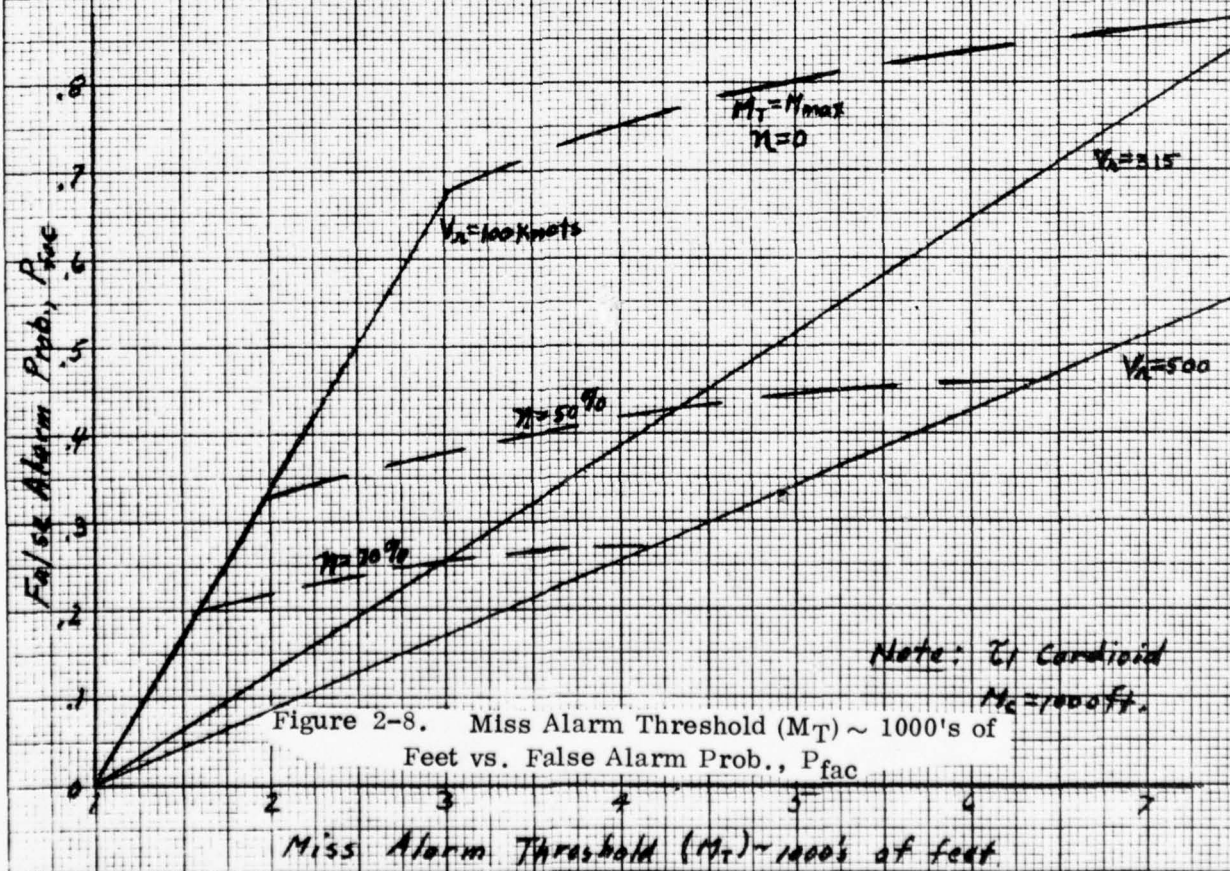
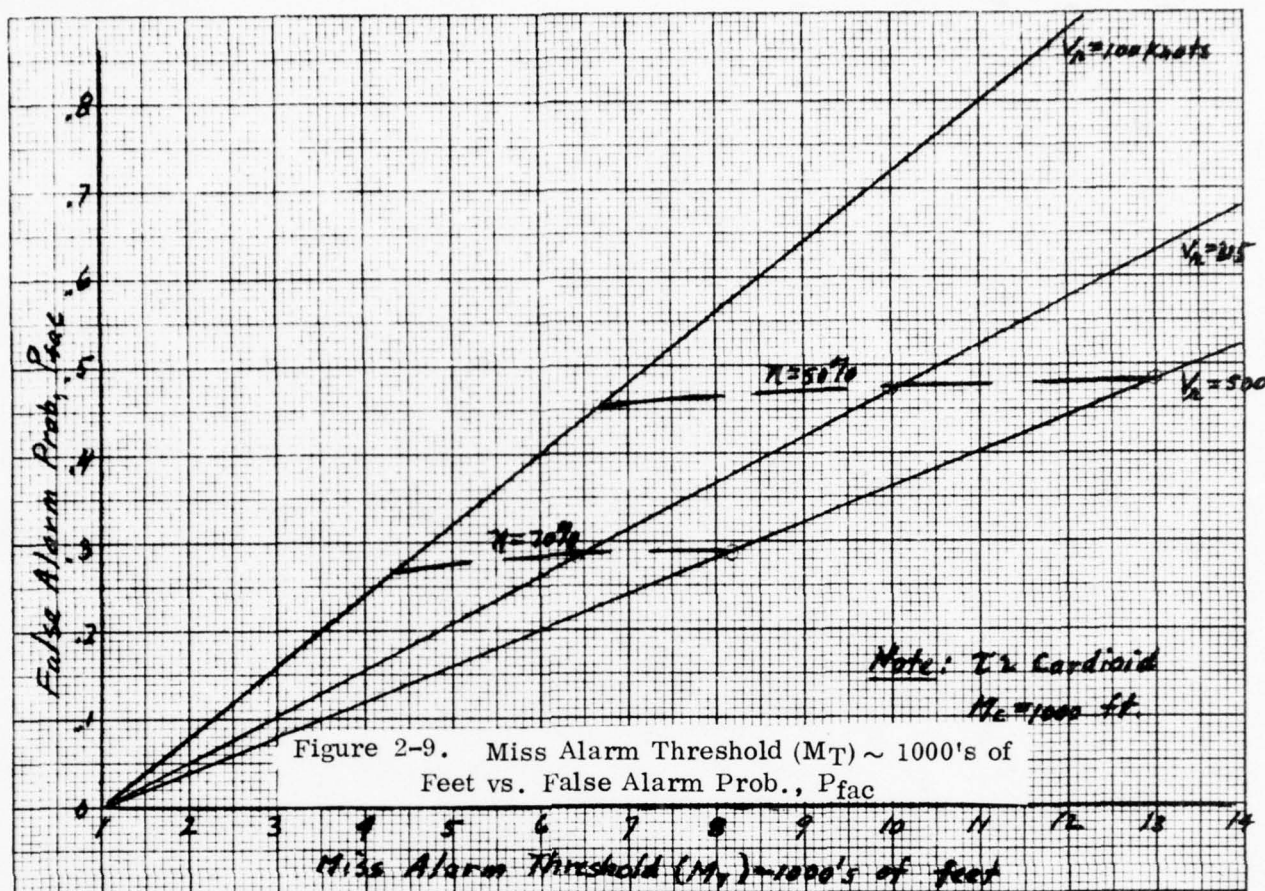


K&E 10 X 10 TO 1/2 INCH 46 1322  
7 X 10 IN. L&E  
KEUFFEL & ESSER CO.











$$\eta (\%) = 100 \left[ 1 - \frac{P_{fac}}{P_{fa\tau}} \right]$$

$\eta$  has been plotted as functions of  $V_r$  and  $M_T$ , in two different manners in Figures 2-10 through 2-13. Superposed on Figures 2-12 and 2-13 is the  $\tau$ -only system false alarm probability,  $P_{fa\tau}$ .

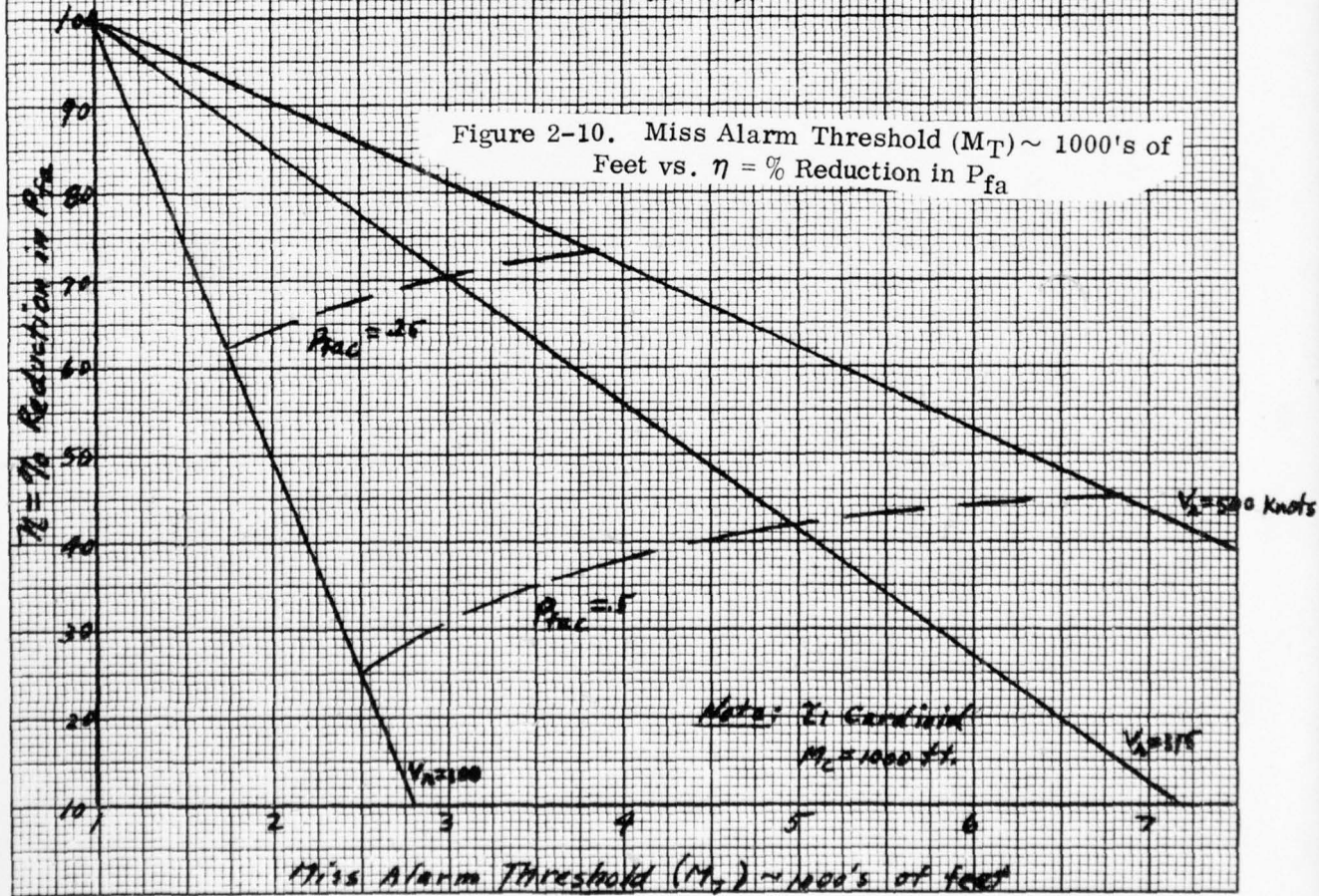
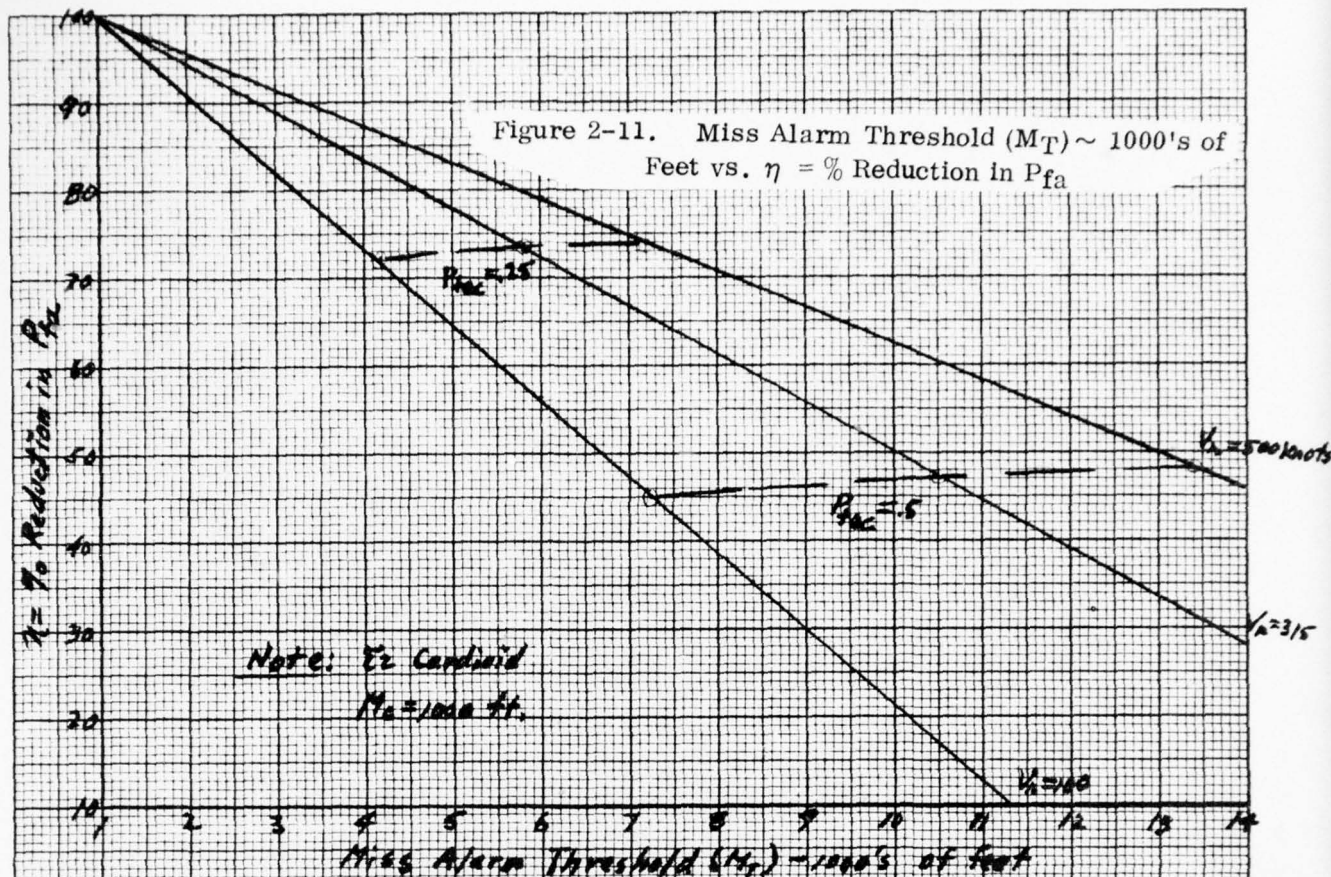
Finally, curves of constant  $P_{fac}$  are superposed on the  $M_T$  vs.  $\sigma(\Delta\beta)$  curves. If a missed alarm probability of .01 is taken as acceptable for the  $\tau_2$  cardioid, then an acceptable  $M_T$  would lie between 7000 and 13000 feet, dependent on  $V_r$ , so as to give about 50% improvement in false alarm probability. The required value of  $\sigma(\Delta\beta)$  lies between .5 and .7 degrees. In like fashion, if a  $P_{fac}$  of .001 is taken as acceptable for the  $\tau_1$  cardioid, the  $M_T$  required to give  $P_{fac} = .5$  must lie between 2500 feet and 7000 feet, with a corresponding  $\sigma(\Delta\beta)$  of between .8 and 1.2 degrees. Results are summarized in Table 2-4 for  $P_{fac} = .5$ .

### 2.3.3 Alarm Probabilities in Traffic Environment

For a system comprised of both range and miss distance alarm thresholds, a probability of potential missed alarm can be derived. This missed alarm occurs when the intruding aircraft has penetrated the Tau alarm cardioid with a projected miss distance less than critical and the computed (estimated) miss distance is indicated as greater than a specified threshold value; so that no alarm is given when it should have been given. Let subscript c denote critical value, subscript t denote true value, and subscript T denote threshold value.  $R_c$  is taken as the range when the intruder penetrates the Tau cardioid at a miss distance  $M_c$  (see Figure 2-1). Thus,

$$\text{Tau 2: } R_c (\text{ft.}) = 1.8 \times 6076 + 40 V_r \cos \alpha_c$$

$$\text{Tau 1: } R_c (\text{ft.}) = .25 \times 6076 + 25 V_r \cos \alpha_c$$





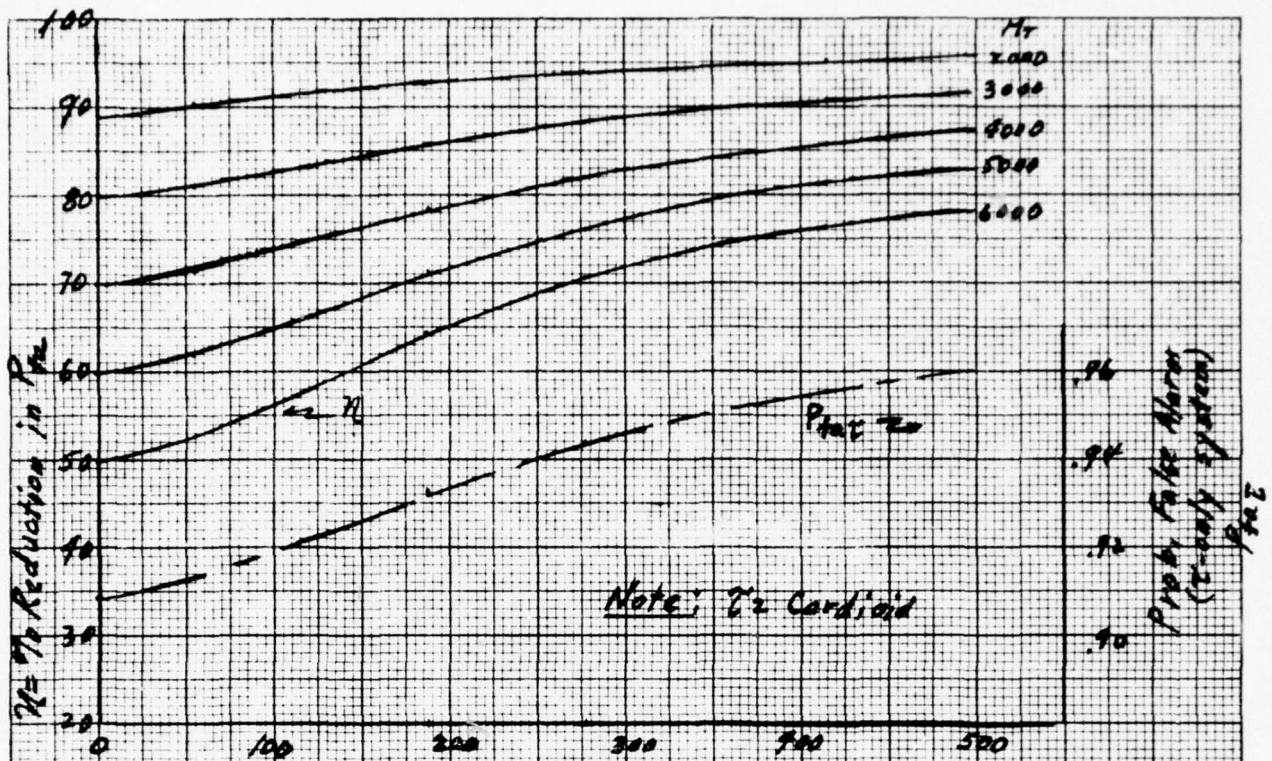


Figure 2-13. Relative Velocity ( $V_r$ ) ~ Knots vs.  $\eta$  = % Reduction in  $P_{fa}$

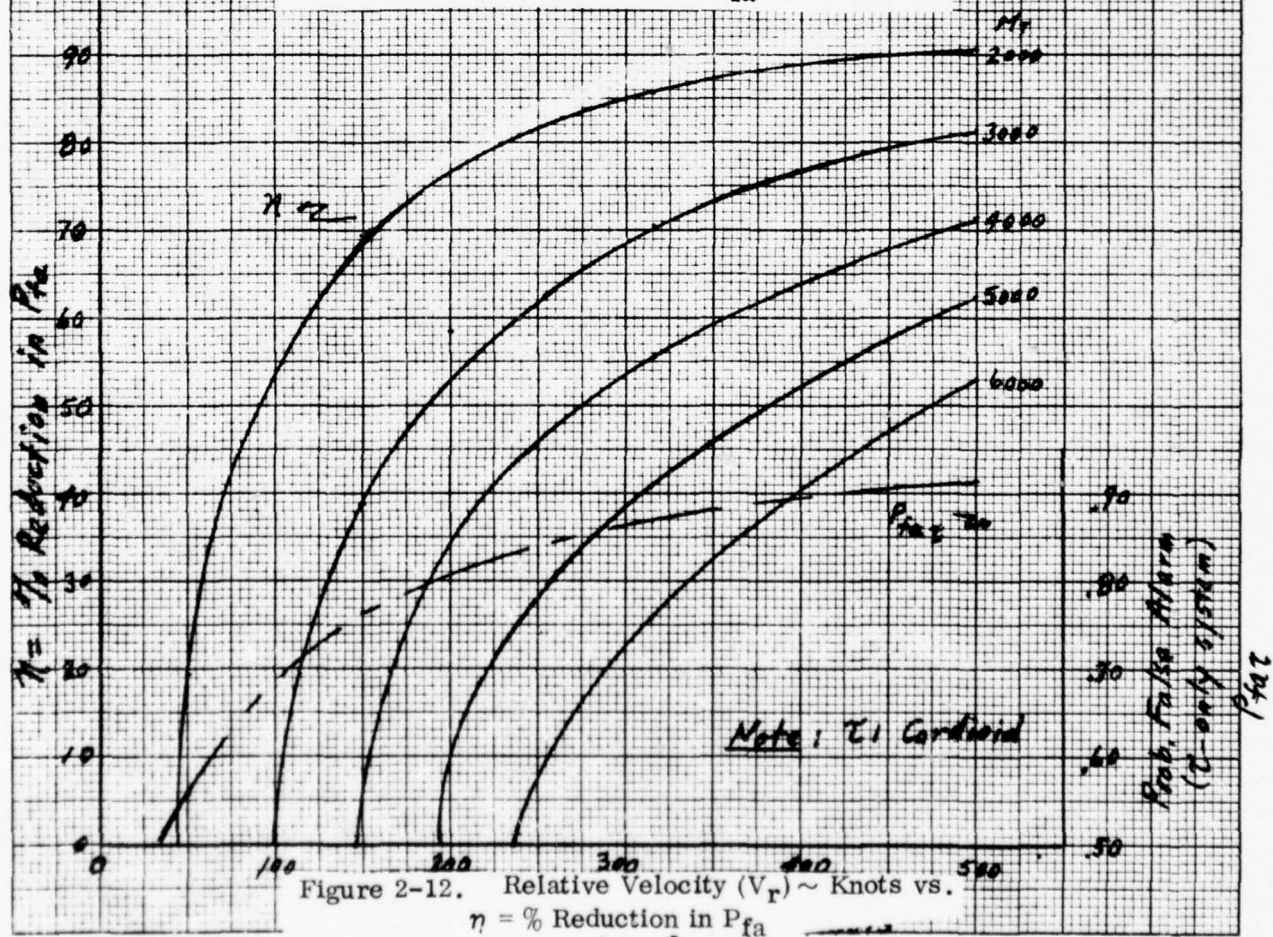


Figure 2-12. Relative Velocity ( $V_r$ ) ~ Knots vs.  $\eta$  = % Reduction in  $P_{fa}$



TABLE 2-4

 $M_T$  AND  $\sigma(\Delta\beta)$  REQUIRED FOR  $P_{fac} = .5$ 

| $\tau$ | $P_{mas}$ | $V_r$   | $M_T$  | $\sigma(\Delta\beta)$ |
|--------|-----------|---------|--------|-----------------------|
| -      | -         | (KNOTS) | (FEET) | (DEG'S.)              |
| 2      | .01       | 500     | 13400  | .68                   |
| 2      | .01       | 315     | 10500  | .63                   |
| 2      | .01       | 100     | 7200   | .44                   |
| 2      | .001      | 500     | 13400  | .53                   |
| 2      | .001      | 315     | 10500  | .50                   |
| 2      | .001      | 100     | 7200   | .35                   |
| 1      | .01       | 500     | 6850   | 1.45                  |
| 1      | .01       | 315     | 4900   | 1.47                  |
| 1      | .01       | 100     | 2500   | 1.20                  |
| 1      | .001      | 500     | 6850   | 1.14                  |
| 1      | .001      | 315     | 4900   | 1.09                  |
| 1      | .001      | 100     | 2500   | .82                   |

with  $V_r$  in fps, and  $\alpha_c$  given by

$$\sin \alpha_c = \frac{M_C}{R_C}$$

and  $M_C$  is taken as 1000 feet. Numerical values of  $R_C$  are given, Table 2-5, for several values of  $V_r$ . In algebraic notation, then

$$P_{MA} = P(R_t < R_C, M_t < M_C) \cdot P(\hat{M} > M_T/R_t = R_C, M_t = M_C)$$

or

$$P_{MA} = \underbrace{P(R_t < R_C) P(M_t < M_C)}_{K_{ma}} \underbrace{[1 - P(\hat{M} < M_T/R_t, M_t)]}_{P_{mas}}$$

$P(R_t < R_C)$  and  $P(M_t < M_C)$  were obtained from the cumulative distribution functions derived for the LAX 1982 traffic model (see Appendix E). Note that  $P(M_t < M_C) = .02$ , necessarily small in a controlled environment, so that  $k_{ma}$  is small, as seen in Table 2-5. Note that  $k_{ma}$  is a function of  $V_r$  and  $\tau$  and  $P_{mas}$  is a function of the statistical error parameters in computed miss, that is  $\sigma(\delta M)$ ,  $\delta \bar{M}$ .

TABLE 2-5

CUMULATIVE PROBABILITIES BASED ON TRAFFIC MODEL

|          | $V_r$   | $R_c$  | $t_c$    | $K_{fa}$ | $K_{ma}$ | $K_{fau}$ | $K_{mau}$ |
|----------|---------|--------|----------|----------|----------|-----------|-----------|
|          | (knots) | (feet) | (sec's.) | —        | —        | —         | —         |
| $\tau 1$ | 100     | 5673   | 33.1     | .9992    | .0008    | .998      | .0023     |
| $\tau 1$ | 315     | 14783  | 27.7     | .9980    | .0020    | .994      | .0059     |
| $\tau 1$ | 500     | 22599  | 26.8     | .9953    | .0047    | .991      | .0090     |
| $\tau 2$ | 100     | 17678  | 104.6    | .9972    | .0028    | .993      | .0071     |
| $\tau 2$ | 315     | 32194  | 60.5     | .9900    | .0100    | .987      | .0129     |
| $\tau 2$ | 500     | 44684  | 52.9     | .9815    | .0185    | .982      | .0179     |

The probability of potential false alarm is the probability that the computed miss will be indicated as less than threshold, when the intruder is outside the Tau cardioid and the true projected miss is greater than critical. Thus

$$\begin{aligned}
 P_{FA} &= P(R_t > R_C, M_t > M_C) \cdot P(M < \hat{M}_T/R_t = R_C, M_t = M_C) \\
 &= \underbrace{[1 - P(R_t < R_C) P(M_t < M_C)]}_{K_{fa}} \cdot \underbrace{P(M < M_T/R_t, M_t)}_{P_M}
 \end{aligned}$$

Evidently  $P_{FA}$  and  $P_{MA}$  are linearly related, for given  $V_r$  and  $\tau$ , since

$$P_{FA} = K_{fa} \left[ 1 - \frac{P_{MA}}{K_{ma}} \right]$$

(see Figure 2-14)

Sample printouts of a combined error and probability program are shown in Tables 2-1, 2-2. Figures 2-15 to 2-18 are plots of  $P_{FA}$  and  $P_{MA}$  for  $k\beta = 0$  only, for  $V_r = 315$  or 500 knots, and for various miss thresholds. In general, for given  $V_r$ ,  $\tau$ , and  $M_T$ , it is seen that  $P_{MA}$  increases,  $P_{FA}$  decreases, with increased  $\sigma(\Delta\beta)$ ; it is seen that  $P_{MA}$  decreases,  $P_{FA}$  increases, with increased  $M_T$ .

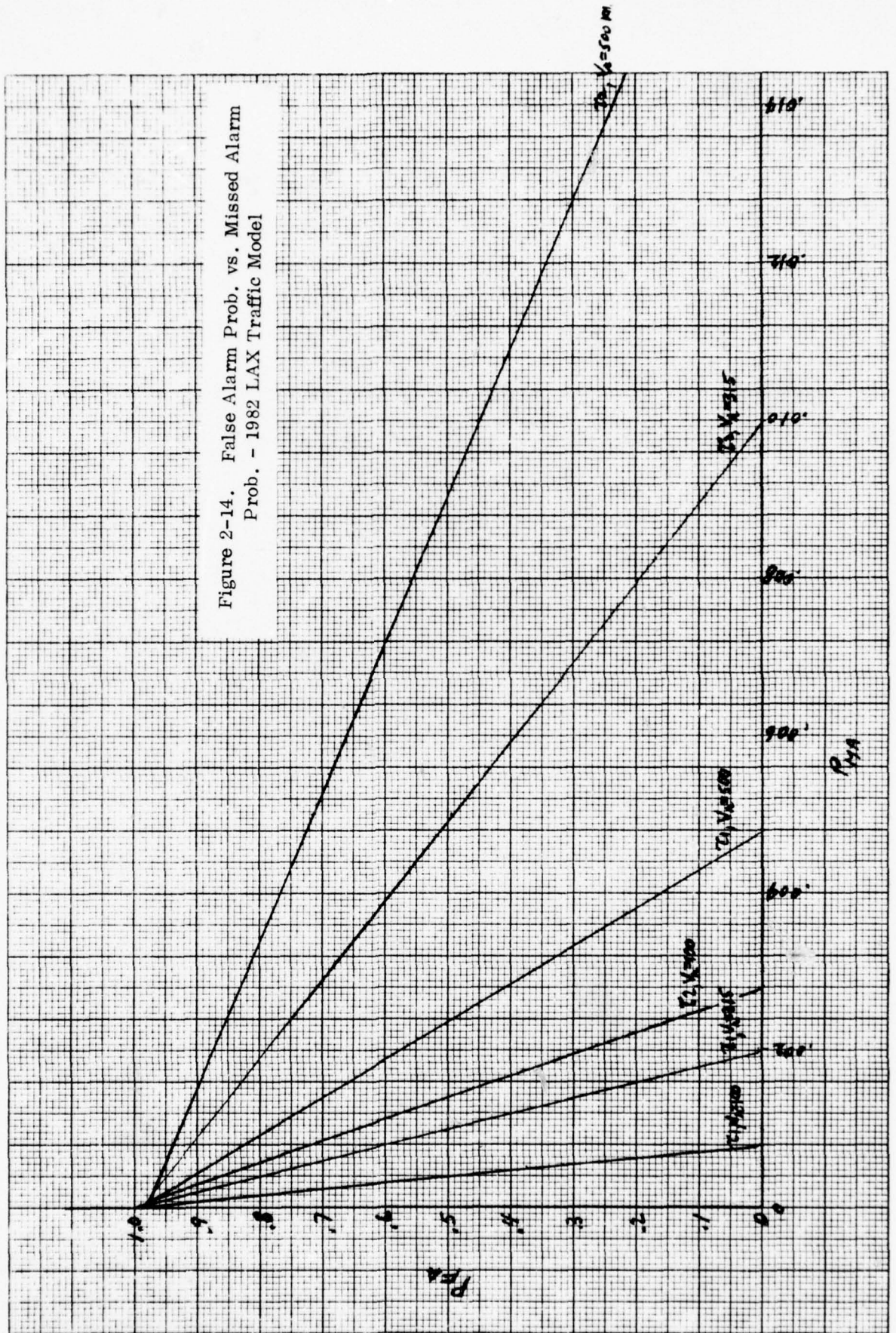
The single conflict missed alarm porbability,  $P_{mas}$ , decreases with increased miss threshold ( $M_T$ ), for given  $\sigma(\delta M)$ , or given  $\sigma(\Delta\beta)$ . But to achieve small  $P_{mas}$ , a sizeable  $P_{FA}$  must be accepted. This is seen from the formula

$$P_{mas} = 1 - P_M = 1 - \frac{P_{FA}}{K_{fa}}$$



K-2 10 X 10 TO 1/2 INCH 46 1322  
 NEUFEL & ESSER CO

Figure 2-14. False Alarm Prob. vs. Missed Alarm Prob. - 1982 LAX Traffic Model



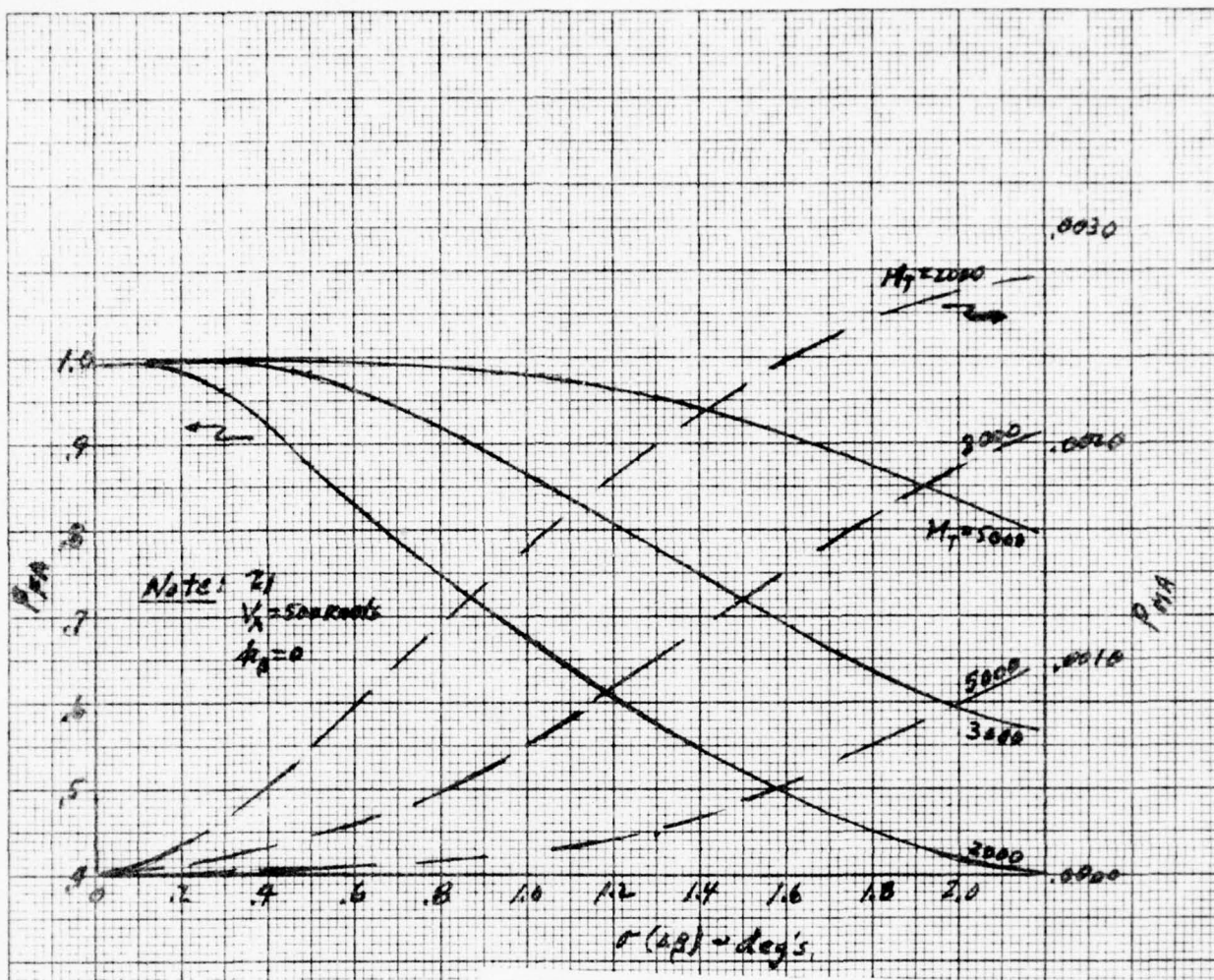


Figure 2-16. Tau 1 False alarm and missed alarm probabilities (500 knots)

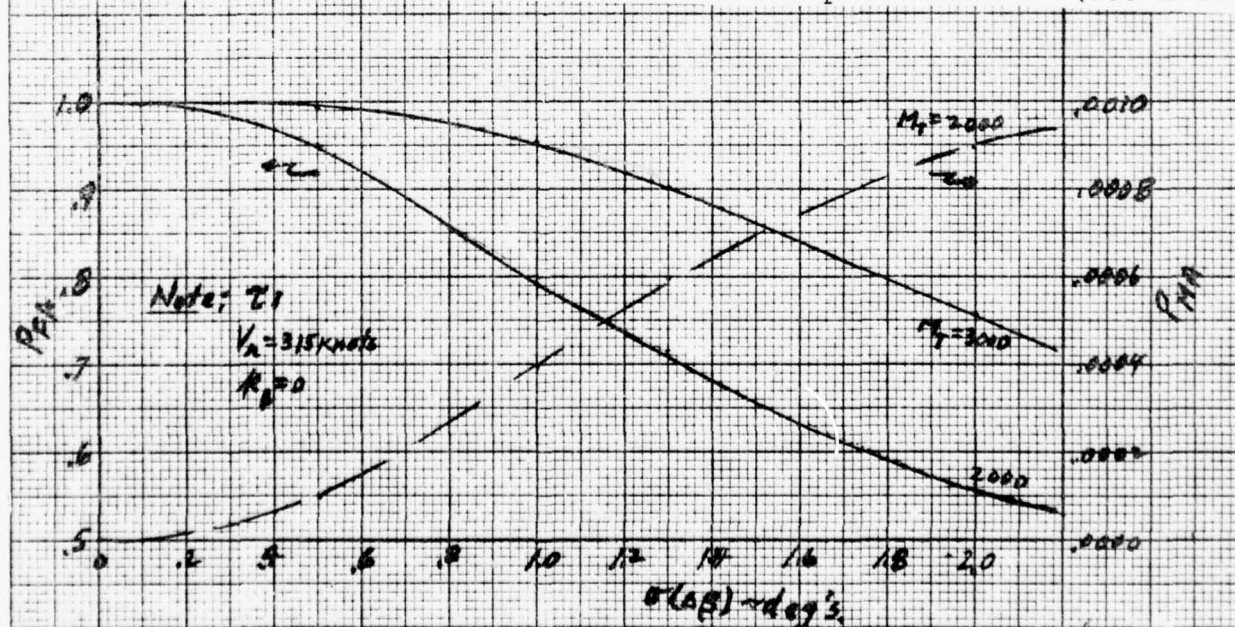


Figure 2-15. Tau 1 False alarm and missed alarm probabilities (315 knots)



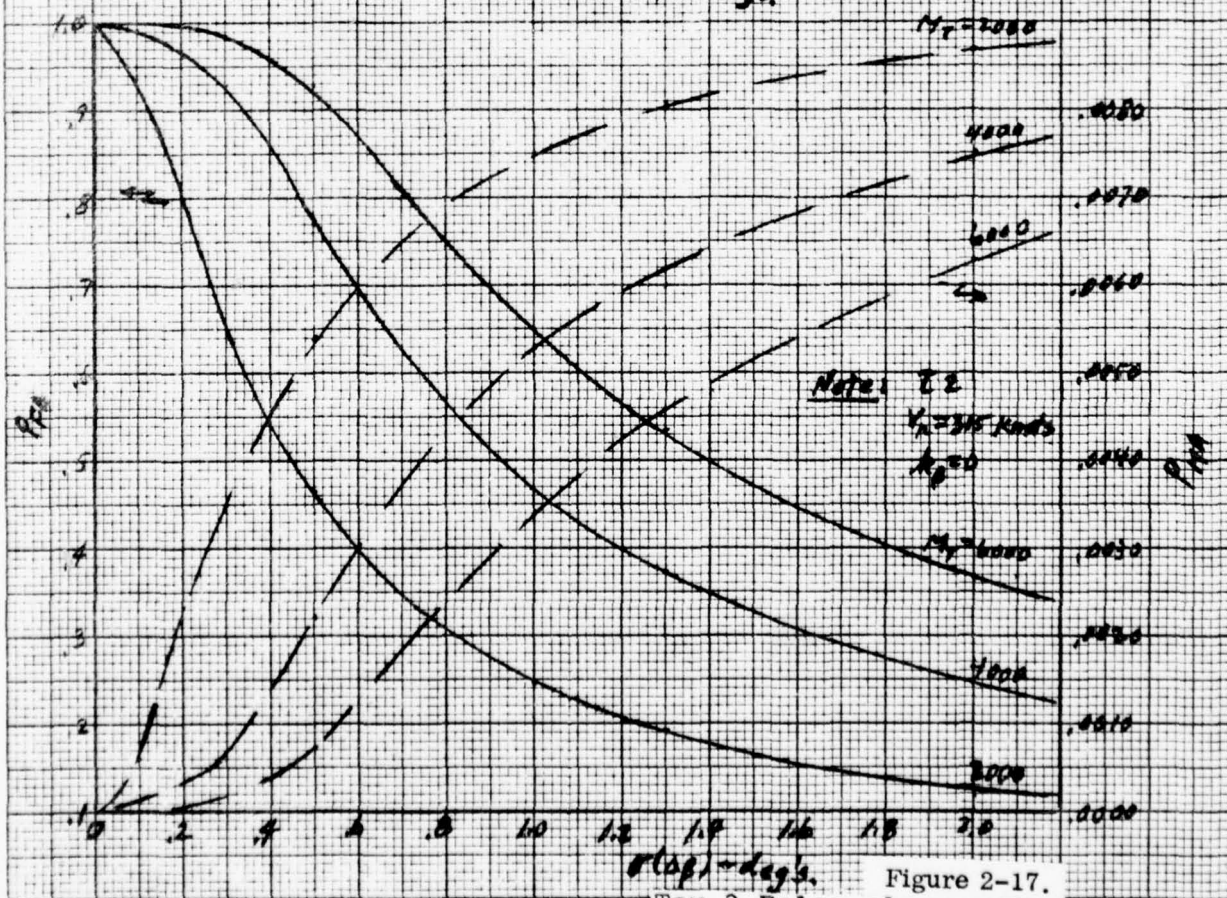
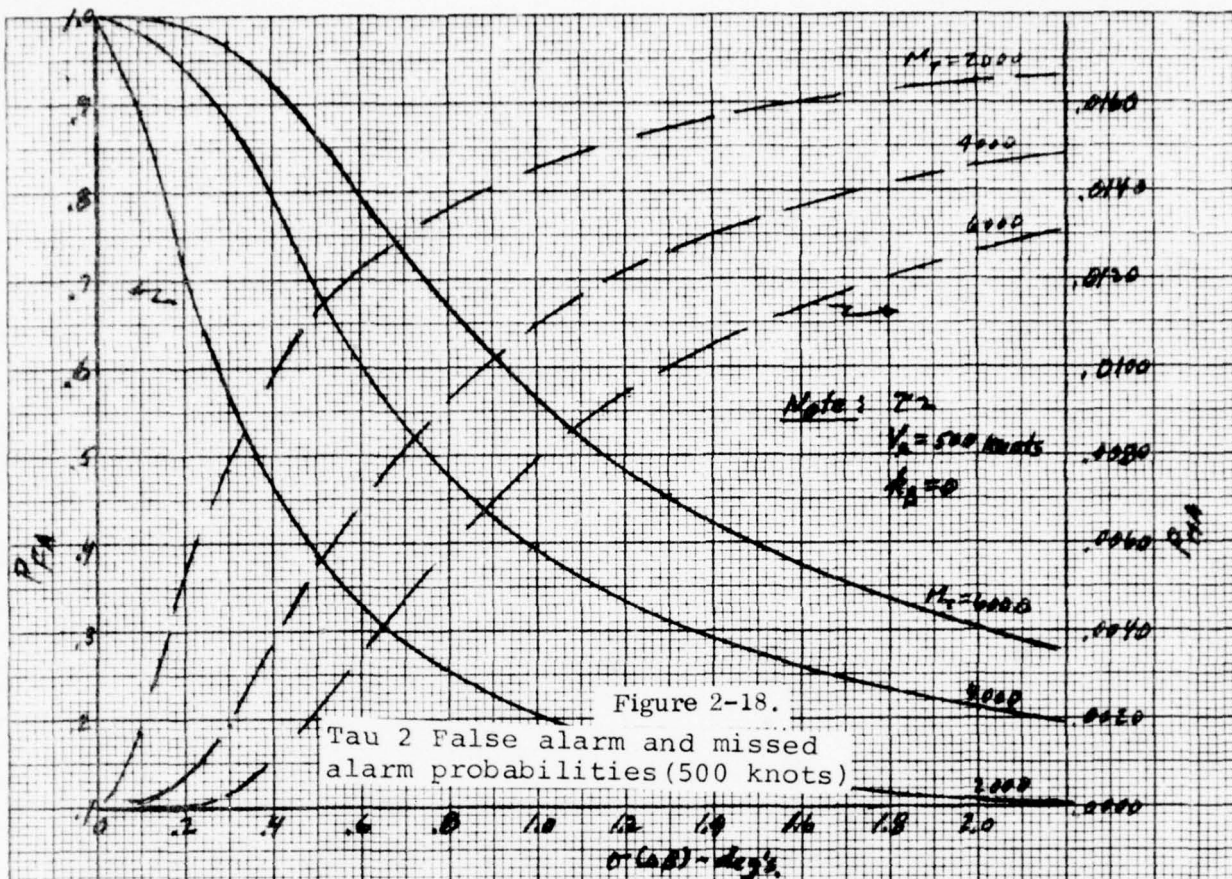


Figure 2-17. Tau 2 False alarm and missed alarm probabilities (315 knots), 9/1/78



Since  $k_{fa} = .99$ , then  $P_{FA} \cong .98$  to obtain  $P_{mas} = .001$ . If  $M_T$  is set by specifying  $P_{fac}$ , then  $\sigma(\Delta\beta)$  is set by specifying either  $P_{FA}$ ,  $P_{MA}$  or  $P_{mas}$ . A comparison is afforded, Table 2-6, where  $P_{fac} \approx .5$  and  $P_{FA}$  is selected as .5; or  $P_{mas}$  is selected as .010 for  $\tau 2$  cardioid, or .001 for  $\tau 1$  cardioid. The latter technique is seen to give a  $\sigma(\Delta\beta)$  requirement of around 1/3 that afforded by the  $P_{FA}$  specification.

TABLE 2-6  
 $\sigma(\Delta\beta)$  REQUIREMENT

|          | $V_r$<br>(knots) | $M_T$<br>(feet) | $P_{fac}$<br>— | $P_{FA}$<br>— | $P_{MA}$<br>—      | $P_{mas}$<br>— | $\sigma(\Delta\beta)$<br>— |
|----------|------------------|-----------------|----------------|---------------|--------------------|----------------|----------------------------|
| $\tau 1$ | 100              | 3000            | .67            | .5            | .0004              | .4996          | >3                         |
| $\tau 1$ | 100              | 3000            | .67            | .998          | $8 \times 10^{-7}$ | .001           | 1.15                       |
| $\tau 1$ | 315              | 5000            | .52            | .5            | .0010              | .4989          | 3.15                       |
| $\tau 1$ | 315              | 5000            | .52            | .997          | $2 \times 10^{-6}$ | .001           | 1.14                       |
| $\tau 1$ | 500              | 6000            | .43            | .5            | .0023              | .4976          | 2.85                       |
| $\tau 1$ | 500              | 6000            | .43            | .994          | $2 \times 10^{-5}$ | .001           | .97                        |
| $\tau 2$ | 100              | 8000            | .56            | .5            | .0015              | .4986          | 1.68                       |
| $\tau 2$ | 100              | 8000            | .56            | .987          | $3 \times 10^{-5}$ | .01            | .49                        |
| $\tau 2$ | 315              | 11000           | .52            | .5            | .0049              | .4949          | 2.1                        |
| $\tau 2$ | 315              | 11000           | .52            | .980          | .0001              | .01            | .66                        |
| $\tau 2$ | 500              | 13000           | .49            | .5            | .0091              | .4906          | 2.0                        |
| $\tau 2$ | 500              | 13000           | .49            | .972          | .0002              | .01            | .66                        |

A maximum detection range of 50000 feet was used in obtaining the cumulative frequency distributions (in range and in miss distance) for the LAX 1982 model (see Appendix D). If uniform distributions are assumed, in both range and miss distance, then

$$P(R_t < R_C) = \frac{R_C}{50000}$$

$$P(M_t < M_C) = \frac{M_C}{50000} = .02, \text{ for } M_C = 1000 \text{ ft.}$$

Then, for the uniform distributions,

$$K_{\text{mau}} = P(R_t < R_C) \cdot P(M_t < M_C) = .02 R_C / 50000$$

$$K_{\text{fau}} = 1 - P(R_t < R_C) \cdot P(M_t < M_C) = 1 - K_{\text{mau}}$$

Numerical values are displayed, Table 2-5. Comparison with the values for the LAX model shows a marked similarity, indicating that the distributions for that model are essentially uniform.

#### 2.3.4 Conclusions

It has been shown that acceptance of a missed alarm probability of 0.01 for  $\tau 2$  cardioid penetration provides a requirement of between  $0.44^\circ$  and  $0.68^\circ$  on  $\sigma(\Delta\beta)$  and of between 7200 feet and 13400 feet on miss threshold, depending on relative speed ( $V_r$ ). Acceptance of  $P_{\text{mas}} = 0.001$  for  $\tau 1$  penetration provides a requirement of  $0.82^\circ$  to  $1.14^\circ$  on  $\sigma(\Delta\beta)$  and of 2500 feet to 6850 on  $M_T$ . The reduction of unnecessary alarms depends directly on the threshold setting that can be used, but this in turn depends on the  $\sigma(\Delta\beta)$  and on the relative speed. In a practical system,  $\sigma(\Delta\beta)$  would be fixed but the threshold could be adjusted to the speed and Tau of the particular encounter. If we base the system design on achieving a  $P_{\text{fac}} = 0.5$  at Tau 1 with  $V_r = 100$  knots and  $P_{\text{mas}} = 0.001$ , the required  $\sigma(\Delta\beta)$  is 0.8 degrees (five second interval). With this constant value, the false alarm probability improvement will differ at other values of relative velocity and Tau, as shown in Table 2-7. The improvement, especially at Tau 1, is substantial.

TABLE 2-7

REDUCTION OF UNNECESSARY ALARMS FOR  $\sigma(\Delta\beta) = 0.8$  DEGREE

|          | $P_{mas}$ | $V_R$   | $M_T$  | $P_{fac}$ | $P_{fa\tau}$ | $\eta$ |
|----------|-----------|---------|--------|-----------|--------------|--------|
|          | —         | (knots) | (feet) | —         | —            | (%)    |
| $\tau 1$ | .001      | 100     | 2500   | .50       | .67          | 25     |
| $\tau 1$ | .001      | 315     | 3800   | .36       | .87          | 59     |
| $\tau 1$ | .001      | 500     | 5100   | .35       | .92          | 62     |
| $\tau 2$ | .01       | 100     | 12500  | .92       | .92          | 0      |
| $\tau 2$ | .01       | 315     | 13300  | .65       | .95          | 32     |
| $\tau 2$ | .01       | 500     | 15800  | .60       | .96          | 38     |

## 2.4 ACCURACY REQUIREMENTS FOR HORIZONTAL MANEUVERING

### 2.4.1 Results of SCI Study

For this task, the requirements for bearing measurement accuracy for use with horizontal maneuvering were to be obtained from the results of a study being performed by Systems Control, Inc. for the DOT Transportation System Center. Through conversation with Mr. Gilbert Gagne at TSC and Dr. John Sorenson at SCI, the results have been received in the form of a few pages of excerpts from the draft final report. Further conversations have also been held with Mr. J. S. Karmarkar at SCI. The conclusion has been reached that the SCI results are not useful for this program.

The portion of the SCI effort applicable to this area involved a Monte Carlo simulation, each encompassing 2,000 samples. In each run, all of the conflict aircraft had the same relative heading and speed and were positioned with miss distances uniformly distributed  $\pm 2,600$  feet from the test aircraft. A Turn Right/Turn Left criterion was used, and although not defined in the material furnished, is somewhat similar to a Tau criterion as



it has a range vs. miss distance shape. A given encounter begins in a straight flight path. When the criterion is satisfied, a standard turn is made in the commanded direction and continues until  $R = 0$ . Runs were made with 9 different relative heading angles. The one at 150 degrees was judged by SCI to be representative of high missed alarm and false alarm rates and was, therefore, used in more detailed sensitivity analyses.

The sensitivity to bearing errors was explored for three values of  $\sigma$ ; 2.5, 5.0, and 7.5 degrees. The results are given in Table 2-8. Although runs were not made for  $\sigma$ s less than 2.5 degrees, the conclusion could be reached that  $\sigma = 2.5$  is a suitable requirement because its performance is acceptable, substantially better than for  $\sigma = 5.0$ . However, after analyzing the method used to develop these results, it was concluded that they are not valid and cannot be used to set the requirement for bearing measurement accuracy for an airborne collision avoidance system.

The reasons for this conclusion are:

1. The analysis assumed that the target's range and bearing were measured and its heading and speed were communicated. The target's relative position vector is measured but its velocity vector is communicated and there are four independent parameters subject to error. In the practical case, the velocity vector is not communicated but must be derived by tracking the range and bearing measurements. There are, therefore, only two parameters involved and their effect is determined by how their error varies over a period of time.
2. The errors were taken by SCI to consist only of a bias, randomly drawn for each aircraft and held constant throughout the encounter. The form of error characteristic is expected in practice to be a random bias on each sample, changing throughout the encounter. Since the bias was not allowed to change during the encounter, the runs are not representative. Furthermore, the results are suspect because they indicate a sensitivity to the value of the

TABLE 2-8. EFFECT OF BEARING ERROR ON HORIZONTAL MANEUVERS  
(Per SCI Study)

| MISS DISTANCE<br>Ft.  | No.<br>In<br>Orig<br>Dist. | DISTRIBUTION AFTER RUN |                     |                     |                   |                   |                   |
|-----------------------|----------------------------|------------------------|---------------------|---------------------|-------------------|-------------------|-------------------|
|                       |                            | $\sigma=2.5$<br>No.    | $\sigma=5.0$<br>No. | $\sigma=7.5$<br>No. | $\sigma=2.5$<br>% | $\sigma=5.0$<br>% | $\sigma=7.5$<br>% |
| 0-300 collision       | 214                        | 1                      | 25                  | 48                  | 0.05              | 1.25              | 2.4               |
| 300-900 near miss     | 671                        | 9                      | 79                  | 116                 | 0.45              | 3.95              | 5.8               |
| 900-2000 unacceptable | 648                        | *                      | *                   | *                   | *                 | *                 | *                 |
| 2000-2600 safe        | 467                        | *                      | *                   | *                   | *                 | *                 | *                 |
| <u>MANEUVERS</u>      |                            |                        |                     |                     |                   |                   |                   |
| Total                 |                            | 1737                   | 1645                | 1513                | *                 | *                 | *                 |
| False                 |                            | 288                    | 317                 | 309                 | 61.67             | 67.88             | 66.17             |
| Incorrect             |                            | 318                    | 512                 | 659                 | 18.31             | 31.12             | 43.56             |
| Incorrect - near miss |                            | 5                      | 94                  | 157                 | 0.15              | 18.36             | 23.82             |
| Acceptable miss       |                            | 1856                   | 1774                | 1720                | 92.8              | 88.7              | 86.0              |
| Excessive miss        |                            | 134                    | 122                 | 116                 | 6.7               | 6.1               | 5.8               |

\* Data not supplied.

Conditions: Velocity aircraft A=425 fps, B=375 fps, relative heading=150 degrees

Error Sigmas: Range=200 ft., heading=5 deg, speed ratio=0.05  
All errors taken to be a constant bias randomly drawn from Gaussian distribution.

bearing measurement bias error whereas it can easily be shown that the measurement of miss distance is independent of a constant bias error in bearing measurement. For a given range and speed, miss distance is determined by the difference between two bearing measurements at different times and a constant bias will drop out.

3. In the SCI runs, both aircraft are equipped and both maneuver. Not only is this not representative of the important case of a fully equipped airliner maneuvering against a minimally equipped general aviation aircraft, but it illustrates the invalidity of the SCI random bias approach. The approach merely tested the randomness of the bias on all four parameters, with a high probability that the values given to one aircraft would compensate for the values given to the other. In fact, in many of the encounters, a fairly large percentage of aircraft turned in the wrong direction but still avoided a near miss because the other errors were so great.

SCI apparently has reduced the operation of a horizontal maneuvering system to the detection of penetration of a range vs. miss distance criterion and the application of a step function maneuver. This has great similarity to the operation of the miss distance discriminator used in conjunction with the Tau criterion, described in Section 2.3. . Because the SCI numerical results are seen to be unusable, the results of the RCA analysis of Section 2.3 will be used as the guide to bearing measurement accuracy requirements.

#### 2.4.2 Erroneous Horizontal Maneuver Effects

This section considers the effect of bearing measurement error in causing an incorrect maneuver, i.e., a turn in the wrong direction.

In Figure 2-19, suppose that the true miss is  $M_C$  and that, therefore, in the absence of measurement errors, a turn to the right would be commanded, so as to increase positive miss. If the miss were computed as being negative, a turn to the left would be commanded. This erroneous turn would be deleterious if it caused the relative path to intersect a



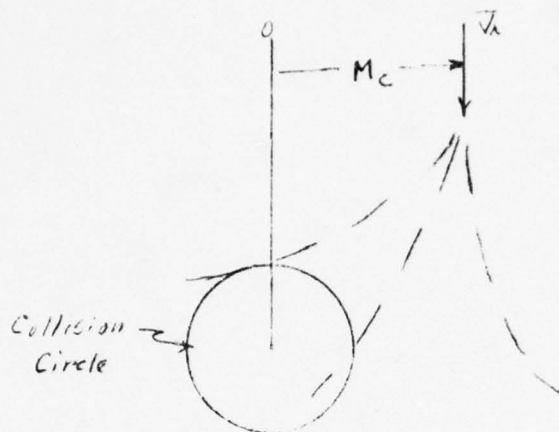


Figure 2-19.  
Erroneous Turn  
Command

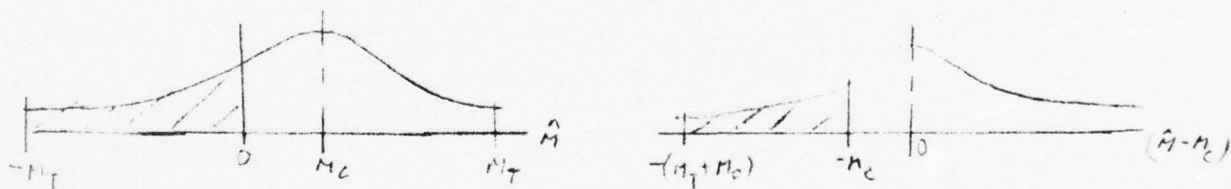


Figure 2-20.  
Left Turn Command  
Probability

"collision" circle, say of radius 300 feet. It is to be emphasized that, in and of itself, a turn in the "wrong" direction is not harmful if the collision circle is avoided. The extent to which measurement errors can cause penetration of the collision circle cannot be explored without specification of a maneuver logic; i.e., turn rate and time of execution of the turn, as well as a statement as to whether one or both aircraft maneuver. These considerations are beyond the scope of the present study; instead, we shall discuss measurement errors in terms of the probability of an erroneous turn command.

If it is assumed that a turn to the left is commanded if the computed miss lies between 0 and  $-M_T$ , and neglecting bias error, then (see Figure 2-20)

$$\begin{aligned} P(-M_T < \hat{M} < 0) &= P[-(M_T + M_C) < \hat{M} - M_C < M_C] \\ &= P[M_C < \hat{M} - M_C < M_T + M_C], \end{aligned}$$

This probability is dependent on miss threshold. If the concept of wrong turn is extended to include "no turn" commanded, then

$$\begin{aligned} \text{Prob. (erroneous command)} &= \text{Prob. (turn left, or no turn to left)} + \text{Prob. (no} \\ &\quad \text{turn to right)} \\ &= P(-\infty < \hat{M} - M_C < M_C) + P(M_T < \hat{M} - M_C < \infty), \end{aligned}$$

Since  $M_T$  will be selected so that  $P_{\text{mas}}$  is small, the second term will be small, and the total probability can be approximated by the first term alone, independent of  $M_T$ . Figure 2-21 is a plot of this probability vs.  $\sigma_M$ . Evidently  $\sigma_M$  (and therefore  $\sigma(\Delta\beta)$ ) would need to be quite small to obtain a small probability.

Suppose a  $\sigma(\Delta\beta) = .8^\circ$  is selected as proposed in Section 2.3.4. From Figure 2-22, for the  $\tau_1$  cardioid and  $P_{\text{mas}} = .001$ , a maximum  $M_T = 5100$  feet is required (corresponding to  $V_r = 500$  knots); from Figure 2-3, the corresponding  $\sigma_M$  is 1400 feet and this gives

PERFORMANCE AS 4074  
 CALCULATED BY J. J. J. J.  
 WE KEEP A RECORD

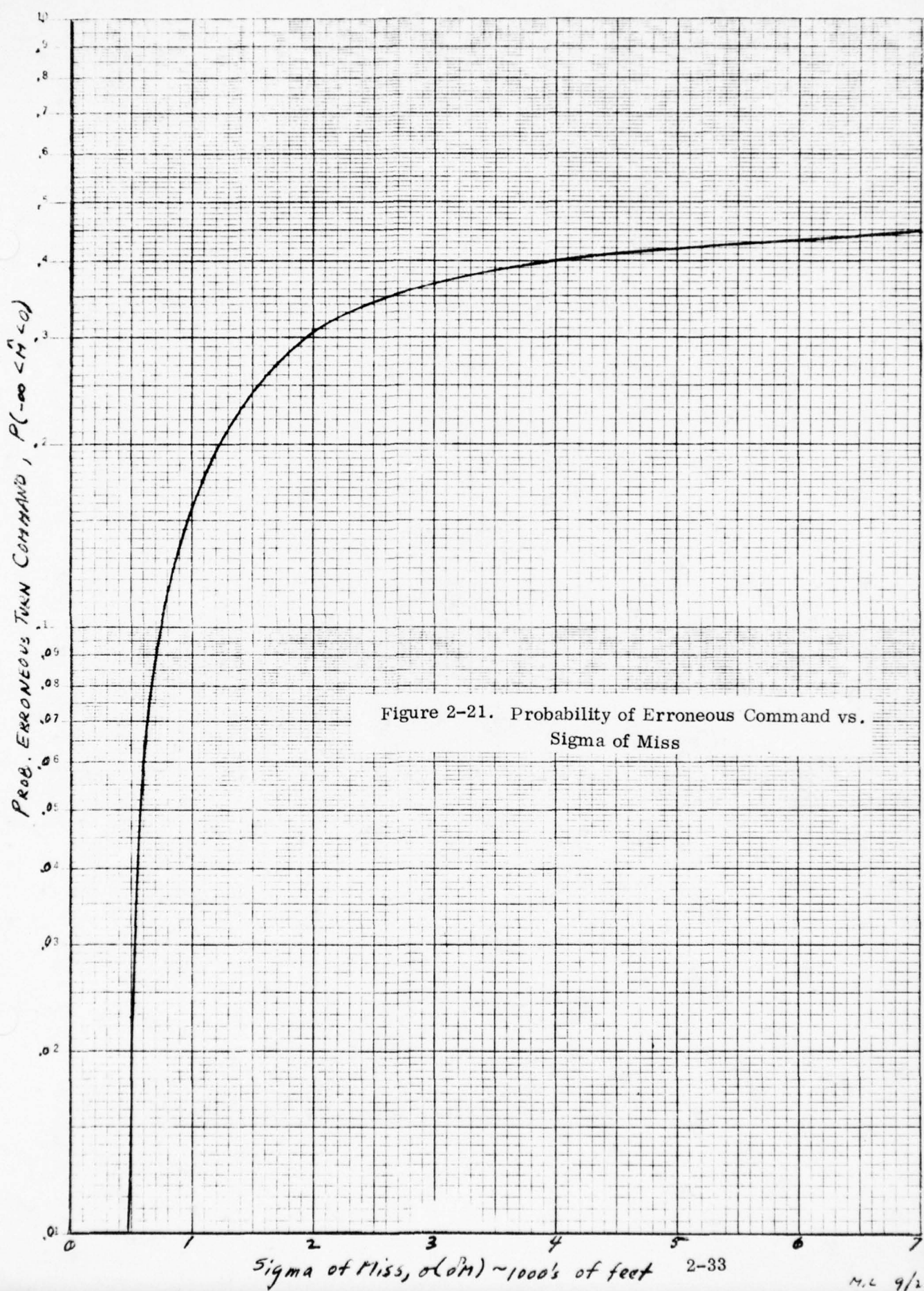


Figure 2-21. Probability of Erroneous Command vs. Sigma of Miss



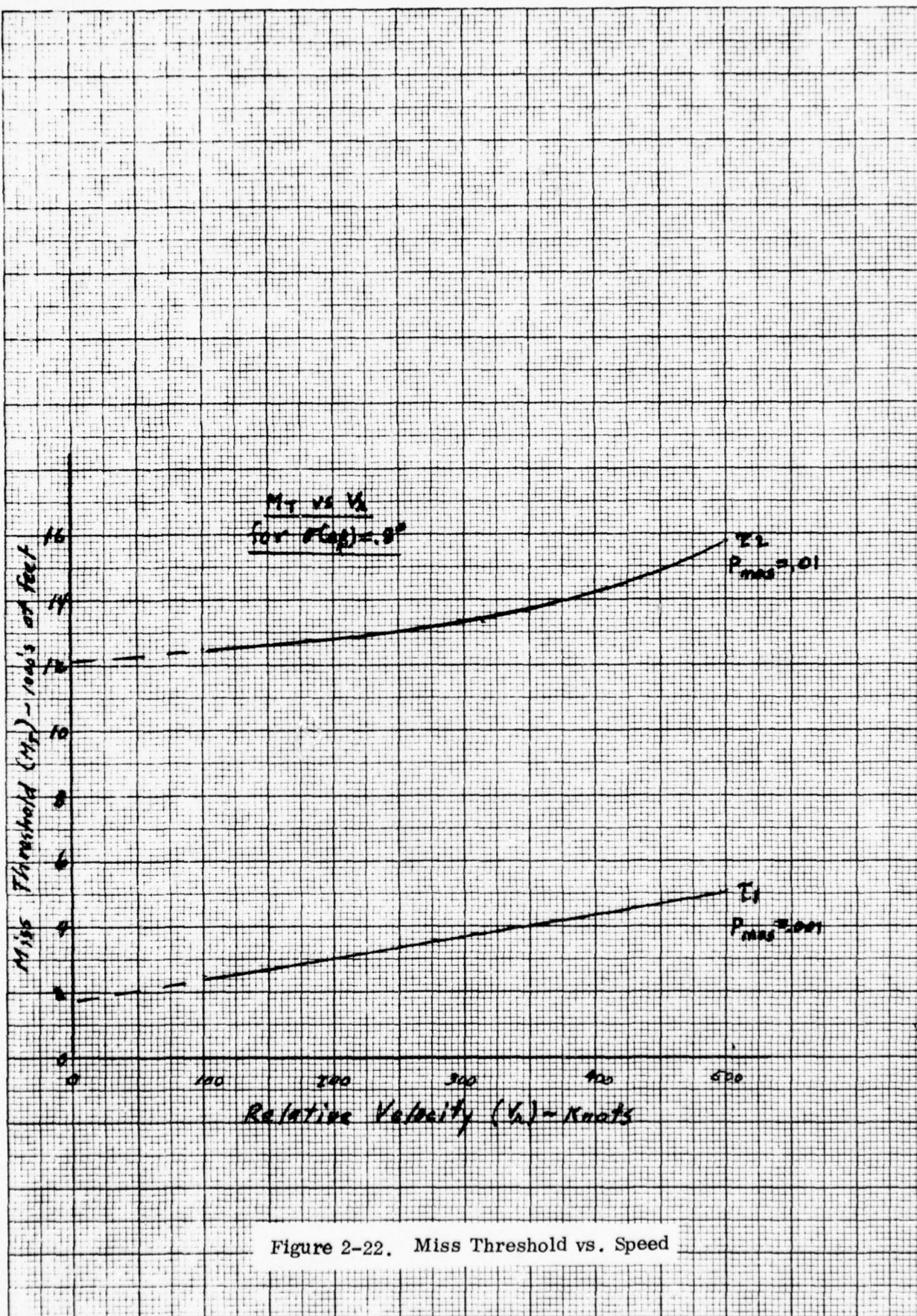


Figure 2-22. Miss Threshold vs. Speed

$P(-\infty < \hat{M} < 0) = .2$ . Similarly, for  $V_r = 500$  knots,  $P_{mas} = .01$  on the  $\tau 2$  cardioid, we have  $M_T = 15800$  feet,  $\sigma_M = 6000$  feet and  $P(-\infty < \hat{M} < 0) = .43$ . Analysis of the acceptability of these probability values is not attempted herein.

## 2.5 SUMMARY OF REQUIREMENTS

The results of the analyses in Sections 2.2, 2.3, and 2.4 set accuracy requirements for each of the functions shown on the first three lines of Table 2-9. From these, the overall accuracy requirement is derived and shown on the fourth line.

The overall requirement is based on the need for a swept bearing accuracy of 0.8 degree which was derived for Tau Warning Reduction and extended to Horizontal Maneuvering. To meet this requirement, the relative bearing measurement must have an accuracy of  $0.8/\sqrt{2}$ , or 0.56 degree, because two such measurements are used to make the swept bearing measurement.

TABLE 2-9  
SUMMARY OF ACCURACY REQUIREMENTS

| Function                  | Requirement<br>Degrees, One Sigma |        |                       |        |
|---------------------------|-----------------------------------|--------|-----------------------|--------|
|                           | Relative Bearing                  |        | Swept Bearing (5 sec) |        |
|                           | Bias                              | Random | Bias                  | Random |
| PWI                       | 15                                |        | n/a                   | n/a    |
| Tau Warning<br>Reduction  | n/a                               | 0.56   | n/a                   | 0.8    |
| Horizontal<br>Maneuvering | *                                 | *      | *                     | *      |
| Overall<br>Requirement    | 15                                | 0.56   | n/a                   | 0.8    |

.\*To have been furnished by another contractor but were not.



## SECTION 3.0

### CONFIGURATION ANALYSIS (TASK 2)

#### 3.1 GENERAL

This subsection provides an introduction to the configuration analysis task by describing the overall bearing measurement concept and trade-off areas. The individual areas of antenna signal processing, and data processing are discussed in subsequent subsections.

Although many techniques exist for measurement of relative bearing by radio direction finding (DF) from airborne platforms, few appear applicable to the SECANT collision avoidance system. One approach for this purpose was originally given in the SECANT "Blue Book"<sup>(1)</sup>, which includes a brief description of means for the related determinations of swept bearing (i.e., bearing increment) and miss distance. It is, however, desirable to examine alternative promising approaches with the objective of identifying a preferred configuration and critical performance parameters of a DF system.

Because a common signal structure is employed in the SECANT CAS and PWI equipments, both would possess essentially similar circuits for the signal processing involved with the function of relative bearing measurement. Significant differences arise, however, mainly in the degree of complexity and extent of hardware implementation associated with the antenna arrays and the bearing data processing applicable to each facility. Thus a simple antenna array, having element spacings small enough to avoid bearing ambiguity, would suffice for the low accuracy requirements of a PWI. But analysis indicates that an additional, co-located antenna array of larger aperture would be mandatory in the case of the full CAS, in order to attain measurement accuracies consistent with a reliable determination of projected miss distance from relative bearing increments. Furthermore, whereas data processing of a phase comparison for target

(1) Refers to Reference 1.

sector identification in a PWI is minimal, comparatively sophisticated digital processing in combination with short-term data storage are required in a full CAS providing miss distance and accurate bearing measurements.

In pursuing the configuration analysis, the various anomalous effects inimical to accurate relative bearing measurement were listed and quantified. Particular consideration was given to the deleterious influences of transient response and nonlinearity in IF circuits, phase delay asymmetry in dual-channel receivers, local multipath (reflections from aircraft surfaces causing "site" errors), noise and fruit interferences, and aircraft attitude variations occurring during measurements of relative bearing and swept bearing.

Major results of the configuration analysis are:

- (a) Selection of key system elements, such as DF antenna structure, receiver arrangement, pulse phase comparator type, etc.
- (b) Formulation of algorithms for improving data quality, eliminating bearing ambiguity, compensating aircraft attitude changes, and computing projected miss distance.
- (c) Preparation of a performance and design specification (Appendix F) covering the bearing and miss distance measuring equipment which interfaces with the DF antenna and with the SECANT correlator, tracking, and data processing system. This specification expresses selection of system elements made by trade-offs among candidates identified in (a).

A basic system operating concept for bearing observations and projected miss distance determinations by a full CAS is described below. Trade-off areas pertaining to adequate reduction of perturbing effects are then outlined against a background of appropriate constraints on the complexity and amount of additional equipment needed to implement bearing

measurement. Subsequent sections detail the trade-offs, interrelated with results of various configuration analyses. These analyses refer to antenna array options, signal processing, data processing, and system errors.

### 3.1.1 General Description of System Concept

#### 3.1.1.1 Dominant Concept Constraints

Adapting a relative bearing measurement capability to the interrogator/transponder signal structure of SECANT restricts the associated techniques to those available in pulsed radio direction finding, and precludes exotic techniques such as synthetic aperture processing, inverse TACAN, rotational doppler, microwave Wullenweber, etc., even though they may possess the potential for superior DF performance.

Furthermore, directional antennas would require prohibitively large apertures at L-band to be consistent with the angular resolution needed. Consequently, fixed omni-directional structures having modest dimensions, acceptable for emplacement on aircraft, must be used in conjunction with suitable signal and data processing to achieve desired relative bearing measurement accuracies. These antenna structures, typified by the crossed-axis interferometer<sup>(1)</sup> originally proposed for SECANT, and by multi-mode ring arrays<sup>(2)</sup>, provide information on the direction-of-arrival in terms of the phase displacement between signals received at the antenna ports.

Matched dual-channel receivers are needed to preserve these phase relationships during signal amplification. A time shared, single-channel system, employing phase lock techniques, would be preferable for freedom from circuit phase variations and for equipment economy, but is not admissible because phase coherence does not exist between the carrier waves of pulses in the SECANT pulse sequence. In order to achieve desired performance levels while handling the bearing data for up to 32 targets per altitude layer (as are detectable in the correlator bins), heavy dependence must be placed on a capability for digital data processing and storage in the full CAS. Further



general constraints are that equipment concepts to implement bearing measurement shall be compatible with form factors envisioned for production versions of SECANT hardware, and shall be cost effective from an overall system viewpoint.

#### 3.1.1.2 Basic System Concept

The above mentioned constraints and the motivation to minimize additional equipment in SECANT lead to the basic system block diagram of Figure 3-1 for a full CAS. It shows the essential elements (solid-line blocks, no's. 1 to 6) of an electrically symmetrical dual-channel receiver, for relative bearing measurement by processing the reply signals ( $P^+$ ,  $P^-$ ,  $Q^+$ ,  $Q^-$ ) impinging on the antenna (block no. 1) in one field. A corresponding receiver (not shown in Figure 3-1 but included in a more detailed diagram Figure F-1 of Appendix F) comprising antenna, dual RF front ends and IF circuits, would be incorporated to serve the other field, with appropriate gating to share the common bearing measurement facility (block no's. 4, 5 and 6). Interfaces are indicated with units (block no's. 7 to 10) performing all other functions of the CAS including those in the present VECAS.

A dual-channel superheterodyne receiver is virtually mandatory because precise phase measurement is difficult at microwave frequencies but is practical at lower frequencies. In this type of receiver in which common local oscillators are employed in conjunction with electrically symmetrical channels, the phase displacement between the input RF signals is preserved between the resulting output IF signals. Components represented by the upper channel consisting of an RF front end and IF circuits, and by block no's. 7, 8 and 9 (shown in dashed line at the top of the diagram) perform the requisite signal and data processing functions of a VECAS. This channel is served by a monopole antenna which would exist as either one antenna element of the interferometer or the center element associated with the ring array, whichever is utilized.



A control connection is shown between the CAS data processor (block no. 9) and the antennas, primarily for the purpose of switching between the wide and narrow aperture arrays which are required to improve resolution of relative bearing measurement and to eliminate bearing ambiguity, respectively. If crossed-axis interferometer arrays were employed, an additional switching operation would be needed to time share the dual-channel receiver between the outputs from the three ports associated with each array. Time sharing could be avoided by including a third receiver channel, but the increased system cost and complexity, and reduced reliability incurred thereby would have to be traded off against the shorter processing time and simplified RF switching.

Subsidiary antenna switching functions may be necessary in a full CAS to permit neutralization of undesirable phase imbalance between the two channels. (As discussed later, such imbalance could seriously degrade the accuracy of relative bearing and swept bearing observations when interferometer arrays are used.) Changes in the scaling of relative bearing measurements, and the application of bearing ambiguity resolution logic must accompany the alternative selection of narrow and wide aperture arrays. Application of these functions is represented by an extension of the antenna switching control to the relative bearing data processor, block no. 5.

Reference and signal pulses from broadband IF amplifiers are applied to inputs of phase detection and measurement circuits in block no. 4, via transmission gates which are enabled by various control signals including those from the range trackers in block no. 8. The purpose of multiple gating is to minimize bearing measurement errors as a result of three processes. In the first, pulses are not admitted to the phase detector until the initial transients of the IF bandpass filters have decayed sufficiently to permit reliable phase measurements between the two channels. The object of the second process is to prevent bearing measurements from being made on signals other than from a particular target of interest selected by range, although infrequent interference from undesired



co-range targets is unavoidable thereby. The third inhibiting process is to minimize interference by fruit and noise pulses which coincide with reply pulses, and false responses when reply pulses are missing. This function is illustrated by the extension of the gate control line shown from block no. 4 to no. 9 wherein the message data circuits provide signals indicating the presence of fruit or noise pulses, and the absence of reply pulses due to blocking.

Several severe constraints drastically reduce the number of candidate methods<sup>(4)</sup> of phase detection and measurement in block no. 4. Significant constraints are the pulsed, noncoherent signal structure of SECANT; the short duration of measurement; and the variability of signal level, especially at longer ranges where hard limiting action at IF is no longer available. These constraints and other considerations discussed later, narrow the selection to the two phase comparison methods shown in Figure 3-2. They are well known zero crossing techniques which can be implemented with either analog or digital outputs, and the quadrature scheme. Both methods were analyzed in<sup>(5)</sup> with respect to white noise interference and were found to be superior to other methods by virtue of relative immunity to noise induced bias error.

Inter-channel phase difference measurements made in block no. 4 are translated into bearing observations relative to the antenna plane by the data processing block no. 5 in Appendix I. A range measurement performed in blocks 8 and 9 on a reply pulse is accompanied by a phase difference measurement in block no. 4. A convenient procedure is to obtain phase measurement data using the wide aperture antenna from one sequence of 62 ranging pulses received during a tracking cycle (Figure 3-3) and the narrow aperture antenna from pulses in the other 62 pulse sequence of the cycle. In all conflict encounters of interest, the bearing change that could develop over the 0.25 second interval separating the two sequences would be too small to impair resolution of ambiguity in relative bearing measurements made with the wide aperture antenna.

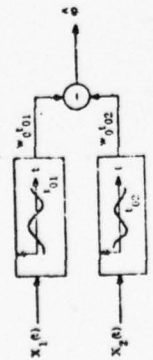
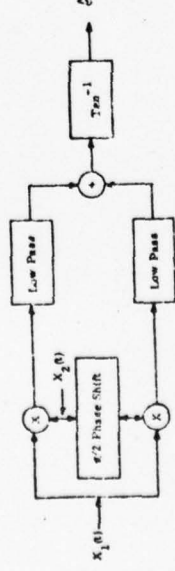
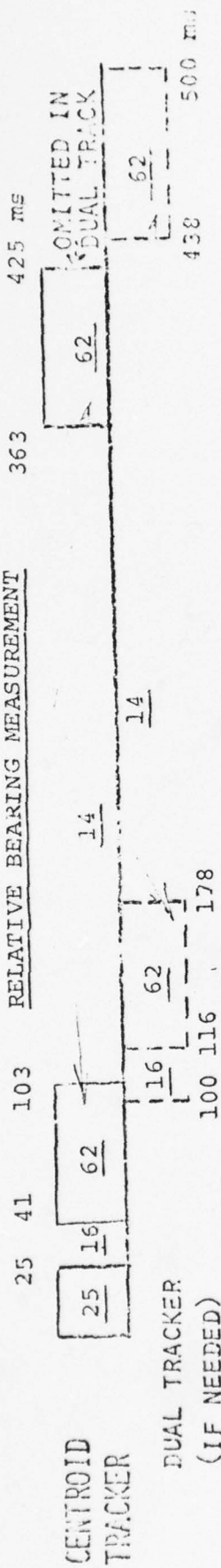
| SCHEMATIC  | EXPECTATION                    | POSITIVE SLOPE ZERO CROSSING | VARIANCE   |
|--|--------------------------------|------------------------------|--|
|   | $\sigma_{mod} \approx 2\sigma$ | POSITIVE SLOPE ZERO CROSSING | Variance<br>$\frac{1}{2} \left[ \frac{1}{(S/N)_1} + \frac{1}{(S/N)_2} \right]$ |
|  | $\sigma_{mod} \approx 2\sigma$ | QUADRATURE                   | $\frac{1}{2} \left[ \frac{1}{(S/N)_1} + \frac{1}{(S/N)_2} \right]$             |

Figure 3-2. NOISE ERRORS FOR TWO TYPES OF PHASE COMPARATOR

# UPFIELD

## SEQUENCES AVAILABLE FOR

### RELATIVE BEARING MEASUREMENT



# DOWNFIELD

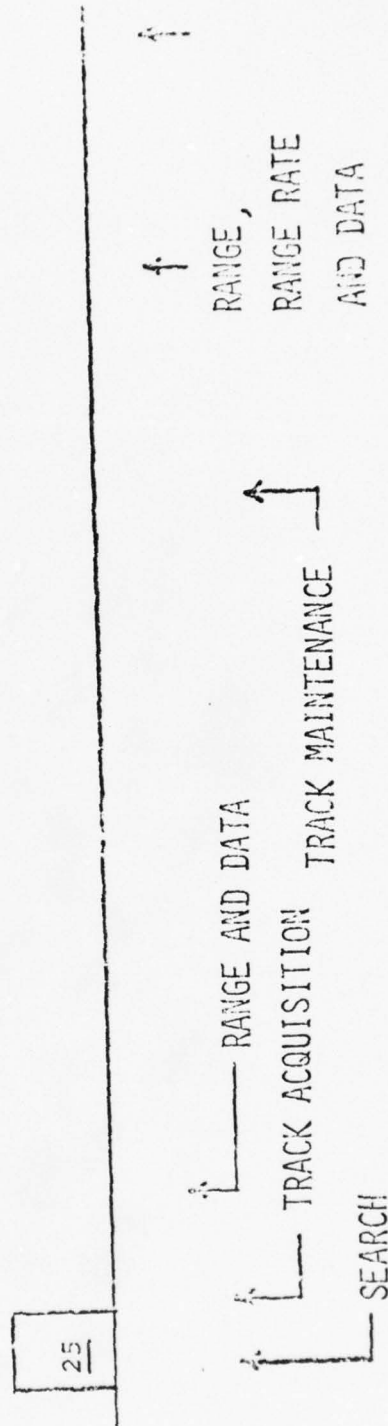


Figure 3-3. PULSE SEQUENCES USED DURING VECAS TRACK

(underlined numbers are the quantity of pulses in each sequence)



Smoothing of phase difference measurements, in combination with statistical rejection of wild bearing data produced by residual fruit and noise pulses, are functions also performed in block no. 5. These functions are vital to successful operation of the bearing subsystem because they fully exploit the intrinsic SECANT integration feature which combats accuracy degradation by random perturbations as the result of averaging a large quantity of data points to provide a desired measurement.

Estimates of horizontal relative bearing and of projected miss distance  $M$  are computed in block no. 6 by utilizing algorithms contained in Section 3.4.2. The requisite inputs to block no. 6 comprise the observed bearings  $\beta$  furnished by block no. 5; and target range  $R$  and altitude difference  $\Delta h$  data from block no. 9. A further input to the miss distance processor is from block no. 10 representing an aircraft attitude sensor which would be either an inertial platform or a gyroscopis reference (6) such as normally supplies roll, pitch and heading data to cockpit displays and to the autopilot. Attitude data is sampled and utilized in the miss distance processor at a time corresponding to the mid point of the pulse sequence from which phase measurements are made in conjunction with the wide aperture antenna.

Data processing of target returns in VECAS includes computation of range and range rate, decoding of messages, and application of ANTC-117 threat logic in combination with digitized data from an on-board altimeter. Block no. 9 retains these functions, but utilizes the horizontal relative bearing and miss distance data from block no. 6. Additional logic could be incorporated to command horizontal maneuvers, and to suppress unnecessary ANTC-117 warnings or vertical maneuver instructions when the computed miss distance is greater than a safe threshold value.

### 3.1.2 Summary of Trade-Offs

#### 3.1.2.1 Trade-Off Approach

The system concept outlined above was formulated to provide relative bearing measurement and be compatible with the existing SECANT CAS while minimizing cost, size and

weight penalties. In view of this overall constraint and of the state-of-the-art in direction finding, the major options are limited to alternative configurations for DF antenna arrays and for phase comparators. However, at the level of the internal configurations of block no's. 2, 3, 4 and 5 in Figure 3-1, subsidiary design options are to be found which reflect strongly on the anticipated performance of the bearing measurement facility. Parametric comparisons and choices involving trade-offs among all known critical options are necessary to achieve the desired performance characteristics. A preamble to these analyses involves the recognition of all significant error sources and of candidate methods to suitably control the errors. These topics are discussed in the next section.

As is typical of system design, an expedient that alleviates an error of one type may exacerbate or introduce other types. In some instances, the cost or complexity of the expedients may be prohibitive. Otherwise, they might raise objections in respect to size, weight, installation and maintenance factors; the tolerable extent of which will depend on the effectiveness of the solution. Clearly, comprehensive system optimization must include trade-offs of factors other than those which pertain solely to system performance. A detailed study of such trade-offs is beyond the scope of the present program. Nevertheless, engineering judgement was exercised in rejecting any option which, while beneficial from a performance viewpoint, would be obviously self defeating in the context of overall system effectiveness.

#### 3.1.2.2 Identification of Errors and Error Control Methods

Several sources of error must be assessed when designing equipment to determine the relative bearing and bearing changes of an L-band emitter by measuring the direction-of-arrival of signals received from that emitter. Table 3-1 lists pertinent error sources while also presenting comments on their salient characteristics and on such means for reducing the error effects as appear possible in the present application. Very approximate estimates of error magnitudes are included for preliminary assessment of their relative significance.

TABLE 3-1. IDENTIFICATION OF BEARING MEASUREMENT ERRORS

| BEARING ERROR CONTRIBUTOR                                      | UNCONTROLLED <sup>1</sup> BEARING ERROR MAGNITUDE (PRELIM EST.-DEGS)                        | BEARING ERROR CAUSES & CHARACTERISTICS  | POSSIBLE MEANS FOR CONTROLLING ERROR  |
|--|---|---|---|
| Propagation  | Fixed bias: 0.1<br>Random <sup>2</sup> : 0.005 (1σ)   | Refractivity changes in troposphere. Fixed bias does not affect swept bearing accuracy.     | No compensation needed, errors are negligible.  |
| Local multi-path ("site" errors).                              | Unpredict. bias: $\pm 1.5$ max.   | Variable bias fluctuates as function of bearing. Due to reflections from aircraft surfaces. | Increase array aperture. Exploit SECANT frequency diversity.  |
| Co-range target interference.                                  | Catastrophic errors.  | Rare occurrence. Resolution for bearing fails before that of range with edge trackers.      | Attempt new meas. in next round. Use ring array antenna to transmit interrogations directionally.       |
| Spontaneous attitude variations of aircraft measuring bearing. | Random: 1 to 2 (1σ) in yaw; depending on size of aircraft.                                  | Atmospheric turbulence. Error is stated for medium turbulence conditions.                   | Interface bearing computer with attitude sensing gyros or inertial platform, to compensate for effect.  |
| Fruit interference   | Random: 2 (1σ) max.   | Fruit distributed over 360° in azimuth in densest region of FAA 1982 LA Basin traffic model | Implement rejection logic for "wild" bearings with objective of reducing error to $\leq 0.2^\circ$ (1σ) |
| Mutual coupling between interferometer monopoles.              | Known bias: $\pm 4$ max. <sup>3</sup>   | Applies to interferometer. Error is a periodic function of bearing.                         | Increasing aperture to 4 wavelengths reduces error to 0.04 degs. max.                                   |
| Ring array non-linearity                                       | Known varying bias: $\pm 2$ max. <sup>3</sup> with H=1 mode.                                | Due to finite number of monopoles. Error is periodic vs. bearing.                           | Increase mode order. Use monopole couplets. Apply theoretical corrections.                              |
| Thermal noise.   | Random: 0.5/n (1σ) <sup>4</sup>   | Based on SNR of 12dB and average of 62 pulses. Error proportional to range.                 | Locate RF front end at antenna. Reduce recvr. noise figure. Pulse integration.                          |
| Phase comparator resolution.                                   | Random: 0.6/n (1σ) for ring array; 1/n (1σ) for interferometer. Both are design objectives. | Max. practical resolution between zero crossings, or errors in analog multipliers.          | Increase mode order of ring array or aperture of interferometer.  |
| Pulse excited transients.                                      | Random: 0.5/n (1σ) design objective.  | Phase perturbations during transient states of IF filters.                                  | Delay phase measurements until transients have decayed. Use linear phase filters.                       |
| IF amplifier saturation.                                       | Variable bias: $\pm 0.5/n$ max. design objective.   | Errors occur at short ranges where hard limiting exists.                                    | Equalize limiter characteristics in both channels. Reduce mid-band 2nd IF.                              |
| Phase unbalance between dual receiver channels.                | Fixed bias: $\pm 2/n$ max.<br>Random: 0.8/n (1σ)<br>Both are design objectives.             | Drifts in receiver parameters. Frequency hopping introduces random error.                   | Locate RF front end at antenna. Increase antenna aperture. Transpose channels.                          |
| Quantization noise.  | Random: 0.1/n (1σ) design objective.  | Based on use of 11-bit word in processing data associated with ring array outputs.          | Use longer word. However, non-linear characteristic of interferometer would offset this remedy.         |

1. Except where error is designated a design objective.
2. All random error estimates given in table are after integration of data from 62 pulses.
3. Depending on choice of antenna type, only one of these errors apply.
4.  $n$  = angle conversion factor or mean rate of change of array output angle with respect to angle of arrival (corresponds to  $H=n$  for ring arrays).



Table 3-1 comprises essentially three groups of errors viz.; errors arising due to exterior or environmental influences (first four items), interface errors associated with the antenna structure, and interior errors (last seven items) caused by limitations of signal and data processing within the receiving equipment. The last group is amenable to diminution by employing an antenna array whose angle conversion factor, as defined in Note 4 of Table 3-1, exceeds unity. An appreciation of the trade-offs involved in controlling all errors except the first and last in the Table will be gained from a later discussion (Section 3.3) of the errors and possible means for alleviating them.

It is necessary to distinguish between three categories of error that arise in relative bearing measurement. They are errors definable as random variables (i.e., noise-like errors), constant bias errors, and bias errors that vary as a function of relative bearing. The latter category may be subdivided into systematic errors whose functional relationships are known, and therefore could be calibrated out; and into bias errors which are unpredictable in the sense that analytical or experimental evaluations of their actual magnitudes cannot be obtained with sufficient confidence to permit corrective actions. Only constant bias errors are completely nullified when computing a swept bearing observation from the difference of two relative bearing measurements, in order to obtain the projected miss distance.

### 3.2 ANTENNA CONFIGURATION ANALYSIS (TASK 2.1)

#### 3.2.1 Summary and Conclusions

The objective of this task was to select an antenna configuration for construction and test. The selection was made among several possible candidates and based on a trade-off analysis to identify the type most likely to succeed. To qualify as a candidate the antenna type had to be characterized by small size, no moving parts, and suitability for installation on the upper or lower surface of an aircraft for the purpose of determining

the relative bearing of a transmitting aircraft over substantial elevation angles relative to the horizontal plane.

A short analysis is first given in Section 3.2.2 of an earlier directing finding concept, the interferometer array. Next, in Section 3.2.3 the present concept of ring modes is discussed and element types are considered. Trade-offs are conducted on the number of elements, feed geometry, and radiation characteristics of dual-mode arrays. Printed circuit designs are studied for this system. A method of improving the azimuth bearing accuracy by increasing the number of elements is described. Higher order modes are then discussed and a fourth order ring mode is described. A short discussion is given on the effect of a finite ground plane on the radiation characteristics.

The analysis of the two-element interferometer array shows that the mutual coupling between the two antennas, spaced one-half wavelength apart, produces a maximum azimuth bearing error of almost  $14^\circ$ . This error can be reduced, however, by increasing the element spacing. It becomes negligible in the 3-element, crossed axis interferometer with elements spaced at four wavelengths.

The study of the ring mode concept has demonstrated that the four element ring array is adequate for generating the two lower order modes of radiation and can produce the desired characteristics. A comparison of the received phases on this two mode antenna gives the azimuth bearing without ambiguity. The maximum bearing error for a practical array geometry is about  $2.3^\circ$ .

An important system consideration is accurate determination of incremental changes in the bearing angle. By the use of a higher order mode, much greater accuracy is theoretically obtainable since the phase change throughout  $360^\circ$  is  $H \times 360$ , where  $H$  is the mode number. A choice of the fourth order mode is an optimum compromise between

increased accuracy and limitations on array size and circuit complexity. In actual practice, after obtaining the bearing direction from the comparison of the first and second order mode phases, the phases of the  $H = 0$  and  $H = 4$  mode antennas are compared. In this case, the phase difference is then four times the bearing direction.

Although the azimuth bearing accuracy of the  $H = 1$  mode can be improved by using a nine element array (a single monopole for the  $H = 0$  mode and eight monopoles in the  $H = 1$  ring) this is not considered necessary since the use of the  $H = 4$  mode gives much greater accuracy. It was, therefore, decided that the antenna selected for construction be a 3 mode ( $H = 0$ ,  $H = 1$ ,  $H = 4$ ) antenna containing 21 monopoles.

### 3.2.2 Analysis of Interferometer Array

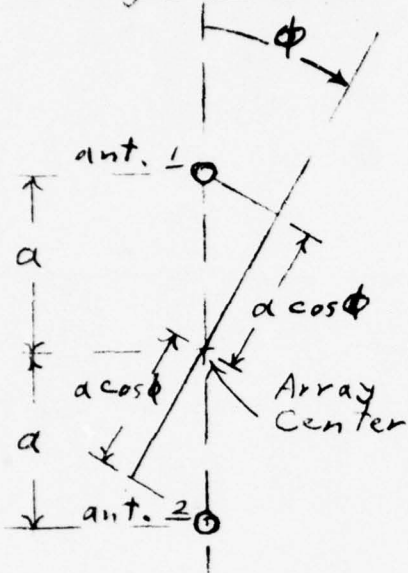
Consideration is first given to the azimuth bearing accuracy of the interferometer array of monopoles over an infinite ground plane. The analysis is given initially for only the simplest type consisting of only two elements. The spacing between the elements has been chosen as one-half wavelength for this particular example. An analysis of the crossed-axis interferometer with various element spacings is given in Appendix G.

The array geometry and coordinate system is shown in Figure 3-4a. A wave arriving from an azimuth direction,  $\theta$ , will induce equal amplitude voltages in the two elements. These voltages are leading and lagging, respectively, in phase by the same value relative to the array center (Figure 3-4b). Hence, the two voltages may be considered as the vector sum of in-phase components and out-of-phase components; the latter are in quadrature with the former.

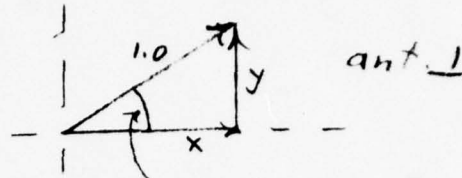
Using the equivalent circuits pictured in Figure 3-4c, the received currents ( $\bar{I}_{++}$  and  $\bar{I}_{+-}$ ) may be found for each of the two voltage components. These currents may then be added vectorily to give the actual received currents,  $\bar{I}_1$  and  $\bar{I}_2$ . Calculations are supplied in Figure 3-5.



(a) Array - Top View



(b) Received voltages

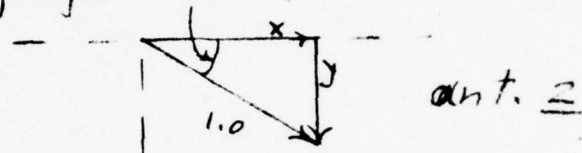


Lead angle =  $a \cos \phi$

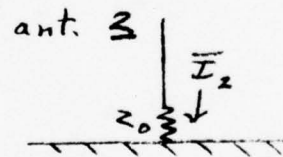
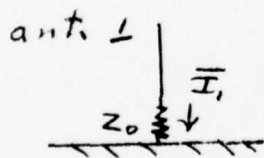
In-phase components,  $|x| = \cos(a \cos \phi)$

Out-of-phase components,  $|y| = \sin(a \cos \phi)$

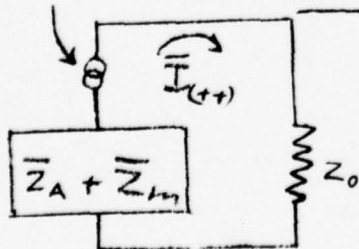
Lag angle =  $a \cos \phi$



(c) Terminated monopoles and Equivalent Circuits  
For In-phase & Out-of-phase Components



In-phase Components  
 $\cos(a \cos \phi)$  ant. 1 and 2



Out-of-phase Components  
 $\sin(a \cos \phi)$  ant. 1 and 2

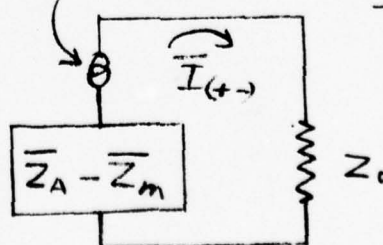


Figure 3-4. Analysis of Two-Element Interferometer Array

$$\bar{I}_{(+)} = \frac{\cos(a \cos \phi)}{(R_0 + R_m) + j(X_0 + X_m) + Z_0}$$

$$\bar{I}_{(-)} = \frac{\pm j \sin(a \cos \phi)}{(R_0 - R_m) + j(X_0 - X_m) + Z_0}$$

$$\bar{I}_1 = \bar{I}_{(+)} + j \bar{I}_{(-)}$$

$$\bar{I}_2 = \bar{I}_{(+)} - j \bar{I}_{(-)}$$

$$\bar{I}_1 = \frac{\cos(a \cos \phi)}{(R_0 + R_m) + j(X_0 + X_m) + Z_0} + \frac{j \sin(a \cos \phi)}{(R_0 - R_m) + j(X_0 - X_m) + Z_0}$$

$$\bar{I}_2 = \frac{\cos a(\cos \phi)}{(R_0 + R_m) + j(X_0 + X_m) + Z_0} - \frac{j \sin(a \cos \phi)}{(R_0 - R_m) + j(X_0 - X_m) + Z_0}$$

$$\bar{I}_1 = \bar{A} [\cos(a \cos \phi)] + j \bar{B} [\sin(a \cos \phi)]$$

$$\bar{I}_2 = \bar{A} [\cos(a \cos \phi)] - j \bar{B} [\sin(a \cos \phi)]$$

where

$$\bar{A} = \frac{[(R_0 + R_m + Z_0) - j(X_0 + X_m)]}{[(R_0 + R_m + Z_0)^2 + (X_0 + X_m)^2]}$$

and

$$\bar{B} = \frac{[(R_0 - R_m + Z_0) - j(X_0 - X_m)]}{[(R_0 - R_m + Z_0)^2 + (X_0 - X_m)^2]}$$

(Note: for no mutual coupling,  $\bar{A} = \bar{B}$ )

Figure 3-5. Analysis of Two-Element Interferometer Array (Continued)

The phases of the received currents are plotted versus the azimuth angle,  $\theta$ , in Figure 3-6 as the solid curves. Also plotted for comparison are the phases assuming no mutual coupling. Data is given only over the  $\theta$  range of  $0^\circ$  to  $90^\circ$  since the curves repeat in each quadrant.

The azimuth error for the actual case is plotted in Figure 3-7 and is seen to reach a maximum value of  $13.8^\circ$  at  $\theta = 60^\circ$ . The magnitude variations as a function of  $\theta$  are given in Figure 3-8 for the two cases.

It appears that the azimuth bearing error is excessive for the proposed system. A greater element spacing would have less error since the mutual impedance diminishes with distance. Also, the crossed-axis configuration which would apply to the present program, results in much lower errors (Appendix G).

Several severe drawbacks concerning the utilization of airborne interferometer arrays were realized at an early stage in the bearing measurement study. These drawbacks, listed in Table 3-2, are not suffered by the omni-directional ring array DF antenna which is treated in the following sections. The data processing and accuracy advantages of the ring array are so significant that the interferometer was not pursued further, despite its constructional simplicity.

### 3.2.3 Analysis of Ring Arrays

The remaining portion of the antenna study was devoted to a preferred alternative system for direction finding in the azimuth plane. This approach uses antennas to generate decoupled, omni-directional patterns that differ in far-field phase. On reception, the measured phase difference defines the azimuth angle of the incoming wave.

#### 3.2.3.1 Mode Definition and Geometry

In this study, a mode is defined as radiation that is omni-directional in the plane normal to a reference axis, and that has an integral number (H) of cycles of phase variation



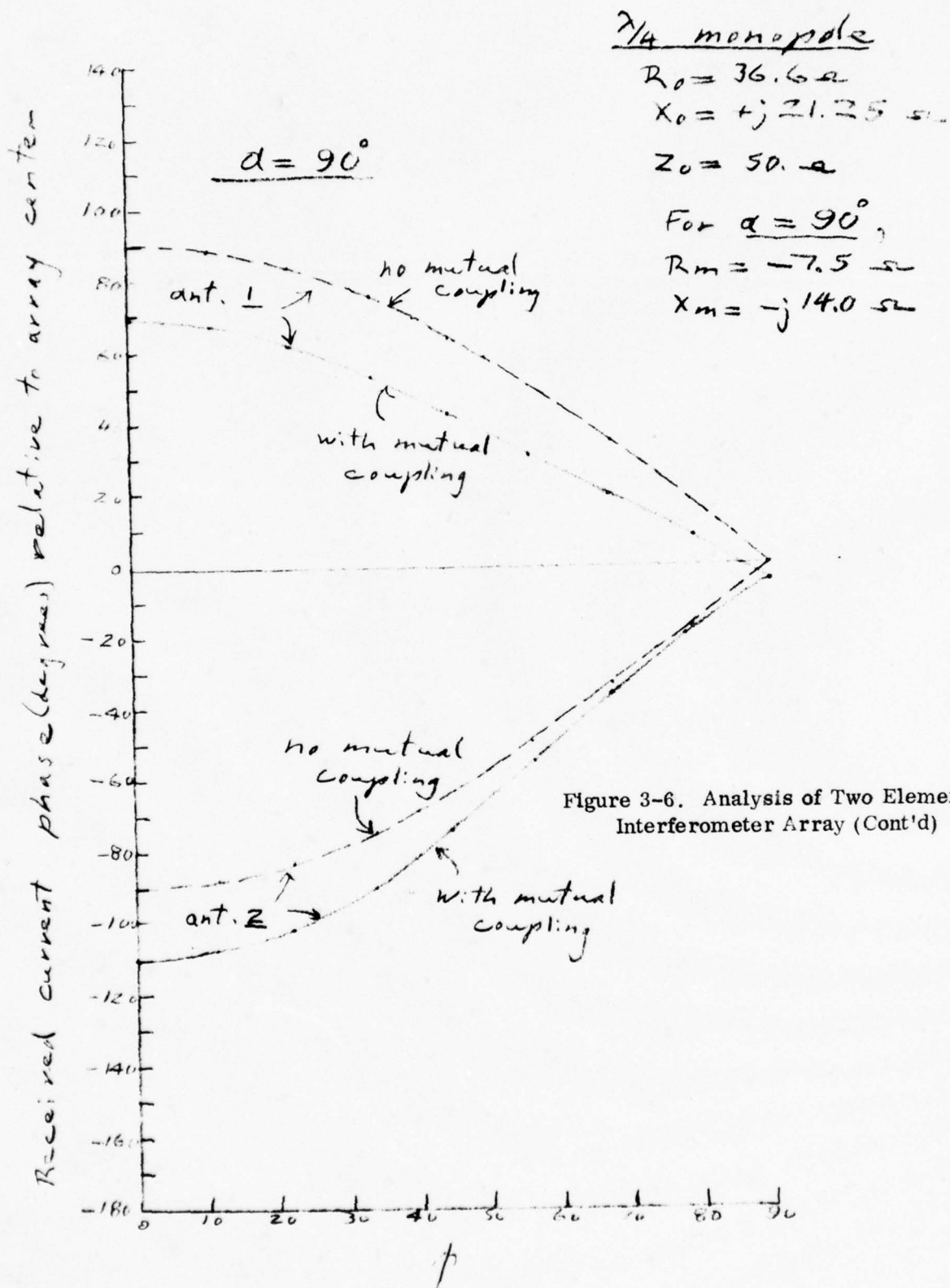


Figure 3-6. Analysis of Two Element-Interferometer Array (Cont'd)

Azimuth error (degrees) caused  
by mutual coupling between monopoles

$$\underline{a = 90^\circ}$$

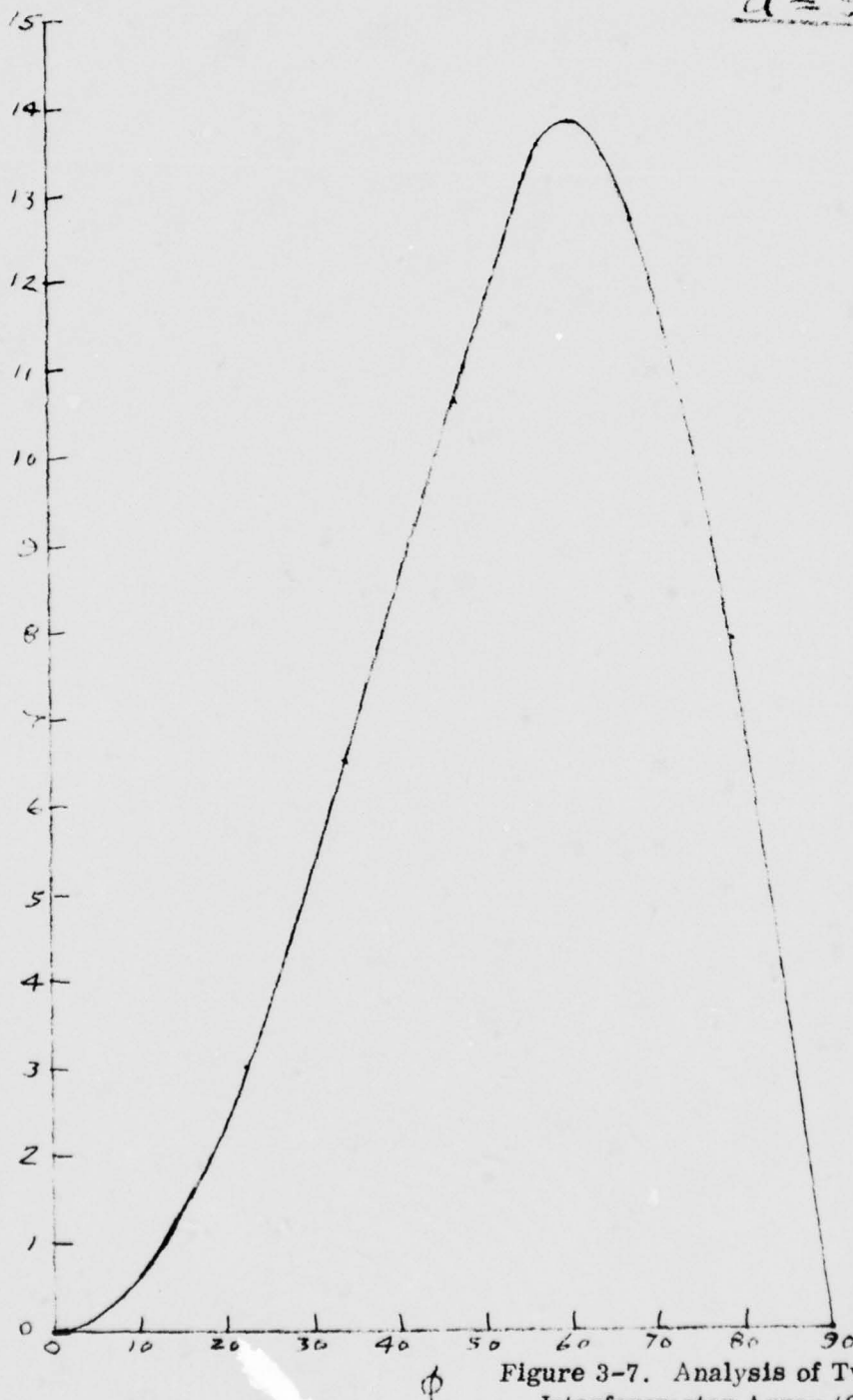


Figure 3-7. Analysis of Two Element Interferometer Array (Cont'd)

Relative Amplitude Changes in Received  
Currents due to mutual coupling

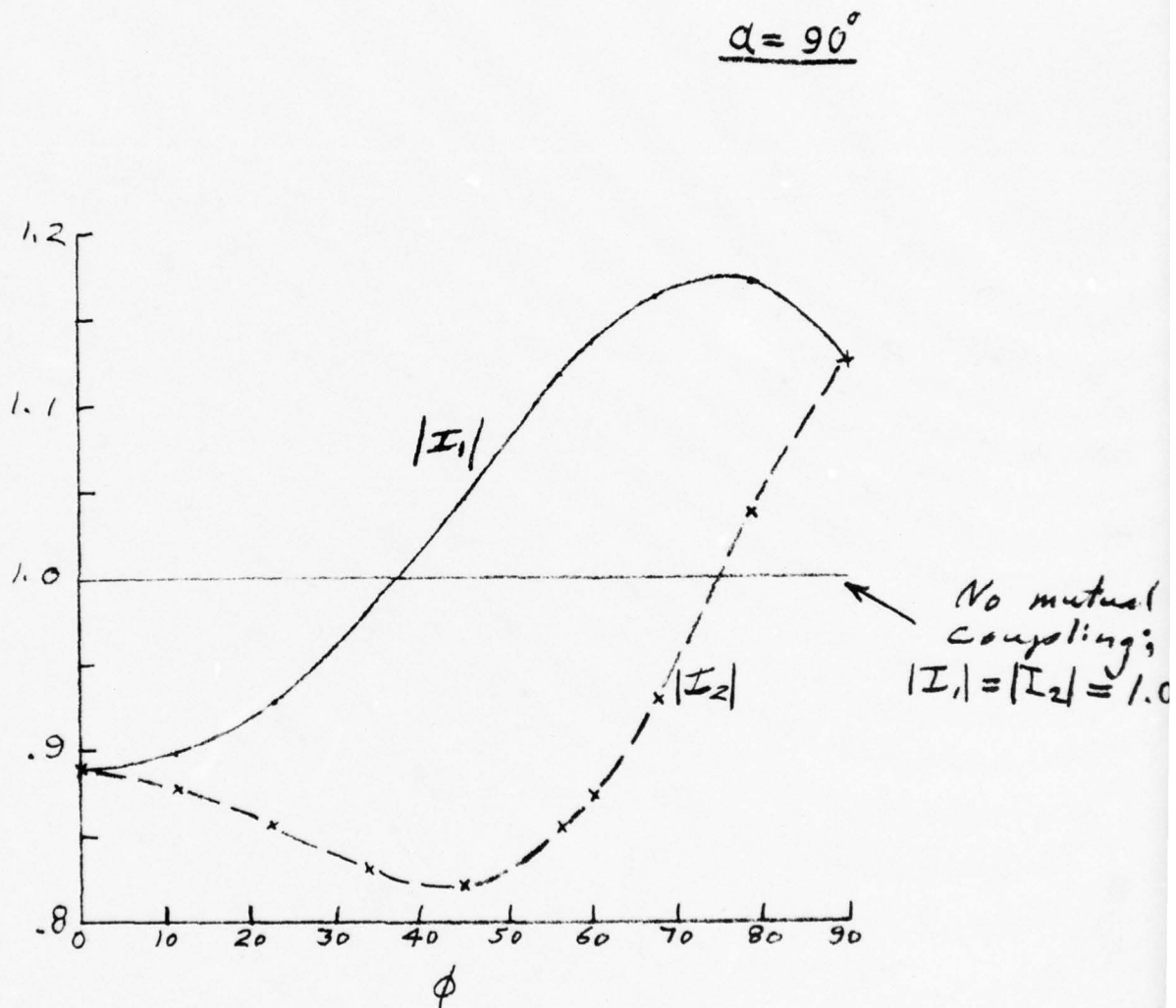


Figure 3-8. Analysis of Two Element Interferometer Array (Cont'd)



TABLE 3-2. COMPARISON OF D.F. ANTENNA ARRAYS

| ARRAY TYPE   | ADVANTAGES   | DISADVANTAGES  |
|--|--|--|
| <u>Crossed-Axis Interferometer</u><br><br>(Wide aperture array + narrow aperture array for quadrant ambiguity resolution). | Low-cost construction - simple mechanical configuration with 5 monopole elements, including those for quadrant ambiguity resolution.                         | Each array has three ports thus requiring three receiver channels or R.F. switching to share one channel of two-channel system.  |
|  | Elevation angle measurable, but with poor accuracy for rays near antenna ground plane (capability not required for CAS application).                         | Excessively complex data processing to extract bearing data from phase difference measurements of signals outputted from array ports.  |
|  |  | Interchannel phase balance correction is necessary for both relative bearing and swept bearing measurements.   |
|  |  | Tangent relationship between phase and DOA inflates bearing error especially at and near 0°, 90°, 180°, 270°.  |
| <u>Ring Mode</u><br><br>(Two concentric monopole rings, H=1 and H=4, with central reference element).                      | Each array has two ports thus eliminating need for switching except for quadrant ambiguity resolution.   | Slightly higher cost than interferometer. Up to 21 monopole elements are required with associated microstrip delay lines and hybrid junctions all mounted on a single printed circuit board. |
|  | Phase difference is proportional to bearing, permitting simple data processing for bearing determination, and avoiding error inflation due to non-linearity. |  |
|  | Interchannel phase imbalance does not affect accuracy of swept bearing (hence miss distance) measurement.  |  |

throughout  $360^\circ$  in the normal plane. This phase variation may be either clockwise (+H) or counterclockwise (-H). The mode identifying integer may also be zero, i.e., the radiation may be constant in phase in all directions.

Such modes may be conceived as emanating from an infinite number of infinitesimal radiators (Hertz dipoles) arranged in a very small circle or ring coaxial to the reference axis. For any given mode, three orthogonal orientations of the radiators are possible, namely, axial, tangential, and radial (Figure 3-9). The radiation geometry can be most conveniently expressed in the usual  $\theta, \phi$  spherical coordinates with the  $\theta = 0^\circ$  axis assumed to be vertical and normal to the ring array lying in the horizontal plane.

It should be pointed out that as the radius,  $a$ , approaches zero, such a ring becomes a supergain antenna (for any  $H$  not zero) that is physically unrealizable. However, these concepts are quite useful as elementary building blocks in a theoretical study; first, because they illustrate the ultimate limitations, and second, because a number of practical antenna configurations have radiation characteristics that closely approximate these idealized patterns. A more detailed study of these ring modes is given in (7).

#### 3.2.3.2 Element Types

It has been shown (8) that only modes  $H = \pm 1$  of the tangential and radial types can radiate in the direction  $\theta = 0^\circ$ ; all other modes have a null in this direction. The two modes to be considered first in this present concept are the  $H = 0$  and  $H = 1$ . Since the  $H = 0$  has a null at  $\theta = 0^\circ$ , then it is desirable that the  $H = 1$  mode also has a null at  $\theta = 0^\circ$  so that the two modes have approximately the same gains and relative pattern shapes. This means that only the axial type of radiator geometry can be used for both desired modes. Thus, slot and loop radiators are eliminated, and only vertical monopoles can be used.

Another reason for this choice is that only the axial type is linearly polarized (vertical) in all directions; the tangential and radial types for the  $H = 1$  mode radiate both horizontal and vertical components of polarization. A specification of the system is that the polarization be linear.

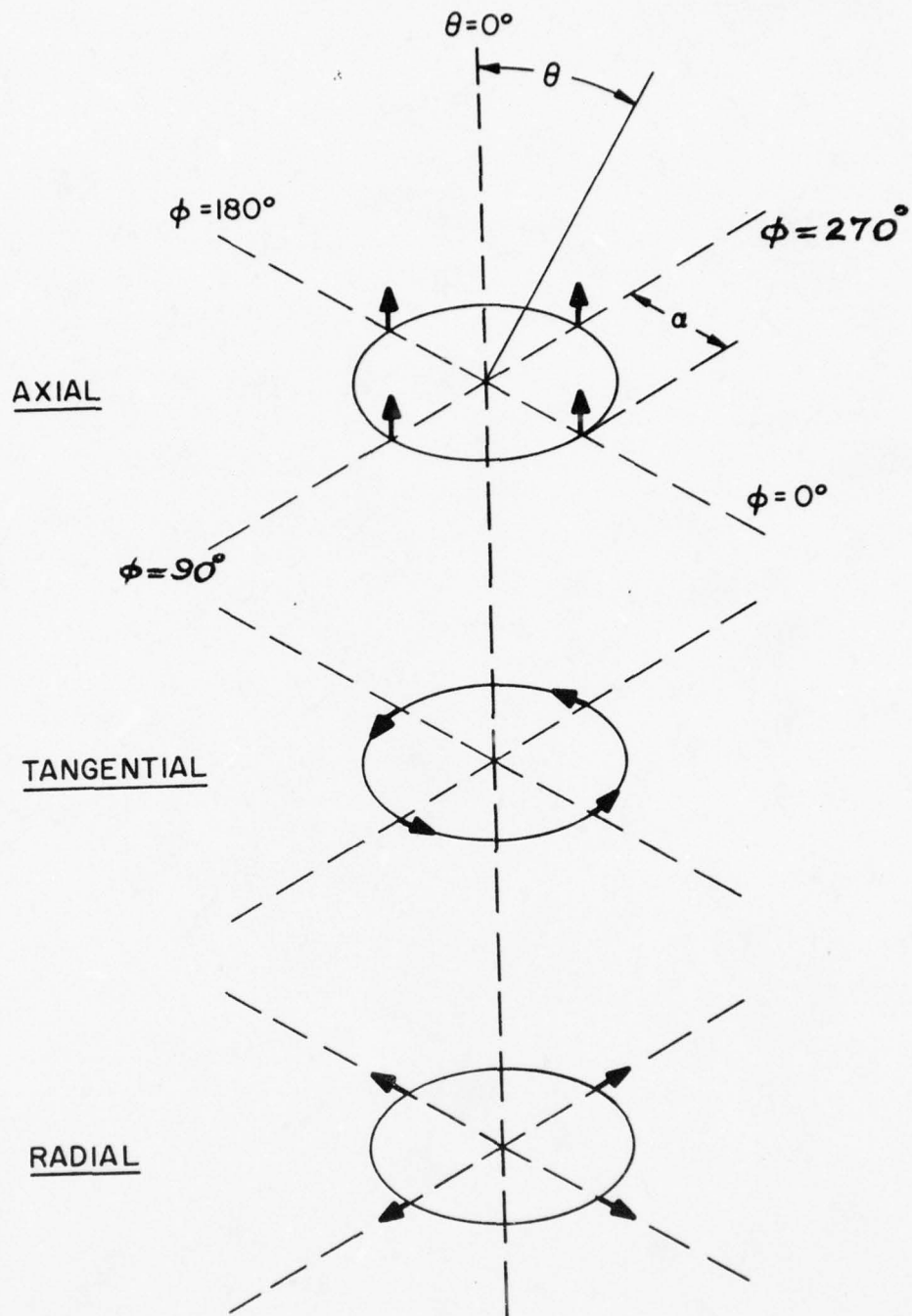


Figure 3-9.  
GEOMETRY OF RING ELEMENTS



3.2.3.3 Trade-offs Between Number of Elements and Feed Circuitry;  
3-Element -- H = 1

All of the radiation characteristics for the various arrangements are calculated for monopoles over a perfect, infinite ground plane. Consideration is given later as to the effect on the patterns of finite ground planes.

First to be studied is a 3-element array of monopoles arranged in an equilateral triangle (Figure 3-10a). This is the minimum number that can produce the  $H = 1$  mode. The elements are located on a circle of radius,  $a$ , and fed in progressive phasing with equal amplitudes. In this and the following sections, the arrays are assumed to be used as transmitting antennas for ease in evaluation. The end results of course apply to the receiving case by reciprocity.

One method of feeding the elements is shown in Figure 3-10b, where the antennas are fed from a common junction by three coaxial cables which differ in length by  $1/3$  wavelength steps; thus, the antennas, if matched, are excited with equal amplitudes and relative phases of  $0^\circ$ ,  $120^\circ$  and  $240^\circ$ . Each antenna sees adjacent antennas differing in phase by either  $\pm 120^\circ$ . Therefore, by symmetry, the radiation impedance of all three antennas are identical for this particular phasing\*.

Now, if the three unit radiators are not perfectly matched, equal amplitude waves of magnitude  $K$  (relative reflection coefficient magnitude) will be reflected back toward the input port. These waves, having traveled twice over the three unequal length feed lines, will arrive at the input port with equal amplitudes in a 3-phase relation having the opposite sense of phase progression.

ORIGINAL PHASING

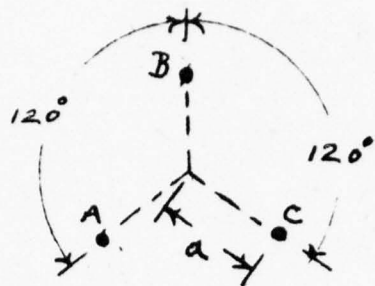
$0^\circ$   
 $120^\circ$   
 $240^\circ$

x2

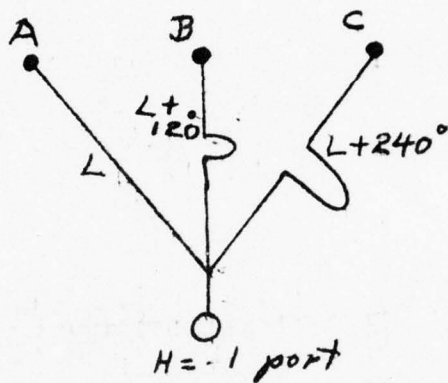
$0^\circ$   
 $240^\circ$   
 $480^\circ = 120^\circ$

\*This equality of radiation impedances also occurs for equal phase excitation.

(a)



(b)



(c)

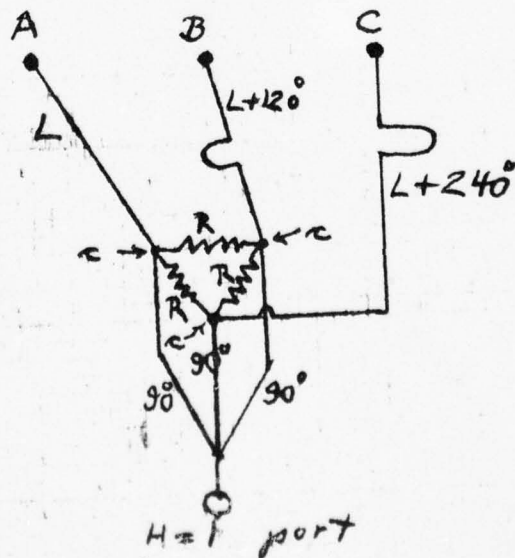


Figure 3-10. 3-Element Array -  $H = 1$

This results in a voltage null at the input port; hence, no reflected wave travels toward the generator.

Next, because of this null or effective short circuit at the input junction, the three waves return to the three radiators. For this case, each equal amplitude wave component has traveled three times over the three separate feed cables.

| <u>ORIGINAL PHASING</u> | <u>x3</u> |
|-------------------------|-----------|
| 0°                      | 0°        |
| 120°                    | 360° = 0° |
| 240°                    | 720° = 0° |

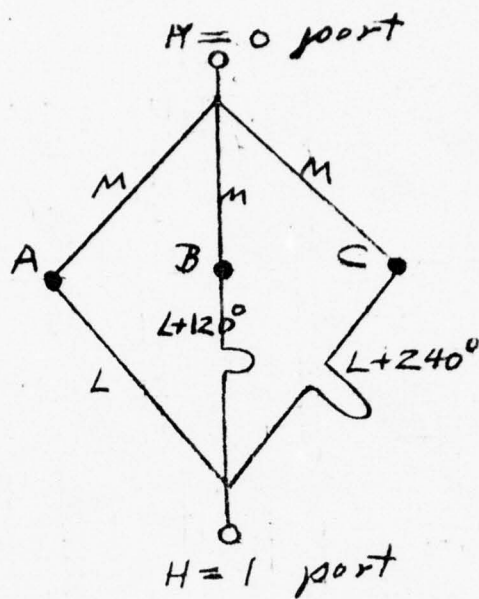
Thus, it is seen that the radiation of these re-reflected waves constitute a  $H = 0$  mode azimuthal pattern. This effective cross-coupling between the two modes is undesired in the proposed system operation.

The circuitry of Figure 3-10c illustrates a means of absorbing the reflected waves from mismatched antennas using a triangular loop of three resistors. Main waves going out from the input port arrive at the corners, c, in-phase; hence, no power is lost in the resistors. However, reflected waves return to the corners in progressive phasing, and are completely absorbed in the resistors.

Next to be discussed are means to operate with both the  $H = 0$  and  $H = 1$  modes. Circuitry such as shown in Figure 3-11a is unsatisfactory since reflected waves from mismatched antennas end up in the  $H = 0$  port. The arrangement of Figure 3-11b is likewise unsatisfactory; although reflected waves are absorbed in the resistors for input at the  $H = 1$  port, power is also lost in the resistors when a signal is applied at the  $H = 0$  port. In addition, no improvement is gained by using a single antenna at the center of the array for the  $H = 0$  mode. Thus far in this study of a triad geometry for the  $H = 1$  mode, no desirable method has been found to generate both modes with simple printed circuit elements.



(a)



(b)

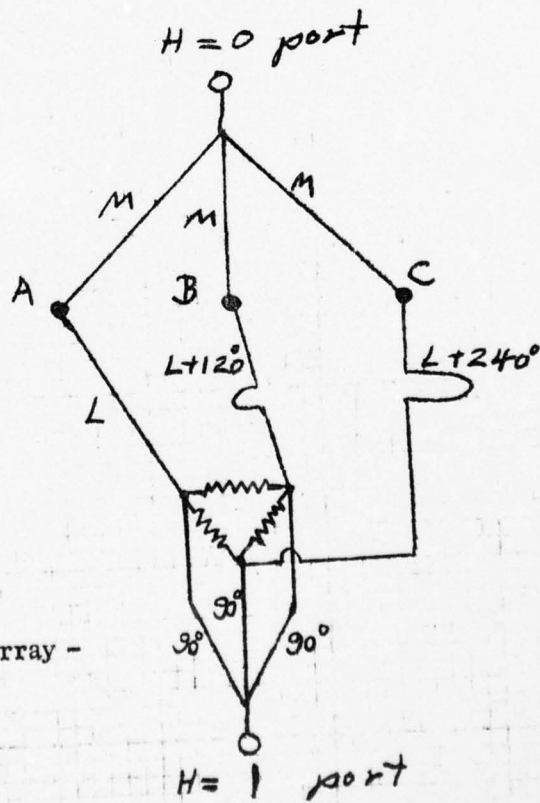


Figure 3-11. 3-Element Array -  
 $H=0$  and  $H=1$

This is not to say, however, that the desired modes cannot be generated by other means. For example, the drawing of Figure 3-12 illustrates one such method. A section of circular waveguide has two mode exciters at one end and three monopole radiators coupled through a shorting plate at the other end. Input from the rectangular waveguide excites a linearly polarized, dominant ( $TE_{11}$ ) mode in the circular waveguide. Ridges aligned at  $45^\circ$  to the base input convert this wave to a circularly polarized  $TE_{11}$  mode which in turn excites the three monopoles in progressive phasing ( $H = 1$  mode). Input at the base through a coaxial probe excites the second order  $TM_{01}$  mode in the circular waveguide. The purity of this mode is unaffected by the ridges and thus the three radiators are fed in-phase ( $H = 0$ ). Mismatches for either mode do not cause mode cross-coupling. In addition, another  $TE_{11}$  port, orthogonal to the one shown, may be added at the base of the circular waveguide to deliver reflected  $TE_{11}$  waves to an absorbing resistor. However, the size and weight of such an approach is less desirable in this system than simple printed circuitry. It is, therefore, concluded at this stage that the triad system is inadequate and that next consideration will be devoted to a 4-element arrangement for exciting the  $H = 1$  mode.

#### 3.2.3.4 4-Element --- $H = 1$ Array

The 4-element array (Figure 3-13a) is most easily excited in progressive phasing by two baluns and a  $90^\circ$  hybrid (Figure 3-13b). These components may be made using printed circuitry as shown in Figure 3-13c. Although the balance quality of this type of balun is frequency dependent, the SECANT band is sufficiently small that no serious problem is presented. A discussion of the balun frequency characteristics is included in Appendix H.

Referring to the circuitry of Figure 3-13c, it is to be noted that a mode conversion problem also exists for unmatched radiators. A main wave from point "a" excites the antennas in phase quadrature. Reflected waves arrive back to point "a" out-of-phase since one has traveled the extra  $90^\circ$  line section twice. This gives a virtual short circuit

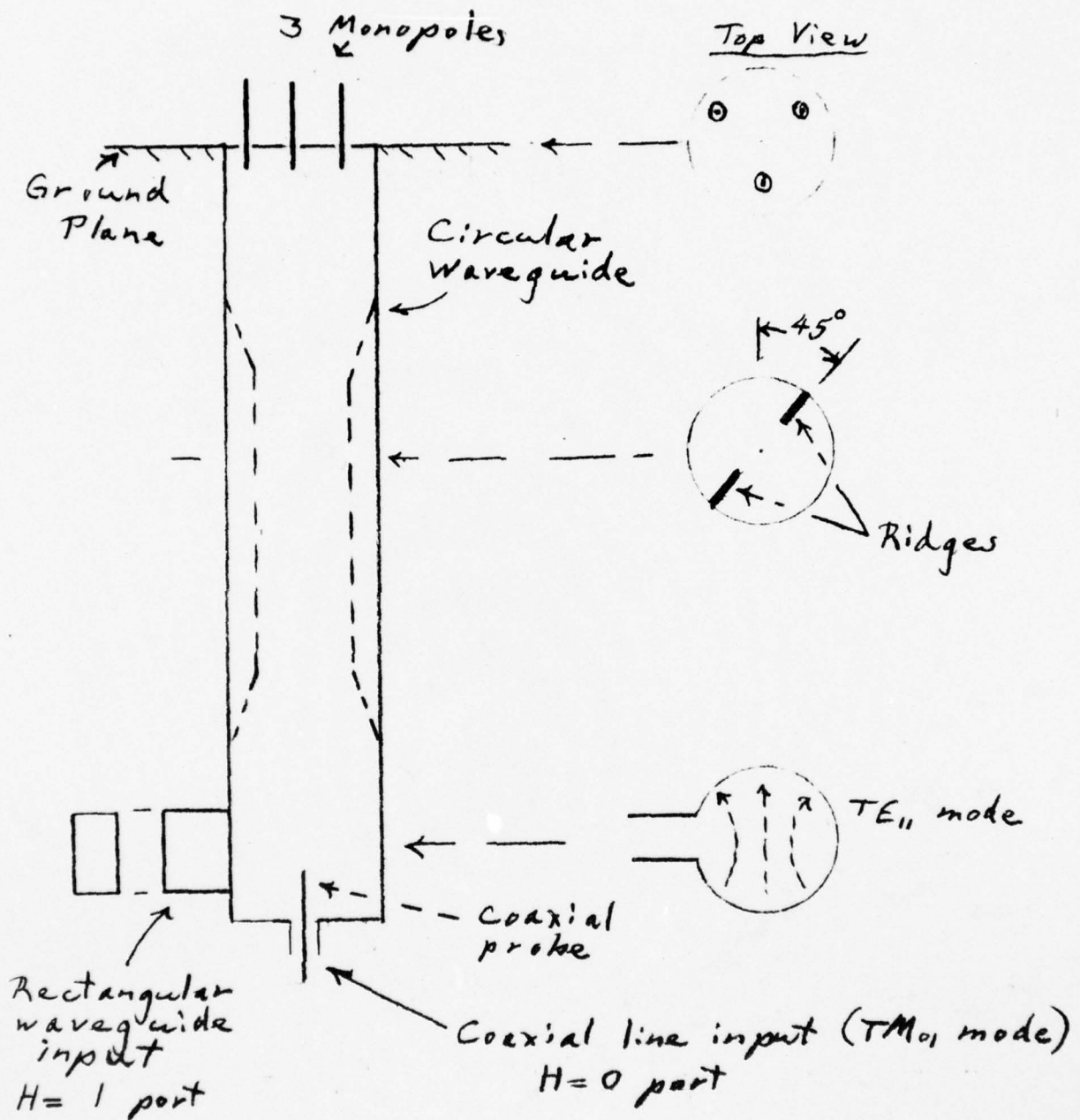


Figure 3-12. 3-Element Array — H = 0 and H = 1



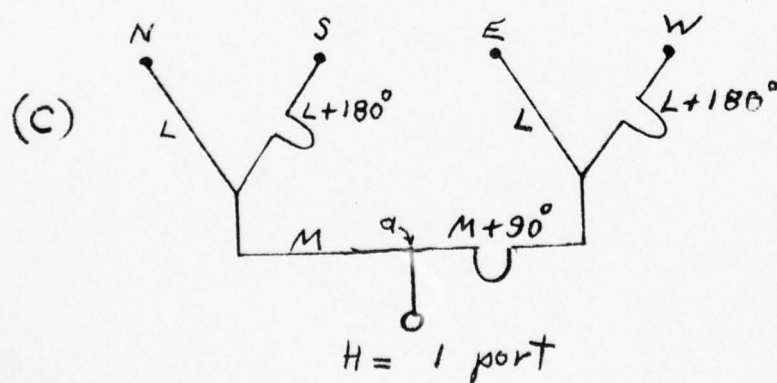
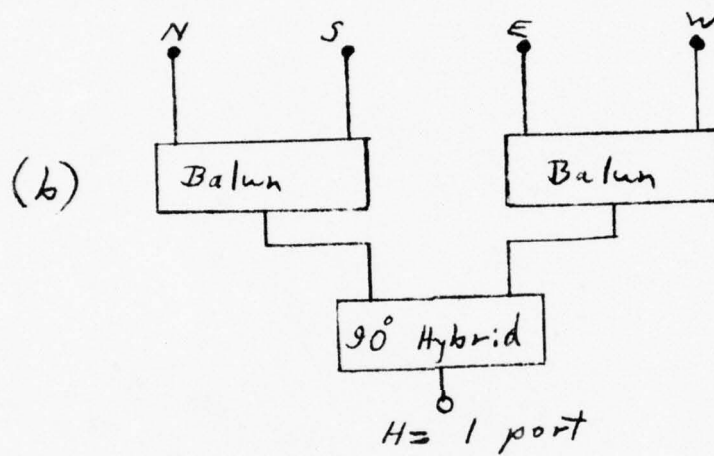
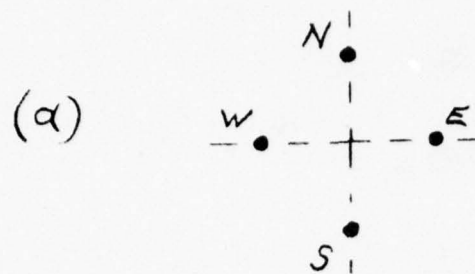


Figure 3-13. 4-Element Array -  $H = 1$

at point "a" and the waves are re-reflected to the antennas with a phase progression opposite in sense relative to that of the main wave excitation. Hence, a  $H = +1$  mode is partially converted to a  $H = -1$  mode if the antennas are mismatched. This action would impair the desired phase linearity with azimuth angle. However, there is no mode conversion to a central element for the  $H = 0$  mode since diametrically opposite radiators of the  $H = 1$  array are out-of-phase and have a neutral plane of zero field midway between them.

This problem may be solved by using a "rat-race" hybrid between the  $H = 1$  port and the radiators as shown in the lower part of Figure 3-14b. Any reflected waves from the antennas are now absorbed in the resistor joined to one port of the hybrid.

Also shown in the upper part of Figure 3-14b is circuitry for exciting the four elements in-phase for the  $H = 0$  mode radiation. The added hybrids between the N-S and E-W elements prevent cross coupling between the two input ports. Line sections M and P may be chosen for optimum impedance matching without affecting the mode purity of either the two modes.

Figure 3-15 shows an alternative method for obtaining both modes; here a central element is added for the  $H = 0$  mode radiation. Thus, the circuitry is simplified at the expense of adding a fifth element.

It is concluded at this point that a 4-element array for the  $H = 1$  mode has distinct advantages over the 3-element systems previously described.

#### 3.2.3.5 Characteristics of 4-Element Array

The vector diagram of Figure 3-16 illustrates that the far-field phase for the  $H = 0$  mode is constant, even for values of the radii,  $a$ , that produce considerably poor azimuth circularity. The relative field pattern at  $\theta = 0^\circ$  is given as the addition of two couplet patterns.

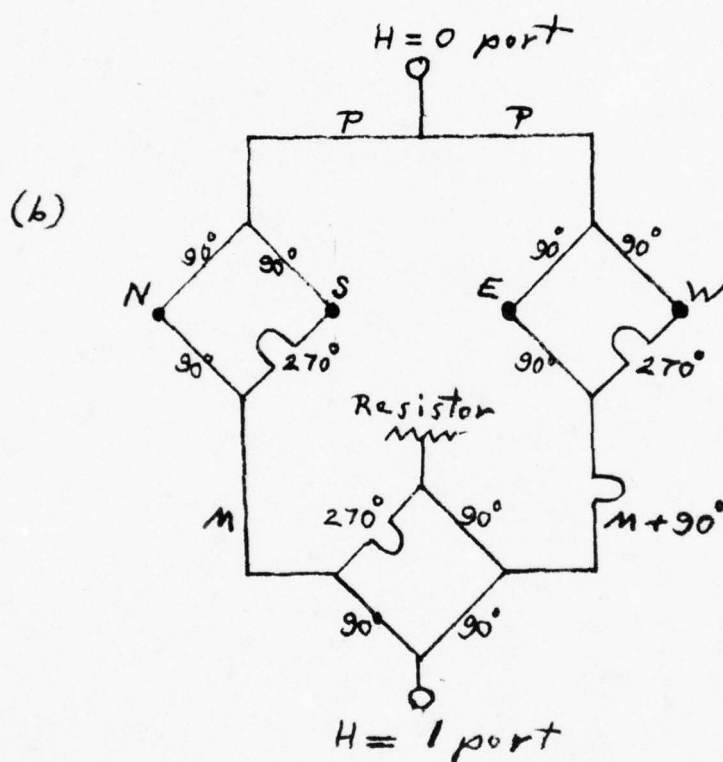
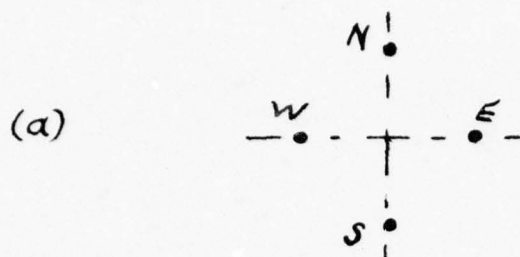


Figure 3-14. 4-Element Array --  $H = 0$  and  $H = 1$



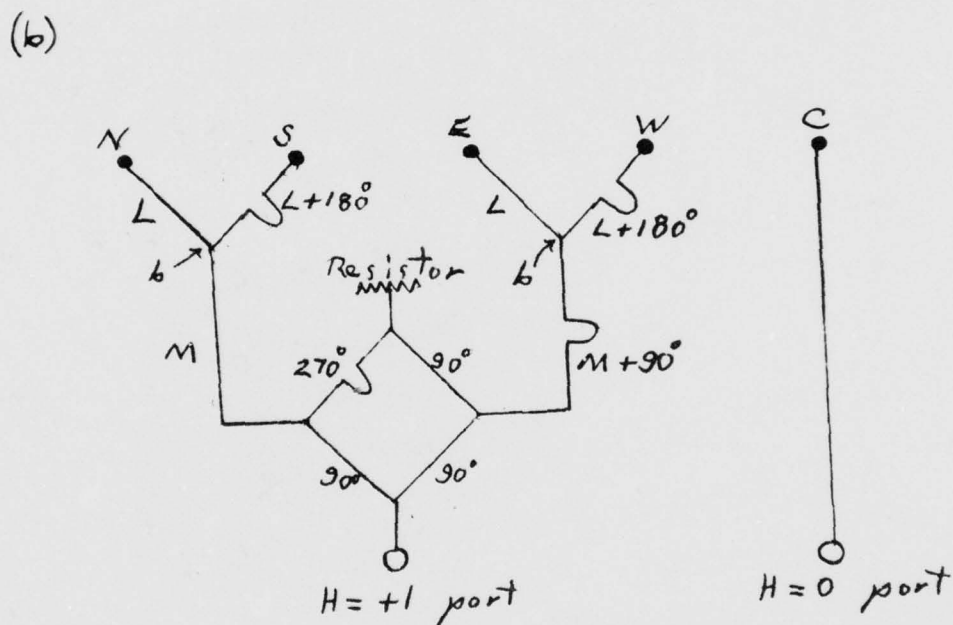
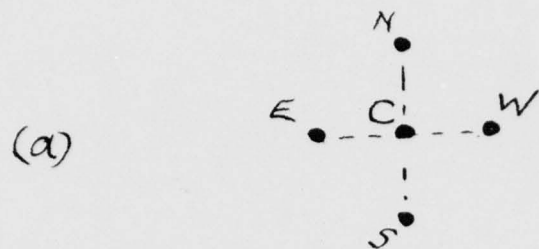
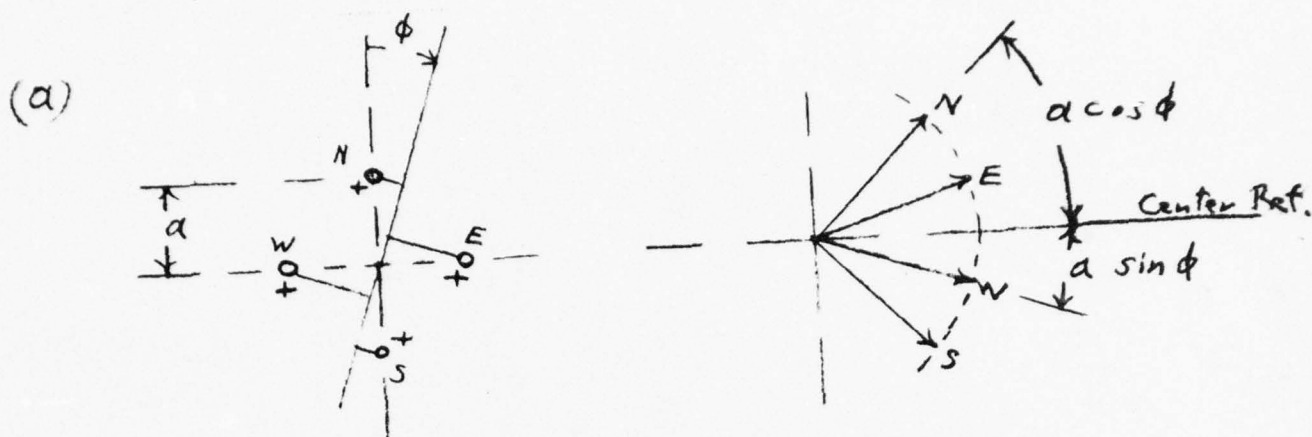


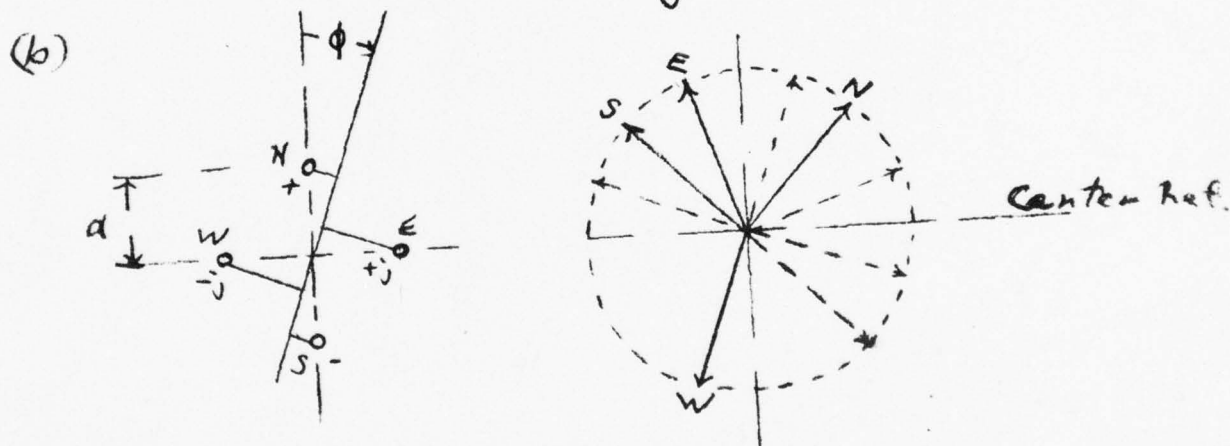
Figure 3-15. 5-Element Array -  $H = 0$  and  $H = +1$



$$\theta = 90^\circ$$

$$F = \cos(a \cos \phi) + \cos(a \sin \phi)$$

4-Element Array --  $H = 1$



$$\theta = 90^\circ$$

$$F = \sin(a \cos \phi) + j \sin(a \sin \phi)$$

Figure 3-16. 4-Element Array --  $H = 0$

The couplet patterns for the  $H = 1$  mode (Figure 3-16a) are figure-eight shapes as shown in Figure 3-17. As depicted by the vector diagram of Figure 3-16b, the N-S couplet pattern is always in phase quadrature relative to the array center. Since the E-W couplet is fed in phase quadrature relative to the N-S couplet, then its couplet pattern is always either in-phase or out-of-phase relative to the array center. The relative field pattern at  $\theta = 90^\circ$  is also given as the vector sum of the two couplet patterns.

Using the field formula of Figure 3-16b, the azimuth bearing errors were calculated at  $\theta = 0^\circ$  and the data plotted in Figure 3-18 versus  $\phi$ . It is seen that no error occurs at  $\phi = 0^\circ, 45^\circ$ , etc., and that the maximum error occurs at  $\phi = 22\text{-}1/2^\circ, 67\text{-}1/2^\circ$ , etc. The maximum values are plotted in Figure 3-19 versus the radii,  $a/\lambda$ . Curves are also shown for  $\theta$  angles other than  $90^\circ$  to illustrate the decreased error at smaller values of  $\theta$ . This reduction takes place because the projected element spacing is reduced at angles above the horizon as a cosine function.

Gain, circularity, and impedance data presented in the following section were obtained from an earlier study at RCA. The data were derived using the mutual impedance method of calculating gain and radiation impedance.

The gain relative to an isotropic source for four elements fed in phase is plotted in Figure 3-20a versus  $a/\lambda$ . Curves are given for  $\phi$  angles of minimum and maximum phase error. The azimuth circularity is shown in Figure 3-20b versus  $a/\lambda$ . Similar data for the  $H = 1$  mode is plotted in Figure 3-21. It is seen that the  $H = 1$  mode has about 1 db greater gain for values of around  $1/8$  wavelength but slightly poorer circularity.

The radiation impedance of each element of a four element array for the  $H = 1$  mode is plotted in Figure 3-22 versus  $a/\lambda$ . It is seen that as the radius decreases the impedance decreases, approaching zero as a limit.

The above data were calculated from theoretical elements of very small diameter. Experimental measurements performed at RCA Laboratories long ago are given in Figure 3-23 for comparison. In this example, two monopoles of relatively thick diameter were



AD-A049 767

RCA ELECTROMAGNETIC AND AVIATION SYSTEMS DIV VAN NUY--ETC F/G 1/2  
BEARING STUDY PROGRAM.(U)

APR 74 E JELLINEK, W KRAM, M LEVINSSEN  
RCA-EASD-TP-2146

N62269-73-C-0906  
NL

UNCLASSIFIED

2 OF 5

AD  
A049 767



$$H=1$$

Rosette Patterns produced  
by Sub-Ring A and Sub Ring B

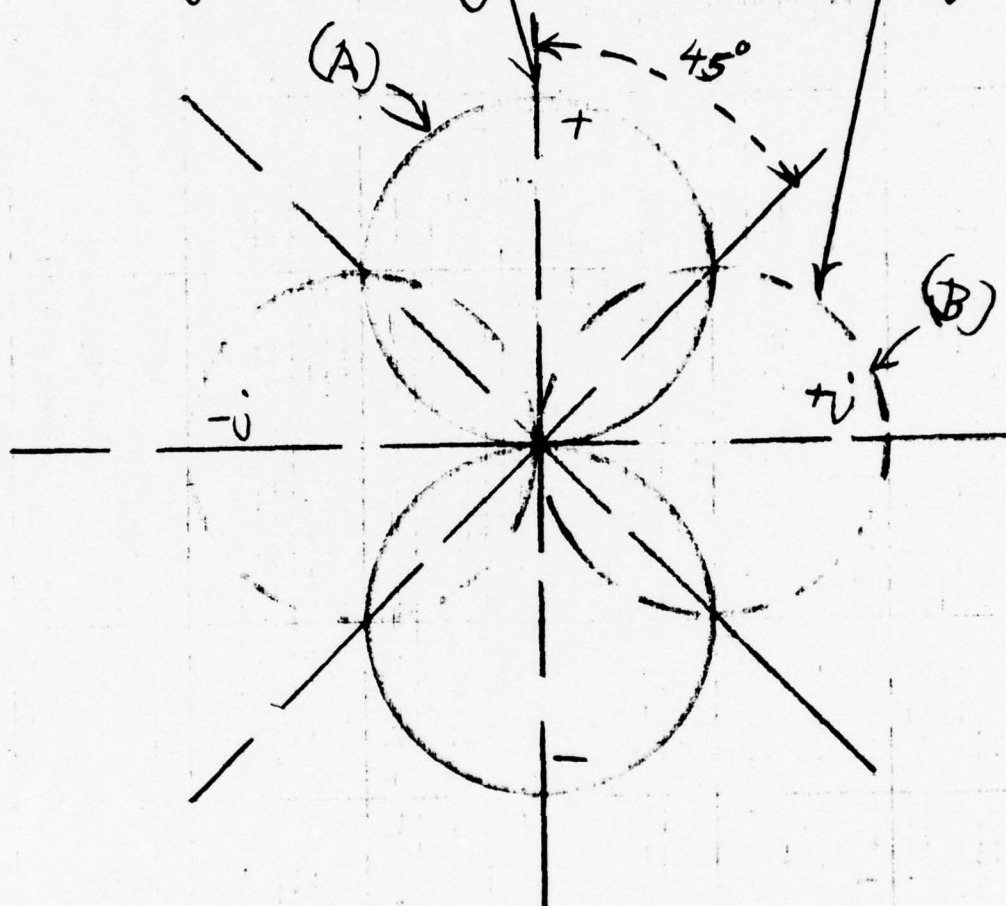


Figure 3-17. Four Element Array,  $H = 1$ , Rosette Patterns  
Produced by Subring A and Subring B

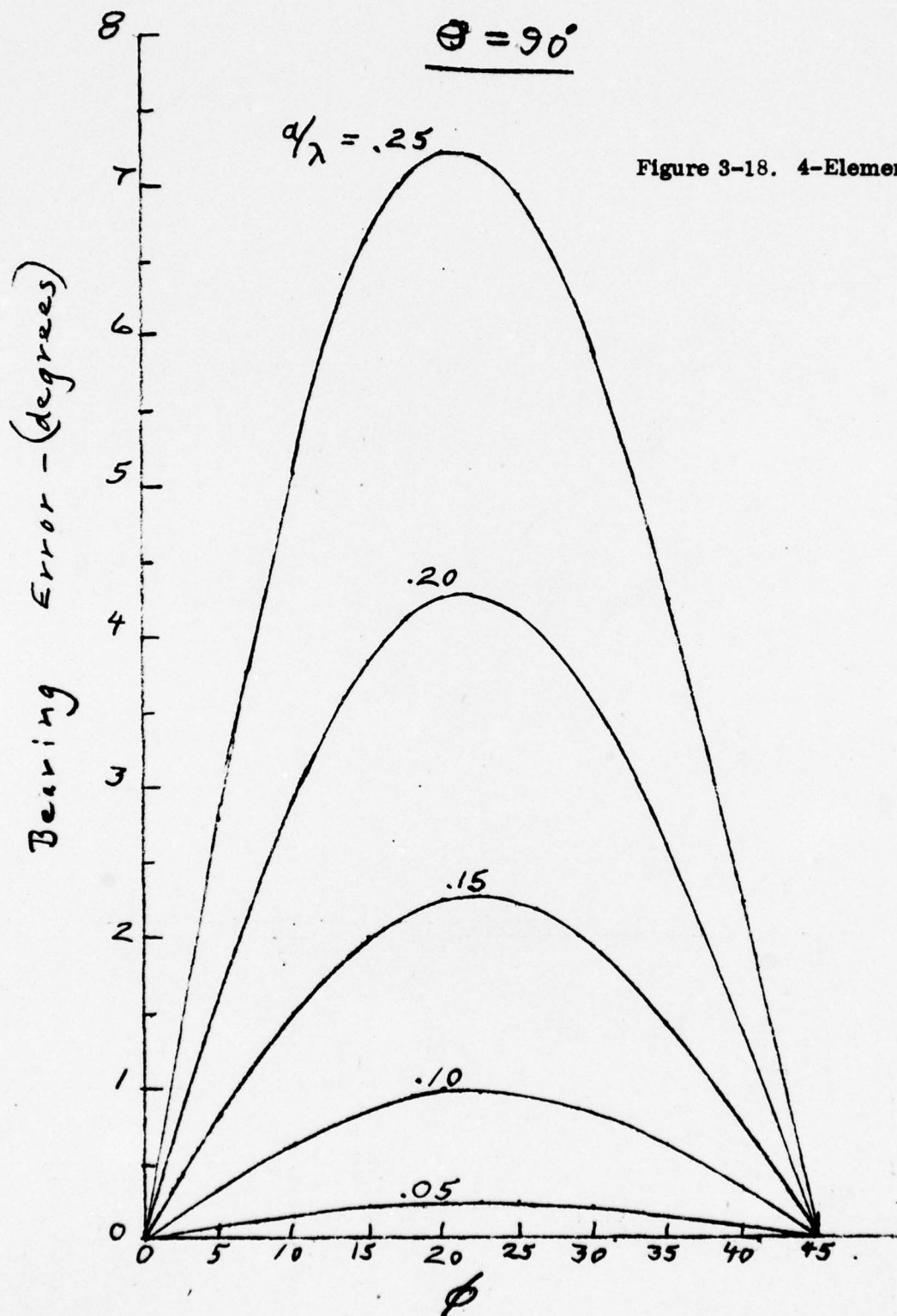
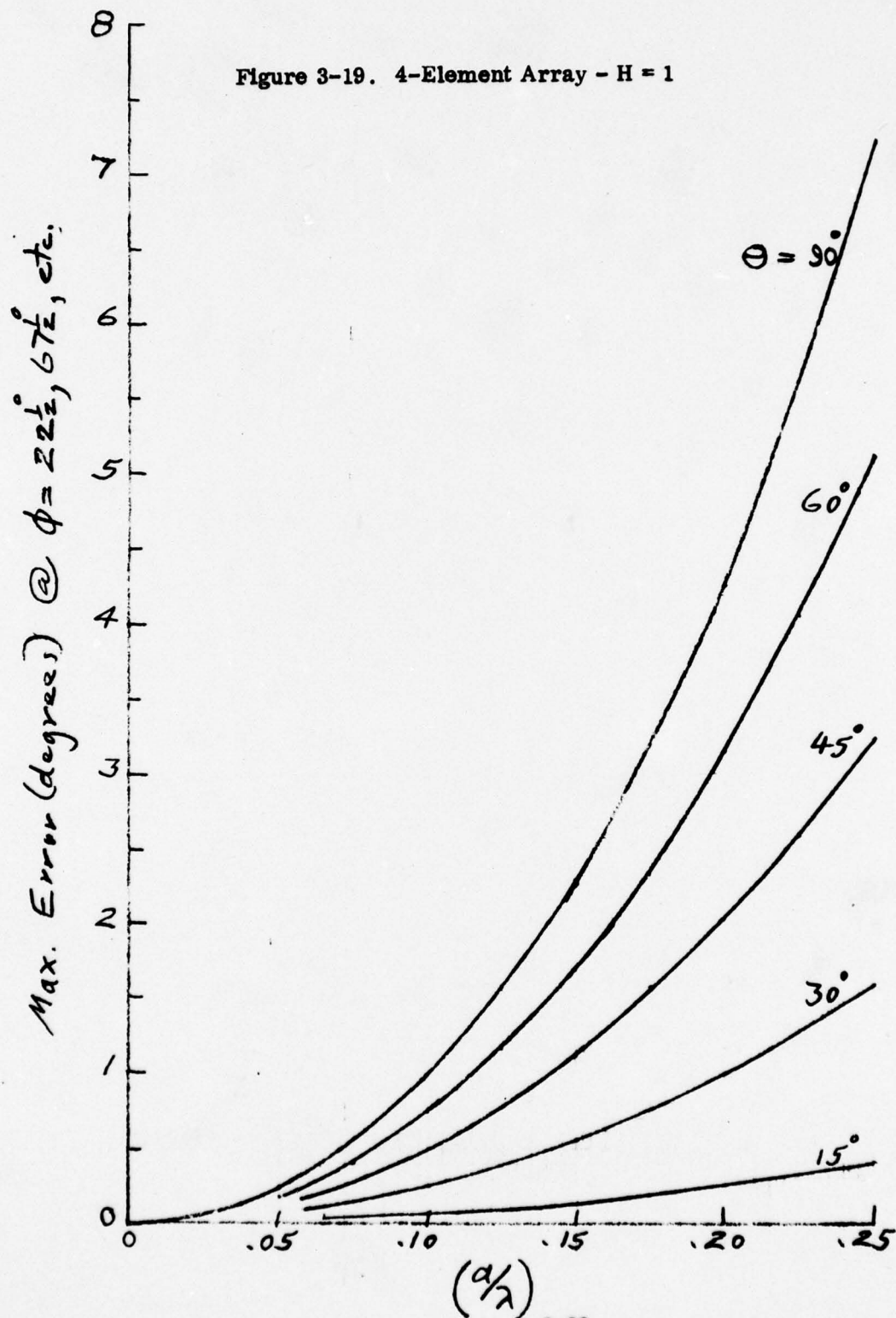


Figure 3-18. 4-Element Array -  $H = 1$



Figure 3-19. 4-Element Array -  $H = 1$



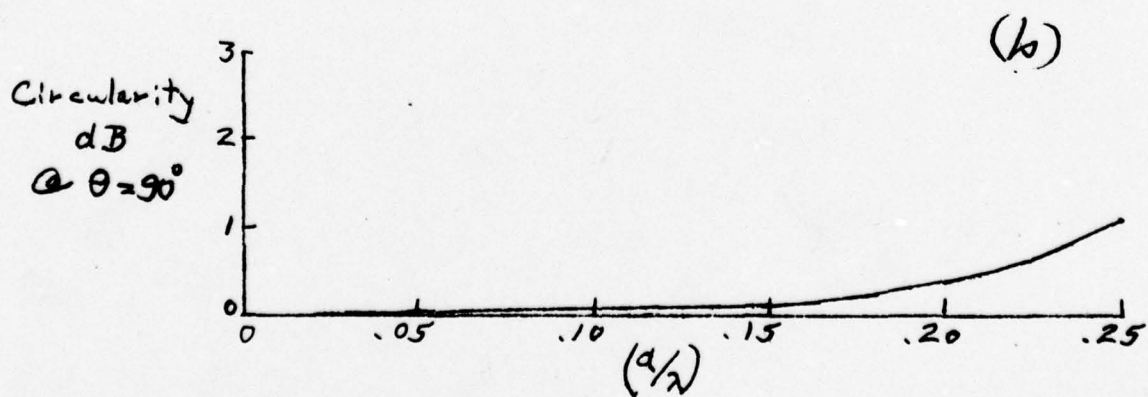
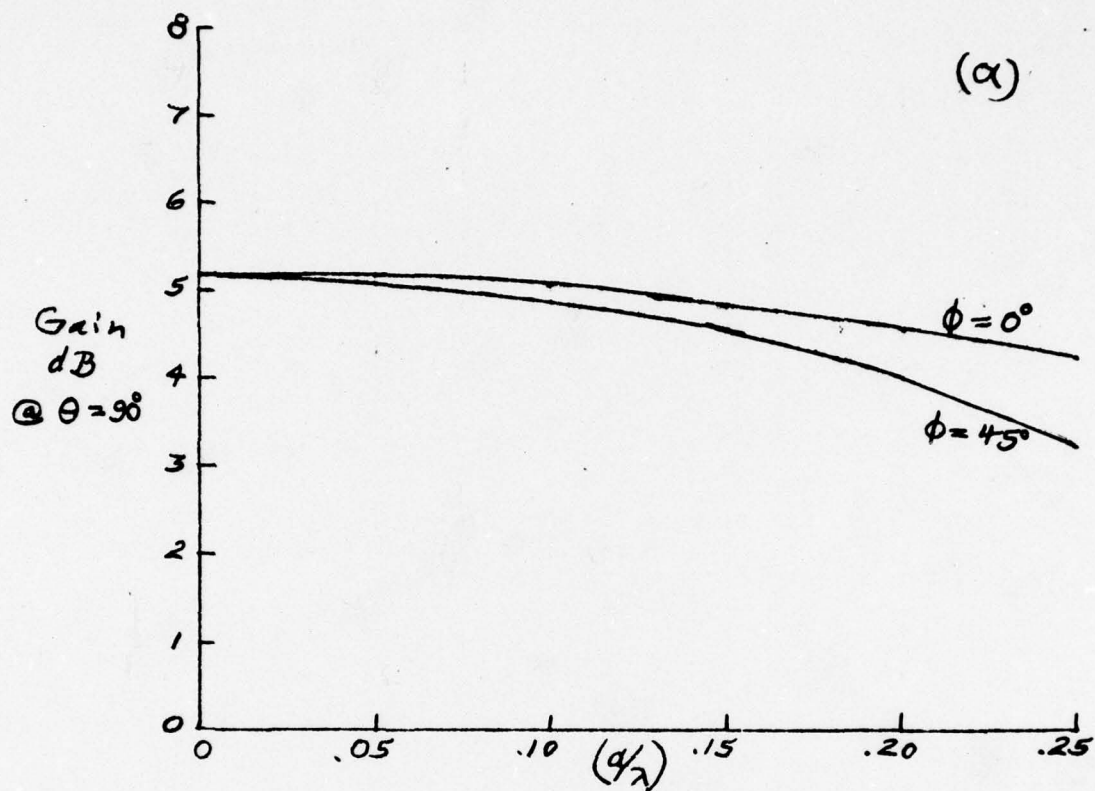


Figure 3-20. 4-Element Array -  $H = 0$

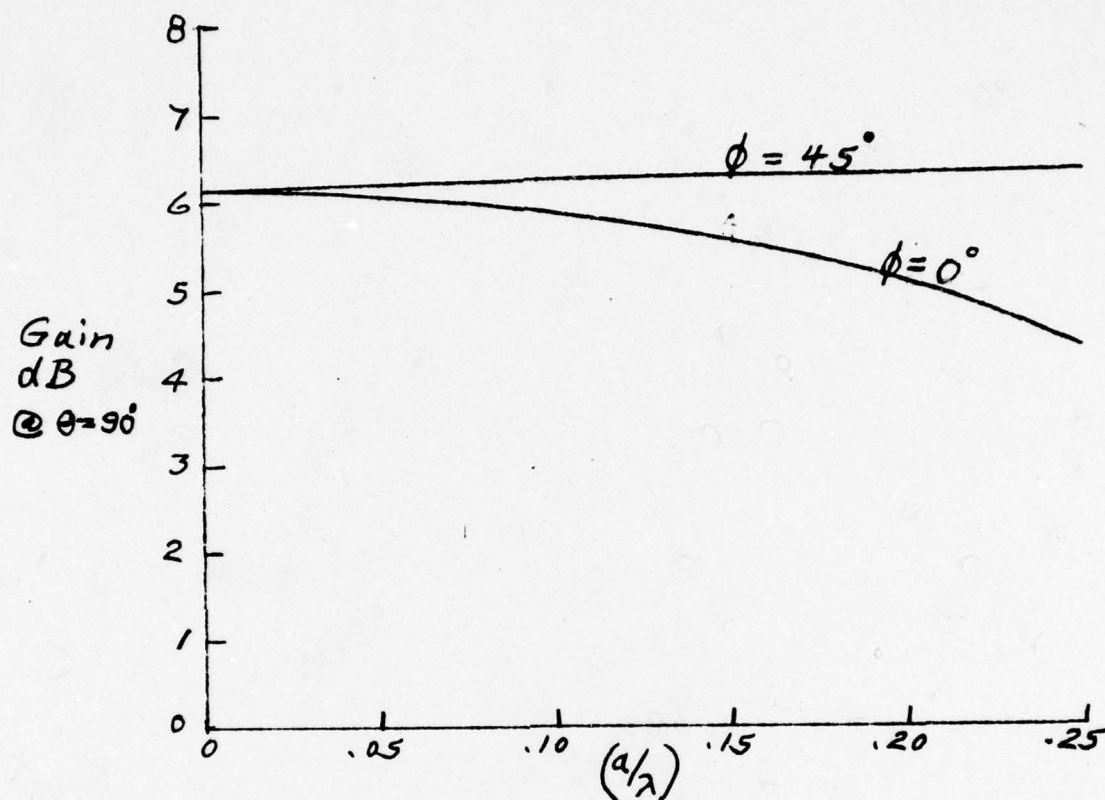
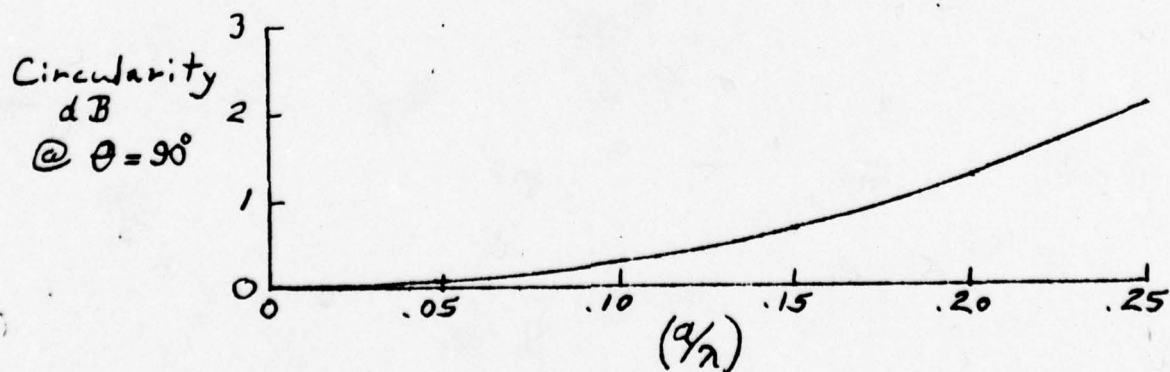


Figure 3-21. 4-Element Array -  $H = 1$



$\lambda/4$  Monopole

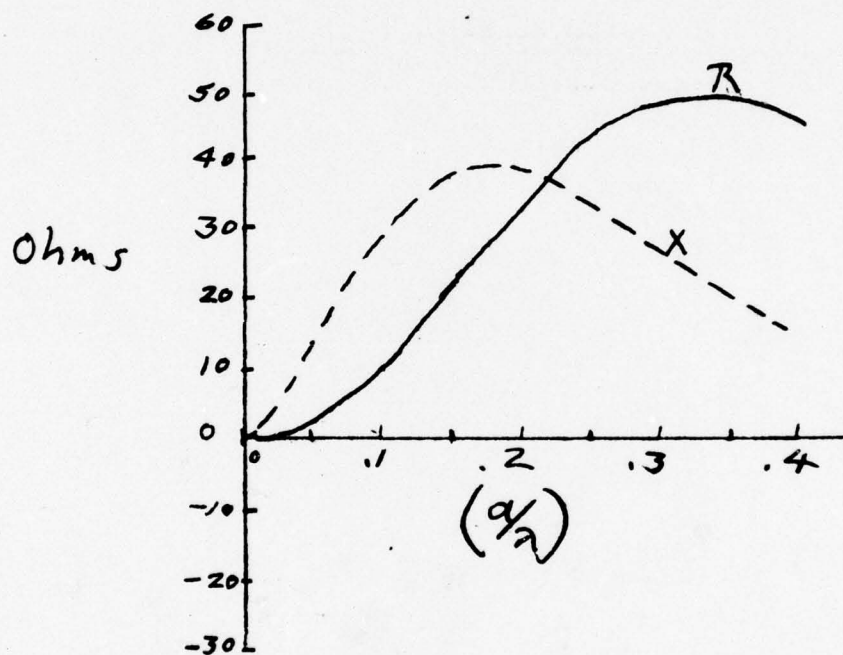


Figure 3-22. 4-Element Array --  $H = 1$



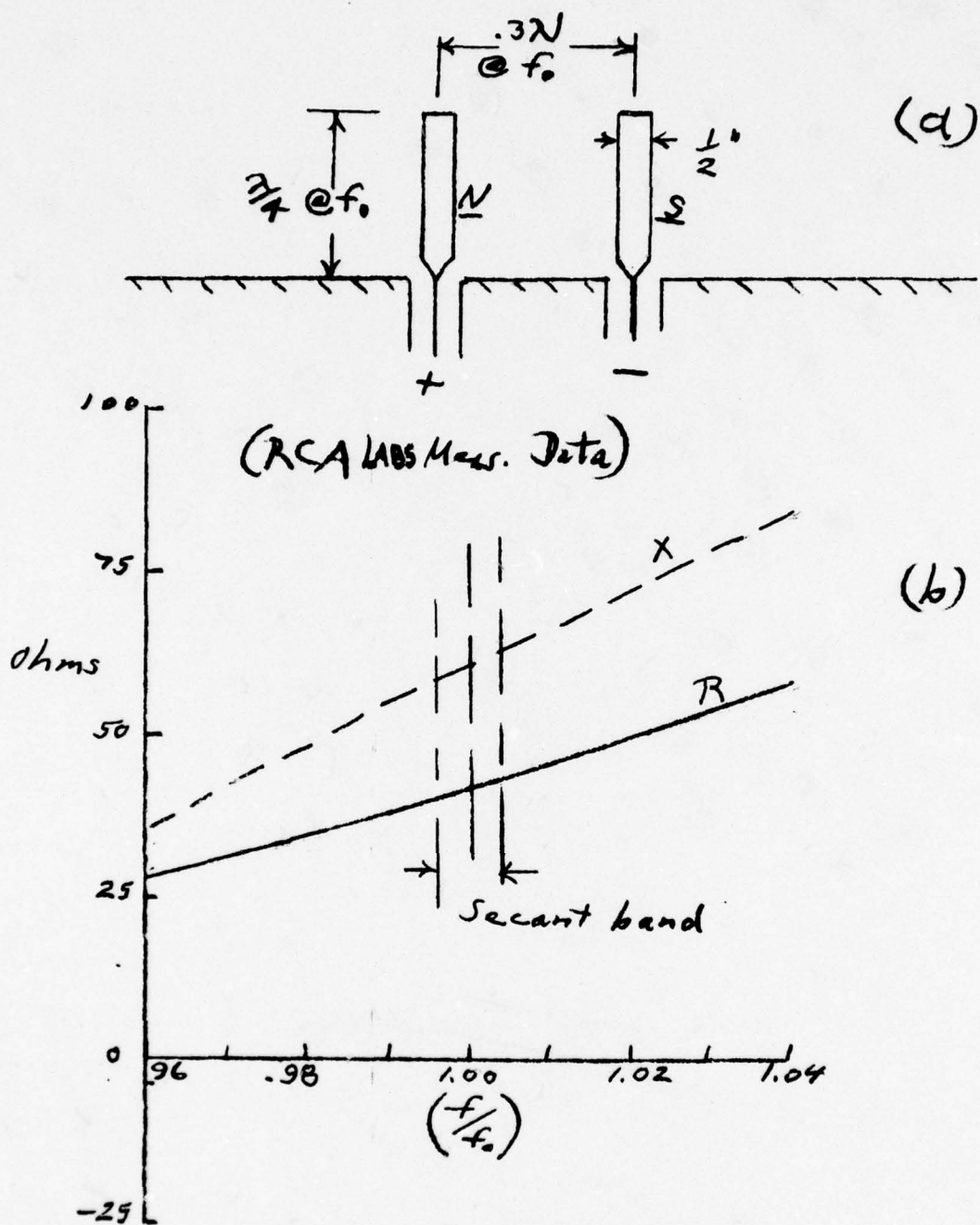


Figure 3-23. 4-Element Array --  $H = 1$

separated  $0.3 \lambda$  (or  $a/\lambda = 0.15$ ) and fed out-of-phase (Figure 3-23a). The impedance of each of the two radiators is plotted in Figure 3-23b versus frequency change. This plot shows the impedance change over the SECANT band of frequencies. In addition, it is to be noted that the measured impedance at  $f/f_0 = 1$  is considerably different than the calculated value given in Figure 3-22 for  $a/\lambda = 0.15$ . This difference is attributed to two factors: the rapid change in impedance with large diameter changes, and the strong influence on the impedance associated with the design of the end seal mounting arrangement of the monopole.

It is believed that the most accurate method of obtaining impedance values for the  $H = 1$  mode is a simple experimental measurement setup as shown in Figure 3-24. Two metal ground planes, each large in terms of wavelengths, intersect at right angles. The test monopole is mounted parallel to, and at a distance,  $a$ , from one plane. The image monopole spaced a distance,  $a$ , behind the plane makes the measured impedance of the fed monopole be identical to that obtained on a setup like Figure 3-24.

In actual practice, the height,  $A$ , of the fed monopole is adjusted for a pure resistance at the coaxial input and then this value used to design the desired feed circuitry. Since the impedance of a quarter-wave monopole for the  $H = 1$  mode is inductive (as shown in Figures 3-22 and 3-23), then shortening the element will make its impedance a pure resistance.

#### 3.2.3.6 Printed Circuit Design of 5-Element Array -- $H = 0$ and $H = 1$

The full size drawing of Figure 3-25 is the printed circuit layout of the circuitry shown in Figure 3-15 for a 5-element array with a ring radius of 1.1 inches. The overall diameter is only 4-1/2 inches and the circuitry is less complex than a 4-element array combining the  $H = 0$  and  $H = 1$  modes. In addition, the impedance of the four ring elements need be adjusted for an optimum match only for the  $H = 1$  mode. The height of the added central element is independently adjusted for best impedance match at the  $H = 0$  mode.

However, an additional problem is introduced by the use of a 5-element array of this type. This effect was first encountered and solved in an earlier RCA work on multi-mode

# Impedance Measurements

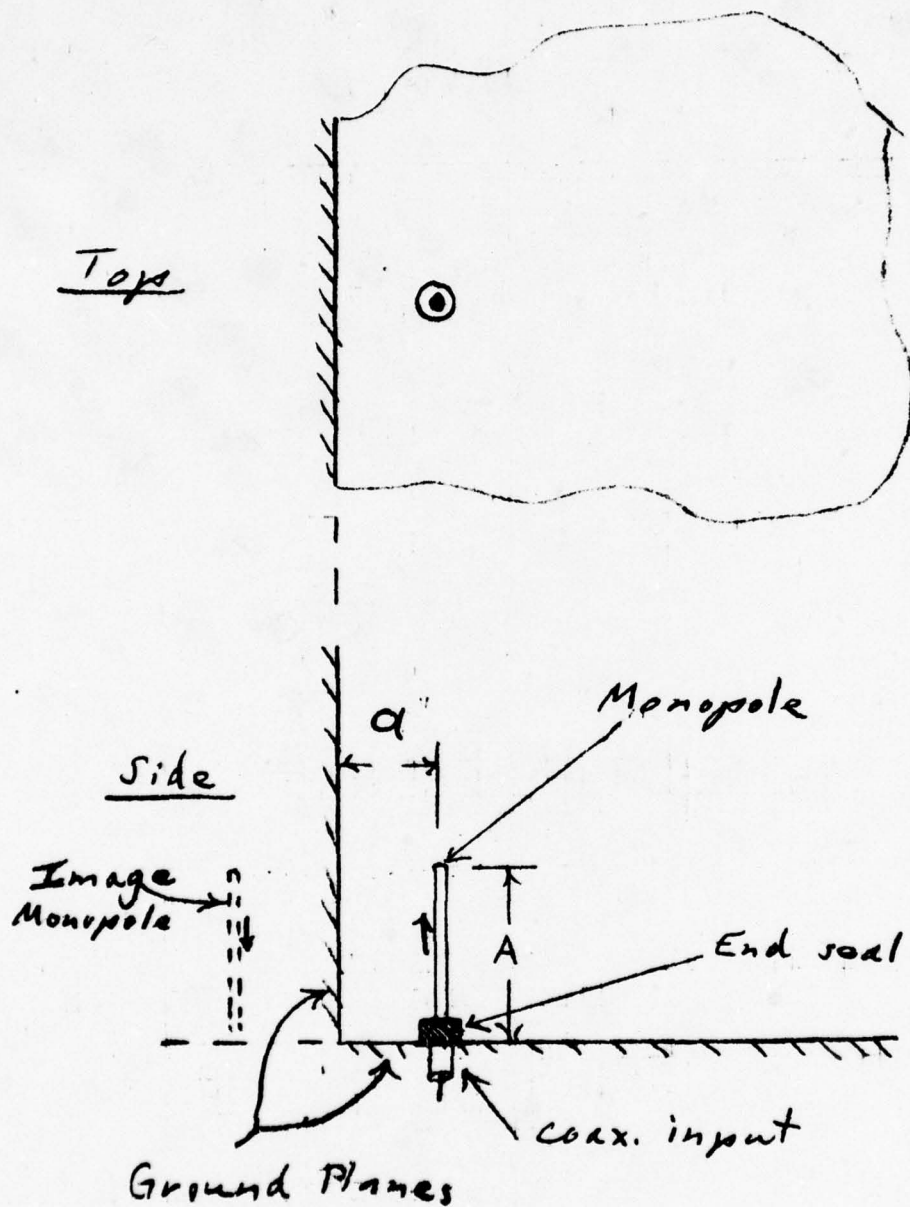


Figure 3-24. Experimental Setup for  $H = 1$

$$a = .15 \lambda$$

Full Size

(All lines are either segments of a radius or a circle.)

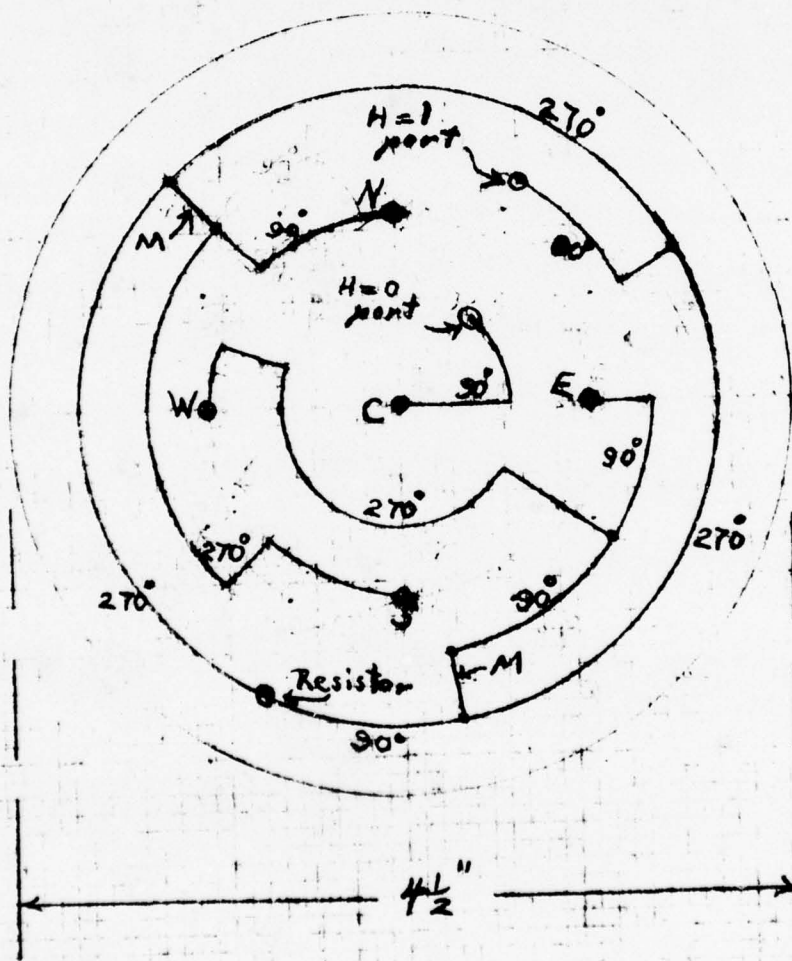


Figure 3-25. 5-Element Array —  $H = 0$  and  $H = 1$



ring arrays<sup>(9)</sup>. Although the two input ports are completely decoupled, the radiation pattern for the  $H = 0$  mode is not independent of the presence of the outer 4-element ring.

Consider first the  $H = 1$  pattern. For this case, the central element lies at a zero potential point, hence the pattern is not affected by the central element. However, the converse is not true.

Excitation of the central element will cause in-phase voltages to be induced in the four ring elements. No power is delivered to the  $H = 1$  port since the ports are decoupled. Therefore, these elements, now functioning as parasitic radiators, will reradiate a  $H = 0$  mode pattern. As described earlier, this pattern has no azimuth bearing error, but the overall effect will be a greater amplitude distortion of the  $H = 0$  pattern and a possible shift in the azimuth direction at which the phases of the  $H = 0$  and  $H = 1$  patterns are the same (defined as the zero reference angle).

This parasitic reradiation phenomena can be minimized by effectively open circuiting the four ring elements for the case of the  $H = 0$  mode operation. This is done by making the line sections,  $L$ , of Figure 3-15 be one-quarter wavelength. Thus, excitation of the central element puts the N-S (and E-W) elements in-phase, point b and a voltage null, and the inputs of the four ring elements are open-circuited. For this open-circuit condition, the quarter-wave monopole element is detuned and will have greatly reduced parasitic reradiation as compared to the case where the monopole base is short circuited. The printed circuitry of Figure 3-25 incorporates this feature.

Some discussion is taken up here as to the shift in the zero reference angle with change of operation frequency. The frequency band has been designated from 1592.5 MHz to 1622.5 MHz. This corresponds to a frequency change of  $\pm 0.933\%$  from the center band frequency,  $f_0$ , of 1607.5 MHz.

Referring now to the circuitry of Figure 3-25, the line length from the  $H = 0$  port to the central element is  $90^\circ$ , and the length from the  $H = 1$  port to the north element is  $480^\circ$  at  $f_0$  (the line segment,  $M$ , is  $30^\circ$ ). The difference between these lengths is then  $390^\circ$  at  $f_0$ .

At the band edges, these differences are:

$$\begin{array}{ll} f_L & 386.361^\circ \\ f_H & 393.639^\circ \end{array}$$

or a maximum difference change of  $\pm 3.639^\circ$  over the band. This is, therefore, equivalent to the change in the zero reference angle. However, this shift can be reduced to zero by adding an external  $390^\circ$  line section to the  $H = 0$  mode port. A possible mechanical design for the antenna of Figure 3-25 is shown in Figure 3-26.

It is concluded that the antenna shown in Figures 3-25 and 3-26 represents the optimum design for the simplest solution to a  $H = 0$  and  $H = 1$  mode operation with moderate azimuth bearing error.

### 3.2.3.7 Higher Order Modes ( $H > 1$ )

Thus far, two preferred designs, using the  $H = 0$  and  $H = 1$  modes, have been discussed:

|          | NUMBER OF<br>ELEMENTS     |                           | MAXIMUM BEARING<br>ERROR ( $a = .15\lambda$ ) |
|----------|---------------------------|---------------------------|---|
|          | <u><math>H = 0</math></u> | <u><math>H = 1</math></u> |   |
| Design 1 | 1                         | 4                         | $2.3^\circ$                                   |
| Design 2 | 1                         | 8                         | $0.029^\circ$                                 |

The rate of change of azimuth bearing is of importance in the system operation, and an approach to increase the accuracy in obtaining this is next discussed.

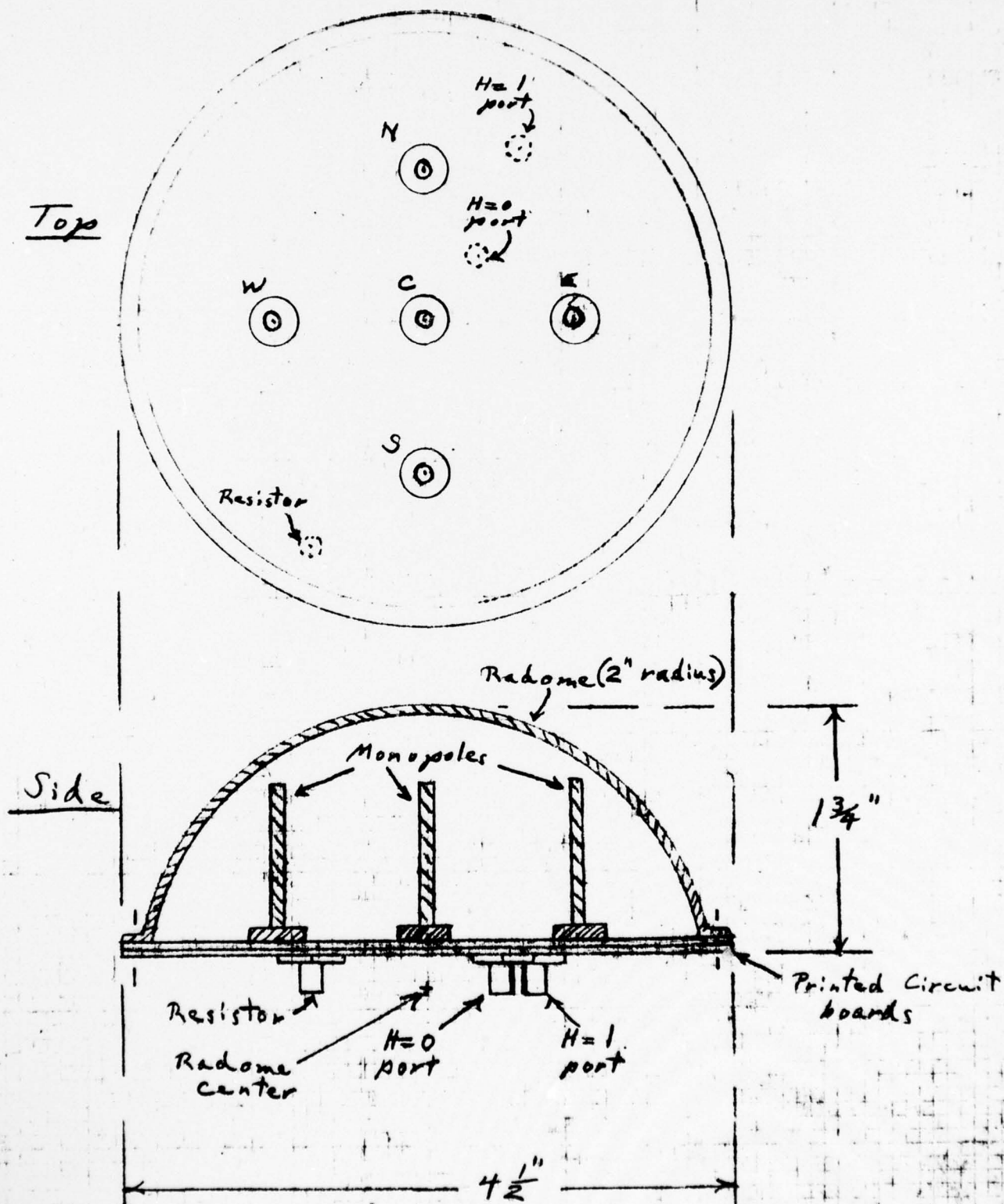


Figure 3-27 shows the far-field phase change with azimuth angle for different higher order modes. The number of degrees change in phase per degree of azimuth angle change is equal to  $H$ . Since the number of complete cycles of phase change occurs  $H$  times around the circle, then there will be  $H$  directions in which the phase relative to a  $H = 0$  mode is the same. These ambiguities can be resolved by operating two arrays sequentially (or possibly simultaneously):

- (1) Using the  $H = 0$  and  $H = 1$  modes to obtain the direction of wave arrival without ambiguity
- (2) Using the  $H = 0$  and  $H = (n > 1)$  modes for obtaining vernier changes in arrival directions.

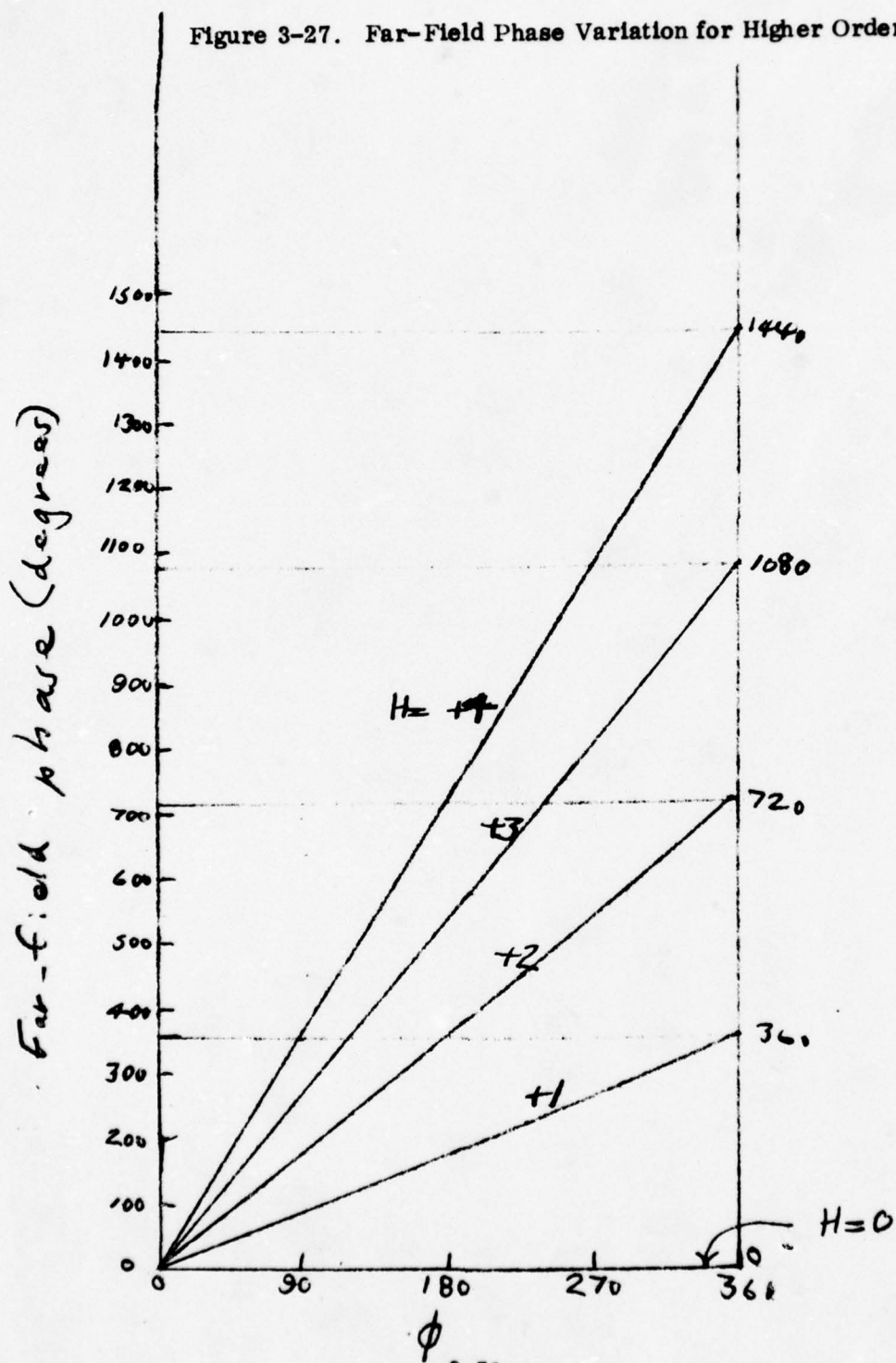
Appendix I gives the mathematical relationships required for ambiguity resolution.

The physical size of higher order mode generators is limited by the available ground plane regions on typical aircraft. Previous work has indicated that the minimum spacing between adjacent elements on the ring is about one-quarter wavelength. The phase difference between these adjacent elements is  $90^\circ$ . Thus, the circumference of the ring is  $H\lambda$ , and the radius of the ring is  $\frac{H\lambda}{2\pi}$ . The number of elements is  $4H$ . A reasonable assumption for the maximum practical array diameter is about eight or ten inches. This limits the highest order mode that can be used at this frequency band to be  $H = 4$ .

Figure 3-28 shows how such a 16-element ring for  $H = 4$  can be made up of two sub-rings, each having 8 elements. The elements of each subring are fed in alternating polarity from half-wave transmission line sections. There will be no cross-coupling between subrings since the elements of one lie in the neutral planes of the other. Two subrings are then fed in quadrature from a hybrid and  $90^\circ$  phasing line. The fourth port of the hybrid is resistance-terminated to absorb any reflected waves.



Figure 3-27. Far-Field Phase Variation for Higher Order Modes



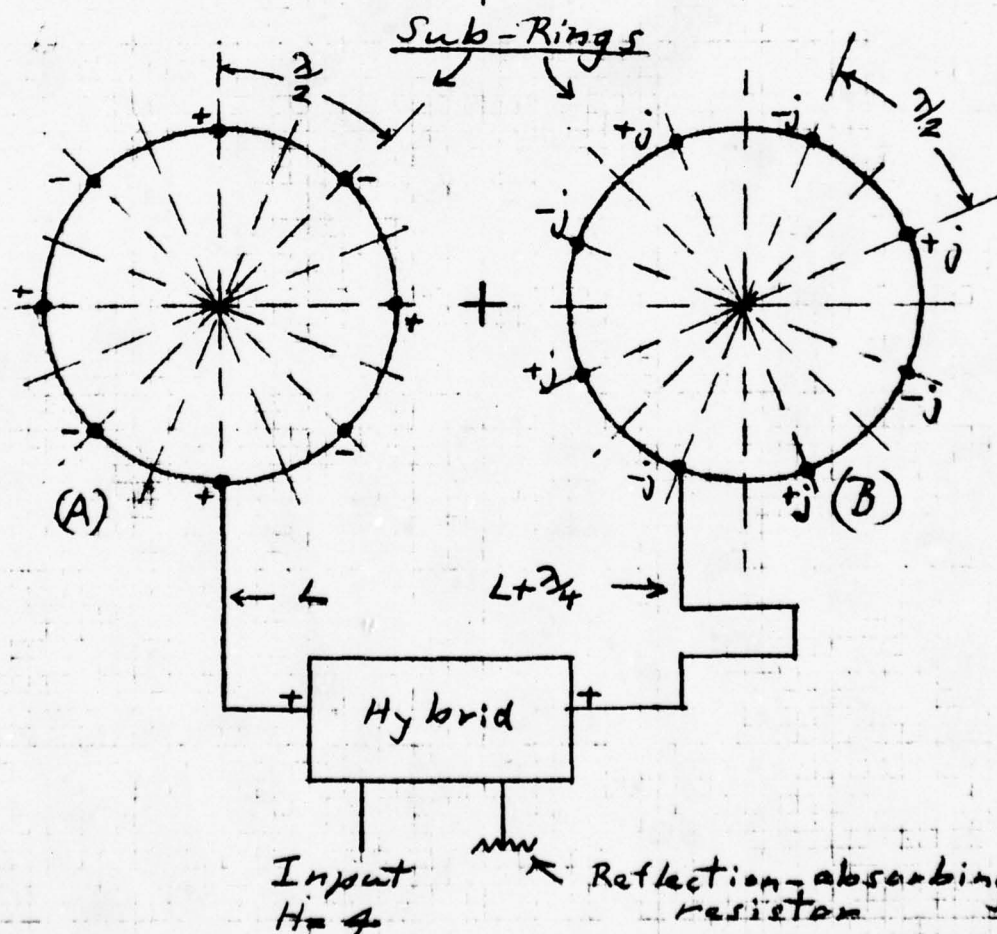
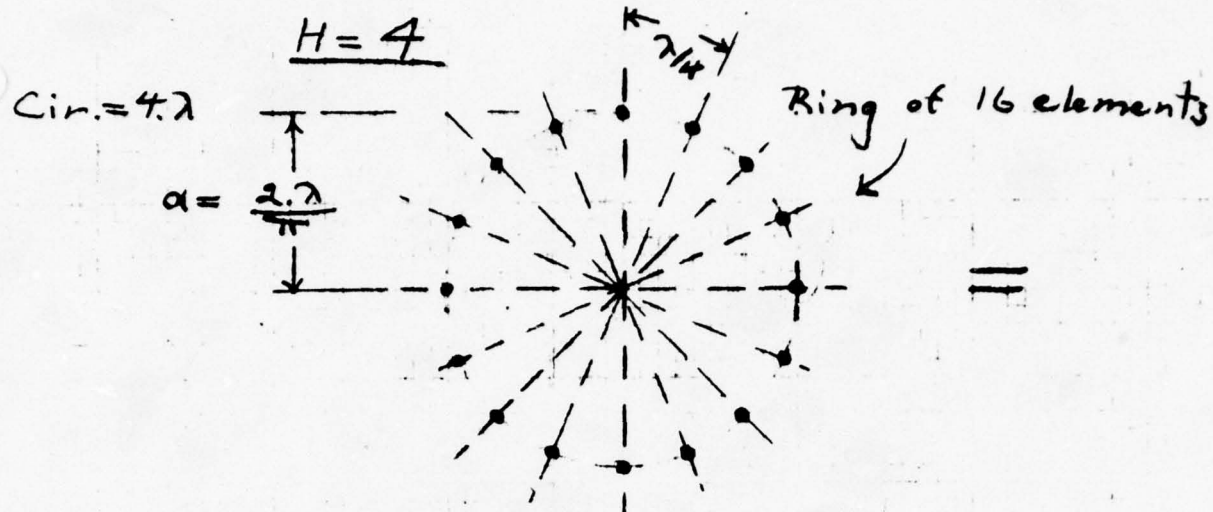


Figure 3-28. Separation of Ring into Two Subrings and Mode Excitation Circuitry

Figure 3-29 shows the rosette field pattern produced by each subring. Figure 3-30 illustrates a simple means of calculating the field pattern of a single subring in terms of the patterns of couplets symmetrically disposed around the ring. The total field pattern from the complete ring is then the vector addition of the radiation from the rosette patterns generated by the two subrings fed in phase quadrature.

The radiation pattern was calculated for a  $\frac{2\lambda}{\pi}$  (4.673 inches at 1607.5 MHz); the maximum bearing error was found to be  $0.0015^\circ$  and the azimuth circularity was  $4.34 \times 10^{-4}$  db. Thus, the ideal mode pattern is almost perfectly achieved.

The elevation pattern was determined using couplet formulas of the type given in Figure 3-30. This pattern was then integrated to give its peak gain, and plotted in Figure 3-31. Also plotted for comparison are the elevation patterns for the  $H = 0$  (single element) and  $H = 1$  modes. For this comparison, the  $H = 1$  elevation pattern is assumed to be independent of angle  $\phi$  and to have a peak gain midway between the curves of Figure 3-21 for  $a/\lambda = 0.15$ . The  $H = 4$  pattern is seen to have a little higher gain than the other two plots.

The differences in amplitude obtained from Figure 3-31 are plotted in Figure 3-32 for the two different operating systems. This difference is of interest since practical phase comparison equipment may not operate properly if the difference is too great (possibly around 10 db). It is seen in Figure 3-32 that the difference between the  $H = 0$  and  $H = 4$  modes exceeds 10 db only in the upper conical sector defined by  $\theta = 40^\circ$ . For the difference between the  $H = 0$  and  $H = 1$  modes, this occurs only in the conical sector defined by  $\theta = 16^\circ$ .

#### 3.2.3.8 Feed Circuitry for the $H = 4$ Ring

The simplest feed circuitry for the  $H = 4$  ring consists of half-wave, phase reversing line segments between adjacent elements. This circuitry (transformed from a circular to linear geometry), is pictured in Figure 3-33. The odd number of  $1/4$  wavelength sections

$$H = 4$$

Rosette Patterns produced  
by Sub-Ring A and Sub-Ring B

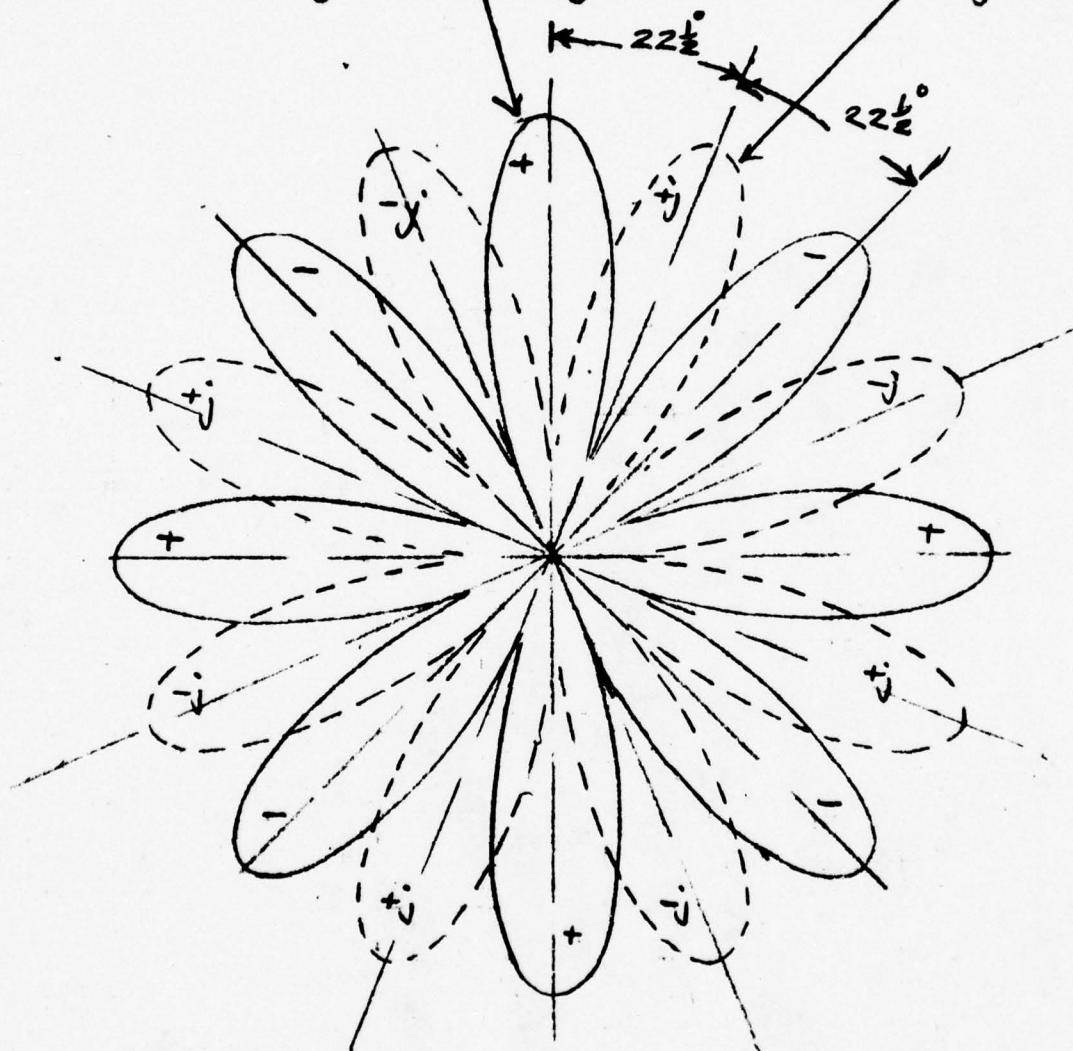
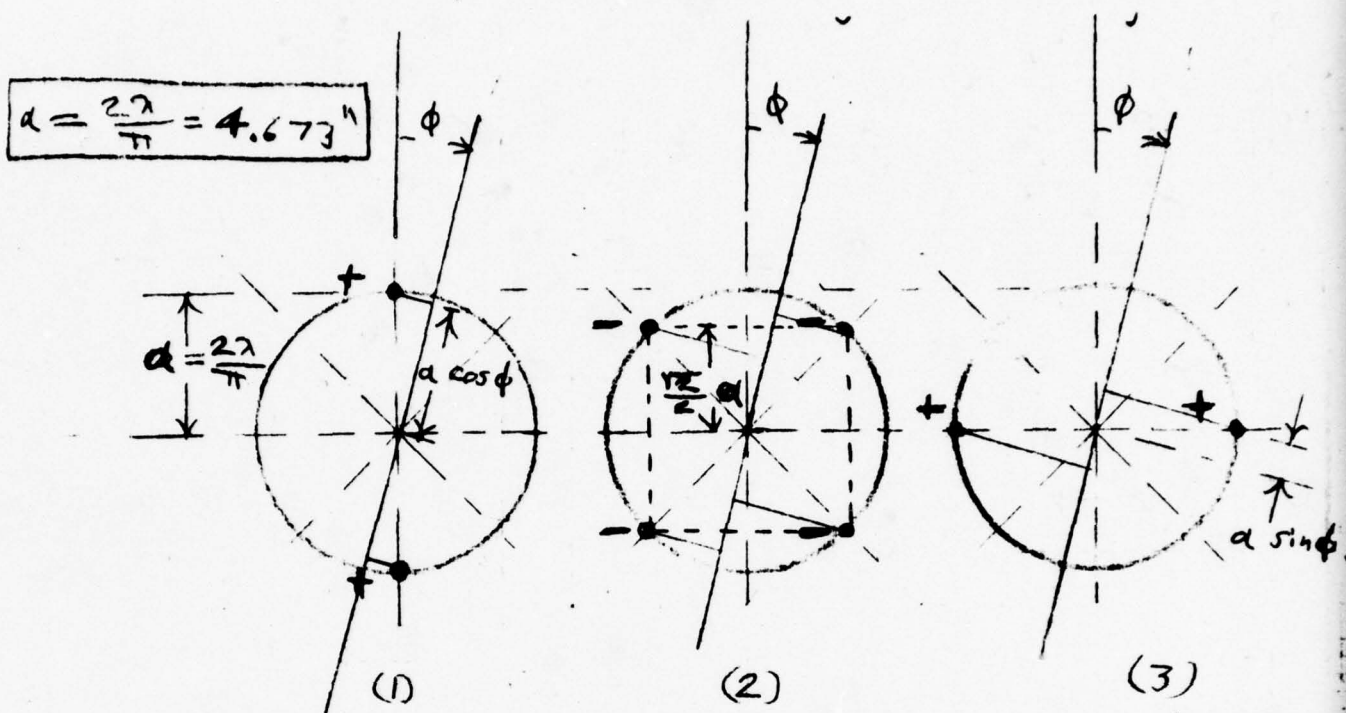


Figure 3-29. Rosette Patterns Produced by Subring A and Subring B





$$F = \left[ 2 \cos\left(\frac{2\lambda}{\pi} \cos \phi\right) \right] - 4 \left[ \cos\left(\frac{2\lambda}{\pi}\right) \left(\frac{12}{2}\right) \sin \phi \right] \cdot \left[ \cos\left(\frac{2\lambda}{\pi}\right) \left(\frac{12}{2}\right) \cos \phi \right] + \left[ 2 \cos\left(\frac{2\lambda}{\pi} \sin \phi\right) \right] =$$

$$\cos(229.183 \cos \phi) - 2 \cdot \cos(162.057 \sin \phi) \cdot \cos(162.057 \cos \phi) + \cos(229.183 \sin \phi)$$

$$\text{Max. } \epsilon = .0015^\circ$$

$$\text{Azimuth circularity} = 4.34 \times 10^{-4} \text{ dB}$$

Figure 3-30. Azimuth Pattern of Single Subring for  $H = 4$

## Theo. Elevation Patterns

for

$H=0$  (central element)

$H=1$  (4 elements,  $a/\lambda = .15$ )

$H=4$  (16 elements,  $a/\lambda = .637$ )

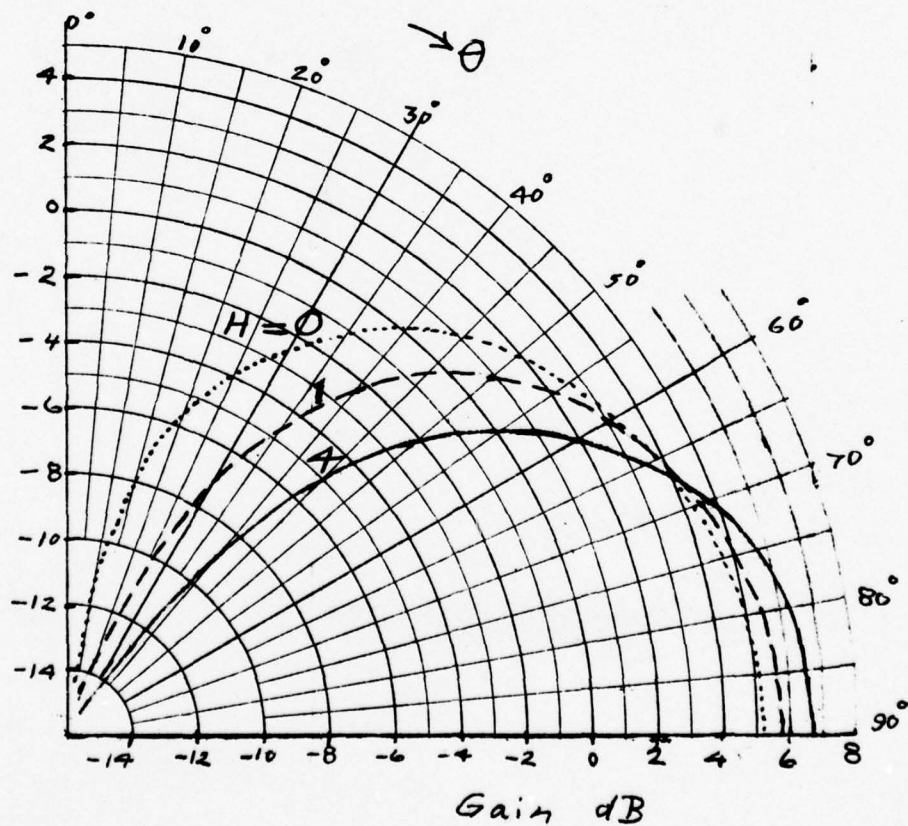


Figure 3-31. Theo. Elevation Patterns

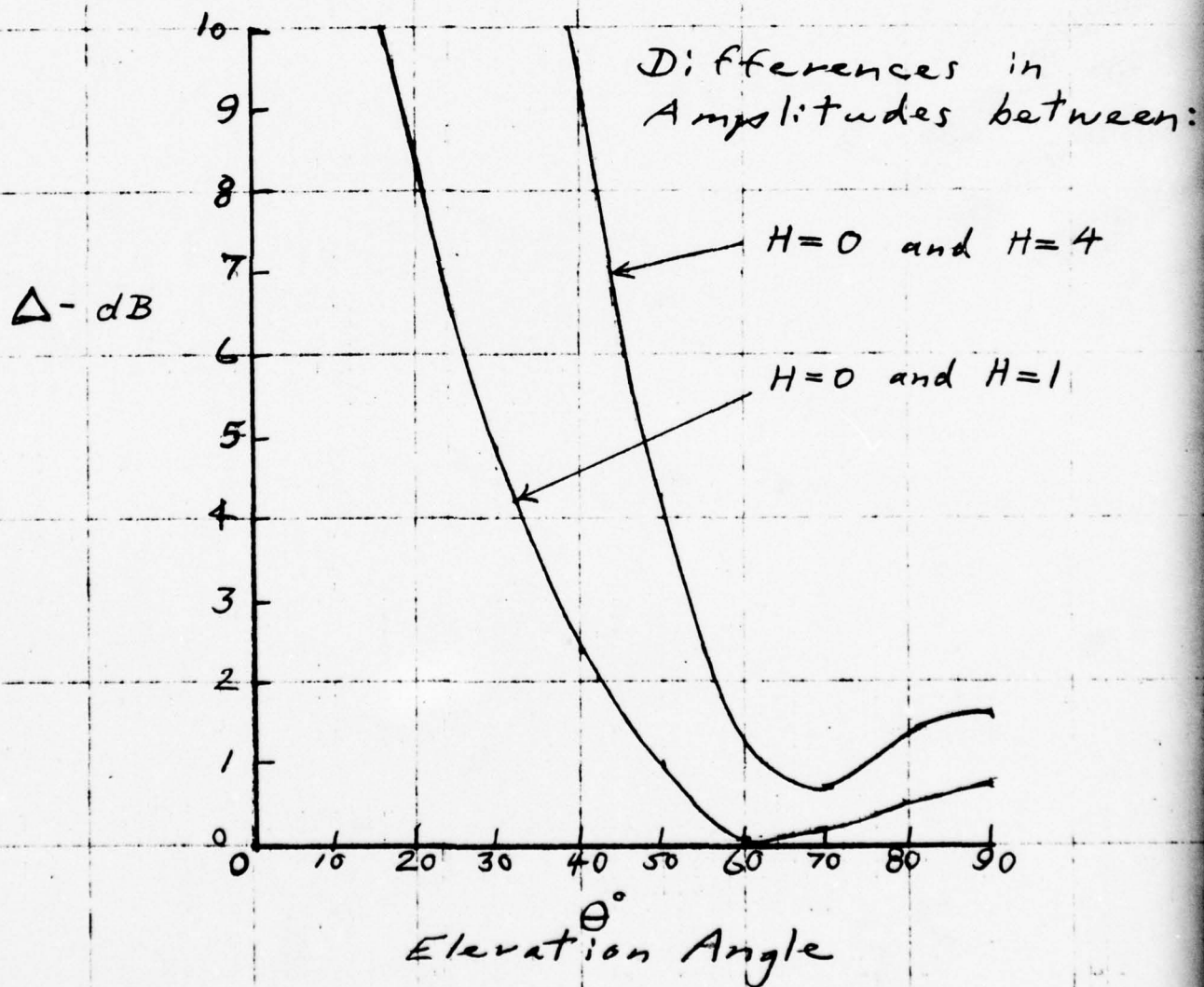
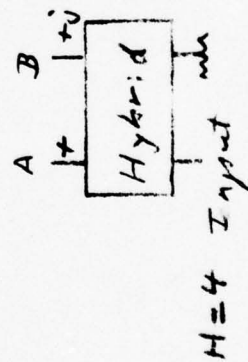
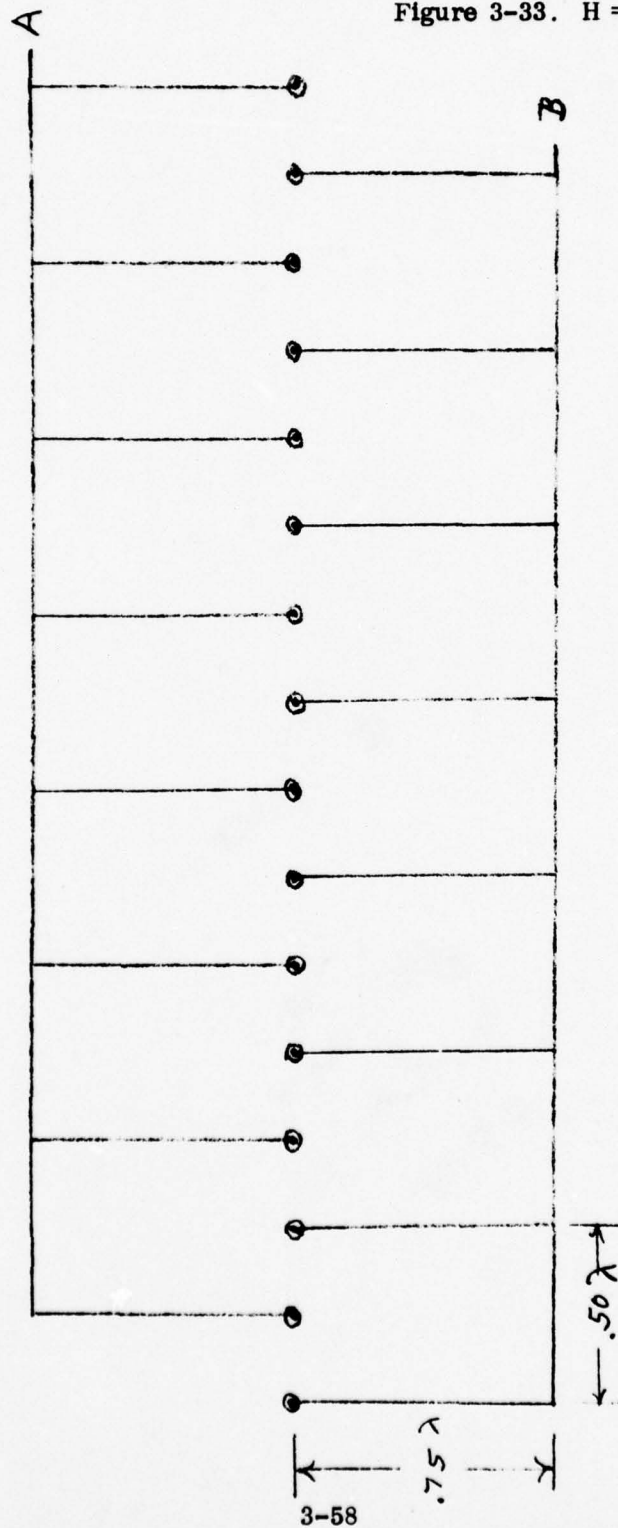


Figure 3-82. Amplitude Difference Comparisons

Figure 3-33.  $H = 4$  Feed Circuitry





between the successive feed points and the antennas are required to reduce the parasitic reradiation as described previously. An equivalent circular layout is given in Figure 3-34. The  $3/4$  wavelength sections are required since one  $\lambda/4$  sections are not long enough physically.

Although this arrangement is perfectly satisfactory for a single frequency, the last-fed elements suffer a phase deterioration from the design value as the frequency is changed. Even for a very small frequency change, the four  $\lambda/4$  baluns in series can introduce a serious phase problem to the last-fed element.

A corporate feed network (Figure 3-35) could be used to solve this difficulty. Although this network is frequency independent, space limitations in this particular design precluded its use. The approach finally selected as optimum is pictured in Figure 3-36. Here, each quadrant of four monopoles is fed from a single input, thus reducing the number of branching feed lines in the remaining corporate feed network. A square hybrid network is used in each quadrant section to provide the required quadrature phasing. This particular hybrid, consisting of four quarter-wave line sections joined in a square, offers a reduced length hybrid to give two equal amplitude outputs in quadrature-phasing by the proper choice of the individual line impedances.

The selected geometry of this quadrant feed circuitry, given in Figure 3-37, offers a compact arrangement for the maximum clearance in the central area for the  $H = 0$  and  $H = 1$  circuitry. The corporate feed network joining the four quadrant sections is installed external to the  $H = 4$  ring. Although occupying slightly more printed circuitry area, the approach was deemed satisfactory in this preliminary experimental design.

A comparison of the rat-race and square hybrids is given in Figure 3-38 as a function of frequency change. Although the rat-race hybrid is seen to be superior over a wide frequency range, the small differences over the relatively small SECANT band range was not considered serious in view of the advantages offered by the square hybrid in effecting the reduced size feed circuitry.

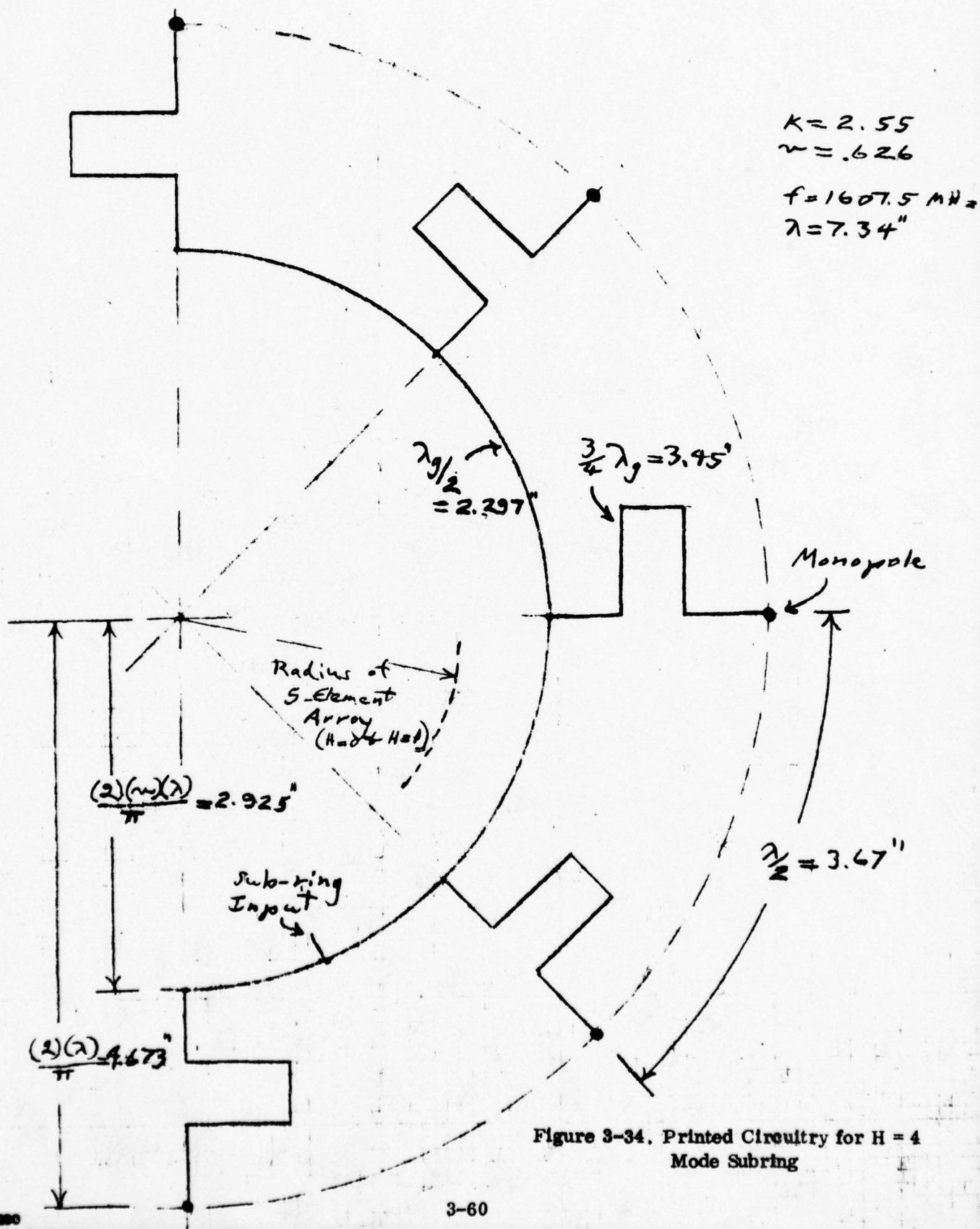


Figure 3-34. Printed Circuitry for  $H = 4$  Mode Subring

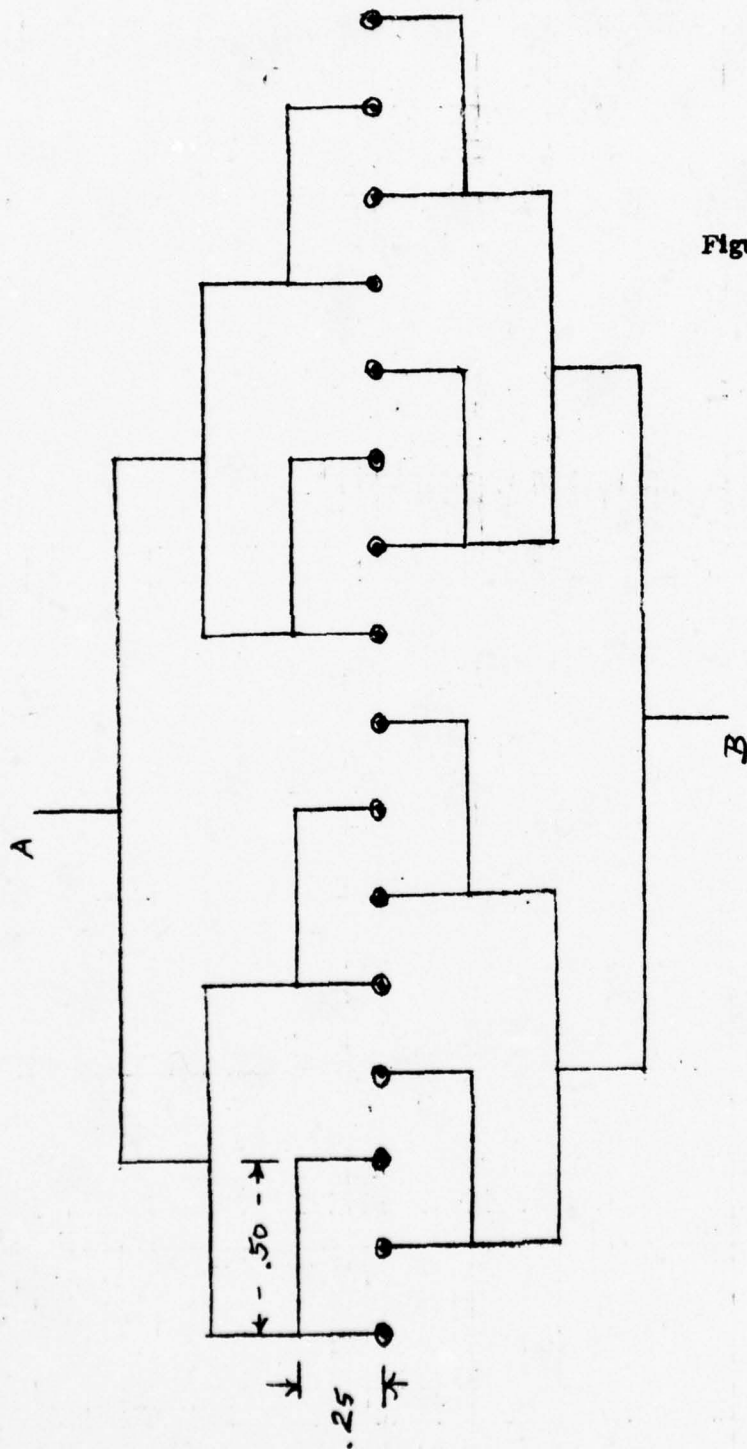
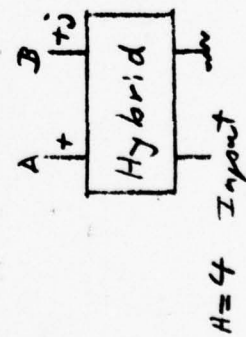


Figure 3-35. H = 4 Feed Circuitry



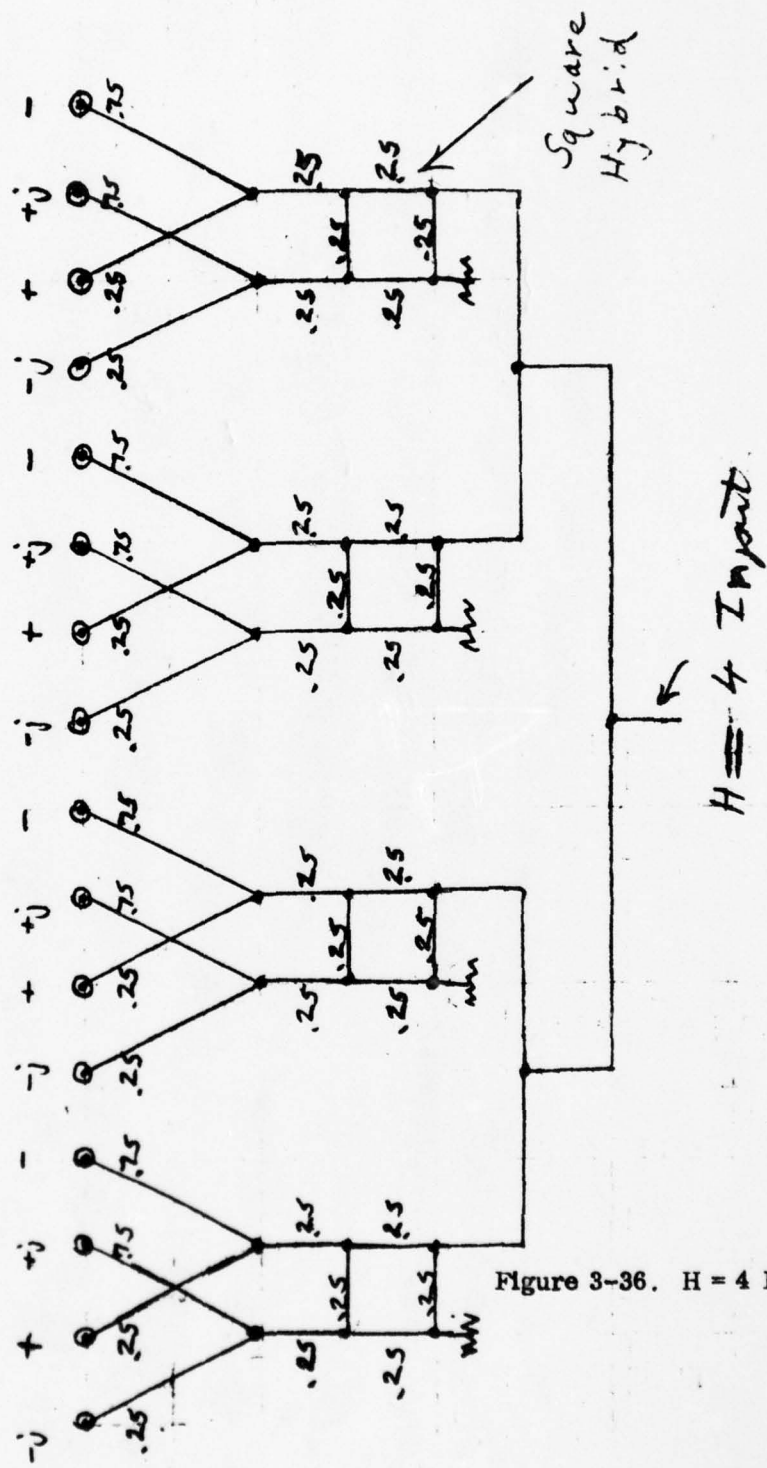
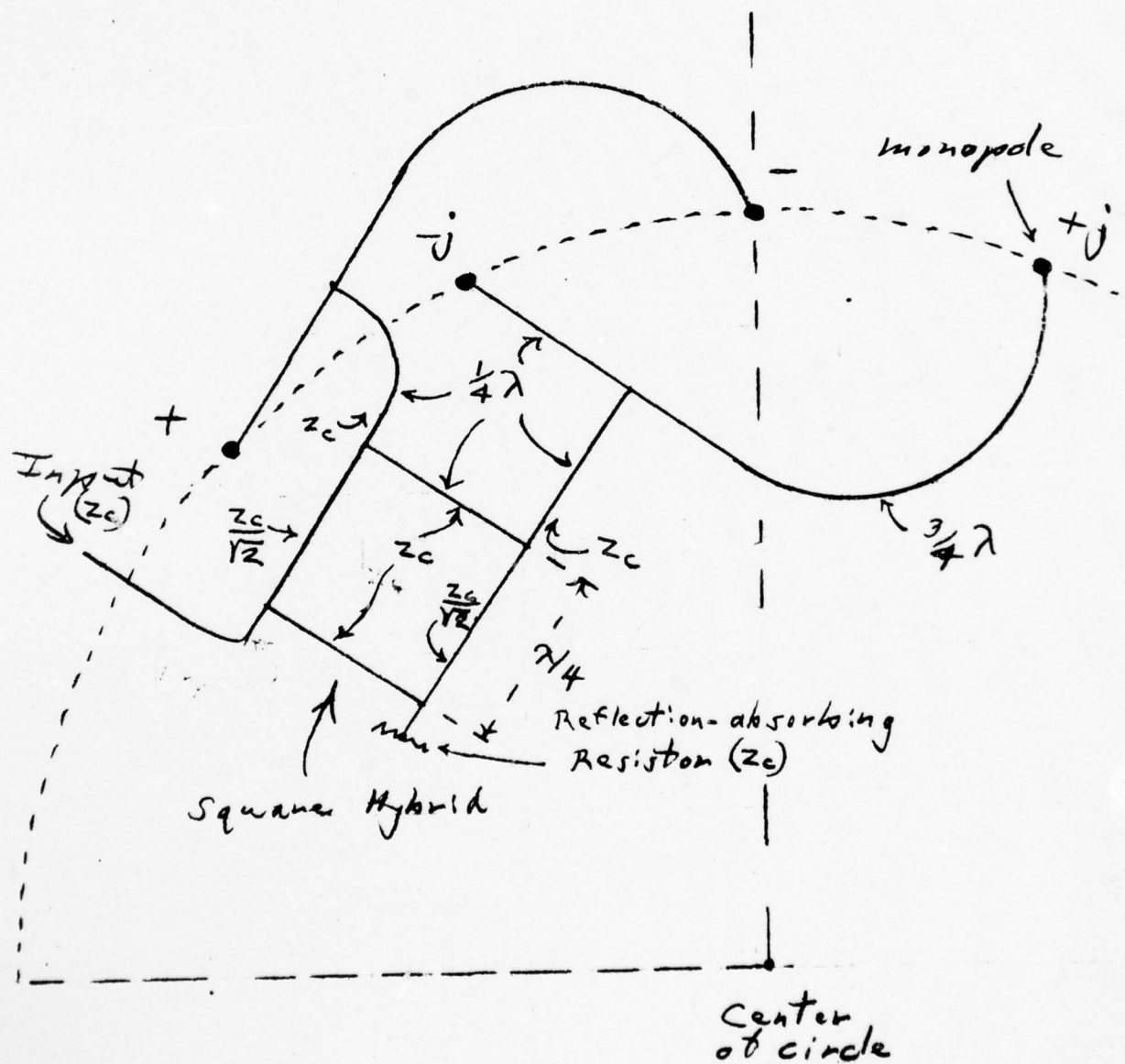
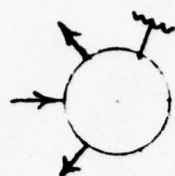


Figure 3-36.  $H = 4$  Feed Circuitry (C)



Figure 3-37. Full Size Layout of Printed Circuitry for 1/4 of the  $H = 4$  Ring



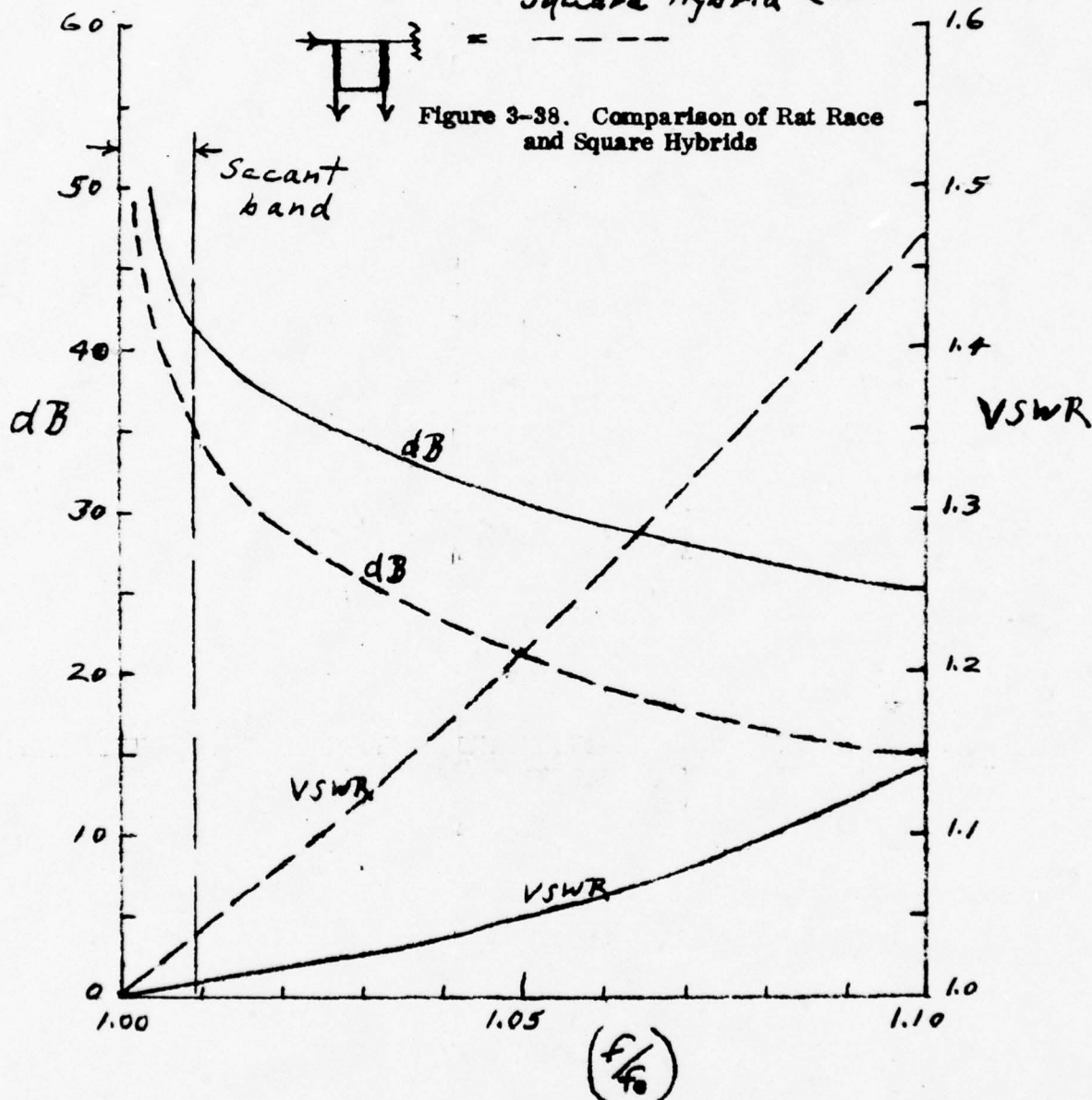


Rat Race Hybrid (Six  $\lambda/4$  sections)



Square Hybrid (Four  $\lambda/4$  sections)

Figure 3-38. Comparison of Rat Race and Square Hybrids



(Data from "A Method of Analysis of Symmetrical Four-Port Networks", J. Read and G. J. Wheeler, IRE Transactions on Microwave Theory and Techniques, Oct. 1956)

### 3.2.3.9 Effect of Finite Ground Planes on Radiation Characteristics

The foregoing studies have been concerned only with the ideal cases of noncurved, infinite ground planes of perfect conductivity. Next to be considered are some observations on changes in the radiation characteristics with finite grounds having surfaces approaching the geometries characterized by practical aircraft fuselage shapes.

It is first to be noted that the actual case is very complex, consisting of finite grounds with different curvatures in orthogonal planes. It is considered that factual data is best secured by experimental measurements. However, certain simple geometries, representing rather extreme conditions, produce radiation properties of known values. This data is touched upon in the belief that the actual case lies somewhere in between this and the ideal assumption.

Only the elevation pattern of a single vertical monopole ( $H = 0$ ) is considered here for the sake of simplicity, since the elevations patterns for the higher order modes of  $H = 1$  and  $H = 4$  do not change radically. Figure 3-39 shows the elevation pattern for such a single monopole under ideal conditions. The elevation pattern for a very small ground plane of two wavelengths diameter is given in Figure 3-40. This shape illustrates the general character of patterns with finite ground planes; an upward tilt of the beam maximum and multi-lobe radiation of reduced amplitudes below the horizontal plane. As the diameter increases (Figure 3-41), the beam maximum drops downward and radiation near the zenith develops small, multi-lobes<sup>(10)</sup>.

The solid curves of Figure 3-42 (from Jasik<sup>(10)</sup>), relates the beam tilt with ground dimensions. The dashed curve at the left was obtained earlier at the RCA Laboratories. This limited data was derived on a theoretical basis and confirmed by experimental measurements. Hence, it is considered to be more accurate than the solid curve in the region of small diameters. However, the general shape of the solid curve is probably reasonably accurate as the diameter of the ground increases.

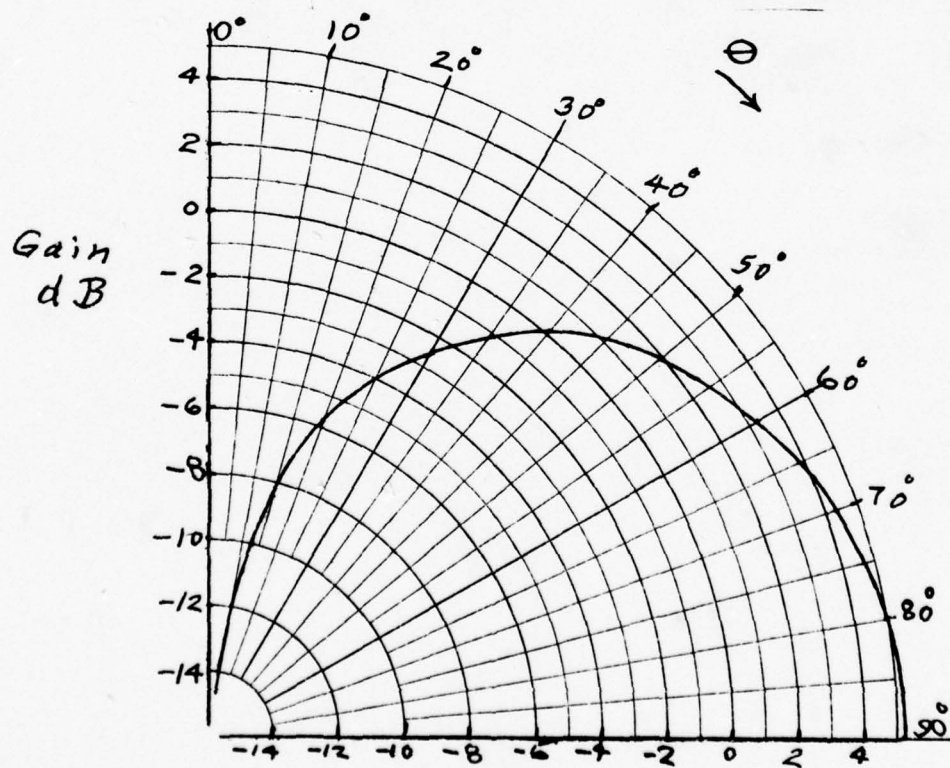
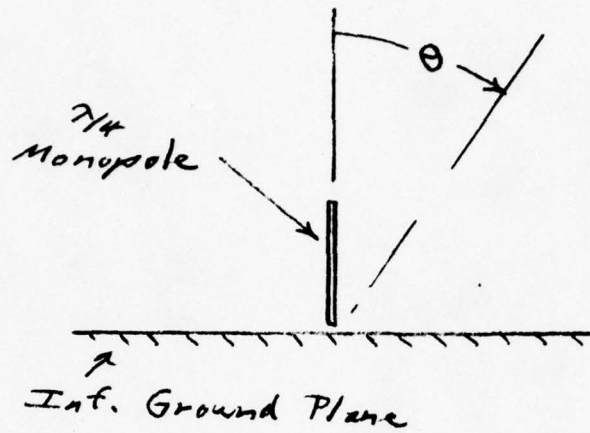


Figure 3-39. Theo. Elevation Pattern



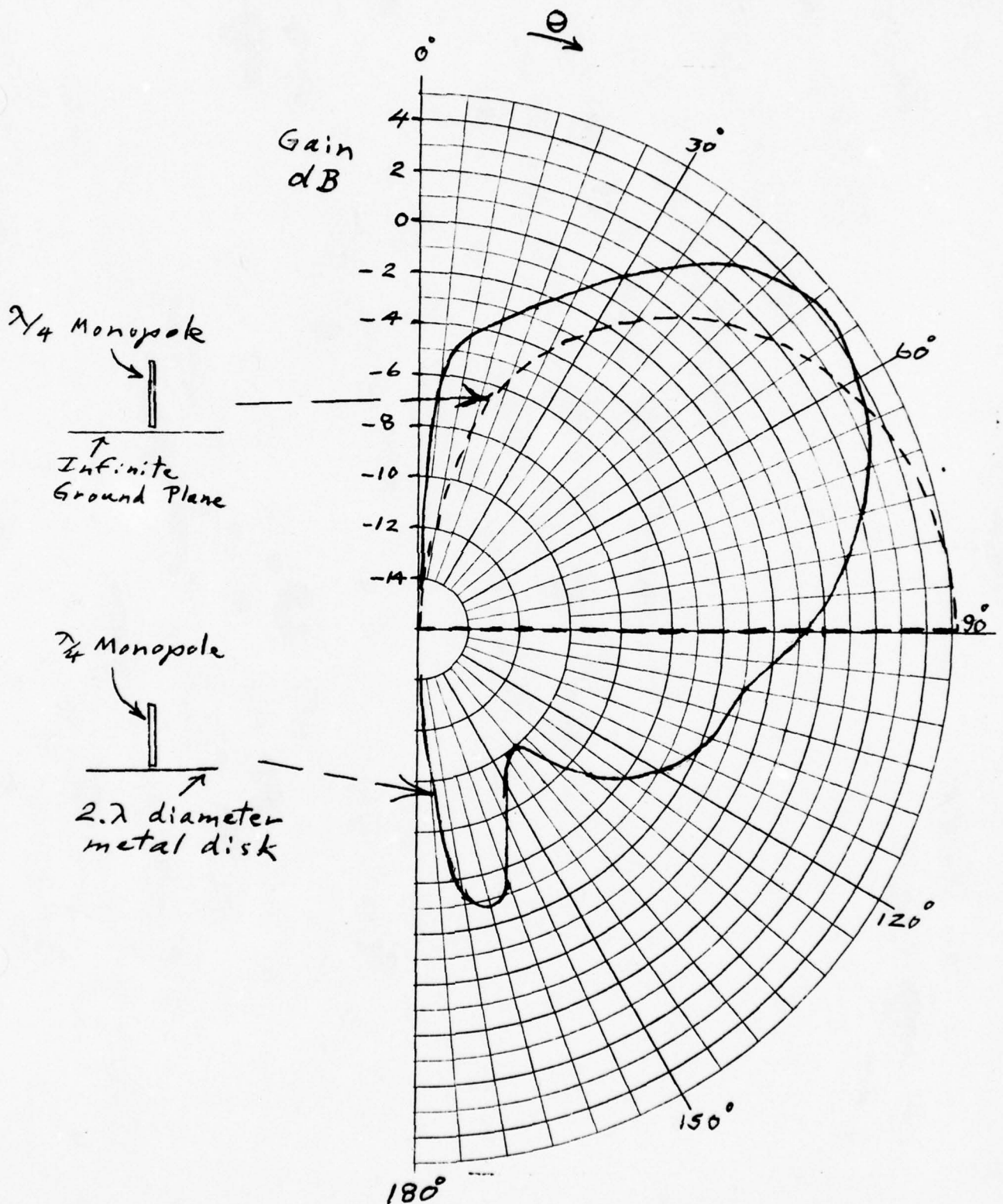


Figure 3-40. Elev. Pattern With Small Ground Plane

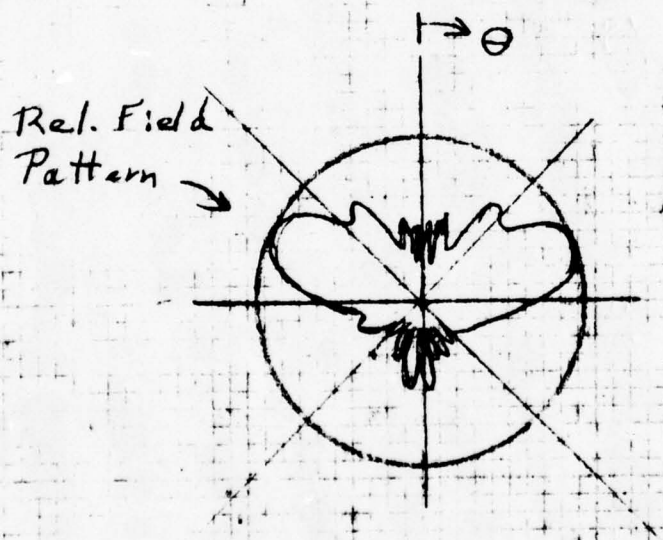
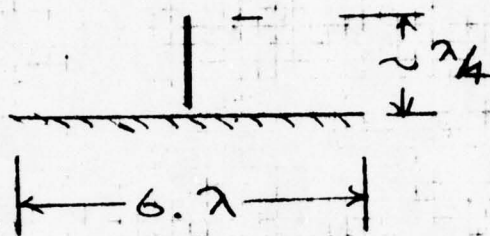


Figure 3-41. Elevation Pattern of  $\lambda/4$  Monopole Over a  $6\lambda$  Diameter Ground Plane

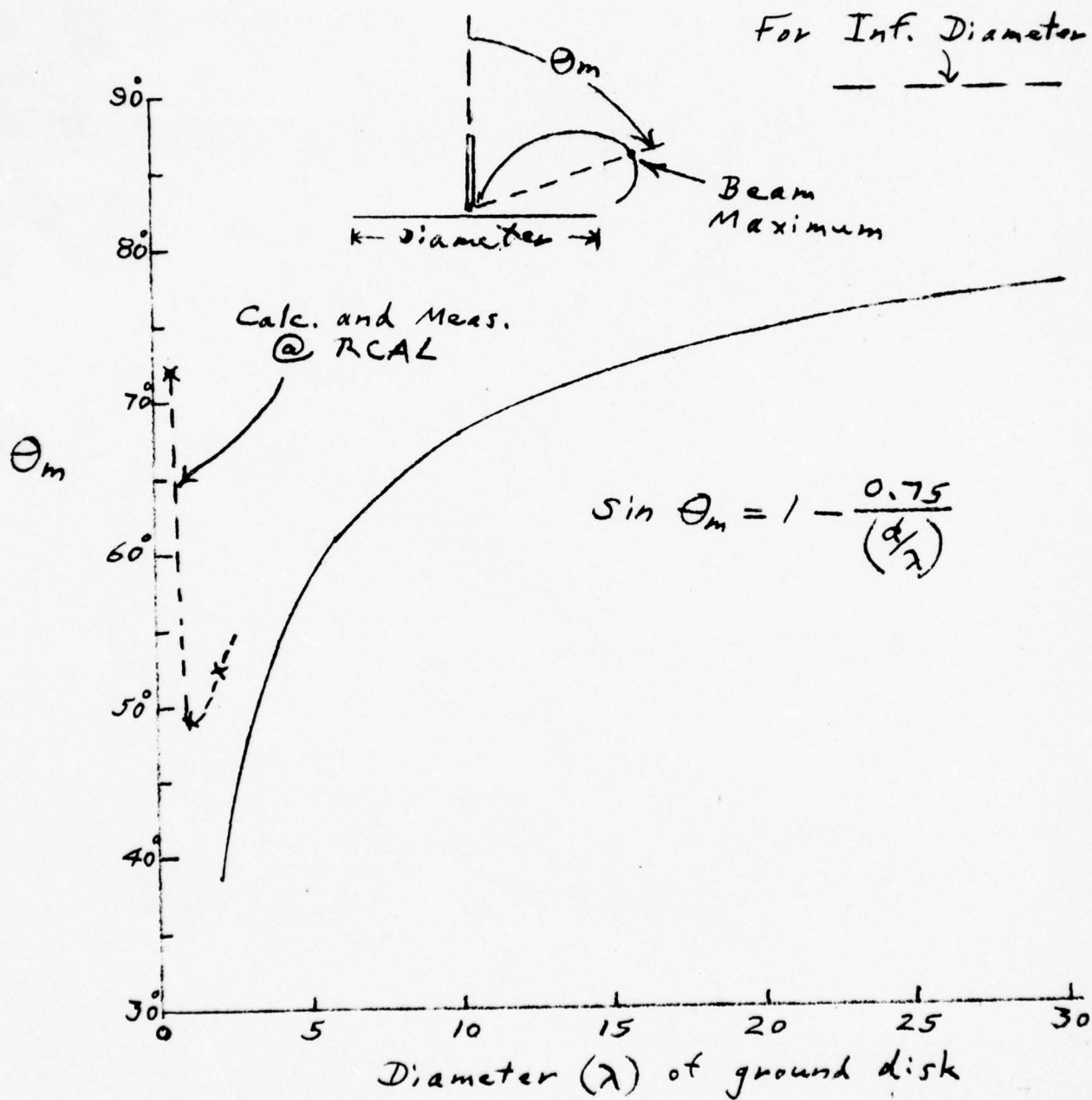


Figure 3-42. Elev. Pattern Vs. Ground Plane Diameter

Since the multi-lobe character near the poles probably exhibits phase changes with elevation angle, additional azimuth bearing errors might be encountered in these regions. Differences are particularly expected in the vertical planes parallel and perpendicular, respectively, to the major axis of the aircraft. These errors may possibly limit the useful operating range of elevation angle to values of  $\theta$  from, say,  $40^\circ - 45^\circ$  to directions near the horizon.

In the final analysis, only experimental measurements on a mock-up section of the aircraft surface can give accurate data as to the spacial regions in which the ideal characteristics can be realized.

### 3.3 SIGNAL PROCESSING CONFIGURATION ANALYSIS (TASK 2.2)

Control of errors, and maintenance of calibration over long operational periods, are predominant factors affecting the level of overall system performance of the bearing and miss distance measurement scheme. Such factors are realizable by a combination of signal processing techniques, data processing algorithms, and judicious choices from candidate hardware options. This section identifies appropriate signal processing methods and associated circuit elements and examines several sources of error which appear amenable to control by such methods. The sequence of addressing the topics corresponds to the listing of Table 3-1; however, owing to their insignificant effect, reference to errors caused by propagation anomalies and quantization is relegated to Section 3.5 on system accuracy analysis.

#### 3.3.1 Local Multipath

Increasing the DF antenna aperture to diminish multipath ("site") errors causes the constant phase wave-front arriving at the antenna to be sampled over a broadside span of several wavelengths instead of merely a fraction of a wavelength as with the interferometer array originally proposed for bearing measurement in SECANT. Spatial corrugations are



created in the wave-front by the combination of the direct ray and reflected rays from the aircraft wings and fuselage. When these corrugations impinge on antenna elements that are closely spaced (in the order of  $1/2$  wavelength or less), the apparent direction-of-arrival (DOA) as denoted by a particular phase difference measured between the emfs induced in the elements, may deviate substantially from the true DOA. The worst deviation occurs if the wave-front is sampled only between adjacent opposing peaks of a corrugation cycle. Clearly, reduction of the deviation may be achieved by increasing the antenna aperture and spacing the antenna elements so as to span many corrugations.

Another method of mitigating DOA errors due to multipath is to change the carrier frequency enough to produce sizable lateral translations of the corrugations relative to the antenna array, to acquire several sample measurements of the apparent DOA for a spread of frequencies, and to compute the average value of the sample. Movement of the corrugations is brought about by virtue of the longer paths taken by the indirect rays compared to the direct ray, which cause the phases of the reflected signals to change more rapidly than the direct signals as the frequency is varied. The extent of the translation depends upon the amount of frequency change and the distances between the reflecting surfaces and the antenna. In SECANT the received carrier is randomly hopped between eight different frequencies (two sets of  $P^+$ ,  $P^-$ ,  $Q^+$ ,  $Q^-$ ) occupying the high and low bands. As presently allocated, however, the four frequencies in a band cover an arbitrary range of only 5 MHz which is insufficient to confer tangible frequency diversity benefit in combating multipath. By an alternative allocation, the four frequencies can be dispersed over a band of at least 21 MHz to improve the benefit.

### 3.3.2 Corange Target Interference

Reference to "catastrophic errors" caused by interference from corange targets should not be construed as vitiating the application of relative bearing measurement to SECANT. A recent unpublished analysis of the altitude coding facility shows that the corange event

is rare under the most congested traffic conditions predicted in the FAA 1982 LA Basin standard traffic model (snapshot #3), and becomes even more so if the event includes persistence of a corange condition beyond a 4 second round time.

Although not embodied in the present configuration concept it is of interest to note that if the ring array antenna were employed reciprocally, (i.e., for transmission as well as reception) a cardioid-like radiation pattern would be created having a null whose azimuthal orientation could be controlled by varying the phase difference between the signals fed to the  $H = 0$  monopole and the  $H = 1$  ring array. There would then exist the potential for aiming the null at an undesired target causing the corange state, so selectively depriving it of interrogation pulses and inhibiting its interference. The crossed-axis interferometer does not conveniently lend itself to a similar reciprocal application as a directionally emissive antenna.

### 3.3.3 Aircraft Attitude Variations

A potentially crucial perturbation of swept bearing measurement develops from spontaneous short term variations of yaw which occur when aircraft are flying nominally straight courses during conditions of atmospheric turbulence. An example provided by Reference 12 gives typical peak-to-peak yaw variations in the order of 5 degrees at angular velocities ranging from 1.32 to 2.59 deg/sec rms for a fighter and a bomber flying in a clear, medium turbulence environment. The seriousness of such angular movement can be judged in relation to the anticipation that swept bearing measurements would be characteristically in a range of 2 to 5 degrees and undertaken over an interval from 3 to 5 seconds. Unless compensated, spontaneous yaw changes could be drastically inimical to miss distance determinations. The necessary compensation can be derived by interfacing the CAS with inertial platforms or integrating rate gyros which normally serve navigational and autopilot equipment in the aircraft. It is essential that the response and resolution characteristics of the yaw pickoff shall match those of the bearing measurement system sufficiently well to limit residual uncompensated angular differences to a budgetary error of 0.1 degrees (one sigma).

Roll and pitch variations occurring about a nominally level and straight flight path would cause relatively insignificant errors in bearing and miss distance measurements. However, large angular deviations (as occur during banking, diving, and climbing) cannot be ignored. Pick-offs for roll, pitch and yaw will be necessary if accurate determination of true\* relative bearing and miss distance are required for nonlevel modes of flight, as is assumed to be the case in the present study.

Signal processing associated with attitude variation compensation is limited to conversion of the signal format of the aircraft attitude sensor to the digital format compatible with data processing in the bearing measurement subsystem, together with such lag correction as may be required.

#### 3.3.4 Fruit Interference

Errors in bearing measurement, caused by fruit pulses overlapping target pulses in the range gate, have magnitudes determined by a complex stochastic process involving four significant random variables (rv) pertaining to the fruit signal. They comprise the time-of-arrival, the direction-of-arrival, the phase displacement of the fruit carrier with respect to the target reply carrier in a receiver channel, and the amplitude of the fruit signal relative to that of the desired reply. Additionally, there is a binominal distribution which gives the probability that one or more fruit pulses (the actual number is another rv) will enter the range gate and interfere with the desired signal pulse. The probability density functions of the first three rv's could reasonably be taken as uniform for an aircraft located at the center of a densely populated traffic model, whereas the density function for the relative fruit amplitude could be ascertained from the histogram of fruit statistics outputted from the SECANT signal environment computer simulation program for a particular traffic model. A further complication is that the last mentioned density function itself is a function of the signal level received by a protected aircraft, and hence of the target range.

---

\* I.e., the relative bearing observed in the horizontal plane, as distinct from that in the azimuthal plane of the antenna. The latter observation is called simply relative bearing herein.



A rigorous error analysis embodying the above mentioned density functions would be rather formidable, especially if undertaken for a variety of target range magnitudes, and would exceed the scope of the present study. A simplified analysis is given in Section 3.5.2.4, however. It proceeds on the assumption that the received fruit pulses essentially causing the interference error are at levels in excess of the signal level received from a target aircraft. This assumption is valid for a target separated by the maximum Tau 2 hazard range (approximately 8 nautical miles in the terminal area) from a protected aircraft located in the densest region of the FAA/MITRE 1982 LA Basin standard traffic model.

Signal processing is essential for reducing fruit interference within the receiver to a level from which associated residual errors can be further diminished to acceptable bounds by data processing. Such signal processing would be implemented by the operation of a gate controlled from the detection and tracking circuits of the SECANT equipment with which the bearing measurement subsystem is integrated. The gate would be enabled to permit a phase measurement only when a reply signal appeared within the SECANT tracking gate in only one of the two active reply channels, corresponding to the condition of valid bit recognition by the SECANT message data processing circuitry. Accordingly, bearing measurements would be permitted only during the interval in which SECANT anticipates and senses the reception of an above threshold reply pulse from a target aircraft. A coincident fruit pulse, then, could not evoke a response unless it were of the same type (domain and message symbol) as the anticipated reply pulse. Only this event or simultaneous interference by a noise pulse could cause an erroneous phase measurement due to interference.

The fruit interference error shown in Table 3-1 would apply, following signal processing, in the most congested region of the traffic model given that fruit signals are uniformly distributed over 360° of azimuth relative to the protected aircraft. This worst case error is an order of magnitude greater than a tolerable budgetary value for the full CAS, but is amenable to adequate reduction by data processing as described



in Section 3.4.1. Thus, digitizing the 62 bearing measurements as discussed in Section 3.1.1.3, and storing the data in temporary memory, provides the opportunity for statistically refining the data points in that "wild" measurements due to fruit and noise can be detected and rejected before final data smoothing is undertaken. Assuming that wild bearings are uniformly distributed in azimuth, a stochastic acceptance window which contracts from  $360^\circ$  to  $4^\circ$  would reduce the random component of bearing error to within a budgetary value of 0.25 degree, one sigma, after averaging the 62 bearing measurements taken with the  $H = 4$  ring array antenna.

### 3.3.5 Mutual Coupling Effects in Interferometer Array

Mutual coupling between the monopole stubs of the crossed axis interferometer array cause cyclic deviations in measured angle from computed values. As shown in Section 3.2, the deviations vary cyclically between limits of  $\pm 4^\circ$  over each  $45^\circ$  azimuthal sector for  $1/4$  wavelength monopoles set at an aperture of  $1/2$  wavelength (9.4 cm at 1.6 GHz). This effect could produce errors of as high as  $\pm 0.5^\circ$  per degree of swept bearing, assuming that the small aperture array was employed for such measurements. The deviation diminishes rapidly as the aperture is widened, such that at four wavelengths its maximum rate of change falls to the negligible theoretical level of  $0.004^\circ$  per degree of azimuth.

Attempts to satisfactorily correct the mutual coupling error in the small aperture interferometer would prove futile because of the large uncertainty in the magnitude of the relative bearing angle measured with the antenna. While this conclusion adds further weight to the argument for disqualifying the small aperture interferometer in making swept bearing measurements, it does not vitiate applications for sector identification in PWI or for angle ambiguity resolution in a full CAS which is also equipped with a wide aperture interferometer for swept bearing measurements and accurate relative bearing measurements.

### 3.3.6 Phase Nonlinearity in Ring Arrays

A theoretical ring array having an indefinitely large number of antenna elements and a moderate number ( $H = n$ ) of phase cycles per  $360^\circ$  of azimuth possesses a linear phase

versus arrival angle characteristic. In practical applications as few as three elements can be employed in a ring for  $H = 1$ . Therefore, a ripple is superimposed on the calibration, whose maximum deviation depends upon the magnitude of  $H$ , the number of elements in the ring, and the ratio of the ring radius to the wavelength  $\lambda$ . Thus, with a 4-element ring array having parameters of  $H = 1$  and  $a/\lambda = 0.15$  (corresponding to a ring radius of " $a$ " = 2.8 cm at 1.6 GHz), the ripple has a computed maximum deviation of  $2.3^\circ$  and passes through four cycles in  $360^\circ$  of azimuth. These numbers imply that deviation errors in swept bearing measurement could reach a maximum rate of  $0.16^\circ$  per degree, which is considerably lower than the rate caused by mutual coupling in a crossed-axis interferometer having a similar aperture. However, the deviation increases sharply with array diameter which, if 9.3 cm ( $a/\lambda = 0.25$ ), would produce an error rate of  $0.5^\circ$  per degree.

Some mitigation of the error could be realized at larger apertures by the device of substituting circumferentially dispersed monopole couplets for each antenna element, but a much more effective remedy is to adopt a higher cyclicity mode. Negligible ripple error results at  $H = 4$  and 25 cm diameter, which are the parameters of the larger ring array antenna investigated in the present study.

### 3.3.7 Thermal Noise Errors

Errors caused by thermal noise will be of concern only at target ranges approaching the maximum Tau 2 hazard range of the ATA ANTC-117 specification. For a closing speed of 550 knots this range is about 8 nautical miles and accounts for a mean signal-to-noise ratio of 18 db in VECAS when range tracking from two paralleled channel filters having a combined noise bandwidth of 2 MHz. Phase difference measurements would be undertaken at larger bandwidths on account of the necessity to reduce the pulse transient settling time to a small fraction of the pulse width, as is discussed in Section 3.3.9. A 3 db IF bandwidth of around 6 MHz is required for this purpose; the SNR would be degraded to about 13 db and the corresponding noise error averaged over 62 samples would be about 1.6 degree one sigma. The 62 bearing samples become available if phase measurements are made for each pulse of a VECAS range track pulse sequence which occurs in the track format.

Eliminating cable losses by locating the RF front end of the receiver at the antenna, and improving the receiver noise figure would serve to restore the SNR to 18 db. An additional, more potent method of bearing error reduction is to utilize an antenna having an angle conversion factor (n) exceeding unity since the noise error is inversely proportional to n. Proceeding on the assumption that  $n = 4$  is a reasonable number for design purposes, its effect would be equivalent to improving the SNR by 12 db and so reducing the random noise error to approximately 0.23 degree one sigma with 62 pulses. As previously noted, the device of increasing n is correspondingly effective for controlling all other interior error sources discussed herein.

### 3.3.8 Phase Comparator Resolution

Resolution limitations of the phase comparator contribute an error component to the relative bearing measurement. The error  $\epsilon_p$  is virtually independent of bearing,  $\theta$ , in the case of ring array antennas. But for crossed axis interferometer of comparable aperture the reflected phase comparator error can reach a value of  $2 \epsilon_p \cos^2 \theta$ , and hence may exceed the corresponding ring array error by as much as 2:1 over a cumulative azimuth range of  $180^\circ$ . This result stems from the condition that, whereas a phase displacement in the measuring system translates linearly into an equivalent change of bearing with the ring array, there is an inverse tangent relationship between a ratio of phase displacements and bearing in the case of the interferometer.

Distinctly different conditions affect resolution limitation in the phase comparator, according to whether it is of the zero crossover type or of the multiplier type. These conditions are discussed in the following subsections.

#### 3.3.8.1 Zero Crossover Phase Comparator

A further distinction regarding resolution capability must be drawn in the case of the zero crossover type depending on the method used to measure the interval between the start crossover of the reference signal and the succeeding (stop) crossover of similar slope in



the comparison signal. One favored method involves initiating a linear ramp waveform at the start crossover and measuring its terminal amplitude when sampled and held at the stop. This crossover amplitude is proportional to the phase difference. An alternative, completely digital method employs a time interval counter to accumulate clock pulses observed between the two crossovers and will be discussed first in the following paragraphs. It is of interest to note that the Hewlett-Packard Company (Reference 13) utilizes a hybrid combination of the counting and vernier ramp sensing techniques in its high precision Model 5360A Computing Counter to greatly improve resolution and accuracy when it is used for phase and other measurements.

#### 3.3.8.1.1 Clocked Crossover Method

The resolution problem of the clocked crossover method arises from the magnitude of the second IF frequencies associated with the  $P^+$ ,  $P^-$ ,  $Q^+$ , and  $Q^-$  replies. These frequencies are 19, 20, 23 and 24 MHz in the present VECAS for which the average period is 53.25 ns. Thus if a free running 100 MHz clock were employed for time interval measurement, its period of 10 ns would correspond to a phase comparison quantum of  $10 \times 360/53.25 = 67.6^\circ$ . Direct counting at much higher rates than 100 MHz is only beginning to become commercially practicable (Reference 3) so that other techniques must be invoked in substantially reducing the quantization error, as appears necessary from the following approximate estimate of the quantization error magnitude.

The phase comparison quantum implies a total resolution error having triangular probability density symmetrically distributed over a range of  $\pm 67.6^\circ$ , and thus a standard deviation of  $67.6/6 = 27.6^\circ$ . Now with 62 independent pulse samples the standard deviation of the averaged result would be  $27.6/62 = 3.5^\circ$ . When divided by an antenna angle conversion factor of four, the resulting error of  $0.9^\circ$  one sigma is in excess of a budgetary goal

---

\*Assuming all clock pulses occurring between start and stop crossovers are counted.



tentatively set at about 0.13 degrees one sigma for each of the interior random error contributors. Nevertheless, this simple exercise demonstrates the remarkable effectiveness of pulse integration and angle conversion when combined to combat such contributors. Reduction of the phase quantum could be accomplished by a dual-channel receiver modification, without a major revision of system frequencies generally, by:

- (a) The addition of two second LO frequencies at 142 MHz and 148 MHz which would generate 17 MHz and 18 MHz instead of the existing (VECAS) 19 MHz and 20 MHz second IF reply frequencies, respectively.
- (b) A third IF section incorporating a third LO frequency of 21 MHz, to serve the phase measurement circuitry only.

The purpose of the modification would be to generate two third IF's of 3 MHz and 4 MHz from the four second IF's of 17, 18, 24 and 25 MHz. The longer resulting periods would reduce the phase comparison quantum to a mean of  $12.6^\circ$  and so almost satisfy the above mentioned budget  $0.13^\circ$  (one sigma) when integrating 62 pulses. Note that although it might appear preferable to remain with the original second IF's of 19, 20, 23 and 24 MHz, the lower third IF would then be 1.5 MHz which would not guarantee availability of a full cycle having two positive going crossovers or two negative going crossovers, but not both, under a  $1 \mu\text{sec}$  pulse while also providing sufficient margin for adequate subsidence of the initial filter transient.

Certain drawbacks are evident in the third IF solution albeit an option which avoids a completely new set of frequencies. One drawback is the additional circuit complexity involved. Another drawback arises from the characteristics of the third IF filter which must possess a sharp cutoff frequency between 4 MHz and 6 MHz in order to suitably attenuate harmonics of the 3 MHz and 4 MHz IF's. Hence the third IF bandwidth may be insufficient for adequate attenuation of filter transients.

A third, but minor drawback, stems from the difference in the periods of the 3 MHz and 4 MHz IF's; which would appear to require compensation by extending either signal processing or data processing. This complication could be avoided if the average of the two periods is employed in computing the phase angle; which procedure introduces an error, however, since the period must be regarded as a random variable. Assuming equal-likelihood of the IF's, integration of 62 pulses, and an angle conversion factor of 4; the related error component in relative bearing and swept bearing is found to be 0.4% (one sigma). This amount corresponds to a worst case error of 1.4° (one sigma) when measuring a relative bearing approaching 360°. By comparison, averaging the periods of the original second IF's (19, 20, 23 and 24 MHz) causes a smaller error of 0.22% one sigma which slightly diminishes the resolution advantage gained in resorting to lower IF's, but only in respect to relative bearing measurement. Negligible error would occur when determining swept bearing because the errors caused by the variable period have high probability of being nearly equal in the differenced relative bearing measurements. This error correlation occurs due to the fact that the sequence of reply symbols is the same for both sets of signals employed when making the relative bearing measurements.

Resolution of the problem of achieving a small enough phase quantum was finally reached by adopting a design plan in which the diversity of SECANT reply frequencies was expanded to control multipath errors as described in Section 3.3.1. Consequently, the constraint on redistribution of LO and IF receiver frequencies vanishes thus allowing the generation of a single IF of 3.5 MHz for phase measurements, and avoiding phase quantum averaging errors.

#### 3.3.8.1.2 Linear Ramp Function Method

This method avoids the use of high speed clocks and counting rates, but would require analog-to-digital conversion of the ramp amplitude in order that bearing data can be processed and smoothed to deliver suitable inputs for the CAS computer. It can be shown that if the angle range of 0 to 360° is quantized in  $L$  levels, the quantizing error

need not exceed  $180/(\sqrt{3})$  degrees one sigma. Therefore, with an angle conversion factor of four and integration of 62 measurements, the relative bearing error caused by quantization would be  $180/(4\sqrt{3} \times 62) = 3.3/4$  degree one sigma. This result means that in order to limit the quantizing error to 0.13 degree:  $\sqrt{3} \geq 26$  (i.e.,  $14^\circ$  per level) and hence a 5-bit A-D converter would be required to process the ramp amplitude.

While the ramp function method may superficially appear an attractive alternative to the clocked crossover method, it is essentially analog in character and requires stabilization or normalization of the terminal amplitude, particularly in regard to measurement of large phase angles where a 2% variation in that amplitude approaches the maximum  $1/2$  quantum digitizer error. Any nonlinearity of the ramp waveform would also contribute to the amplitude error, so that it is evidently appropriate to specify a tolerance of 1% of full scale for the amplitude bias error and linearity bias error, individually. In normal practice this requirement may be too onerous for a ramp whose time base is only 53.25 nanoseconds, corresponding to the average period of the second IF's in the present VECAS. Consequently, it would be necessary to extend the average period as, for example, by the third IF down conversion described above. The problem of maintaining a stable reference to support the amplitude accuracy appears more difficult than that of assuring linearity, but could be overcome utilizing a normalization process in which the mean amplitude of the ramp at the stop crossover is divided by a calibration amplitude generated from the ramp signal source over a full mean period. The arithmetic operation would be a digital computation conducted in the bearing data processor, and the calibration amplitude would be updated from time to time by integration of the standard number (62) of ramp samples. Normalization implies the use of the same ramp signal source and A-D converter when making a calibration amplitude measurement as when measuring the ramp amplitude at the stop crossover.

The above remarks concerning drawbacks of the ramp method have negligible significance when it is used as a vernier in combination with the clocked crossover method.



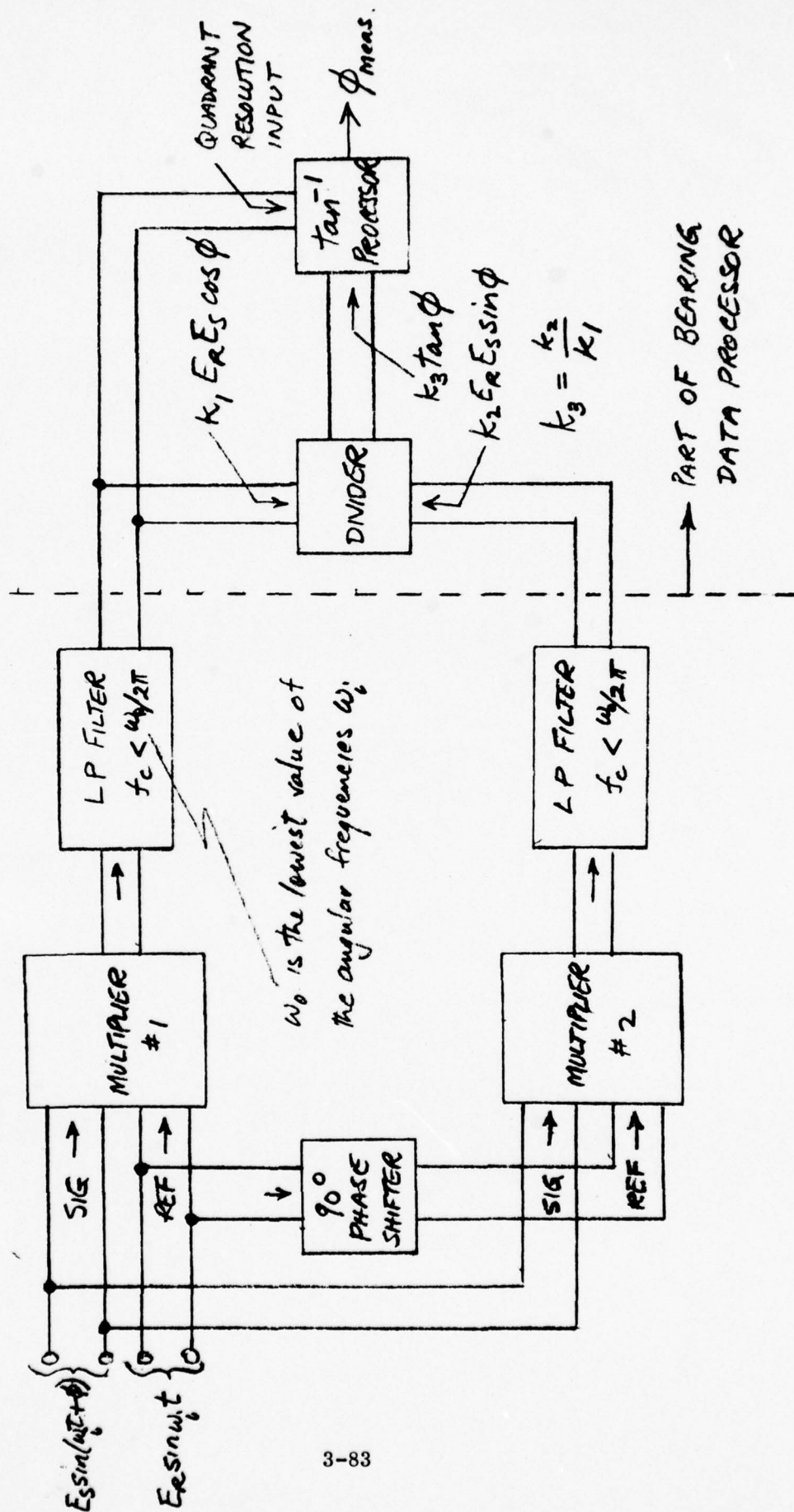
### 3.3.8.2 Multiplier Phase Comparator

On forming the product of two sinusoids,  $E_R \sin \omega t$  and  $E_S \sin (\omega t + \theta)$ , the resulting potential contains a dc component which is proportional to  $E_R E_S \cos \theta$ . Thus, if  $E_R$  and  $E_S$  are maintained at predetermined fixed magnitudes when applied to the two input ports of an electronic multiplier having stable characteristics; its output, after being filtered to reject ac components, could be calibrated to measure  $\theta$  albeit ambiguous in sign. In its simplest form, therefore, the multiplier phase comparator is deficient on three counts with respect to the types of zero crossing phase comparators discussed above. It is inferior in that a severely nonlinear relationship exists between the measured and actual values of phase angle  $\theta$ , variations of levels affect the phase indication, and response to  $\theta$  values from  $0^\circ$  to  $360^\circ$  is subject to ambiguity in quadrant identification. All three deficiencies are intolerable for the present application, and eliminating them leads to the so called quadrature phase comparator ... a configuration of substantially increased complexity which is depicted by Figure 3-43.

Two multipliers having matched electrical parameters are shown in the diagram. Both receive the reference and phase displaced second IF signals from the dual-channel receiver. One, however, has a  $90^\circ$  phase shifter inserted in series with its reference channel input. The phase shifter is designed to provide a  $90^\circ$  displacement which is independent of frequency over the IF band to be processed. A low pass filter at each multiplier output extracts the dc component which for both multipliers is proportional to the product of the input signal amplitudes. The outputs differ, however, in that multiplier #2 receiving the quadrature input thereby yields a dc component depending on  $\sin \theta$ . Thus by computing the quotient of the multiplier outputs in the divider unit an output  $K_3 \tan \theta$  is obtained. The constant  $K_3$  depends on the transfer characteristics of the  $90^\circ$  phase shifter and of the multipliers, and is made unity by appropriate design. Inverse tangent processing to recover the measured value of  $\theta$  would be undertaken in the bearing angle data processor, and since  $\tan^{-1} \theta$  has two solutions within a period, sign information must be supplied from a multiplier output to the data processor which applies an algorithm to correctly identify the quadrant occupied by  $\theta$ .



FIG. 3-43. BASIC SCHEME OF QUADRATURE PHASE COMPARATOR  
 (Sample-and-hold and A-D conversion at outputs of LP filters are not represented)



Actually, with SECANT signals the multiplier output signals will be unipolar pulses having durations shorter than 1 microsecond by the interval that must be allowed for the settling time of the IF filters. Moreover, since it is necessary to measure the output pulse amplitude before perturbing effects associated with the lagging edge are encountered, a sample-and-hold technique must be utilized, which implies that A-D conversion will be required at the multiplier outputs. Provision would be made to initiate the sample-and-hold action at a controlled time lag following the emergence of the leading edges of the pulses from the multiplier outputs. As the multiplier outputs would then be rendered in digital form it would be appropriate to undertake the quotient processing in the bearing angle processor also.

#### 3.3.8.3 Comparison of Phase Detectors

As compared with the clocked crossover phase detector described above, the multiplier type suffers from serious drawbacks. It involves considerably more complex circuitry, is prone to accuracy deterioration due to unavoidable instabilities of its analog multipliers and divider, and incurs the additional complication of inverse tangent data processing. No advantage has been shown in regard to improved performance with noisy signals, and its only merit is that a clock signal source is rendered unnecessary. In view of these considerations the clocked crossover phase detector is identified as the preferred device in the present program.

#### 3.3.9 Errors Encounterable with Pulsed Waves

Two conceivable complications arise with phase measurements made between pairs of pulses in the dual receiver channels. First, because of the short pulse duration and the requirement to measure phase up to the full  $360^\circ$  limit, phase measurement cannot be conducted on frequencies below 3 MHz. This limitation results in the circuit elaborations discussed in the preceding subsections on phase comparators, which are needed to realize sufficient resolution for maintaining accurate bearing measurements.

The other complication concerns ringing effects due to the excitation of IF filter transients by the received pulse modulated carrier. Such transients combine with the true (i.e., forced oscillation) signal and cause phase distortion which, if not controlled or averted, may induce significant bearing errors.

Accordingly, IF bandpass filters - incorporated in the dual channel receiver (block #3 of Figure 3-1 ) to serve the bearing determination circuitry - must be designed to insure that the transient settling time occupies a limited portion of the pulsewidth, thereby affording a steady state interval of adequate duration for completing a satisfactory phase measurement before the transient due to the pulse lagging edge is encountered. The existing 5-pole Butterworth filters used in VECAS have a bandwidth of only 1 MHz, from which it follows that the combined rise and settling time is in excess of the 1  $\mu$ sec pulse width. Therefore, phase measurements must be made in the receiver at a point ahead of the 1 MHz filters (which are exclusively associated with signal processing (Block #7 of Figure 3-1 ) for range measurement and message data acquisition). IF filters dedicated to the bearing measurement channels would possess broader bandwidths to control transient decay times. For a specified bandwidth, and for a given number of poles, the rise and settling times increase in the filter order: Bessel (linear phase) Butterworth-Chebyshev. However, the rapidity of roll-off also increases in the same order, so that a trade-off in filter type selection will be necessary to minimize the error due to a combination of transient and noise effects.

Another type popular in IF amplifier applications is the 4-pole double tuned filter which, while conveniently amenable to closed-form analysis of transient effects, also provides a basis for assessing the magnitude of the transient phase error at a condition believed intermediate between extremes posed by the Bessel and Chebyshev types. Appendix J presents the derivation of phase perturbation effects in synchronous double-tuned filters having bandwidths of 5 MHz and 10 MHz. Results are parameterized also for several values of the epoch of the carrier wave as referred to the leading edge of a rectangular



modulating pulse. Two values of the filter damping factor that are compatible with acceptable overcoupled ripple magnitudes of the filter, are invoked to reveal the influence of filter skirt selectivity on the transient phase error.

Figure 3-44 shows the transient phase shifts which could occur in a receiver channel at the mid-band frequency of an overcoupled double-tuned filter having a spacing of 5 MHz between its response maxima. A particular case is presented in which the leading edge of the modulating pulse occurs at the  $45^\circ$  phase epoch of the carrier, the transient phase being plotted as a function of the interval  $\Delta T$  between phase angle observation and the time the leading edge enters the filter. Curves are shown for damping factors of 0.05 and 0.1. At any given observation time the total phase measurement error caused by the transients could reach a value exceeding the value shown in Figure 3-44 by the magnitude of the transient phase shift simultaneously occurring in the other channel of the dual-channel receiver. The additional phase shift will depend on the phase epoch that exists for the carrier in the second channel at the instant of leading edge impingement on the filter in that channel, but will be in the same order as that in the aforementioned channel for  $\Delta T \geq 0.3$  microseconds. It would appear from Figure 3-44 that even with the higher damping factor, an interval in the order of  $\Delta T = 0.5$  microseconds must be allowed to elapse in order to insure that the transient will have decayed sufficiently to permit phase measurements to be made with requisite accuracy. At lower damping, as may be necessary to control noise levels, practically the full 1 microsecond of measurement opportunity is apparently lost on account of the transient.

Fortunately, the situation is rendered considerably less critical by virtue of the fact that the phase epoch would be a random variable uniformly distributed from  $0^\circ$  to  $360^\circ$  in phase. Consequently, the transient phase error, being a function of the phase epoch at a selected  $\Delta T$  value, is also random and, therefore, the variance of its mean value would be reduced in inverse proportion to the number of measurement samples integrated to give a relative bearing measurement. In the case of swept bearing determinations,

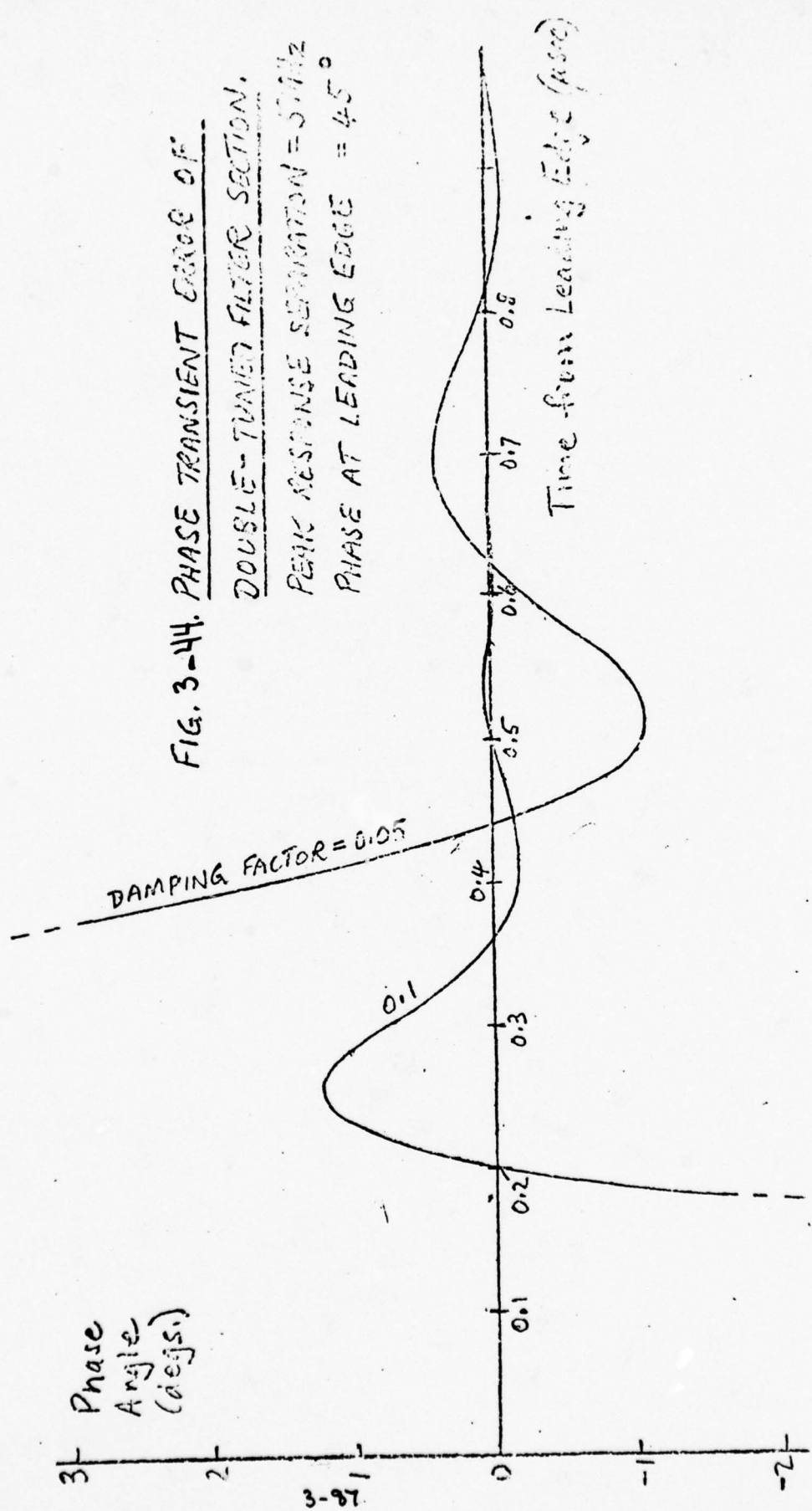


FIG. 3-44. PHASE TRANSIENT ERROR OF

DOUBLE-TUNED FILTER SECTION.

PEAK RESPONSE SEPARATION = 5.71 Hz

PHASE AT LEADING EDGE =  $45^\circ$



a further reduction of 4 to 1 is effected on account of the angle conversion factor of the  $H = 4$  ring array antenna. This advantage is slightly diminished by the fact that both channels contribute to the random error which is thus inflated by a factor of  $\sqrt{2}$ .

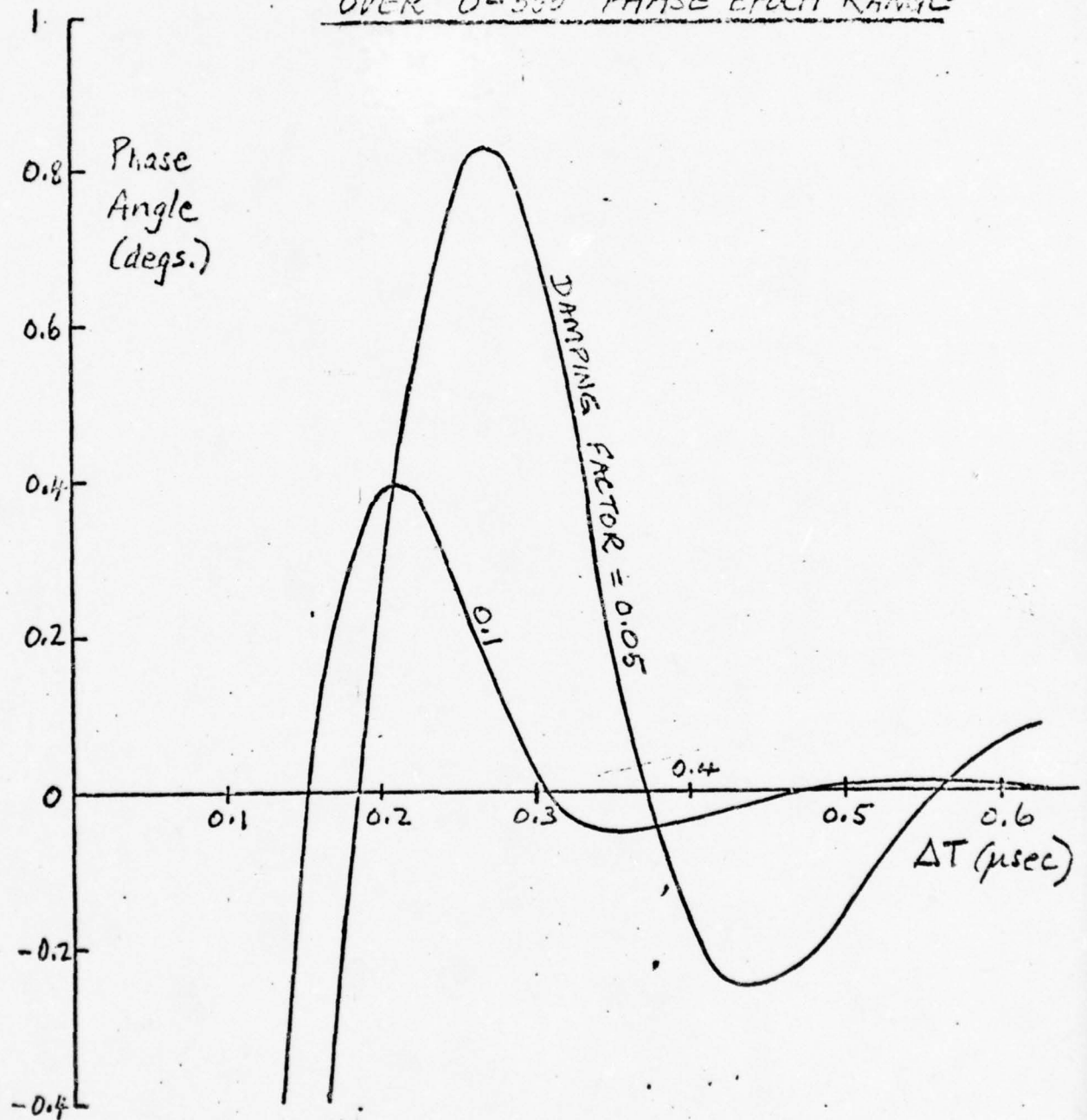
The integration process when applied to the transient phenomenon introduces a phase bias whose error influence is also reducible by the angle conversion factor for swept bearing measurements. This bias, expressed in terms of phase measurement error, is plotted versus  $\Delta T$  in Figure 3-45 for the case of the double tuned IF filter, with various combinations of bandwidth and damping factor. In an ideal situation, whereby the dual-channel receiver has perfectly symmetrical characteristics, the same bias would occur in both channels and its effect would be nullified. However, it must be assumed that incidental differences in the channels' parameters will cause a residual bias error to exist. In order to avoid a lengthy variability analysis, it is reasonable to allow for a residual of 40% of the estimated bias in one channel as representing the maximum system bias error effect due to the transients.

The conclusion reached in this analysis is that provision should be made, in designing an engineering model of the dual-channel receiver and associated bearing measurement equipment, for effecting an adjustable delay of phase comparator operation by the interval  $\Delta T = 0.4 - T_g \pm 0.15$  microseconds beyond the instant that the pulse leading edge is sensed at the interface between the filter and the comparator. In this expression for  $\Delta T$ ,  $T_g$  is the group delay (in the order of 0.15 microseconds for a 5 MHz bandpass section) of the filter causing the transient, while the  $\pm 0.15$  microsecond variability term implies the temporary availability of delay lines having that range of adjustment in each channel. The correct settings of the delay lines would be established on a one-time basis during bench tests on the equipment, and fixed networks having corresponding delays would be substituted for the delay lines in subsequent prototype models.

#### 3.3.10 Phase Variations in IF Limiter-Amplifiers

The phamp, i.e., the change of phase shift with signal amplitude in multi-stage limiter-amplifier, must be suitably bounded in order to control bearing measurement errors which

FIG. 3-45. MEAN PHASE TRANSIENT ERROR  
OVER 0-360° PHASE EPOCH RANGE



can arise within the dual-channel receivers represented in Figure 3-1. Data are lacking, as yet, on phamp characteristics pertaining to the type of limiter-amplifier employed in VECAS, and hence its qualifications for retention in the bearing subsystem are questionable.

Phamp is caused by relaxation due to charge storage in transistors and diodes, Miller capacitance variation in the presence of reactive coupling or terminating networks, and RC time constants which induce bias variations as a function of signal level. There is a paucity of literature on (References 15 and 16) phamp, particularly in respect to analytical versus experimental results. This situation is understandable in view of the highly nonlinear nature of the mechanism causing phamp. However, some quantitative data and commentary have been supplied by RCA specialists in monopulse radar, who are confronted with the utilization of limiters in systems having onerous dynamic ranges 40 to 50 db in excess of that arising in the present application. Their experience shows that in regard to typical bandpass limiters having 60 MHz center frequency and 20 MHz bandwidth, the differential phase between the outputs of two such limiters when excited from a common signal source can be held to 3 degrees peak-to-peak over a dynamic range of -70 to zero dbm in the input level. The transmission phase through a particular limiter could shift typically in the order of 20 degrees over the same dynamic range, but owing to the tracking afforded by a dual-channel receiver configuration that incorporates a limiter in each channel, only differential phase variation is of consequence.

Most of the phase variation in multi-stage limiters typically occurs during the last 10 db or so at the high level end of the dynamic range. It is hypothesized that this effect could be ascribed to the onset of saturation conditions in the final stage whose output impedance changes and interacts with the load impedance to produce further phase variations. On this assumption, the phamp effect could be substantially reduced in the present instance where the maximum dynamic range is only 30 db, thus permitting the final stage to be



operated in its linear region as an output buffer. Additional error mitigation is apparent in the present application, since such high levels will normally exist at target ranges shorter than Tau 1 hazard ranges on which occasions precise bearing measurements would not be required.

From the above observations, it appears reasonable to set a design goal of 1 degree peak-to-peak for the differential phase variation between the transmission characteristics of the limiter amplifiers employed in the bearing measurement system. This goal is expressed in Table 3-1 by the anticipated maximum bias error of  $\pm 0.5/n$  degrees which is  $\pm 0.13$  degrees when bearing measurements are made using the  $H = 4$  antenna array. However, some reservation should be maintained when accepting this low error, in that the error estimate assumes equal signal levels at the inputs to the limiter-amplifiers whereas, in the operational environment, the levels could differ by several db.

This discussion of the phamp effect concerns absolute bearing accuracy primarily. Its influence on the measurement of swept bearing would be insignificant unless substantial variations in level differential accompanied the angle change.

### 3.3.11 Effects of Interchannel Phase and Delay Imbalances

#### 3.3.11.1 Phase Imbalance (Bias Error Generation)

When the phase displacements in the channels of the dual-channel receiver are unequal, the resulting interchannel phase offset translates directly into a systematic or bias bearing error on a degree-to-degree basis when a  $H = 1$  ring array is being utilized for DF purposes. The error is reduced in inverse proportion to the H-number for higher order ring arrays. However, the accuracy of miss distance determinations, which depend essentially on measurements of bearing increments (i.e., swept bearings), would not be adversely affected by the bias error.

By comparison, the crossed axis interferometer performs very poorly when swept bearings are being measured in the presence of interchannel phase imbalance. Appendix K indicates that in the case of the interferometer, errors of up to 50% in swept bearing, and hence in miss distance, are possible irrespective of azimuth. Accordingly, while phase imbalance correction would be essential with the interferometer, regardless of whether it is used for absolute bearing or swept bearing measurement, such corrective action would be unnecessary in relation to ring array antenna utilization unless accurate absolute bearing measurements were required. This consideration, incidentally, constitutes an important trade-off factor in the selection of an optimum antenna configuration.

An interchannel phase offset observed during a preflight alignment procedure could be readily eliminated, but the corrective action would not ensure the avoidance of offsets developing subsequently as the result of aging effects, mechanical disturbances, and environmental factors as may affect the channeling equipment. These considerations apply with equal force to long runs of RF coaxial cable if installed in the aircraft to connect antennas to remotely located receiver inputs. The influence of temperature differentials between a pair of long cables extending to the dual-channel receiver could be highly critical as is illustrated by the following example:

Assuming that the cables are constructed with solid dielectric to improve mechanical stability, it is found that, subject to conditions:

|   |   |            |
|---|---|------------|
| Cable pair length                       | = | 50 ft      |
| Dielectric permittivity                 | = | 2.2        |
| Frequency                               | = | 1600 MHz   |
| Temperature coefficient of permittivity | = | 150 ppm/°C |

a temperature differential between the two cables would cause a phase offset of 3.3 degrees of arc per deg°C. Such a great temperature sensitivity would probably be intolerable even if the cable were of the twin coax type to minimize temperature differences.

One possible remedy is to locate the RF and IF stages of the receivers in close proximity to the antennas and employ the long cables for transmitting the first or second IF signals, the center frequency of which would typically be at least an order of magnitude lower than the RF carrier. Accordingly, the temperature sensitivity would be reduced in the ratio of RF to IF, and adequate stability would then appear achievable.

For many airframe structures the above solution may be unattractive or even inadmissible on account of problems in accommodating and providing maintenance access to receivers collocated with the antennas. An alternative solution would involve converting the  $H = 1, 4$  antenna switch from 2-pole to 3-pole operation so allowing its use for repetitive phase checks in which both RF cables would be connected in parallel to a common antenna port. In this condition the phase imbalance could be detected or measured by built in test facilities and would be automatically compensated either by adjustment of a variable delay line or by a computing operation in the bearing data processor.

In the case of the ring array, but not the interferometer, a simpler technique for phase imbalance compensation is feasible. By means of a crossover switch, transpose the two channel inputs of the dual-channel receiver at the mid interval point of the phase measurement sequence associated with a particular bearing observation, and compute the mean of those measurements. If the transposition were effected in the channel paths at points ahead of cables or circuits prone to phase drifts, and if the process were carefully designed to avoid the introduction of significant phase shifts on its own account, the averaging procedure would eliminate the deleterious influence of the imbalance owing to its change of sign during transposition.

#### 3.3.11.2 Group Delay Differences (Random Error Generation)

Random errors will arise from the existence of an inter-channel group delay differential, owing to frequency hopping in the SECANT signal structure. Thus, for a delay difference

$\Delta D_i$  and frequency shift  $\Delta f_i$  associated with the  $i$ th section (RF or IF) of the channels, the phase differential over all  $n$  sections is:

$$\Delta \theta = 2 \pi \sum_{i=1}^n \Delta f_i \Delta D_i \text{ radians}$$

If  $\Delta f_i$  is the same for all  $n$  sections (as in the case of the present VECAS) then  $\Delta \theta$  is simply the product of the angular frequency shift  $2 \pi \Delta f$  and the total delay difference  $\Delta D$  between the channels.

It is readily shown that for consistency with the random error limit denoted as a design goal in Table 3-3, the standard deviation of  $\Delta \theta$  may not exceed  $4.4^\circ$ . A more practical specification is rendered in terms of the permissible limit to the channel delay difference  $\Delta D$ . Assuming the four reply frequencies ( $P^+$ ,  $P^-$ ,  $Q^+$ ,  $Q^-$ ) are equiprobable, the standard deviation of the contributed error in the smoothed (integrated 62 pulse) phase measurement is given by:

$$\sigma(\theta) = \frac{180 \sqrt{5}}{\sqrt{62}} \Delta D \Delta f \text{ (deg.)}$$

where :

$\Delta D$  = Delay differential between channels

$\Delta f$  = Frequency spacing between adjacent reply frequencies

$\Delta f = 7$  MHz in the design plan of Section 5.0, so that with the object of limiting  $\sigma(\theta)$  to  $0.8^\circ$  maximum (corresponding to  $0.2^\circ$  with the  $H = 4$  ring array antenna, as entered in Table 3-3) the following condition must be satisfied:

$$\begin{aligned} \Delta D &\leq \frac{62 \times 0.8 \times 10^9}{180 \sqrt{5} \times 7 \times 10^6} \\ &\leq 2.23 \text{ nanoseconds} \end{aligned}$$



Conforming to this tight differential delay tolerance on a long term basis should not be difficult since it is anticipated that the group delay of the receiver (RF and first IF stages, but not including external cabling) would be only in the order of 40 nanoseconds. This viewpoint is valid provided no frequency hopping is allowed in the second IF stages ... a condition satisfied by the design plan of Section 5.0, where a single second IF carrier of 3.5 MHz is indicated. Difficulty with delay differentials in cables can be avoided by collocating receiver front ends and IF stages with the antenna, or can be satisfactorily minimized by installing twin-coax when long cable runs are unavoidable.

### 3.4 DATA PROCESSING CONFIGURATION ANALYSIS (TASK 2.3)

This section derives the data processing algorithms required for phase measurement and for miss distance and horizontal bearing computation.

#### 3.4.1 Phase Measurement Data Processing

##### 3.4.1.1 Purpose

The overall purpose of the Phase Measurement Data Processing algorithm is to generate the required smoothed estimated  $\theta_1$  and  $\theta_4$  of the phase displacement occurring at the ports of the H = 1 and H = 4 antennas from the phase difference measurements  $\theta_1^{(j)}$  ( $j = 1, 2, \dots, 10$ ), and  $\theta_4^{(j)}$  ( $j = 1, 2, \dots, 62 \text{ max.}$ ), respectively. In performing this function the algorithm accounts for  $0^\circ/360^\circ$  ( $0/2\pi$  radian) discontinuities among a set of measurements, identifies and rejects outlying data points resulting from residual fruit pulses and noise, and determines the mean values of all accepted data points. A tally is kept of rejected data points, which when found excessive, results in recycling the algorithm with a new reference datum on the assumption that the previous one selected was spurious, i.e., "wild".

##### 3.4.1.2 Description

A two section flowchart of the algorithm is shown in Figures 3-46 and 3-47. Groups of decision and operation symbols enclosed by the chain-dotted boundaries pertain to  $0^\circ/360^\circ$

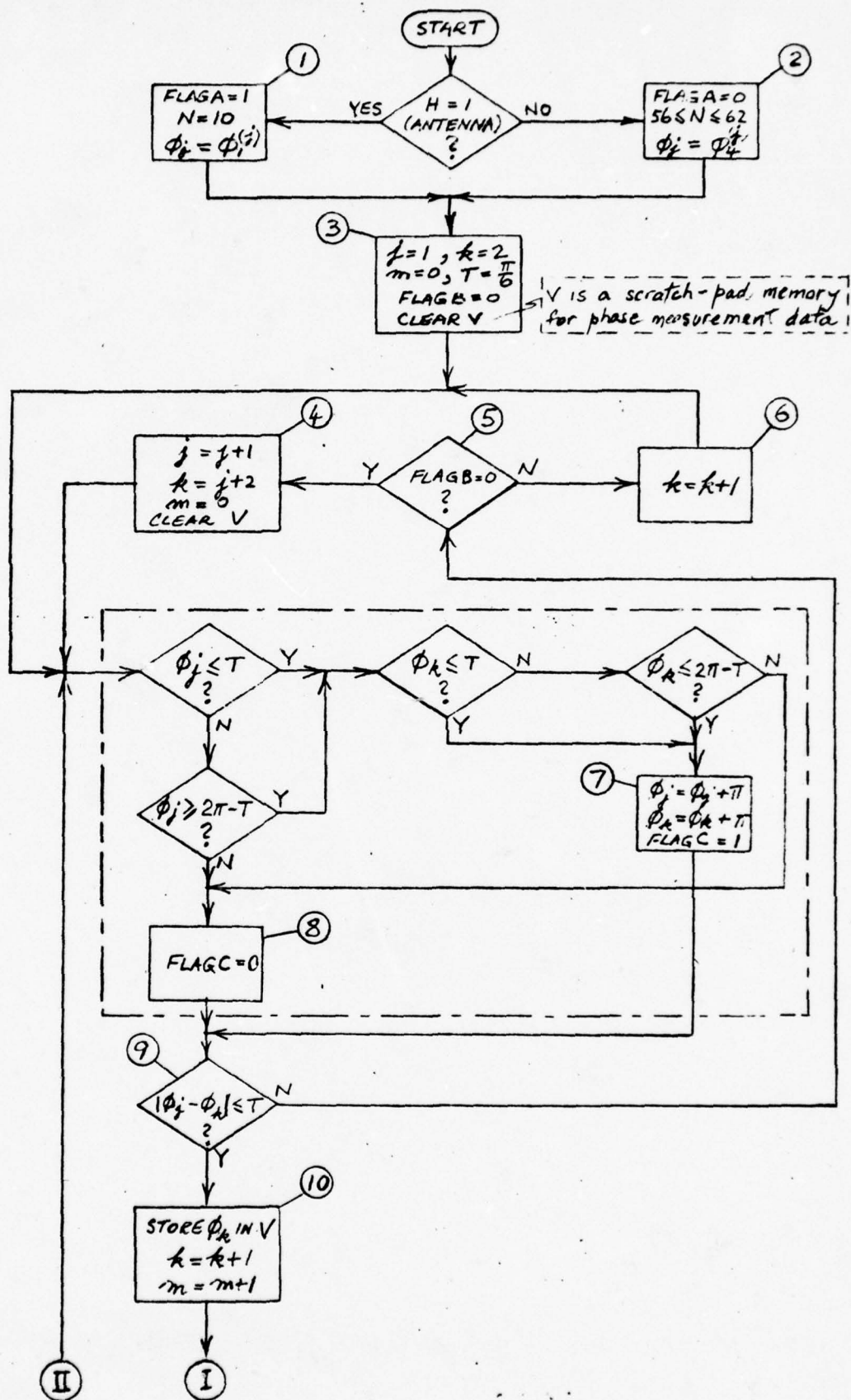


FIG. 3-46.  $\phi$ -Meast. Data Processing. Part 1.

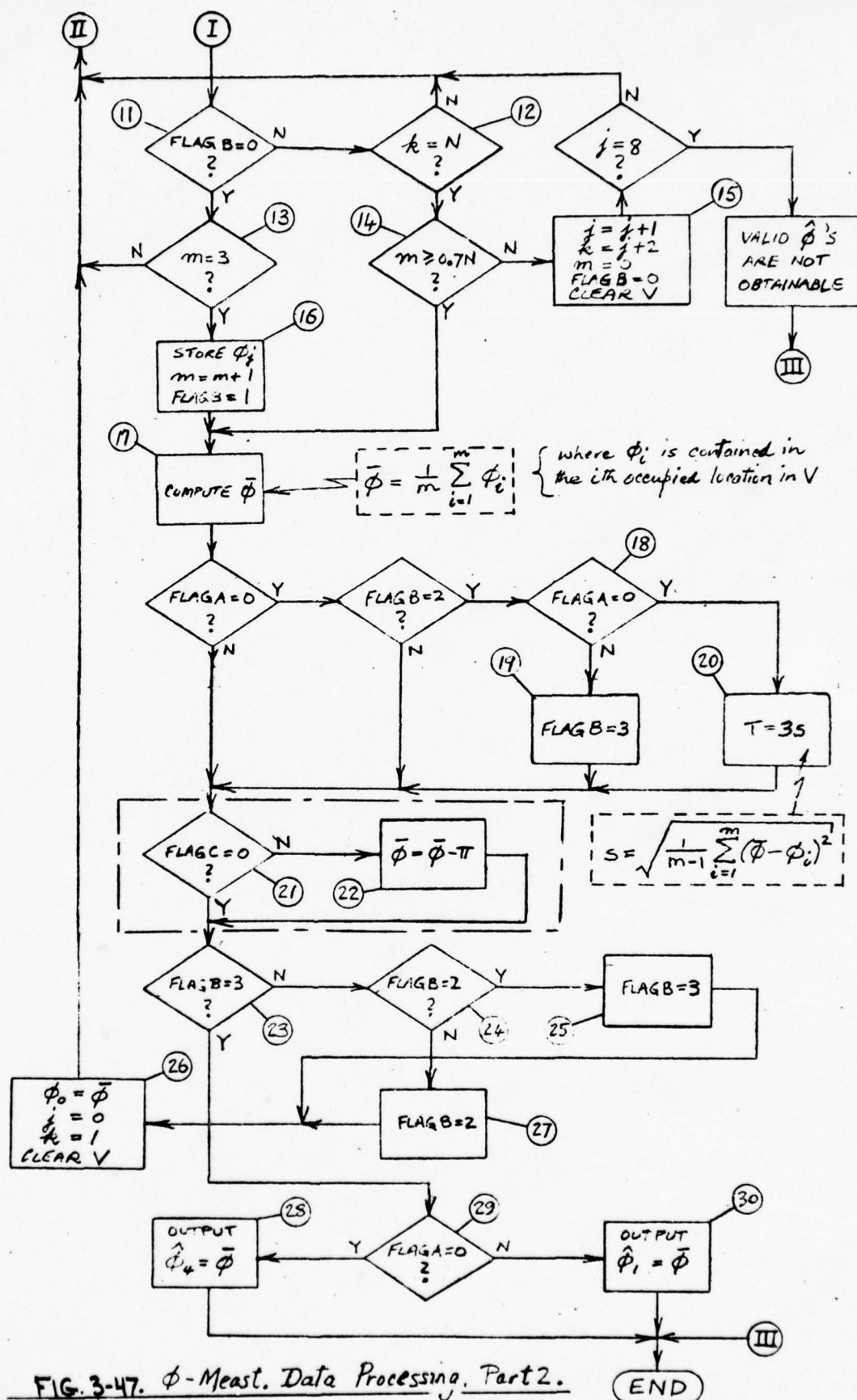


FIG. 3-47.  $\phi$ -Meas. Data Processing, Part 2.

discontinuity management and are bypassed in the initial descriptive matter and discussed subsequently.

The algorithm has two modes of operation: one for the data acquired with the  $H = 1$  antenna (FLAG A = 1 in flowchart symbol #1, Figure 3-46) and the other for the  $H = 4$  antenna (FLAG A = 0 in #2, Figure 3-46). While the latter mode is the more involved one, it employs most of the logic associated with the former. In either mode the first phase measurement  $\theta_1$  originating from a given antenna is selected (#3 in Figure 3-46) as a preliminary screening reference against which the three succeeding measurements are compared and stored (#9 and #10 in Figure 3-46, and #11 and #13 in Figure 3-47) in conjunction with  $\theta_1$  (#16 in Figure 3-47) provided all four measurements occur within a sector of  $\pi/3$  radians, i.e.,  $T = \pm\pi/6$  (#3 in Figure 3-46) about  $\theta_1$ . If this threshold criterion is not satisfied (#9 in Figure 3-46) the reference phase measurement is advanced one position (#4 and #5 in Figure 3-46), and the screening process is reiterated until the criterion is met.

At this juncture the average value  $\bar{\theta}$  of the four accepted measurements is computed (#17 in Figure 3-46) for provisional use on FLAG B = 2 (#27 in Figure 3-47) as a final refined screening reference for all 10  $H = 1$  measurements, and as an intermediate reference for all 62  $H = 4$  measurements. This second screening cycle normally flows via #26 in Figure 3-47, #9 and #10 in Figure 3-46, and #12 and #14 in Figure 3-47; and is followed by a new computation of  $\bar{\theta}$  (#17 Figure 3-47). If outliers beyond the  $\pm T$  limits are encountered in the second screening cycle they are rejected by #9 in Figure 3-46. The process is then resumed via #6 in Figure 3-46, and accepted measurements are counted by the index  $m$  (#10 in Figure 3-46). Excessive rejection of data, as denoted by  $m <$  for  $H = 4$ , following completion of the second cycle (#12 in Figure 3-47), is assumed to indicate selection of an invalid screening reference; whereupon the complete process is reinitiated by #11 in Figure 3-47 which in effect, replaces #3 in Figure 3-46 and selects a new preliminary



screening reference measurement. In the absence of such a rejection condition, and assuming control had selected the  $H = 1$  antenna (FLAG A = 1), the value of  $\bar{\theta}$  computed at this stage is outputted as  $\theta_1$  via the decisions and operations of #18, #19, #23, #29, and #30 in Figure 3-47.

If the  $H = 4$  antenna has been selected (FLAG A = 0) a refinement of the threshold T is computed (#20 in Figure 3-47) during the second cycle in terms of 3 times the unbiased estimate of the standard deviation of the M selected measurements. Since operations #19 and #20 are mutually exclusive, the screening process enters a third cycle (via #23, #24, #25 and #26 in Figure 3-47) in which the computed T is the screening threshold. The ensuing third computation of  $\bar{\theta}$  (#17 in Figure 3-47) then becomes the desired "best" estimate  $\theta_4$  of the phase displacement produced in the  $H = 4$  antenna, which estimate is outputted by the action of #23, #29, and #28 of Figure 3-47.

Flowchart symbols relating to correction of  $0^\circ/360^\circ$  discontinuities are contained within the chain-dotted outlines of Figures 3-46 and 3-47. Both the reference measurement  $\theta_j$  and the measurement under test  $\theta_k$  are examined (Figure 3-46) to determine whether they lie within limits of  $\pm T$  radians about zero phase angle. If so, both are augmented by  $\pi$  radians and the assignment FLAG C = 1 is made (#7 in Figure 3-46). If one or the other, or both, do not lie within  $\pm T$ , no action is taken and FLAG C = 0 (#8 in Figure 3-46) is assigned. Subsequent processing of  $\bar{\theta}$  under conditions of  $\pi$  augmentation requires subtraction of  $\pi$  at a suitable point in the flow as indicated by #21 and #22 in Figure 3-47.

Reduction of memory requirements of the processor employed for the algorithm may be realized by eliminating storage of  $\theta_j$  (#16 in Figure 3-47) and the  $\theta_k$  (#10 in Figure 3-45), which is permitted when computing  $\bar{\theta}$  (#17 in Figure 3-47) and s (#20 in Figure 3-47), by use of the following recursion formulas:

$$\bar{\theta} = \frac{1}{r} [(r-1)\bar{\theta}_{r-1} + \theta_r]$$

$$s_r = \sqrt{\left(\frac{r}{r-1} s_{r-1}^2 + \frac{1}{r} (\bar{\theta}_{r-1} - \theta_r)^2\right)}$$

in which  $r = 2, 3, \dots, m$

and where:

$$\bar{\theta}_m = \bar{\theta} \text{ in \#17}$$

with

$$\bar{\theta}_1 = \theta_j \text{ in \#16}$$

Note that the  $\theta_r$  comprise the sequence of accepted  $\theta_k$  which would be otherwise stored as in #10.

Also

$$s_m = s \text{ in \#20}$$

$$s_1 = 0$$

#### 3.4.1.3 Comments on Algorithm Requirements

The program constants in #1, #2, #13, #14, and #20 should be regarded as provisional and subject to revision as a result of possible design changes following the conclusion of any tests that may be undertaken. Flexibility of program modification in this respect is essential.

The algorithm shall not be activated unless external control logic determines that 10 measurements of  $\theta_1$ , and from 56 to 62 measurements of  $\theta_4$  are available for processing by the algorithm.

#### 3.4.1.4 $\bar{\theta}$ Computation in Block #17

The wild data rejection algorithm finds an initial estimate of the correct phase angle  $\theta$  from the mean  $\bar{\theta}$  of the first encountered succession of four ( $m + 1$ , and  $m = 3$  in #16 and 13, respectively) phase measurements  $\theta_j$ ,  $\theta_{j+1}$ ,  $\theta_{j+2}$ , and  $\theta_{j+3}$ , such that, in general terms

$$|\theta_{j+k} - \theta_j| < T, (k = 1, 2, \dots s) \quad (3.4-1)$$

i.e., each  $\theta_{j+k}$  must fall within  $\pm T$  radians of  $\theta_j$ .

We then ask: What is the probability ( $p_f$ ) that, owing to wild data, a succession of  $s$  data points complying with inequality (3.4-1) is not found among  $r$  ( $n \geq s$ ) independent measurements of  $\theta$ ? Note that  $s = 4$  and  $n = 10$  in the algorithm.

Let the probability that  $\theta_j$  is a valid (i.e. not "wild") measurement =  $p_v$ , and select the magnitude of the acceptance arc  $2T$  such that other valid measurements fall within limits  $\theta_j + T$  and  $\theta_j - T$  with probability very closely approaching unity.

Assume "wild" measurements are uniformly distributed over  $2\pi$  radians

$$\text{Now } P_r(\text{wild measurement}) = p_w = 1 - p_v \quad (3.4-2)$$

Write:

$A_k$  is the event that  $\theta_{j+k}$  is accepted

$B$  is the event that  $\theta_j$  is valid, i.e.,  $P(B) = p_v$

$W$  is the event that a wild measurement is accepted

$$\text{Then: } P(W) = p_w \frac{T}{\pi} \quad (3.4-3)$$

$$\text{and } P(A_k | B) = p_v + p_w \frac{T}{\pi} \quad (3.4-4)$$

From 3.4-3 and 3.4-4:

$$P(A_k | B) = 1 - p_w \left(1 - \frac{T}{\pi}\right) \quad (3.4-5)$$

Hence the joint probability:

$$\begin{aligned} P(A_k, B) &= P(A_k | B) P(B) \\ &= \left[1 - p_w \left(1 - \frac{T}{\pi}\right)\right] (1 - p_w) \end{aligned} \quad (3.4-6)$$

If  $p_w \ll 1$  we may write

$$p_1 = P(A_k, B) \cong [1 - p_w (2 - \frac{T}{\pi})] \quad (3.4-7)$$

Evidently, since the  $A_R$  are independent the probability that all  $s-1$   $\theta_{j+k}$  measurements are accepted, jointly with the condition that  $\theta_j$  is valid, is given by:

$$p_2 = p_1^{s-1} \quad (3.4-8)$$

From 3.4-7 and 3.4-8

$$p_2 \cong [1 - p_w (s-1) (2 - \frac{T}{\pi})] \quad (3.4-9)$$

Thus the probability,  $p_3$ , that a trial denoted by the sequence of  $s$  measurements does not satisfy 3.4-1 while  $\theta_j$  is valid, is given by the complement of  $p_2$ , or:

$$p_3 \cong p_w (s-1) (2 - \frac{T}{\pi}) \quad (3.4-10)$$

Assuming that wild bearings are almost certainly due to undetected fruit, and addressing worst case fruit interference in the FAA 1982 LA Basin standard traffic model (snapshot #3),  $p_w$  will correspond to  $p = 0.026$  as estimated in Section 3.5.2.4. Whence, with  $s = 4$ , and selecting  $T = \frac{\pi}{6}$ :

$$\begin{aligned} p_3 (\text{max}) &\cong 0.026 \times 3 (2 - \frac{1}{6}) \\ &\cong 0.143 \end{aligned}$$

Now with  $n = 10$ , as in the algorithm (#1 in Figure 3-46), 6 trials to obtain an initial  $\bar{\theta}$  can be made before all ten measurements are exhausted. And since the result of any



trial is independent of those preceding it, the probability of not computing  $\bar{\theta}$  is  $p_f = (0.143)^s = 8.6 \times 10^{-6}$  even under worst case circumstances.

With:  $s = 5, p_f = 252 \times 10^{-6}$

or with:  $s = 6, p_f = 3,230 \times 10^{-6}$

so that, although the estimator  $\bar{\theta}$  is improved slightly by averaging a larger number of measurements than 4, the price paid in increased risk if not computing  $\bar{\theta}$  becomes rapidly unacceptable. An offsetting option is then to increase  $n$  beyond 10, but this measure imposes added cost for data storage and longer processing time.

#### 3.4.2 Miss Distance and Horizontal Bearing Data Processing

In this section, a computational procedure is provided for the determination of horizontal bearing angle and of the horizontal component of projected miss distance. These quantities are obtained from sequential measurements of range, bearing and altitude difference; the bearing measurement being that defined in the aircraft wing plane. A detailed derivation of the equations is presented in Appendix L.

##### Nomenclature

$\Delta h(t_1) = h_B - h_s$  = altitude difference with respect to own altitude; (feet)

$\beta(t_1)$  = bearing angle; angle in antenna ground plane from aircraft longitudinal axis to projection of range line; measured positive clockwise

$R(t_1)$  = range, own aircraft to intruder aircraft; (feet)

$\psi(t_1)$  = yaw angle, at time  $t_1$

$P(t_1)$  = pitch angle, at time  $t_1$

$r(t_1)$  = roll angle, at time  $t_1$

$E(t_1)$  = elevation angle of range line, determined in vertical plane

$\epsilon(t_1)$  = elevation angle of range line, in plane containing range line and normal to antenna ground plane

$\delta_{12}$  = angle between range lines at times  $t_1$  and  $t_2$

$V_r$  = magnitude of relative velocity vector; (f.p.s.)

$\gamma_v$  = path angle of  $\bar{V}_r$

$M$  = miss distance; shortest range to intruder; (feet)

$M_H$  = horizontal component of  $\bar{M}$ ; (feet)

$M_v$  = vertical component of  $\bar{M}$ ; (feet)

$\Delta t_{12} = t_2 - t_1$ , estimation time interval; (sec's.)

$t_1$  = time at which  $\beta_1$  is estimated (mid point of track pulse sequence);  $i = 1, 2$

$\delta_{12H}$  = angle between horizontal projections of  $R_1$  and  $R_2$

$\theta_s$  = angle between horizontal projections of range line and aircraft longitudinal axis

Computational Sequence:

Inputs  $\Delta h, \Delta h_2; \beta_1, \beta_2; R_1, R_2$   
 $\psi_1, \psi_2; P_1, P_2; r_1, r_2; \Delta t_{12}$

1) Find  $\sin E_1, \sin E_2$ :

$$\sin E_1 = \left( \frac{\Delta h_1}{R_1} \right)$$

$$\sin E_2 = \left( \frac{\Delta h_2}{R_2} \right)$$

2) Find  $\epsilon_1, \epsilon_2$ :

$$\theta_1 = \tan^{-1} [P_1^r \cos \beta_1 - r_1^r \sin \beta_1]; 0 \leq |\theta_1| \leq 90^\circ$$

$$\epsilon_1 = \sin^{-1} [\sin E_1 \cos \theta_1] - \theta_1; 0 \leq |\epsilon_1| \leq 90^\circ$$

$$\theta_2 = \tan^{-1} [P_2^r \cos \beta_2 - r_2^r \sin \beta_2]; 0 \leq |\theta_2| \leq 90^\circ$$

$$\epsilon_2 = \sin^{-1} [\sin E_2 \cos \theta_2] - \theta_2; 0 \leq |\epsilon_2| \leq 90^\circ$$

3) Find  $\cos \delta_{12}, \sin \delta_{12}$ :

$$\cos \delta_{12} = \cos \epsilon_1 \cos \epsilon_2 \cos (\beta_2 - \beta_1) + \sin \epsilon_1 \sin \epsilon_2$$

$$- (\psi_2 - \psi_1)^r \cos \epsilon_1 \cos \epsilon_2 \sin (\beta_2 - \beta_1)$$

$$+ (P_2 - P_1)^r [\sin \epsilon_1 \cos \epsilon_2 \cos \beta_2 - \sin \epsilon_2 \cos \epsilon_1 \cos \beta_1]$$

$$+ (r_2 - r_1)^r [\sin \epsilon_2 \cos \epsilon_1 \sin \beta_1 - \sin \epsilon_1 \cos \epsilon_2 \sin \beta_2]$$

$$\sin \delta_{12} = \sqrt{1 - \cos^2 \delta_{12}}$$

4) Find  $\delta_{12H}, \theta_{s1}, \theta_{s2}$ :

$$\theta_{s1} = \tan^{-1} \left[ \frac{\sin \beta_1 \cos \epsilon_1 + r_1^r \sin \epsilon_1}{\cos \beta_1 \cos \epsilon_1 - P_1^r \sin \epsilon_1} \right]$$

$$\theta_{s2} = \tan^{-1} \left[ \frac{\sin \beta_2 \cos \epsilon_2 + r_2^r \sin \epsilon_2}{\cos \beta_2 \cos \epsilon_2 - P_2^r \sin \epsilon_2} \right]$$

quadrants from num. and den. signs

$$\delta_{12H} = (\psi_2 - \psi_1) + (\theta_{s2} - \theta_{s1})$$

5) Find  $V_r \Delta t_{12}$ :

$$V_r \Delta t_{12} = \sqrt{R_1^2 + R_2^2 - 2 R_1 R_2 \cos \delta_{12}}$$

6) Find M:

$$M = \frac{R_1 R_2 \sin \delta_{12}}{V_r \Delta t_{12}}$$

7) Find  $\sin \gamma_v$ :

$$\sin \gamma_v = \frac{(\Delta h_2 - \Delta h_1)}{V_r \Delta t_{12}}$$

8) Find  $M_v$ :

$$M_v = \Delta h_2 + \sqrt{R_2^2 - M^2} \sin \gamma_v$$

9) Find  $M_H$ :

$$M_H = \pm \sqrt{M^2 - M_v^2}$$

Take sign of  $\delta_{12H}$

10) Find  $V_r$ :

$$V_r = \frac{(V_r \Delta t_{12})}{\Delta t_{12}}$$



11) Find  $M_T$ :

$$\text{At } \tau_2 \text{ Alarm: } M_{T2} = 11,200 + 4.73 V_r$$

$$\text{At } \tau_1 \text{ Alarm: } M_{T1} = 1700 + 4.14 V_r, \text{ for } M_{T1} > 3038 \text{ ft.}$$

$$= 3038, \text{ if } M_{T1} < 3038$$

NOTE: Superscript  $r$ , on angular quantities, means that the angle is to be inputted in radians.

### 3.5 ACCURACY ANALYSIS (TASK 2.4)

This section reports on the results of the theoretical analyses undertaken in Task 2.4 to provide predictions of system measurement accuracies in relative bearing and swept bearing.

The analysis deals quantitatively with random and systematic errors attributable to eleven contributing sources, and shows how the errors may be combined to give overall estimates. Thus, postulating acceptable physical conditions for bounding the predominant random error due to local multipath, it is found that the overall (random and bias) relative bearing error prediction is approximately one degree, one sigma. Four of the error sources contribute 90% of the overall error; and as few as two, namely multipath and antenna imperfections, contribute 70%. A maximum random error of 0.8 degree one sigma is predicted for swept bearing measurements, with local multipath accounting for over 70% of the error.

Section 3.5.1 provides a summary of the individual error allocations. Each is briefly discussed with regard to sources of random and systematic components and a reference is made to the section of the report where a more detailed analysis is given. This section

also provides the rationale for computing the predicted overall error in relative bearing measurement, and a discussion of possible further improvement of accuracy with calibration of the antenna. Section 3.5.2 is devoted to detailed analyses of the three most significant sources of error in the measurement of relative bearing and swept bearing; namely, local multipath, aircraft attitude effects, and fruit interference in dense traffic environments.

### 3.5.1 Error Allocations

#### 3.5.1.1 Estimates of Error Contributions

Table 3-3 summarizes estimates of system random and bias errors stemming from anomalous effects which were investigated in the configuration analyses of the H = 4 ring array antenna. An analysis of the errors associated with the antenna configuration is provided in Section 3.2 and of candidate signal processing techniques in Section 3.3. Additional error estimates are derived from the error analysis (Section 3.5.2) and from considerations advanced in this section. The Table presents individual estimates of random and bias (systematic) errors in relative bearing, and of the swept bearing errors. Assuming stationarity, the latter errors are  $\sqrt{2}$  times the random errors of corresponding relative bearing error components; since taking the difference of two successive relative bearings to obtain the incremental, (i.e., swept bearing) eliminates the bias component. However, the bias component of the multipath error is not stationary between relative bearing measurements taken several seconds apart. Hence the swept bearing error contributed by multipath must be estimated by  $\sqrt{2}$  times the rss of the random and bias components.

The error contributor items in the first column of Table 3-3 are discussed below.

#### Item 1 - Propagation

Tropospheric propagation errors encountered when measuring azimuth in the microwave spectrum have not been previously discussed because of their negligible influence in

TABLE 3-3. ERROR ANALYSIS RESULTS

| ITEM | ERROR CONTRIBUTING CAUSE                   | RELATIVE BEARING ERROR (degs.)                  |             | SWEPT BEARING ERROR (degs.1σ) | RELATED REPORT SECTIONS  |
|------|--|---|-------------|-------------------------------|--------------------------|
|      |  | RANDOM (1σ)                                     | BIAS LIMITS |                               |                          |
| 1    | Propagation                                | 0.005   | ± 0.1       | 0.007                         | 3.1.1                    |
| 2    | Attitude Variations                        | 0.15  | 0           | 0.21                          | 3.3.3, 3.5.2.4           |
| 3    | Fruit Interference                         | 0.20  | 0           | 0.28                          | 3.5.2.3                  |
| 4    | H=4 Ring Array Imperfections               |   |             |                               | 3.2,4.5                  |
|      | (a) Non-linearity                          | 0   | ± 0.5       | 0                             |                          |
|      | (b) Elevation anomalies                    | 0   | ± 0.5       | 0                             |                          |
|      | (c) Reproducibility                        | 0   | ± 1.0       | 0                             |                          |
|      | (d) Boresighting                           | 0   | ± 0.1       | 0                             |                          |
| 5    | Thermal Noise                              | 0.23  | 0           | 0.32                          | 3.3.7                    |
| 6    | Phase Comparator Resolution                | 0.017   | 0           | 0.02                          |                          |
| 7    | Phase Transients                           | 0.022   | ± 0.03      | 0.03                          | 3.3.9                    |
| 8    | Phamp                                      | 0   | ± 0.13      | 0                             | 3.3.10                   |
| 9    | Interchannel Phase & Delay Imbalances      | 0.20  | ± 0.5       | 0.28                          | 3.3.11.1, 3.3.11.2       |
| 10   | Quantization Noise                         | 0.026   | 0           | 0.037                         | Table 3.1-1              |
| 11   | Local Multipath                            | 0.28  | ± .29       | 0.57                          | 2.3, 3.3.1, 3.2, 3.5.2.1 |
| 12   | Total Random Error (1σ)                    | 0.485   | —           | 0.8                           |                          |
| 13   | Est. Std. Deviation of A Priori Bias Error | —   | 0.79        |                               |                          |
| 14   | Est. of Overall Error In Relative Bearing  | $(.485^2 + .79^2)^{1/2} = 0.93^\circ (1\sigma)$ |             |                               |                          |

respect to accuracy requirements indicated by the present study. The error magnitudes shown are for worst case environmental conditions, but with the benefit of integration applied to the random error component. Barton's (16) treatment of the subject has been followed to provide the essential data on propagation errors.

#### Item 2 - Attitude Variations

An analysis of relative bearing measurement errors due to unintentional short term departures of the measuring aircraft from a rectilinear flight path appears in Section 3.5.2.4, where the ARINC specification no. 417 for autopilots is invoked to estimate residual variations of yaw, pitch and roll remaining after corrective action. The analysis shows that these uncompensated attitude variations cause errors in bearing measurement amounting to  $0.125^\circ$  ( $1\sigma$ ) by yaw, and  $0.06^\circ$  ( $1\sigma$ ) individually and independently by pitch and roll. Hence the combined relative bearing error due to attitude variations is  $\sqrt{0.125^2 + 0.06^2 + 0.06^2} = 0.15^\circ$  ( $1\sigma$ ) which appears in Table 3-3. Drift errors, which would introduce bias errors in the measurement of true bearing, for example, do not effect the measurement of relative bearing. Consequently the relative bearing bias error is zero.

#### Item 3 - Fruit Interference

The random error given in the table pertains to a CAS equipped aircraft exposed to fruit in the densest traffic region of the FAA/MITRE 1982 LA Basin Standard Traffic Model (Snapshot #3). A uniform random distribution of fruit in azimuth is assumed, and the effect of wild data rejection is operative in phase measurement data processing. In view of the linear response of the phase measuring system to bearing magnitude, no bias error can arise from fruit interference.

#### Item 4 - H = 4 Ring Array Imperfections

Laboratory measurements (Section 3.2) undertaken with the experimental H = 4 ring array antenna at an elevation of  $15^\circ$  above the ground plane, gave azimuth readings



which exhibited gradual departures of up to  $\pm 1^\circ$ , maximum, from the rotational angle applied to the test turntable. Approximately half of this nonlinearity is attributable to anomalies in the microstrip antenna hybrid junctions. The anomalies are mechanical and would be eliminated in production versions of the antenna. The residual nonlinearity of  $\pm 0.5^\circ$ , maximum, is cyclic in azimuth and changes by an insignificant amount over azimuthal increments corresponding to typical swept bearing values. Hence nonlinearity introduces a bias which is to be accounted for only in respect to its influence on the accuracy of relative bearing measurement. Nonlinearity in the  $H = 1$  antenna is of no concern when it is used in conjunction with the  $H = 4$  antenna, because the errors are not significant in respect to data processing whereby quadrant ambiguity of the  $H = 4$  antenna is resolved.

An additional bias error allocation is necessary to account for variation of evaluation angle from the antenna ground plane up to, say,  $45^\circ$ . It is expected that by optimizing the antenna design, and effecting phase measurements between two modes of opposite polarity available with a single array, the bias error associated with elevation angle change can be held to limits of  $\pm 0.5^\circ$ .

By virtue of extensive experience in the manufacture of a wide variety of microwave antenna types, RCA's antenna skill center conservatively estimates that reproducibility of the multimode ring array antenna could be such that differences between bearing performance characteristics of production versions would be contained within a range of  $2^\circ$ . Accordingly, a bias error of  $\pm 1.0^\circ$ , maximum, has been included in Table 3-3 to allow for the effect of dimensional and electrical tolerances.

A further bias error component of  $\pm 0.1^\circ$  is shown to account for boresighting the electrical axis of the antenna in parallelism with the longitudinal axis of the aircraft. Bore-sighting to this order of precision can be conveniently achieved without resorting to elaborate methods demanded in mechanically aligning airborne weapons with high accuracy.

#### Item 5 - Thermal Noise

The estimate given in Table 3-3 for the random relative bearing error due to thermal noise applies for a target range of 8 nmi which is the maximum hazard range corresponding to initiation of a Tau 2 alert (12) at a closing speed of 550 knots. At this range, and for a bandwidth of 6 MHz, the signal-to-noise ratio is taken as 18 db, i.e., approximately 63 to 1.

A basis for the estimate is given by the variance equation of Figure 3-2 as reproduced from (5). The upper schematic of Figure 3-2 is applicable because the zero axis cross-over phase comparator has been selected in the present study. Since it is reasonable to assume that the signal-to-noise ratios would be the same for both channels of the receiver we can write  $(S/N)_1 = (S/N)_2 = S/N$ , whereby the standard deviation of the thermal noise error for the zero crossover method simplifies to  $\sqrt{1/(S/N)}$  radians. The numerical value of the error (as entered in Table 3-3 ) is:

$$\begin{aligned}\epsilon_N &= \sqrt{\frac{1}{63}} \times \sqrt{\frac{1}{62}} \times \frac{1}{4} \times \frac{180}{\pi} \\ &= 0.23^\circ \text{ one sigma} \quad .\end{aligned}$$

The first factor used in the above calculation involves the signal-to-noise ratio, the second the 62 pulse integration advantage, and the third the error reduction effect of the H = 4 ring array antenna.

#### Item 6 - Phase Comparator Resolution

The phase comparator configuration described in Section 5.3 will permit phase measurements to be made with a resolution which contributes only about a 0.02 degree, one sigma, random component to the measurement error. This low error is realized by employing a 100 MHz clock combined with a 1 to 10 ramp vernier to time the interval between successive zero crossovers detected by the comparator, thus providing a resolution of 1

nanosecond. Correspondingly, at the planned IF of 3.5 MHz, the phase angle resolution is  $360 \times 3.5 \times 10^6 \times 10^{-9} = 1.26^\circ$ .

Clearly, the error caused by the discrete sampling of the time interval has a uniform distribution so that its standard deviation is  $1.26/2\sqrt{3} = 0.36^\circ$ . Furthermore, the combination of 62 point integration and  $H = 4$  antenna phase magnification results in an additional reduction of the error to  $0.36/(4\sqrt{62}) = 0.012^\circ$  one sigma. However, two crossovers contribute to the overall error effect of finite resolution, which is thus  $0.012 \times \sqrt{2} = 0.017^\circ$  one sigma.

Bias errors occurring at the two crossovers are equal and of the same sign. They cancel as a result of the subtraction involved in obtaining the phase measurement.

#### Item 7 - Phase Transients

Worst case random and bias errors due to phase variations in the pulse responses of receiver IF's, were estimated as follows:

Figure 3-44 shows that for a damping factor of 0.1, and at  $\Delta T = 0.25$  microseconds, viz. the earliest instant at which phase measurements would be enabled, the maximum phase transient per channel is  $1.2^\circ$  approximately. Since we are concerned with the phase difference between two channels, the maximum transient departure is  $2.4^\circ$ . Now assuming the actual departure has a uniform density function, its standard deviation is  $2.4/(2\sqrt{3}) = 0.69^\circ$ . As a result of 62 pulse integration and 4X phase amplification by the  $H = 4$  antenna, the random error in relative bearing contribution is reduced to  $0.69/(4\sqrt{62}) = 0.022^\circ$  one sigma.

Figure 3-45 indicates a maximum bias error of  $0.3^\circ$  at  $\Delta T = 0.25$  microseconds when the filter damping factor is 0.1. Using the arbitrary reduction factor of 40% as suggested in Section 3.3.9, the net maximum bias error between a pair of channels is  $0.3 \times 0.4 = 0.12^\circ$ . Finally, the  $H = 4$  antenna causes a further reduction of 4 to 1 leaving a residual bias of  $0.03^\circ$ .

#### Item 8 - Phamp

A design choice (Section 5.2) of 3.5 MHz for the second IF in the receiver phase channels is much lower than that of the VECAS receiver. Consequently the severity of amplifier phase shift as a function of signal level is considerably mitigated, and there should be no difficulty of operating within the design goal of  $0.13^\circ$  (Section 3.3.10) for the bias error due to the effect when the  $H = 4$  antenna is being utilized.

#### Item 9 - Interchannel Phase and Delay Imbalances

By using automatic, built-in means for periodically sensing the correcting any gradual degeneration of phase equality between both channels of the dual channel receiver, no difficulty should be encountered in limiting phase drifts of one channel with respect to the other to  $\pm 2^\circ$ . Reflected into relative bearing measured with the  $H = 4$  antenna, the limiting phase departure translates into a bipolar bias error of  $0.5^\circ$  maximum.

Regarding the random error component caused by frequency hopping in the presence of incidental phase delay unbalance, the discussion of the effect in Section 3.3.11.2 is pertinent. It assures that, with the phase amplification provided by the  $H = 4$  antenna and the additional advantage of data integration by 62 pulses, the error can be limited in practice to a maximum of 0.2 degree one sigma.

#### Item 10 - Quantization Noise

An estimate of the error to be expected from digital encoding of the relative bearing data is simply calculated on the basis of a uniform density function for the encoding instant. Thus, using a twelve bit word to represent the full  $360^\circ$  range of relative bearing, the standard deviation of the random quantization error incurred when measuring relative bearing is:

$$\begin{aligned}\sigma_1 (B) &= \frac{360}{4096} \times \frac{1}{2\sqrt{3}} \\ &= 0.0254^\circ\end{aligned}$$



Quantization of the phase measurement data prior to bearing determination is specified by means of a 9 bit word for the full 360° range of phase angle. But owing to the ameliorative effect of integration combined with the phase amplification of the H = 4 ring array antenna the associated relative bearing error has a standard deviation of only:

$$\begin{aligned}\sigma_2(B) &= \frac{360}{512} \times \frac{1}{2\sqrt{3}} \times \frac{1}{\sqrt{62}} = \frac{1}{4} \\ &= 0.0032^\circ\end{aligned}$$

Hence the combined quantization error may be estimated by

$$\sqrt{0.0254^2 + 0.0032^2} = 0.0256^\circ$$

#### Item 11 - Local Multipath

The error caused by multipath will depend on the geometry of the reflecting surface relative to the transmitter and to the receiving antenna array. Because this geometry varies with installation conditions, the multipath error component of the overall error will be a variable. A more practical approach to error analysis is to bound this error component to a value which permits the overall error to meet its required value of 0.8° one sigma. The geometry limitations applicable to the boundary value, if practical and realizable, can then be specified.

When considering the multipath geometry affecting a forward, top mounted DF antenna on an aircraft in the Boeing 707 class, for example, no reflecting surface other than the fuselage on which the antenna is mounted can be within closer line-of-sight proximity than 150 inches, assuming that other antennas are mounted outside this range. Now, following the analysis of Section 3.5.2.1.5; and in particular, referring to the graph of Figure 3-70b for the frequency set B; it is seen that the swept bearing error, caused

by a reflector having a reflection coefficient of about 0.05 and separated from the antenna by 150 inches, is  $0.57^\circ$  one sigma. Furthermore, the error first diminishes at greater separations, goes through a minimum of  $0.1^\circ$  one sigma, and at a separation of 730 inches reaches a value of  $0.57^\circ$  again. The latter error magnitude is important because the root-sum-square of it and all other swept bearing error contributions (Items 1, 2, 3, 5, 6, 7, 9 and 10) is an overall error of  $0.8^\circ$  one sigma which is a magnitude found acceptable by the conclusions of Section 2.3.4 concerning the reduction of unnecessary pilot alarms. The  $0.57^\circ$  error magnitude is, therefore, entered for Item 11 as an allocated error.

An analysis (Appendix L) of an antenna pattern for a top mounted monopole on a Boeing 707 indicates that, except for the vertical stabilizer, no major reflecting surface which is exposed to the antenna possesses a reflection coefficient significantly in excess of 0.05. Hence it is reasonable to expect that an optimal location can be found for the top antenna, in the sense that no reflector in a range of 150 to 730 inches from the antenna will produce a multipath error greater than  $0.57^\circ$  one sigma. This conclusion would be reinforced if the effect of the evidently worst offender, namely the vertical stabilizer, were minimized by locating the antenna about 40 ft. from it so as to derive the fullest error reduction (approximately 5 to 1) indicated at the trough of the curve in Figure 3-70b for frequency set B.

#### 3.5.1.2 Estimate of Overall Error in Relative Bearing

In view of the large measurement sample size of up to 62 points and of the Central Limit Theorem, the total random error (Item 12 of Table 3-3) in relative bearing, representing the root-sum-squared value of contributing Items 1 through 11, will approach a normal distribution even when the probability density functions of the several individual error contributors are markedly non-normal. The standard deviation of the total random error is  $0.485^\circ$ .

In the case of bias (or systematic) errors  $b_1, b_2, \dots, b_n$ , only the positive and negative limits  $+B_1, +B_2, \dots, +B_n$  between which each  $b_i$  can lie are predictable since no

before the fact knowledge (as from calibration data on a particular system) of their actual individual or total ( $b_T = \sum_{i=1}^n b_i$ ) values is available. Hence, for the purpose of characterizing the a priori distribution of  $b_T$ , it is legitimate to treat the  $b_i$  as random variables. Furthermore, there is reason to believe that each  $b_i$  assumes any value between the limits  $\pm B_i$  with equal probability. Accordingly, by the relationship for the standard deviation of a uniform density function:

$$\sigma(b_i) = \frac{1}{\sqrt{3}} B_i$$

and, therefore, the standard deviation of  $b_T$  is estimated by:

$$\hat{\sigma}(b_T) = \sqrt{\frac{1}{3} \sum_{i=1}^n B_i^2}$$

Using the  $B_i$  values shown in the column "BIAS (SYSTEMATIC) LIMITS" of Table 3-3 for Items 1, 4, 7, 8 and 9 the computed  $\hat{\sigma}(b_T) = 0.79^\circ$ .

Now the overall error in relative bearing can be estimated from the square root of the summed variances of the above total random error and the total a priori bias error, i.e.:

$$\begin{aligned} \epsilon_B &= \sqrt{0.485^2 + 0.79^2} \\ &= 0.93 \text{ degree one sigma} \end{aligned}$$

### 3.5.1.3 Overall Error Estimate With Calibration Corrections

Reduction of the overall error could conceivably be accomplished by means of a factory calibration of the antenna. This procedure, including the appropriate utilization of its results, would be beneficial only in respect to minimizing the rather substantial invariant bias errors stemming from antenna nonlinearity (Item 4a) and from antenna

reproducibility limitations (Item 4c). Assuming this were done and produced irreducible bias errors of the order  $\pm 0.15^\circ$  and  $\pm 0.3^\circ$ , respectively, the estimated standard deviation of the a priori bias error (Item 13) would contract to  $0.5^\circ$ , and the overall relative bearing error (Item 14) to  $0.7^\circ$ . Little benefit would accrue to the accuracy of swept bearing error from the calibration action, and so it is doubtful whether the improvement of relative bearing accuracy would be justifiable in view of the expense in acquiring the calibration data, and the complication of correcting measurements with it during in-flight data processing. Nevertheless, there remains the prospect that a production version of the antenna could be designed with preset trimming devices whereby deleterious effects of antenna imperfections would be intrinsically compensated during factory test and alignment procedures. Error reduction of the order indicated above would then be realizable without further burden on data storage and processing in the airborne equipment.

### 3.5.2 Major Error Contributors - Summary of Analyses

This section provides theoretical analyses of error sources external to the receiver equipment. Error effects from some of these sources attain no benefit from integration of pulse samples. Furthermore, these externally caused effects are not attenuated by reason of the  $H = 4$  antenna phase amplification. The error effects treated are ripple nonlinearity due to the finite number of monopoles in the  $H = 4$  mode ring array (Section 3.5.2.1.2); local multipath for the  $H = 4$  mode (Sections 3.5.2.1.3 through 3.5.2.1.5); ripple, and local multipath for the  $H = 1$  mode (Section 3.5.2.2); fruit (Section 3.5.2.3); and aircraft attitude influence (Section 3.5.2.4).

For the  $H = 4$  antenna, the deviation of phase difference measurement from linearity, with respect to bearing angle, was shown to be negligible. Using the mathematical model of a vertical plane reflector, which produces indirect EM reception at the antenna, multipath effects were investigated. By employing (random) frequency diversity, and by



taking cognizance of the variability of initial bearing and swept bearing values, the rms value of mean error in swept bearing was determined to be not more than  $.6^\circ$ , for expected values of antenna-to-reflector spacings.

The multipath error for the  $H = 1$  antenna was also explored. Using the same reflector model, at reasonably expected spacing and for the frequency set selected, the peak mean (over frequency) bearing error is  $5.6^\circ$ , of which nonlinearity (ripple) contributes a peak error of  $2.3^\circ$ . It was not considered necessary to analyze the statistical effect of the variability in bearing angle itself, for the Mode 1 analysis of multipath effect, since the peak mean error has an acceptable value for PWI operation or for the ambiguity resolution function.

Fruit signals that are not detected and discarded by the logic available in the SECANT message processing circuitry can cause the appearance of "wild" bearing data which, in general, are distributed over  $360^\circ$  in azimuth. The analysis given below permits estimates of the resulting error due to fruit, with particular reference to the densest region of the FAA/MITRE 1982 LA Basin Standard Traffic Model (Snapshot #3). An order of magnitude reduction in the error is shown to be attainable by application of the wild data rejection algorithm described in Section 3.4.1.

An analysis of the effect of the neglect of attitude angle compensation in the determination of horizontal miss (Appendix L) was made. It was ascertained that the accuracy in this determinator (and therefore the efficiency of the hazard discriminator in the reduction of false alarm probability) would be significantly impaired if compensation were not afforded. Assuming attitude angle measurements at the mid point of bearing sample set, residual attitude error sensitivity effects on horizontal miss and horizontal bearing were analyzed. Acceptable one sigma values have been selected, as a consequence of this analysis, and are  $.13^\circ$  in yaw measurement and  $.3^\circ$  in pitch or roll measurement.

### 3.5.2.1 Ripple and Multipath Errors

#### 3.5.2.1.1 Abstract and Summary

Ripple error is defined as the deviation of measured phase angle from linearity, with respect to bearing angle. This error is much reduced by utilizing more elements in the ring array and operating at higher mode. The 16-element, Mode 4 antenna is analyzed herein, and is found to produce negligible ripple error.

Derivations have been developed for the multipath interference error caused by a vertical plane reflector. In the SECANT system, the reply pulse carrier frequency varies randomly among four possible values; and 62 independent phase difference measurements are made and averaged to obtain a bearing estimate. The mean error in the average is taken as most probable value, with respect to the frequency set. It is shown that increasing the spread of the frequency diversity produces a significant improvement in the mean error, especially over the range of expected antenna-to-reflector spacings.

Considering the randomness of both initial bearing and subsequent swept bearing values, in a conflict situation, an expected value of the mean multipath error, with respect to those random variables, can be defined. It is shown that on an rms basis, the multipath error, for the proposed frequency set, is less than  $.6^\circ$ , over the expected range of antenna-to-reflector spacings.

#### 3.5.2.1.2 Ripple Error Analysis

Figure 3-48 is a representation of a ring array of 16 antenna elements mounted normal to the plane surface. Taking element 1 as reference, let the difference in path length between the advancing signal wave front impinging at element 1 and that at any other element  $j$  be denoted  $Z_{1j}$ . From Figure 3-48a

$$\begin{aligned} Z_{1j} &= d_{1j} \cos \left[ 180 - \theta - \left( 90 - \frac{\delta_{1j}}{2} \right) \right] \\ &= 2r \sin \frac{\delta_{1j}}{2} \sin \left( \theta - \frac{\delta_{1j}}{2} \right) \end{aligned} \quad (3.5-1)$$

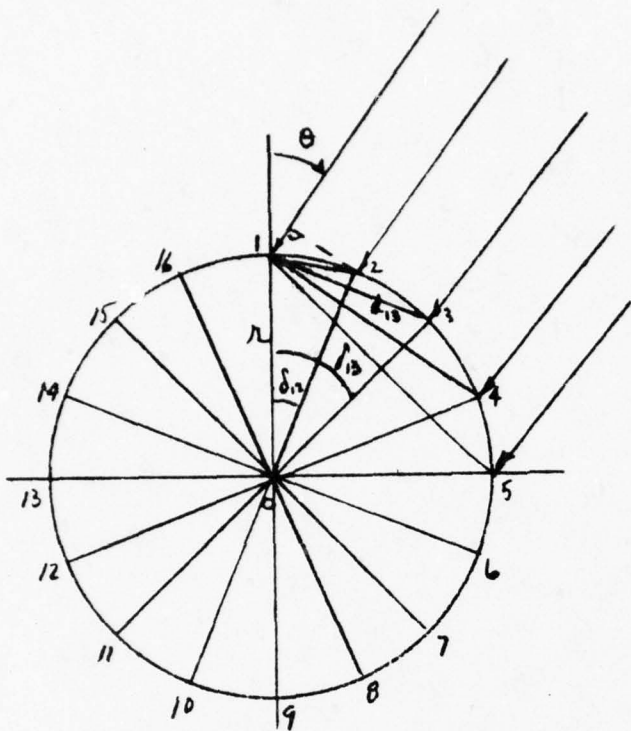


FIG 3-48a

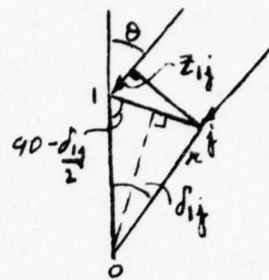


FIG. 3-48a

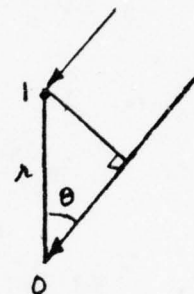
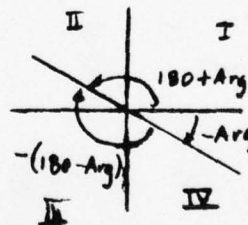
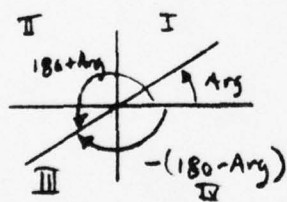


FIG. 3-48b

MODE 4 RING ARRAY  
FIG. 3-48.



$$\text{Arg} = \tan^{-1} \left[ \frac{s_1}{1+s_2} \right]$$

FIG. 3-49  
AMBIGUITY IN  $\Phi$

where

$r$  = radius of ring array

$\delta_{1j}$  = central angle, from element 1 to element  $j$

$\theta$  = bearing angle of direct signal

For  $m = 16$  elements,

$$\delta_{1j} = (j - 1) \frac{360}{m} = (j - 1) \times 22.5^\circ \quad (3.5-2)$$

$$j = 2 \text{ to } 16$$

In addition to the phase lead (or lag) due to path length difference, each  $j^{\text{th}}$  element has its signal delayed, in mode 4, by an amount

$$\frac{2\pi(j-1)}{m} \times 4 = \frac{\pi}{2} (j-1); \text{ radians}$$

Let the potential at element 1, due to the direct wave, be

$$e_1' = E_1 \cos \omega t \quad (3.5-3)$$

where  $\omega = 2\pi f$ , and  $f$  is the carrier frequency. Then the potential received at element  $j$ , after delay and transmission to a common port, is

$$\begin{aligned} e_j' &= E_1 \cos \left[ \omega t + \frac{2\pi}{\lambda} Z_{1j} - \frac{\pi}{2} (j-1) \right] \\ &= E_1 \cos [\zeta_1 + a_j + b_j] \end{aligned} \quad (3.5-4)$$



where:

$$\lambda = c/f; c = 3 \times 10^{10} \text{ cm/sec}$$

$$\zeta_1 = \omega t$$

$$a_j = \frac{2\pi r}{\lambda} [\sin \delta_{1j} \sin \theta - (1 - \cos \delta_{1j}) \cos \theta]$$

$$b_j = -\frac{\pi}{2} (j - 1)$$

The vector sum of all signals, from elements 1 through 16, is

$$\begin{aligned} e &= e_1' + \sum_{j=2}^m e_j' = E_1 [\cos \zeta_1 + \sum_{j=2}^m \cos (\zeta_1 + a_j + b_j)] \\ &= E_1 \left\{ 1 + \sum_{j=2}^{16} \cos (a_j + b_j) \right\} \cos \zeta_1 - \sin \zeta_1 \cdot \sum_{j=2}^{16} \sin (a_j + b_j) \\ &= E_1 N \cos (\Phi + \zeta_1) \end{aligned} \quad (3.5-5)$$

where:

$$N = \left\{ \left[ 1 + \sum_{j=2}^{16} \cos (a_j + b_j) \right]^2 + \left[ \sum_{j=2}^{16} \sin (a_j + b_j) \right]^2 \right\}^{1/2} \quad (3.5-6)$$

$$\Phi = \tan^{-1} \left\{ \frac{\sum_{j=2}^{16} \sin (a_j + b_j)}{1 + \sum_{j=2}^{16} \cos (a_j + b_j)} \right\} = \tan^{-1} \left[ \frac{S_1}{1 + S_3} \right] \quad (3.5-7)$$

The phase of the combined signal is compared with the received signal at the center element 0, to obtain a measure of the bearing angle. From Figure 3-48b, the signal at element 0 is spatially delayed, relative to that of element 1, by the path difference  $r \cos \theta$ , so that

$$\begin{aligned} e_0' &= E_1 \cos \left[ \omega t - \frac{2\pi r}{\lambda} \cos \theta \right] \\ &= E_1 \cos \zeta_0 \end{aligned} \quad (3.5-8)$$

Taking the difference of the phase angles given by equations 3.5-5 and 3.5-8

$$\Phi + \zeta_1 - \zeta_0 = \Phi + \frac{2\pi r \cos \theta}{\lambda} \quad (3.5-9)$$

By analyzing equation 3.5-9 for  $\theta = 0, 22-1/2^\circ, 45^\circ, 67-1/2^\circ$  and  $90^\circ$  (since at these values, ripple error theoretically vanishes) it was determined that the bearing angle estimate is given, for mode 4, by

$$\hat{\theta} \text{ (degrees)} = \frac{A^r}{4} \times \frac{180}{\pi} = \frac{45}{\pi} A^r \quad (3.5-10)$$

where

$$A^r = 2\pi - \left[ \Phi + \frac{2\pi r \cos \theta}{\lambda} \right] \quad (3.5-11)$$

The deviation of  $\theta$  (in the absence of any other errors) from its true value (i.e., the deviation from linearity) is defined as ripple error

$$d\theta_r = \hat{\theta} - \theta_t$$

where subscript t denotes true value.

The phase angle given by equation 3.5-9 is automatically determined by the phase comparator of the receiving system. A possible ambiguity exists in distinguishing between  $0^\circ$  and  $360^\circ$ . For the purpose of analysis, however, an inverse tangent function (equation 3.5-7) must be evaluated. This can assume one of three possible values (Figure 3-49):

$$\Phi = \text{Arg.}; \Phi = 180 + \text{Arg.}; \Phi = -(180 - \text{Arg.})$$

It was ascertained by means of the  $d\theta_r = 0$  analysis previously mentioned, that the proper quadrant determination is given by the following rule:

$$\text{If } \frac{S_1}{1 + S_3} = 0, \Phi = 0$$

$$\text{If } \frac{S_1}{1 + S_3} = +, \Phi \text{ in quadrant I}$$

$$\text{If } \frac{S_1}{1 + S_3} = -, \Phi \text{ in quadrant II, for } 0 \leq \theta \leq 45^\circ$$

$$\Phi \text{ in quadrant IV, for } 45^\circ \leq \theta \leq 90^\circ$$

That is,

$$0 \leq \Phi \leq \pi, \text{ for } 0 \leq \theta < 45^\circ$$

$$-\frac{\pi}{2} \leq \Phi \leq \frac{\pi}{2}, \text{ for } 45^\circ \leq \theta < 90^\circ$$

Table 3-4 shows a computer printout, executed in double precision, for the ripple error. The radius  $r = 5''$ ;  $\lambda$  corresponds to a nominal frequency of 1600 megahertz, so that

$$\lambda_{\text{nom.}}'' = \frac{3 \times 10^{10}}{1600 \times 10^3} \times \frac{1}{2.54} = 7.38''$$

The error is cyclic, with a period of  $22.5^\circ$ ; zero crossings occur at increments of  $11-1/2^\circ$ . The magnitude of maximum and minimum values is  $.00057^\circ$ , virtually negligible.

TABLE 3-4

## RIPPLE ERROR AT 1600 MHz

350 -  
F=1600.D0  
R=5.D0  
THLO=0.D0  
THHI=90.D0  
THINC=1.D0

RUN #1

|       | $\delta\phi$ | $\phi$ | $\delta\phi$ |
|-------|--------------|--------|--------------|
| 0.00  | -0.0000000 ← | 46.00  | -0.0001575   |
| 1.00  | -0.0001575   | 47.00  | -0.0003028   |
| 2.00  | -0.0003028   | 48.00  | -0.0004247   |
| 3.00  | -0.0004247   | 49.00  | -0.0005136   |
| 4.00  | -0.0005136   | 50.00  | -0.0005628   |
| 5.00  | -0.0005628   | 51.00  | -0.0005683   |
| 6.00  | -0.0005683   | 52.00  | -0.0005299   |
| 7.00  | -0.0005299   | 53.00  | -0.0004503   |
| 8.00  | -0.0004503   | 54.00  | -0.0003359   |
| 9.00  | -0.0003359   | 55.00  | -0.0001955   |
| 10.00 | -0.0001955   | 56.00  | -0.0000399   |
| 11.00 | -0.0000399 ← | 57.00  | 0.0001188 ←  |
| 12.00 | 0.0001188    | 58.00  | 0.0002683    |
| 13.00 | 0.0002683    | 59.00  | 0.0003970    |
| 14.00 | 0.0003970    | 60.00  | 0.0004949    |
| 15.00 | 0.0004949    | 61.00  | 0.0005545    |
| 16.00 | 0.0005545    | 62.00  | 0.0005711    |
| 17.00 | 0.0005711    | 63.00  | 0.0005435    |
| 18.00 | 0.0005435    | 64.00  | 0.0004738    |
| 19.00 | 0.0004738    | 65.00  | 0.0003673    |
| 20.00 | 0.0003673    | 66.00  | 0.0002324    |
| 21.00 | 0.0002324    | 67.00  | 0.0000795 ←  |
| 22.00 | 0.0000795 ←  | 68.00  | -0.0000795 ← |
| 23.00 | -0.0000795   | 69.00  | -0.0002324   |
| 24.00 | -0.0002324   | 70.00  | -0.0003673   |
| 25.00 | -0.0003673   | 71.00  | -0.0004738   |
| 26.00 | -0.0004738   | 72.00  | -0.0005435   |
| 27.00 | -0.0005435   | 73.00  | -0.0005711   |
| 28.00 | -0.0005711   | 74.00  | -0.0005545   |
| 29.00 | -0.0005545   | 75.00  | -0.0004949   |
| 30.00 | -0.0004949   | 76.00  | -0.0003970   |
| 31.00 | -0.0003970   | 77.00  | -0.0002683   |
| 32.00 | -0.0002683   | 78.00  | -0.0001188 ← |
| 33.00 | -0.0001188 ← | 79.00  | 0.0000399 ←  |
| 34.00 | 0.0000399 ←  | 80.00  | 0.0001955    |
| 35.00 | 0.0001955    | 81.00  | 0.0003359    |
| 36.00 | 0.0003359    | 82.00  | 0.0004503    |
| 37.00 | 0.0004503    | 83.00  | 0.0005299    |
| 38.00 | 0.0005299    | 84.00  | 0.0005683    |
| 39.00 | 0.0005683    | 85.00  | 0.0005628    |
| 40.00 | 0.0005628    | 86.00  | 0.0005136    |
| 41.00 | 0.0005136    | 87.00  | 0.0004247    |
| 42.00 | 0.0004247    | 88.00  | 0.0003028    |
| 43.00 | 0.0003028    | 89.00  | 0.0001575    |
| 44.00 | 0.0001575    | 90.00  | -0.0000000 ← |
| 45.00 | -0.0000000 ← |        |              |



In the operating system, bearing measurements are made every millisecond over a span of 61 milliseconds. At each measurement, one of four possible frequencies may be employed, the selection being purely random. Denoting measurements containing ripple error only by subscript  $t$ , the value at the mid point of the block of measurements (assuming constant bearing rate) is given by the average over the time interval:

$$\begin{aligned}\hat{\theta} &= \frac{1}{4} A_{t\text{ave}} = \frac{1}{4} \left[ \frac{1}{62} \sum_{i=1}^{62} A_{t_i} \right] \\ &= \frac{1}{4} \left\{ 2\pi - \frac{1}{62} \left[ \sum_i \Phi_{t_i} + 2\pi r \cos \theta \cdot \sum_i \frac{1}{\lambda_i} \right] \right\} \quad 3.5-12\end{aligned}$$

The error in this average is

$$d\hat{\theta} = \frac{A_{t\text{ave}}}{4} - \theta_t = \frac{\sum_i A_{t_i}}{4 \cdot 62} - \theta_t = \frac{\sum_i \frac{A_{t_i}}{4} - \theta_t}{62} = \frac{\sum_i d\theta_i}{62}$$

where  $d\theta_i$  is the error in the  $i^{\text{th}}$  determination. Assuming stationary statistics over the sampling interval of 62 milliseconds, the probabilistic mean error,  $\overline{d\theta_i}$ , is constant over that interval. Taking expectations,

$$\overline{d\hat{\theta}} = \frac{\overline{\sum_i d\theta_i}}{62} = \overline{d\theta_i} = \frac{\sum_{k=1}^n d\theta_k}{n}$$

where  $n$ , usually 4, is the number of possible frequencies, each equally likely to occur, at any given sampling instant. But

$$d\theta_k = \frac{A_{tk}}{4} - \theta_t$$

Whence

$$\overline{d\hat{\theta}} = \frac{\sum_{k=1}^n \frac{A_{tR}}{4}}{n} - \theta_t$$

or, the mean ripple error in the average is

$$\overline{d\hat{\theta}}_r \text{ (deg's)} = 57.2958 \left[ \frac{\sum_{k=1}^n A_{t_k}}{4n} \right] - \theta_t^\circ \quad (3.5-13)$$

In this equation, for each frequency,

$$A_{t_k} = 2\pi - \left[ \Phi_{t_k} + \frac{2\pi r \cos \theta}{\lambda_k} \right]$$

where

$$\Phi_{t_k} = \tan^{-1} \left[ \frac{S_1}{1 + S_3} \right]_k$$

Since the operating frequencies are near the nominal 1600 MHz value, with a total spread of not more than 30 MHz, it would be expected that  $\overline{d\theta}_r$  would attain essentially the same value as for the single nominal frequency. This is borne out by the various computer runs made, in which  $\overline{d\theta}_r$  was computed as part of an overall multipath error program. The results of these runs will be discussed subsequently. Peak  $d\theta_r$  was not more than .0006 degrees.

A standard deviation (sigma) of the ripple error, in the time average, can be obtained as follows. Over 62 sample points, assuming uncorrelated measurements, we have

$$\sigma^2 (d\hat{\theta})_r = \frac{1}{(62)^2} \sum_i \sigma^2 (d\theta_i) = \frac{1}{62} \sigma^2 (d\theta)_\lambda$$

where it has been assumed that, for stationarity, all  $i^{\text{th}}$  sigmas are equal; that is,

$$\sigma(d\theta)_i = \sigma(d\theta)_\lambda$$

The latter quantity is the sigma taken over the various frequencies; that is, the variance is given by

$$\begin{aligned} \sigma^2(d\theta)_\lambda &= \frac{\sum_k d\theta_k^2}{n} - \overline{(d\theta_r)^2} \\ &= \frac{1}{n} \sum_k \left[ \frac{A_{t_k}}{4} - \theta_t \right]^2 - \left[ \frac{\sum_k A_{t_k}}{4n} - \theta_t \right]^2 \\ &= \frac{1}{16n} \left[ \sum_k A_{t_k}^2 - \frac{1}{n} (\sum_k A_{t_k})^2 \right] \end{aligned} \quad (3.5-14)$$

The quantity  $\sigma(d\theta)_\lambda$  was not numerically evaluated, particularly in view of the diminution caused by dividing by  $\sqrt{62}$  to obtain  $\sigma(d\hat{\theta})_r$ . Instead the effect is considered in obtaining an overall sigma, including both ripple and multipath error effects, as discussed subsequently.

#### 3.5.2.1.3 Multipath Error Effects (Mode 4)

In Figure 3-50, the point A represents an antenna stub viewed in the horizontal plane. The reflecting surface R-R' is situated at a distance l from point A, in a direction normal to

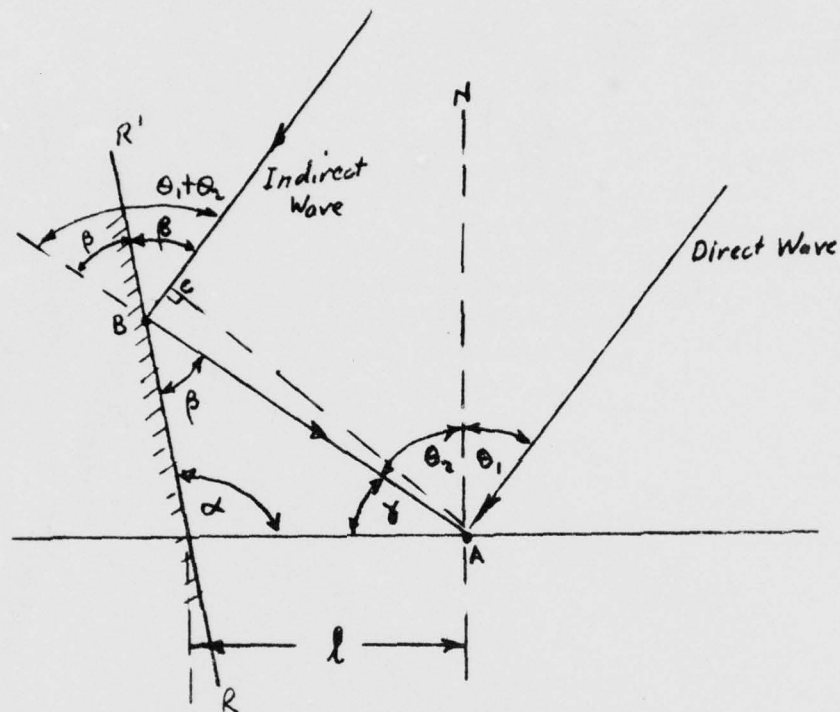


FIG. 3-50. Interference Model

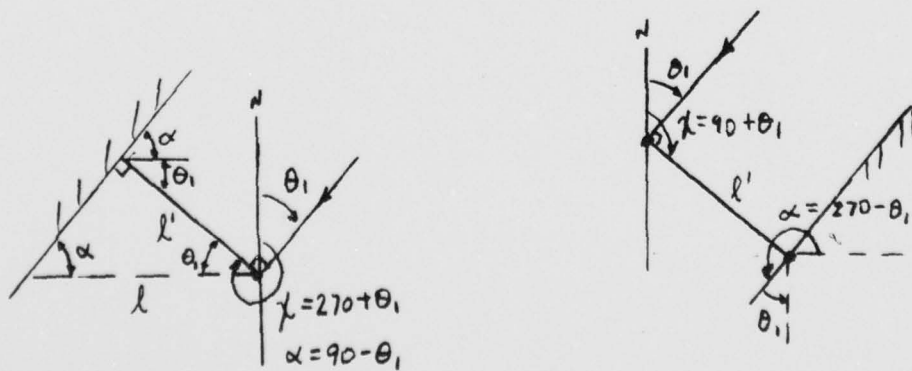


FIG. 3-51 Reflector Limits



the aircraft's longitudinal axis NA. The direct signal arrives at element A making an angle  $\theta_1$  (bearing) with the axis. An indirect signal impinges at A by being reflected at the point B (defined by Snell's law of reflection). This indirect signal, therefore, has a phase lag with respect to the direct signal, which is proportional to the distance

$$s = CB + BA$$

It can be shown, (see Appendix M), that

$$s = -2L \sin \alpha \cos (\theta_1 + \alpha)$$

The phase lag, with respect to direct signal, is therefore

$$\psi = \frac{2\pi s}{\lambda} = -\frac{4\pi L}{\lambda} \sin \alpha \cos (\theta_1 + \alpha) \quad (3.5-15)$$

Thus, if the potential at A, due to the direct wave, is

$$e' = E_1 \cos \omega t$$

then the potential due to the indirect wave is

$$e'' = E_2 \cos (\omega t - \psi) = \rho E_1 \cos (\omega t - \psi)$$

where  $\rho$  is a reflection coefficient. The total potential received is

$$e = e' + e''$$

If R-R' is to be a bona fide reflector, a restriction on  $\alpha$  is imposed:

$$90 - \theta_1^\circ < \alpha^\circ < 270 - \theta_1^\circ \quad .$$

Parameters  $\iota$  and  $\alpha$ , which specify the location and orientation of the reflector, may be replaced by the more convenient specification of  $\iota'$ ,  $X$  (see Figure 3-51). Thus

$$\iota' = \sin \alpha$$

$$X = 360 - \alpha$$

where,

$$90 + \theta_1 < X < 270 + \theta_1$$

Referring now to Figure 3-52, the transverse distance  $\iota_j$  from any element  $j$  to the reflector, is related to the normal distance  $\iota'$  by

$$\begin{aligned} \iota_j &= \iota' \csc \alpha + r \sin \delta_{1j} - r \cos \delta_{1j} \cot \alpha \\ &= -\iota' \csc X + r \sin \delta_{1j} + r \cos \delta_{1j} \cot X \end{aligned} \quad (3.5-16)$$

valid for  $j = 1$  through 16. For the center element,

$$\iota_0 = \iota' \csc \alpha = -\iota' \csc X \quad (3.5-17)$$

Substitution of  $\iota_j$  or of  $\iota_0$ , for  $\iota$  in equation 15, gives

$$\psi_j = \frac{-4\pi}{\lambda} [\iota' - r \cos (X - \delta_{1j})] \cos (X - \theta_1) \quad (3.5-18)$$

$$\psi_0 = \frac{-4\pi}{\lambda} \iota' \cos (X - \theta_1) \quad (3.5-19)$$

AD-A049 767

RCA ELECTROMAGNETIC AND AVIATION SYSTEMS DIV VAN NUY--ETC F/G 1/2  
BEARING STUDY PROGRAM.(U)

APR 74 E JELLINEK, W KRAM, M LEVINSEN  
RCA-EASD-TP-2146

N62269-73-C-0906  
NL

UNCLASSIFIED

3 OF 5

AD  
A049 767



Dropping the prime notation from  $\iota'$ , as well as the subscript notation from  $\theta_1$ , we have, in particular, for  $X = 180^\circ$ , the following:

$$\psi_j = \frac{4\pi}{\lambda} [\iota + r \cos \delta_{1j}] \cos \theta \quad (3.5-20)$$

$$\psi_0 = \frac{4\pi \iota}{\lambda} \cos \theta \quad (3.5-21)$$

These equations can be verified directly by referring to Figure 3-53. Note that analysis need be conducted only for  $0 < \theta < 90^\circ$ , since negative  $\theta$  will produce symmetrical results.

The potential due to the indirect wave, received at element 1, is

$$e''_1 = \rho E_1 \cos (\omega t - \psi_1) \quad (3.5-22)$$

where

$$\psi_1 = \frac{4\pi}{\lambda} [\iota + r] \cos \theta \quad (3.5-23)$$

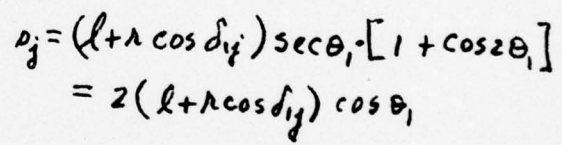
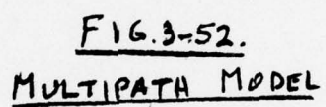
The potential due to indirect wave, produced at any other element  $j$  ( $j = 2$  through 16), is

$$e''_j = \rho E_1 \cos \left[ \omega t + \frac{2\pi}{\lambda} Z_{1j} - \frac{\pi}{2} (j - 1) - \psi_j \right] \quad (3.5-24)$$

where  $Z_{1j}$  is given by equation 1 and  $\psi_j$  is given by equation 3.5-20 sum of all signals, both direct and indirect, from element 1 through 16, utilizing equations 3.5-3, -4, -22 and 24,

$$e = e'_1 + e''_1 + \sum_{j=2}^{16} (e'_j + e''_j)$$





$$s_0 = l \sec \theta_1 \cdot [1 + \cos 2\theta_1] = 2l \cos \theta_1$$

FIG. 3-53  
MULTIPATH MODEL  
for  $\gamma = 180^\circ$

$$\begin{aligned}
&= E_1 \left[ \cos \zeta_1 + \sum_{j=2}^{16} \cos (\zeta_1 + a_j + b_j) \right] \\
&\quad + \rho E_1 \left[ \cos (\zeta_1 - \psi_1) + \sum_{j=2}^{16} \cos (\zeta_1 + a_j + b_j - \psi_j) \right] \\
&= E_1 N' \cos (\Phi_{\text{IND}} + \zeta_1)
\end{aligned} \tag{3.5-25}$$

where

$$\zeta_1 = \omega t$$

$$\Phi_{\text{IND}} = \tan^{-1} \left[ \frac{S_1 + \rho (S_2 - \sin \psi_1)}{1 + S_3 + \rho (S_4 + \cos \psi_1)} \right] \tag{3.5-26}$$

$$S_1 = \sum_{j=2}^{16} \sin (a_j + b_j)$$

$$S_2 = \sum_{j=2}^{16} \sin (a_j + b_j - \psi_j)$$

$$S_3 = \sum_{j=2}^{16} \cos (a_j + b_j)$$

$$S_4 = \sum_{j=2}^{16} \cos (a_j + b_j - \psi_j)$$

and where  $a_j$ ,  $b_j$  have the defining equations given in the previous section. The quadrant of  $\Phi_{\text{IND}}$  is obtained as for  $\Phi_t$  in the previous section.

The phase angle of  $e_1$ , in equation 3.5-25, is to be compared with the phase angle of the received potential at the central element. We have, summing direct and indirect potential at element 0,

$$\begin{aligned} e_0 &= e'_0 + e''_0 = E_1 \cos \left( \omega t - \frac{2\pi r \cos \theta}{\lambda} \right) \\ &+ \rho E_1 \cos \left( \omega t - \frac{2\pi r \cos \theta}{\lambda} - \psi_0 \right) \\ &= E_1 N_0 \cos (\zeta_0 - \mu_0) \end{aligned} \quad (3.5-27)$$

where

$$\begin{aligned} \zeta_0 &= \zeta_1 - \frac{2\pi r \cos \theta}{\lambda} \\ \mu_0 &= \tan^{-1} \left[ \frac{\rho \sin \psi_0}{1 + \rho \cos \psi_0} \right] \end{aligned}$$

(quadrant from signs of numerator and denominator)

The difference in phase angles of  $e$  and  $e_0$  is

$$\Phi_{\text{IND}} + \zeta_1 - \zeta_0 + \mu_0 = \Phi_{\text{IND}} + \frac{2\pi r \cos \theta}{\lambda} + \mu_0 \quad (3.5-28)$$

The estimated bearing angle is

$$\hat{\theta}(\text{deg's.}) = \frac{180}{\pi} \times \frac{r}{4} \frac{A_{\text{IND}}}{A_{\text{IND}}} \quad (3.5-29)$$

where

$$A_{IND_k}^r = 2\pi - [\Phi_{IND} + \frac{2\pi r \cos \theta}{\lambda} + \mu_0]_k \quad (3.5-30)$$

The subscript  $k$  denotes that  $A_{IND}$  has a value, at each sampling instant, which is dependent on the carrier frequency at that instant.

Of the  $n$  possible frequencies, one can produce a maximum deviation, and another can produce an (algebraic) minimum deviation; that is,

$$d\theta_{T_{max}}^{\circ} = \frac{180}{4\pi} A_{IND_k} l_{max} - \theta_t$$

$$d\theta_{T_{min}}^{\circ} = \frac{180}{4\pi} A_{IND_k} l_{min} - \theta_t$$

where  $d\theta_T$  denotes total error, including ripple error effect. The deviation of the time average estimate of bearing must be between the two extremes. The most probable deviation is the mean value of the error in the average. We have

$$d\hat{\theta}_T = \frac{A_{IND} l_{AVE}}{4} - \theta_t = \frac{\sum_{j=1}^{62} \left( \frac{A_{IND_j}}{4} - \theta_t \right)}{62} = \frac{\sum_{j=1}^{62} d\theta_j}{62}$$

Taking expectations and assuming stationarity,

$$\overline{d\hat{\theta}_T} = \frac{\sum_{j=1}^{62} \overline{d\theta_j}}{62} = \overline{d\theta_1} = \frac{\sum_{k=1}^n d\theta_k}{n} = \frac{\sum_k A_{IND} l_k}{4n} - \theta_t$$



or

$$\overline{d\hat{\theta}_T} (\text{deg's.}) = \frac{180}{4\pi} \left[ \frac{\sum_k A_{\text{IND}} ]_k}{n} \right] - \theta_t^\circ \quad (3.5-31)$$

where  $A_{\text{IND}} ]_k$  is given by equation 3.5-30. The mean error in the average, due to multipath only, is

$$\begin{aligned} d\hat{\theta}_M &= d\hat{\theta}_T - d\hat{\theta}_r = \frac{1}{4n} \left[ \sum_{k=1}^n (A_{\text{IND}_k} - A_{t_k}) \right] \\ &= \frac{1}{4n} \left[ \sum_{k=1}^n (\Phi_{t_k} - \Phi_{\text{IND}_k} - \mu_{\sigma_k}) \right] \end{aligned} \quad (3.5-32)$$

Similar to the derivation of equation 3.5-14, the sigma of the error in the average, when both multipath and ripple errors are present, is

$$\sigma(d\hat{\theta})_T = \frac{1}{4\sqrt{62n}} \left[ \sum_{k=1}^n A_{\text{IND}_k}^2 - \frac{1}{n} \left( \sum_{k=1}^n A_{\text{IND}_k} \right)^2 \right]^{1/2} \quad (3.5-33)$$

This may be interpreted as a measure of the spread in the error in the average, about the mean error.

Since the error due to multipath only is

$$d\hat{\theta}_M = d\hat{\theta}_T - d\hat{\theta}_r = \frac{\sum \left( \frac{A_{\text{IND}}}{4} \right)_i}{62} - \frac{\sum \left( \frac{A_t}{4} \right)_i}{62}$$

and assuming stationarity, then

$$E(d\hat{\theta}_M^2) = \frac{1}{16n} \frac{\sum_k (A_{\text{IND}_k} - A_{t_k})^2}{62}$$

Thus

$$\sigma^2 (\hat{d\theta})_M = E (\hat{d\theta}_M^2) - \overline{(\hat{d\theta}_M)^2} / 62 \quad (3.5-34)$$

where  $\overline{\hat{d\theta}_M}$  is given by equation 3.5-32, and

$$A_{IND_k} - A_{t_k} = \Phi_{t_k} - \Phi_{IND_k} - \mu_{\sigma_k}$$

#### 3.5.2.1.4 Quantitative Results

In Figure 3-54, assume an extended vertical reflecting surface is located a distance of  $l$  inches from the center of the ring antenna array. The point of reflectance of the indirect ray moves further from the center line, as the bearing angle increases. Since the extended surface is limited in length, say  $w$  feet, a limiting bearing angle is attained beyond which reflection cannot occur. This limit is given by

$$\tan \theta_{LIM} = \frac{w \text{ (ft.)} - r \text{ (ft.)}}{(l''/12)} \approx \frac{w}{(l''/12)}$$

The limit angle is given, Table 3-5, for a wing length of 100 feet.

TABLE 3-5

#### DIRECTION OF ARRIVAL REFLECTION LIMITS

| $l''$ | $\theta_{LIM}^\circ$ |
|-------|----------------------|
| 104   | 85.1                 |
| 208   | 80.2                 |
| 416   | 70.9                 |
| 624   | 62.7                 |
| 832   | 55.3                 |

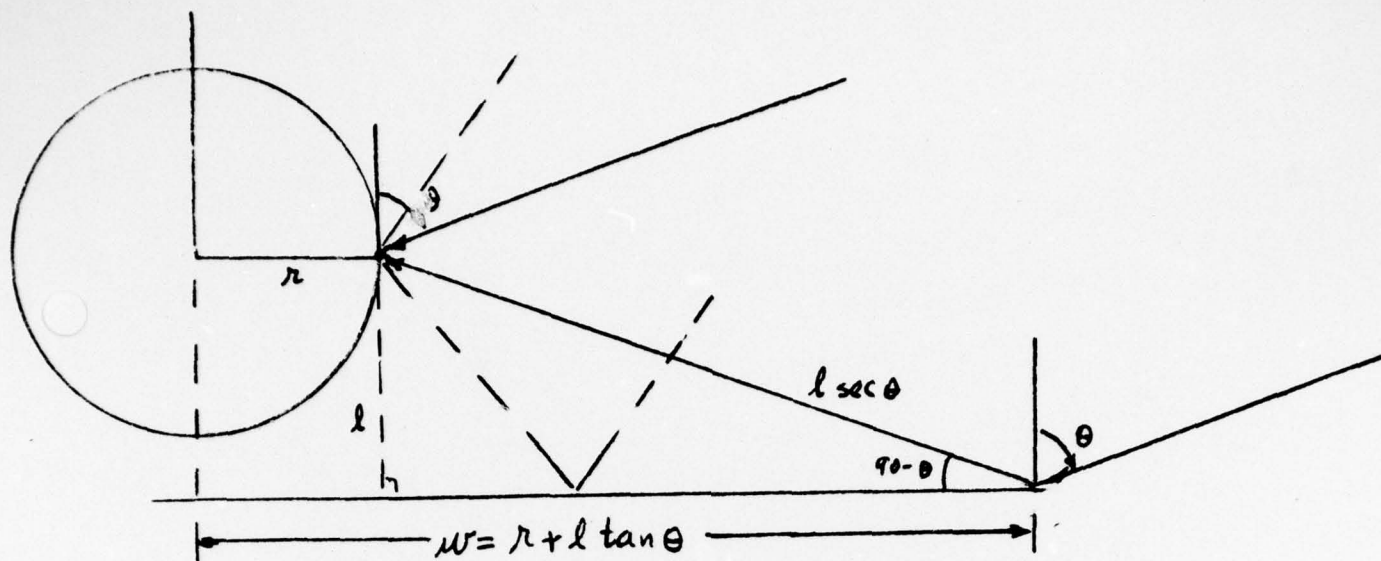


FIG. 3-54  
REFLECTION LIMIT

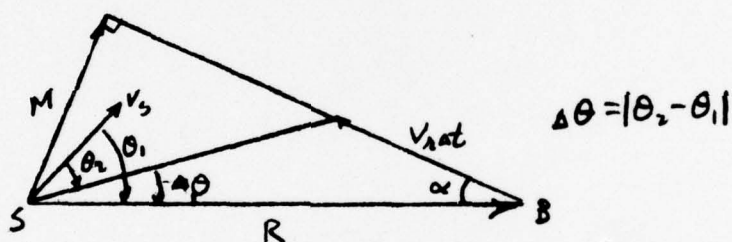


FIG. 3-65  
CONFLICT TRIANGLE

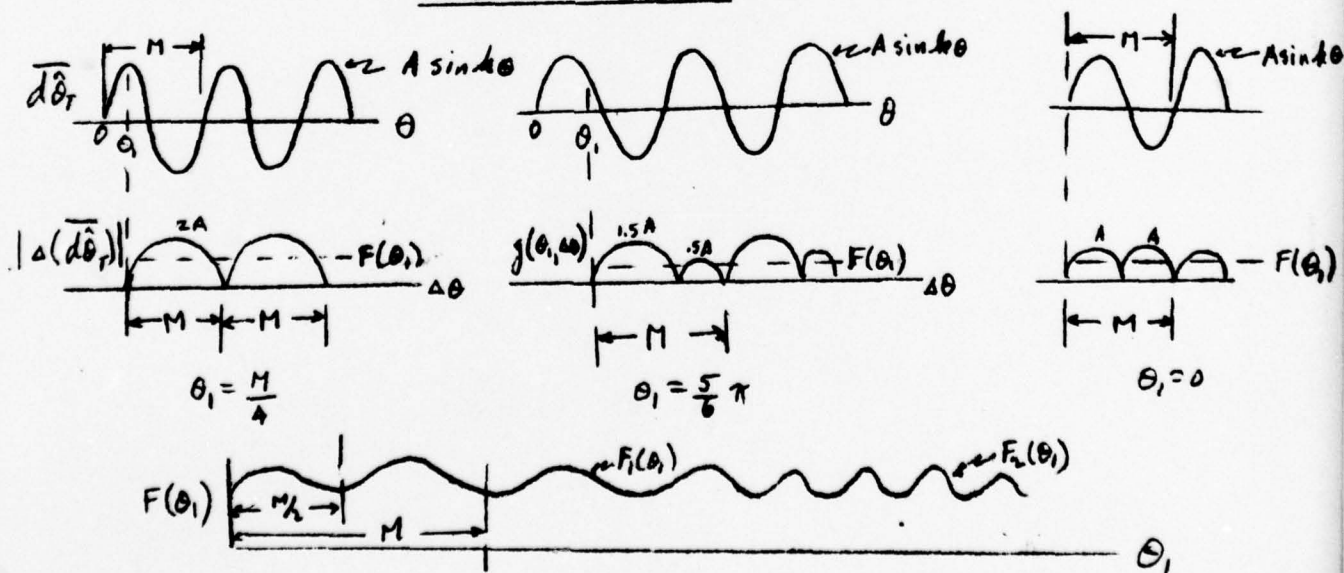


FIG. 3-67, DERIVATION OF F(θ)

Actually, if the antenna is always located fore of the wing, a large  $\iota$  of 800" would correspond to the distance to a tail surface, in which case  $\theta_{LIM}$  would be on the order of 27°.

Computer runs were made in increments of .5 degrees over a range of  $\theta$  from 0 to  $\theta_{LIM}$ , and for various sets of frequencies, so as to determine the effect of frequency spread on the mean error  $\overline{d\hat{\theta}_T}$  in the time averaged bearing estimate. These frequency sets were selected so as to cause a minimal change in the present SECANT frequency allocation for replies. Table 3-6 lists the sets investigated; set A is presently specified

TABLE 3-6  
TRANSMISSION SETS

| <u>FREQUENCY SET</u> | <u>FREQUENCIES (MHz)</u> |
|----------------------|--------------------------|
| A                    | 1599, 1600, 1603, 1604   |
| B                    | 1596, 1604, 1611, 1619   |
| C                    | 1611, 1612, 1615, 1616   |
| D                    | 1600, 1604, 1612, 1616   |
| E                    | 1596, 1604, 1612, 1620   |

Runs were also made, with sets A and B, varying the antenna-to-reflector spacing. A portion of a representative computer printout is presented in Table 3-7, for set B and  $\iota = 416''$ . An explanation of column headings follows (all angles in degrees):

THETA =  $\theta$  = True bearing angle

DTHR =  $\overline{d\hat{\theta}_T}$  = Mean ripple error in time averaged bearing estimate ( $\hat{\theta}$ )

DTH (MAX) =  $d\theta_{Tmax}$  = Max. possible error in  $\hat{\theta}$ , including ripple and multipath error effects



THLD=0.  
THHI=71.  
THINC=.5

TABLE 3-7. Ripple & Multipath Error

RUN #6

F(K)= 1596., 1604., 1611., 1619.,  
L = 416. RHO= 0.05

| THETA | DTHR     | DTH(MAX) | DTH(MIN) | DTHT     | 2DDTHT   | SIG     |
|-------|----------|----------|----------|----------|----------|---------|
| 0.00  | -0.00000 | 0.00000  | -0.00000 | 0.00000  | 0.00000  | 0.00000 |
| 0.50  | -0.00008 | 0.05167  | -0.04737 | 0.00054  | 0.00108  | 0.00604 |
| 1.00  | -0.00016 | 0.10009  | -0.09479 | -0.00157 | -0.00422 | 0.01175 |
| 1.50  | -0.00024 | 0.13886  | -0.14267 | -0.00846 | -0.01378 | 0.01649 |
| 2.00  | -0.00032 | 0.15650  | -0.18372 | -0.02203 | -0.02713 | 0.01911 |
| 2.50  | -0.00038 | 0.13765  | -0.20537 | -0.04242 | -0.04077 | 0.01805 |
| 3.00  | -0.00044 | 0.06846  | -0.18865 | -0.06550 | -0.04616 | 0.01200 |
| 3.50  | -0.00049 | 0.00360  | -0.16168 | -0.08087 | -0.03074 | 0.00785 |
| 4.00  | -0.00054 | 0.17773  | -0.30317 | -0.07407 | 0.01360  | 0.02457 |
| 4.50  | -0.00057 | 0.37889  | -0.41652 | -0.03670 | 0.07473  | 0.04583 |
| 5.00  | -0.00059 | 0.51313  | -0.46828 | 0.01952  | 0.11245  | 0.06035 |
| 5.50  | -0.00060 | 0.54217  | -0.42596 | 0.06480  | 0.09055  | 0.05576 |
| 6.00  | -0.00059 | 0.34955  | -0.18408 | 0.08339  | 0.03718  | 0.02526 |
| 6.50  | -0.00058 | 0.42139  | -0.24606 | 0.08873  | 0.01068  | 0.03294 |
| 7.00  | -0.00055 | 0.70101  | -0.59026 | 0.06683  | -0.04380 | 0.07732 |
| 7.50  | -0.00052 | 0.66514  | -0.68504 | -0.03422 | -0.20209 | 0.08033 |
| 8.00  | -0.00047 | 0.15853  | -0.44813 | -0.15492 | -0.24140 | 0.02876 |
| 8.50  | -0.00041 | 0.43869  | -0.64504 | -0.12332 | 0.06319  | 0.05873 |
| 9.00  | -0.00035 | 0.87677  | -0.80654 | 0.03732  | 0.32129  | 0.10441 |
| 9.50  | -0.00028 | 0.63135  | -0.40259 | 0.11666  | 0.15867  | 0.05419 |
| 10.00 | -0.00020 | 0.72609  | -0.49691 | 0.11791  | 0.00252  | 0.06653 |
| 10.50 | -0.00012 | 0.97000  | -0.91825 | 0.00409  | -0.22765 | 0.11714 |
| 11.00 | -0.00004 | 0.12690  | -0.49308 | -0.19031 | -0.38880 | 0.02904 |
| 11.50 | 0.00004  | 0.86951  | -0.96472 | -0.07024 | 0.24015  | 0.10925 |
| 12.00 | 0.00012  | 0.95621  | -0.72991 | 0.11900  | 0.37848  | 0.09786 |
| 12.50 | 0.00020  | 0.78813  | -0.53058 | 0.13167  | 0.02534  | 0.07290 |
| 13.00 | 0.00028  | 1.04430  | -1.08575 | -0.03989 | -0.34313 | 0.13034 |
| 13.50 | 0.00035  | 0.19941  | -0.57498 | -0.19449 | -0.30920 | 0.03914 |
| 14.00 | 0.00041  | 1.22108  | -1.11510 | 0.06450  | 0.51798  | 0.14614 |
| 14.50 | 0.00047  | 0.46561  | -0.18353 | 0.14179  | 0.15459  | 0.03219 |
| 15.00 | 0.00052  | 1.20440  | -1.20819 | -0.01454 | -0.31266 | 0.15068 |
| 15.50 | 0.00055  | 0.30162  | -0.65531 | -0.18213 | -0.33518 | 0.05296 |
| 16.00 | 0.00058  | 1.25019  | -1.07124 | 0.09455  | 0.55336  | 0.14376 |
| 16.50 | 0.00059  | 0.99487  | -0.75324 | 0.12311  | 0.05712  | 0.10588 |
| 17.00 | 0.00060  | 0.66942  | -0.93590 | -0.13791 | -0.52205 | 0.09760 |
| 17.50 | 0.00059  | 1.24765  | -1.30178 | -0.03132 | 0.21318  | 0.16057 |
| 18.00 | 0.00057  | 0.20292  | 0.06449  | 0.13377  | 0.33018  | 0.00667 |
| 18.50 | 0.00054  | 1.18646  | -1.28696 | -0.05131 | -0.37016 | 0.15658 |
| 19.00 | 0.00049  | 1.00207  | -1.16906 | -0.08394 | -0.06525 | 0.13755 |
| 19.50 | 0.00044  | 0.35765  | -0.11283 | 0.12259  | 0.41305  | 0.02777 |
| 20.00 | 0.00038  | 1.26065  | -1.34006 | -0.04274 | -0.33066 | 0.16358 |
| 20.50 | 0.00032  | 1.16934  | -1.28125 | -0.05994 | -0.03440 | 0.15262 |
| 21.00 | 0.00024  | 0.32866  | -0.11102 | 0.10924  | 0.33836  | 0.02167 |
| 21.50 | 0.00016  | 0.94340  | -1.09492 | -0.08023 | -0.37893 | 0.12259 |
| 22.00 | 0.00008  | 1.43278  | -1.42723 | 0.00461  | 0.16968  | 0.18080 |
| 22.50 | -0.00000 | 1.18624  | -1.07280 | 0.06189  | 0.11456  | 0.13469 |
| 23.00 | -0.00008 | 0.22708  | -0.38763 | -0.08112 | -0.28603 | 0.02818 |
| 23.50 | -0.00016 | 0.89567  | -0.77050 | 0.06715  | 0.29654  | 0.09184 |
| 24.00 | -0.00024 | 1.31854  | -1.37342 | -0.03274 | -0.19978 | 0.16285 |
| 24.50 | -0.00032 | 1.40626  | -1.42615 | -0.01618 | 0.03314  | 0.17737 |
| 25.00 | -0.00038 | 1.25726  | -1.22690 | 0.02337  | 0.07910  | 0.14456 |
| 25.50 | -0.00044 | 0.80379  | -0.85734 | -0.02590 | -0.09855 | 0.08577 |
| 26.00 | -0.00049 | 0.36816  | -0.28392 | 0.04332  | 0.13845  | 0.03091 |
| 26.50 | -0.00054 | 0.59783  | -0.60918 | -0.00318 | -0.09300 | 0.05591 |
| 27.00 | -0.00057 | 0.96242  | -0.95006 | 0.01413  | 0.03462  | 0.09879 |
| 27.50 | -0.00059 | 1.15875  | -1.18300 | -0.00333 | -0.03492 | 0.12871 |
| 28.00 | -0.00060 | 1.24949  | -1.29808 | -0.01768 | -0.02871 | 0.14597 |
| 28.50 | -0.00059 | 1.27623  | -1.32523 | -0.01339 | 0.00858  | 0.15370 |

DTH (MIN) =  $d\theta_{T_{\min}}$  = Min. possible error in  $\hat{\theta}$

DTHT =  $\overline{d\hat{\theta}_T}$  = Mean error in  $\hat{\theta}$ , including both ripple and multipath mean errors

2DDTHT = Approximate rate of change of  $\overline{d\hat{\theta}_T}$  with respect to  $\theta$

SIG =  $\sigma(d\theta)_T$  = Standard deviation of error in  $\hat{\theta}$

#### NOTE

If subscript u represents values along any row in Table 3-7, then for a given  $\theta$ ,

$$\left. \frac{\overline{d\hat{\theta}_T}}{d\theta} \right|_u \approx \frac{\Delta(\overline{d\hat{\theta}_T}) \ln .5^*}{.5} = 2\Delta(\overline{d\hat{\theta}_T}) = \frac{\overline{d\hat{\theta}_T}_u - \overline{d\hat{\theta}_T}_{u-1}}{\theta_u - \theta_{u-1}}$$

Pertinent results from all of the runs are summarized in Table 3-8. Since frequency sets C and D did not show marked improvement in peak-to-peak excursion of  $\overline{d\hat{\theta}_T}$ , but set E does provide improvement in comparison to the result for set A, at  $\iota = 104''$ , it was decided to make further comparison runs only with sets A and B (set B is essentially the same as set E).

The standard deviation is quite small compared to  $\overline{d\hat{\theta}_T}$  max, indicating a clustering of error near the mean value. The most significant parameter is the peak-to-peak excursion of  $\overline{d\hat{\theta}_T}$  since this indicates the largest probable error in swept bearing. For set A, it is seen to diminish continuously as the antenna-to-reflector spacing increases; for set B, a minimum is reached at about  $\iota = 500''$  (The columns in Table 3-8, labeled  $\bar{B}$ ,  $\alpha_\beta$  etc. will be explained in the next section.) Comparing runs 6 and 9, it is seen that doubling the reflection coefficient ( $\rho$ )\*, resulted in double the peak-to-peak excursion of  $\overline{d\hat{\theta}_T}$ .

\*A value of  $\rho = .05$  was selected for most runs; this value was deduced from consideration of the radiation pattern of the top mounted (stick) antenna on a Boeing 707; see Appendix N.

TABLE 3-8: SUMMARY, MODE 4

| Run No. | Freq. Set | $l''$ | Max $d\theta_{\max}$ | Min $d\theta_{\min}$ | Max $d\theta_T$<br>Peak-to-Peak | Max $\sigma(d\theta)_T$ | $\bar{B}$ | $\sigma_B$ | $\sqrt{B^2 + \sigma_B^2}$ | $\sqrt{B^2 + (3\sigma_B)^2}$ |
|---------|-----------|-------|----------------------|----------------------|---------------------------------|-------------------------|-----------|------------|---------------------------|------------------------------|
| 2B      | A         | 104   | 1.42                 | -1.42                | 2.81                            | .04                     | .68       | .73        | 1.00                      | 2.30                         |
| 2T      | C         | 104   | 1.42                 | -1.39                | 2.70                            | .04                     |           |            |                           |                              |
| 3       | D         | 104   | 1.40                 | -1.39                | 2.54                            | .10                     |           |            |                           |                              |
| 4       | E         | 104   | 1.43                 | -1.43                | 2.49                            | .13                     |           | .56        | .78                       | 1.75                         |
| 5       | A         | 416   | 1.43                 | -1.43                | 2.60                            | .13                     | .52       | .52        | .74                       | 1.35                         |
| 15      | A         | 624   | 1.43                 | -1.42                | 1.98                            | .16                     | .26       | .34        | .42                       | 1.04                         |
| 7       | A         | 832   | 1.43                 | -1.43                | .30                             | .16                     | .06       | .10        | .11                       | .30                          |
| 6       | B         | 416   | 1.43                 | -1.43                | .33                             | .18                     | .06       | .09        | .11                       | .30                          |
| 16      | B         | 624   | 1.41                 | -1.42                | .64                             | .14                     | .09       | .14        | .16                       | .42                          |
| 17      | B         | 750   | 1.37                 | -1.43                | 2.20                            | .14                     | .52       | .54        | .75                       | 1.70                         |
| 18      | B         | 800   | 1.43                 | -1.43                | 2.52                            | .11                     |           |            |                           |                              |
| 8       | B         | 832   | 1.40                 | -1.42                | 2.78                            | .09                     |           |            |                           |                              |
| *9      | B         | 416   | 2.86                 | -2.87                | .68                             | .35                     |           |            |                           |                              |

\* $\rho = .10$



Plots of  $\overline{d\hat{\theta}_T}$  versus  $\theta$  are presented in Figures 3-55 through 3-64, for all run numbers except 2T, 3 and 18. All the graphs exhibit a type of "beat" frequency pattern. Improvement due to frequency diversity, for set A, is evident only at the higher spacing ( $\iota$ ). For set B, the improvement is quite marked in the region of  $\iota = 400''$  to  $600''$ .

#### 3.5.2.1.5 Effect of Variability in Bearing and Swept Bearing Probabilistic Analysis

In the case of swept bearing determination, the multipath (and ripple) error effect must be the algebraic difference, at two sequential points, of a function such as those depicted in Figures 3-55 through 3-64. This difference (residual error) must, therefore, depend on the times at which the bearing measurements are made, as well as the relative kinematic geometry; that is, upon the initial bearing angle and the swept bearing itself. These latter quantities cannot be known, a priori, and are, therefore, random variables. If the swept bearing in a miss determination situation can attain, at most, a value greater than half the oscillation (high frequency) period of the mean error function, then the residual error can be at most equal to some peak-to-peak difference along the function, dependent on initial  $\theta$ . From the curves, it is seen that the half period can be  $5^\circ$ , or less, depending on initial  $\theta$ , frequency set, and antenna-reflector spacing. It then is advisable to ascertain the maximum swept bearing to be expected in a declared conflict situation, so as to afford a comparison.

From the conflict triangle in Figure 3-65(see page 3-140). From this, the following relations can be derived:

$$\tan \Delta\theta = \frac{V_r \Delta t \sin \alpha}{R - V_r \Delta t \cos \alpha} \quad (3.5-35)$$

where

$$\sin \alpha = M/R \quad (3.5-36)$$



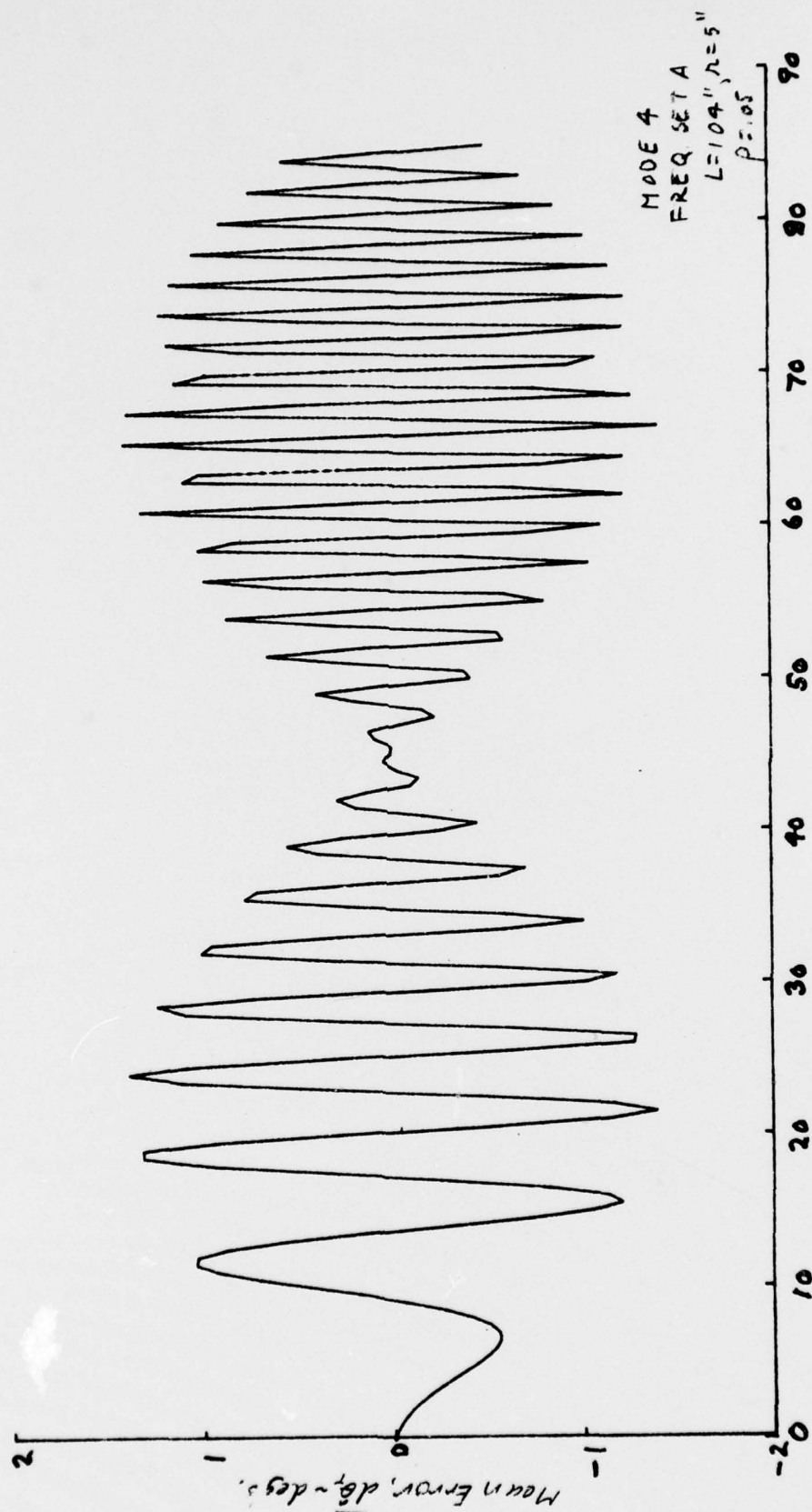
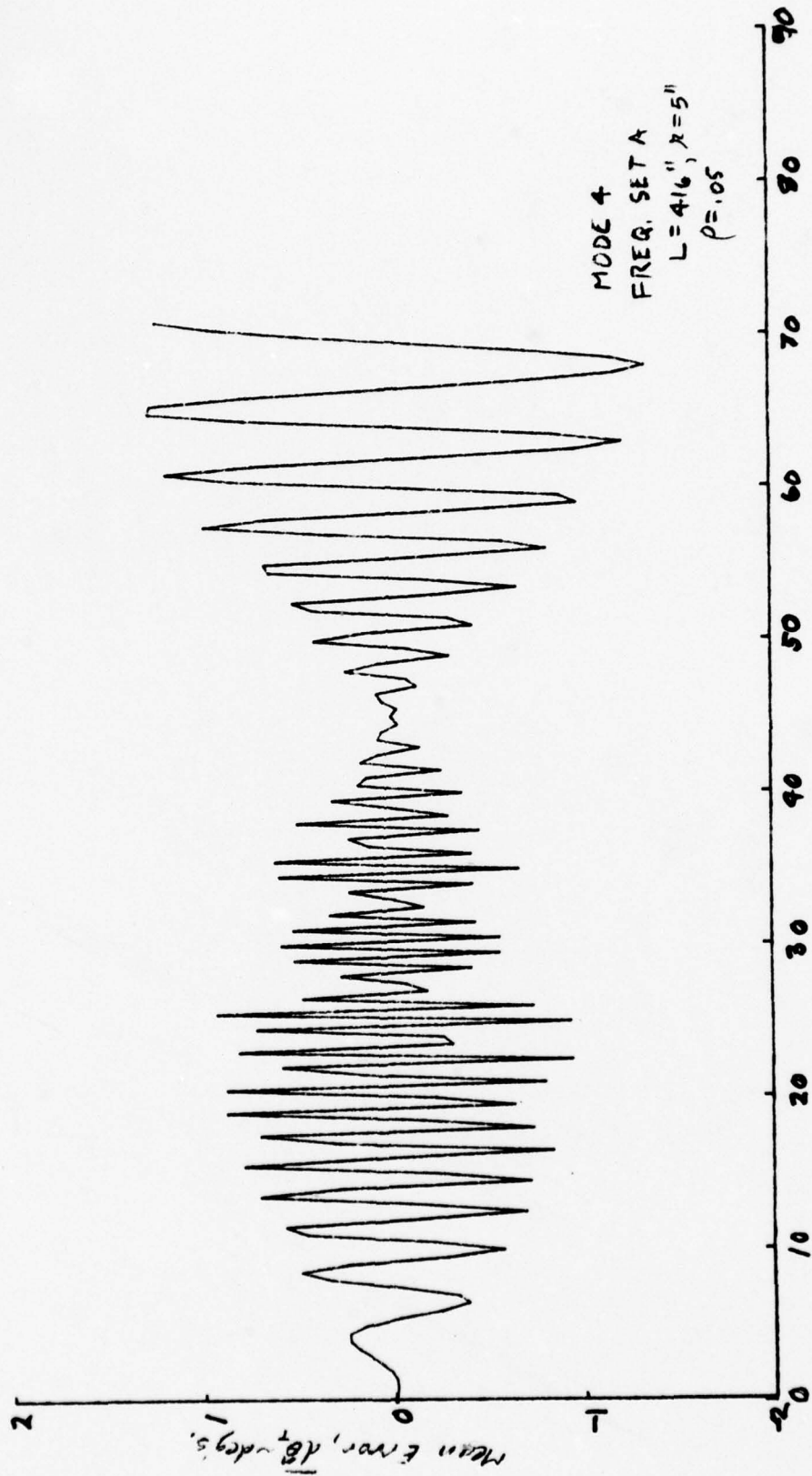


FIG. 3-55, RUN # 2B

MEAN ERROR vs BEARING ANGLE



**FIG. 3-56** RUN #5

MEAN ERROR VS BEARING ANGLE

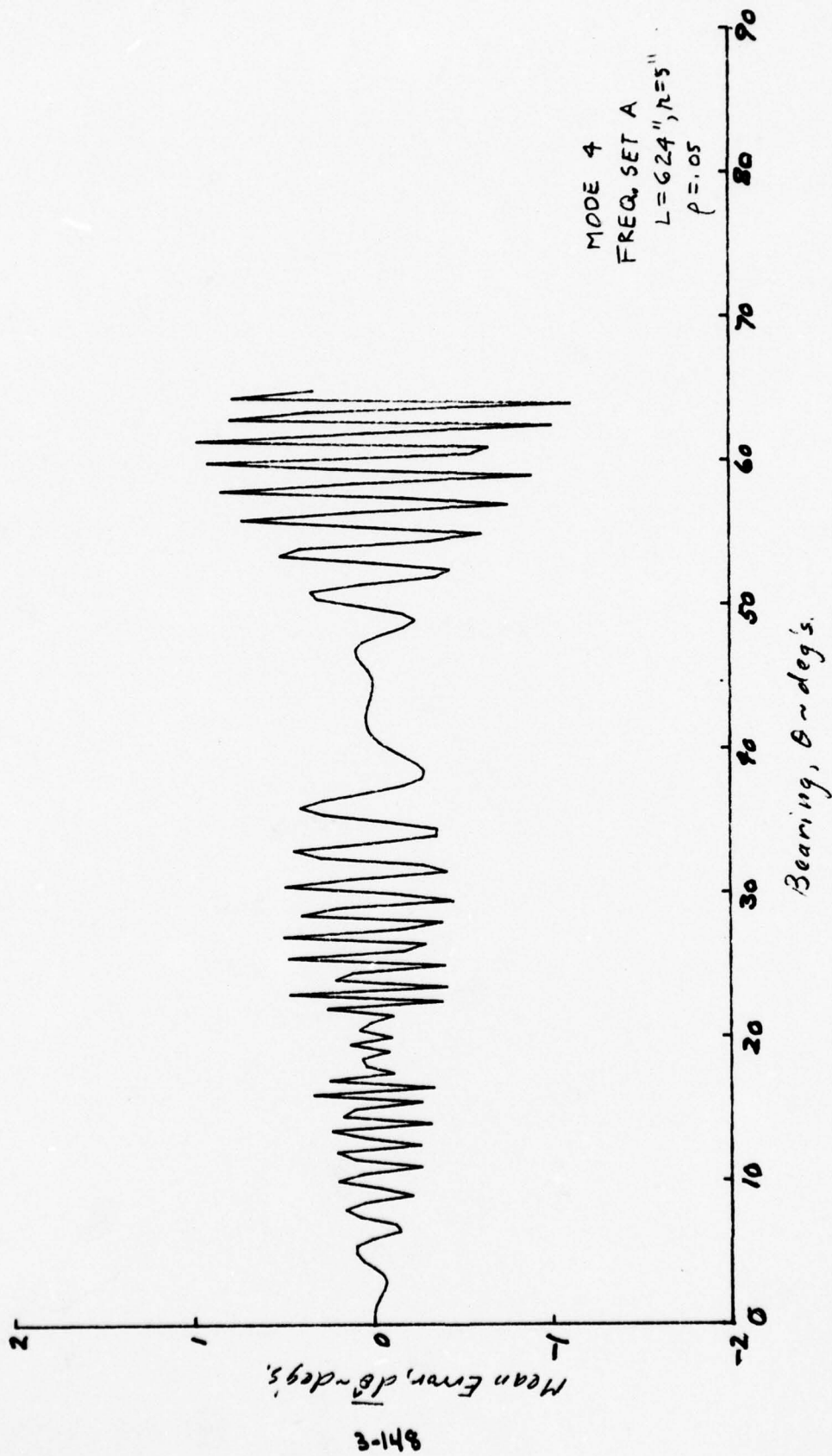


FIG 3-57, RUN # 15

MEAN ERROR VS. BEARING ANGLE

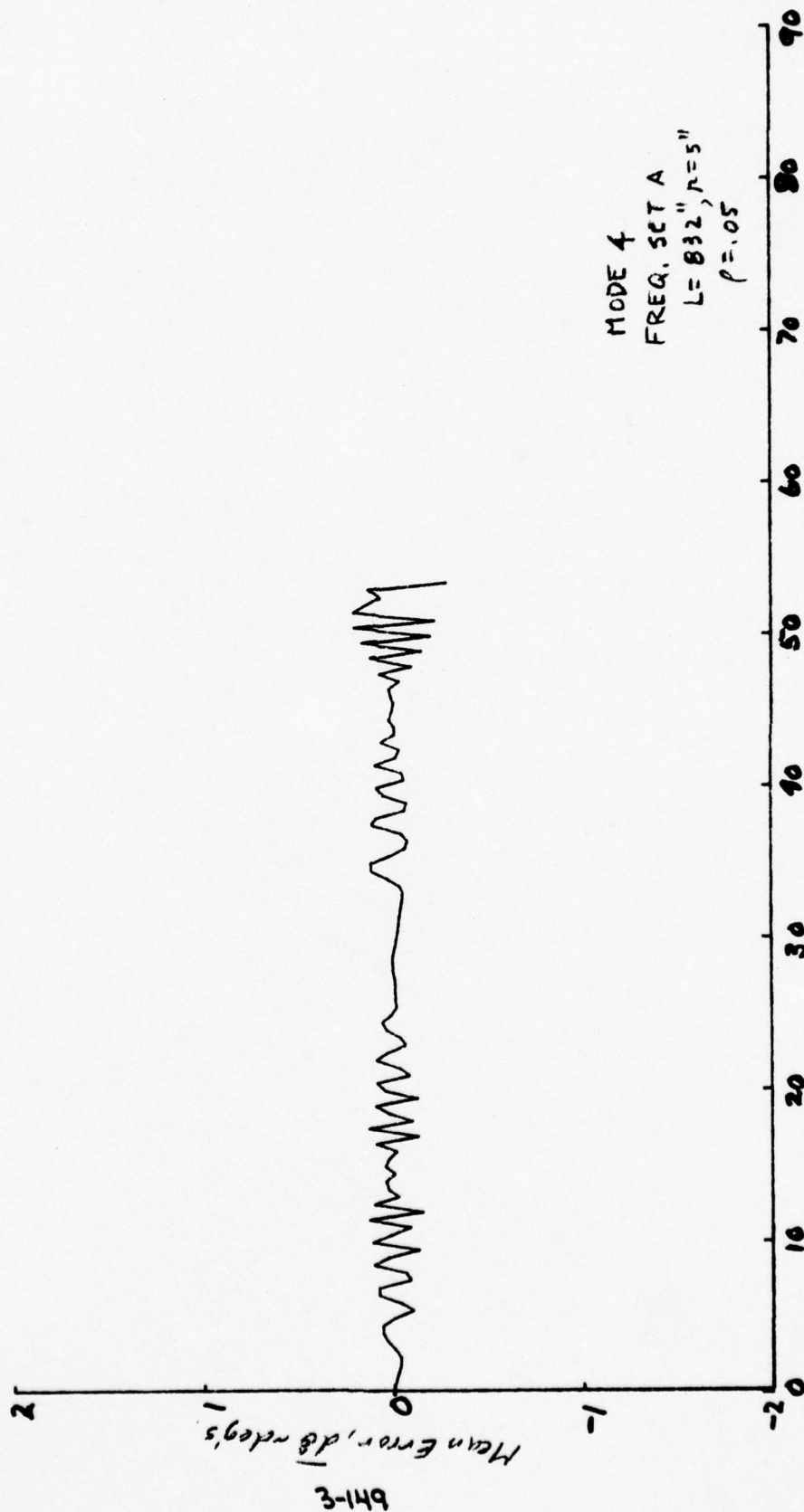


FIG. 3-58, RUN # 7

MEAN ERROR VS BEARING ANGLE



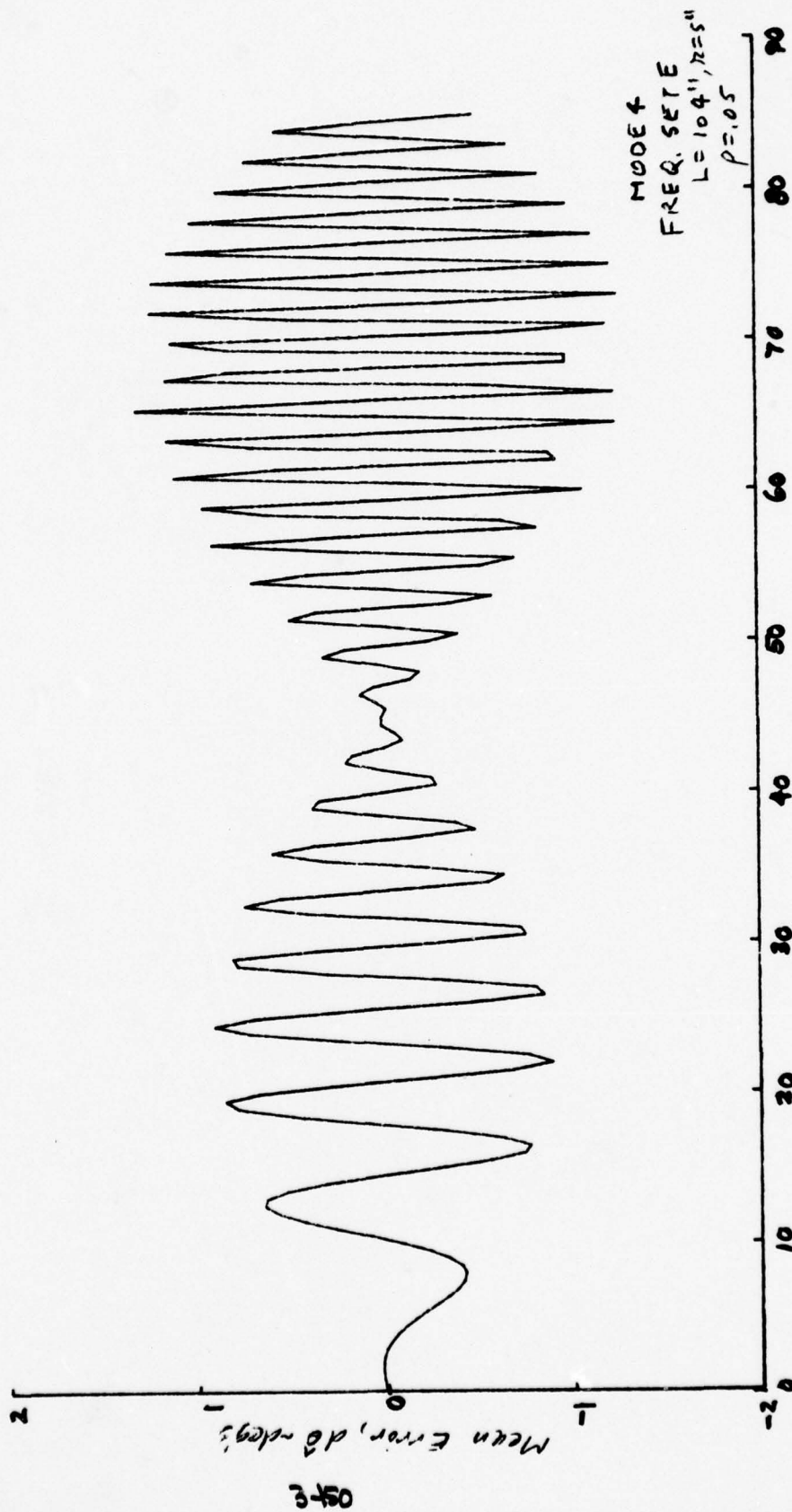
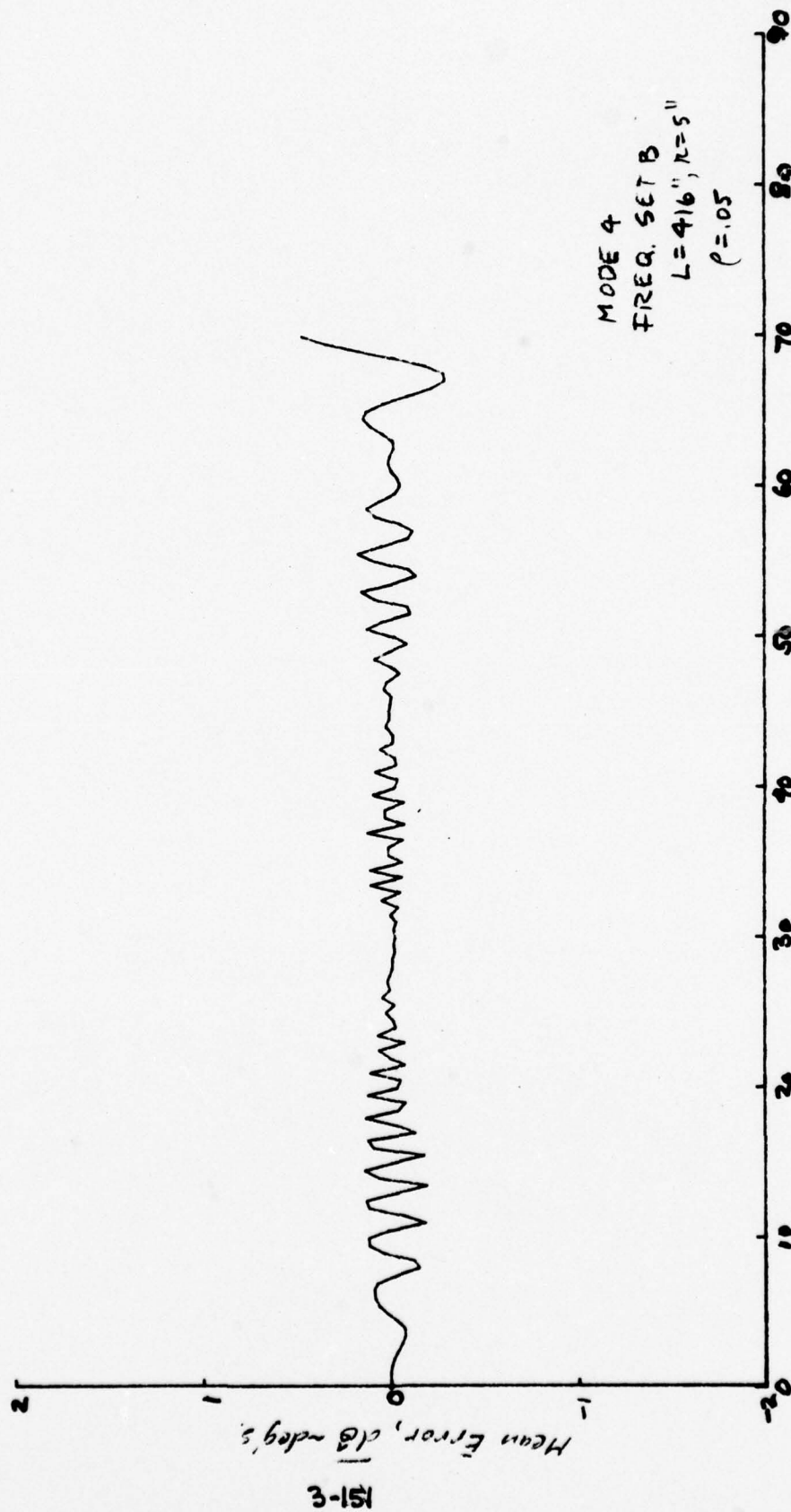


FIG. 3-59, RUN #4

MEAN ERROR VS. BEARING ANGLE



Bearing, 0-deg's

FIG. 3-60, RUN #6

MEAN ERROR VS. BEARING ANGLE

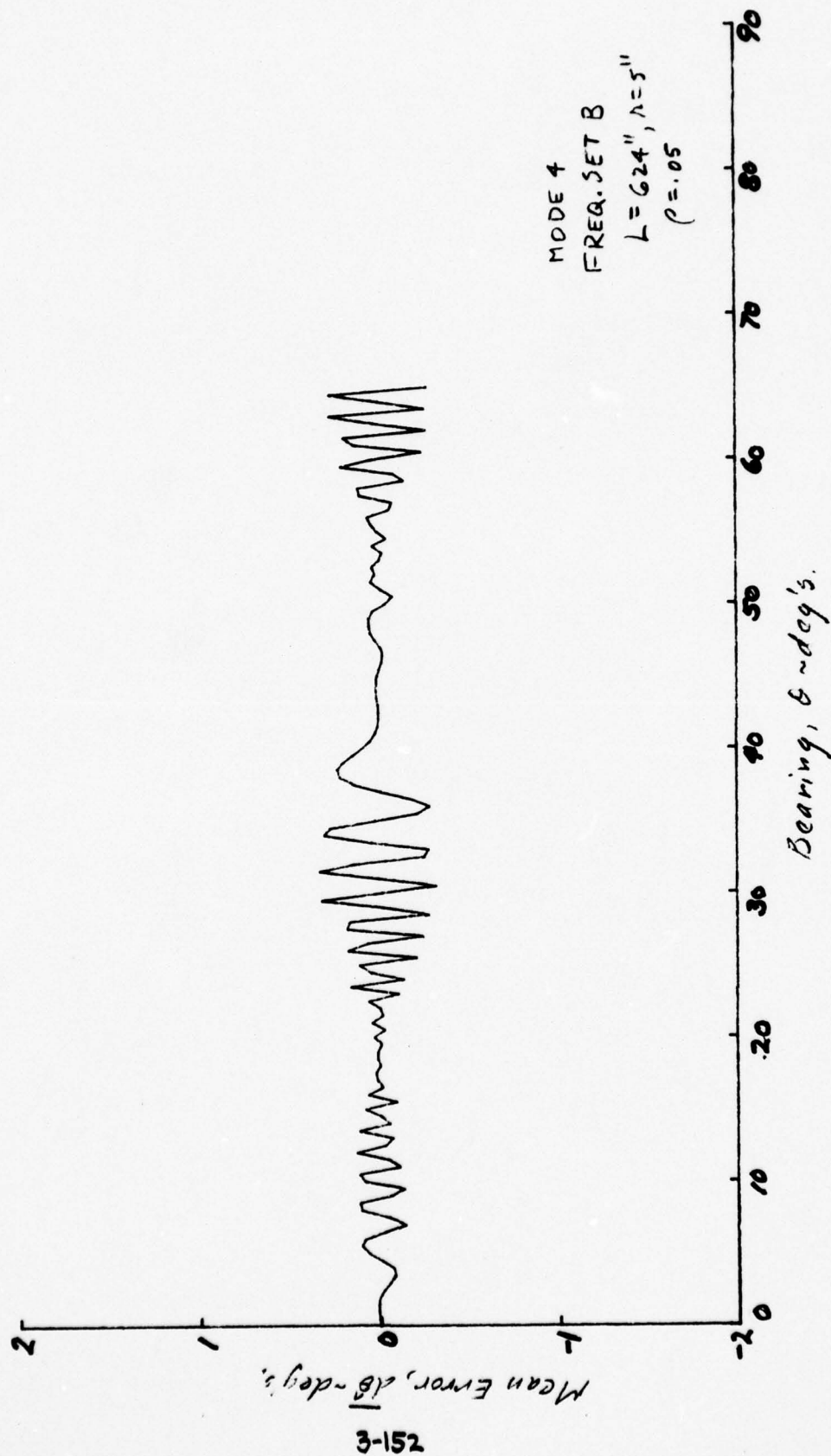


**FIG. 3-61, RUN# 16**

MEAN ERROR VS. BEARING ANGLE

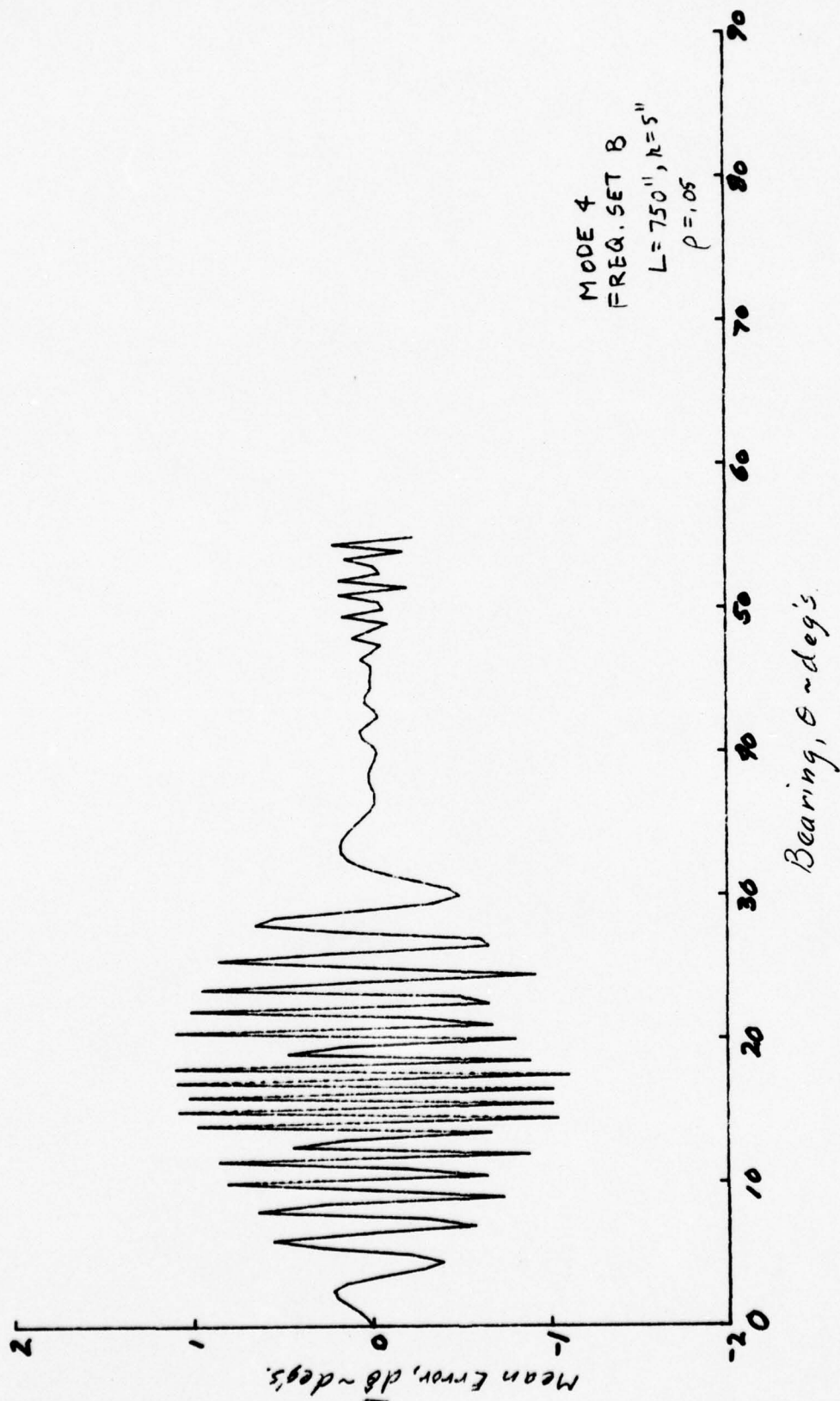
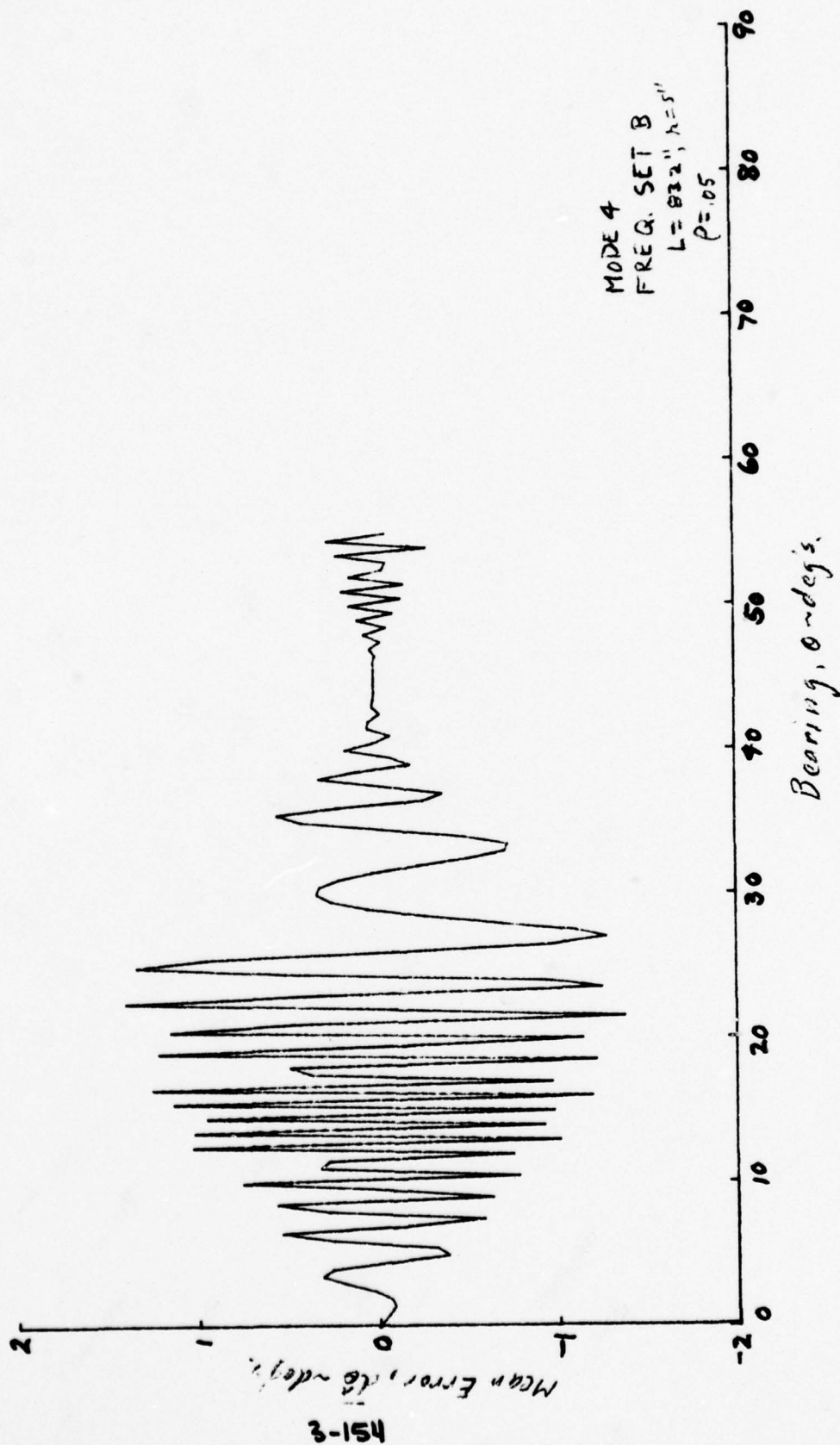


FIG. 3-62 RUN #17

MEAN ERROR VS. BEARING ANGLE





**FIG. 3-63, RUN #8**

MEAN ERROR VS. BEARING ANGLE

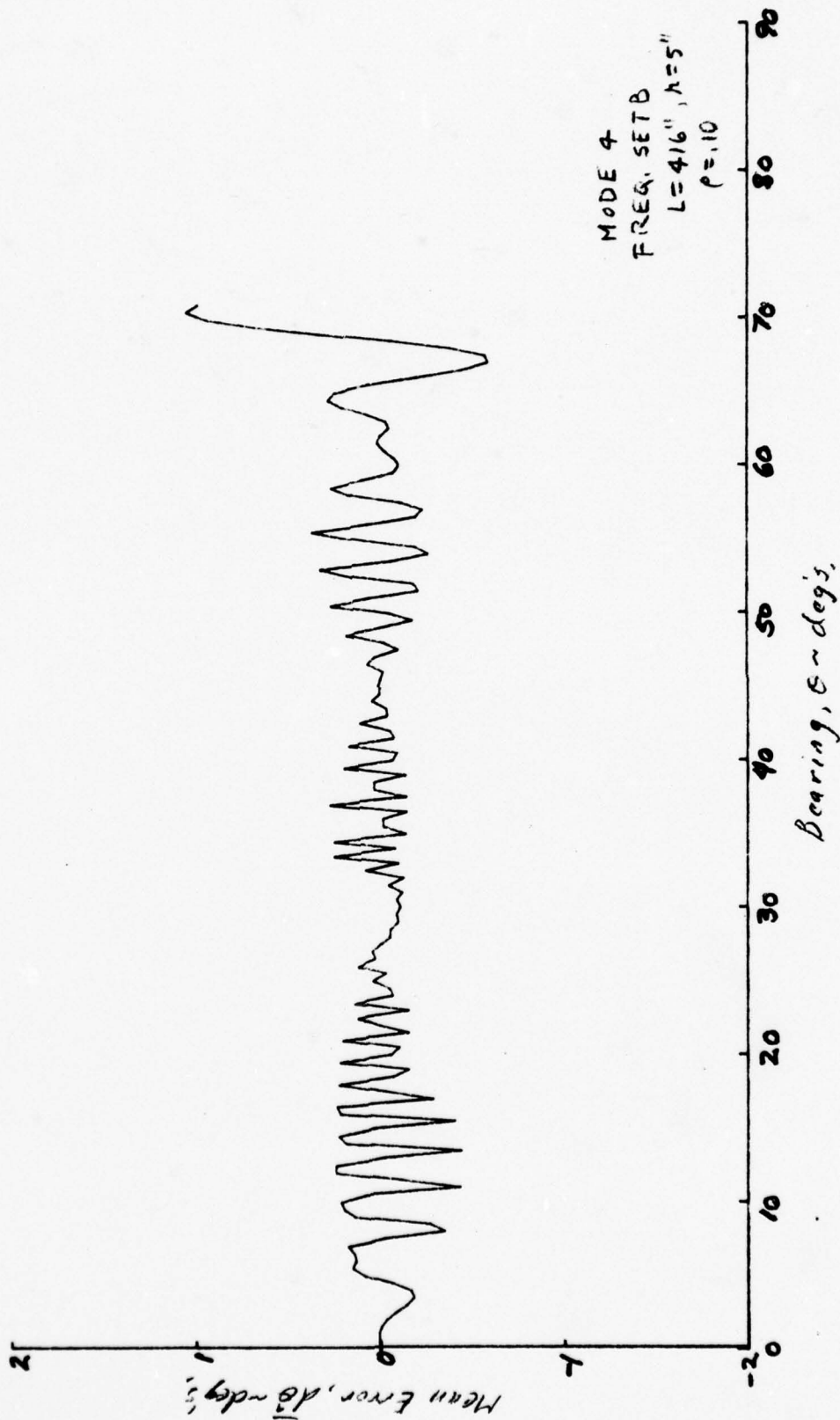


**FIG. 3-64, RUN #9**

MEAN ERROR VS. BEARING ANGLE

In a modified Tau-alarm system, an alarm is given if both a range threshold and a miss threshold are crossed. The range alarms are given by

$$\left. \begin{array}{l} \text{For Tau 2:} \quad R_{AL} \text{ (ft.)} = 10,937 + 40 V_R \text{ (f.p.s.)} \cos \alpha \\ \text{For Tau 1:} \quad R_{AL} \text{ (ft.)} = 1519 + 25 V_R \text{ (f.p.s.)} \cos \alpha \end{array} \right\} \quad (3.5-37)$$

The proposed miss thresholds are given by

$$\left. \begin{array}{l} \text{For Tau 2:} \quad M_T \text{ (ft.)} = 11,200 + 8 V_R \text{ (knots)} \\ \text{For Tau 1:} \quad M_T \text{ (ft.)} = 1700 + 7 V_R \text{ (knots)} \end{array} \right\} \quad (3.5-38)$$

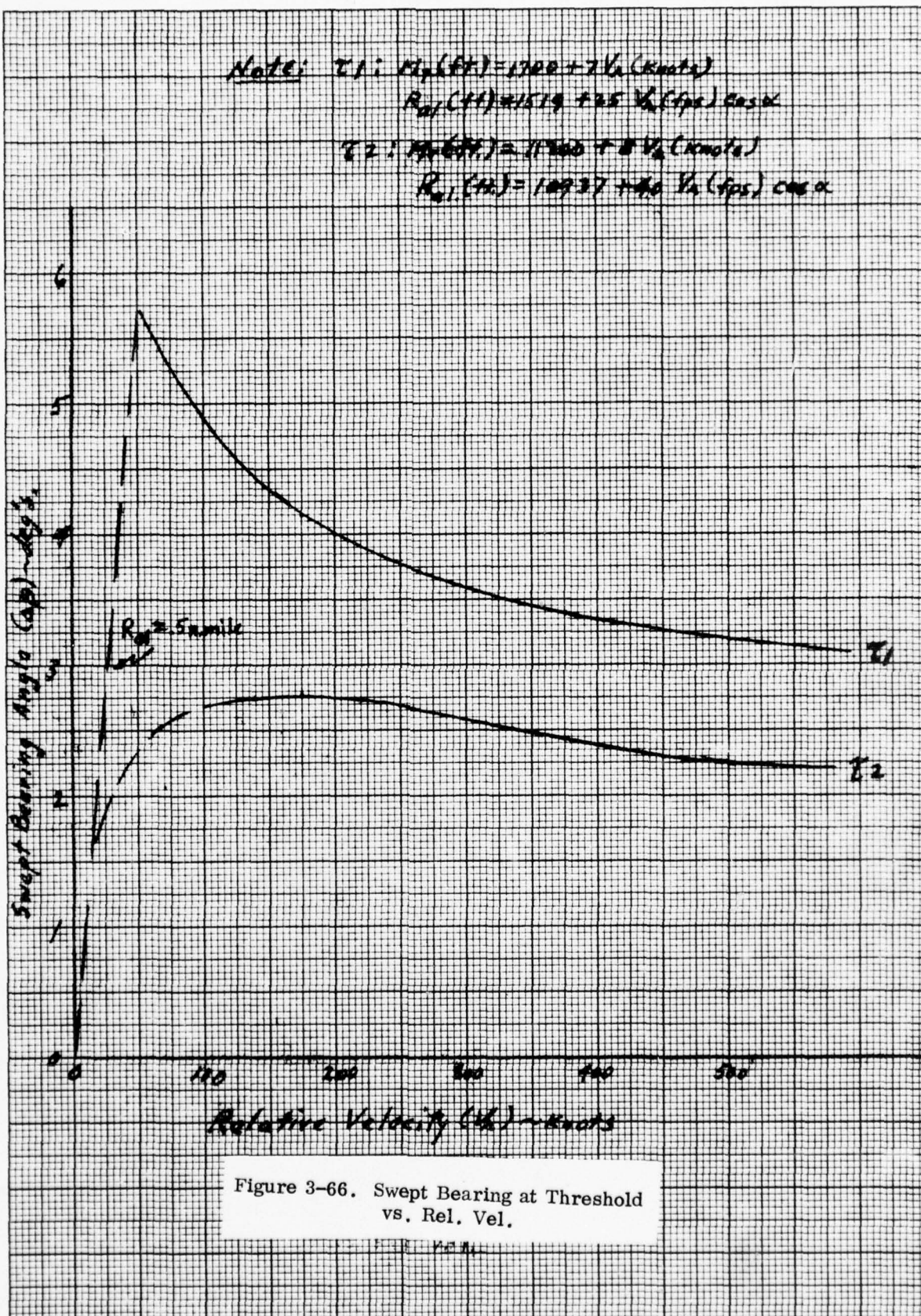
To obtain the value of  $\Delta\theta$  at miss and range threshold penetration,  $M_T$  is substituted for  $M$  and  $R_{AL}$  for  $R$  in equations 3.5-35 and 3.5-36. This leaves  $\alpha$  and  $\Delta\theta$  as unknowns, with  $V_R$  a parameter and  $\Delta t$  specified, say, at 5 seconds. By a trial and error/iteration process these equations were solved, and the functions shown in Figure 3-66 were obtained. It is seen that, in comparison to the half periods evidenced on the multipath error curves, the Tau 1 situation is of greater concern than the Tau 2 situation, since there is more chance in the former for a multipath half period to be exceeded.

If a bearing measurement  $\theta_1$  has been made, and a bearing measurement  $\theta$  is measured  $\Delta t_{12}$  seconds later, then the magnitude of the mean multipath error is

$$g(\theta_1, \Delta\theta) = |\Delta(\overline{d\hat{\theta}_T})| = |\overline{d\hat{\theta}_T}(\theta) - \overline{d\hat{\theta}_T}(\theta_1)|$$

If it is assumed there is equal probability that  $\theta_1$  can have a value anywhere between  $-90^\circ$  and  $+90^\circ$ , insofar as multipath error is concerned; and if further, a miss computation is called for and it is assumed uniformly likely that  $\Delta\theta$  will have a value between  $0^\circ$  and  $6^\circ$ , then the expectation of the mean bearing error is







$$\begin{aligned}
\bar{g} &= \iint g(\theta_1, \Delta\theta) P(\theta_1, \Delta\theta) d\theta_1 d\Delta\theta \\
&= \iint g(\theta_1, \Delta\theta) P_{\theta_1}(\theta_1) P_{\Delta\theta}(\Delta\theta) d\theta_1 d\Delta\theta \\
&= \frac{57.3}{6} \times \frac{1}{\pi} \int_{-90}^{90} \left[ \int_0^6 g(\theta_1, \Delta\theta) d\Delta\theta \right] d\theta_1
\end{aligned}$$

Assume that a particular  $\widehat{d\theta}_T$  function has a constant amplitude (A) and denote

$$F_1(\theta_1) = \frac{1}{M_1} \int_0^{M_1} g_1(\theta_1, \Delta\theta) d\Delta\theta \quad (3.5-39)$$

$$F_2(\theta_2) = \frac{1}{M_2} \int_0^{M_2} g_2(\theta_1, \Delta\theta) d\Delta\theta \quad (3.5-40)$$

where  $M_1$  and  $M_2$  are the respective (high frequency) periods respectively of the two sets of cycles such as shown in Figure 3-55.  $F_1(\theta_1)$  and  $F_2(\theta_2)$  give the same values as would be obtained by averaging over  $\Delta\theta = 6^\circ$ , assuming even multiples of  $M_1$  or of  $M_2$  in a  $6^\circ$  span. Symmetry of the  $\widehat{d\theta}_T$  function about the  $\theta = 0$  axis is assumed, so that

$$\bar{g} = \frac{2}{\pi} \left[ \int_0^{45} F_1(\theta_1) d\theta_1 + \int_{45}^{90} F_2(\theta_1) d\theta_1 \right]$$

Suppose that  $\widehat{d\theta}_T$  has  $M_1$  cycles in the region  $\theta = 0^\circ$  to  $45^\circ$ , and  $M_2$  cycles in the region  $\theta = 45^\circ$  to  $90^\circ$ . (It will be demonstrated later that  $F_1$  and  $F_2$  have the same periodicity as  $\widehat{d\theta}_T$ .)

Then

$$\bar{g} = \frac{2}{\pi} \left[ M_1 \int_0^{M_1} F_1(\theta_1) d\theta_1 + M_2 \int_{45}^{45+M_2} F_2(\theta_1) d\theta_1 \right]$$

But

$$M_1 = (\pi/4)/M_1^r; \quad M_2 = (\pi/4)/M_2^r$$

whence

$$\begin{aligned} \bar{g} &= \frac{1}{2} \left[ \frac{1}{M_1^r} \int_0^{M_1} F_1(\theta_1) d\theta_1 + \frac{1}{M_2^r} \int_0^{M_2} F_2(\theta_1) d\theta_1 \right] \\ &= \frac{1}{2} (\bar{g}_1 + \bar{g}_2) . \end{aligned} \quad (3.5-41)$$

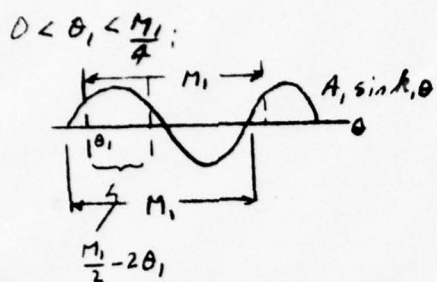
By extension of the analysis, if there are three sets of cycles in the  $\overline{d\hat{\theta}_T}$  function,

$$\bar{g} = \frac{1}{3} (\bar{g}_1 + \bar{g}_2 + \bar{g}_3) .$$

Figure 3- (see page 3-140) shows a geometric interpretation to  $F(\theta_1)$ ; it is seen that the period is reduced to  $M/2$ . Thus, for two sets of cycles,

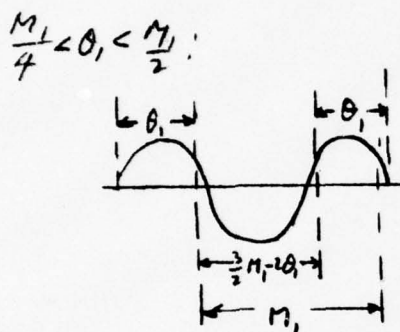
$$\begin{aligned} \bar{g} &= \frac{1}{2} \left[ \frac{2}{M_1^2} \int_0^{\frac{M_1}{2}} \left\{ \int_0^{M_1} g_1(\theta_{11}, \Delta\theta) d\Delta\theta \right\} d\theta_1 \right. \\ &\quad \left. + \frac{2}{M_2^2} \int_{45}^{45 + \frac{M_2}{2}} \left\{ \int_0^{M_2} g_2(\theta_1, \Delta\theta) d\Delta\theta \right\} d\theta_1 \right] \end{aligned} \quad (3.5-42)$$

Figure 3-68 indicates two regions of validity for the  $F_1$  function; that is for  $0 < \theta_1 < (M_1)/4$  and for  $(M_1)/4 < \theta_1 < (M_1)/2$ . Moreover, because of the absolute nature of the  $g$  function, integration must take place in parts. Performing the indicated integrations, noting that  $\theta = \theta_1 + \Delta\theta$ , we have



$$\frac{F_1 M_1}{A_1} = \int_0^{\frac{M_1}{2} - \theta_1} [\sin k_1 \theta - \sin k_1 \theta_1] d\theta$$

$$+ \int_{\frac{M_1}{2} - \theta_1}^{M_1} [\sin k_1 \theta - \sin k_1 \theta_1] d\theta$$



$$\frac{F_1 M_1}{A_1} = \int_0^{\frac{3}{2} M_1 - 2\theta_1} [\sin k_1 \theta - \sin k_1 \theta_1] d\theta$$

$$+ \int_{\frac{3}{2} M_1 - 2\theta_1}^{M_1} [\sin k_1 \theta - \sin k_1 \theta_1] d\theta$$

FIG. 3-68.  
REGIONS OF VALIDITY  
OF  $F_1$  FUNCTION



FIG. 3-69.  
EFFECT OF VARIABLE  
AMPLITUDE OF  $d\delta_T$

For  $0 < \theta_1 < \frac{M_1}{4}$ :

$$\begin{aligned} \frac{F_1 M_1}{A_1} &= \frac{2}{K_1} \cos K_1 \left( \frac{M_1}{2} - \theta_1 \right) + 4\theta_1 \sin K_1 \theta_1 \\ &\quad + \frac{\cos K_1 \theta_1}{K_1} + \frac{\cos K_1 (\theta_1 + M_1)}{K_1} \end{aligned} \quad (3.5-43)$$

For  $\frac{M_1}{4} < \theta_1 < \frac{M_1}{2}$ :

$$\begin{aligned} \frac{F_1 M_1}{A_1} &= (2M_1 - 4\theta_1) \sin K_1 \theta_1 + \frac{2}{K_1} \cos K_1 \left( \frac{3}{2} M_1 - \theta_1 \right) \\ &\quad - \frac{1}{K_1} \cos K_1 \theta_1 - \frac{1}{K_1} \cos K_1 (\theta_1 + M_1) \end{aligned} \quad (3.5-44)$$

Integration of  $F_1$  with respect to  $\theta_1$ , between the limits of 0 and  $(M_1)/2$ , leads to:

$$\begin{aligned} \bar{g}_1 &= \frac{2}{M_1} \int_0^{\frac{M_1}{2}} F_1 d\theta_1 \\ &= \frac{2A_1}{(M_1 K_1)^2} \left[ 12 \sin \frac{K_1 M_1}{4} - 7 \sin \frac{K_1 M_1}{2} + 4 \sin \frac{5}{4} K_1 M_1 \right. \\ &\quad \left. - \sin \frac{3}{2} K_1 M_1 - 3 \sin K_1 M_1 \right] \end{aligned} \quad (3.5-45)$$

Noting that  $M_1 K_1 = 2\pi$ ,

$$\bar{g}_1 (\text{deg's.}) = \frac{8}{\pi^2} A_1 (\text{deg's.}) = .8106 A_1^\circ \quad (3.5-46)$$

thus affording a ratio of probabilistic average to amplitude of the  $\overline{d\hat{\theta}_T}$  function. Evidently  $\bar{g}_2$  bears the same relation to  $A_2$ .

Since the amplitude of  $\overline{d\hat{\theta}_T}$  is actually a function of  $\theta$ , a variable value of  $\bar{g}_1$  (and of  $\bar{g}_2$ ) was found for each cycle of the  $\overline{d\hat{\theta}_T}$  plots involving frequency sets A and B.  $\bar{g}_1(\theta_1)$  and  $\bar{g}_2(\theta_2)$  were plotted (see illustration, Figure 3-69). Average ordinates were found by eye, and



overall averages were found by the latter expression, equation 3.5-41. Quantitative results are given under the column labeled  $\bar{B} = \bar{g}$ , the expected bias error, in Table 3-8.

The measure of the spread of  $g$ , about its mean value, is given by

$$\sigma^2(g) = (\overline{g^2}) - (\bar{g})^2$$

where,

$$(\overline{g^2}) = \iint g^2(\theta_1, \Delta\theta) \rho_{\theta_1}(\theta_1) \rho_{\Delta\theta}(\Delta\theta) d\theta_1 d\Delta\theta$$

By direct analogy to the derivation of equation 3.5-42, we have

$$\begin{aligned} (\overline{g^2}) &= \frac{1}{2} \left[ \frac{2}{M_1} \int_0^{\frac{M_1}{2}} U_1(\theta_1) d\theta_1 + \frac{2}{M_2} \int_{45}^{\frac{M_2}{2} + 45} U_2(\theta_1) d\theta_1 \right] \quad (3.5-47) \\ &= \frac{1}{2} \left[ \overline{g_1^2} + \overline{g_2^2} \right] \end{aligned}$$

for the case of two sets of cycles  $\widehat{d\theta_1}$  in the region  $\theta = 0^\circ$  to  $\theta = 90^\circ$ . In this equation,

$$\begin{aligned} U_1(\theta_1) &= \frac{1}{M_1} \int_0^{M_1} g_1^2(\theta_1, \Delta\theta) d\Delta\theta d\theta_1 \\ &= \frac{A_1^2}{M_1} \int_0^{M_1} [\sin K_1 \theta_1 - \sin K_1 \theta_1]^2 d\Delta\theta \quad (3.5-48) \end{aligned}$$

with like expression for  $U_2(\theta_1)$ . Substituting  $\theta = \theta_1 + \Delta\theta$ , and performing the integration,

$$\frac{U_1 M_1}{A_1^2} = \frac{M_1}{2} + M_1 \sin^2 K_1 \theta_1 + (\sin^2 K_1 \theta_1 - \cos^2 K_1 \theta_1) \frac{\sin 2 K_1 M_1}{4K_1} \\ - 2 \frac{\sin K_1 M_1 \sin^2 K_1 \theta_1}{K_1} - 3 (1 - \cos 2 K_1 M_1) \frac{\sin 2 K_1 \theta_1}{4K_1} \quad (3.5-49)$$

Integration of this equation with respect to  $\theta_1$ , recognizing that  $K_1 M_1 = 2\pi$ , gives ultimately

$$\overline{g_1^2} = \frac{2}{M_1} \int_0^{\frac{M_1}{2}} U_1(\theta_1) d\theta_1 = A_1^2$$

Similar to the process described before, the square of the amplitudes of each cycle of the  $\overline{d\hat{\theta}_T}$  plots were calculated and plotted. The average ordinates of these mean square curves were determined by eye and  $\sigma(g)$  was calculated. Results are shown by the values given in the column labeled  $\sigma_B = \sigma(g)$ , in Table 3-8.

Using an allowable sigma of  $.8^\circ$  in swept bearing error, previously proposed for reduction of false alarm probabilities, allowable values of  $\overline{B}$  and  $\sigma_B$  can be specified. Either an rms criterion or a maximum probable error criterion can be set. Considering only major contributors to swept bearing error, a feasible value for residual yaw measurement error may be taken as  $\sigma_Y = .5^\circ$ , and an allowable thermal noise sigma,  $\sigma_N = .3^\circ$  can be specified. Thus, by the rms criterion, we set

$$(\sqrt{(\overline{B})^2 + \sigma_B^2 + \sigma_Y^2 + \sigma_N^2})_{ALL} = .8^\circ$$

$$(\sqrt{(\overline{B})^2 + \sigma_B^2})_{ALL} = .56^\circ$$

By the maximum probable error criterion,

$$(\sqrt{(B)^2 + (3\sigma_B)^2 + (3\sigma_\gamma)^2 + (3\sigma_N)^2})_{ALL} = 3 \times .8^\circ \quad (\sqrt{(B)^2 + (3\sigma_B)^2})_{ALL} = 1.64^\circ$$

The statistical criteria are shown plotted in Figures 3-70a and 3-70b, with antenna-to-reflector spacing as the ordinate for the two frequency sets. By either criterion, frequency set B permits a considerable range of spacing, the optimum spacing being about 500".

### 3.5.2.2 Addendum. Mode 1 Multipath Analysis

The difference in phase angles of the signal received at the center element and the summed signal of the Mode 4 outer ring antenna elements, is proportional to four times the actual bearing angle. From equation 3.5-9, let

$$\Phi' = \Phi + q \cos \theta \quad (3.5-50)$$

where  $q = \frac{2\pi r}{\lambda}$ . From equations 3.5-10 and 3.5-11,

$$\theta = \frac{A^0}{4} = \frac{360 - \Phi'}{4} \quad (3.5-51)$$

whence,

$$\Phi'_t = 360 - 4\theta \quad (3.5-52)$$

However,  $\Phi'$  is read out modulo  $360^\circ$ . A three-fold ambiguity could, therefore, exist in the determination of  $\theta$ ; this ambiguity being a multiple of  $90^\circ$ . To resolve this ambiguity, an inner ring array, 1/5 the diameter of the outer array, is utilized, which operates in Mode 1. The bearing angle obtained from this inner array as given by

$$\theta = A_1 = 90 - \Phi'_1$$

where  $\Phi'_1$  is the phase difference between the summed signal of inner array ring elements and that of the signal of the central element.



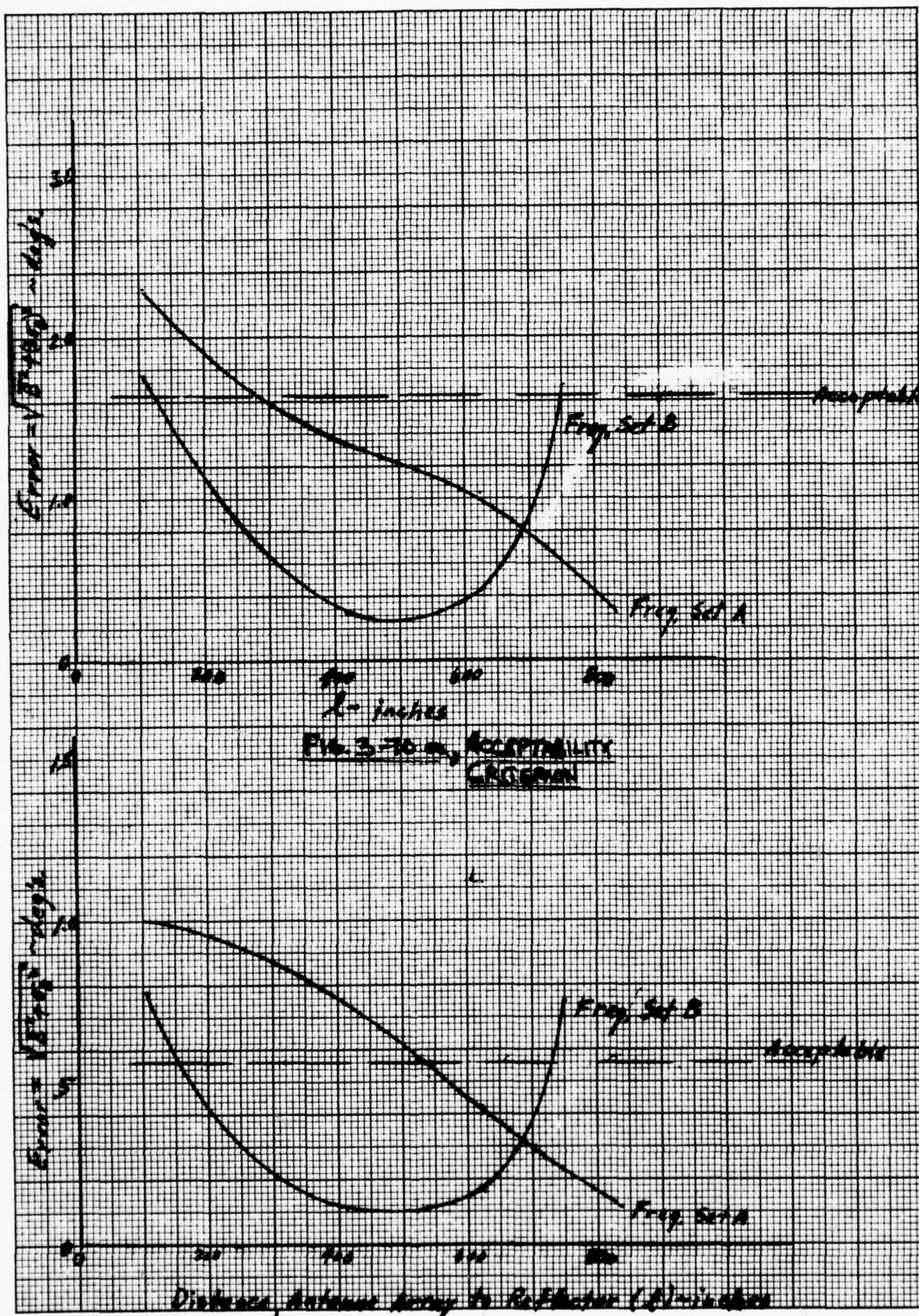


FIG. 3-70b 3-165 ACCEPTABILITY CRITERION



From the viewpoint of ambiguity resolution only, the Mode 1 array phase difference read-out would not require an accuracy of better than  $\pm 45^\circ$ . However, for PWI usage, the accuracy limits should be better than  $\pm 15^\circ$ . The equations developed for multi-path error effects for the Mode 4 array will be modified in this section to provide an analysis of Mode 1 operation. Computer runs have been made to quantitatively assess the mean error in the time averaged bearing angle. For the antenna-to-reflector spacings taken, it is shown that the error does not exceed  $6^\circ$  (using frequency set B).

#### 3.5.2.2.1 Ripple Error

In Figure 3-71, consider a ring array of  $m = 4$  elements. Relative to the arrival of the signal at element 1, the signals at the other elements have phase delays, due to path differences, which are given by

$$\begin{aligned} a_j &= \frac{2\pi}{\lambda} Z_{1j} + \frac{2\pi}{\lambda} d_{1j} \sin \left( \theta - \frac{\delta_{1j}}{2} \right) \\ &= \frac{4\pi r}{\lambda} \sin \frac{\delta_{1j}}{2} \sin \left( \theta - \frac{\delta_{1j}}{2} \right), \end{aligned} \quad (3.5-53)$$

where

$$\delta_{1j} = (j - 1) \times \frac{360}{m} = (j - 1) \times 90^\circ$$

$$j = 2 \text{ to } 4$$

Thus

$$\left. \begin{aligned} a_2 &= q (\sin \theta - \cos \theta) \\ a_3 &= -2q \cos \theta \\ a_4 &= -q (\sin \theta + \cos \theta) \end{aligned} \right\} \quad (3.5-54)$$



where

$$q = \frac{2\pi r}{\lambda} .$$

The signal at each  $j^{\text{th}}$  element is also further delayed in transmission to a common port by an amount, in Mode 1, of

$$b_j = \frac{-2\pi}{m} (j - 1) \times 1 = \frac{-\pi}{2} (j - 1) \quad (3.5-55)$$

since  $m = 4$ .

Similar to equation 3.5-7 of Section 3.5, the phase angle of the sum of the signals received at elements 1 through 4, after delays and transmission to a common port, is given by

$$\zeta' = \Phi + \zeta_1$$

where  $\zeta_1 = \omega t = 2\pi ft$ , and where

$$\Phi = \tan^{-1} \left[ \frac{S_1}{1 + S_3} \right] \quad (3.5-56)$$

$$S_1 = \sum_{j=2}^4 \sin(a_j + b_j) \quad (3.5-57)$$

$$S_3 = \sum_{j=2}^4 \cos(a_j + b_j) . \quad (3.5-58)$$

Utilizing equation 3.5-55,

$$S_1 = -\cos a_2 - \sin a_3 + \cos a_4 \quad (3.5-59)$$

$$S_3 = \sin a_1 - \cos a_3 - \sin a_4 \quad . \quad (3.5-60)$$

The difference in phase angles between the summed ring element signals and that at the central element, is (see equations 3.5-8 and 3.5-9)

$$(\Phi - \zeta_1) - (\zeta_2 - q \cos \theta) = \Phi + q \cos \theta \quad . \quad (3.5-61)$$

By analyzing equation 3.5-50, utilizing equations 3.5-54, -59, -61 and -56, it was determined that the bearing estimate is given by

$$\hat{\theta} = A = \frac{\pi}{2} - [\Phi + q \cos \theta] \quad . \quad (3.5-62)$$

The ripple error is  $d\theta_r = \hat{\theta} - \theta_t$ , where subscript  $t$  denotes true value. The angle  $\Phi$  is taken such that

$$-\frac{\pi}{2} \leq \Phi \leq \frac{\pi}{2} \quad .$$

Table 3-9 shows numerical values of the ripple error for  $\theta$  in increments of .5 degrees, for a nominal frequency of 1607.5 MHz ( $\lambda = 7.347''$ ), and for  $r = .15 \lambda (= 1.102'')$ . Peak values occur at  $\theta = 22^\circ$  and  $\theta = 68^\circ$ , with a magnitude of about  $2.3^\circ$ . The ripple error vanishes at  $\theta = 0^\circ, 45^\circ$  and  $90^\circ$ .

If the frequency is randomly varied from sample to sample, the time averaged estimate of bearing angle is (over .062 seconds)

$$\begin{aligned} \hat{\theta} &= \frac{1}{62} \sum_{i=1}^{62} A_{ti} \\ &= \frac{1}{62} \left[ \sum_i \Phi_{ti} + 2\pi r \cos \theta \sum_i \frac{1}{\lambda_i} \right] \quad . \quad (3.5-63) \end{aligned}$$



RIPPLE ERROR PROGRAM MODE 1

THLO=0.  
THHI=90.  
THINC=.5

TABLE 3-9.

RUN #10  
 $f_{nom} = 1607.5 \text{ MHz}$

| THETA | DTHR   | $\theta$ | $d\theta$ | $\theta$ | $d\theta$ |
|-------|--------|----------|-----------|----------|-----------|
| 0.00  | -0.000 |          |           | 60.50    | -1.968    |
| 0.50  | 0.082  |          |           | 61.00    | -2.006    |
| 1.00  | 0.165  | 30.50    | 1.886     | 61.50    | -2.042    |
| 1.50  | 0.247  | 31.00    | 1.842     | 62.00    | -2.075    |
| 2.00  | 0.328  | 31.50    | 1.796     | 62.50    | -2.105    |
| 2.50  | 0.410  | 32.00    | 1.747     | 63.00    | -2.133    |
| 3.00  | 0.491  | 32.50    | 1.697     | 63.50    | -2.159    |
| 3.50  | 0.571  | 33.00    | 1.644     | 64.00    | -2.182    |
| 4.00  | 0.650  | 33.50    | 1.590     | 64.50    | -2.203    |
| 4.50  | 0.728  | 34.00    | 1.534     | 65.00    | -2.220    |
| 5.00  | 0.806  | 34.50    | 1.477     | 65.50    | -2.236    |
| 5.50  | 0.882  | 35.00    | 1.417     | 66.00    | -2.248    |
| 6.00  | 0.957  | 35.50    | 1.356     | 66.50    | -2.258    |
| 6.50  | 1.031  | 36.00    | 1.294     | 67.00    | -2.265    |
| 7.00  | 1.104  | 36.50    | 1.230     | 67.50    | -2.270    |
| 7.50  | 1.175  | 37.00    | 1.165     | 68.00    | -2.272    |
| 8.00  | 1.244  | 37.50    | 1.098     | 68.50    | -2.270    |
| 8.50  | 1.312  | 38.00    | 1.031     | 69.00    | -2.267    |
| 9.00  | 1.378  | 38.50    | 0.962     | 69.50    | -2.260    |
| 9.50  | 1.442  | 39.00    | 0.892     | 70.00    | -2.251    |
| 10.00 | 1.504  | 39.50    | 0.821     | 70.50    | -2.238    |
| 10.50 | 1.564  | 40.00    | 0.749     | 71.00    | -2.223    |
| 11.00 | 1.622  | 40.50    | 0.677     | 71.50    | -2.206    |
| 11.50 | 1.678  | 41.00    | 0.603     | 72.00    | -2.185    |
| 12.00 | 1.732  | 41.50    | 0.529     | 72.50    | -2.162    |
| 12.50 | 1.784  | 42.00    | 0.455     | 73.00    | -2.136    |
| 13.00 | 1.833  | 42.50    | 0.380     | 73.50    | -2.107    |
| 13.50 | 1.879  | 43.00    | 0.304     | 74.00    | -2.076    |
| 14.00 | 1.924  | 43.50    | 0.229     | 74.50    | -2.042    |
| 14.50 | 1.966  | 44.00    | 0.153     | 75.00    | -2.005    |
| 15.00 | 2.005  | 44.50    | 0.076     | 75.50    | -1.966    |
| 15.50 | 2.042  | 45.00    | 0.000     | 76.00    | -1.924    |
| 16.00 | 2.076  | 45.50    | -0.076    | 76.50    | -1.880    |
| 16.50 | 2.107  | 46.00    | -0.152    | 77.00    | -1.833    |
| 17.00 | 2.136  | 46.50    | -0.229    | 77.50    | -1.784    |
| 17.50 | 2.162  | 47.00    | -0.304    | 78.00    | -1.732    |
| 18.00 | 2.185  | 47.50    | -0.380    | 78.50    | -1.679    |
| 18.50 | 2.206  | 48.00    | -0.455    | 79.00    | -1.623    |
| 19.00 | 2.223  | 48.50    | -0.529    | 79.50    | -1.564    |
| 19.50 | 2.238  | 49.00    | -0.603    | 80.00    | -1.504    |
| 20.00 | 2.251  | 49.50    | -0.677    | 80.50    | -1.442    |
| 20.50 | 2.260  | 50.00    | -0.749    | 81.00    | -1.378    |
| 21.00 | 2.267  | 50.50    | -0.821    | 81.50    | -1.312    |
| 21.50 | 2.270  | 51.00    | -0.892    | 82.00    | -1.244    |
| 22.00 | 2.272  | 51.50    | -0.962    | 82.50    | -1.175    |
| 22.50 | 2.270  | 52.00    | -1.031    | 83.00    | -1.104    |
| 23.00 | 2.265  | 52.50    | -1.098    | 83.50    | -1.031    |
| 23.50 | 2.258  | 53.00    | -1.165    | 84.00    | -0.958    |
| 24.00 | 2.248  | 53.50    | -1.230    | 84.50    | -0.882    |
| 24.50 | 2.236  | 54.00    | -1.294    | 85.00    | -0.806    |
| 25.00 | 2.220  | 54.50    | -1.356    | 85.50    | -0.729    |
| 25.50 | 2.202  | 55.00    | -1.417    | 86.00    | -0.650    |
| 26.00 | 2.182  | 55.50    | -1.477    | 86.50    | -0.571    |
| 26.50 | 2.159  | 56.00    | -1.534    | 87.00    | -0.491    |
| 27.00 | 2.133  | 56.50    | -1.590    | 87.50    | -0.410    |
| 27.50 | 2.105  | 57.00    | -1.644    | 88.00    | -0.329    |
| 28.00 | 2.075  | 57.50    | -1.697    | 88.50    | -0.247    |
| 28.50 | 2.042  | 58.00    | -1.747    | 89.00    | -0.165    |
| 29.00 | 2.006  | 58.50    | -1.796    | 89.50    | -0.082    |
| 29.50 | 1.968  | 59.00    | -1.842    | 90.00    | -0.000    |
| 30.00 | 1.929  | 59.50    | -1.886    |          |           |
|       |        | 60.00    | -1.929    |          |           |

The mean ripple error in the average is

$$\overline{d\hat{\theta}_r} (\text{deg's.}) = 57.2958 \left[ \frac{\sum_{k=1}^n A_{t_k}}{n} \right] - \theta_t^\circ \quad (3.5-64)$$

where  $n$  = number of frequencies available at each sampling instant ( $n$  is usually taken as 4). In this equation, for the  $k^{\text{th}}$  frequency,

$$A_{t_k} = \frac{\pi}{2} - \left[ \Phi_{t_k} + \frac{2\pi r \cos \theta}{\lambda_k} \right] \quad (3.5-65)$$

$$\Phi_{t_k} = \tan^{-1} \left[ \frac{S_1}{1 + S_3} \right]_k \quad (3.5-66)$$

Computer runs made with the two sets of frequencies (A and B) show the same periodicity in  $\overline{d\hat{\theta}_r}$  as for the single nominal frequency, and the peak amplitude remains at about  $2.3^\circ$ . The sigma of the ripple error in the time average bearing estimate was not computed, but is part of an overall sigma which includes the multipath error effect.

#### 3.5.2.2.2 Multipath Error

The configuration of a plane reflector located at a distance  $l$  from the center element, and normal to the line defined by the 1-3 elements, is depicted in Figure 3-72. The analysis of Section 3.5.3.1 holds, with some modification for Mode 1 operation. Thus, at a specified (true) bearing angle  $\theta$ , and for a particular ( $k^{\text{th}}$ ) frequency, a possible bearing estimate obtained by phase difference measurement, in the presence of multipath, is

$$A_{\text{IND}_k} = \frac{\pi}{2} \left[ \Phi_{\text{IND}_k} + \mu_{\text{OK}} + \frac{2\pi r \cos \theta}{\lambda_k} \right] \quad (3.5-67)$$

where

$$\Phi_{\text{IND}_k} = \tan^{-1} \left[ \frac{S_1 + \rho (S_2 - \sin \psi_1)}{(1 + S_3) + \rho (S_4 + \cos \psi_1)} \right]_k \quad (3.5-68)$$

$$-\frac{\pi}{2} \leq \Phi_{\text{IND}_k} \leq \frac{\pi}{2}$$

$$\mu_{o_k} = \tan^{-1} \left[ \frac{\rho \sin \psi_o}{1 + \rho \cos \psi_o} \right]_k \quad (3.5-69)$$

$$-\frac{\pi}{2} \leq \mu_{o_k} \leq \frac{\pi}{2}$$

and where (see main text following equation 3.5-26)

$$S_{1k} = [-\cos a_2 - \sin a_3 + \cos a_4]_k \quad (3.5-70)$$

$$S_{2k} = [-\cos(\psi_2 - a_2) + \sin(\psi_3 + a_3) + \cos(\psi_4 - a_4)]_k \quad (3.5-71)$$

$$S_{3k} = [\sin a_2 - \cos a_3 - \sin a_4]_k \quad (3.5-72)$$

$$S_{4k} = [-\sin(\psi_2 - a_2) - \cos(\psi_3 - a_3) + \sin(\psi_4 - a_4)]_k \quad (3.5-73)$$

From equations 3.5-54

$$a_{2k} = q_k (\sin \theta - \cos \theta) \quad (3.5-74)$$

$$a_{3k} = 2 q_k \cos \theta \quad (3.5-75)$$

$$a_{4k} = -q_k (\sin \theta + \cos \theta) \quad (3.5-76)$$

where

$$q_k = \frac{2\pi r}{\lambda_k} \quad (3.5-77)$$

From equations 3.5-20, -21, -23 of Section 3.5.3.1,

$$\psi_{0k} = \psi_{2k} = \psi_4 = \frac{4\pi l \cos \theta}{\lambda_k} \quad (3.5-78)$$

$$\psi_{1k} = \frac{4\pi}{\lambda_k} (l + r) \cos \theta \quad (3.5-79)$$

$$\psi_{3k} = \frac{4\pi}{\lambda_k} (l - r) \cos \theta \quad (3.5-80)$$

where

$$\lambda_k \text{ (inches)} = \frac{3 \times 10^{10}}{2.54 \lambda_k}$$

$f_k$  being one of four possible frequencies.

At a specified  $\theta_1$ , one of the frequencies can produce a maximum deviation from true value, and another frequency will produce a minimum deviation:

$$d\theta_{T_{\max}} = 57.2958 A_{\text{IND}_k} l_{\max} - \theta^\circ ; \text{deg's.} \quad (3.5-81)$$

$$d\theta_{T_{\min}} = 57.2958 A_{\text{IND}_k} l_{\min} - \theta^\circ ; \text{deg's.} \quad (3.5-82)$$

(Subscript T denotes total error, including both ripple and multipath errors.)



The time averaged estimate of bearing is

$$\hat{\theta} = A_{\text{IND}} ]_{\text{AVE}} = \frac{1}{62} \sum_{i=1}^{62} A_{\text{IND}} ]_i \quad (3.5-83)$$

where  $A_{\text{IND}i}$  has one of the  $k$  possible (random) values given by equation A-17, at each of the 62 sampling times. The mean error in the time average (see derivation leading to similar result, Equation 3.5-31) is

$$\overline{d\hat{\theta}}_T (\text{deg's.}) = \frac{180}{\pi} \left[ \frac{\sum_{k=1}^4 A_{\text{IND}k}}{4} \right] - \theta^\circ \quad (3.5-84)$$

The standard deviation of the error in the time average (see derivation leading to similar result, Equation 3.5-33) is

$$\sigma(d\hat{\theta})_T (\text{deg's.}) = \frac{57.2958}{2\sqrt{62}} \left[ \sum_{k=1}^4 A_{\text{IND}k}^2 - \frac{1}{4} \left( \sum_{k=1}^4 A_{\text{IND}k} \right)^2 \right]^{\frac{1}{2}} \quad (3.5-85)$$

#### 3.5.2.2.3 Quantitative Evaluation

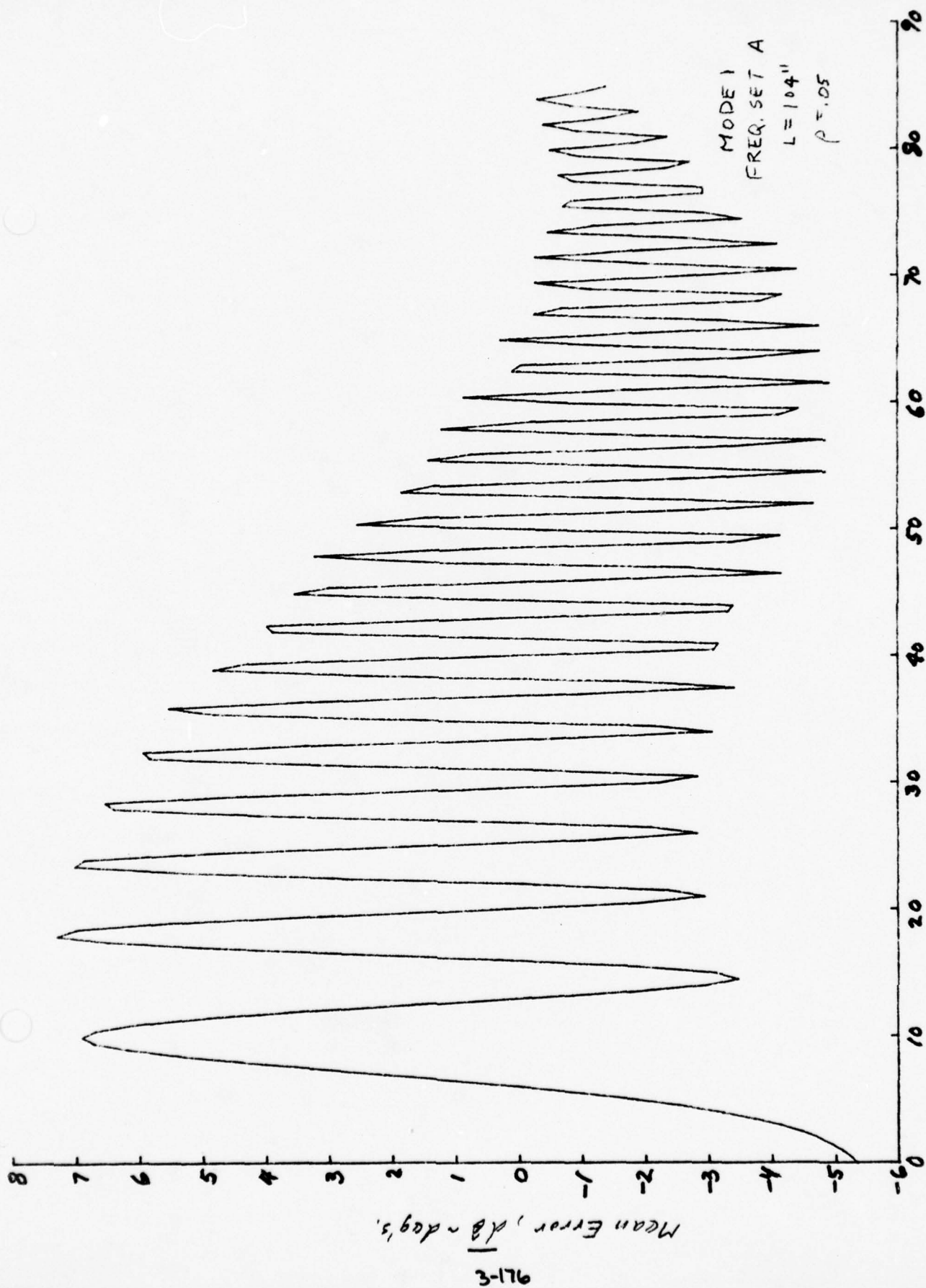
Computer runs were made for  $\iota = 104''$  and for  $\iota = 416''$ , and for the two sets (A and B) of frequencies, varying  $\theta$  in  $.5^\circ$  increments to an appropriate  $\theta_{\text{LIM}}$ . A portion of a print-out ( $\iota = 416''$ , set B,  $\rho = .05$ ) is presented in Table 3-10. Figures 3-73 through 3-76 are plots of mean bearing error versus actual bearing angle. It is seen that the maximum amplitude of error decreases as  $\theta$  increases, and also decreases as reflector-to-antenna spacing is increased. Frequency set B provides a smaller maximum amplitude, for given spacing. Pertinent results are summarized in Table 3-11. If an allowable error of  $15^\circ$ , at any  $\theta$ , is assumed to be a  $3\sigma$  limit; and if the major multipath contributor has a spacing on the order of  $400''$ , then frequency set B certainly provides acceptable accuracy for the Mode 1 antenna operation as PWI. It should be noted that the mean ripple error can be a substantial portion of the total mean error, particularly for run #14.

F(1)=1596.,1604.,1611.,1619.  
R=1.10205  
L=416.  
RD=.05  
THLO=0.  
THHI=71.  
HINC=.5

RUN #14

TABLE 3-10. Mean Bearing Error (DTHT) as  
Function of Bearing Angle (Theta)

| THETA | DTHR     | DTHT     | DTHMAX  | DTHMIN   | SIGMA   |
|-------|----------|----------|---------|----------|---------|
| 0.00  | -0.00000 | -1.11650 | 0.35932 | -2.55777 | 0.13927 |
| 0.50  | 0.08846  | -1.02680 | 0.65709 | -2.66317 | 0.15179 |
| 1.00  | 0.16480  | -0.92376 | 1.25970 | -3.02597 | 0.19336 |
| 1.50  | 0.24692  | -0.79205 | 2.14667 | -3.59750 | 0.27383 |
| 2.00  | 0.32870  | -0.60942 | 3.25953 | -4.27993 | 0.38786 |
| 2.50  | 0.41003  | -0.35101 | 4.47216 | -4.90628 | 0.51785 |
| 3.00  | 0.49080  | 0.00316  | 5.56503 | -5.23022 | 0.63500 |
| 3.50  | 0.57090  | 0.45717  | 6.22269 | -5.14515 | 0.69329 |
| 4.00  | 0.65022  | 0.98390  | 6.33959 | -4.71998 | 0.66500 |
| 4.50  | 0.72865  | 1.50453  | 5.89333 | -3.14309 | 0.49663 |
| 5.00  | 0.80609  | 1.87418  | 4.06253 | -0.41575 | 0.20640 |
| 5.50  | 0.88244  | 1.91697  | 4.47477 | -0.78602 | 0.25050 |
| 6.00  | 0.95758  | 1.55123  | 6.40635 | -3.62272 | 0.57635 |
| 6.50  | 1.03143  | 0.91888  | 6.64253 | -4.68061 | 0.69744 |
| 7.00  | 1.10388  | 0.35049  | 4.86161 | -3.93928 | 0.48652 |
| 7.50  | 1.17485  | 0.18487  | 1.23651 | -0.88070 | 0.10968 |
| 8.00  | 1.24423  | 0.59662  | 5.48222 | -4.10746 | 0.54846 |
| 8.50  | 1.31193  | 1.48657  | 6.89624 | -4.18324 | 0.68235 |
| 9.00  | 1.37788  | 2.31949  | 5.10198 | -0.56052 | 0.28544 |
| 9.50  | 1.44199  | 2.25614  | 5.86736 | -1.55846 | 0.40309 |
| 10.00 | 1.50417  | 1.36081  | 7.01045 | -4.16140 | 0.69266 |
| 10.50 | 1.56435  | 0.72355  | 3.32114 | -1.78732 | 0.25750 |
| 11.00 | 1.62245  | 0.98469  | 5.47216 | -3.40538 | 0.51079 |
| 11.50 | 1.67841  | 2.04304  | 7.12486 | -3.20600 | 0.62248 |
| 12.00 | 1.73216  | 2.66592  | 4.06963 | 1.18736  | 0.13247 |
| 12.50 | 1.78362  | 1.78991  | 7.27123 | -3.78684 | 0.68895 |
| 13.00 | 1.83275  | 1.07330  | 3.06022 | -0.84606 | 0.19592 |
| 13.50 | 1.87949  | 1.50506  | 6.74309 | -3.65857 | 0.63764 |
| 14.00 | 1.92378  | 2.67023  | 5.60119 | -0.30176 | 0.33051 |
| 14.50 | 1.96558  | 2.32153  | 7.09884 | -2.61137 | 0.59205 |
| 15.00 | 2.00483  | 1.38278  | 4.37150 | -1.53366 | 0.33832 |
| 15.50 | 2.04150  | 1.68111  | 6.74440 | -3.36176 | 0.62564 |
| 16.00 | 2.07556  | 2.81730  | 4.73292 | 0.91267  | 0.21322 |
| 16.50 | 2.10696  | 2.12000  | 7.45081 | -3.27551 | 0.67472 |
| 17.00 | 2.13568  | 1.56339  | 2.22174 | 0.86332  | 0.06779 |
| 17.50 | 2.16169  | 2.32441  | 7.36542 | -2.70689 | 0.63373 |
| 18.00 | 2.18496  | 2.66188  | 6.11181 | -0.84930 | 0.43425 |
| 18.50 | 2.20549  | 1.74731  | 4.29625 | -0.75546 | 0.31726 |
| 19.00 | 2.22326  | 2.10022  | 7.44167 | -3.24110 | 0.67531 |
| 19.50 | 2.23825  | 2.77324  | 5.04848 | 0.53353  | 0.27906 |
| 20.00 | 2.25045  | 1.88181  | 4.95605 | -1.23354 | 0.38064 |
| 20.50 | 2.25987  | 2.15243  | 7.46122 | -3.15521 | 0.66941 |
| 21.00 | 2.26650  | 2.64815  | 5.86526 | -0.56195 | 0.38574 |
| 21.50 | 2.27035  | 1.97514  | 3.56002 | 0.34451  | 0.17316 |
| 22.00 | 2.27142  | 2.37938  | 7.09364 | -2.44420 | 0.58626 |
| 22.50 | 2.26972  | 2.28206  | 7.30915 | -2.76627 | 0.62515 |
| 23.00 | 2.26527  | 2.05641  | 5.11736 | -0.96566 | 0.34101 |
| 23.50 | 2.25808  | 2.63006  | 3.84743 | 1.34736  | 0.11470 |
| 24.00 | 2.24818  | 2.08152  | 6.03386 | -1.92808 | 0.45764 |
| 24.50 | 2.23557  | 2.17565  | 7.22153 | -2.98523 | 0.63169 |
| 25.00 | 2.22030  | 2.18533  | 7.15099 | -2.81633 | 0.60609 |
| 25.50 | 2.20239  | 2.10931  | 6.12499 | -1.90301 | 0.44731 |
| 26.00 | 2.18187  | 2.36769  | 4.69808 | 0.02505  | 0.22269 |
| 26.50 | 2.15878  | 2.20528  | 3.32704 | 1.03242  | 0.11490 |
| 27.00 | 2.13314  | 2.24145  | 4.95597 | -0.58313 | 0.26706 |
| 27.50 | 2.10501  | 2.12907  | 5.91489 | -1.79192 | 0.40516 |



Bearing,  $\theta$  - deg's.  
FIG. 3-13.  $\delta$  vs  $\theta$

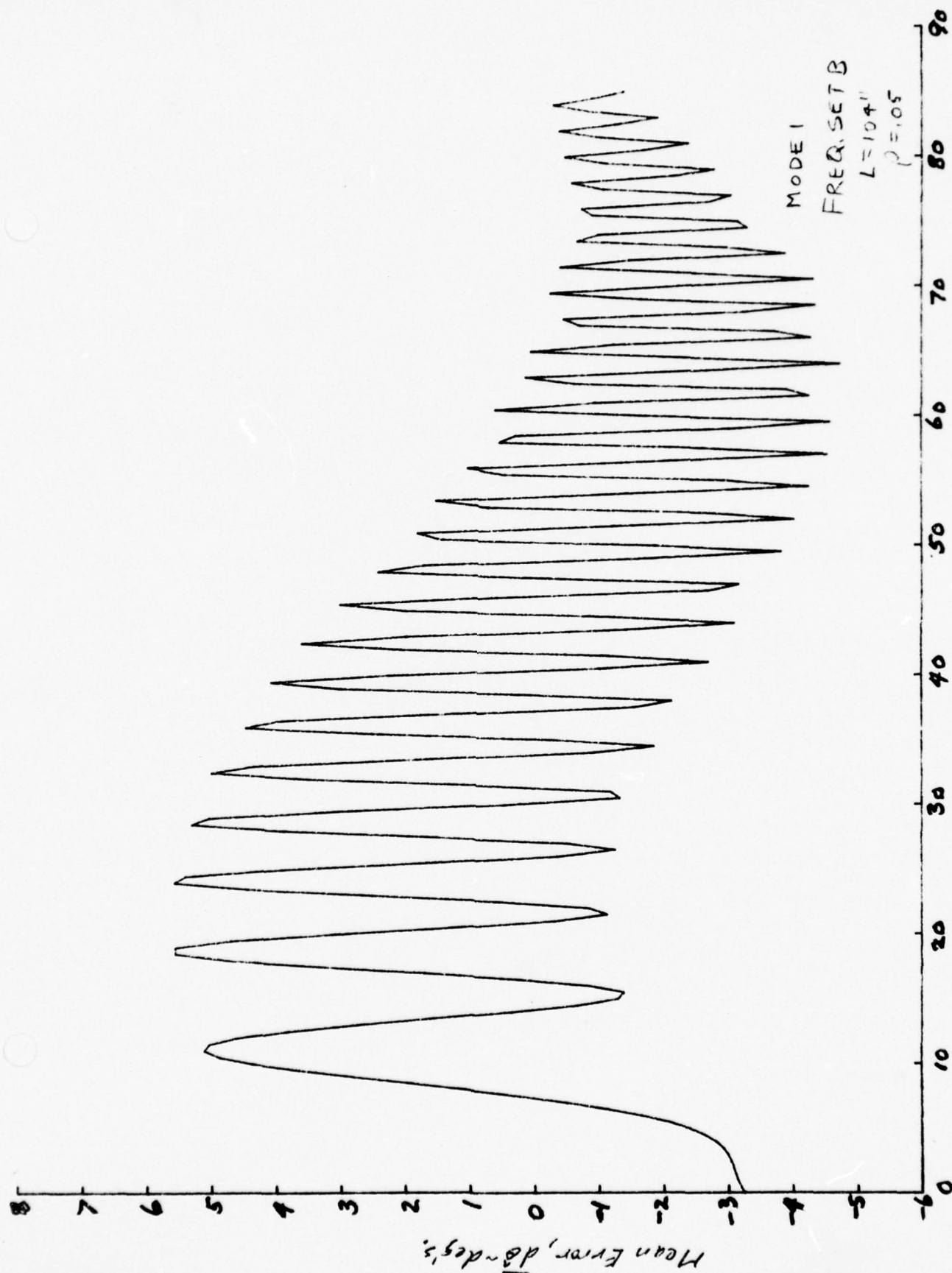


FIG. 3-74.  $\overline{\delta\theta}$  vs.  $\theta$



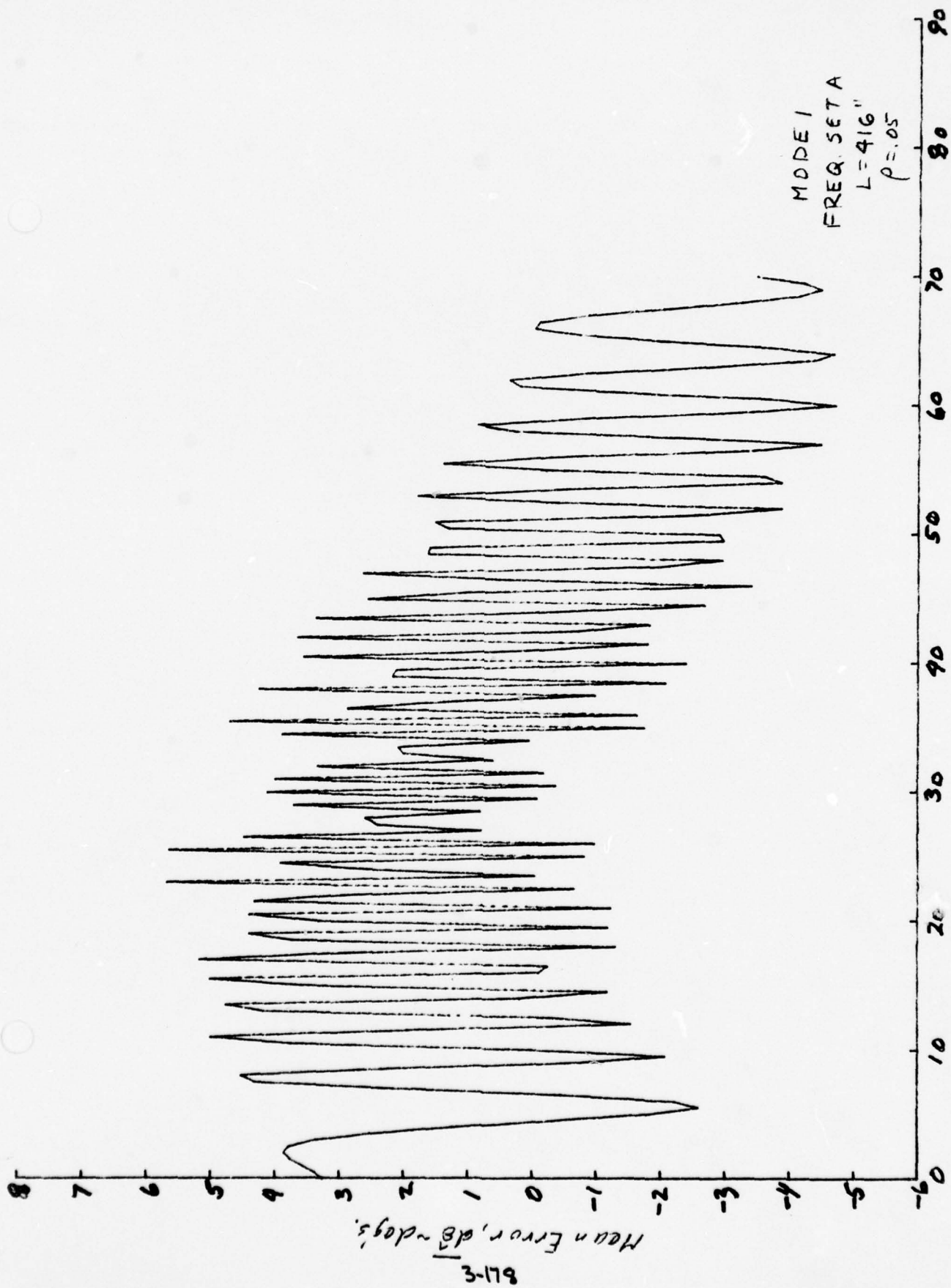
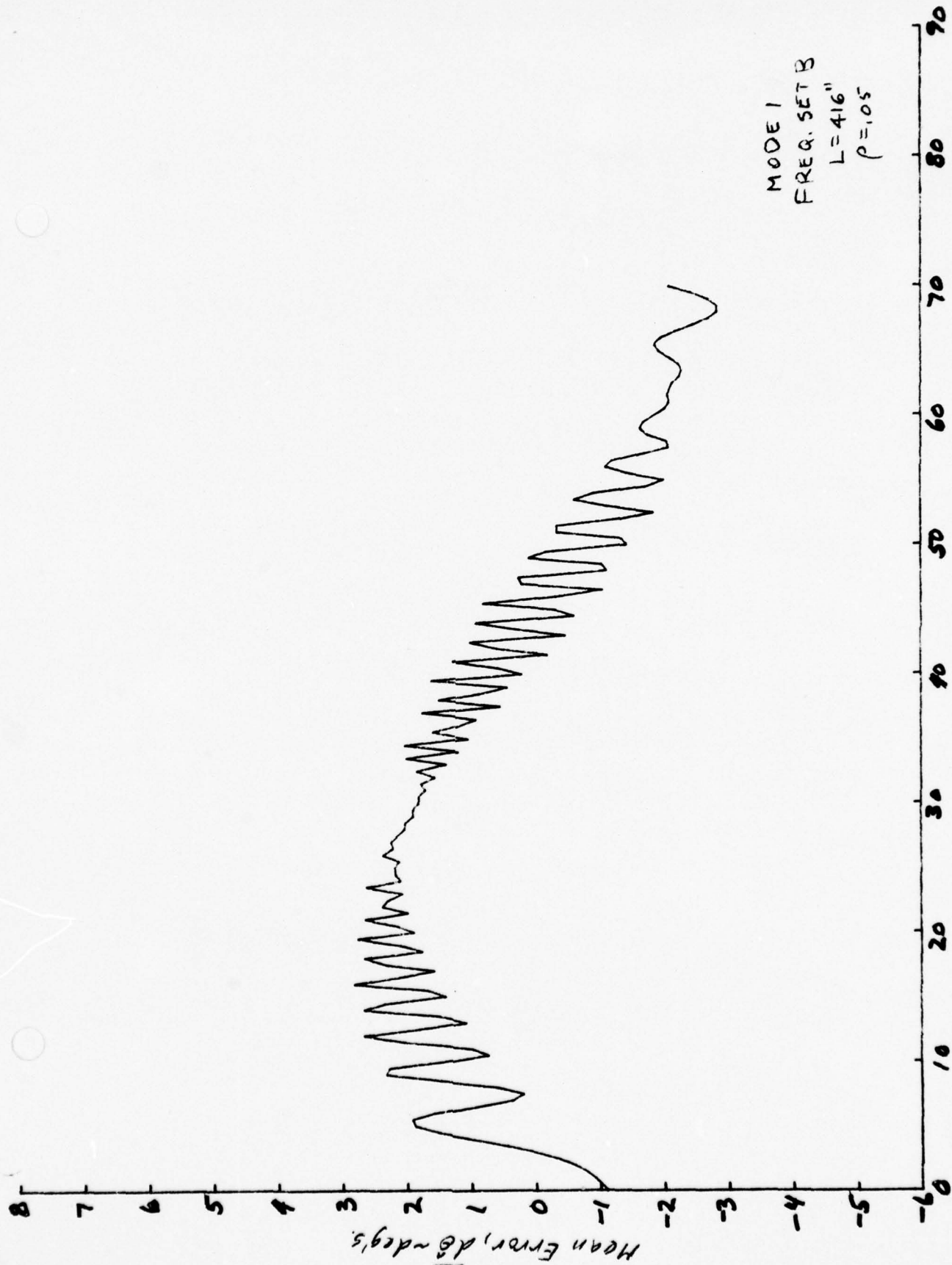


FIG. 3-75.  $\overline{dB}$  vs  $\theta$



Bearing,  $\theta$  ~ deg's,  
Fig. 3-76.  $\overline{\delta}$  vs.  $\theta$

Table 3-11. Summary, Mode 1

| Run No. | Freq. Set | $\ell''$ | Max $d\theta_{\max}$ | Min $d\theta_{\min}$ | Max $ d\theta_T $ | Max $\sigma(d\hat{\theta})_T$ | Max $d\hat{\theta}_2$ |
|---------|-----------|----------|----------------------|----------------------|-------------------|-------------------------------|-----------------------|
| 11      | A         | 104      | 7.44                 | -5.73                | 7.31              | .16                           | 2.25                  |
| 13      | A         | 416      | 7.43                 | -5.02                | 5.69              | .55                           | 2.25                  |
| 12      | B         | 104      | 7.45                 | -5.72                | 5.58              | .52                           | 2.27                  |
| 14      | B         | 416      | 7.46                 | -5.12                | 2.84              | .70                           | 2.27                  |

Set A: 1599, 1600, 1603, 1604 MHz

Set B: 1596, 1604, 1611, 1619 MHz

#### 3.5.2.2.4 Calibration Constant Compensation

If the aircraft longitudinal axis is aligned with the 0-1 axis of the ring array (see Figures 3-48 and 3-71), then the direction-of-arrival angle  $\theta$  is identical with relative bearing angle (as measured in a plane parallel to the wing plane). As indicated in Section 3.5.2.2, the angle  $\theta$  is given, for Mode 1 operation, by

$$\theta^{(1)} = 90^\circ - \Phi_1' = 90^\circ - (\zeta' - \zeta_0)_1$$

where  $\zeta'$  is the phase angle of the summed signals received by all outer elements,  $\zeta_0$  is the phase angle of the signal at the center element 0, all relative to the phase angle of element 1.

It would, therefore, be necessary to subtract the output phase difference  $\Phi_1'$  from  $90^\circ$ , in the data processor, in order to obtain true bearing angle. The same effect can be achieved more expeditiously by simply physically aligning the 0-2 axis of the ring array with the aircraft axis and taking the phase difference as  $\zeta_0 - \zeta'$ . This result can be seen from Figure 3-77, since

$$-\theta_t = 90^\circ - \theta^{(1)} = (\zeta' - \zeta_0)_1$$

and by this means a direct measure of true bearing angle is obtained.

In like fashion, for the Mode 4 antenna, we have by equation 3.5-51,

$$\theta^{(4)} = 90^\circ - \Phi_4' = 90 - \frac{1}{4} (\zeta' - \zeta_0)_4$$

Compensation is effected by aligning the 0-5 axis of the array with the aircraft axis (Figure 3-77). Thus

$$-\theta_t = 90^\circ - \theta^{(4)} = \frac{(\zeta' - \zeta_0)_4}{4},$$

making the bearing angle directly proportional to the measured phase difference.



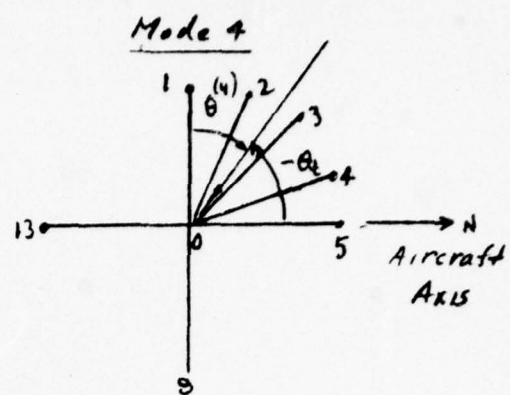
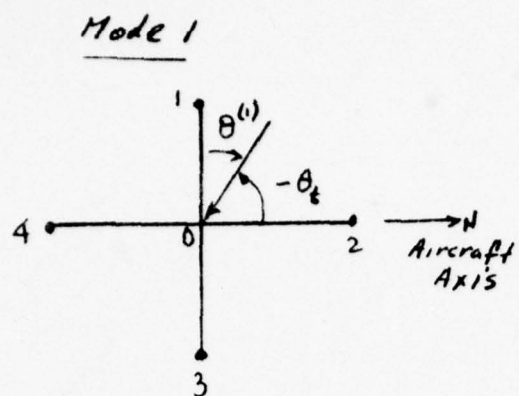


FIG. 3-77.  
ORIENTATION OF RING ARRAYS  
WITH RESPECT TO AIRCRAFT AXIS

The alignments indicated can be accomplished by optical boresighting techniques, which should achieve an alignment accuracy of a few minutes of arc.

### 3.5.2.3 Estimation of Fruit Errors in Bearing Measurement

#### 3.5.2.3.1 Assumptions

Fruit wave fronts will impinge on the protected aircraft with arrival angles which can reasonably be taken as uniformly distributed in a statistical sense over  $0^\circ$  to  $360^\circ$  in azimuth when the aircraft is centered in a dense traffic region. It will also be assumed that reply pulses and fruit pulses received above threshold level are processed in a manner which permits them to contribute linearly with equal weights to a smoothed bearing reading. As a result of the integration(smoothing),the variability of the bearing measurement, caused by the fruit signals, will be substantially diminished. In fact, the measurement can be regarded as being the mean value of  $n$  individual bearing measurements comprising a group of reply bearings from a selected target combined with much fewer fruit bearings. By virtue of the range gating process used in the bearing measurement,only those undetected fruit pulses that fall in the range gate can produce adverse effects. When such events occur,it will be assumed that the resulting measurements have random values with a uniform distribution from  $0^\circ$  to  $360^\circ$ . This assumption is a worst case one which results in a somewhat exaggerated estimate of the fruit error as compared with the error obtained when the distribution of fruit arrival angles is assumed to be leptokurtic (peaky) and having its mode coincident with the true bearing. In this respect, a triangular distribution is intuitively more realistic since it would tend to characterize the effect of combination of the true vector signal with the random fruit vector, and to allow for the effects of subthreshold fruit.

#### 3.5.2.3.2 Analysis

Let  $\rho$  = ratio of fruit pulses to reply pulses entering a phase gate

$n$  = number of reply pulses and fruit pulses contributing to a relative bearing measurement ( $= n_R + n_F$ )

Then 
$$n_R = \frac{n}{1 + \rho} \quad (3.5-86)$$

and 
$$n_F = \frac{\rho n}{1 + \rho} \quad (3.5-87)$$

Based on the above mentioned assumption of a linear combination of reply and fruit bearings in the measured integrated bearing result, the latter is given by:

$$\beta_{FR} = \frac{1}{n} \sum_{i=1}^{n_R} (\beta_R)_i + \frac{n_F}{\sum_{i=1}^{n_F} (\beta_F)_i} \quad (3.5-88)$$

in which  $\beta_R$  is the bearing of a reply, and  $\beta_F$  the bearing of a fruit strike.

Equation 3.5-88, written in terms of the mean  $\bar{\beta}_R$ , is

$$\begin{aligned} \beta_{FR} &= \frac{n_R}{n} \bar{\beta}_R + \frac{1}{n} \sum_{i=1}^{n_F} \beta_{F_i} \\ \therefore \beta_{FR} - \bar{\beta}_R &= \left( \frac{n_R}{n} - 1 \right) \bar{\beta}_R + \frac{1}{n} \sum_{i=1}^{n_F} \beta_{F_i} \\ &= - \frac{n_F}{n} \bar{\beta}_R + \frac{1}{n} \sum_{i=1}^{n_F} \beta_{F_i} \quad (3.5-89) \end{aligned}$$

Equation 3.5-89 expresses the error caused in the measured bearing by fruit. Its mean is given by:

$$\begin{aligned} \bar{\epsilon}_\beta &= \overline{\beta_{FR} - \bar{\beta}_R} = - \frac{n_F}{n} \bar{\beta}_R + \frac{n_F}{n} \bar{\beta}_F \\ &= \frac{n_F}{n} (\bar{\beta}_F - \bar{\beta}_R) \\ &= \frac{\rho}{1 + \rho} (\bar{\beta}_F - \bar{\beta}_R) \quad . \end{aligned} \quad (3.5-90)$$

It is observed from Equation 3.5-90 that, in measuring a swept bearing  $\Delta\beta_R$  from two successive measurements of  $\beta_R$ , a bias error

$$\bar{\epsilon}\Delta\beta = \frac{\rho}{1+\rho} \Delta\beta_R \quad (3.5-91)$$

will occur.

However, interest is primarily in the variability of  $\beta_{FR}$ ; thus, an expression for its variance is sought. From Equation 3.5-89 and assuming independent fruit strikes, the variance of the measurement error is:

$$\begin{aligned} \sigma^2(\epsilon_\beta) &= \sigma^2(\beta_R - \bar{\beta}_R) = \frac{n_F}{n^2} \sigma^2(\beta_F) \\ &= \frac{1}{n} \left( \frac{\rho}{1+\rho} \right) \sigma^2(\beta_F) \end{aligned} \quad (3.5-92)$$

Expressed as a standard deviation:

$$\sigma(\epsilon_\beta) = \sqrt{\frac{1}{n} \cdot \frac{\rho}{1+\rho}} \sigma(\beta_F) \quad (3.5-93)$$

For  $\beta_F$  uniformly distributed over  $0^\circ$  to  $360^\circ$ ,

$$\sigma(\beta_F) = \frac{360}{2\sqrt{3}} \text{ degrees.}$$

An estimated value for  $\rho$  was obtained from a SECANT signal environment simulation (computer run no. 5-3) pertaining to the most densely populated region of the FAA/MITRE 1982 LA Basin Standard Traffic Model, Snapshot #3.  $\rho$  may be considered as equivalent



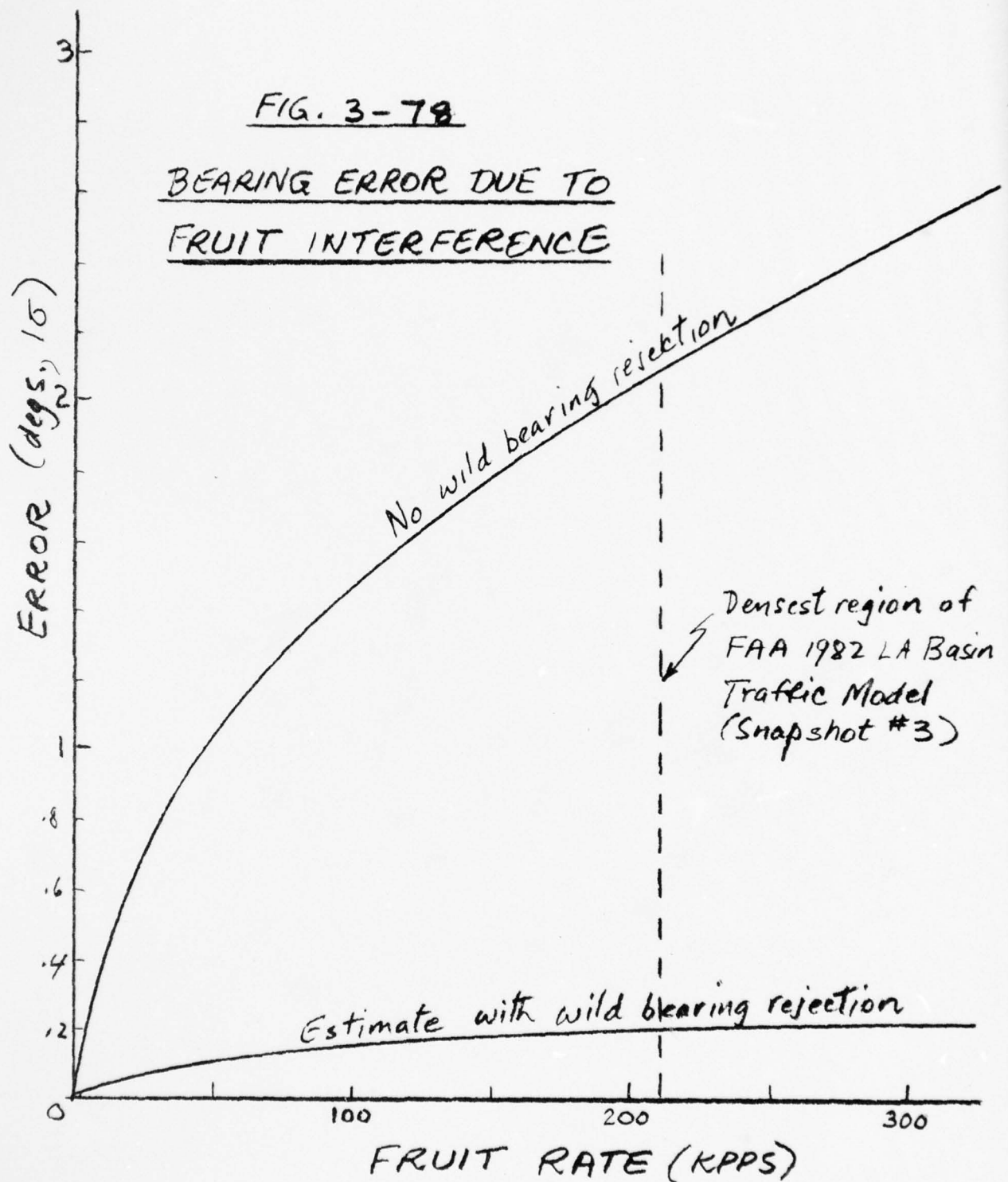
to the probability that an undetected fruit pulse will be received during the time interval in which a reply pulse is being phase detected. Taking this interval as 0.5 microsecond and using a worst case fruit rate given by the simulation as 211 kpps (being the modified value with average probe rate of 538 pps and extended system range margins),  $\rho = 0.5 \times 0.25 \times 10^{-8} \times 211 \times 10^3 \cong 0.026$ . The factor of 0.25 in this calculation accounts for the system's capability of detecting a coexisting fruit pulse in any of the reply channels other than that from which the reply signal is being processed, and depends on the validity of  $P^+$ ,  $P^-$ ,  $Q^+$  and  $Q^-$  replies being equiprobable. Then using  $n = 62$ , Equation 3.5-93 gives:

$$\sigma(\epsilon_\beta) = .0202 \sigma(\beta_F) \quad .$$

The upper curve of Figure 3-78 shows  $\sigma(\epsilon_\beta)$  plotted versus fruit rate. If a triangular distribution rather than a uniform one is assumed for  $\beta_F$ , then  $\sigma(\beta_F) = 180 / \sqrt{6}$  in which instance  $\sigma(\epsilon_\beta)$  is  $1.5^\circ$ .

#### 3.5.2.3.3 Conclusions

Application of wild data rejection logic described in Section 3.4.1 will have a powerful influence in reducing fruit errors to acceptable levels. Based on a total estimated random error of 0.56 degree ( $1\sigma$ ) in relative bearing, the computed threshold of the wild bearing rejection algorithm will approach  $T \cong 3 \times 0.56 \cong 1.7$  degree. Hence acceptance of fruit bearings will be reduced in the ratio  $(2 \times 1.7) - 360 = 1/110$ , with corresponding reduction in the accepted fraction of the worst case fruit rate. For conditions as stated above, the random error component due to fruit will then be reduced to  $2.1 \times \sqrt{1/110} = 0.2^\circ$  one sigma, which is an acceptable budgetary magnitude. At other fruit rates, the reduced random error is shown by the lower curve of Figure 3-78.



#### 3.5.2.4 Attitude Errors

##### 3.5.2.4.1 Abstract and Summary

The equations for the miss distance algorithm have been presented in Section 3.4.2; the derivation of these equations and the need for measurement of attitude angles and compensation for their effects is demonstrated in Appendix L. A question then arises on the precision with which the attitude measurements should be made. This can be answered by an analysis of residual error effects, assuming attitude compensation to be effected.

Error sensitivity equations are presented in this section, and some worst case kinematic conditions of conflict geometry are investigated. For a horizontal direct collision course, the horizontal miss distance error sensitivity to yaw error can be as high as 11630 ft./°. Since the corresponding miss threshold (Tau 2 cardioid) is about equal in numerical value, an order of magnitude reduction is afforded by specifying a yaw precision requirement of  $\sigma(\psi) = .13^\circ$ , the value attainable for autopilots, according to specification ARINC #417.

Although yaw error predominates in its effect on horizontal miss determination, roll and pitch errors can have a significant effect on horizontal bearing angle determination unless controlled. An acceptable value for roll or pitch measurement precision is .3 to .5°, per ARINC #417. For worst case condition, the resultant error in horizontal bearing is .06 to .1°, an order of magnitude less than the overall bearing error limit specification arrived at in Section 2.3.

##### 3.5.2.4.2 Horizontal Bearing Error

It is desired to find the error in the determination of  $\theta_s$ , the horizontal bearing angle, as function of the errors in measured pitch (p) and roll (r). From Appendix L, Equation L-29 indicates that  $\theta_s = f(\beta, \epsilon, p, r)$ ; while Equation L-19 shows that elevation angle  $\epsilon = f(\beta, p, r)$ . Assuming  $\epsilon$  and  $d\epsilon$  small, terms in  $p \sin \epsilon d\epsilon$  and  $r \sin \epsilon d\epsilon$  may be neglected;

whereupon differentiation of Equation L-19, with respect to p and r only, gives

$$d\epsilon \approx dr \sin \beta - dp \cos \beta \quad . \quad (3.5-94)$$

Neglecting terms involving products such as  $pd\theta_s$ ,  $pd\epsilon$  and  $rd\epsilon$ , differentiation of Equation L-29 and subsequent substitution of Equation 3.5-94 yields

$$d\theta_s = \cos(\theta_s - \beta) \cos \theta_s \tan \epsilon [dp \tan \beta + dr] \quad (3.5-95)$$

which may be evaluated at either time  $t_1$  or  $t_2$ .

For numerical examples, suppose  $\Delta h = 600$  ft. and  $R \cos \epsilon = 3000$  ft., so that  $\tan \epsilon = 1/5$ . Then,

Case 1:  $\theta_s = \beta = 0$ ,  $dp = 0$ ; then

$$d\theta_s = \frac{1}{5} dr$$

Case 2:  $\theta_s = \beta = 90^\circ$ ,  $dr = 0$ ; then

$$d\theta_s = dp \sin \beta \tan \epsilon = \frac{1}{5} dp \quad .$$

For a roll or pitch measurement error of  $.3^\circ$ , the resultant error in  $\theta_s$ , in either case, would be only  $.06^\circ$ ; a probably acceptable value insofar as maneuver error effect is concerned.

#### 3.5.2.4.3 Horizontal Miss Component Error

Referring again to Appendix L, the following equations have the functional relations indicated:

$$S = V_r \Delta t_{12} = f(R_1, R_2, \delta_{12}) \quad (L-30)$$

$$M = f(R_1, R_2, \delta_{12}, S) \quad (L-31)$$



$$\gamma_v = f(\Delta h_1, \Delta h_2, s) \quad (L-5)$$

$$M_v = f(\Delta h_2, R_2, M, \gamma_v) \quad (L-4)$$

$$M_H = f(M, M_v) \quad (L-6)$$

Differentiation of these equations and subsequent elimination of  $ds$ ,  $d\sigma_v$ ,  $dM$  and  $dM_v$  leads to  $dM_H = f(d\delta_{12})$ , with range and altitude difference error effects not considered:

$$dM_H = \frac{R_1 R_2 \sin \delta_{12} \cdot d\delta_{12}}{M_H S^2 \sqrt{R^2 - M^2}} \left[ (R_1 R_2 \cos \delta_{12} - M^2) (\sqrt{R_2^2 - M^2} + M_v \sin \gamma_v) + M_v (R_2^2 - M^2) \sin \gamma_v \right] \quad (3.5-96)$$

$$= F_H \sin \delta_{12} \cdot d\delta_{12}$$

Now, from Equation L-26, it is seen that

$$\delta_{12} = f[\beta_1, \beta_2, \epsilon_1, \epsilon_2, (\psi_2 - \psi_1), (P_2 - P_1), (r_2 - r_1)]$$

and it is desired to find  $\frac{\partial \delta_{12}}{\partial \psi_1}$ ,  $\frac{\partial \delta_{12}}{\partial P_1}$ ,  $\frac{\partial \delta_{12}}{\partial r_1}$ .

Differentiating Equation 3.4-1.26 with respect to  $\epsilon_1$ ,  $\psi_1$ ,  $p_1$ ,  $r_1$  and eliminating  $d\epsilon_1$  through the use of Equation 3.5-86, and neglecting terms involving  $(p_2 - p_1) d\epsilon_1$ ,  $(r_2 - r_1) d\epsilon_1$  results in

$$\begin{aligned} \frac{\sin \delta_{12} \cdot d\delta_{12}}{\sin (\beta_2 - \beta_1)} &= \cos \epsilon_1 \cos \epsilon_2 \cdot d(\psi_2 - \psi_1) \\ &+ (dp_2 \sin \beta_2 + dr_2 \cos \beta_2) \sin \epsilon_2 \cos \epsilon_1 \\ &- (dp_1 \sin \beta_1 + dr_1 \cos \beta_1) \sin \epsilon_1 \cos \epsilon_2 \quad (3.5-97) \end{aligned}$$

Substitution into Equation 3.5-88 leads to identification of the desired partials (sensitivities), viz.:

$$\frac{\partial M_H}{\partial(\psi_2 - \psi_1)} = -F_H \sin(\beta_2 - \beta_1) \cos \epsilon_1 \cos \epsilon_2$$

$$\frac{\partial M_H}{\partial P_1} = -F_H \sin(\beta_2 - \beta_1) \sin \beta_1 \sin \epsilon_1 \cos \epsilon_2$$

$$\frac{\partial M_H}{\partial r_1} = F_H \sin(\beta_2 - \beta_1) \cos \beta_1 \sin \epsilon_1 \cos \epsilon_2$$

$$\frac{\partial M_H}{\partial p_2} = F_H \sin(\beta_2 - \beta_1) \sin \beta_2 \sin \epsilon_2 \cos \epsilon_1$$

$$\frac{\partial M_H}{\partial r_2} = F_H \sin(\beta_2 - \beta_1) \cos \beta_2 \sin \epsilon_2 \cos \epsilon_1$$

Evidently, considering purely random errors only in the (independent) attitude measurements,

$$\begin{aligned} \sigma^2(M_H) &= 2 \left[ \frac{\partial M_H}{\partial(\psi_2 - \psi_1)} \right]^2 \sigma^2(\psi) \\ &+ \left[ \left( \frac{\partial M_H}{\partial P_1} \right)^2 + \left( \frac{\partial M_H}{\partial P_2} \right)^2 \right] \sigma^2(P) \\ &+ \left[ \left( \frac{\partial M_H}{\partial r_1} \right)^2 + \left( \frac{\partial M_H}{\partial r_2} \right)^2 \right] \sigma^2(r) . \end{aligned} \quad (3.5-98)$$

Several subcases are of special interest:

Case 1: Horizontal Plane Conflict (Figure 3-79)

$$\epsilon_1 = \epsilon_2 = 0; p_1 = p_2 = 0; r_1 = r_2 = 0; \psi_2 - \psi_1 = 0; \gamma_V = 0; \delta_{12} = \beta_2 - \beta_1$$

From Equation L-3,

$$M_H = M \frac{R_1 R_2 \sin(\beta_2 - \beta_1)}{s}$$

and Equation 3.5-97 gives

$$d\delta_{12} = d(\psi_2 - \psi_1) \quad . \quad .$$

Substitution in Equation 3.5-96 leads to

$$\sigma(M_H) = \frac{\sqrt{5}}{s} (R_1 R_2 \cos \delta_{12} - M_H^2) \sigma(\psi) \quad . \quad (3.5-99)$$

In particular, if additionally  $\delta_{12} = 0$ , then  $M_H = 0$  (pure collision course) and

$$\sigma(M_H) = \frac{\sqrt{2}}{s} R_1 R_2 \sigma(\psi) \quad (3.5-100)$$

or

$$\frac{\sigma(M_H)}{\sigma(\psi)} \text{ (ft./deg.)} = \frac{\sqrt{2}}{57.3} \frac{R_1 R_2}{s} \quad .$$

Case 2:  $V_r$  Horizontal and Above Wing Plane (Figure 3-80),

$$\delta_{12} \neq \beta_2 - \beta_1; \epsilon_1 = E_1; \epsilon_2 = E_2; P_1 = P_2 = 0; r_1 = r_2 = 0; \psi_2 - \psi_1 = 0; \gamma_V = 0, M_V = \Delta h.$$

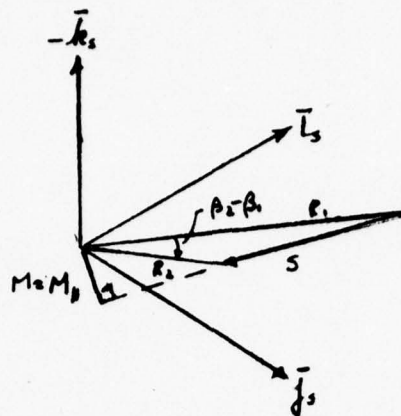


FIG. 3-79. HORIZONTAL PLANE  
CONFLICT  
(Case 1)

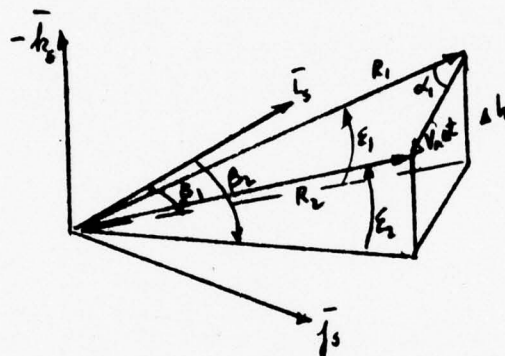


FIG. 3-80.  $V_h$  HORIZONTAL, DISPLACED  $\Delta h$   
(Case 2)

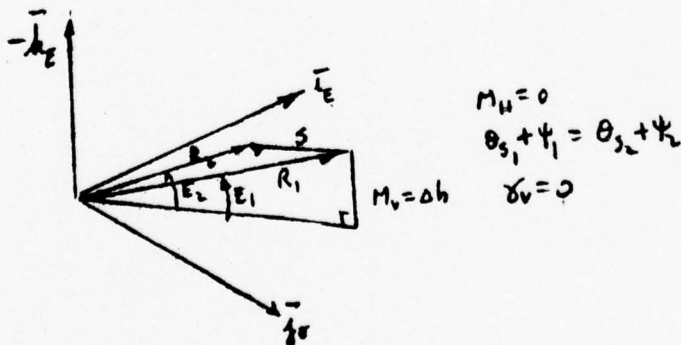


FIG 3-81.  $V_h$  HORIZONTAL,  $M_h = 0$   
(Case 3)  
3-193



Using Equations 3.5-96 and 3.5-97,

$$\frac{\sigma(M_H)}{\sigma(\psi)} = \sqrt{2} Q \cos E_1 \cos E_2 \quad (3.5-101)$$

$$\frac{\sigma(M_H)}{\sigma(P)} = Q [ \sin^2 \beta_2 \sin^2 E_2 \cos^2 E_1 + \sin^2 \beta_1 \sin^2 E_1 \cos^2 E_2 ]^{1/2} \quad (3.5-102)$$

$$\frac{\sigma(M_H)}{\sigma(r)} = Q [ \cos^2 \beta_2 \sin^2 E_2 \cos^2 E_1 + \cos^2 \beta_1 \sin^2 E_1 \cos^2 E_2 ]^{1/2} \quad (3.5-103)$$

where,

$$Q = \frac{R_1 R_2}{M_H S^2} [ R_1 R_2 \cos \delta_{12} - M^2 ] \sin (\beta_2 - \beta_1) \quad (3.5-104)$$

Note that for the same values of  $(\beta_2 - \beta_1)$ , the quantitative values of  $\frac{\sigma(M_H)}{\sigma(p)}$  and  $\frac{\sigma(M_H)}{\sigma(r)}$  are interchanged when  $\beta_1 = 0^\circ$  and when  $\beta_1 = 90^\circ$ .

Case 3: Vertical Plane Conflict,  $V_r$  Horizontal,  $M_H = 0$  (Figure 3-81),

$$\gamma_v = 0; \delta_{12} = E_2 - E_1; M = M_v$$

In this case, Equation 3.5-96 cannot be used because of the zero term in the denominator. Differentiation of Equation L-3, after some manipulation, gives

$$dM = \frac{V_r t_{c1} t_{c2}}{\Delta t_{12}} \cdot d\delta_{12} \quad (3.5-105)$$

and differentiation of Equation L-4 gives

$$dM_v = \frac{-(t_{c2} + t_{c1})}{\Delta t_{12}} M \sin \gamma_v \cdot d\delta_{12} \quad (3.5-106)$$

where

$$t_{c1} = R_1 \cos \alpha_1 / V_r \quad (3.5-107)$$

$$t_{c2} = \sqrt{R_2^2 - M^2} / V_r \quad (3.5-108)$$

The above equations are perfectly general.

Noting that

$$M_H^2 = M^2 - M_V^2$$

and taking perturbations, we have, for  $M_H = 0$  and  $M = M_V$ ,

$$\Delta M_H^2 = \Delta M (\Delta M + 2M) - \Delta M_V (\Delta M_V + 2M_V) \quad (3.5-109)$$

For  $\gamma_V = 0$ ,  $\Delta M_V$  must be zero. Substituting Equation 3.5-105 into Equation 3.5-109,

$$\Delta M_H^2 = \frac{V_r t_{c1} t_{c2}}{\Delta t_{12}} d\delta_{12} \left[ \frac{V_r t_{c1} t_{c2}}{\Delta t_{12}} d\delta_{12} + 2M_V \right] \quad (3.5-110)$$

For the special case of the vertical plane conflict,

$$t_{c1} = \frac{R_1 \cos E_1}{V_r}; t_{c2} = \frac{R_2 \cos E_2}{V_r}.$$

Assuming purely random attitude errors,  $\overline{d\delta_{12}} = 0$ , so that the expectation of Equation 3.5-110 gives the rms error in  $M_H$ :

$$\sqrt{\Delta M_H^2} = \frac{R_1 R_2 \cos E_1 \cos E_2}{V_r \Delta t_{12}} \sigma(\delta_{12}) \quad (3.5-111)$$

where

$$\begin{aligned} \sigma^2 (d\delta_{12}) \frac{\sin^2 (E_2 - E_1)}{\sin^2 (\beta_2 - \beta_1)} &= 2 \cos \epsilon_1 \cos^2 \epsilon_2 \sigma^2 (\psi) \\ &+ (\sin^2 \beta_2 \sin^2 \epsilon_2 \cos^2 \epsilon_1 + \sin^2 \beta_1 \sin^2 \epsilon_1 \cos^2 \epsilon_2) \sigma^2 (P) \\ &+ (\cos^2 \beta_2 \sin^2 \epsilon_2 \cos^2 \epsilon_1 + \cos^2 \beta_1 \sin^2 \epsilon_1 \cos^2 \epsilon_2) \sigma^2 (r) . \end{aligned} \quad (3.5-112)$$

#### 3.5.2.4.4 Quantitative Results

Case 1: For  $V_r$  horizontal and in the wing plane, we assume the condition of a Tau 2 cardioid penetration, so that

$$R_1 = R_{AL} \text{ (ft.)} = 10936.8 + 67.5 V_r \quad (3.5-113)$$

with  $V_r$  in knots. Then

$$S = 1.688 V_r \Delta t_{12} \quad (3.5-114)$$

with  $V_r$  in knots and  $\Delta t_{12}$  in seconds, and

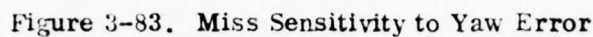
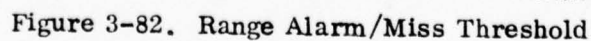
$$R_2 = R_1 - S . \quad (3.5-115)$$

Miss threshold, at Tau 2 penetration, is taken as

$$T_{T2} \text{ (ft.)} = 11,200 + 8 V_r \quad (3.5-116)$$

with  $V_r$  in knots. This can be used to compare with the horizontal miss error per degree of yaw error. Range alarm and miss threshold at Tau 2 cardioid penetration are shown as a function of relative velocity in Figure 3-82.







The miss error sigma per degree of yaw error, for  $M = 0$ , is computed from Equation 3.5-100 and is shown graphically in Figure 3-83.

Normalizing by dividing by  $M_T$  enables determination of relative effect, as shown in the figure. Thus, in order not to significantly decrease the efficiency of the miss hazard evaluator in reducing false alarm probability, the effect of yaw attitude error should produce, say, an order of magnitude less of miss error as compared to threshold value. Taking the sensitivity ratio at lowest  $V_r$ , we set

$$\frac{\frac{\sigma(M_H)}{[\frac{M}{M_T}]}}{\sigma(\psi)} = \frac{.1}{\sigma(\psi)} = 1.002$$

so that  $\sigma(\psi) = .1^\circ$  is certainly acceptable under the stated geometric condition.

Case 2: Taking  $\gamma_v = 0$ ,  $M_v = \Delta h = 600$  ft.,  $\beta_1 = 0$  (or  $90^\circ$ ) and all attitude angles at both sampling times zero; and taking penetration of the Tau 2 cardioid as a kinematic condition, then;

$$R_1 = R_{AL} \text{ (ft.)} = 10936.8 + 67.5 V_r \cos \alpha_1 \quad (3.5-117)$$

where

$$\alpha_1 = \sin^{-1} \left( \frac{M}{R_1} \right) = \sin^{-1} \left( \frac{M_{T_2}}{R_{AL}} \right) \quad (3.5-118)$$

with  $M_{T_2}$  given by Equation 3.5-116. For a specified  $V_r$  (hence  $M_T$ ), Equations 3.5-117 and 3.5-118 can be solved by a trial and error/iteration process to give  $R_1$  and  $\alpha_1$ . The remaining parameters required for calculating the sensitivities, Equations 3.5-101 through 3.5-104 are  $S$ ,  $E_1$ ,  $\delta_{12}$ ,  $R_2$ ,  $E_2$ ,  $\beta_2$ ,  $M_H$ , obtained from

$$S = V_r \Delta t_{12} \quad (3.5-119)$$

$$\delta_{12} = \tan^{-1} \left[ \frac{S \sin \alpha_1}{R_1 - S \cos \alpha_1} \right] \quad (3.5-120)$$

$$\epsilon_1 = E_1 = \sin^{-1} \left( \frac{\Delta h}{R_1} \right) \quad (3.5-121)$$

$$R_2 = S \sin \alpha_1 / \sin \delta_{12} \quad (3.5-122)$$

$$\epsilon_2 = E_2 = \sin^{-1} \left( \frac{\Delta h}{R_2} \right) \quad (3.5-123)$$

$$\beta_2 = \beta_1 + \cos^{-1} \left[ \frac{(R_1 \cos E_1)^2 + (R_2 \cos E_2)^2 - S^2}{2R_1 R_2 \cos E_1 \cos E_2} \right] \quad (3.5-124)$$

$$M_H = \sqrt{M_T^2 - \Delta h^2} \quad (3.5-125)$$

For Tau 1 cardioid penetration, we have the same set of equations, except that in lieu of Equations 3.5-116 and 3.5-117 we have

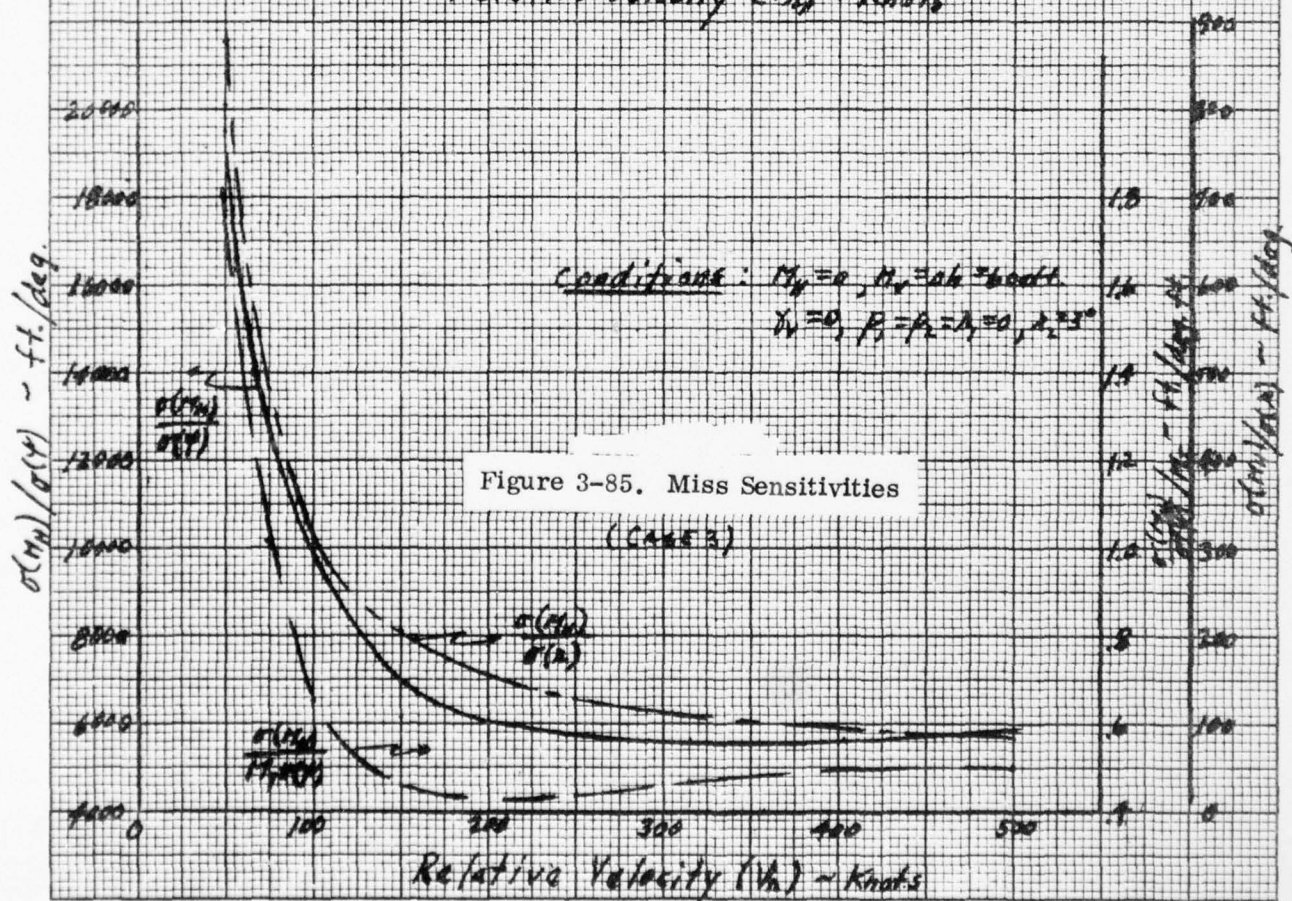
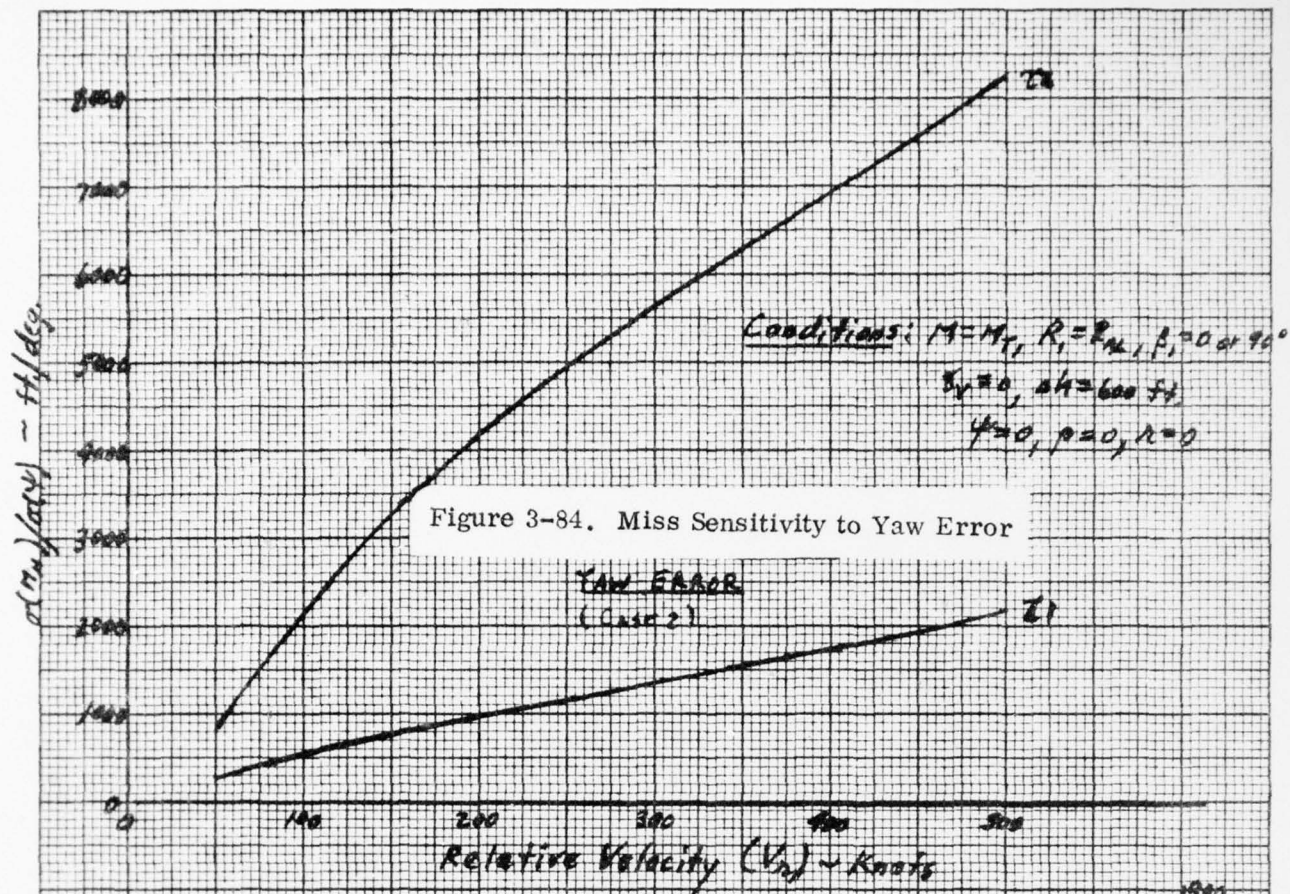
$$M_{T1} \text{ (ft.)} = 1700 + 7 V_R \quad (3.5-126)$$

with  $V_R$  in knots, and

$$R_1 = R_{AL} \text{ (ft.)} = 1519 + 42.2 V_R \cos \alpha_1 \quad (3.5-127)$$

with  $V_R$  in knots.

The miss sensitivity to yaw error is depicted in Figure 3-84, for both  $\tau_1$  and  $\tau_2$  penetration. Comparing the sensitivity curves of Figures 3-83 and 3-84 (for  $\tau_2$ ), it is seen that the latter is monotonically increasing with  $V_R$ , the extremum being 8290 ft./deg., and the normalized ratio to  $M_T$  (at 500 knots) is .55. The extremum in Figure 3-83 (at  $V_R = 50$  knots) is 11630 ft./deg., with a normalized ratio of 1.0. A measure of comparison of the extrema (at





$V_r = 500$  knots) of the  $\tau_1$  and  $\tau_2$  curves, in Figure 3-84, is obtained by noting that the normalized ratio for the  $\tau_1$  point is .42 (i.e., less than the .55 value for the  $\tau_2$  curve).

For  $\beta_1 = 0$ , the roll sensitivity at  $\tau_2$  is at most (over the 50 to 500 knot regime) 123 ft./deg.; for  $\tau_1$  penetration, the largest roll sensitivity is 67 ft./deg. The pitch sensitivities are less than 4 ft./deg., but note that the roll and pitch sensitivity values are interchanged if  $\beta_1 = 90^\circ$ .

Case 3: Consider the geometric condition displayed in Figure L-9 (or L-10) of Appendix L, where  $\psi_1 = \psi_2 = 0$ ,  $p_1 = p_2 = 0$ ,  $r = 0$ ,  $r_2 = 3^\circ$ ,  $\beta_1 = 0$ ,  $\gamma_v = 0$ ,  $\delta_{12} = E_2 - E_1$ ,  $M = M_v$  =  $\Delta h$ . Letting  $\Delta h = 600$  ft. and considering  $\tau_2$  penetration,

$$R_1 = R_{AL} = 10936.8 + 67.5 V_r \cos E_1$$

$$\approx 10936.8 + 67.5 V_r$$

with  $V_r$  in knots. Note that

$$\epsilon_1 = E_1 = \sin^{-1} \frac{\Delta h}{R_1}$$

and  $E_2$  is given by

$$E_2 = \tan^{-1} \left[ \frac{\Delta h}{R_1 \cos E_1 - S} \right], \quad (3.5-128)$$

where  $S = 1.688 V_r \Delta t_{12}$ , with  $V_r$  in knots and  $\Delta t_{12} = 5$  seconds.  $\epsilon_2$  and  $\beta_2$  are given respectively by

$$\epsilon_2 = \sin^{-1} [\sin E_2 \cos r_2] \quad \text{and} \quad (3.5-129)$$

$$\beta_2 = \tan^{-1} [-\tan E_2 \sin r_2] \quad (3.5-130)$$



Finally,

$$R_2 = \frac{\Delta h}{\sin E_2} \quad (3.5-131)$$

and all parameters for sensitivity evaluation can be determined for specified  $V_r$ .

Miss error sensitivities were calculated using Equations 3.5-111 and 3.5-112, and are depicted in Figure 3-85. The sensitivity to roll error is now fairly significant, attaining an extremum of 876 ft./deg. for  $V_r = 50$  knots. The sensitivity to pitch error is negligible. (Note that if all attitude angles are zero except that  $p_2 = 3^\circ$ , and  $\beta_1 = 90^\circ$ , the sensitivity roles would be interchanged.) The sensitivity to yaw error is somewhat higher than that in Case 1, reaching an extremum of 20,580 ft./deg.; or with respect to miss threshold, a ratio of 1.77. Taking an allowable  $\sigma(\psi) = .13^\circ$  (ARINC Spec 117, Autopilots), the normalized ratio at the extreme condition is

$$\frac{\sigma(M_H)}{M_T} = 1.77 \times .13 = .23$$

which may be considered acceptable at the very low  $V_r$ . (Note from Figure 3-85 that  $\frac{\sigma(M_H)}{\sigma(\psi)}$  drops off very rapidly with increasing  $V_r$ , attaining a value - beyond  $V_r = 150$  knots - of about 1/3 that at  $V_r = 50$  knots.)

## SECTION 4.0

### BREADBOARD ANTENNA (TASK 3.1)

#### 4.1 SUMMARY

A breadboard antenna array having  $H = 0$ ,  $H = 1$ , and  $H = 4$  modes was built and tested over a relatively wide frequency range several times greater than the required band. The measurements included VSWR at each port, cross-coupling between ports, azimuth and elevation patterns for each port, and miscellaneous experiments to aid in the study of the data.

The analysis of the data showed that the basic concept evolved in the study program was validated. Areas in which the circuitry could be improved were also identified. Additional experiments were conducted to aid in evaluating bearing measurement error caused by reflection from objects such as the vertical stabilizer.

#### 4.2 CONCLUSIONS

The antenna was found to be broadband in operation. The VSWR at the various ports was around 1.2 or better; the cross-coupling between different mode ports varied from 30 db to 50 db. The phase linearity of the four-cycle mode (used in the fine measure of azimuth bearing) was very good in spite of a small amplitude unbalance in the hybrids. The time scope of the program did not permit full analysis of all of the accumulated data. However, a preliminary study of a small portion of the data indicated a maximum bearing error of  $\pm 1^\circ$  of which one-half can be attributed to correctable amplitude unbalance in the hybrids.

The phase linearity of the one-cycle mode (used in the coarse measurement of bearing and for resolving bearing ambiguity of the four-cycle mode) showed undesirably high ripples at certain azimuth angles. Experimental work indicated that this distortion was caused by reradiation from the outer ring of monopoles. It is expected that this anomaly can be eliminated by installing diode switches in the four-cycle array to provide short-circuits when the one-cycle mode is being used.

These anomalies are to be expected in a short data gathering program. They are correctable by relatively small modifications which would take more time than presently available. The antenna concept was proven to be practical and future work could be directed to correction of the anomalies, and to tests more representative of the curved ground plane and multipath sources of an aircraft.

#### 4.3 ANTENNA MECHANICAL DESIGN

The antenna assembly (Figure 4-1) consists of 21 monopoles mounted on the ground plane with a strip transmission line feed and 5 TNC stripline connectors. The diameter of the assembly is 15.00" and the height is 3.167".

Two sheets of .031" thick dielectric substrates were used, the top clad with 1 oz. (.0014" thick) copper one side, and .062" aluminum on the other side. The bottom sheet has only .062" aluminum clad to one side. The aluminum serves as the ground plates for the stripline and as the ground plates for the monopoles. It also imparts mechanical stability to the assembly and minimizes warpage during circuit etching operations. The pattern of the transmission lines, shown in Figure 4-2, is transferred to the copper and the remaining copper etched away. The dielectric is RT/Duroid 5870, a polytetrafluoroethylene laminate reinforced with randomly oriented microglass fibers.

For each  $H = 1$  and  $H = 4$  monopole, a .250" diameter hole is bored through the aluminum ground plane, followed by an .083" diameter hole through the Duroid and the copper pad. The monopole is then centered by a Teflon bushing and its bottom end is soldered to the copper pad. The Rexolite sleeve is then bonded to the monopole and to the ground plane to provide support. The  $H = 0$  monopole is soldered directly to a TNC center conductor rather than to a copper pad. It is located in the center of the disk and has no printed circuitry associated with it.

For joining the TNC stripline connectors to the printed copper paths, the so called Fuzz Button is used, rather than soldering the center conductors to the copper paths. This is



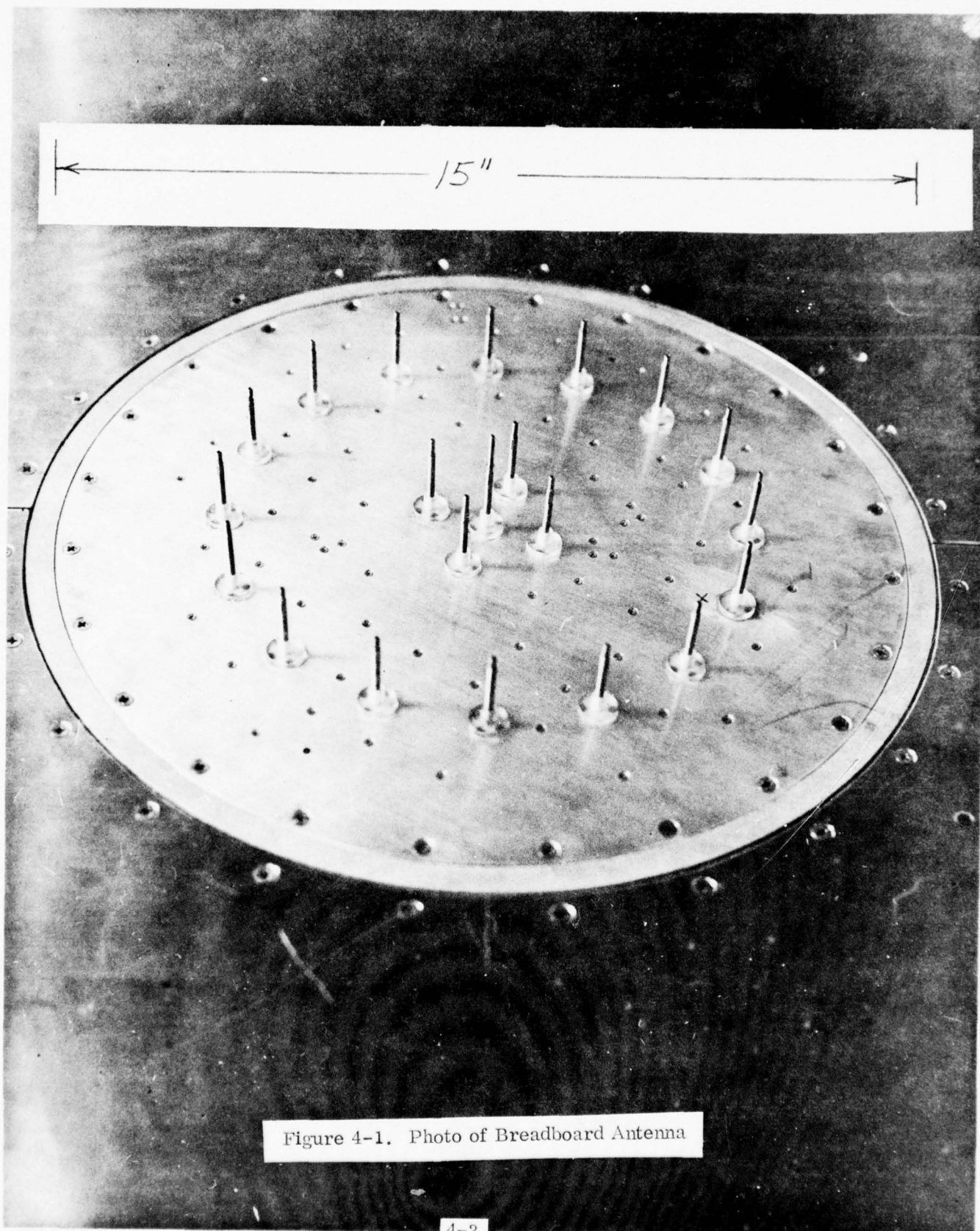


Figure 4-1. Photo of Breadboard Antenna



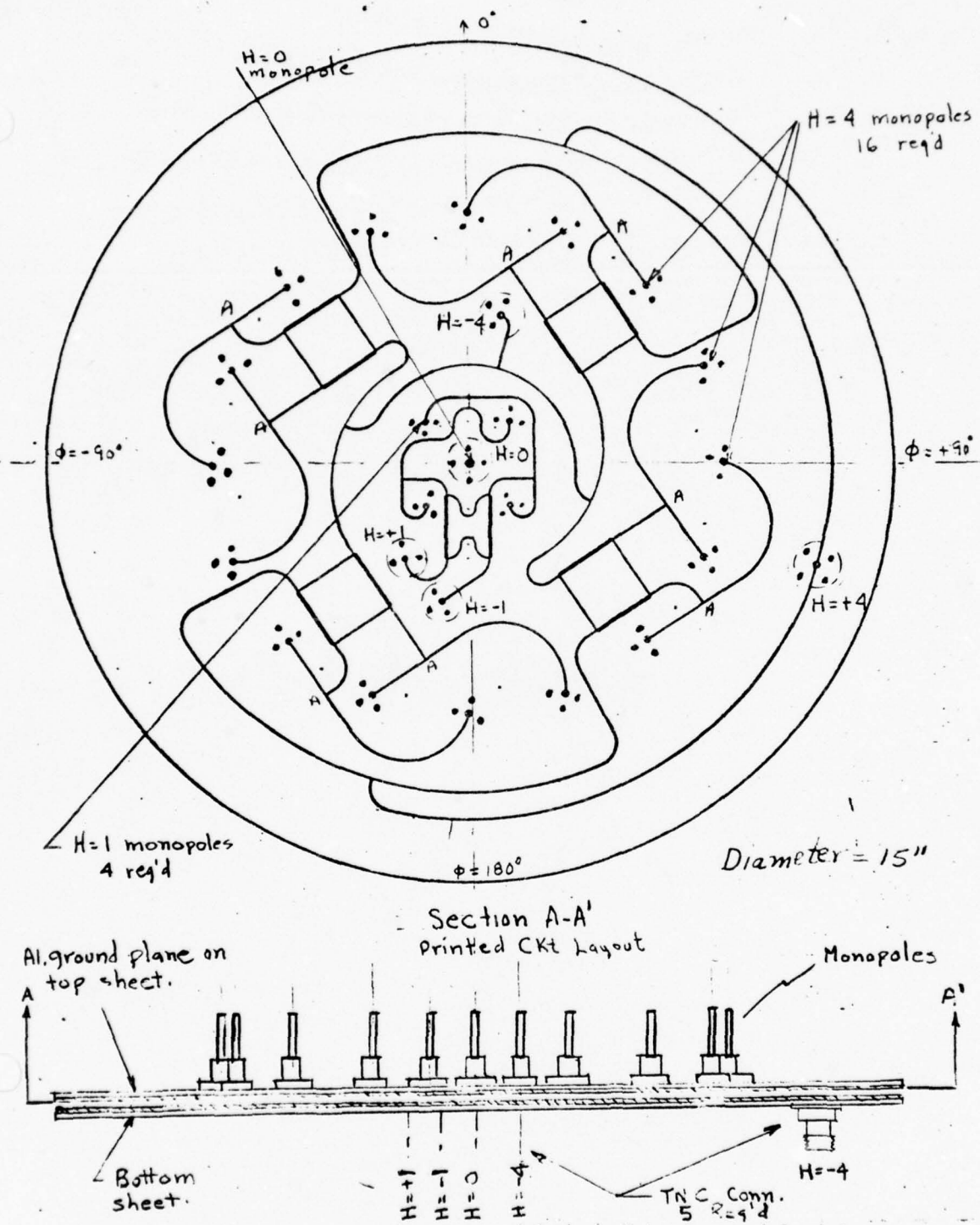


Figure 4-2. Construction of Breadboard Antenna

a loosely woven button consisting of gold plated fine copper wire, inserted into the .083 diameter hole drilled in the bottom layer of dielectric, which exposes the copper path printed on the top dielectric layer. On securing the TNC connector, its center conductor compresses the Fuzz Button assuring good contact.

An antenna of this type would be quite practical to produce and to utilize on an aircraft. The strip transmission lines would be sandwiched by heat bonding. All holes would be drilled after bonding. The holes required for the monopoles and the TNC connectors would be masked, and the remaining holes used for mode suppression would be plated through. After removing the masking, the connectors would be assembled and the monopoles soldered. The entire assembly, except for a surface on the periphery which is required for grounding to the skin of the aircraft, would be sprayed with a polyurethane resin (MFP). Finally the radome would be epoxied to the ground plane.

The radome would be constructed of a thin epoxy fiberglass dome. The entire structure would be reinforced with a fire retardant polyurethane foam that completely fills the inside of the radome. The foam material has sufficient structural properties to provide substantial support to the monopoles. The radome would be a truncated sphere of 15" diameter and extending 3" above the ground plane, and will present minimum aerodynamic drag.

#### 4.4 TEST PROCEDURES

The ground plane was mounted perpendicular to the floor in the microwave laboratory, and cross-coupling measurements made between the  $H = +4$  and  $H = -4$  ports versus frequency. For this test, all monopoles in the outer ring were set to the length determined from the earlier test using the  $45^\circ$  corner reflector. In this and all following tests, all of the unused ports were terminated with nominally matched loads (VSWR between 1.05 and 1.09). At the frequency of minimum cross-coupling, the monopoles were adjusted in height to further reduce the cross-coupling. For this height, the final cross-coupling and VSWR data were taken versus frequency and plotted in Figure 4-3.

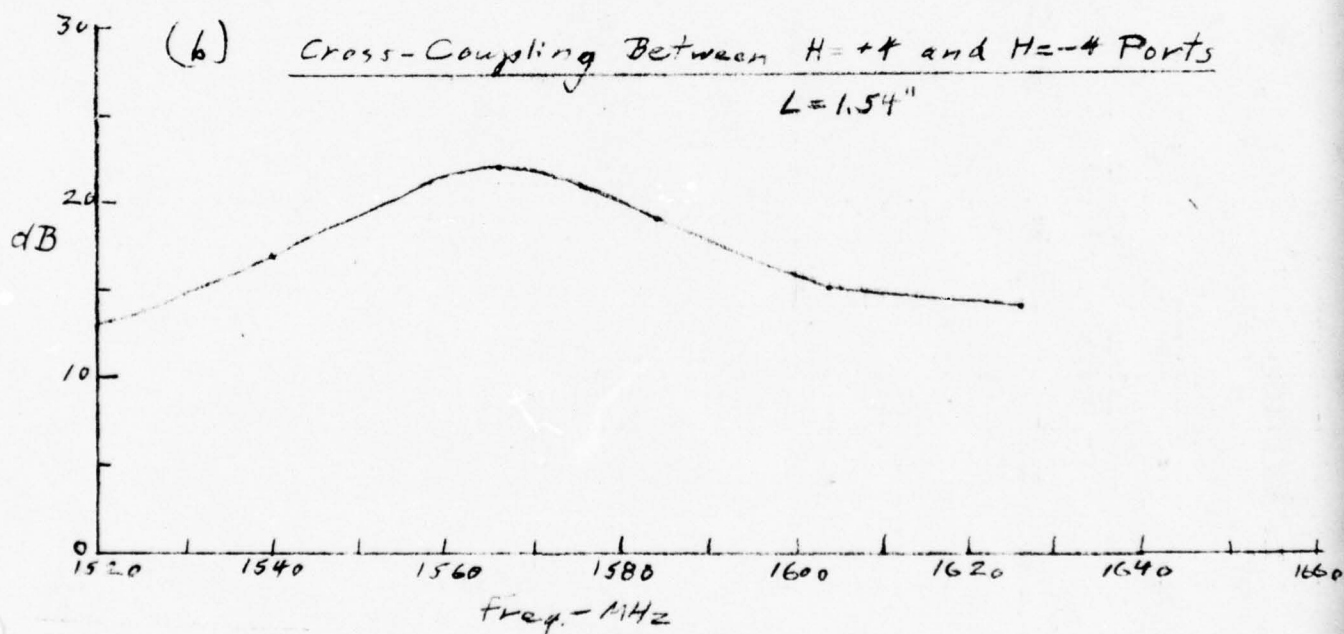
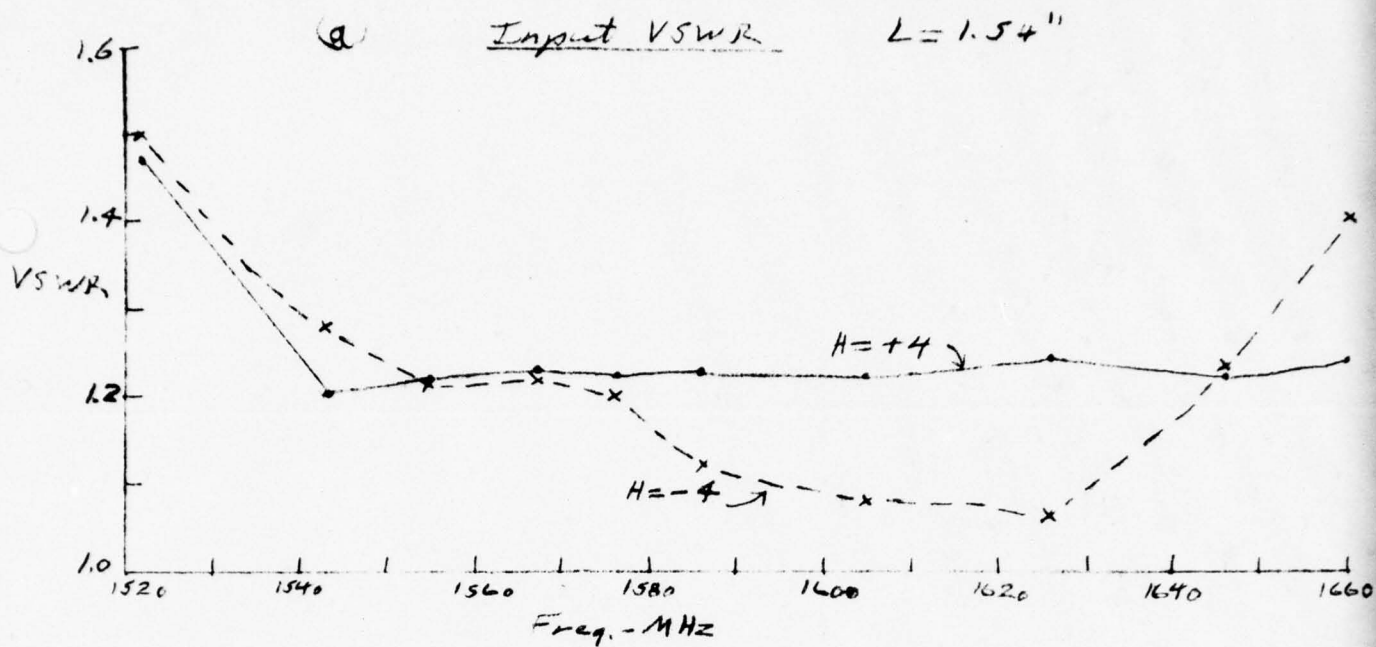


Figure 4-3. Complete Antenna Assembly

The VSWR (Figure 4-3) is seen to be about 1.2 or better over a wide frequency band. The frequency of minimum cross-coupling is about 2.5% below the frequency determined from previous measurements made with the circuit analyzer. A possible explanation for this shift may be that the corporate feed network joining the four circuit groups is not exactly symmetrical; however, this is not serious in the system operation as long as only one of the  $H = 4$  ports is used at a time.

Similar measurements were then made on the  $H = 1$  ring and the height of the center monopole was adjusted for minimum VSWR. The measured VSWR data is plotted in Figure 4-4 and the cross-coupling data in Figure 4-4. It is seen from the latter curve that the frequency of minimum cross-coupling is quite a bit lower than the design frequency. This was found to be caused by reradiation from the  $H = 4$  monopoles and associated circuitry, as explained in Section 4.5.1.

Next, the cross-coupling between ports of different modes was measured versus frequency and plotted in Figure 4-5. These values varied from about 30 db to 50 db over a wide frequency band. Some of the variations in the curves are probably due to small room reflections which show up at the low levels of cross-coupling but are of second order effect in the VSWR measurements.

For elevation pattern measurements, the antenna and ground plane assembly was installed perpendicular to the horizontal turntable in the anechoic chamber. Elevation patterns were taken at each port over a frequency range from 1540 to 1620 MHz for a total of 25. The output of a signal generator was fed to the source horn at the far end of the chamber and a receiver was connected in turn to each of the three ports of the antenna. A small sample from the signal generator was fed to the receiver as a reference to measure the relative phase of the received signal. The  $\theta = 0^\circ$  coordinate was designated as the normal to the ground plane; hence, the ground plane itself is designated  $\theta = 90^\circ$ . All of these patterns show the typical effects due to the diameter



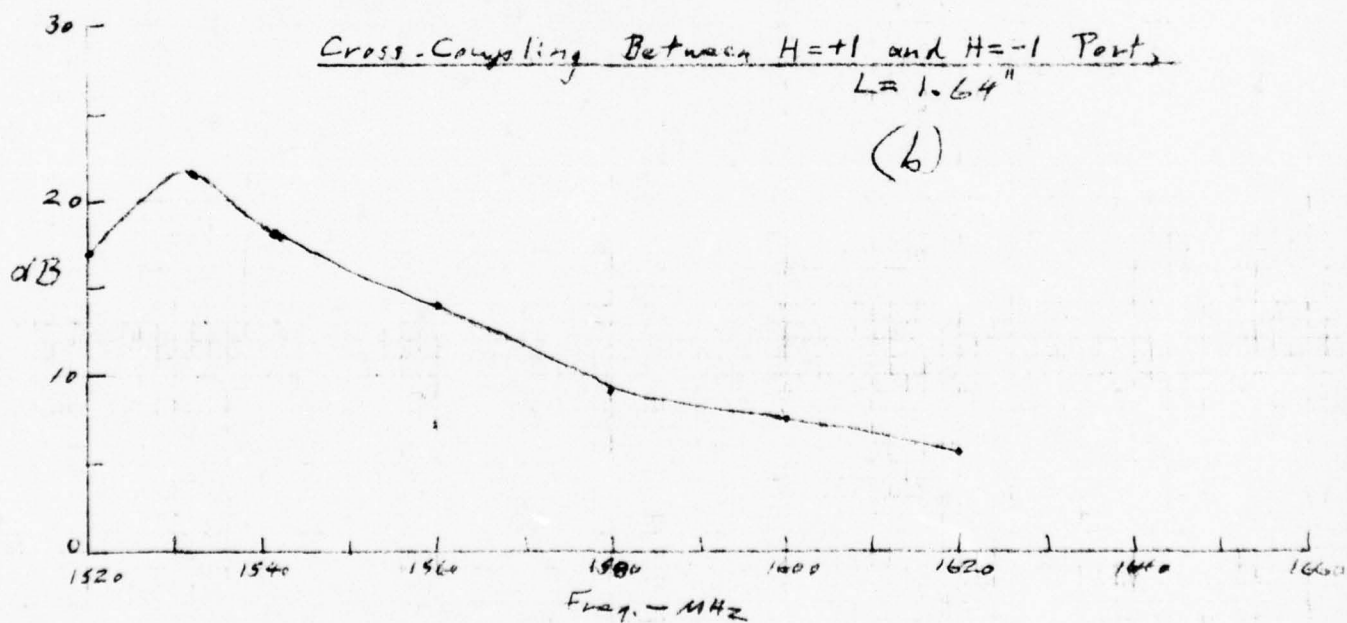
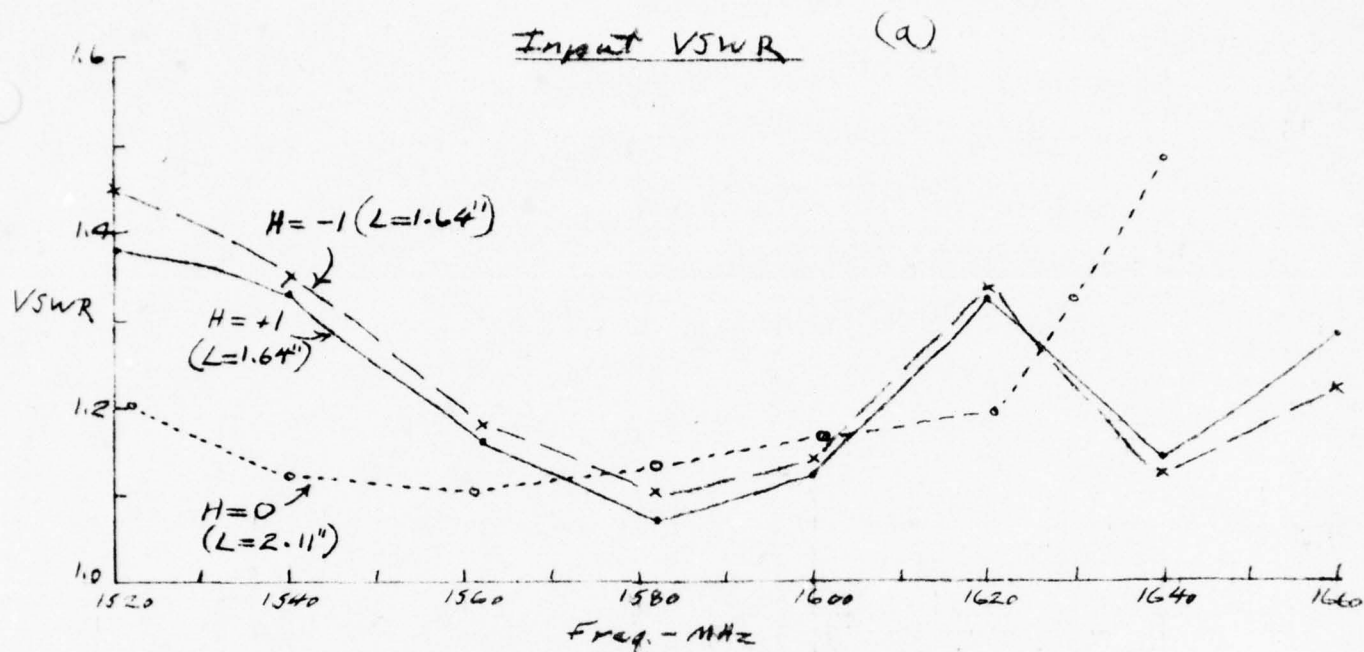


Figure 4-4. Complete Antenna Assembly

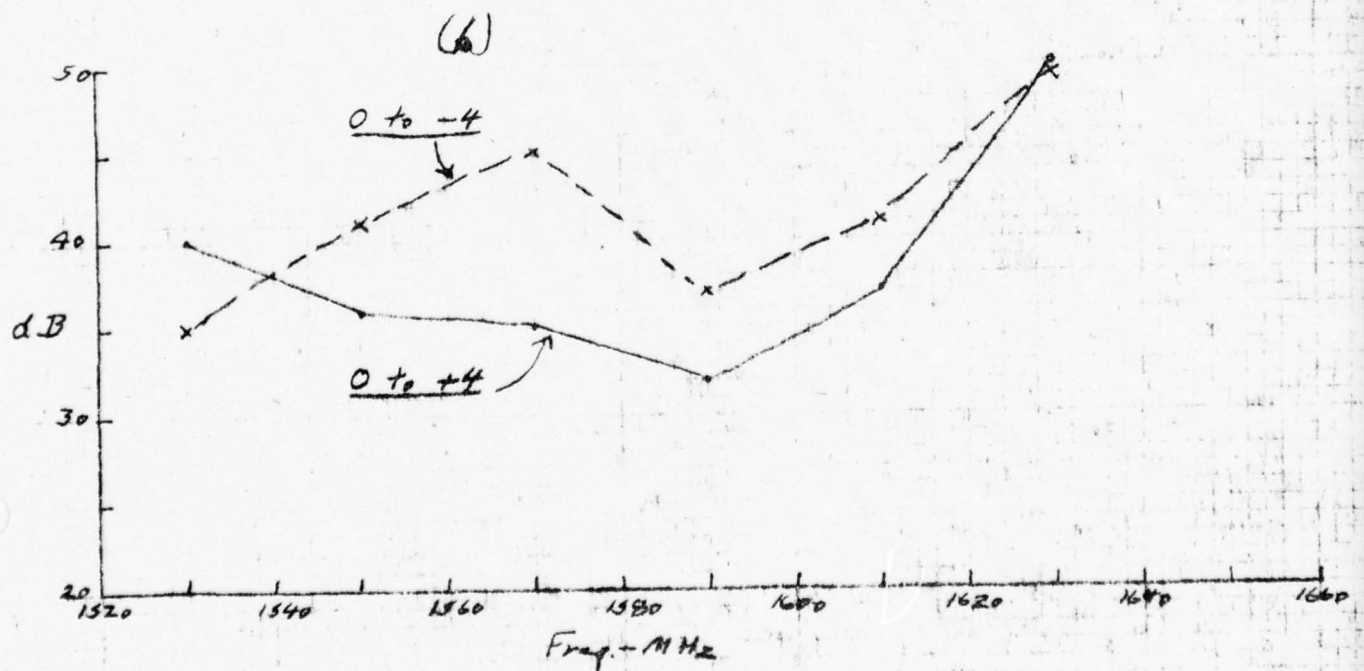
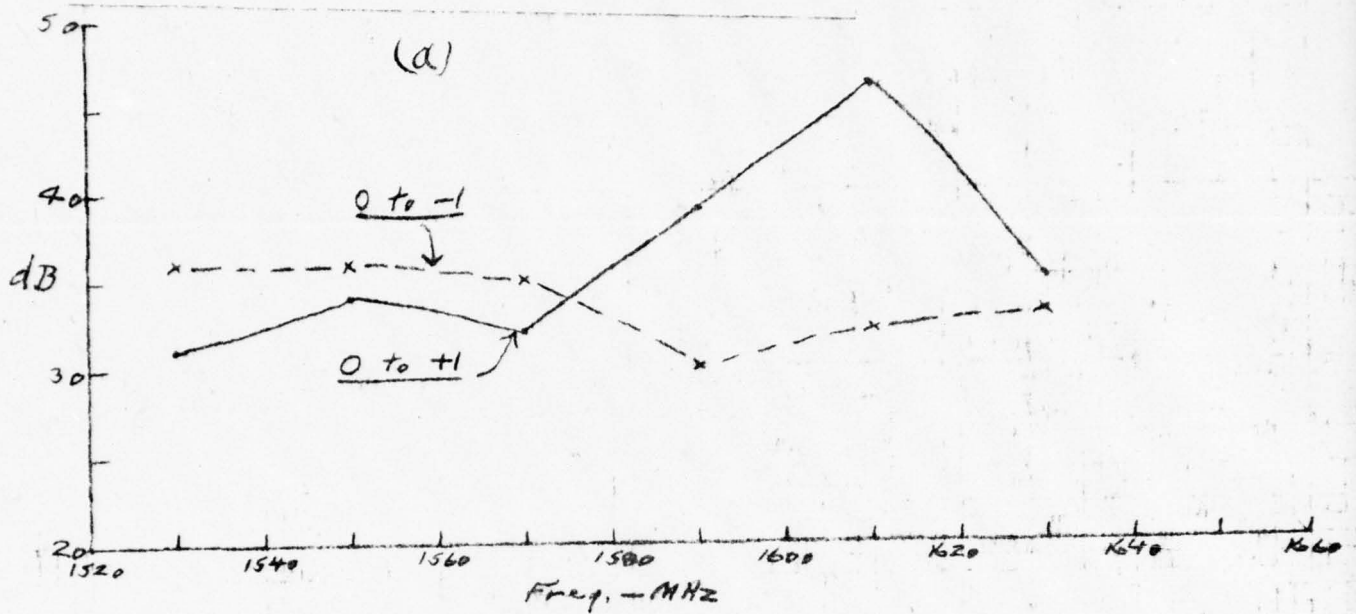


Figure 4-5. Cross-Coupling Between Different Modes

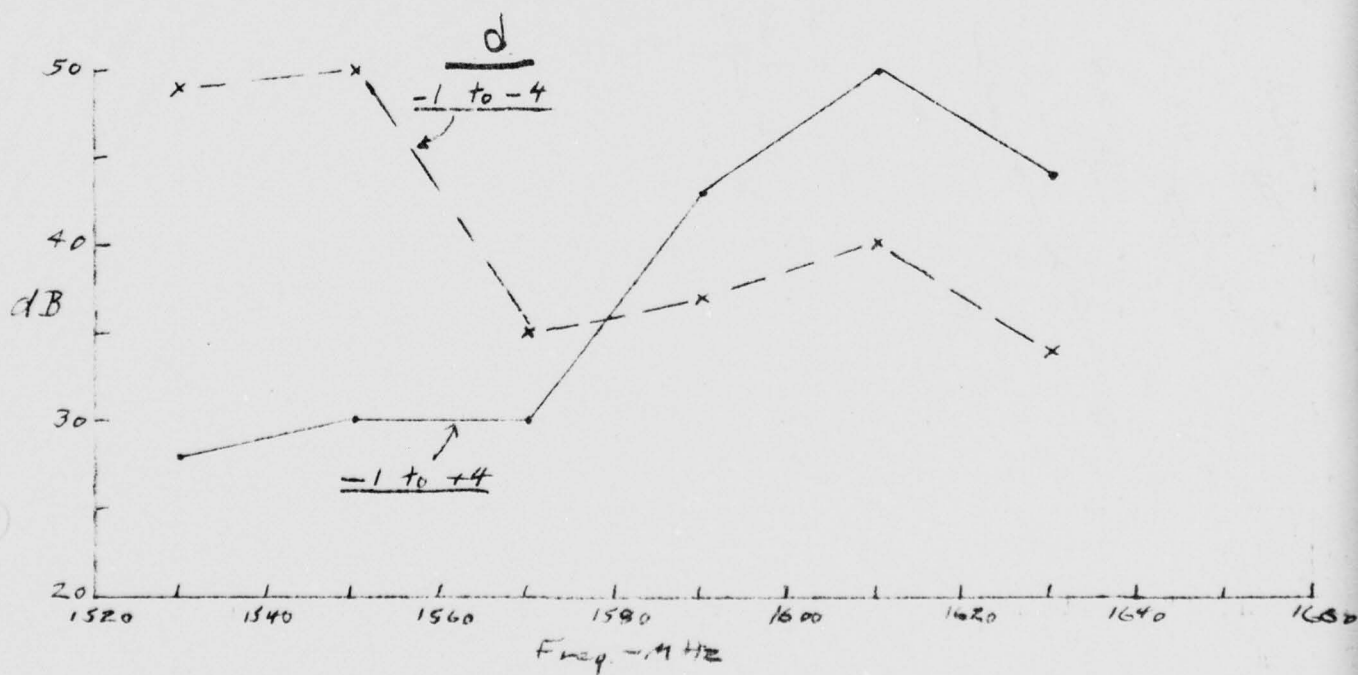
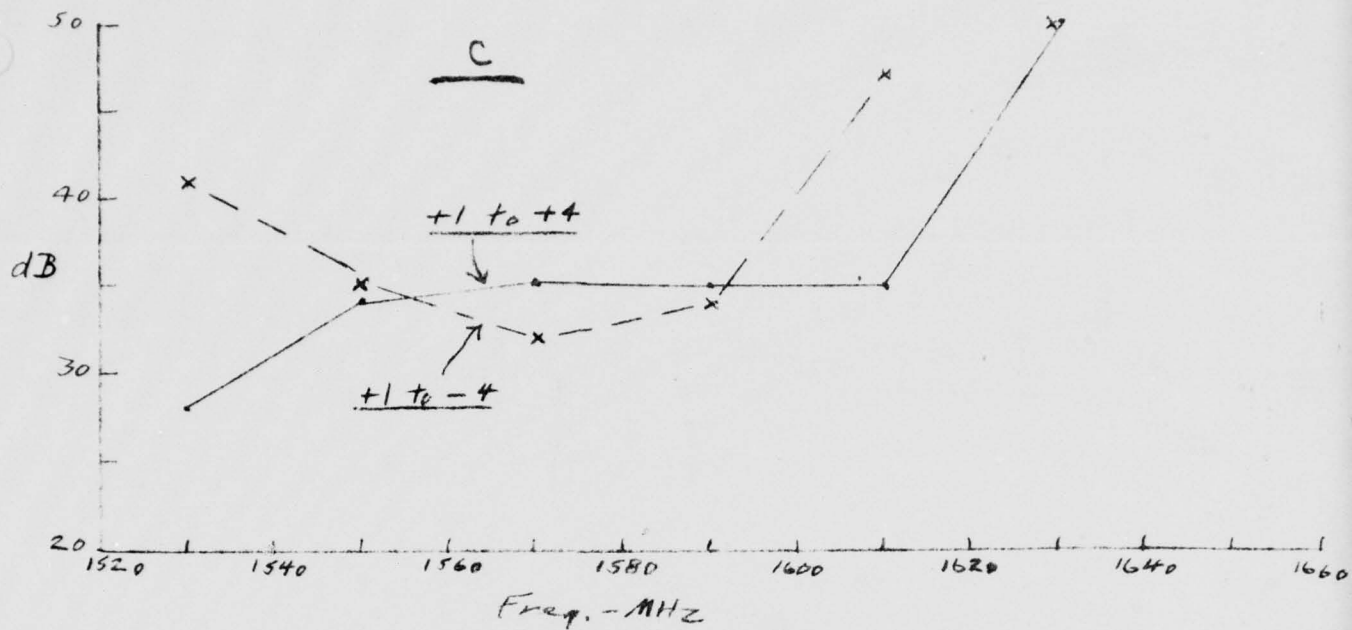


Figure 4-5. Cross-Coupling Between Different Modes (Continued)

of the ground plane being finite; an upward tilt of the beam maximum and ripples in both amplitude and phase on the beam shape. Each of the low level lobes below the ground plane exhibit a complete phase reversal.

For azimuth patterns, the ground plane was mounted about three feet above and parallel to the top of the turntable. The turntable was tilted in elevation to an angle of  $\theta \approx 78^\circ$  which was chosen from inspection of the elevation patterns to provide a tilt angle near the peak of the beam and where the phase curve was nearly flat. This would not have been necessary if the ground plane were larger.

Azimuth patterns were taken for each port at frequencies from 1540 to 1620 MHz for a total of twenty five. At each frequency, the phase plot of the  $H = 0$  mode was set near the center of the phase graph. This phase control was not changed while taking the patterns for the four other ports at this same frequency.

Hence, the phase difference between any two of the curves will give the characteristic that would be obtained if a phase-comparison instrument were joined to the respective two ports. The phase difference could not be measured directly because only one slip ring was available on the turntable.

#### 4.5 RESULTS OF THE PATTERN MEASUREMENTS

##### 4.5.1 H = 0 Mode

From the azimuth patterns, it was seen that the phase vs. bearing response of the  $H = 0$  mode was not flat as expected. There was a variation of ten degrees with one maximum and one minimum per revolution. This was found to be caused by the array not being exactly over the center of rotation. A physical check was made in which a fixed pointer was suspended directly over the tip of the center monopole. The nutation of this monopole was found to be about 0.2 inch for one revolution of the turntable. At this frequency this would produce about ten degrees phase change, which checks very



closely with the patterns. Also, the high and low values of phase on the patterns corresponded to the azimuth angles at which the monopole was closest and furthest from the source horn.

There were also some smaller ripple effects that are attributable to minor physical ripples in the circular ground plane and possibly also to small reflections from the walls of the anechoic chamber.

A typical plot of the azimuth bearing data versus azimuth angle is presented in Figure 4-6. It is seen that the maximum departure from the ideal characteristic is about 16 degrees at certain azimuth angles. Repeating the plots at three different frequencies showed that the ripple characteristic is fairly independent of frequency.

Tests indicated the fault to be caused by unsymmetrical reradiation from the outer ring of 16 monopoles and its associated circuitry. The base of all sixteen monopoles in the outer ring were shorted to the ground plane. Azimuth patterns were then measured and considerable improvement in amplitude and phase linearity was found. As a further experimental check, one diagonal pair of the  $H = 1$  monopoles was shorted to ground. Two azimuth patterns were then measured with the receiver at the  $H = 1$  port. In one, the sixteen outer elements were shorted and in the other, the shorts were removed from the outer ring.

The amplitude characteristic of the shorted case was very close to calculated values for a two-element array, and the phase curve was fairly flat as it should be. However, with the shorts removed from the outer ring elements, considerable distortion occurred in both the amplitude and phase characteristic.

It is, therefore, concluded that the major problem lies in the reradiation from the outer assembly. Radiation from the  $H = \pm 1$  ports excites the sixteen outer elements with equal amplitudes but progressively phased in  $22\text{-}1/2$  degree steps around the circle. Now, if the outer elements are either shorted to ground or are open-circuited, then by symmetry the reradiated wave from the outer ring will also be a pure  $H = \pm 1$  mode. Hence, no pattern distortion will occur.

$$\text{Azi. Bearing} = (Ph_{-1}) - (Ph_0)$$

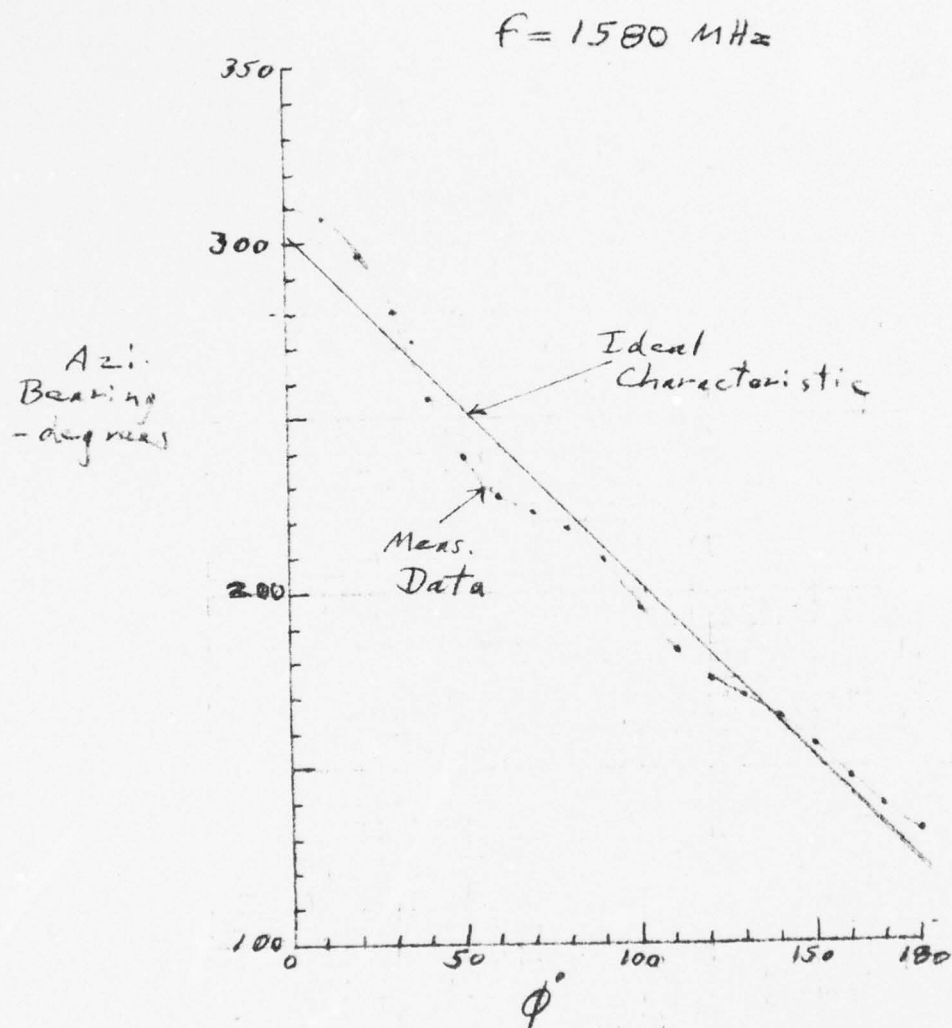


Figure 4-6. Azimuth Bearing Versus Phase Difference for  $H=0$ ,  $H=-1$

In the present case, however, little or no signal arrives at the  $H = \pm 4$  ports with excitation of the  $H = \pm 1$  ports. This means that there are no resistive losses (other than from normal line losses) in the hybrid circuits for the  $H = \pm 4$  modes. Thus, in effect, the input ports to each of the four outer hybrids are terminated with reactances, the magnitudes of which depend on the lengths of the corporate feed network legs joining the hybrids to common ports. Since the four monopoles of each quadrant are joined together through a hybrid and hence intercoupled, then the reradiated signals may take a complex variety of relative amplitudes and phases, resulting in higher mode distortion components.

One option to solve the anomaly, using the present circuitry, is described below. If eight short circuits are applied at the points marked A in Figure 4-2, then the hybrids would be eliminated from the circuitry when it is desired to employ only the  $H = 0$  and  $H = \pm 1$  modes for approximate azimuth bearing without ambiguity. The shorts would then be removed when using the  $H = 0$  and  $H = +4$  mode mode (or  $H = -4$  mode). These shorts could be obtained by the use of remotely-controlled diode switches.

Another advantage is obtained by applying the shorts at the indicated points. The electrical length from point A to the two fed elements are  $1/4\lambda$  and  $3/4\lambda$ , respectively. Hence, a short at A, open-circuits the base of each of the fed monopoles, thus reducing their reradiation.

It is to be noted that the present circuitry automatically prevents higher mode reradiation when the  $H = 0$  mode is fed. For this case, all sixteen of the outer elements are fed in phase with equal amplitudes. Thus the signals arriving at point A cancel and automatically give an effective short circuit at that point.

#### 4.5.2 $H = 4$ Mode

The phase slopes for the  $H = \pm 4$  modes showed much closer conformance to the calculated values than did the  $H = \pm 1$  mode. The graph of Figure 4-7 compares the measured  $H = 0$ ,  $H = 4$  azimuth pattern data with the ideal characteristic at one frequency of operation. (A

$$\text{Azi. Bearing} = \frac{(Ph_{-t}) - (Ph_o)}{4}$$

$$f = 1580 \text{ MHz}$$

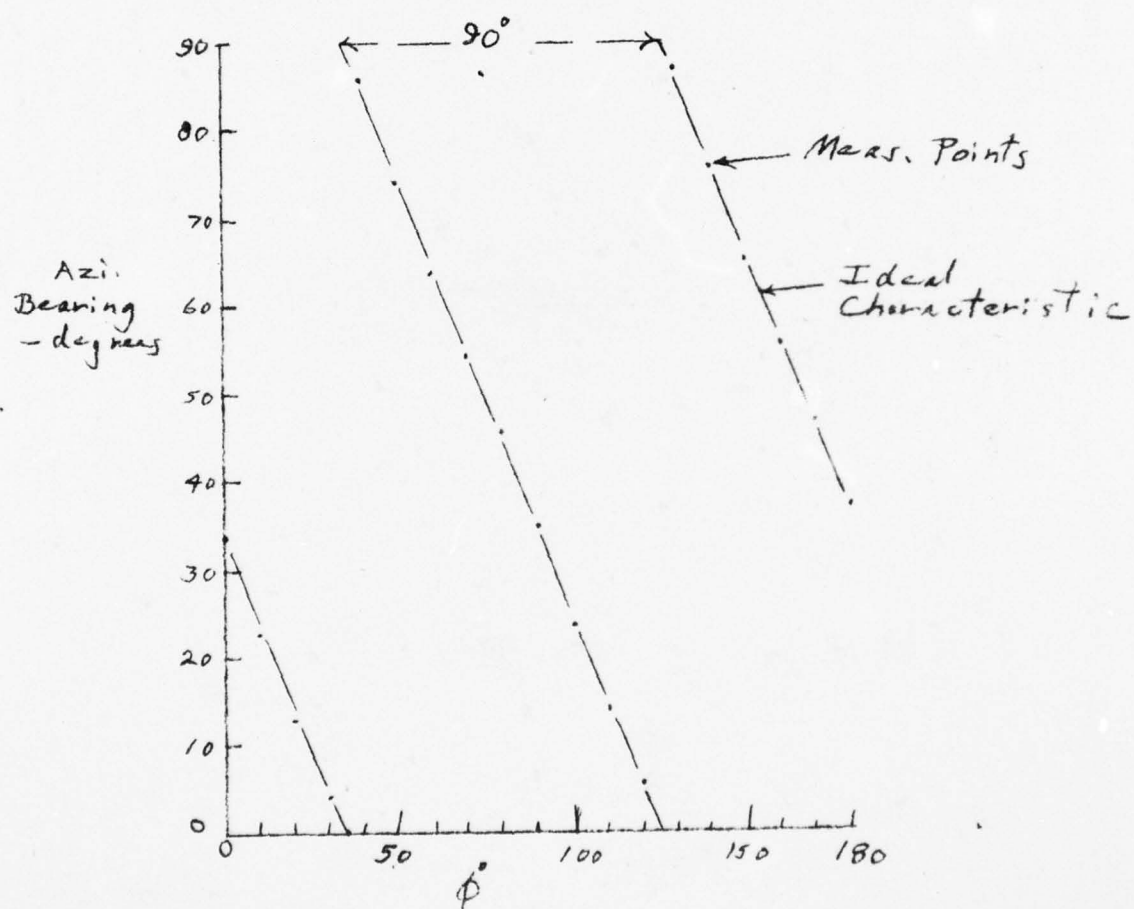


Figure 4-7. Bearing Versus Phase Difference for  $H=0$ ,  $H=-4$



more accurate determination of the bearing error may be derived from the expanded data given in Section 4.5.3.)

The  $H = +4$ ,  $H = -4$  azimuth pattern data presented in Figure 4-8 confirms a hypothesis for a possible alternative system. In this alternative, the phase difference is measured between the  $+4$  and  $-4$  ports, which would provide a multiplication factor of eight instead of four and also would decrease bearing error resulting from elevation angle change. However, to achieve this goal, the cross-coupling between the  $+4$  and  $-4$  ports must be much better than obtained with this first breadboard model.

#### 4.5.3 Multipath Effects

A limited experiment was performed to determine the effect of multipath. A grounded parasitic radiator, in the form of a conical monopole, was mounted off center on the ground plane and azimuth patterns were measured. Because of space limitations, the monopole was only three feet from the center of the array under test. This is not sufficiently representative of an aircraft structure and consequently the improvement from frequency diversity, predicted for greater spacings, was not achieved.

A cone was used because it presents a constant aperture and reflection angle as it rotates around the antenna whereas a flat reflector would not.

The resulting patterns showed increased ripple (in the normal cone regions) in both amplitude and phase introduced by the cone reradiation. It was found that the cone reradiation introduces an amplitude ripple of about  $\pm 0.5$  db which checks very well with the predicted value of  $\pm 5.6\%$  in field (or  $\pm 0.47$  db).

To determine the effect of frequency diversity, additional patterns were taken at 1596, 1604, 1611, and 1619 MHz. For these, the azimuth scale was expanded for the  $H = \pm 4$  patterns to secure greater accuracy in resolving the azimuth bearing error. The data

$$\text{Azi. Bearing} = \frac{(Ph_{+4}) - (Ph_{-4})}{8}$$

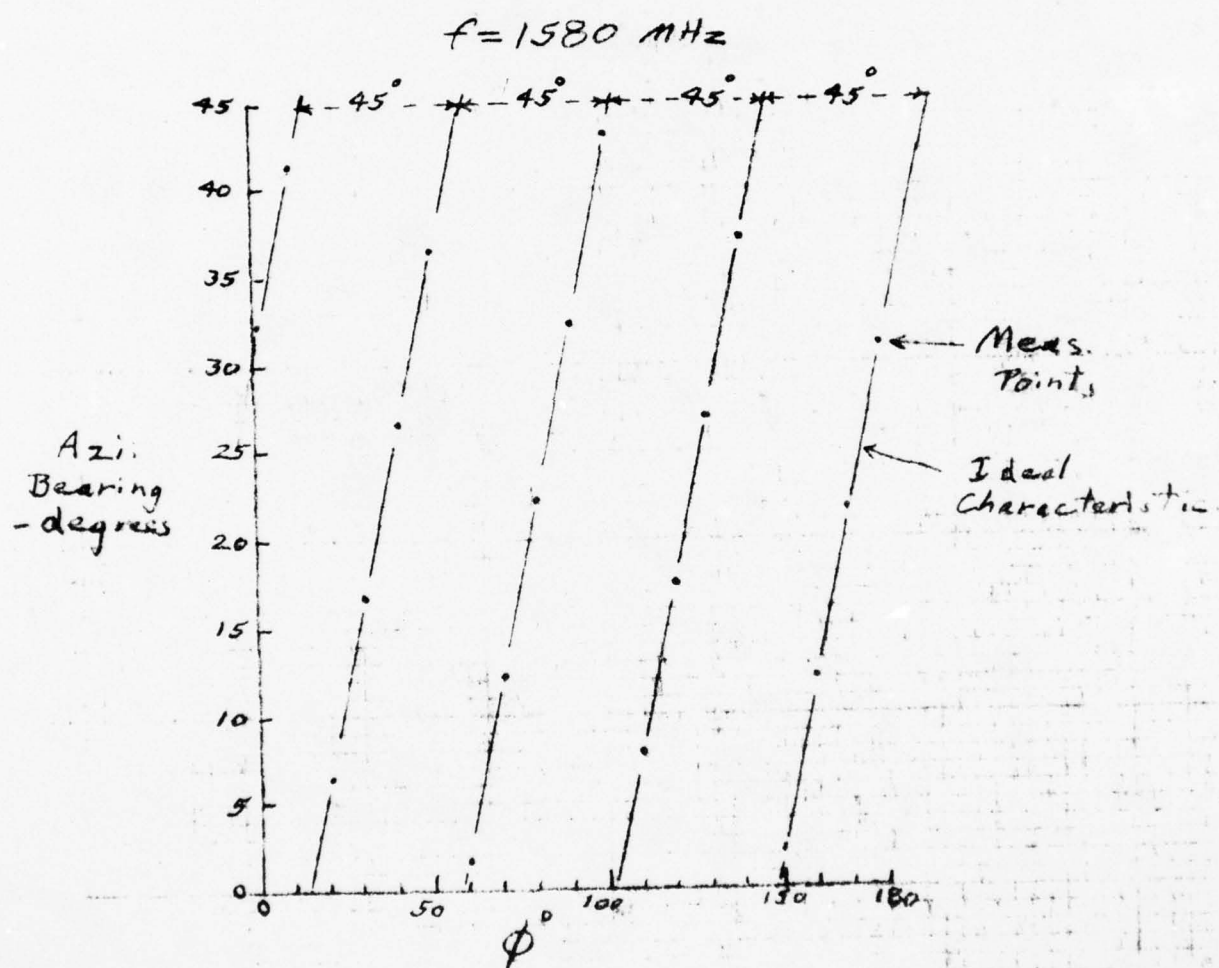


Figure 4-8. Bearing Versus Phase Difference for  $H = -4$ ,  $H = +4$

was taken both with and without the cone parasitic radiator in place. Figure 4-9 shows a pattern trace of the quadrant where the deviation from linearity was most pronounced, at 1604 MHz, and with the cone. The phase differences were scaled from these patterns and their departure from linearity plotted, as in Figure 4-10.

Figure 4-10 shows the error curves resulting from patterns made with and without the cone, at 1604 MHz. The results of the latter would be expected to represent only ripple error with a cyclicity of  $22.5^\circ$ , but instead had a cyclicity of  $45^\circ$ . Also, the peak-to-peak amplitude, after deducting the effect of unequal amplitude division of hybrids, is about  $\pm .5^\circ$ , which agrees with the value determined analytically in Appendix O.

It was, therefore, concluded that the lower curve contains unintentional multipath effects due to turntable edge effects and imperfections in the anechoic chamber.

Examining the upper curve for the introduced multipath effect, and subtracting the  $0.5^\circ$  experimental error, leaves a peak error of  $2^\circ$ , which agrees with the value determined analytically in Appendix O. This also compares with the  $1.4^\circ$  maximum, at any frequency and any bearing, as given in the analytic results, Table 3-8 of Section 3.5.2.1. The upward shift of the curve, indicating a positive bias, has not been explained.

A composite picture of multipath errors at four different frequencies, is depicted in Figure 4-11. A mean value (solid lines) is also shown. All of the plots have the same cyclicity. The predicted significant compensation expected from the use of frequency diversity was not achieved, probably due to the closeness of the cone radiator to the antenna structure. It was previously shown, in Table 3-8, that generally (up to a certain point) frequency diversity has a greater effect on error reduction, at greater antenna-to-reflector spacings, which are more typical of aircraft installations.

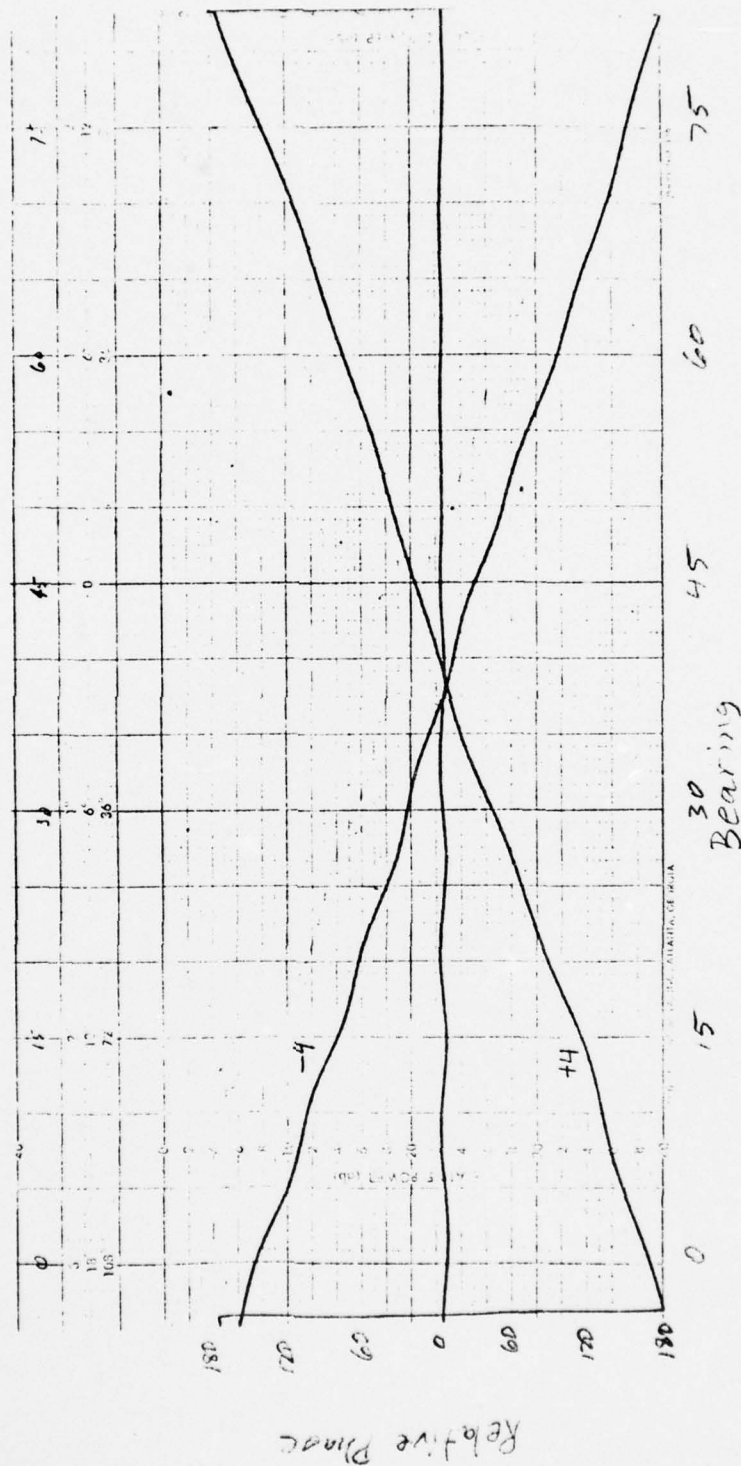


Figure 4-9. Bearing Versus Phase for  $H = 0$ ,  $H = -4$ ,  $H = +4$  at 1604 MHz, With Cone



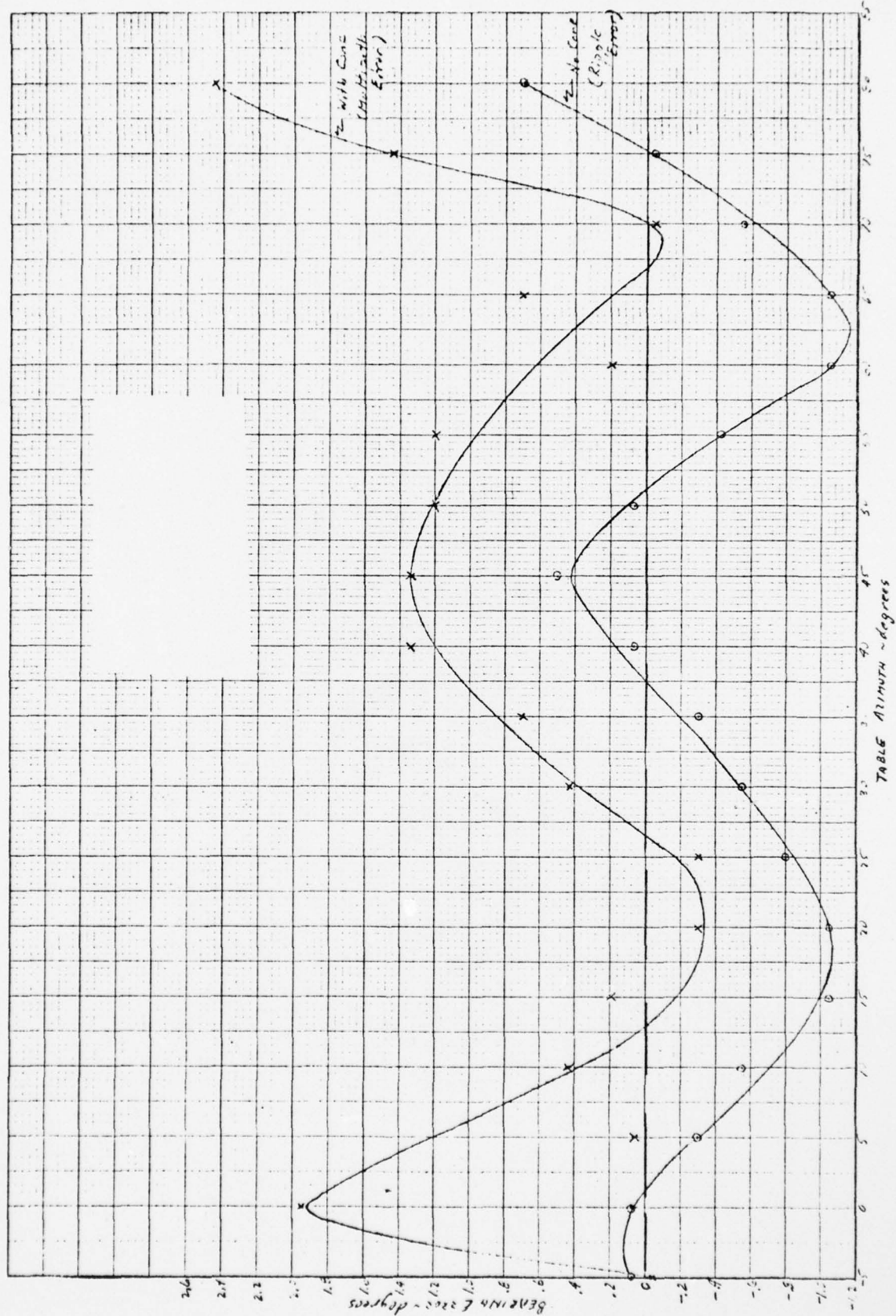


Figure 4-10. Multipath and Ripple Error at 1604 MHz

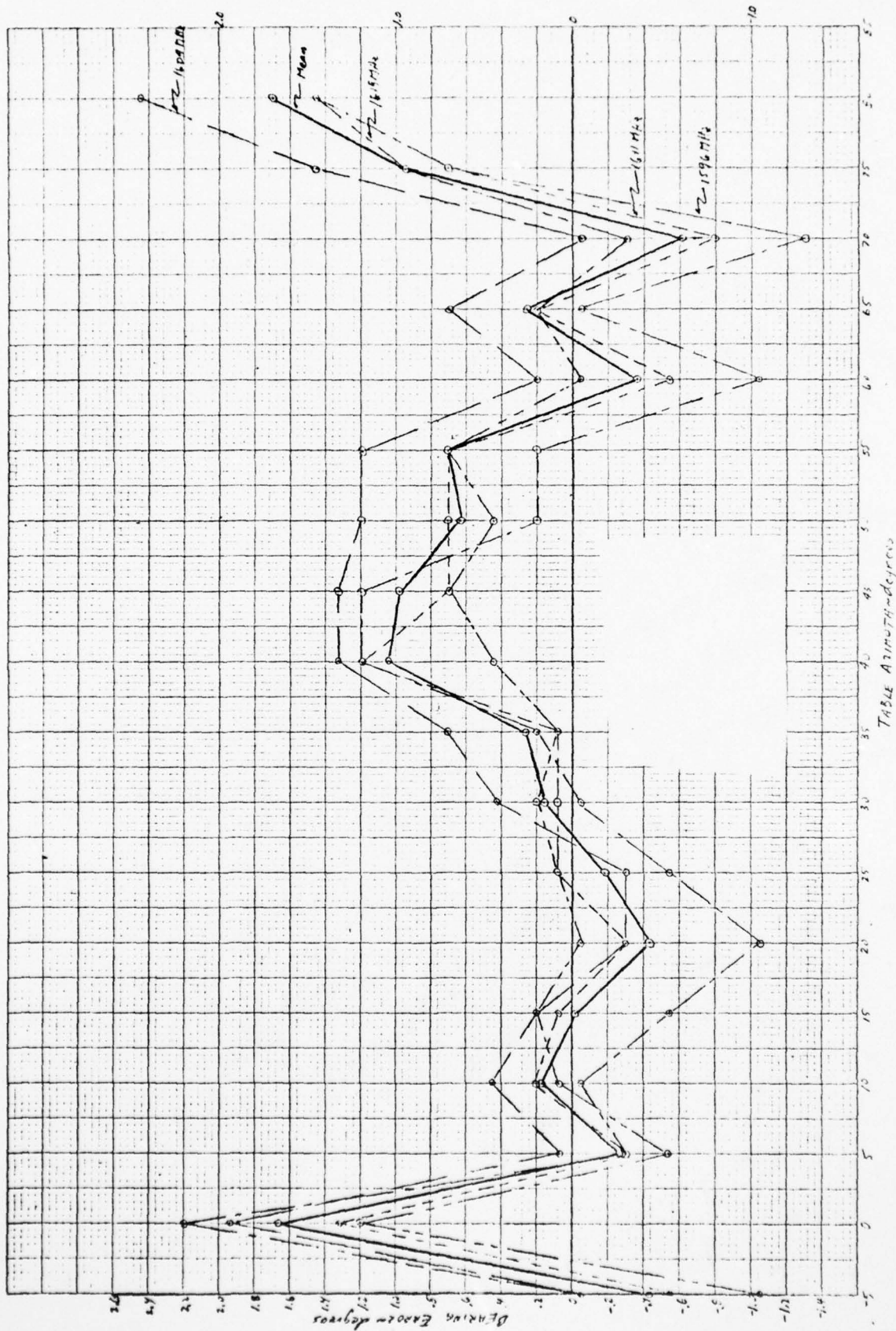


Figure 4-11. Multipath Error at Various Frequencies

If  $.5^\circ$  is subtracted from the peak of the mean function, the result is a value of  $1.2^\circ$ . This compares with half the maximum peak-to-peak mean error of  $1.25^\circ$  shown for run 4, frequency set E, antenna spacing of 104" in Table 3-8. Thus, considerable credence to the analytical results of Section 3.5.2.1 is afforded by the test results.

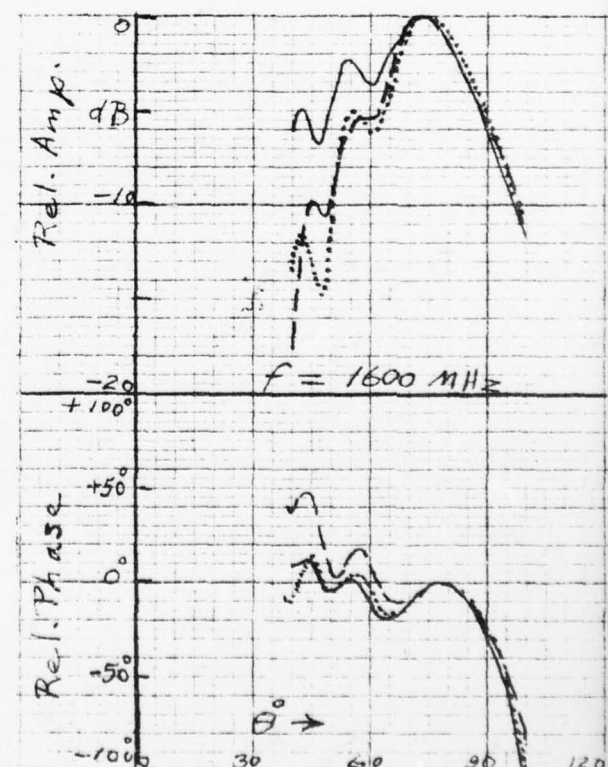
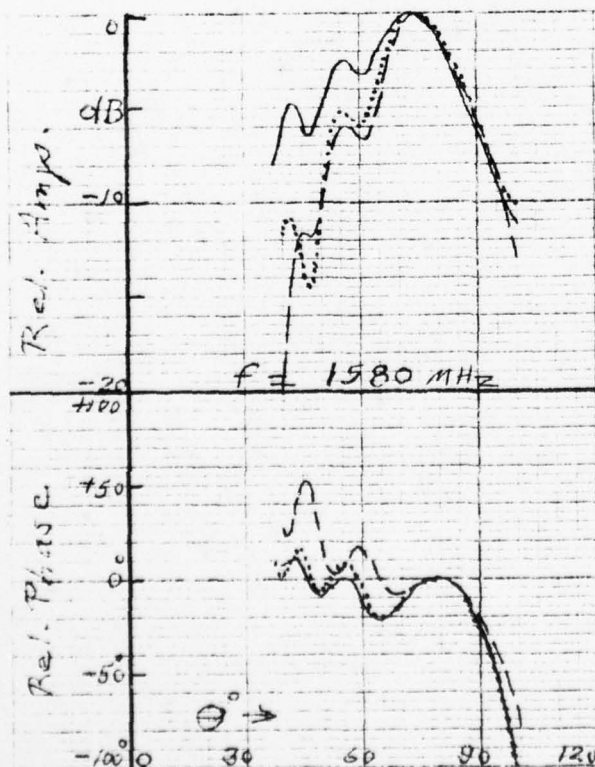
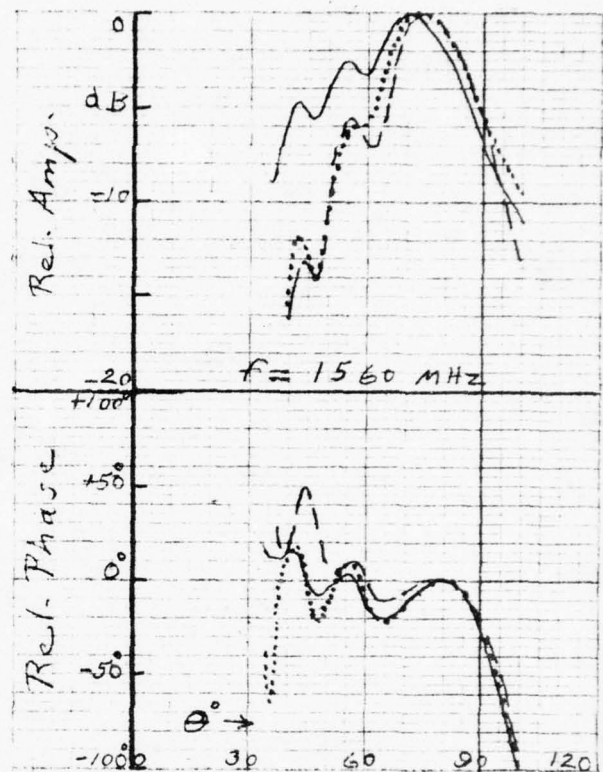
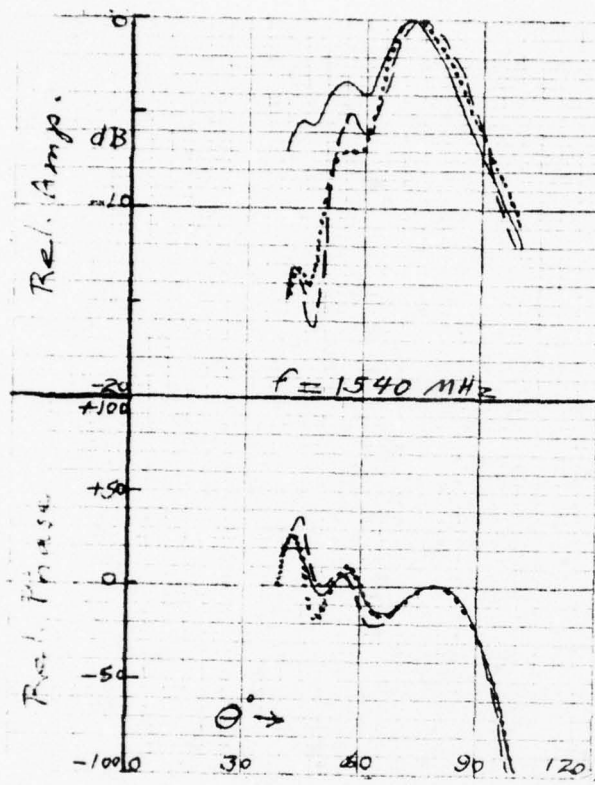
#### 4.5.4 Effect of Elevation Angle on Azimuth Patterns

The antenna must perform properly for targets at various elevation angles. A comparison of the amplitude and phase changes as a function of elevation angle ( $\theta$ ) is given in Figure 4-12 for each of the three modes over the frequency range of 1540 to 1620 MHz. Since the pattern shapes are different for different modes, then the phase characteristics differ also. It is seen, however, that the phase difference between the  $H = 0$  and  $H = +4$  is small over the  $\theta$  range of greatest interest; this is important in avoiding apparent azimuth angle changes with a change in elevation angle.



Figure 4-12. Elev. Patt. --  $\Phi$  Cus =  $-67.5^\circ$   
Comparison of Amp. & Phase for Different Modes

—  $H=0$   
- - -  $H=+1$   
...  $H=+4$





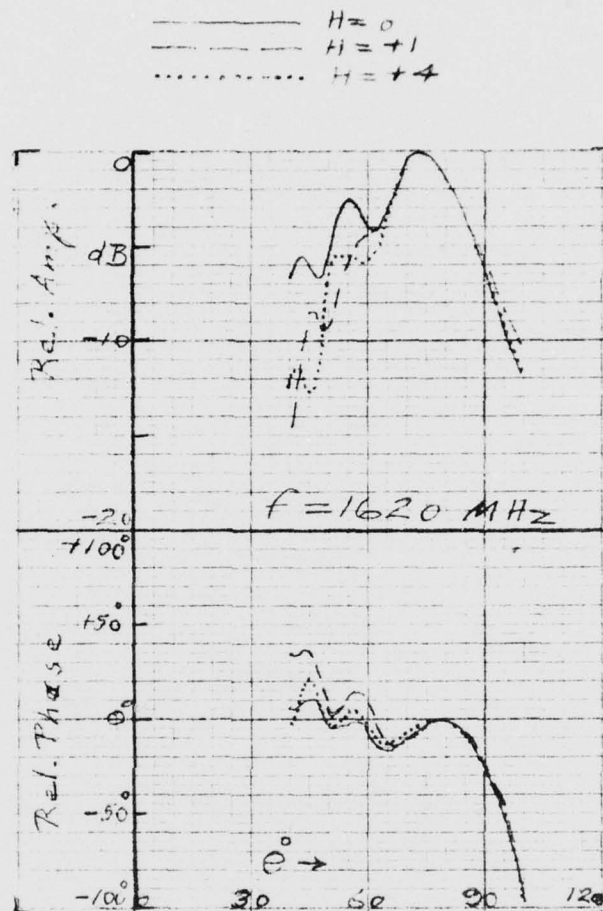


Figure 4-12. Elev. Patt. --  $\Phi$  Cus =  $-67.5^\circ$  Comparison of Amp. & Phase for Different Modes (Continued)

## SECTION 5.0

### HARDWARE CHARACTERISTICS FOR RECEIVER, SIGNAL PROCESSOR AND DATA PROCESSOR (TASKS 3.2, 3.3, 3.4)

#### 5.1 GENERAL

This section describes the implementation and configuration projected for the receiver, signal processor and data processor portions of the Bearing Measurement/Miss Distance Subsystem. These portions receive signals from the three ports of the ring antenna array and provide an output of miss distance and horizontal relative bearing for each target in accordance with the Subsystem Specification. A description of a PWI configuration is provided in Section 5.5. They are completely compatible with other members of the SECANT family.

The following material describes the subsystem as it might be associated with VECAS. It utilizes a dual channel receiver in place of the single channel VECAS receiver so that the instantaneous phase difference between signals received in two rings of the array can be taken. This receiver will also provide reply signals to the correlator, tracker, and data channels of VECAS, and probe signals to the reply generation channels. The VECAS tracker will control gates of the subsystem to coordinate phase measurements for the targets being tracked. These VECAS channels are not described herein but the interfaces to the subsystem are shown.

A block diagram of the Bearing/Miss Distance Subsystem is presented in Figure 5-1. The receiving system was configured to achieve the 0.8 degree sweep bearing measurement accuracy requirement defined in Section 2.5. Fabrication costs are minimized by sharing signal processing functions between the VECAS and bearing subsystems.

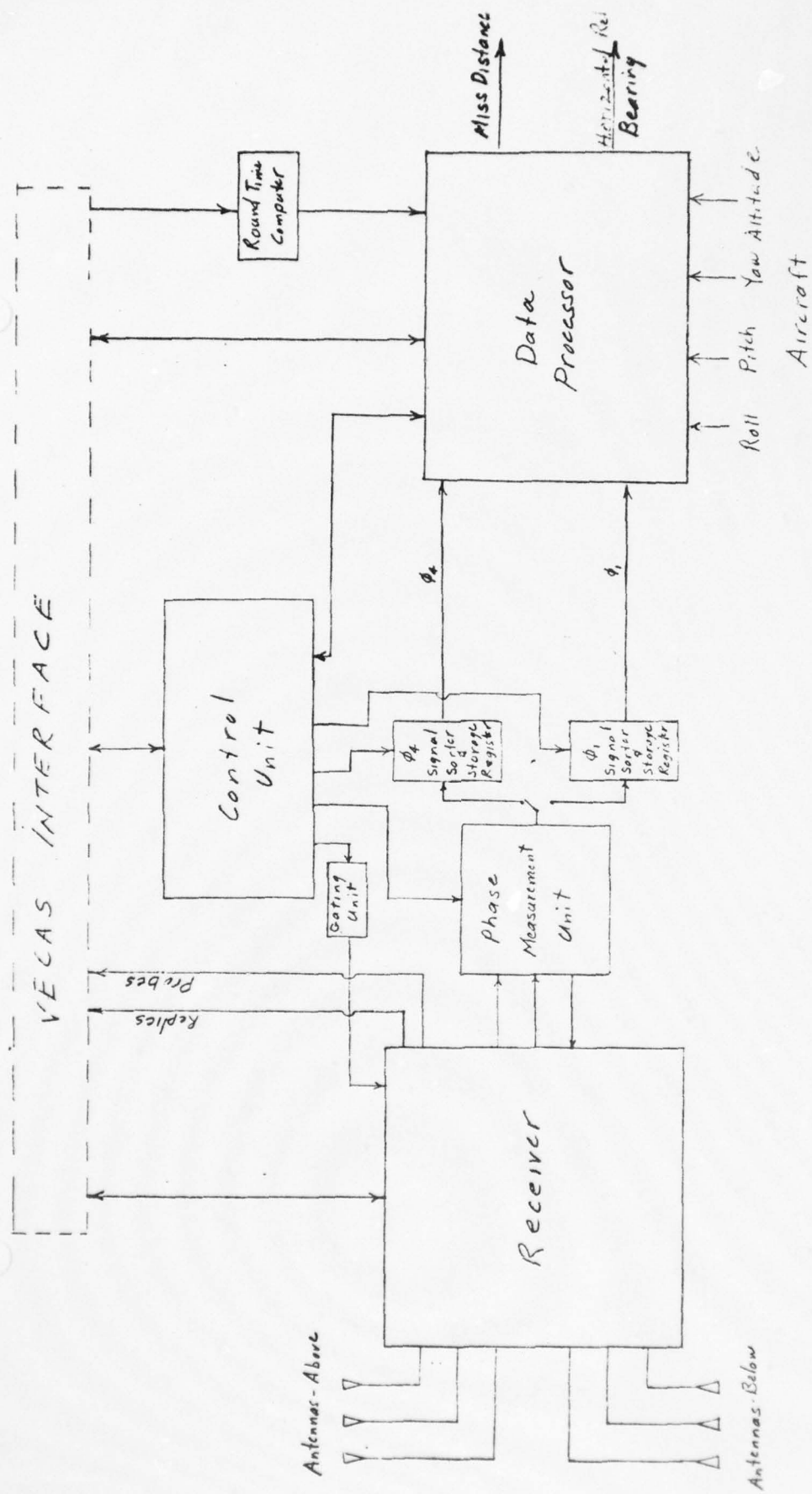


Figure 5-1. SECANT Bearing Block Diagram

AD-A049 767

RCA ELECTROMAGNETIC AND AVIATION SYSTEMS DIV VAN NUY--ETC F/G 1/2  
BEARING STUDY PROGRAM.(U)  
APR 74 E JELLINEK, W KRAM, M LEVINSSEN  
RCA-EASD-TP-2146

N62269-73-C-0906

NL

UNCLASSIFIED

4 OF 5

AD  
A049 767





As described previously, the antenna configuration consists of zero, single, and four mode ( $H = 0$ ,  $H = 1$ ,  $H = 4$ ) ring arrays. The phase of the signal output of the zero mode array is independent of the direction of arrival (DOA) of the incident wave, while the phase of the signal from the single mode array exhibits a nominally linear relationship with the DOA of the wave. Thus, an evaluation of the phase difference ( $\phi_1$ ) in the signal outputs of these two arrays will provide a direct bearing measurement without ambiguity. The four mode array yields four times the phase displacement of the single mode configuration. Therefore, measurement of the phase difference ( $\phi_4$ ) between the outputs of the  $H = 0$  and  $H = 4$  arrays will provide a more sensitive bearing evaluation. This higher phase versus bearing sensitivity is highly advantageous in achieving accurate bearing and miss distance assessments.

The receiver, under direction of the control unit, provides gated signals to the phase measurement unit from the  $H = 0$ , and from either the  $H = 1$  or the  $H = 4$  array. In addition, the receiver processes signals which are utilized in correlation, tracking, and reply transmitting. Separate antennas and receiver channels are utilized for the top and bottom fields. As the bandpass filters in the receiver channels will introduce maximum phase distortion at the beginning and end of pulses, a gating unit generates a sampling gate which extracts a measurement sample from the central segment of the pulse which has low phase distortion. The dual bearing receiver channels are phase matched. One of the channels is time shared between the  $H = 1$  and  $H = 4$  antennas to perform  $\phi_1$  and  $\phi_4$  measurements respectively. The other is connected to the  $H = 0$  antenna full time.

The phase measurement unit (PMU) measures the phase differences between the signals in the two channels from the time interval between the zero crossings of the two signals using digital counter techniques. The required resolution is achieved by utilizing analog verniers to expand the time intervals between pulse and clock edges and employing

averaging techniques. The total clock count, together with the number of measurements used in obtaining the total count are combined in word format for subsequent evaluation in the data processor.

The standard SECANT system tracking format is shown in Figure 5-2. This format utilizes two groups of 62 interrogation probes separated by a 260 ms time period. Range gates and circuitry are provided for tracking and measuring the range and bearing of up to 32 targets. In order to have an adequate number of most recent samples for high accuracy,  $\theta_4$  target bearing data is obtained on each of the reply pulses for the latter 62 probe group (Group B). As  $\theta_1$  data is utilized only to resolve the quadrant of the target bearing, its accuracy requirement is much lower. Therefore,  $\theta_1$  target bearing data is obtained only on the reply pulses for the first ten probes of Group A. As data for up to 32 targets can be obtained on each probe, each output of the phase measurement unit is stored in separate storage registers for subsequent data processing. A set of aircraft attitude data is also stored for each track format sequence.

The data processor, under direction of the control unit processes the individual samples and rejects wild readings, to derive a bearing for each target. The derived values, together with target range and altitude information and the aircraft's roll, pitch, and yaw data, are utilized to evaluate the target miss distance vector and horizontal relative bearing. The data processor can be implemented by a special purpose micro-processor together with special purpose, hard wired logic (e.g., signal sorter, gating unit, round time computer) to decrease the data processing time and to alleviate software costs.

## 5.2 RECEIVER CONFIGURATION

A block diagram of the receiver which processes bearing and other signals utilized in a SECANT system is shown in Figure 5-3. This unit furnishes reply signals via the dual, phase-matched, channels to the phase measurement unit. Other channels are provided for furnishing replies to the correlator and tracker, and received probes to the reply generator. Separate dual receiver channels are provided for the upper and the lower antennas.

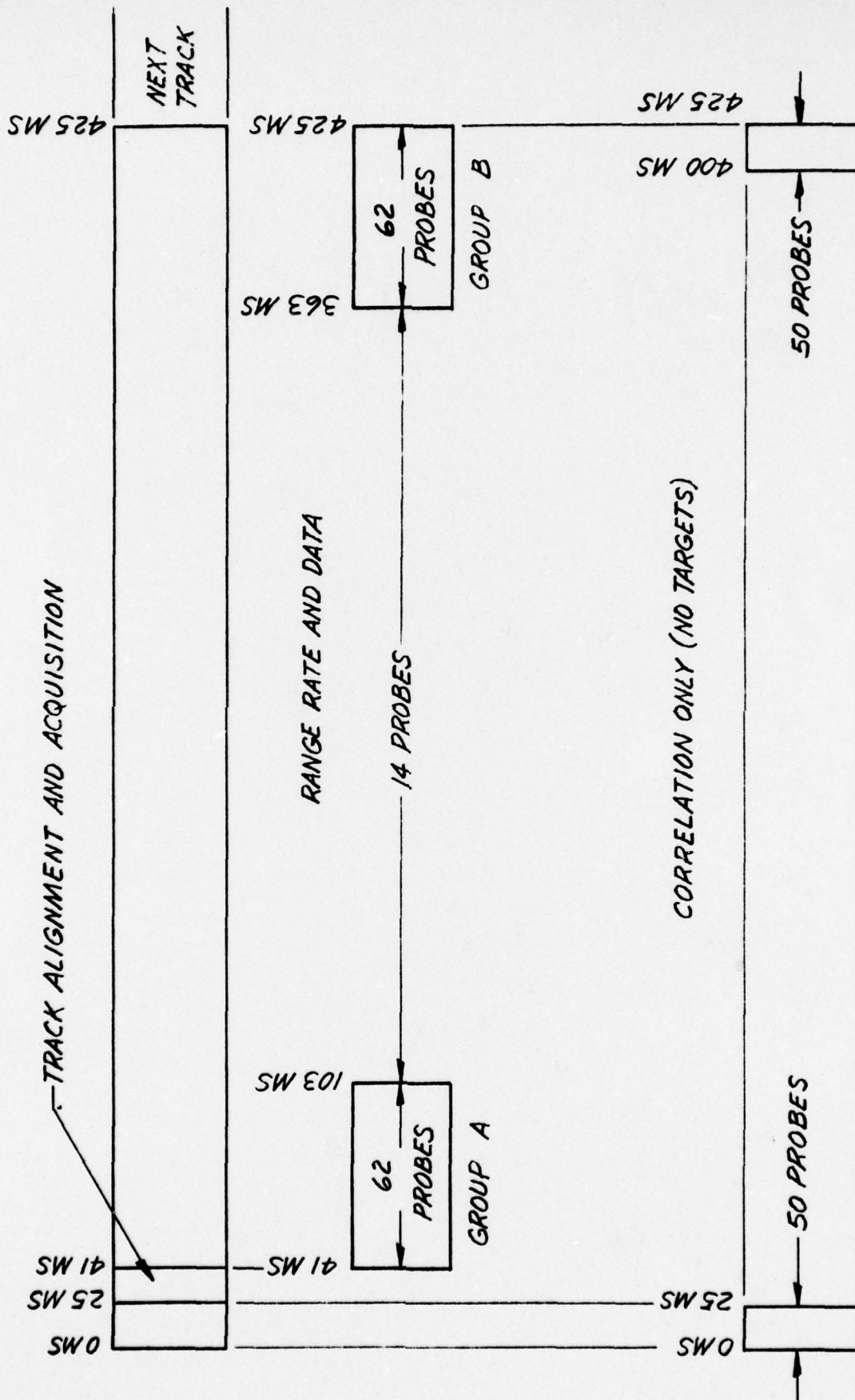


Figure 5-2. VECAS TRACK FORMAT









The front end of the receiver is located at the antenna to minimize noise interference and phase errors introduced by VSWR variations and changes in the electrical length of long cables carrying 1600 MHz signals. Even at a 173 MHz IF frequency, it will be desirable to bind the cables for both channels in a common jacket to produce similar temperature changes and vibration induced stresses for both long cable runs. As phase measurement accuracy is a function of the signal/noise ratio at the phase detector, low noise preamplifiers would be located at the outputs of each antenna. Double conversion, superheterodyne receivers would be utilized. Common local oscillators would be employed so that the oscillator voltages applied to the mixers in the two receiver channels would have equal phase. In this way, the IF voltages in the two receivers will maintain the same phase difference as existed in the RF signals at the antenna outputs.

Both manual and automatic phase adjustment is incorporated to minimize the effects of both long-term and short-term phase drifts in the bearing channels. The manual phase adjustment would be first set after the SECANT equipment is installed, to correct for the initial phase shift in the two paths from the antenna, to the signal delivered to the phase measurement unit. This manual phase alignment would then be performed at periodic intervals (e.g., annually) to correct for long term phase changes caused by such factors as drifts in filter components, dielectric changes in cables, etc.

Automatic phase adjustment updating is incorporated to equalize the smaller, short-term phase drifts between the two receiver channels. The updating would be performed during 10 ms time slots just prior to the 62 probe sequence during which  $\theta_4$  target bearing data is obtained. Phase correction is accomplished by a feedback control system. During updating, the signal from a signal generator is transmitted near the antenna arrays of both receiver channels. At this time, the output of the phase detector will indicate the phase difference between the two channels. This error signal is amplified and used to drive a phase shift network in one of the channels to null out the phase error.

The first and second IF frequencies are selected in accordance with CAS input data on probe type (i.e., P or Q), and the band and field mode of operation. These are listed in Table 5-1. For example, a first L.O. frequency of 1434 MHz is employed when operation with the top (above) antennas and the high band is required. The second IF of the two bearing channels is selected from four oscillators to limit the signal input to the phase measurement unit to a single frequency (i.e., 3.5 MHz). Thus, a second L.O. frequency of 167.5 MHz is selected when a Q probe is transmitted in the high band, top antenna operating mode. However, this frequency is 181.5 MHz for a P probe under the same operating conditions.

The crosstalk between the  $H = 0$  and  $H = 1$ , (or  $H = 4$ ) channels of the dual bearing receiver will not exceed -40 db. Isolation amplifiers will be incorporated in all of the local oscillator feeder lines and in the inter-channel sampling gate wires to inhibit signal coupling. The two channel chains will be mounted on separate chassis, and shielding enclosures and shielded wiring will be utilized to minimize radiation pickup between them. Separate, controlled, ground systems and individual power supply regulators will be utilized in the two receiver chains to inhibit cross coupling through common impedances of the two channels.

The bandwidth of the bandpass filters in the dual bearing channels will be 6 ( $\pm 0.5$ ) MHz between the -3 db point on the skirts. The bandwidth of the filters at the outputs of the probe and reply channels which receive data for the correlator trackers, transmitters, etc., will be 1 ( $\pm 0.05$ ) MHz between the -3 db points.

### 5.3 SIGNAL PROCESSING CONFIGURATION

A flow diagram of the bearing signal and data processing system is shown in Figure 5-4. This diagram exhibits all the input and output signals of the bearing subsystem and indicates signal utilization within the system.



TABLE 5-1

## RECEIVER FREQUENCIES FOR REPLIES

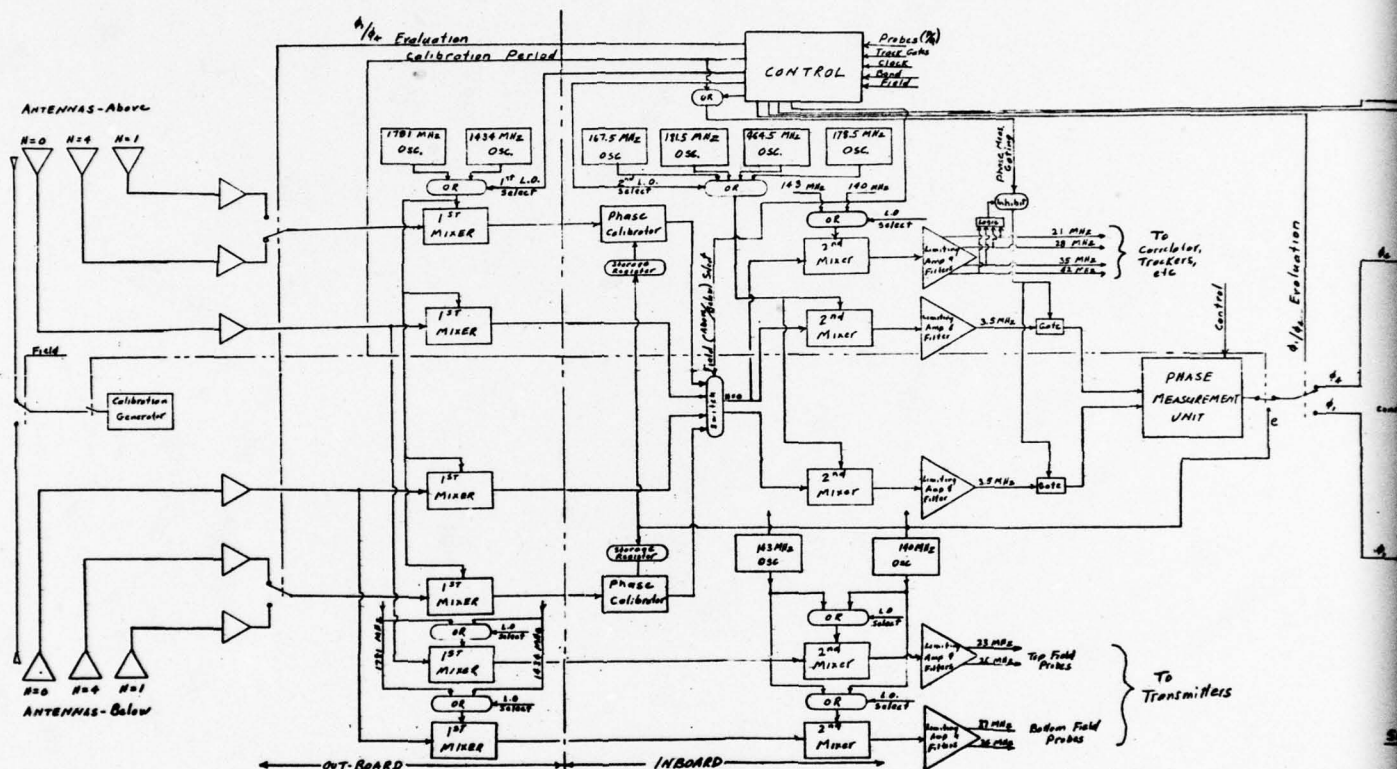
## Bearing Measurement Correlator &amp; Tracker

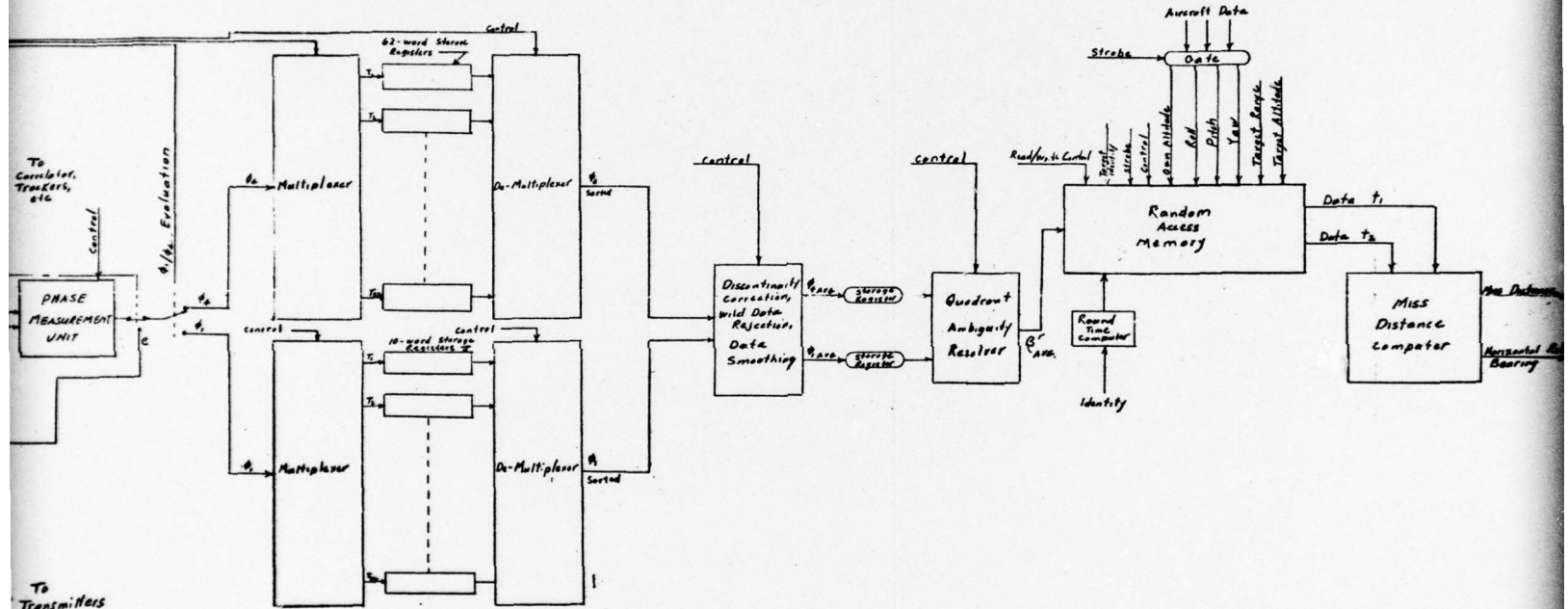
| Type | Band - Antenna | Freq. | Reply          | 2nd L.O. |        |          |        | 2nd IF   |        |          |        |
|------|----------------|-------|----------------|----------|--------|----------|--------|----------|--------|----------|--------|
|      |                |       |                | 1st L.O. | 1st IF | 2nd L.O. | 2nd IF | 2nd L.O. | 2nd IF | 2nd L.O. | 2nd IF |
| N    | High - above   | 1598  | Q <sup>+</sup> | 1434     | 164    | 167.5    | 3.5    | 143      | 21     | 143      | 21     |
|      | "              | 1605  | Q <sup>-</sup> | 1434     | 171    | 167.5    | 3.5    | 143      | 28     | 143      | 28     |
|      | "              | 1612  | P <sup>+</sup> | 1434     | 178    | 181.5    | 3.5    | 143      | 35     | 143      | 35     |
|      | "              | 1619  | P <sup>-</sup> | 1434     | 185    | 181.5    | 3.5    | 143      | 42     | 143      | 42     |
| X    | High - below   | 1617  | Q <sup>+</sup> | 1781     | 164    | 167.5    | 3.5    | 143      | 21     | 143      | 21     |
|      | "              | 1610  | Q <sup>-</sup> | 1781     | 171    | 167.5    | 3.5    | 143      | 28     | 143      | 28     |
|      | "              | 1603  | P <sup>+</sup> | 1781     | 178    | 181.5    | 3.5    | 143      | 35     | 143      | 35     |
|      | "              | 1596  | P <sup>-</sup> | 1781     | 185    | 181.5    | 3.5    | 143      | 42     | 143      | 42     |
| Y    | Low - above    | 1620  | Q <sup>+</sup> | 1781     | 161    | 164.5    | 3.5    | 140      | 21     | 140      | 21     |
|      | "              | 1613  | Q <sup>-</sup> | 1781     | 168    | 164.5    | 3.5    | 140      | 28     | 140      | 28     |
|      | "              | 1606  | P <sup>+</sup> | 1781     | 175    | 178.5    | 3.5    | 140      | 35     | 140      | 35     |
|      | "              | 1599  | P <sup>-</sup> | 1781     | 182    | 178.5    | 3.5    | 140      | 42     | 140      | 42     |
| Z    | Low - below    | 1595  | Q <sup>+</sup> | 1434     | 161    | 164.5    | 3.5    | 140      | 21     | 140      | 21     |
|      | "              | 1602  | Q <sup>-</sup> | 1434     | 168    | 164.5    | 3.5    | 140      | 28     | 140      | 28     |
|      | "              | 1609  | P <sup>+</sup> | 1434     | 175    | 178.5    | 3.5    | 140      | 35     | 140      | 35     |
|      | "              | 1616  | P <sup>-</sup> | 1434     | 182    | 178.5    | 3.5    | 140      | 42     | 140      | 42     |

## Notes:

Guard Bands = 1593, 1594, 1621, 1622  
 AGC Frequencies = 1607, 1608







SIGNAL FLOW DIAGRAM  
Fig. 5-4

As shown, two antenna arrays are employed to provide full coverage. One array is mounted on top of the aircraft for reception in the upper hemisphere (or field) and the other on the bottom to cover the lower field. For fruit rejection, different sets of frequencies are assigned to these fields so that only top antennas can receive probes and replies from bottom transmitter antennas. Similarly, only bottom antennas will receive transmissions from top antennas. Also, to minimize fruit, SECANT uses two bands of frequencies for flight altitude discrimination. One band of frequencies is assigned for altitudes below 10,000 feet; the other band for altitudes above 10,000 feet. As aircraft replies can be in four different forms ( $P^+$ ,  $P^-$ ,  $Q^+$  and  $Q^-$ ), the bearing receiver channels must accommodate 16 different frequencies.

Table 5-1 denotes the  $P^+$ ,  $P^-$ ,  $Q^+$  and  $Q^-$  bearing reply frequencies for the four band and field combinations categorized as W, X, Y, and Z. The corresponding first and second local oscillator and resultant first and second IF bearing frequencies are also listed. These frequencies were selected to conform with the subsystem signal frequency requirements designated in paragraph 3.4.4.2 of the SECANT Bearing Performance Specification, Appendix F. As an additional constraint, the frequencies must be contained within the 30 MHz (1592.5 to 1622.5 MHz) frequency interval allocated by the FCC to the anti-collision function. To insure compliance with this FCC allocation, frequency intervals (guard bands) from 1592.5 to 1594 MHz and 1621 to 1622.5 MHz were not assigned. Also, the mid-band frequencies of 1607 and 1608 MHz were not allotted as they are used in the AGC circuits of the receiver.

The spread of RF signals in each of the subgroups W, X, Y, and Z is 21 MHz and the difference between adjacent frequencies within any subgroup is 7 MHz. This satisfies the minimum value requirements of 20 MHz and 5 MHz specified in paragraph 3.4.4.2.1 of the subsystem specification. The final IF frequency of 3.5 MHz satisfies all the requirements of paragraph 3.4.4.2.2 of the specification. The generation of a single

frequency from the final IF stage of the bearing channels minimizes the complexity of the phase measurement unit and data processing system. A low frequency was selected to enhance the resolution of the phase measurement.

Different second L.O. and second IF frequencies are used to process the replies for correlation and tracking.

The frequency sets designated for the probe receiver channels is shown in Table 5-2. The output from this dual receiver signifies the field (i.e., top or bottom) and sense (i.e., P or Q) of the probe. This information is sent to the SECANT transmitters.

The Phase Measurement Unit (PMU) measures the time interval ( $t$ , Figure 5-5) between the zero crossovers of the dual 3.5 MHz bearing output signals by digital counter techniques. The resolution of the measurement is increased by utilizing analog verniers to expand the time intervals between pulse and clock edges and employing averaging techniques. The sampling gate is generated in accordance with paragraph 3.4.4.7.1 of the Bearing Performance Specification to extract a measurement sample from a section of the pulse which has low phase distortion. The sampling gate is formed by generating a 0.65  $\mu$ sec pulse, 0.25  $\mu$ sec after the leading edge of the track gate. The phase measurement gate is also closed during the calibration period. For fruit rejection, the sampling gate will be inhibited if no signal, or two or more signals, appear simultaneously at the output of the correlator/tracker receiver channel.

High resolution measurements of time  $t$  is made from this sample by the technique illustrated in Figure 5-6(a) and (b). As shown in (a), the width of pulse  $t$  is equal to the time intervals  $t_1$  plus  $t_2$  minus  $t_3$ . Measurement of  $t_2$  is done by counting the output pulses of a crystal-controlled clock. Time periods  $t_1$  and  $t_3$ , which are smaller than a period of the clock, are expanded by a factor of ten by the mechanism illustrated in (b). When used to expand  $t_1$ , flip-flop A is set by the leading edge of the input pulse and reset by the leading edge of the next clock pulse. However, when a similar circuit is employed to expand  $t_3$ , the trailing edge of the signal pulse sets the flip-flop which, in



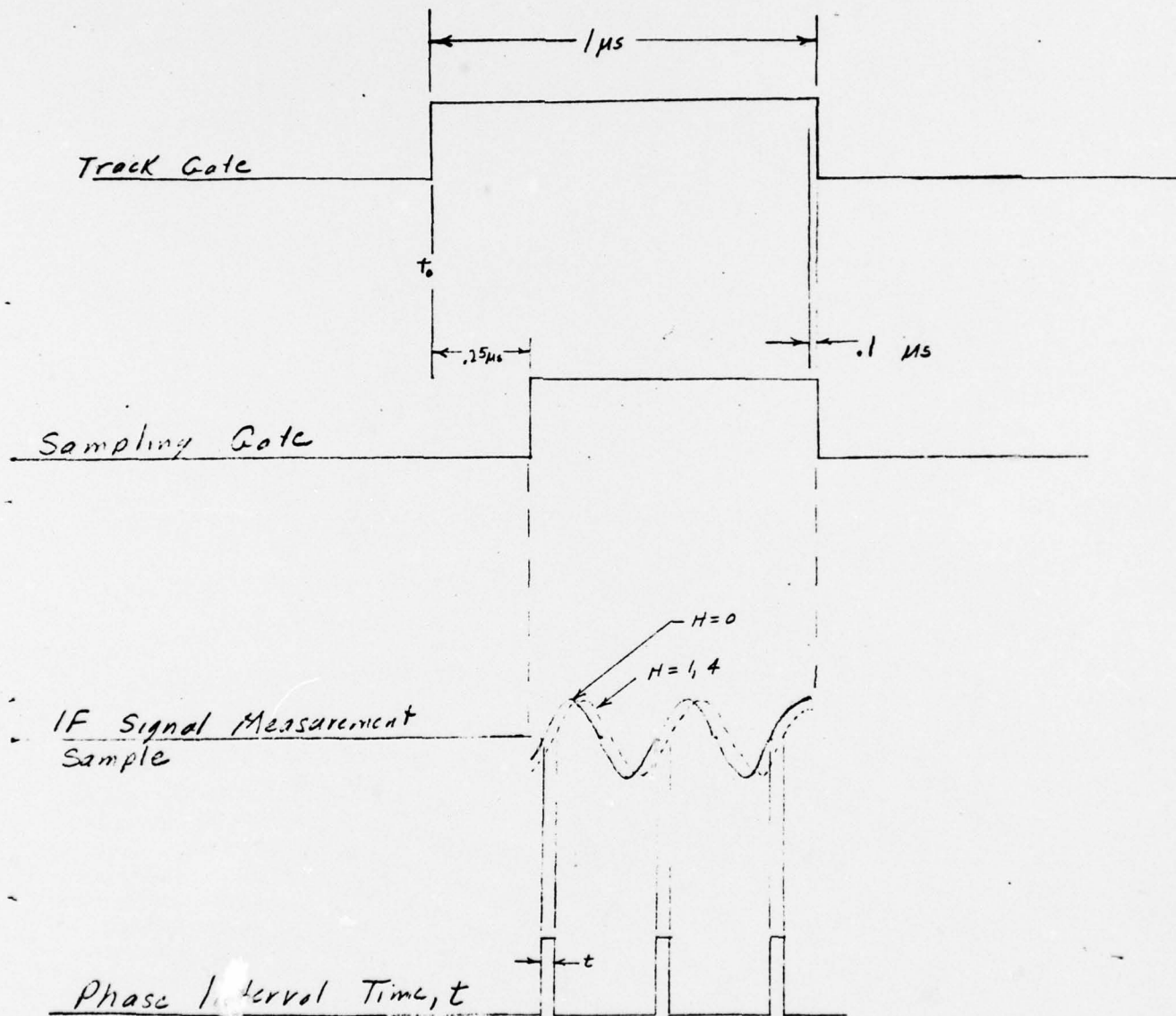
TABLE 5-2

## RECEIVER FREQUENCIES - PROBES

| <u>Type</u> | <u>Band - Antenna</u> | <u>Freq.</u> | <u>Probe</u> | <u>1st L.O.</u> | <u>1st IF</u> | <u>2nd L.O.</u> | <u>2nd IF</u> |
|-------------|-----------------------|--------------|--------------|-----------------|---------------|-----------------|---------------|
| <u>W</u>    | High - Above<br>"     | 1597         | P            | 1434            | 163           | 140             | 23            |
|             |                       | 1600         | Q            | 1434            | 166           | 140             | 26            |
| <u>X</u>    | High - Below<br>"     | 1601         | P            | 1781            | 180           | 143             | 37            |
|             |                       | 1604         | Q            | 1781            | 177           | 143             | 34            |
| <u>Y</u>    | Low - Above<br>"      | 1618         | P            | 1781            | 163           | 140             | 23            |
|             |                       | 1615         | Q            | 1781            | 166           | 140             | 26            |
| <u>Z</u>    | Low - Below<br>"      | 1614         | P            | 1434            | 180           | 143             | 37            |
|             |                       | 1611         | Q            | 1434            | 177           | 143             | 34            |

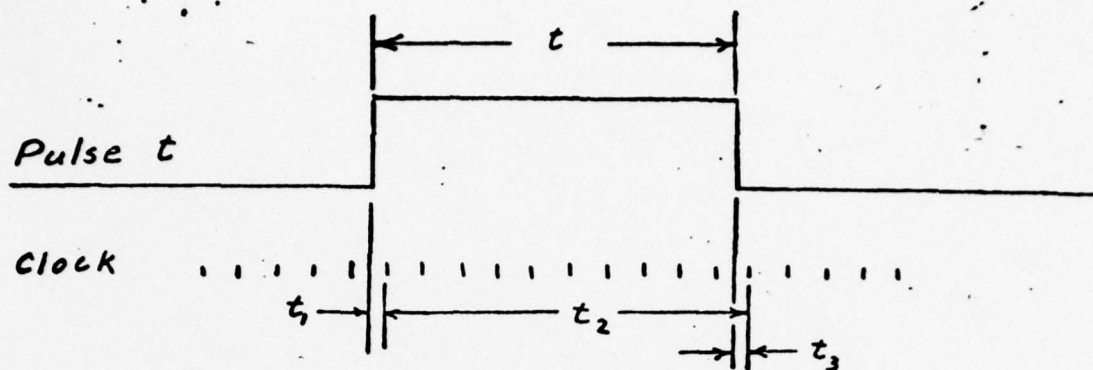
## Notes:

Guard Bands - 1593, 1594, 1621, 1622  
AGC Frequencies = 1607, 1608



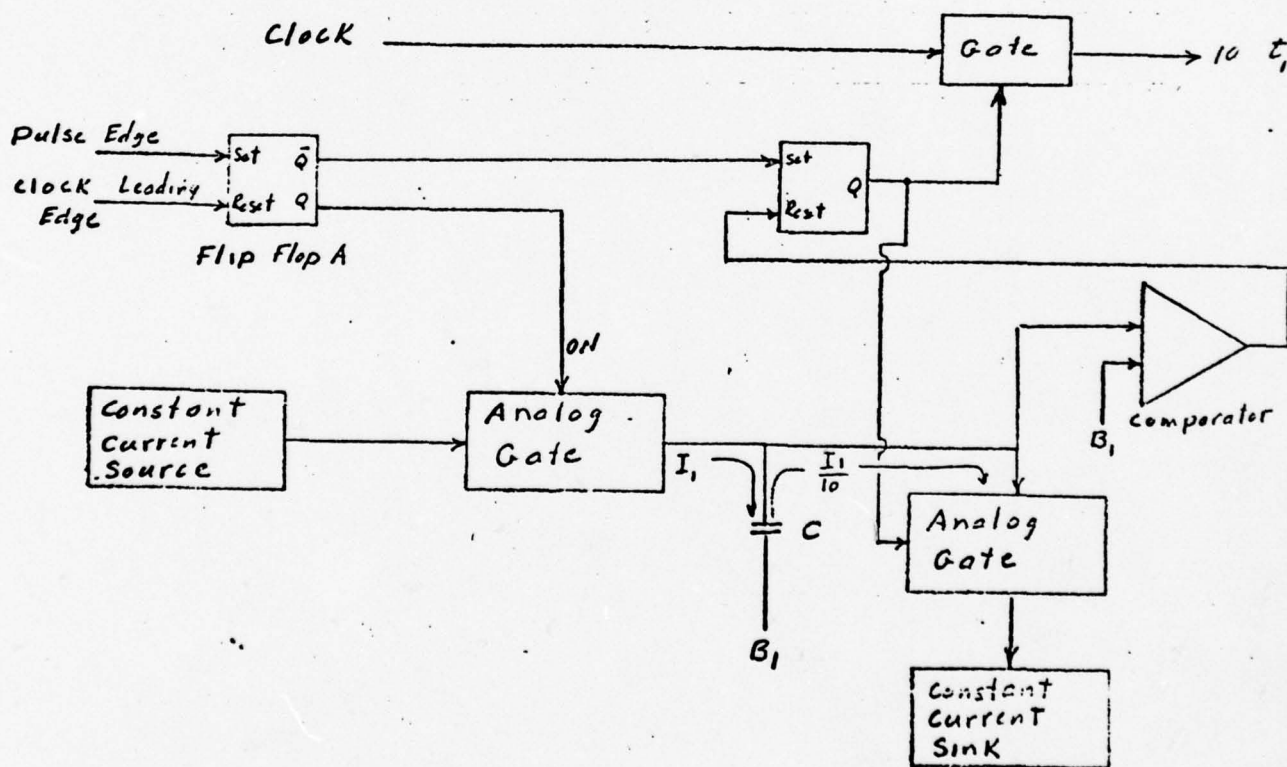
Sampling Gate and Phase Interval Generation

Figure 5-5.



$$t = t_1 + t_2 - t_3$$

(a)



(b)

Figure 5-6.

High Resolution, Digital, Pulse Width Detector Vernier

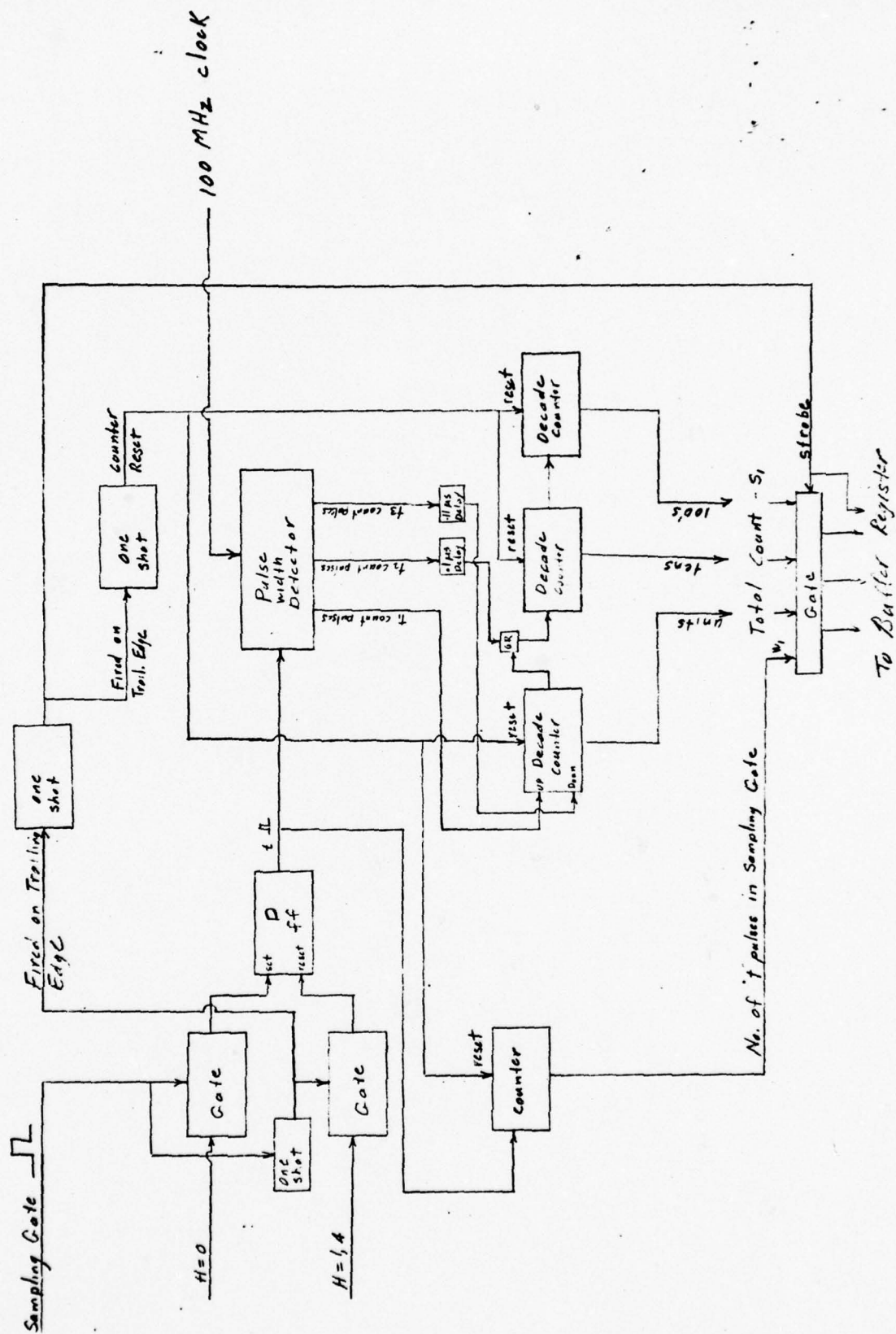
turn, is reset by the leading edge of the following clock pulse. During the time flip-flop A is high, a constant current ( $I_1$ ) charges capacitor C. When the flip-flop goes low, this capacitor is discharged with a second constant current which is ten times smaller than  $I_1$ . Thus, the time taken to discharge C to its initial state will be ten times longer than the charging time. The expanded time ( $10t$ ) is measured by counting the number of clock pulses occurring during the discharge time interval. The vernier counts, appropriately weighted, are combined to evaluate the pulse width. Separate verniers would be employed to resolve the pulse's leading and trailing edges in a pulse width detector configuration.

A block diagram of the phase measurement unit is shown in Figure 5-7. The sampling gate passes a segment of the bearing receiver signals to the D flip-flop which generates a set of two or three  $t$  pulses for each bearing receiver segment. The flip-flop is set and reset by the positive-going axis transitions of the  $H = 0$  and  $H = 1$  (or  $H = 4$ ) waves, respectively. In this way, the pulse width ( $t$ ) is indicative of the phase displacement between the dual bearing signals. As discussed above, the pulse widths are evaluated in the pulse width detector. The serial outputs of the detector, appropriately weighted, are added in the decade counter. Simultaneously, the number of  $t$  pulses generated during the bearing signal segment ( $W_1$ ) are counted. At the end of the sampling period, the total phase count ( $S_1$ ) and number of  $t$  pulses ( $W_1$ ) are sent to a buffer register for subsequent data processing. All counters are reset after the transfer to enable the unit to process the next bearing sample.

Pulse width can be resolved to 1.0 ns with a 100 MHz clock and a vernier magnification factor of ten. Therefore, at signal frequencies of 3.5 MHz, phase angle can be resolved to a resolution of  $1.26^\circ$ . Also, it has been shown that the mean of a number of noisy quantized measurements possesses higher resolution than the quantizing increment. As



Figure 5-7. PHASE MEASUREMENT UNIT  
BLOCK DIAGRAM



62 phase angle measurements of noisy signals would be averaged in the evaluation of  $\phi_4$ , it is indicated that the quantization error contribution is  $0.16^\circ$  one sigma. As  $\phi_4$  has an angle conversion factor of four, bearing measurements will have a resolution of  $0.04^\circ$  one sigma.

#### 5.4 DATA PROCESSING CONFIGURATION

Bearing values from the phase measurement unit are processed together with target and aircraft data to evaluate target miss distance and true bearing. The evaluation is accomplished by a data-sorter, a mini-computer and a hard-wired round-time-computer.

The bearing information received from the phase measurement unit is first sent to a buffer register. Each word contains the total phase count ( $S_1$ ) and number of  $t$  pulses ( $W_1$ ) contained within a sampling gate. The phase angle ( $\phi$ ) delineated by each word is computed from the equation:

$$\phi = \frac{2\pi S_1}{W_1 f_c T} \quad \text{radians}$$

with  $f_c = 10^9$ , and  $T = \frac{1}{3.5 \text{ MHz}}$

$$\phi = .02199 \frac{S_1}{W_1} \quad \text{radians}$$

Each word, in turn, is shifted from the buffer register and its data is used to compute the corresponding phase angle. These values are sorted into  $\phi_1$  and  $\phi_4$  storage registers assigned to each target. The sorting is accomplished by two one-line to 32-line multiplexers. In this way, the 62 samples of all  $\phi_4$  data for each target are stored in 32 separate 62 word storage registers. Similarly, the ten samples obtained in the

collection of  $\theta_1$  phase values for each target are stored in 32 separate ten word storage registers.

A data smoothing computer, under command of the control unit, sequentially requests, through the 32-line to 1-line demultiplexer,  $\theta_1$  and  $\theta_4$  phase information on each target. This data is first processed in accordance with the "Algorithm for Phase Measurement Data Processing" referenced in the System Specification to obtain average  $\theta_1$  and  $\theta_4$  phase values. These values are obtained by: (1) conditioning the measurements to circumvent the discontinuity that occurs at  $360^\circ/0^\circ$ , (2) rejecting wild data caused by residual fruit and noise, and (3) averaging the resultant phase values.

The  $\theta_{1avg}$  and  $\theta_{4avg}$  phase values for each target are then combined to obtain a non-ambiguous target bearing angle ( $\beta^r$  avg). In this process,  $\theta_{1avg}$  is utilized to resolve the quadrant of the bearing angle, while the more accurate  $\theta_{4avg}$  reading determines its actual value. The result is stored in a memory register for the particular target. Enough registers are provided to store the relative bearing readings for all targets. The aircraft's attitude parameters must also be stored for eventual compensation of each of these bearing readings. Only one set of attitude data registers will be needed per altitude zone instead of one set per target.

For miss distance determination, two sets of the above data must be taken on successive rounds and stored separately. However, when the round time is less than four seconds, as is possible in light or moderate traffic, the resulting time base will not be sufficient to provide the required accuracy. A round time computer is used to keep track of the round time and inhibit the loading of new bearing values for old targets for at least four seconds. In this way the resulting time base will be between four and eight seconds. The memory furnishes both sets of data and the length of the time base to the miss distance computer.



The miss distance computer performs the algorithm that computes miss distance and relative horizontal bearing for each target. These are outputted to registers for each target. With additional logic they may be used for false alarm reduction, horizontal maneuver, or display purposes.

Bearing data collection is completed and stored at the end of each track cycle. This data is then processed during the 425 ms of the next cycle. Detailed study of the number and cycle time for all operations is beyond the scope of this program but a preliminary time allocation schedule indicates that the processing can be accomplished within the 425 ms available.

#### 5.5 PWI BEARING RECEIVER AND INFORMATION PROCESSING CONFIGURATION

The Proximity Warning Inductor (PWI) is intended for general aviation and provides intruder warning protection at low cost. It will alert the pilot when a threat has penetrated a range "shield" selected by the pilot. The bearing subsystem will provide the pilot with the relative bearing of the intruder as an aid to visual acquisition. Threat assessment and avoidance maneuver procedures are left to the discretion of the pilot.

Prime requisites of the PWI are low cost, small size, and low weight to enhance its suitability and acceptability for small aircraft. To achieve this, bearing requirements for the PWI system are minimized to achieve simplicity in the equipment. Thus, a bearing accuracy of  $\pm 15^\circ$ , and a maximum capacity of eight simultaneous targets, have been adopted for the PWI bearing system.

A functional block diagram of the PWI relative bearing measurement system is shown in Figure 5-8. The antenna configuration consists of only zero and single mode ( $H = 0$ ,  $H = 1$ ) ring arrays, as the higher accuracy obtained through the incorporation of a  $H = 4$  antenna is not required in this system. All data processing is accomplished with hard-wired logic and a mini-computer or micro-processor will not be needed.



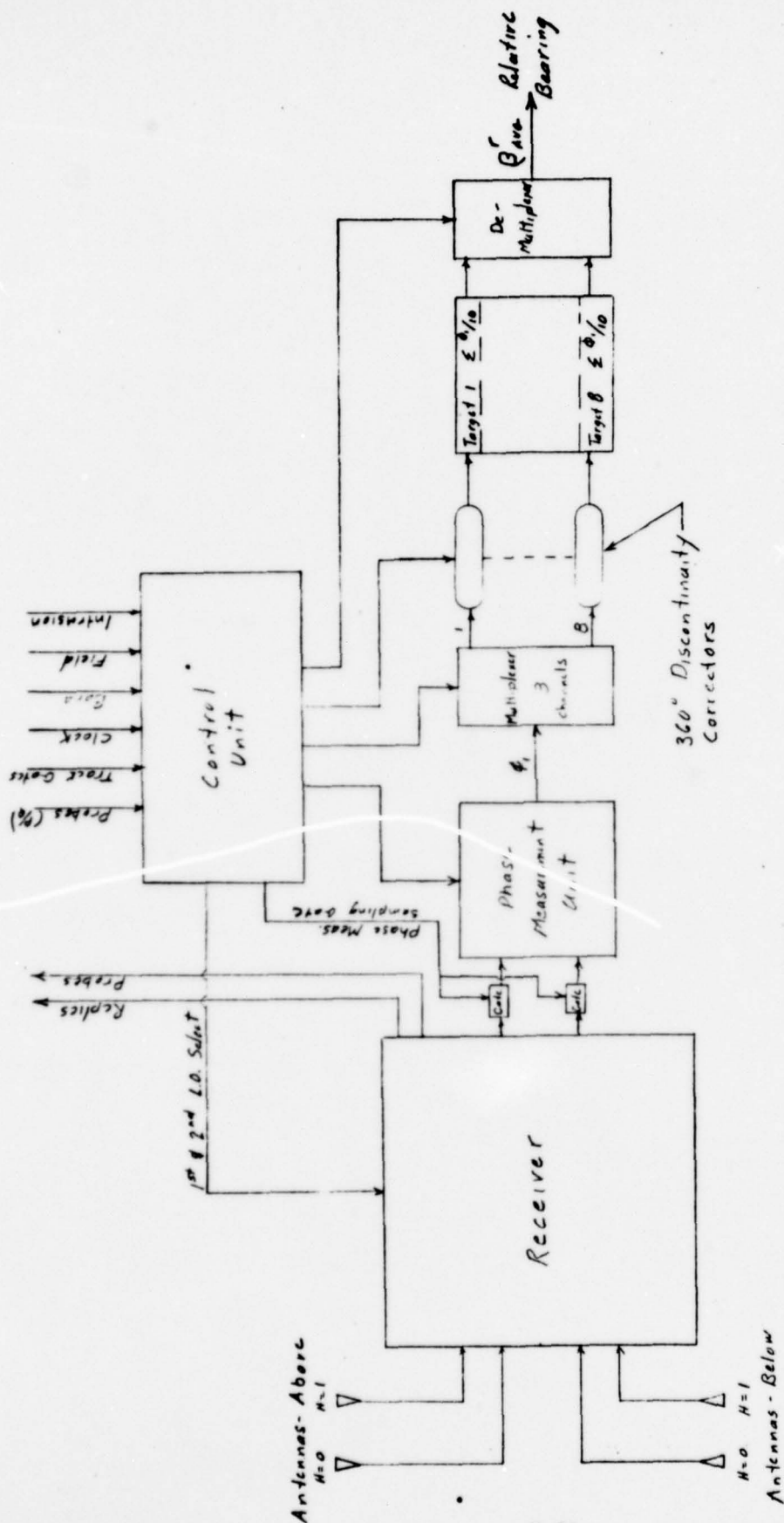


Figure 5-8.  
BLOCK DIAGRAM OF  
PWI BEARING MEASUREMENT SYSTEM

The receiver is the same as the configuration shown in Figure 5-3 and described in Section 5-2 with a few exceptions. Due to the lower PWI bearing accuracy requirements, the automatic phase adjustment servo would not be incorporated. To minimize fabrication costs, only the receiver preamplifier stages would be located at the antenna site. Also, the  $H = 4$  channel would not be provided. The receiver, under direction of the control unit, provides dual, gated signals to the phase measurement unit; replies for the correlator and tracker; and probes for the reply generation units of the PWI system. The latter functions are similar to those in VECAS, however, the tracker is much simplified as it provides only a range gate for fruit rejection, without a servoed range rate measuring capability.

The phase measurement unit (PMU) is similar to the PMU described in Section 5.3 and shown in Figure 5-7. However, the pulse width detector vernier would be eliminated as the increased resolution it provides is not required in the PWI system. Also, the width of the phase measurement sampling gate would be reduced from  $0.65 \mu s$  to  $0.5 \mu s$  to insure that a set of only two  $t$  pulses is always generated in each bearing signal measurement sample. This decreases system complexity by eliminating the need to count the number of  $t$  pulses in the sampling gate and simplifies the evaluation of the phase angle ( $\theta$ ). Thus, as the number of  $t$  pulses ( $W$ ) within a sampling gate will always be two, the phase angle ( $\theta$ ), can be found by:

$$\theta = .011 S_t \text{ radians}$$

where  $S_t$  is the total phase count. Therefore, only a scale factor is required to convert phase count to phase angle.

This digital PMU has measurement discontinuities ( $360^\circ$  to  $0^\circ$ ) at target bearing angles of  $360^\circ/0^\circ$ . These discontinuities can introduce bearing errors when measurements are averaged. The logic shown in Figure 5-9 would condition the measurement to circumvent

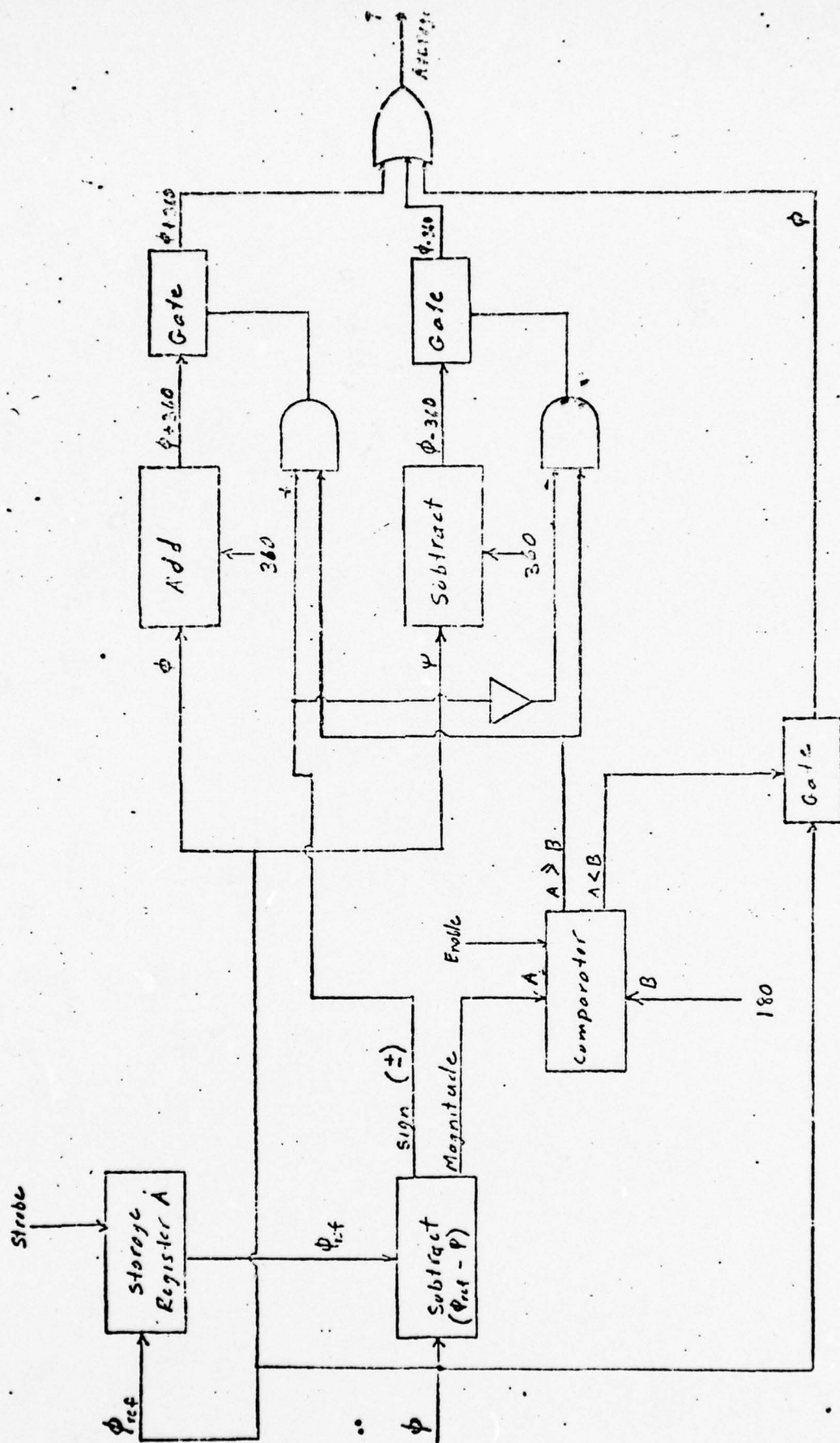


Figure 5-9. 360° Discontinuity Corrector

this discontinuity error. In operation, the first bearing reading ( $\theta_{\text{ref}}$ ) in a probe sequence is stored in Storage Register A. All subsequent measurements ( $\theta$ ) in the sequence are, in turn, subtracted from  $\theta_{\text{ref}}$ . If  $\theta_{\text{ref}} - \theta$  exceeds  $180^\circ$ , a discontinuity has been crossed. The sign ( $\pm$ ) of the difference is indicative of the direction of the crossing (i.e.,  $359^\circ \rightarrow 0^\circ$  or  $0^\circ \rightarrow 359^\circ$ ). In the logic shown in Figure 5-9, if the difference of  $\theta_{\text{ref}} - \theta$  exceeds  $180^\circ$  and the sign is negative,  $360^\circ$  is subtracted from  $\theta$  before this value is sent to the averaging accumulator. Similarly, if the difference exceeds  $180^\circ$  and the sign is positive,  $360^\circ$  is added to  $\theta$  before averaging. As shown,  $\theta$  would be gated directly to the averager when  $\theta_{\text{ref}} - \theta$  is less than  $180^\circ$  as, in this case, no discontinuity has been incurred.

Target bearing data will be obtained for up to eight targets during ten probes of the short track cycle used by the PWI. As shown in Figure 5-8, the phase angle output of the PMU is sorted into channels assigned to each of the eight targets by a one-line to 8-line multiplexer. The ten collated phase data samples for each target are conditioned to circumvent the discontinuity that occurs at  $360^\circ/0^\circ$  and averaged to obtain the relative bearing value,  $\beta^{\text{r}}_{\text{avg}}$ . The relative bearing of each intruder is extracted from these values by the demultiplexer and is sent to display panel registers to aid the pilot in the visual acquisition of threats. These bearing values are updated on each correlation cycle.



APPENDIX A  
WORK STATEMENT

**TASK 1 - ANALYSIS OF BEARING MEASUREMENT REQUIREMENTS**

The purpose of this task is to define the accuracy requirement for the measurement of bearing and bearing rate in airborne anti-collision systems. The interest in making these measurements stems from RCA's advocacy of a horizontal maneuvering capability for a full CAS system. However, these measurements can also be utilized for two other significant functions:

- a. Indicate to the pilot the approximate direction of the threat which will facilitate his visual acquisition of the target (PWI) and his execution of the maneuver decision (CAS).
- b. Eliminate alarms caused by the TAU criterion when the projected miss distance is sufficient. (The TAU criterion cannot distinguish between these and true threats and therefore often alarms unnecessarily.)

The requirements for bearing measurement accuracy for horizontal maneuvering are being defined in the Horizontal Maneuver Study presently being performed by SCI, Inc., and therefore will be utilized in this program. The requirements for Function (a) will be defined and based upon operational and human factor requirements. The accuracy requirements of Function (b) will be determined after an analysis of the expected false alarm rate is determined from the new dynamic FAA 1982 LAX Traffic Model.

Task 1 will consist of the following subtasks:

- 1.1 Analysis of the warning locus for the TAU criteria and the determination of the portions where a warning based solely on TAU is unnecessary.
- 1.2 Definition of a family of warning loci for various combinations of TAU and miss distance criteria.
- 1.3 Evaluation of the above loci in the dynamic FAA 1982 LAX Traffic Model to determine the number of unnecessary warnings each would cause. Select the optimal criterion.
- 1.4 Definition of the accuracy required in the measurement of bearing and bearing rate in the implementation of the optimal criterion.

#### TASK 2 - BEARING MEASUREMENT CONFIGURATION ANALYSIS

This task will provide comparative analysis of several possible approaches for the implementation of bearing and bearing rate measurement. It will consider 3, 4, and 5 element antennas and define their configuration and associated block diagrams for signal processing and data processing. The configurations will consider potential effects of loss of signals and multipath in order to minimize degradation of accuracy.

Task 2 will consist of the following subtasks:

- 2.1 Definition of antenna configurations.
- 2.2 Definition of signal processing approach for each configuration.
- 2.3 Definition of data processing approach for each configuration.
- 2.4 Determination of expected accuracy in the measurement of bearing and bearing rate for each configuration.

### TASK 3 - HARDWARE CHARACTERISTICS FOR BEARING MEASUREMENT

Hardware characteristics have a controlling influence on the choice of system used to obtain bearing. This task will determine several specific performance characteristics and breadboard the antenna configuration chosen.

Task 3 will consist of the following subtasks:

- 3.1 Determine hardware characteristics of possible antenna configurations for use with the SECANT system. A laboratory model of one of these configurations will be breadboarded and bench tested.
- 3.2 Determine characteristics and performance specifications of the receiver required with the above antenna.
- 3.3 Determine instrumentation techniques for processing the bearing signals.
- 3.4 Determine the circuit requirements for handling the bearing data.

### TASK 4 - FINAL REPORT

A final report will be prepared including the results of each study task performed on this program.

## APPENDIX B

### PROBABILITY ANALYSIS

The purpose of this appendix is to derive an expression for single conflict missed alarm probability, as function of critical miss and of computed miss error sigma. This is used to provide a quantitative (parameterized) assessment, presented in Section 2.3.2.

If both range and swept bearing errors are assumed to have Gaussian distributions, then the error in computed miss must also be Gaussian as it is a linear function of those errors.

In Figure B-1, let  $M$  denote the computed value of miss, subscript  $t$  denote true value, and subscript  $T$  denote threshold value. An alarm is indicated if  $-M_T < \hat{M} < M_T$ . The probability of this occurrence is:

$$\begin{aligned}
 P_M &= P(-M_T < \hat{M} < M_T) = P(-M_T - M_t < \hat{M} - M_t < M_T - M_t) \\
 &= \frac{1}{\sqrt{2\pi} \sigma_M} \int_{-(M_T + M_t)}^{(M_T - M_t)} e^{-(x - \bar{\delta}_M)^2 / 2\sigma_M^2} dx \\
 &= \frac{1}{\sqrt{2\pi}} \int_{-(M_T + M_t + \bar{\delta}_n)/\sigma_M}^{(M_T - M_t - \bar{\delta}_M)/\sigma_M} e^{-\zeta^2/2} d\zeta
 \end{aligned}$$



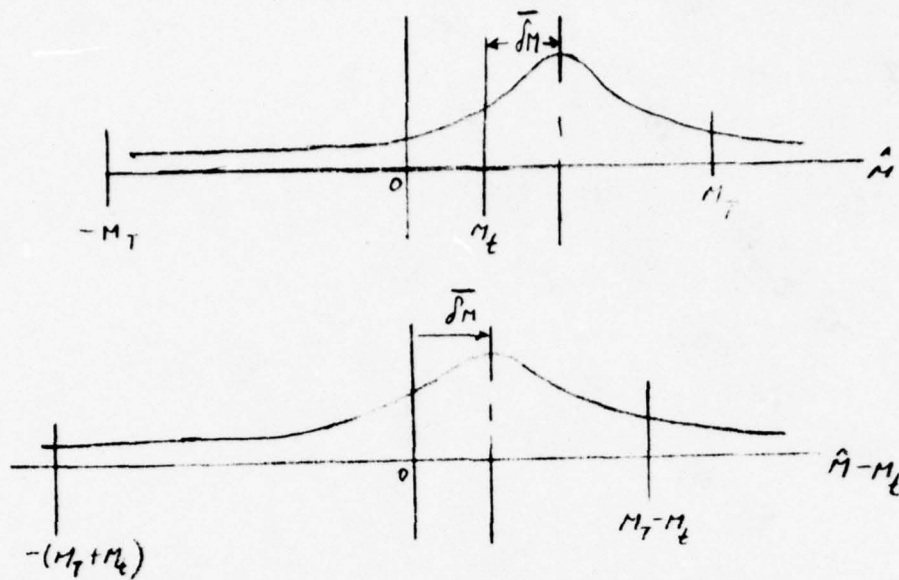


Fig. B-1

Gaussian Distribution of Error

In Computed Miss

$$= \frac{1}{\sqrt{2\pi}} \int_{-Z_1}^{Z_2} e^{-\zeta^2/2} d\zeta = \frac{1}{\sqrt{2\pi}} \left[ \int_0^{Z_1} e^{-\zeta^2/2} d\zeta + \int_{Z_0}^{Z_2} e^{-\zeta^2/2} d\zeta \right]$$

where

$$Z_1 = \frac{1}{\sigma_M} [M_T + M_t + \bar{\delta}_M]$$

$$Z_2 = \frac{1}{\sigma_M} [M_T - M_t - \delta_M]$$

Let

$$\nu^2 = \zeta^2/2, d\zeta = \sqrt{2} d\nu$$

Then

$$P_M = 1/2 \left[ \frac{2}{\sqrt{\pi}} \int_0^{Z_1/\sqrt{2}} e^{-\nu^2} d\nu + \frac{2}{\sqrt{\pi}} \int_0^{Z_2/\sqrt{2}} e^{-\nu^2} d\nu \right]$$

$$= 1/2 [\operatorname{erf} X_1 + \operatorname{erf} X_2]$$

where  $X_1 = Z_1/\sqrt{2}$ ,  $X_2 = Z_2/\sqrt{2}$  and  $\operatorname{erf} X$  stands for error function. The single conflict missed alarm probability is simply

$$P_{\text{mas}} = 1 - P_M$$

Note that  $\operatorname{erf} (-X) = -\operatorname{erf} (X)$ . The computer program for evaluating the error function utilizes the convergent series expansion:

$$\operatorname{erf} X = \frac{2}{\sqrt{\pi}} \left( X - \frac{X^3}{3.1!} + \frac{X^5}{5.2!} - \frac{X^7}{7.3!} + \dots \right)$$

# APPENDIX C

## ERROR ANALYSIS

It is the purpose of this appendix to present the equations which show the relationships of computed miss to errors in range and bearing measurements. A quantitative assessment is made of miss error,  $\sigma(\delta M)$ , as a function of swept bearing error sigma,  $\sigma(\Delta\beta)$ . The results are then used to relate missed alarm probability and miss threshold to  $\sigma(\Delta\beta)$ , as indicated in Figures 2-4 thru 2-7 of Section 2.3.2.

The conflict triangle S-B<sub>1</sub>-B<sub>2</sub> is depicted in Figure C-1.  $\bar{V}_r$  is taken as a constant vector, so that the displacement B<sub>1</sub>B<sub>2</sub> is just  $V_r\Delta t$ . The sensitivities of computed miss, M, to measured quantities, will be obtained. Attitude perturbations, or attitude error effects, are not considered. The analysis is confined to two-dimensional geometry (i.e., to the horizontal plane). The measured quantities are the ranges and bearing angles at times  $t_1$  and  $t_2$ .

$V_r\Delta t$  is obtainable from

$$V_r \Delta t = \sqrt{R_1^2 + R_2^2 - 2 R_1 R_2 \cos \Delta\beta} \quad (C-1)$$

$\alpha_2$  is obtainable from

$$\sin \alpha_2 = R_1 \sin \Delta\beta / V_r \Delta t \quad (C-2)$$

Then M may be computed from

$$M = R_2 \sin \alpha_2 \quad (C-3)$$

$$\begin{aligned}
 & \left. \begin{aligned} R_2 \sin \alpha_2 &= R_1 \sin \alpha_1 \\ R_2 \cos \alpha_2 + V_1 t &= R_1 \cos \alpha_1 \end{aligned} \right\} \\
 & \left. \begin{aligned} V_1 t \sin \alpha_1 &= R_2 \sin \alpha_2 \\ R_2 \cos \alpha_2 + V_1 t \cos \alpha_1 &= R_1 \end{aligned} \right\} \\
 & \left. \begin{aligned} R_1 \sin \alpha_2 &= V_1 t \sin \alpha_1 \\ R_1 \cos \alpha_2 &= R_2 + V_1 t \cos \alpha_1 \end{aligned} \right\} \\
 & \alpha_2 = \alpha_1 + \alpha\beta
 \end{aligned}$$

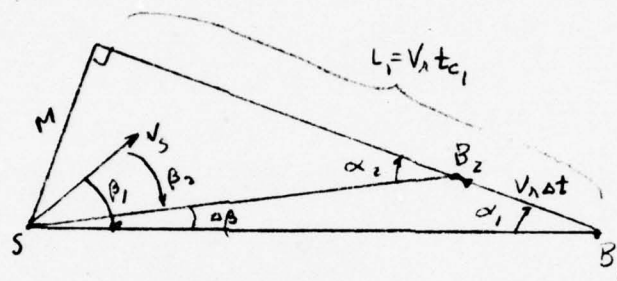


Fig. C-1

Conflict Triangle

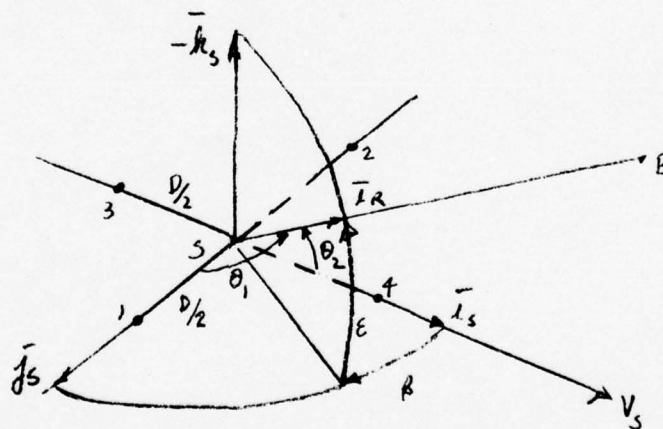


Fig. C-4

Crossed Axis Interferometer



Simultaneous differentiation of these equations leads to expressions for the error sensitivities:

$$\frac{\partial M}{\partial R_1} = (1 - \frac{t_{c1}}{\Delta t}) \sin \alpha_1 \quad (C-4)$$

$$\frac{\partial M}{\partial R_2} = (\frac{t_{c1}}{\Delta t}) \frac{R_1 \sin \Delta \beta}{V_r \Delta t} \quad (C-5)$$

$$\frac{\partial M}{\partial \beta} = V_r t_{c1} (\frac{t_{c1}}{\Delta t} - 1) \quad (C-6)$$

These expressions can be shown to be functions only of  $M$ ,  $\bar{V}_r$ ,  $\Delta t$ , and  $t_{c1}$ . To demonstrate, from the relations given in Figure C-1.

$$\tan \alpha_1 = M / V_r t_{c1} = f(M, V_r, t_{c1}) \quad (C-7)$$

$$\tan \Delta \beta = V_r \Delta t \sin \alpha_1 / (R_1 - V_r \Delta t \cos \alpha_1) = f(M, V_r, t_{c1}, \Delta t, R_1) \quad (C-8)$$

$$R_1 = V_r t_{c1} / \cos \alpha_1 = f(M, V_r, t_{c1}) \quad (C-9)$$

If  $\bar{\delta R}_1 = \bar{\delta R}_2 = \bar{\delta R}$  is the range bias error, and  $\bar{\delta(\Delta \beta)}$  is the bias error in swept bearing, then the bias error in predicted miss is

$$\bar{\delta M} = [\frac{\partial M}{\partial R_1} + \frac{\partial M}{\partial R_2}] \bar{\delta R} + \frac{\partial M}{\partial \Delta \beta} \bar{\delta(\Delta \beta)} \quad (C-10)$$

Taking  $\sigma R_1 = \sigma R_2 = \sigma R$  and assuming random range errors to be uncorrelated (based upon autocorrelation time being much smaller than the time between range samples), then

$$\sigma^2(\delta M) = [(\frac{\partial M}{\partial R_1})^2 + (\frac{\partial M}{\partial R_2})^2] \sigma R^2 + (\frac{\partial M}{\partial \Delta \beta})^2 \sigma^2 \Delta \beta \quad (C-11)$$

The partials are given by equations C-4, C-5, and C-6.

Typical values for range errors are given as

$$\sigma_R = 15 \text{ feet}$$

$$\overline{\delta R} = \underline{+100} \text{ feet}$$

Substituting numerical values,

$$\overline{\delta M} = A_M + B_M k_\beta \sigma_{\Delta\beta}^\circ$$

$$\sigma(\delta M) = [C_M + D_M \sigma_{\Delta\beta}^2]^{1/2}$$

wherein  $A_M$  and  $C_M$  are dependent on the values of range error statistical parameters, and  $k_\beta$  is the ratio of swept bearing bias error to sigma value.

Statistical errors were evaluated for a critical miss distance  $M_C = 1000$  feet, and for a time-to-go  $t_C$  corresponding to initial penetration of either the Tau 2 or Tau 1 cardioid. The following equations can be written:

$$\text{Tau 2: } R_C (\text{ft}) = 10936.8 + 40 V_R (\text{knots}) \times \frac{6076}{3600} \cos \alpha_C$$

$$\text{Tau 1: } R_C (\text{ft}) = 1519 + 25 V_R (\text{knots}) \times \frac{6076}{3600} \cos \alpha_C$$

For specified  $V_R$ , selecting different values of  $\alpha_C$ , one can solve the preceding  $R_C$  equations, as well as equations C-7 and C-9, sequentially for  $R_C$ ,  $t_C$ ,  $M_C$ ; interpolation then provides values of  $\alpha_C$ ,  $R_C$ ,  $t_C$  at the specified  $M_C = 1000$  feet. Results are shown in Table C-1. Then the coefficients  $A_M$ ,  $B_M$ ,  $C_M$ ,  $D_M$  were evaluated for  $\sigma_R = 15$  feet,

Table C-1

## Kinematic &amp; Error Sensitivity Parameters

at  $\tau$  Cardioid Penetration

| $V_R$<br>(knots) | $t_c$<br>(sec's) | $\alpha_c$<br>(deg's) | $R_c$<br>(feet) | $\Delta\beta$<br>(deg's) | $A_n$<br>(feet) | $E_M$<br>(ft/deg) | $C_M$<br>(ft. <sup>2</sup> ) | $D_M$<br>(ft/deg) <sup>2</sup> |
|------------------|------------------|-----------------------|-----------------|--------------------------|-----------------|-------------------|------------------------------|--------------------------------|
| $\tau_1$<br>↓    | 100              | 33.08                 | 5673            | 1.760                    | 19.95           | 547               | 725.73                       | 299,559                        |
|                  | 315              | 27.74                 | 14783           | .849                     | 14.96           | 1171              | 68.34                        | 1,370,702                      |
|                  | 500              | 26.75                 | 22599           | .582                     | 9.85            | 1714              | 27.39                        | 2,938,094                      |
| $\tau_2$<br>↓    | 100              | 104.6                 | 17678           | .162                     | 11.316          | 6134              | 633.96                       | 37,623,616                     |
|                  | 315              | 60.5                  | 32194           | .160                     | 6.493           | 6236              | 64.56                        | 38,890,190                     |
|                  | 500              | 52.9                  | 44684           | .134                     | 4.711           | 7474              | 25.75                        | 55,862,171                     |

$\overline{\delta R} = 100$  feet, and  $\Delta t = 5$  seconds. These results are also shown in Table C-1.

Equation C-8 was solved for  $\Delta\beta$ . It is seen that  $\Delta\beta$  is quite small under the stipulated condition (penetration of cardioid for  $M_c = 1000$  feet, and  $\Delta t = 5$  seconds).

Figure C-2 shows  $\sigma(\delta M)$  as well as  $\overline{\delta M}$ , for several values of  $k_\beta$ , for  $V_r = 315$  knots and  $\tau_1$  cardioid.  $\sigma(\delta M)$  is essentially linear with respect to  $\sigma(\Delta\beta)$ , for given  $V_r$  and  $t_c$ . Figure C-3 shows the  $\sigma(\delta M)$  variation as  $V_r$  is increased, or for a change in  $\tau$  cardioid penetration. In general, for given  $\sigma(\Delta\beta)$ , the value of  $\sigma(\delta M)$  increases with increased  $V_r t_c$ ; that is, at longer range. The variation of  $\sigma(\delta M)$ ,  $\overline{\delta M}$  with miss, say between 0 and 1000 feet, for fixed  $k_\beta$  and  $V_r$ , is not significant, and is not shown. Evidently, miss errors will increase substantially if  $\Delta t$  is decreased, as can be seen from the expressions for the error sensitivities.

If the antenna elements used to measure bearing are arranged in the form of a crossed interferometer, with orthogonal legs (Figure C-4), then the bearing angle  $\beta$  in the wing-plane (and the cross-plane bearing angle  $\epsilon$ ) can be obtained from phase difference measurements. Thus

$$\cos \theta_1 = \cos \epsilon \sin \beta = \phi_{12} / \left( \frac{2\pi}{\lambda} \right) D \quad (C-12)$$

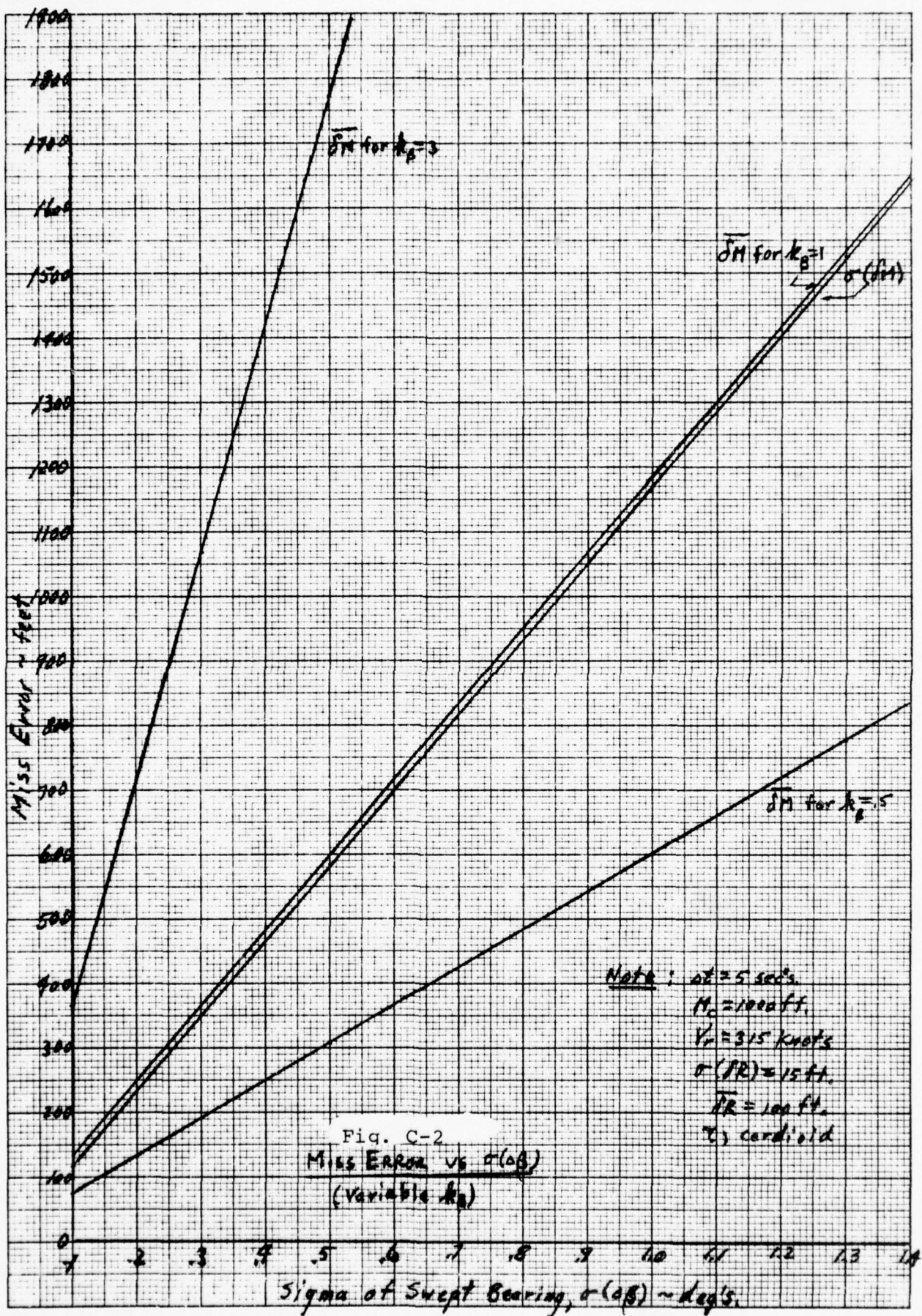
$$\cos \theta_2 = \cos \epsilon \cos \beta = \phi_{34} / \left( \frac{2\pi}{\lambda} \right) D \quad (C-13)$$

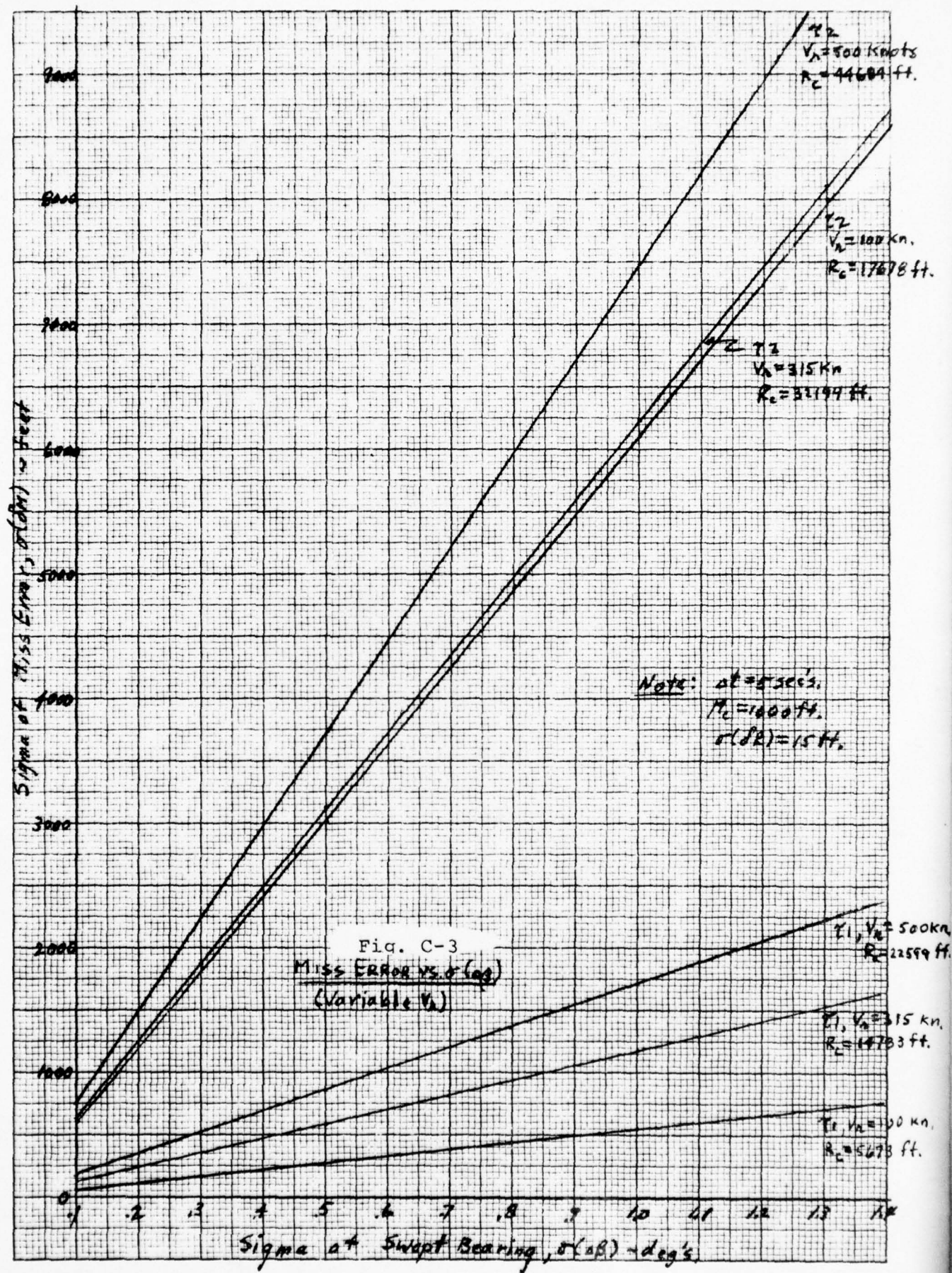
where  $\lambda$  is the wave length of the incoming signal, and  $D$  is antenna spacing. Then

$$\tan \beta = \frac{\cos \theta_1}{\cos \theta_2} = \frac{\phi_{12}}{\phi_{34}} \quad (C-14)$$

$$\sigma(\beta) = \sigma(\phi_{12}) / \left( \frac{2\pi}{\lambda} \right) D \cos \epsilon \quad (C-15)$$









If  $\beta_1$  and  $\beta_2$  are assumed independent, then

$$\sigma(\Delta\beta) = \sqrt{2} \sigma(\beta)$$

Thus, a specification on  $\sigma(\Delta\beta)$  provides a specification on the precision requirement of the phase difference measurements.

It should be noted that for the ideal ring antenna array, the instantaneous  $\sigma(\beta)$  is directly proportional to the sigma of the measured phase difference, and is independent of elevation angle.

## APPENDIX D

### DETERMINATION OF THE MAXIMUM MISS DISTANCE ( $M_{MAX}$ ) OF THE TAU CRITERION

It is the purpose of this appendix to provide equations for the determination of  $M_{max}$  on the  $\tau$  cardioid.  $M_{max}$  is used in numerically defining the false alarm probabilities presented in Section 2.3.2.

The range alarm threshold is given by

$$R_T = R_0 + T (-\dot{R}) \quad (D-1)$$

where  $\dot{R} = V_r \cos \alpha$ . With  $R$  in seconds,  $\dot{R}$  in nautical miles/seconds,  $R_0$  in nautical miles, parameter values are

$$\text{for } \tau_2 \text{ alert: } R_0 = 1.8, T = 40$$

$$\text{for } \tau_1 \text{ alarm: } R_0 = .25, T = 25$$

(An alarm is given if measured range is less than  $R_T$ , using present  $\dot{R}$ .) With an aircraft stationed at the origin in Figure D-1, a coordinate system L-M can be defined such that the ordinate L axis is parallel to  $\overline{V_r}$ , and the abscissa M axis is perpendicular to  $\overline{V_r}$ . Then

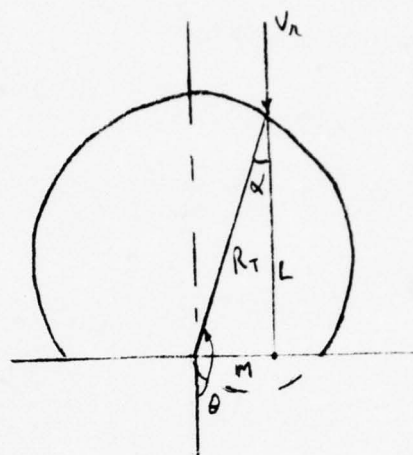
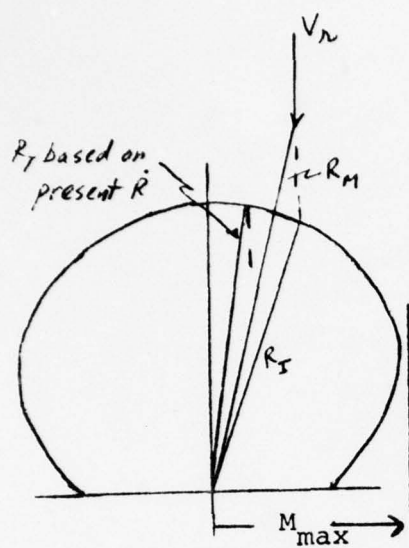
$$M = R_T \sin \alpha \quad (D-2)$$

$$L = R_T \cos \alpha \quad (D-3)$$

Eliminating  $\alpha$  between equations D-2 and D-3

$$M^2 + L^2 = R_T^2 \quad (D-4)$$





$$L = V_n t_c$$

$$= \text{Distance to go}$$

Fig. D-1

Tau Cardioid

Eliminating  $\alpha$  between equations D-1 and D-2

$$R_T = R_0 + V_r TL / R_T \quad (D-5)$$

Eliminating  $R_T$  between equations D-4 and D-5

$$(M^2 + L^2) - R_0 \sqrt{M^2 + L^2} - V_r TL = 0 \quad (D-6)$$

(The locus of  $R_T$ , represented in cartesian coordinates by equations D-6, can be shown to be a cardioid. Thus rewriting equation D-1,

$$\begin{aligned} R_T &= R_0 \left[ 1 + \frac{TV_r}{R_0} \cos \alpha \right] \\ &= R_0 \left[ 1 - \frac{TV_r}{R_0} \cos \theta \right] \end{aligned}$$

which is the equation of a cardioid in polar coordinates.)

To find the maximum width of the cardioid, we differentiate equation D-6 with respect to  $L$ , to find  $dM/dL$  and set this derivative equal to zero. The condition is obtained

$$\sqrt{M^2 + L^2} = R_0 L / 2 \left( L - \frac{T}{2} V_r \right) \quad (D-7)$$

Making use of equations D-3, D-4 to eliminate  $M$  and  $L$ , and equation D-1 to eliminate  $R_T$ , an expression is obtained in  $\alpha$  only:

$$2 T V_r \cos^2 \alpha + R_0 \cos \alpha - T V_r = 0 \quad (D-8)$$

From this, the value of  $\alpha$  for  $M_{\max}$  is given by

$$\cos \alpha |_{M_{\max}} = (-R_0 + \sqrt{R_0^2 + 8 V_r^2 T^2}) / 4 V_r T \quad (D-9)$$

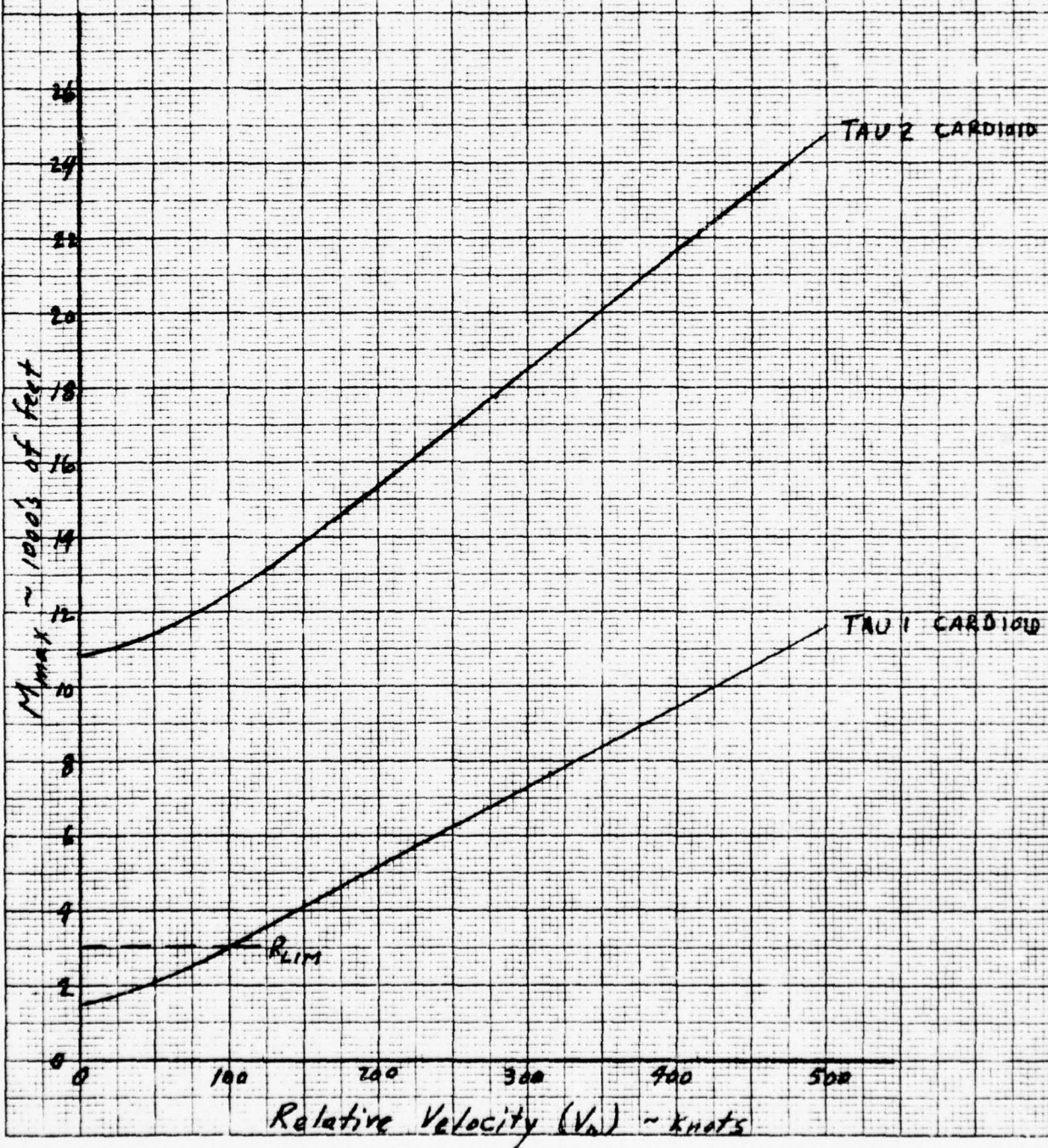
with  $V_r$  in nautical miles/seconds. The value of  $R$ , at which  $M_{\max}$  occurs, is

$$R_T|_{M_{\max}} = \frac{3R_0}{4} + \frac{\sqrt{R_0^2 + 8 V_r^2 T^2}}{4} \quad (D-10)$$

$M_{\max}$  is most conveniently found from equation D-2, using equation D-9 to find  $\alpha$ , and either equation D-5 or D-10 to find  $R_T$ .  $M_{\max}$  is displayed in Figure D-2. Note that the condition  $\alpha|_{M_{\max}} = 90^\circ$  occurs as a limit as  $V_r$  approaches zero.

Fig. D-2

MAX. MISS ON  
RANGE ALARM CARDIOW





# APPENDIX E SIMULATION EQUATIONS

The purpose of this appendix is to derive kinematic quantities (horizontal miss, relative range) and to quantitatively assess these for a sample distribution of aircraft in the 1982 LAX traffic model. Frequency histograms were developed and utilized to obtain potential false and missed alarm probabilities in a traffic environment as discussed in Section 2.3.3.

The input information supplied for each aircraft in the traffic model are position data, relative to the LAX center, and vector velocity. These are given as ground range ( $R_G$ ) from center, azimuth or bearing ( $A$ ) measured from north, altitude ( $h$ ) above sea-level; speed ( $V$ ), heading ( $H$ ), path angle  $\gamma$ . Figure E-1 depicts these quantities. (Bank angle is also supplied as an input, but is not used in this simulation. Bank angle,  $B$ , could be used to obtain aircraft turn rate, since  $\omega = (g \tan B)/V$ .) The objective of the simulation is to obtain values of relative range and horizontal miss for the three-dimensional "picture", i.e., with non-coaltitude aircraft and with some of the aircraft in diving/climbing orientations.

From Figure E-1,

$$\left. \begin{aligned} X_1 &= (R_G)_1 \sin A_1 \\ Y_1 &= (R_G)_1 \cos A_1 \\ Z_1 &= h_1 \end{aligned} \right\} \quad (E-1)$$

With the  $R_G$  in nautical miles and  $h_1$  in feet,

$$\left. \begin{aligned} X_1 &= (X_1 - X_S) \times 6076 \\ Y_1 &= (Y_1 - Y_S) \times 6076 \\ Z_1 &= (Z_1 - Z_S) = h_1 - h_S \end{aligned} \right\} \quad (E-2)$$

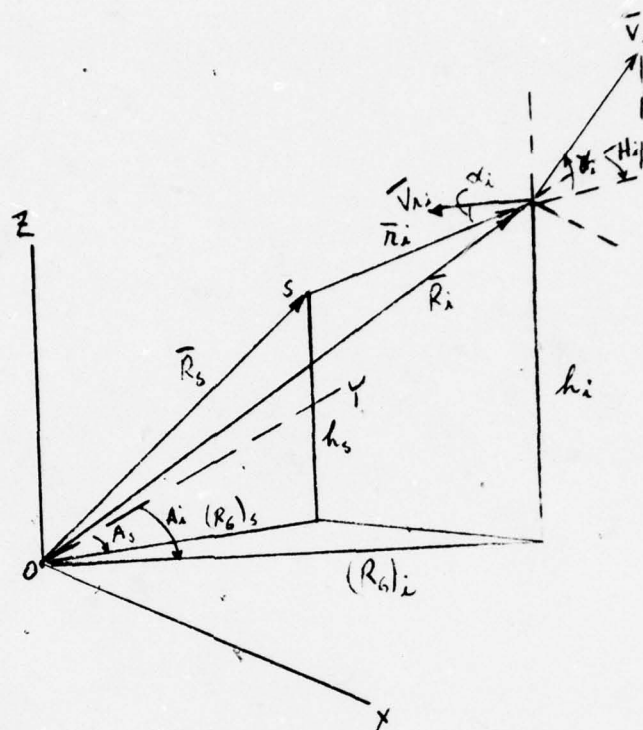


Fig. E-1

Relative Range Determination

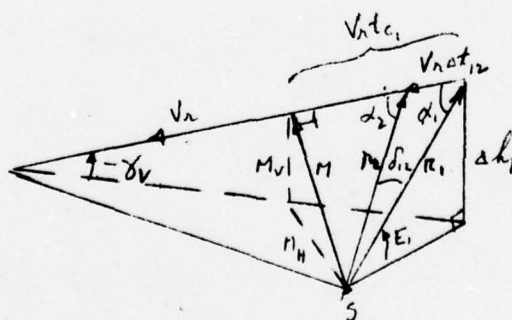


Fig. E-2

Miss Component Determination

and the slant (relative) range between aircraft (S) and  $i^{\text{th}}$  aircraft is simply

$$r_i = \sqrt{X_i^2 + Y_i^2 + Z_i^2} \quad (\text{E-3})$$

Again, from the diagram,

$$\left. \begin{aligned} \dot{X}_i &= V_i \sin H_i \cos \gamma_i \\ \dot{Y}_i &= V_i \cos H_i \cos \gamma_i \\ \dot{Z}_i &= V_i \sin \gamma_i \end{aligned} \right\} \quad (\text{E-4})$$

With  $V_i$  in knots,

$$\left. \begin{aligned} \dot{X}_i &= (\dot{X}_i - \dot{X}_S) \times \frac{6076}{3600} \\ \dot{Y}_i &= (\dot{Y}_i - \dot{Y}_S) \times \frac{6076}{3600} \\ \dot{Z}_i &= (\dot{Z}_i - \dot{Z}_S) \times \frac{6076}{3600} \end{aligned} \right\} \quad (\text{E-5})$$

and the magnitude of the velocity of the  $i^{\text{th}}$  aircraft relative to the S aircraft is

$$V_{ri} = \sqrt{\dot{X}_i^2 + \dot{Y}_i^2 + \dot{Z}_i^2} \quad (\text{E-6})$$

in feet/second. Range rate is given by

$$\dot{r}_i = \bar{V}_{ri} \cdot \bar{r}_i / r_i = (X_i \dot{X}_i + Y_i \dot{Y}_i + Z_i \dot{Z}_i) / r_i \quad (\text{E-7})$$

whence

$$\tau_i = r_i / -\dot{r}_i \quad (\text{E-8})$$

The aspect angle between  $-\bar{r}_i$  and  $\bar{V}_{ri}$  is simply

$$\alpha_i = \cos^{-1} (r_i/V_{ri}); 0 \leq \alpha_i < 90^\circ \quad (E-9)$$

The path angle of  $\bar{V}_{ri}$  (see Figure E-2) is

$$\gamma_{V_i} = \sin^{-1} (\dot{Z}_i/V_{ri}); 0 \leq |\gamma_{V_i}| < 90^\circ \quad (E-10)$$

The elevation angle of the line-of-sight is given by

$$E_i = \sin^{-1} (Z_i/r_i); 0 \leq |E_i| < 90^\circ \quad (E-11)$$

By definition, the total miss (distance at closest approach) is

$$M = r_i \sin \alpha_i$$

where  $\alpha_i$  is given by equation E-9. From Figure E-2, it is readily seen that the evaluation of  $\bar{M}$  is

$$E_{M_i} = \sin^{-1} \left[ \frac{r_i}{M_i} (\sin E_i + \cos \alpha_i \sin \gamma_{V_i}) \right]; 0 \leq |E_{M_i}| < 90^\circ \quad (E-12)$$

The horizontal and vertical components of miss are then simply

$$M_{H_i} = M_i \cos E_{M_i} \quad (E-13)$$

$$M_{V_i} = M_i \sin E_{M_i} \quad (E-14)$$

At the time of the "snapshot", the time to closest approach is

$$t_{c_i} = r_i \cos \alpha_i / V_{ri} \quad (E-15)$$



The Tau 2 range alarm is given (in feet) by

$$r_T = 1.8 \times 6076 - 40 \dot{r} = 10936.8 - 40 \dot{r} \quad (E-16)$$

and may be used in assessing an alarm condition by comparison with present actual relative range.

In performing the simulation, various rejection constraints were applied so as to conform to a realistic CAS system approach:

- 1) Reject all intruding aircraft for which the altitude difference is greater than 2500 feet in magnitude.
- 2) Of the remaining aircraft, reject those for which the range is greater than a maximum detection value of 50,000 feet.
- 3) Of the remaining aircraft, reject all those having a positive range rate, since these do not constitute threats.

#### Traffic Model Simulation and Cumulative Frequency Diagrams

A static simulation of kinematic parameters was conducted for "snapshot #3" of the LAX 1982 aircraft distribution model, with each of two aircraft selected as the "protected" aircraft. One of these was taken in the southwest quadrant at the center of the densest region; the other aircraft was taken in the northwest quadrant, at the center of the Van Nuys concentration. Parameters of these aircraft are listed below:

| <u>A/C No.</u> | <u>Ground Range<br/>(n. miles)</u> | <u>Bearing<br/>(deg's)</u> | <u>Altitude<br/>(feet)</u> | <u>Speed<br/>(knots)</u> | <u>Heading<br/>(deg's)</u> | <u>Pitch<br/>(deg's)</u> |
|----------------|------------------------------------|----------------------------|----------------------------|--------------------------|----------------------------|--------------------------|
| 49             | 20.1                               | 137.04                     | 2888                       | 104.9                    | 314.3                      | 4                        |
| 710            | 15.9                               | 333.77                     | 3997                       | 92.4                     | 125.5                      | 0                        |

After application of the altitude difference constraint ( $\pm 2500$  ft.), detection range constraint (50,000 ft.) and the closing range rate constraint, a total of 41 potential threats existed for A/C #49, and a total of 23 potential threats existed for A/C #710.

According to the ANTC-117 threat logic, a Tau 2 alarm would be given if present (slant) range is less than the alarm range:

$$R_T \text{ (feet)} = 10936.8 - 40 R$$

This value is shown for AC #710, in the accompanying printout (Table E-1). AC #328 and #703 have slant ranges (S/R) less than  $R_{TO}$  but the altitude differences ( $\Delta h = M_V$ ) relative to AC #710 are more than 600 feet; hence these are not present threats. Of more consequence is a comparison of  $M_H$  with  $M_{max}$ , since this indicates eventual penetration of the Tau 2 cardioid. Seven aircraft fall in this category, but of these, only two have altitude differences less than 600 feet. Furthermore, if a horizontal miss threshold of, say 3,000 feet is applied, only one (AC #514) remains as an alarm for the combined Tau/Miss hazard criteria system. A similar analysis was not conducted for AC #49 as protected aircraft, because of the complexity attendant to a non-zero pitch angle.

Figures E-3 and E-4 show frequency histograms in relative range for the two aircraft. Figures E-5 and E-6 are corresponding histograms in horizontal miss. Averaging the separate cumulative frequency functions for the two aircraft gives the results shown in Figures E-3 and E-5. Almost triangular functions lends credence to an assumption of a uniform spatial distribution of aircraft.

PROG. NAME: ROOT

DATE: AUG. 1, 1973

| A/C | S/R   | ROST   | VR    | ALFA | BAMMA | E    | EM    | TAU   | M      | MH     | W      | TC     | R <sub>TO</sub> | M <sub>max</sub> |
|-----|-------|--------|-------|------|-------|------|-------|-------|--------|--------|--------|--------|-----------------|------------------|
| 101 | 44394 | -25.5  | 93.4  | 74.2 | 0.0   | 0.0  | -0.5  | -0.7  | 1741.0 | 42718. | 42718. | -490.8 | 129.3           | 11500            |
| 111 | 27009 | -266.2 | 308.1 | 20.7 | 0.0   | 0.0  | 2.1   | 6.0   | 93.7   | 9501.  | 9501.  | 997.   | 82.0            | x14800           |
| 194 | 40903 | -286.6 | 317.3 | 25.3 | 0.0   | 0.0  | -0.7  | -1.7  | 142.6  | 17458. | 17458. | -506.8 | 116.6           | 22413            |
| 243 | 31166 | -269.1 | 321.0 | 33.3 | 2.2   | 2.2  | 4.5   | 11.6  | 115.8  | 17104. | 17104. | 3450.  | 80.9            | 21701            |
| 328 | 13971 | -251.8 | 353.3 | 46.4 | 0.0   | 0.0  | 10.3  | 13.7  | 55.5   | 10532. | 10532. | 2496.  | 24.0            | x16200           |
| 358 | 21452 | -234.9 | 306.9 | 40.1 | 0.0   | 0.0  | -4.0  | -6.3  | 91.4   | 13812. | 13812. | -1504. | 53.5            | 20833            |
| 400 | 27423 | -111.5 | 130.4 | 31.0 | -3.0  | -3.0 | -13.0 | 245.2 | 14135. | 13745. | 13745. | -317.1 | 130.3           | x14800           |
| 481 | 41332 | -305.9 | 305.0 | 1.6  | 0.0   | 0.0  | -1.4  | -61.0 | 135.2  | 11138. | 11138. | -1003. | 138.1           | 11900            |
| 502 | 14935 | -118.3 | 287.7 | 24.6 | 0.0   | 0.0  | -0.5  | -0.3  | 379.7  | 36859. | 36859. | -424.8 | 127.2           | 23173            |
| 514 | 35586 | -386.9 | 387.6 | 3.5  | 0.0   | 0.0  | 0.8   | 13.4  | 92.0   | 2197.  | 2197.  | 508.2  | 191.6           | 16677            |
| 531 | 24849 | -97.4  | 349.3 | 73.8 | 4.1   | 4.1  | 3.2   | 4.5   | 254.9  | 23859. | 23859. | 1877.  | 19.9            | 26413            |
| 552 | 17430 | -21.1  | 377.3 | 46.1 | 2.3   | 2.3  | 3.3   | 3.3   | 857.1  | 17858. | 17858. | 1080.  | 4.0             | 14841            |
| 564 | 36723 | -77.8  | 133.1 | 24.2 | -4.9  | -4.9 | -1.1  | -4.9  | 472.0  | 29796. | 29796. | -530.  | 151.3           | 11781            |
| 584 | 24538 | -115.6 | 129.0 | 27.0 | -5.0  | -5.0 | -4.4  | -13.7 | 212.3  | 11207. | 11207. | -3787. | 158.0           | 14800            |
| 594 | 21492 | -55.9  | 120.4 | 63.8 | 5.0   | 5.0  | -6.7  | -4.7  | 384.5  | 19213. | 19213. | -1563. | 75.2            | 14049            |
| 599 | 40151 | -104.0 | 135.3 | 39.8 | -4.3  | -4.3 | -0.9  | -7.2  | 366.0  | 25677. | 25677. | -3206. | 228.2           | 15561            |
| 605 | 25282 | -67.7  | 108.1 | 50.4 | 0.0   | 0.0  | 3.3   | 4.2   | 388.2  | 20241. | 20241. | 1499.  | 158.0           | 13173            |
| 703 | 24082 | -392.8 | 356.0 | 9.3  | 0.0   | 0.0  | 4.4   | 28.5  | 1058.7 | 42074. | 42074. | 2029.  | 51.0            | 10993            |
| 724 | 18648 | -17.0  | 86.6  | 78.7 | -6.3  | -6.3 | -1.7  | -3.0  | 1058.4 | 18286. | 18286. | -954.  | 42.2            | 13645            |
| 745 | 37861 | -95.6  | 130.4 | 42.9 | -3.0  | -3.0 | -1.9  | -6.0  | 396.1  | 25762. | 25762. | -2715. | 212.7           | x26569           |
| 760 | 25428 | -193.2 | 230.4 | 50.6 | 0.0   | 0.0  | -2.8  | -3.7  | 136.8  | 20423. | 20423. | -1303. | 55.1            | 11617            |
| 773 | 37037 | -277.9 | 320.5 | 29.9 | 2.2   | 2.2  | 1.3   | 6.5   | 133.3  | 18460. | 18460. | 2134.  | 100.2           | 14761            |
| 774 | 28953 | -378.3 | 468.0 | 36.2 | 0.0   | 0.0  | 0.0   | 0.0   | 76.5   | 17109. | 17109. | 61.8   | 49.8            | 18665            |
|     |       |        |       |      |       |      |       |       |        |        |        |        |                 | 22053            |
|     |       |        |       |      |       |      |       |       |        |        |        |        |                 | 26069            |
|     |       |        |       |      |       |      |       |       |        |        |        |        |                 | X17750           |

Note: R<sub>TO</sub> = Range Alarm at t<sub>0</sub>

Results:

No true alarm  
One potential alarm, combined system  
Two potential alarms, Tau only systems

Table E-1

Kinematic Quantities & Miss Components  
of Intruder Aircraft in Traffic Environment



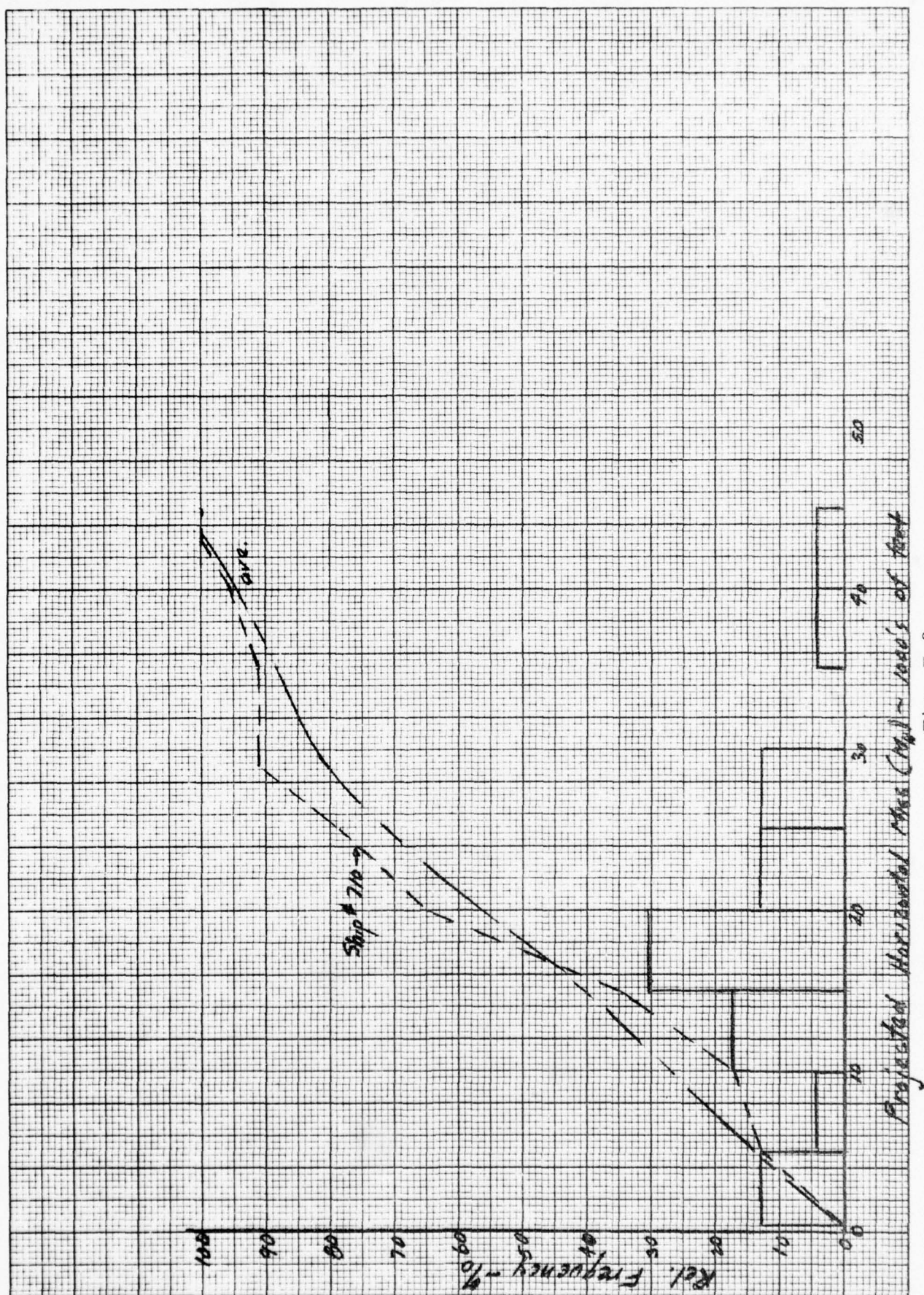


Fig. E-3  
Frequency Histogram of Relative Range - A/C #710



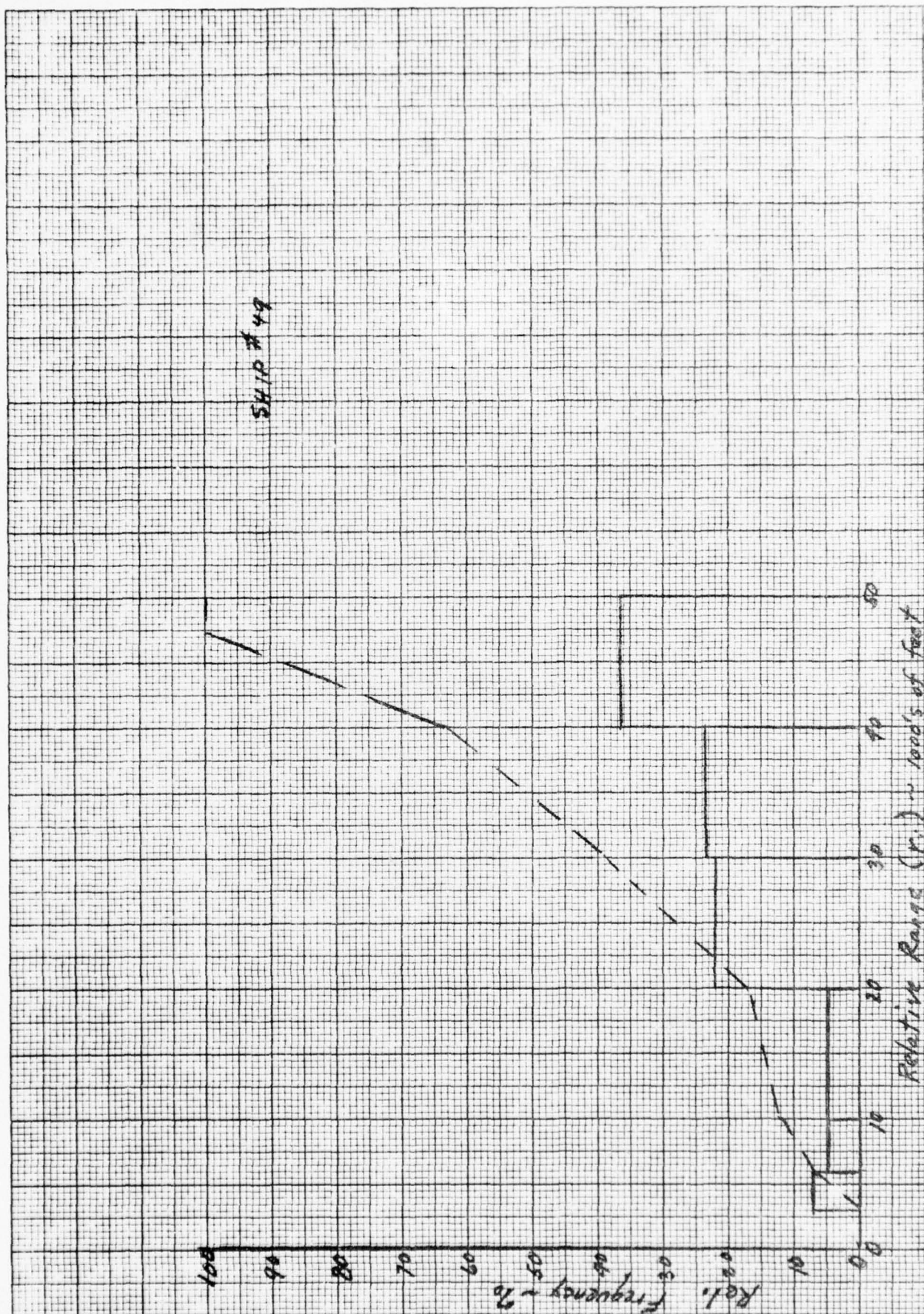


Fig. E-4  
Frequency Histogram of Relative Range - A/C #49

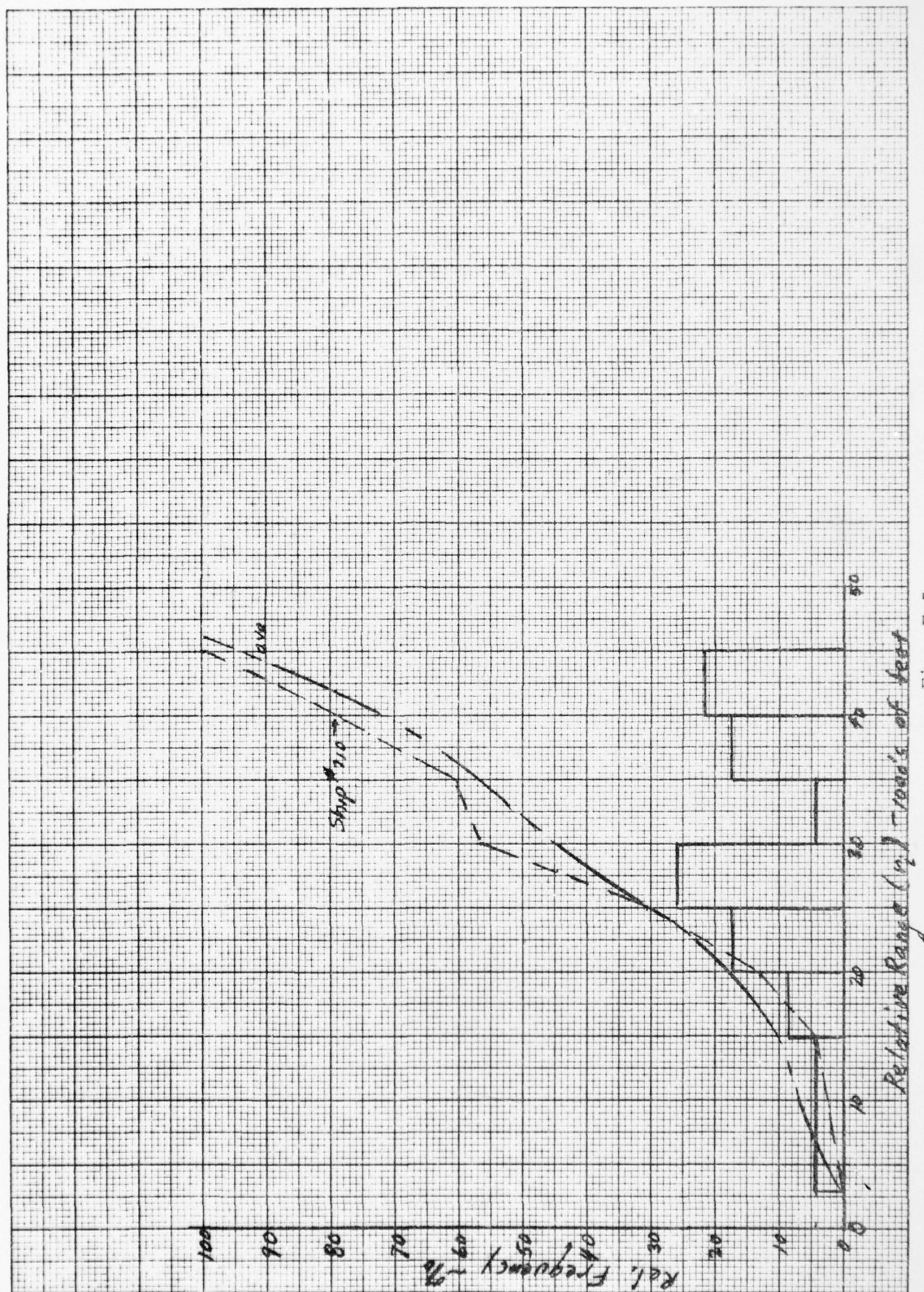
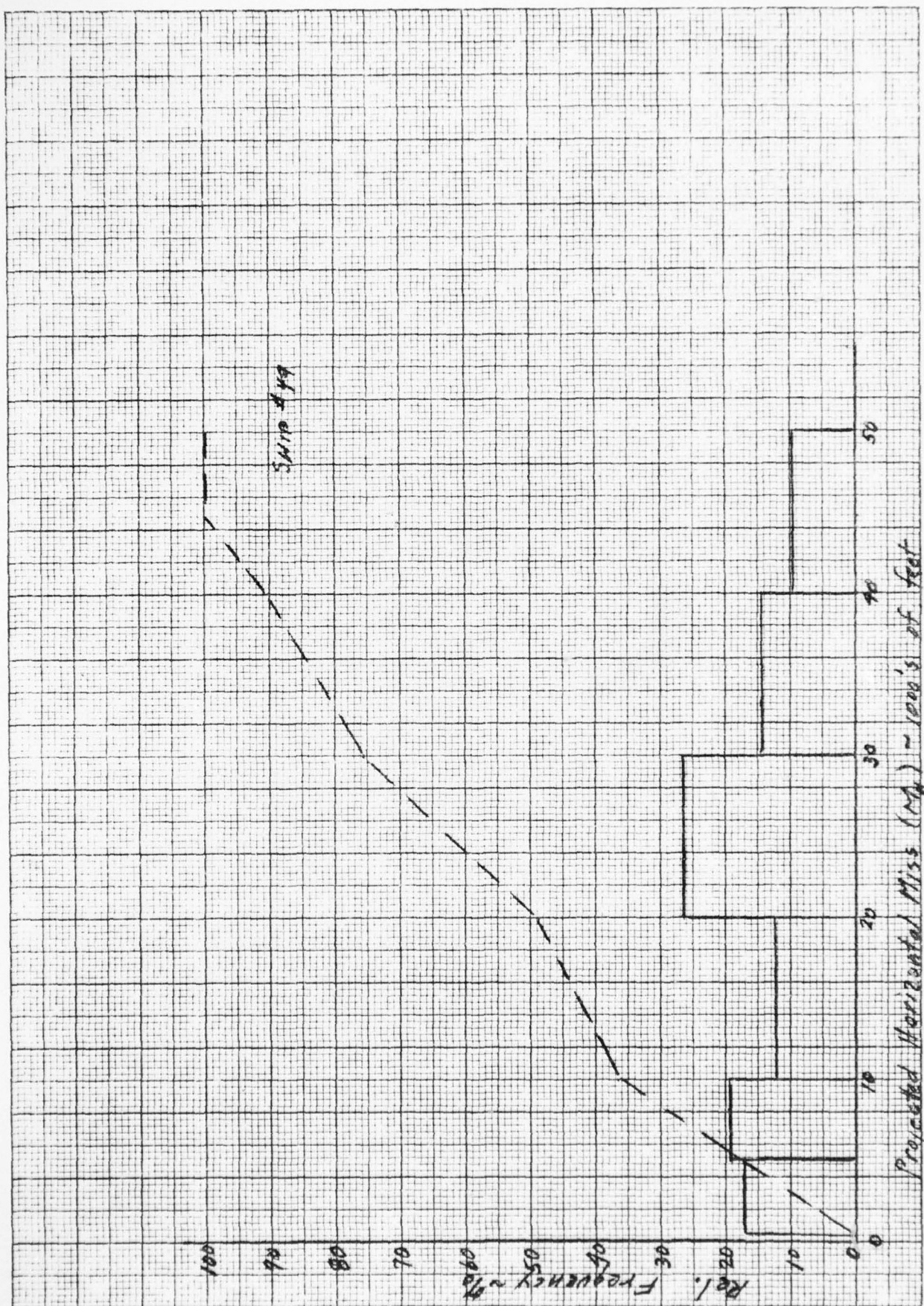


Fig. E-5  
 Frequency Histogram of Horizontal Miss - A/C #710



10 x 10 TO 1/2 INCH 46 1322  
K. E. H. M. S.  
KEUFFEL & ESSER CO.



E-11

Fig. E-6  
Frequency Histogram of Horizontal Miss - A/C #49

## APPENDIX F

### PERFORMANCE SPECIFICATION FOR A SECANT BEARING AND MISS-DISTANCE PROCESSING SUBSYSTEM OF A FULL CAS

Issue: 2 Date: 6 February 1974

#### 1.0 SCOPE

This specification covers the salient performance and general design requirements for a bearing measurement and miss-distance processing subsystem (hereafter referred to as the Bearing Subsystem) comprising two dual channel receivers, bearing signal processor, bearing data processor, and miss distance data processor. The Bearing Subsystem is generally compatible with VECAS, and provides digital outputs of relative bearing and miss distance for each target.

#### 2.0 APPLICABLE DOCUMENTS

The following documents form a part of this specification to the extent specified herein.

##### Military

|             |  |
|-------------|--|
| MIL-W-5088  | Wiring, Aircraft, Installation of                        |
| MIL-E-5400  | Electronic Equipment, Aircraft, General Specification of |
| MIL-T-5422  | Testing, Environmental, Aircraft Electronic Equipment    |
| MIL-C-6781  | Control Panel, Aircraft Equipment                        |
| MIL-A-25708 | Antenna AT-741-A   |

##### Standards

|             |   |
|-------------|---|
| MIL-STD-461 | Electromagnetic Interference Characteristics, Requirements of Equipment |
| MIL-STD-462 | Electromagnetic Interference Characteristics, Measurement of            |
| MIL-STD-463 | Definition and System of Units, Electromagnetic Interference Technology |



|             |  |
|-------------|--|
| MIL-STD-704 | Electric Power, Aircraft, Characteristics and Utilization of     |
| MIL-STD-794 | Parts and Equipment, Procedures for Packaging and Packing        |
| MS 25212    | Control Panel, Console Type, Aircraft Equipment Basic Dimensions |

Naval Air Systems Command

|       |   |
|-------|---|
| AR-10 | Maintainability of Avionics Equipment and Systems, General Requirements for |
|-------|---|

RCA Corporation

SECANT Status Report, TP2118, August 1973

3.0      REQUIREMENTS

3.1      General

The prime design objective of the full Bearing Subsystem shall be as follows:

- a)    To provide the capability of measuring relative bearing and miss distance for targets within the Tau 2 maximum hazard range from the densest region of the FAA/MITRE 1982 LA Basin Standard Traffic Model (Snapshot #3).
- b)    To integrate the Bearing Subsystem with the VECAS design while not adversely affecting the performance of its vertical escape logic.
- c)    To minimize fabrication costs by sharing, where possible, signal and data processing functions between the vertical escape subsystem and the Bearing Subsystem.

3.2      Materials and Parts

Components, materials and parts employed in the Bearing Subsystem shall satisfy the same requirements as for the VECAS equipment.

### 3.3 Design and Construction

This equipment shall conform with design and construction requirements as specified in the applicable procurement specification.

### 3.4 Performance

#### 3.4.1 Power Input

The Bearing Subsystem shall operate satisfactorily and meet all performance requirements when supplied by power sources having similar ratings and characteristics as those employed in VECAS. Where practicable, the Bearing Subsystem and the associated VECAS circuitry shall draw power from common supplies.

#### 3.4.2 Signal Input

##### 3.4.2.1 General

The Bearing Subsystem shall operate satisfactorily and meet all performance requirements, with RF reply signal inputs having the same structure and minimum levels at the receiver terminals applicable to the VECAS design except for such changes of reply ( $P^+$ ,  $P^-$ ,  $Q^+$ ,  $Q^-$ ) carrier frequencies as arise from this specification.

##### 3.4.2.2 Classification and Utilization of Input Signals

The  $P^+$ ,  $P^-$ ,  $Q^+$ ,  $Q^-$  reply frequencies for a given field and altitude zone are categorized into 4 groups W, X, Y, and Z as shown in Table F-1, for a total of 16 types. Each of these is further categorized by the suffix X into 3 additional types (for a total of 48) according to which of the 3 antenna ports provides the signal.

Provision shall be made for processing the RF inputs from the three (3) ports of the top ring array antenna, and from the three (3) ports of the bottom ring array antenna. Each bearing measurement shall be performed by processing a pair of signal inputs both of

TABLE F-1. GENERIC TYPES OF SIGNAL INPUTS

| SIGNAL<br>INPUT<br>TYPE                 | GROUP<br>CATEGORY | BAND <sup>(1)</sup><br>LOW/HIGH | FIELD<br>ABOVE/BELOW | REPLY <sup>(2)</sup><br>TYPE   |
|---|-------------------|---------------------------------|----------------------|--|
| W1x <sup>(3)</sup><br>W2x<br>W3x<br>W4x | W<br>W<br>W<br>W  | H<br>H<br>H<br>H                | A<br>A<br>A<br>A     | P <sup>+</sup><br>P <sup>-</sup><br>Q <sup>+</sup><br>Q <sup>-</sup> |
| X1x<br>X2x<br>X3x<br>X4x                | X<br>X<br>X<br>X  | H<br>H<br>H<br>H                | B<br>B<br>B<br>B     | P <sup>+</sup><br>P <sup>-</sup><br>Q <sup>+</sup><br>Q <sup>-</sup> |
| Y1x<br>Y2x<br>Y3x<br>Y4x                | Y<br>Y<br>Y<br>Y  | L<br>L<br>L<br>L                | A<br>A<br>A<br>A     | P <sup>+</sup><br>P <sup>-</sup><br>Q <sup>+</sup><br>Q <sup>-</sup> |
| Z1x<br>Z2x<br>Z3x<br>Z4x                | Z<br>Z<br>Z<br>Z  | L<br>L<br>L<br>L                | B<br>B<br>B<br>B     | P <sup>+</sup><br>P <sup>-</sup><br>Q <sup>+</sup><br>Q <sup>-</sup> |

Notes:

1. L for < 10Kft, H for > 10Kft
2. Direct replies. Inverse replies have opposite sign.
3. Suffix x=a pertains to the H=0 antenna.  
Suffix x=b pertains to the H=1 antenna.  
Suffix x=c pertains to the H=4 antenna.

which result from the same target pulse. One input of the pair shall originate from the H = 0 mode antenna port, thus deriving from an input signal type with suffix letter (a). The other input shall originate from either the H = 1 mode antenna port or the H = 4 antenna port, thus deriving from an input signal type with suffix letter (b) or (c), respectively.

#### 3.4.3 Data Input

The Bearing Subsystem shall operate satisfactorily and meet all performance requirements when supplied with:

- a) Target range and altitude difference data supplied in digital format at available resolutions by the SECANT CAS subsystem acquiring these data.
- b) Roll, pitch, and yaw data from external sensors and digital format with compatible resolution and digital format.

#### 3.4.4 Operational Characteristics

##### 3.4.4.1 General

The Bearing Subsystem shall meet or have operational performance requirements as specified below. Figure F-1 is included to facilitate comprehension of nomenclature, and of the overall system concept upon which this specification rests. Component blocks of the Bearing Subsystem are shown in full line and connote system integration philosophy rather than implementation guidance. Thus, for example, the designer may elect to adopt three IF's rather than two as indicated in Figure F-1. Note that no reference is made to the probe receive channels which do not constitute part of the Bearing Subsystem. Also, representation of reply channels associated with double probing provisions are omitted.

Each channel of the Dual Receive Channels shall possess transfer characteristics similar to those of the experimental VECAS equipment insofar as they conform with system phase stability requirements.



# LEGEND

$R$  = Range data  
 $\Delta h$  = Altitude difference  
 $M$  = Miss distance vector  
 $\beta_0$  = Observed relative bearing  
 $\theta_0$  = True relative bearing  
 $t_s$  = Time of trigger for sampling attitude data  
 $t_A$  = Estimation time interval  
 $\Delta t_{12}$

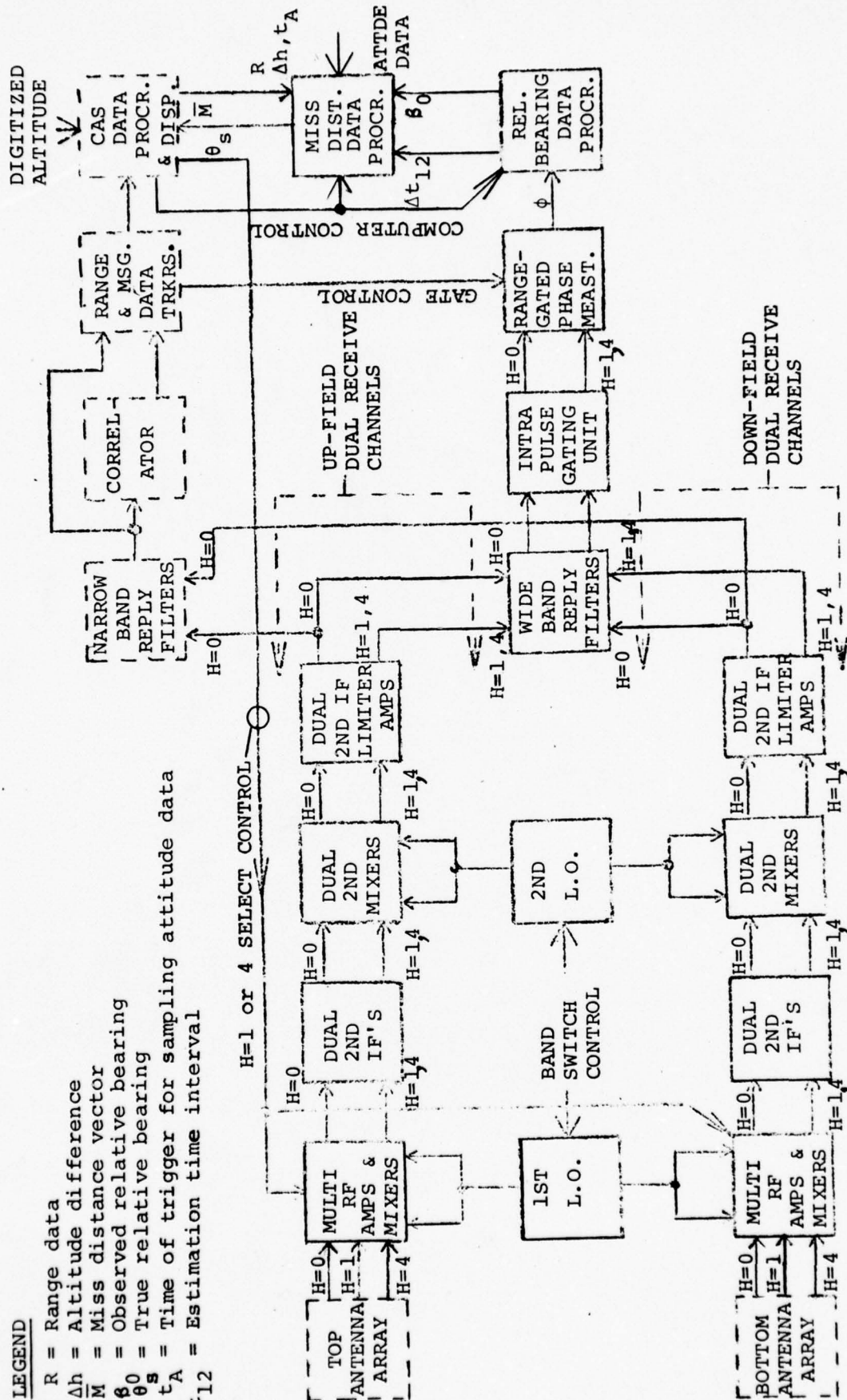


FIG. F-1. BASIC CONCEPTUAL SCHEME FOR BEARING SUBSYSTEM

### 3.4.4.2 Subsystem Signal Frequencies

#### 3.4.4.2.1 Carrier Frequencies

The spread of frequency of the RF input reply signals in each of the subgroups W, X, Y, and Z shall not be less than 20 MHz, and the difference between adjacent frequencies within any subgroup shall not be less than 5 MHz.

#### 3.4.4.2.2 Receiver Intermediate Frequencies

Each RF subgroup W, X, Y, and Z shall generate the same frequency or set of frequencies from the final IF stage. The final IF stage mid-band frequency or frequencies shall not be less than 3 MHz, while the remaining frequencies of a set (if employed) shall be such that:

$$f_{\max} \leq \frac{4}{3} f_{\min} ,$$

where

$f_{\max}$  = maximum frequency of the set

$f_{\min}$  = minimum frequency of the set

Frequencies of earlier intermediate stages and of associated local oscillators shall be selected to minimize their variety, and to be consistent with the foregoing specifications of carrier and final IF frequency or frequencies.

#### 3.4.4.3 Antenna Loading

The load impedances presented to the active individual antenna ports by the receiver inputs, including any associated switches, T/R circulators, interconnection cables, etc., shall be 50 ohm, nominal, with VSWR's not exceeding 1.5. However, the idle H = 1 or H = 4 port shall be either terminated or open circuited at the option of the designer.

#### 3.4.4.4 Channel Interference and Noise Effects

##### 3.4.4.4.1 Inter-channel Crosstalk

The crosstalk between the  $H = 0$  channel and  $H = 1, 4$  channel of the dual receivers, serving the upper and lower fields, shall not exceed  $-40$  db when measured at the inputs to the range gated Phase Measurement unit with regard to each of the 16 (sixteen) carrier frequencies.

##### 3.4.4.4.2 Transmitter Leakage

Prior to initiation of the phase measurement process associated with the acquisition of fresh bearing data, peak amplitudes of transients induced in the receiver channels by leakage from the transmitter shall have subsided to less than 6 db below the receiver noise level.

##### 3.4.4.4.3 Thermal Noise and Spurious Responses

The minimum signal-to-noise ratio occurring at the inputs to the Range Gated Phase Measurement unit shall not be less than 12 db when the Bearing Subsystem is receiving replies from targets at ranges of 15 nm. or less.

#### 3.4.4.5 Interchannel Phase and Delay Balance

##### 3.4.4.5.1 Phase Balance

The magnitude of the difference in steady-state phase shifts occurring in the two paths commencing at the inputs of the Dual Receive Channels and ending at the inputs of the Range gated Phase Measurement unit shall not exceed 2 degrees. This specification shall apply to the high band Dual Receive Channels for input signals at the 8 (eight) reply frequencies in subgroup categories W and X of Table 1, and at any level between

-90 dbm and -60 dbm; and to the low band Dual Receive Channels for input signals at the 8 (eight) reply frequencies in subgroup categories Y and Z of Table 1, and at any level between -84 dbm and -60 dbm.

In order that this specification shall be adhered to throughout the normal operating life of the Bearing Subsystem, consideration shall be given to minimizing the effects of long-term phase drifts by:

- a) Locating RF stages and first IF mixers of the dual-channel receivers in close proximity to the antenna array in order to reduce or eliminate cable runs at the L-band frequencies, and/or:
- b) Providing automatic means for periodic application of built-in test of phase balance and for its restoration when required. (An alternative technique is to transpose the two channels of a dual-channel receiver at the mid interval of the 62-pulse sequence used with the H = 4 ring array antenna, and determine the mean of the phase measurements thus obtained).

#### 3.4.4.5.2 Delay Balance

The delay differential between the Dual Receive Channels for those portions of the channels subject to carrier frequency (RF or IF) changes resulting from reception of different reply frequencies shall not exceed 2.3 nanoseconds.

#### 3.4.4.6 Wideband Reply Filter(s)

##### 3.4.4.6.1 Bandwidth and Selectivity

The bandwidth of the Wideband Reply Filter(s) shall be  $6 \text{ MHz} \pm 0.5 \text{ MHz}$  between the -3 db points on the skirts, and not greater than 10 MHz between the -20 db points.



#### 3.4.4.6.2 Phase Transient Conditions

The magnitude of the departure of the phase from its steady-state value occurring at the filters' output terminals shall not exceed 2 degrees at any time 0.2 microseconds or more later than the instant  $t_0$  at which the leading edge of the pulse envelope at the filter output terminals reaches its maximum slope.

#### 3.4.4.7 Intra-Pulse Width Gating Unit

##### 3.4.4.7.1 Operation

The Intra-Pulse Width Gating Unit shall be designed to:

- a) Apply the  $H = 0$  mode IF signals, and  $H = 1$  or 4 mode IF signals to the inputs of the Range Gated Phase Measurement unit at time  $t_x + 0.25 \pm 0.05$  microseconds (where  $t_x$  is the time of the leading edge of the track gate).
- b) Interrupt these signals at time  $t_x + \Delta T + 0.05$  microseconds, where  $\Delta T$  is the interval between the instant  $t_x$  and the instant at which a transient is initiated at the output of the Wideband Reply Filters due to the lagging edge of the pulse envelope.

##### 3.4.4.7.2 Switching Noise

Peak levels of transients generated by the Intra-Pulse Width Gating unit shall not exceed the threshold level established for the crossover sensing circuit of the Range Gated Phase Measurement unit.

#### 3.4.4.8 Range Gated Phase Measurement Unit

##### 3.4.4.8.1 General

Primary consideration shall be given to a design for a Range Gated Phase Measurement Unit (PMU) which operates by detecting the zero crossovers in the two input channels to

the PMU and estimating the interval (and hence phase for a given frequency) between the crossovers from discrete counts of a free running clock.

#### 3.4.4.8.2 Crossover Detections and Associated Phase Sampling

Reference crossover detections shall be accomplished at the instant of positive-going or negative-going (but not both) axis transitions of the  $H = 0$  wave received from the Intra-Pulse Width Gating Unit. Comparison crossover detections shall be accomplished at the instant of the positive-going or negative-going (whichever sign is employed for corresponding reference crossover detections) axis transitions of the  $H = 1$  wave or  $H = 4$  wave. Phase displacements between the  $H = 0$  wave and  $H = 1$  wave (or the  $H = 4$  wave) shall be measured by counting clock pulses generated in the interval between a pair of crossovers, one of the pair being the reference crossover and the other being the first comparison crossover encountered after the reference crossover. At least one pair of crossovers shall be detected during the reception of a carrier pulse by the PMU.

#### 3.4.4.8.3 Crossover Thresholds

The trigger levels between which the zero crossovers are detected shall be set at  $\pm 0.5 V_p$ , where  $V_p$  is the nominal pulse amplitude of signals presented to the PMU when the Bearing Subsystem is receiving replies at a minimum level of  $-90$  dbm.

#### 3.4.4.8.4 Gating Provisions

The PMU shall be primed at an anticipatory time of  $0.3 \pm 0.1$  microseconds prior to the leading edge mid points of desired pulses received from the Intra-Pulse Width Gating Unit, and shall be deactivated at the end of an elapsed interval of  $1.6 \pm 0.1$  microseconds. The PMU shall not output any spurious responses caused by the deactivation process. Desired pulses shall be recognized by the simultaneous appearance of pulses within the range gates of the SECANT tracker unit, and the trigger signal required to prime the PMU shall be derived from this unit. The PMU shall be inhibited when conditions are such as to cause a bit erasure in the CAS message processing circuits.

#### 3.4.4.8.5 Clock Rate and Counter Capacity

The clock rate to be employed by the PMU shall be fixed at a value  $f_c$  given by:

$$f_c \geq \frac{7_0}{\sqrt{T} \sqrt{3 - 4 T}} \quad (\text{MHz})$$

if two or more frequencies are generated in the final IF stage (Section 3.4.4.2.2),

where  $\bar{T}$  = mean period of the set of final IF frequencies expressed in microseconds.

Otherwise,

$$f_c \geq \frac{28.5}{T} \quad (\text{MHz})$$

where  $T$  = period of single mid band frequency of the final IF stage.

The counter employed to determine the number of clock pulses occurring between start-stop pairs of crossovers, and accumulated during a carrier pulse shall have a capacity of  $C_{\max}$  counts given by

$$C_{\max} \geq \frac{17.5}{T} \sqrt{3 - 4 T}$$

when two or more IF's are generated, or  $C_{\max} \geq 23 f_F$  for a single IF ( $= f_F$ ).

#### 3.4.4.9 Relative Bearing Data Processor

##### 3.4.4.9.1 Phase Count Accumulation

Register or computer memory locations shall be provided for temporary storage of the clock count words inputted by the Range Gated Phase Measurement Unit. These words shall pertain to a particular target bearing and shall arise from crossover pairs formed

with respect to at least 10 pulses contained in one ranging sequence of the VECAS tracking cycle. These pulses shall be derived from signals received via the H = 1 antenna.

A second temporary memory bank shall be provided to individually store a sample of clock count words inputted in respect to the same target and to crossover pairs formed with up to the full quantity ( $\geq 62$ ) of pulses contained in the other ranging sequence of the VECAS tracking cycle. These pulses shall be derived from signals received via the H = 4 antenna.

The phase difference determined by means of the H = 1 antenna shall be computed from:

$$\theta_1^{(j)} = \frac{2\pi S_1^{(j)}}{W_1^{(j)} f_c \tau} \text{ radians}$$

where

$\theta_1^{(j)}$  = Phase difference measurement from the jth pulse in one ranging sequence of the tracking cycle (rads)

$S_1^{(j)}$  = Total clock count between crossover pairs from the jth pulse of the said ranging sequence

$W_1^{(j)}$  = Number of words used to produce the  $S_1^{(j)}$  (one word per each crossover pair detected).

$f_c$  and  $\tau (= T \text{ or } \overline{T})$  are defined in paragraph 3.4.4.8.5.  $\theta_1$  shall be encoded as a word of not less than 7 bits covering the range from 0 to  $2\pi$  radians.

Each per pulse phase difference  $\theta_4$ , obtained by means of the H = 4 antenna, shall be encoded as a word of not less than 9 bits covering the range 0 to  $2\pi$  radians after being computed from:

$$\theta_4^{(j)} = \frac{2\pi S_4^{(j)}}{W_4^{(j)} f_c \tau}$$



where

$\phi_4^{(j)}$  = Phase difference measurement from the jth pulse in the other ranging sequence of the tracking cycle (rads.).

$S_4^{(j)}$  = Total clock count obtained between crossover pairs from the jth pulse.

$W_4^{(j)}$  = Number of words used to produce  $S_4^{(j)}$  (one word per each crossover pair detected).

All the  $\phi_1^{(j)}$  and  $\phi_4^{(j)}$  measurements acquired during the two ranging sequences of the VECAS track cycle shall be subjected to  $0^\circ/360^\circ$  ( $0/2\pi$  radian) discontinuity correction when needed, "wild" data (outlier) rejection, and data smoothing by a computer subroutine conforming to the algorithm given in Supplement A of this specification.

The smoothed differenced  $\hat{\phi}_1$  and  $\hat{\phi}_4$  so computed shall then be outputted in digital words of not less than 12 bits and utilized in computing an unambiguous estimate of the relative bearing observation  $\beta_0$  from the following expressions:

$$\beta_1 = \frac{\hat{\phi}_4}{4} + \hat{\phi}_1 + \frac{\pi}{4} - \frac{1}{4} \left\{ [4(\hat{\phi}_1 + \frac{\pi}{4}) \text{ modulo } 2\pi] \right\}$$

$$\beta_2 = \frac{\hat{\phi}_4}{4} + \hat{\phi}_1 - \frac{\pi}{4} - \frac{1}{4} \left\{ [4(\hat{\phi}_1 - \frac{\pi}{4}) \text{ modulo } 2\pi] \right\}$$

$$\beta_0 = \beta_1 \text{ modulo } 2\pi, \text{ if } |\hat{\phi}_1 - \beta_2| > |\hat{\phi}_1 - \beta_1|$$

$$\beta_0 = \beta_2 \text{ modulo } 2\pi, \text{ if } |\hat{\phi}_1 - \beta_2| < |\hat{\phi}_1 - \beta_1|$$

$\beta_0$  shall be outputted from the Relative Bearing Data Processor as a 12 bit word in radians over the full azimuth range.

#### 3.4.4.9.3 Control and Timing Provisions

The CAS Data Processor shall provide the Relative Bearing Data Processor with control signals which shall steer clock count words to memory locations preassigned to targets whose bearings are being determined, and to cause proper sequencing of arithmetic operations for bearing computations.

The estimation time of  $\hat{\phi}_4$ , computed as in paragraph 3.4.4.9.2, shall be acquired and stored in conjunction with the clock count words and shall correspond to the mid point of the ranging sequence processed to produce  $\hat{\phi}_4$  from which a bearing observation is made.

Output from the Relative Bearing Data Processor shall also be controlled from the CAS Data Processor. Thus, two bearing observations, as are required for miss distance computation of a particular target, shall be separated by an estimation time interval  $\Delta t_{12} = t_2 - t_1$  seconds under control by the CAS Data Processor, such that:

$$\Delta t_{12} \geq 4, \text{ with } \Delta t_{12} = nT_R$$

where  $n$  is an integer,  $T_R$  is the round time encountered by the VECAS subsystem, and  $t_1$  and  $t_2$  are the times, at the mid points of the VECAS tracking pulse sequences, used to obtain two values of  $\hat{\phi}_4$  (paragraph 3.4.4.9.2 herein) from which the said bearing observations are derived.

Storage shall not be furnished for target clock count words at estimation times other than  $t_1$  and  $t_2$ .

#### 3.4.4.10 Miss Distance Data Processor

##### 3.4.4.10.1 General

When supplied with input data comprising observed relative bearings; estimation time and time interval; aircraft yaw, pitch and roll; and target ranges and relative altitudes, the

Miss Distance Data Processor shall output miss distance data and true relative bearing data to the CAS data processor for utilization by its threat logic.

#### 3.4.4.10.2 Computation Provisions

Computation of miss distance and its horizontal and vertical components, and of true relative bearings at estimation times  $t_1$  and  $t_2$  shall be executed in accordance with the expressions given by Supplement B of this specification, and under control by the CAS Data Processor. The latter shall also supply interrupts at times  $t_A$  ( $= t_1$  or  $t_2$ ) to permit inputting the attitude data at those times to the Miss Distance Data Processor.

#### 3.4.5 Bearing Accuracy - Bench Testing

When measured at the output of the Relative Bearing Data Processor with precision test equipment, the Bearing Subsystem shall have the performance indicated by Table F-2 when its RF inputs are fed from the SECANT VECAS Calibration Generator. Coordinated L-band phase shifters, which have been accurately calibrated at the frequencies stated in Table F-1, shall be inserted in series with the  $H = 1$  and  $H = 4$  inputs in order to simulate bearings from 0 to 360°. The tests shall be conducted over this entire bearing range, and any offset due to phase unbalance between dual receiver channels shall be compensated or allowed for prior to determining the Bearing Subsystem errors.

TABLE F-2. BEARING SUBSYSTEM BENCH TEST ACCURACY REQUIREMENTS

| CONDITIONS                         | SIGNAL LEVEL<br>(dBm) | MEASURED ERROR<br>(deg) |
|------------------------------------|-----------------------|-------------------------|
| High-band<br>Up-field & Down-field | -90 to -60            | $\pm 1.4$               |
| ditto                              | -84 to -54            | $\pm 1.0$               |
| Low-band<br>Up-field & Down-field  | -84 to -60            | $\pm 1.0$               |
| ditto                              | -78 to -54            | $\pm 0.8$               |



SUPPLEMENT A (APPENDIX F)

ALGORITHM FOR PHASE MEASUREMENT  
DATA PROCESSING

(This algorithm is given in Section 3.4.1 of the Bearing  
Measurement Study)

SUPPLEMENT B (APPENDIX F)

ALGORITHMS FOR MISS DISTANCE AND BEARING DETERMINATIONS  
ASSOCIATED WITH THE MISS DISTANCE DATA PROCESSOR

Nomenclature

$\Delta h(t_i) = h_B - h_S =$  altitude difference with respect to own altitude (feet)

$\beta(t_i) =$  bearing angle; angle in antenna ground plane from aircraft longitudinal axis to projection of range line; measured positive clockwise

$R(t_i) =$  range, own aircraft to intruder aircraft (feet)

$\psi(t_i) =$  yaw angle, at time  $t_i$

$P(t_i) =$  pitch angle, at time  $t_i$

$r(t_i) =$  roll angle, at time  $t_i$

$E(t_i) =$  elevation angle of range line, determined in vertical plane

$\epsilon(t_i) =$  elevation angle of range line, in plane containing range line and normal to antenna ground plane

$\delta_{12} =$  angle between range lines at times  $t_1$  and  $t_2$

$V_r =$  magnitude of relative velocity vector (f.p.s.)

$\gamma_v =$  path angle of  $\bar{V}_r$

$M =$  miss distance; shortest range to intruder (feet)

$M_H =$  horizontal component of  $\bar{M}$  (feet)

$M_V =$  vertical component of  $\bar{M}$  (feet)

$\Delta t_{12} = t_2 - t_1$ , estimation time interval (seconds)

- $t_i$  = time at which  $\beta_i$  is estimated (mid point of track pulse sequence);  $i = 1, 2$   
 $\delta_{12H}$  = angle between horizontal projections of  $R_1$  and  $R_2$   
 $\theta_s$  = angle between horizontal projections of range line and aircraft longitudinal axis (horizontal relative bearing)

Computational Sequence:

Inputs:  $\Delta h_1, \Delta h_2; \beta_1, \beta_2; R_1, R_2$   
 $\psi_1, \psi_2; P_1, P_2; r_1, r_2; \Delta t_{12}$

- 1) Find  $\sin E_1, \sin E_2$ :

$$\sin E_1 = \left( \frac{\Delta h_1}{R_1} \right)$$

$$\sin E_2 = \left( \frac{\Delta h_2}{R_2} \right)$$

- 2) Find  $\epsilon_1, \epsilon_2$ :

$$\theta_1 = \tan^{-1} [ P_1^r \cos \beta_1 - r_1^r \sin \beta_1 ]; 0 \leq |\theta_1| \leq 90^\circ$$

$$\epsilon_1 = \sin^{-1} [ \sin E_1 \cos \theta_1 ] - \theta_1 ; 0 \leq |\epsilon_1| \leq 90^\circ$$

$$\theta_2 = \tan^{-1} [ P_2^r \cos \beta_2 - r_2^r \sin \beta_2 ]; 0 \leq |\theta_2| \leq 90^\circ$$

$$\epsilon_2 = \sin^{-1} [ \sin E_2 \cos \theta_2 ] - \theta_2 ; 0 \leq |\epsilon_2| \leq 90^\circ$$

- 3) Find  $\cos \delta_{12}, \sin \delta_{12}$ :

$$\cos \delta_{12} = \cos \epsilon_1 \cos \epsilon_2 \cos (\beta_2 - \beta_1) + \sin \epsilon_1 \sin \epsilon_2$$

$$- (\psi_2 - \psi_1)^r \cos \epsilon_1 \cos \epsilon_2 \sin (\beta_2 - \beta_1)$$

$$+ (P_2 - P_1)^r [ \sin \epsilon_1 \cos \epsilon_2 \cos \beta_2 - \sin \epsilon_2 \cos \epsilon_1 \cos \beta_1 ]$$

$$+ (r_2 - r_1)^r [ \sin \epsilon_2 \cos \epsilon_1 \sin \beta_1 - \sin \epsilon_1 \cos \epsilon_2 \sin \beta_2 ]$$

$$\sin \delta_{12} = \sqrt{1 - \cos^2 \delta_{12}}$$

4) Find  $\delta_{12H}$ ,  $\theta_{S1}$ ,  $\theta_{S2}$ :

$$\theta_{S1} = \tan^{-1} \left[ \frac{\sin \beta_1 \cos \epsilon_1 + r_1^r \sin \epsilon_1}{\cos \beta_1 \cos \epsilon_1 - P_1^r \sin \epsilon_1} \right]$$

$$\theta_{S2} = \tan^{-1} \left[ \frac{\sin \beta_2 \cos \epsilon_2 + r_2^r \sin \epsilon_2}{\cos \beta_2 \cos \epsilon_2 - P_2^r \sin \epsilon_2} \right]$$

quadrants from num. and den. signs

$$\delta_{12H} = (\psi_2 - \psi_1) + (\theta_{S2} - \theta_{S1})$$

5) Find  $V_r \Delta t_{12}$ :

$$V_r \Delta t_{12} = \sqrt{R_1^2 + R_2^2 - 2 R_1 R_2 \cos \delta_{12}}$$

6) Find M:

$$M = \frac{R_1 R_2 \sin \delta_{12}}{V_r \Delta t_{12}}$$

7) Find  $\sin \gamma_v$ :

$$\sin \gamma_v = \frac{(\Delta h_2 - \Delta h_1)}{V_r \Delta t_{12}}$$



- 8) Find  $M_V$ :

$$M_V = \Delta h_2 + \sqrt{R_a^2 - M^2} \sin \gamma_V$$

- 9) Find  $M_H$ :

$$M_H = \pm \sqrt{M^2 - M_V^2}$$

Take sing of  $\delta_{12H}$

- 10) Find  $V_r$ :

$$V_r = \frac{(V \Delta t_{12})}{\Delta t_{12}}$$

- 11) Find  $M_T$ :

$$\text{At } \tau_2 \text{ Alarm: } M_{T2} = 11,200 + 4.73 V_r$$

$$\text{At } \tau_1 \text{ Alarm: } M_{T1} = 1700 + 4.14 V_r, \text{ for } M_{T1} > 3038 \text{ ft.}$$

$$= 3038, \text{ if } M_{T1} < 3038$$

NOTE: Superscript r, on angular quantities, means that the angle is to be inputted in radians.

## APPENDIX G

### MUTUAL COUPLING EFFECTS IN CROSSED-AXIS INTERFEROMETER

#### INTRODUCTION AND SUMMARY

An earlier analysis (Section 3.2.2) of mutual coupling between the monopoles of a 2-element single axis interferometer array showed that, with a spacing of one half wavelength between the monopoles, the mutual coupling could cause systematic bearing errors approaching 14° maximum. This appendix extends the investigation to determine corresponding errors for the more applicable structure of the orthogonally crossed-axis interferometer for a generalized spacing between elements lying on the same axis. A simplification made, whereby no coupling is assumed to exist between the elements of one axis with those of the other axis, is justified for the following reason: Phase differences would be measured sequentially from each axis element pair, and any unused element would be deliberately open circuited during its interval of inactivity.

The results of the analysis indicate much lower, but still significant, systematic bearing errors with the crossed-axis configuration having half-wavelength spacing than with the single-axis one. However, using a spacing of four wavelengths (commensurate with the diameter of the H = 4 ring array antenna) the systematic bearing errors are reduced to negligible proportions. Hence, if this larger aperture structure were employed for vernier bearing measurements, and the half-wavelength one for bearing ambiguity resolution, no calibration corrections would be required.

#### Analysis

Except where indicated, the notation definitions for the following analysis is the same as those employed in the analysis of the single-axis interferometer array.

Writing

$$C_1 = \cos (\alpha \cos \theta) \quad (G-1)$$

and

$$S_1 = \sin (\alpha \cos \theta) \quad (G-2)$$

Then,

$$\bar{I}_{11} = \bar{A}C_1 + j\bar{B}S_1 \quad (G-3)$$

$$\bar{I}_{21} = \bar{A}C_1 - j\bar{B}S_1 \quad (G-4)$$

Now,

$$\bar{A} = \frac{1}{Z_p^2} (R_p - jX_p) \quad (G-5)$$

$$\bar{B} = \frac{1}{Z_n^2} (R_n - jX_n) \quad (G-6)$$

where:

$$\left. \begin{aligned} R_p &= R_o + R_m + Z_o \\ X_p &= X_o + X_m \\ R_n &= R_o - R_m + Z_o \\ X_n &= X_o - X_m \end{aligned} \right\} \quad (G-7)$$

$$\therefore \bar{I}_{11} = \frac{1}{Z_p^2} (R_p - jX_p) C_1 + \frac{j}{Z_n^2} (R_n - jX_n) S_1 \quad (G-8)$$

and

$$\bar{I}_{21} = \frac{1}{Z_p^2} (R_p - jX_p) C_1 - \frac{j}{Z_n^2} (R_n - jX_n) S_1 \quad (G-9)$$

where:

$$Z_p^2 = R_p^2 + X_p^2 \quad (G-10)$$

and

$$Z_n^2 = R_n^2 + X_n^2$$

whence  $\arg(\bar{I}_{11} - \bar{I}_{21})$ ; i.e., the phase difference between the phasors  $\bar{I}_{11}$  and  $\bar{I}_{21}$  is:

$$\theta_{12} = -\tan^{-1} \frac{X_p Z_n^2 C_1 - R_n Z_p^2 S_1}{R_p Z_n^2 C_1 + X_n Z_p^2 S_1} + \tan^{-1} \frac{X_p Z_n^2 C_1 + R_n Z_p^2 S_1}{R_p Z_n^2 C_1 - X_n Z_p^2 S_1} \quad (G-11)$$

By a procedure similar to the above, a corresponding expression for  $\theta_{13}$ , the phase difference between elements 1 and 3 lying in the orthogonal axis, was obtained. It is:

$$\theta_{13} = \tan^{-1} \frac{X_p Z_n^2 C_2 - R_n Z_p^2 S_2}{R_p Z_n^2 C_2 + X_n Z_p^2 S_2} + \tan^{-1} \frac{X_p Z_n^2 C_2 + R_n Z_p^2 S_2}{R_p Z_n^2 C_2 - X_n Z_p^2 S_2} \quad (G-12)$$

where

$$C_2 = \cos(\alpha \sin \theta) \quad (G-13)$$

and

$$S_2 = \sin(\alpha \sin \theta) \quad (G-14)$$

Now the orthogonally crossed-axis interferometer delivers an apparent bearing angle  $\theta_{app}$  expressed by:

$$\theta_{app} = \tan^{-1} \frac{\theta_{12}}{\theta_{13}} \quad (G-15)$$

in which  $\theta_{12}$  and  $\theta_{13}$  are given in G-11 and G-12, respectively. The systematic bearing error introduced by inter-element mutual coupling will accordingly be:

$$\epsilon_m = \theta_{app} - \theta$$

or

$$\epsilon_m = \tan^{-1} \frac{\theta_{12}}{\theta_{13}} - \theta \quad (G-16)$$

In computing  $\epsilon_m$  for several cases of differing spacings between quarter-wavelength monopole antenna elements, the values taken for  $r_m$  and  $X_m$  in equation set G-7 were

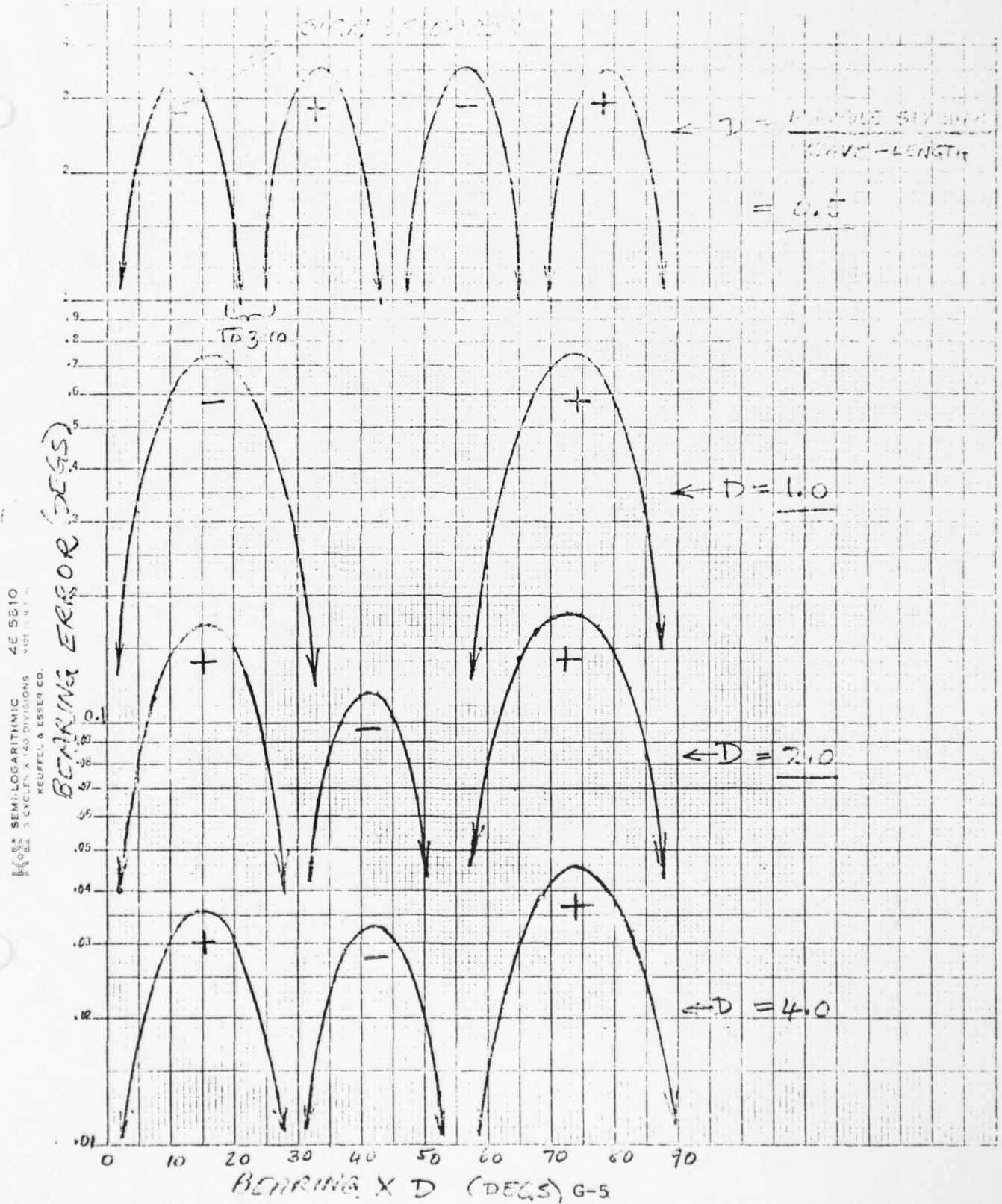


those given in Table G-1. Results given by a computer program coded in conformance with the above expressions are summarized in Figure G-1. The constant between errors in the currently pertinent cases of  $D = 0.5$  and  $D = 4$  is seen to be two orders of magnitude, and approaching three orders when comparison is made with the maximum error originally obtained for the single axis case.

TABLE G-1  
MUTUAL IMPEDANCE DATA

| $\underline{(2d/\lambda)}$ | $\underline{a^\circ}$ | $\underline{R_{m \Omega}}$ | $\underline{X_{m \Omega}}$ |
|----------------------------|-----------------------|----------------------------|----------------------------|
| 1.0                        | 180°                  | +1.5                       | +8.7                       |
| 1.5                        | 270°                  | -1.0                       | -6.0                       |
| 2.0                        | 360°                  | +0.5                       | +4.7                       |
| 2.5                        | 450°                  | -0.35                      | -3.7                       |
| 3.0                        | 540°                  | +0.24                      | +3.1                       |
| 3.5                        | 630°                  | -0.18                      | -2.7                       |
| 4.0                        | 720°                  | +0.14                      | +2.4                       |

Figure G-1. Magnitude of Error in Crossed Axis Interferometer Due to Mutual Coupling Between Axial Monopole Pairs



## APPENDIX H

### BALUN FREQUENCY CHARACTERISTICS

Figures H-1 and H-2 give the relative amplitudes and phases as calculated between the two loads of a half-wave balun as a function of frequency change. It is assumed here that there is no mutual coupling between the two loads. The circuitry is shown at the bottom of Figure H-1. At centerband frequency, the line section is one-half wave long and the balance quality is perfect (i.e., the magnitudes are equal and fed out-of-phase). As the frequency changes, this relationship is impaired, both in amplitude and phase. The curves of the two figures illustrate the effect in terms of the parameter,  $Z_C/Z_O$ , where  $Z_C$  is the characteristic impedance of the balun line and  $Z_O$  is the magnitude of the load impedance.

From Figure H-1, it is seen that the ideal amplitude characteristic is obtained for  $Z_C/Z_O = 1.0$ . On the other hand, Figure H-2 shows that the ideal phase characteristic is approached as the ratio  $Z_C/Z_O > 0$ ; i.e., the load impedances become high relative to the line impedance. In the present application, however, the bandwidth is small (about  $\pm 1\%$ ) and the balance deterioration is considered not serious for values of  $Z_C/Z_O$  considerable less than unity.

The data supplied in Figure H-1 gives the frequency characteristics of the  $\lambda/2$  balun proposed for use in this application. However, this chart does not give sufficient detailed information as to the balance quality change over the present narrow band. Therefore, an expanded chart of the central region of this graph, more applicable to the narrow-band of SECANT, is given in Figure H-3. This data shows: (1) that the amplitude differences are very small, even for a relatively large variation in the ratio ( $Z_C/Z_O$ ), and (2) that the least phase variation from the desired  $180^\circ$  differential is obtained for small values of ( $Z_C/Z_O$ ); i.e., for the antenna impedance to be large relative to the characteristic impedance of the  $\lambda/2$  balun line.

Figure H-1.  $\lambda/2$  Balun Frequency Characteristics (Magnitude)

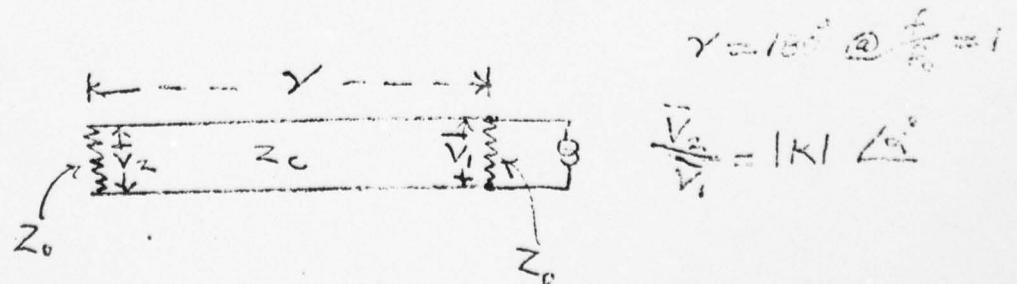
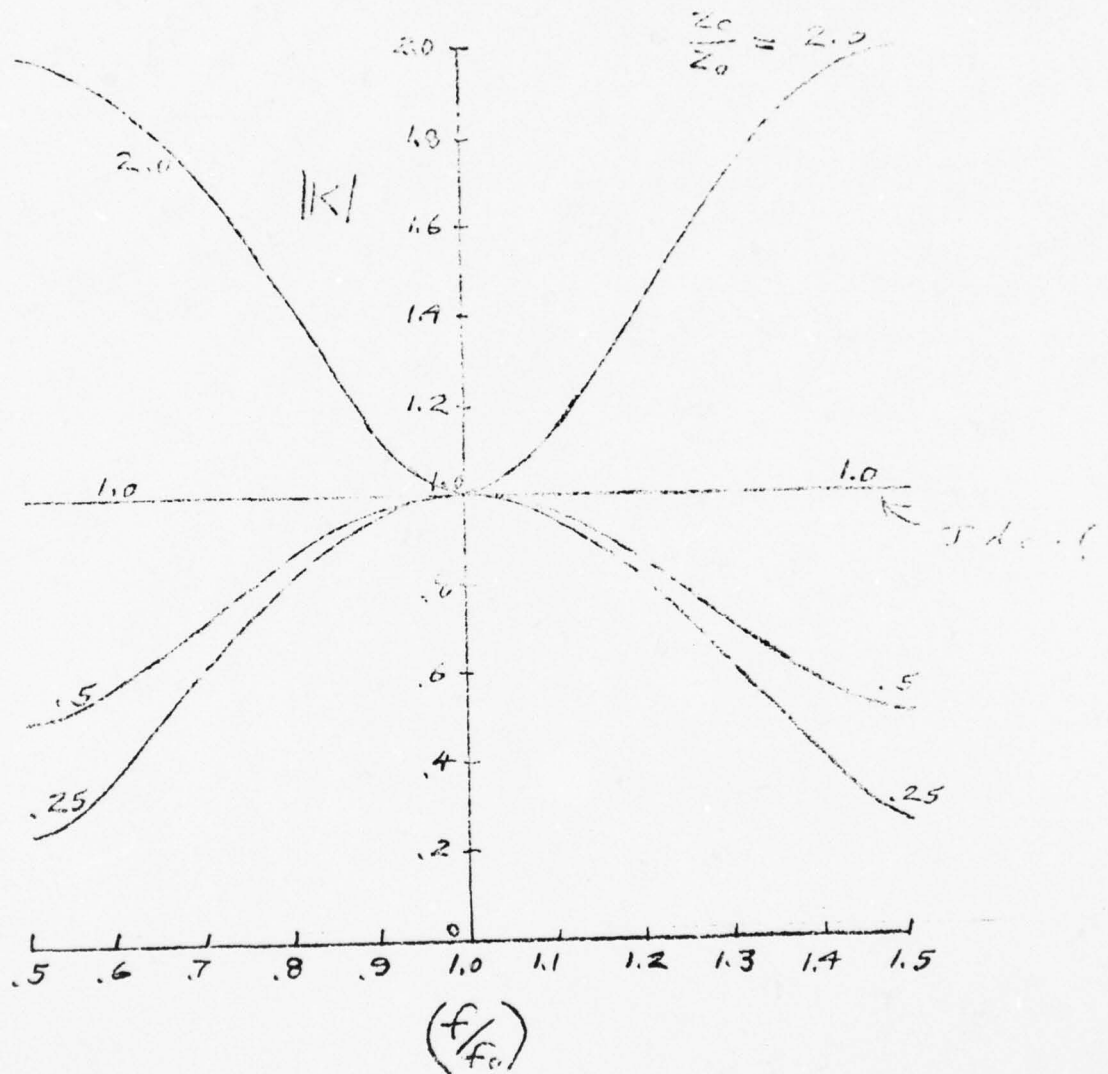
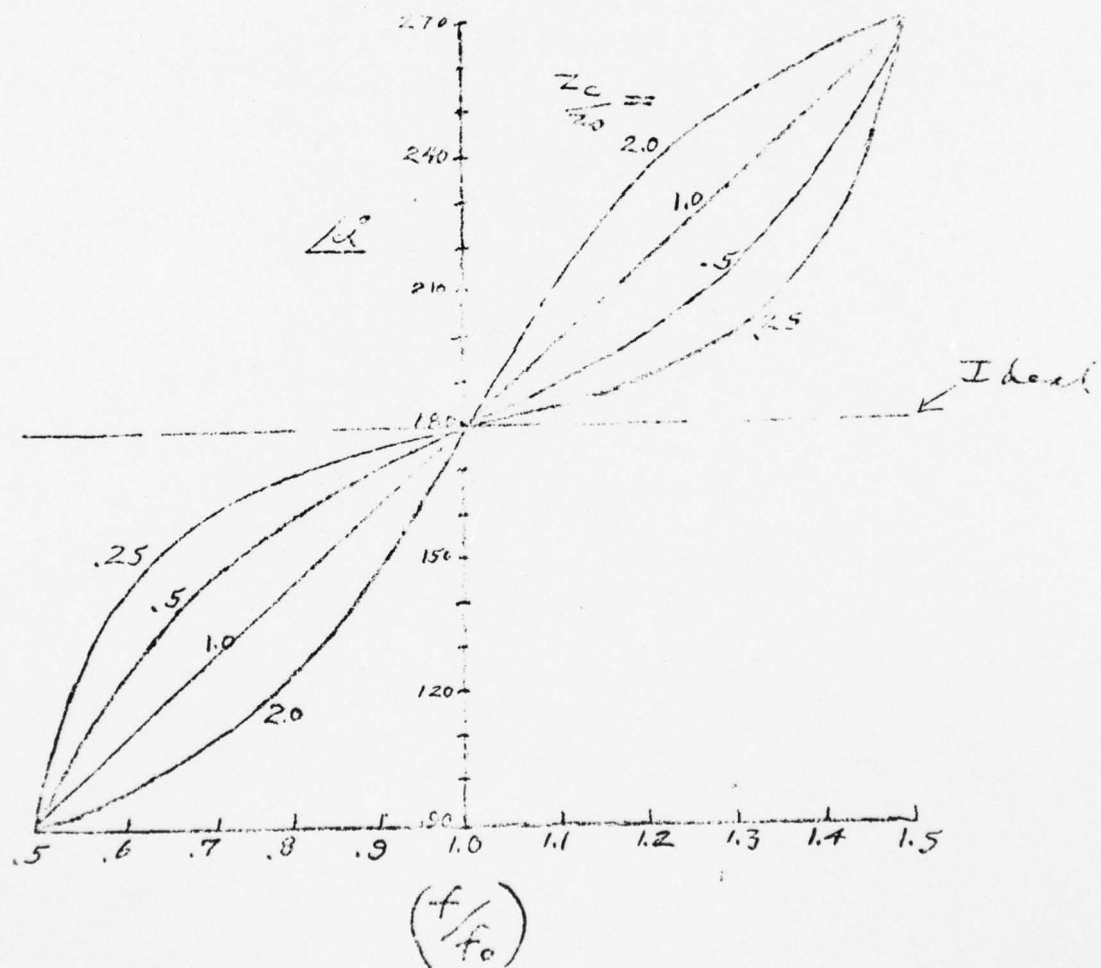




Figure H-2.  $\lambda/2$  Balun Frequency Characteristics (Phase)



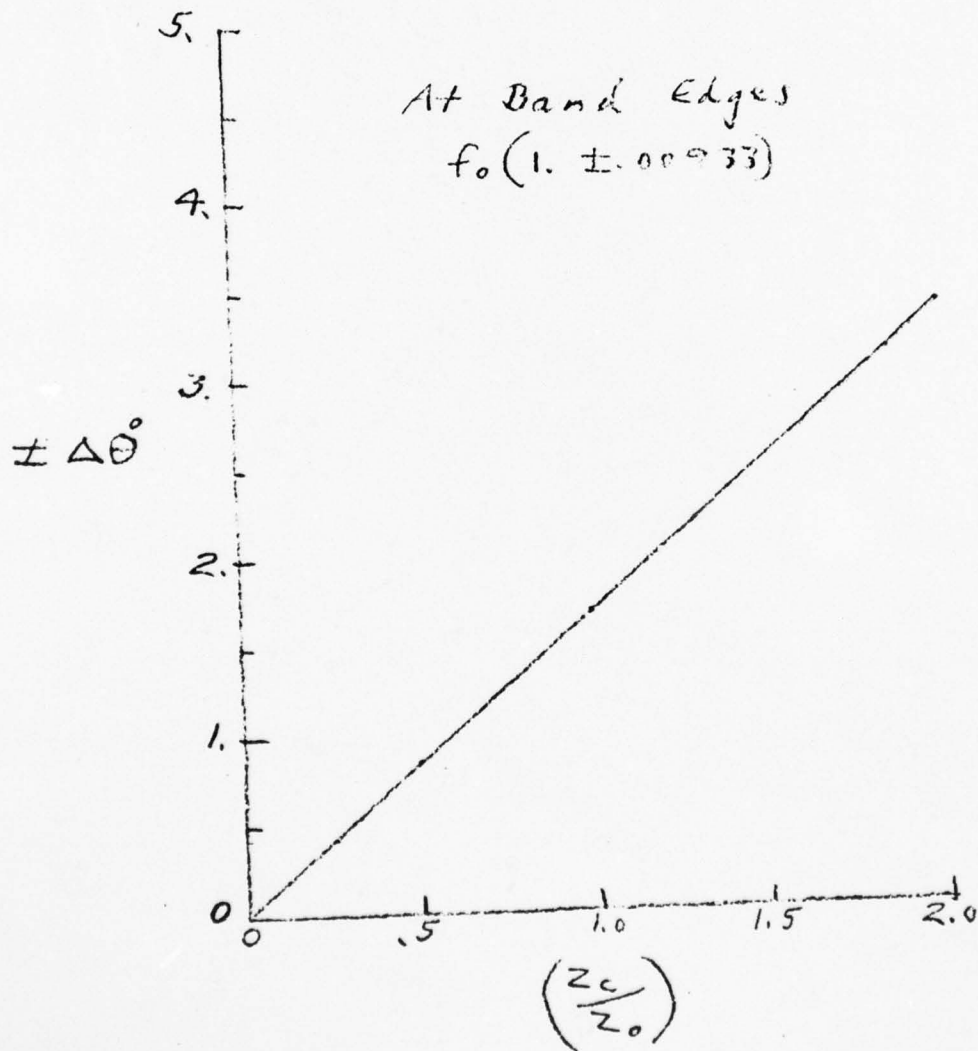
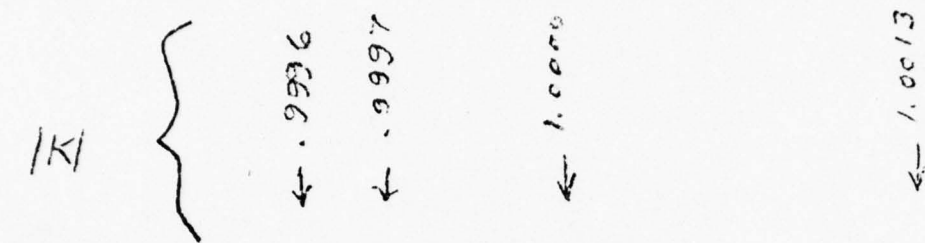


Figure H-3.  $\lambda/2$  Balun Frequency Characteristics

## APPENDIX I

### EXPRESSIONS FOR UNAMBIGUOUS RELATIVE BEARING USING RING ARRAY ANTENNAS AND CROSSED-AXIS INTERFEROMETER

#### Case 1:      Ring Arrays

Consider two concentric ring arrays, one having a single cycle of phase variation ( $H = 1$ ), and the other having  $n$  cycles ( $H = n$ ), where  $n$  is an integer greater than unity. Assume their common mounting surface lies parallel to the wing plane of the aircraft, and their orientation is such that a wave arriving from a direction corresponding to zero relative bearing produces zero phase differences of signals appearing at the antennas' ports.

Then the relative bearing  $\beta_R$  (measured in degrees) for a single return pulse from a target aircraft is found as follows:

Let  $\phi_1$  = phase difference (deg.) measured from  $0^\circ$  to  $360^\circ$  when using the  
           $H = 1$  ring array antenna

$\phi_n$  = phase difference (deg.) measured from  $0^\circ$  to  $360^\circ$  when using the  
           $H = n$  ring array antenna

$\epsilon$  = error in  $\phi_1$ , i.e.,  $\phi_1 = \beta_R + \epsilon$

Disregarding the error in  $\phi_n$ :

$$\begin{aligned}\phi_n &= (n\beta_R) \text{ modulo } 360 \\ &= [n(\phi_1 - \epsilon)] \text{ modulo } 360\end{aligned}$$

Thus the number of complete phase cycles in  $n\beta_R$  is:

$$C = \frac{n(\phi_1 - \epsilon) - [n(\phi_1 - \epsilon)] \text{ modulo } 360}{360} \tag{I-1}$$

Now

$$\theta_n = n\beta_R - 360C$$

or

$$n\beta_R = \theta_n + 360C \quad (I-2)$$

Substituting I-1 into I-2 and solving for  $\beta_R$  gives:

$$\beta_R = \frac{\theta_n}{n} + (\theta_1 - \epsilon) - \frac{1}{n} ([n(\theta_1 - \epsilon)] \text{ modulo}) \quad (I-3)$$

$\epsilon$  is not known but may be bounded, say  $\pm 30^\circ$ . Replacing  $\epsilon$  in I-3 by these bounds gives two values of  $\beta_R$  represented by  $\beta_1$  and  $\beta_2$ . One of them is the correct bearing ( $\beta_{\text{true}}$ ).

It is readily shown that if

$$|\theta_1 - \beta_2| > |\theta_1 - \beta_1|, \beta_{\text{true}} = \beta_1 \text{ modulo } 360 \quad (I-4)$$

and if

$$|\theta_1 - \beta_2| < |\theta_1 - \beta_1|, \beta_{\text{true}} = \beta_2 \text{ modulo } 360$$

#### Case 2: Crossed Axis-Interferometers

Alternatively, block no. 1 could contain crossed-axis interferometer arrays, each composed of a triad of antenna monopoles. When, as indicated in Figure I-1, the elements have axes intersecting at an angle  $\psi$  ( $\psi \leq 90^\circ$ ), are symmetrical with the longitudinal axis of the aircraft, and are mounted in a plane parallel to that of the wings, the ideal (i.e., error-free) expression for the measured relative bearing in degrees is readily shown to be:

$$\beta_I = 90 - \frac{\psi}{2} + \arctan \left[ \frac{\theta_{12}}{\theta_{13}} \left( \frac{\sin \psi}{1 + \frac{\theta_{12}}{\theta_{13}} \cos \psi} \right) \right] \quad (I-6)$$



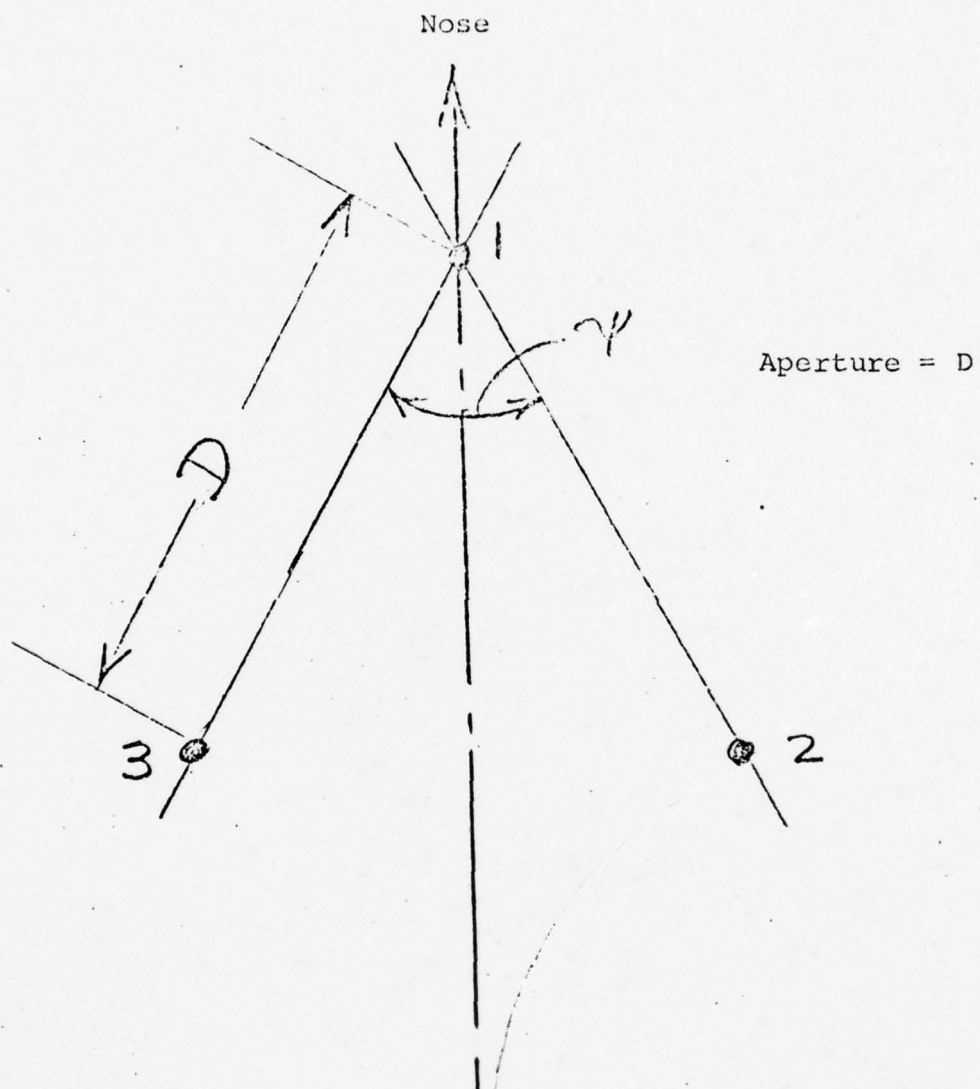


FIGURE I-1. Geometry of Crossed-Axis Interferometer

and for orthogonal axes ( $\psi = 90^\circ$ ) is:

$$\beta_I = 45 + \arctan \left( \frac{\phi_{12}}{\phi_{13}} \right) \quad (\text{I-7})$$

where:

$\phi_{12}$  = phase difference between elements 1 and 2

$\phi_{13}$  = phase difference between elements 1 and 3

Equations I-6 and I-7 are independent of the interferometer aperture (D), and also of the elevation of the target with respect to the wing plane. However, phase comparison devices are intrinsically incapable of resolving phase angles exceeding  $360^\circ$ . Yet, such angles will occur in an interferometer having D larger than half the free-space wavelength of the carrier, as in the present case. Consequently, a secondary interferometer with  $D < \frac{\lambda}{2}$  (where  $\lambda$  = wavelength) would be employed to verify the true magnitude of  $\phi_{12}$  or  $\phi_{13}$  as follows:

Given a phase comparator able to measure phase differences from  $0^\circ$  to  $360^\circ$  without ambiguity, the phase angle values (in degrees) to be inserted in I-6 or I-7 would, similarly to I-3, be computed from:

$$\phi_{12} = \frac{\phi'_{12}}{\rho} + (\phi'_{12} \pm \epsilon_B) - \frac{1}{\rho} ([\rho (\phi'_{12} - \epsilon_B)] \text{ modulo } 360) \quad (\text{I-8})$$

and

$$\phi_{13} = \frac{\phi''_{13}}{\rho} + (\phi'_{13} \pm \epsilon_B) - \bar{\rho} ([\rho (\phi'_{13} - \epsilon_B)] \text{ modulo } 360) \quad (\text{I-9})$$

with verifying qualifications corresponding to those of expressions I-4 and I-5, and in which:

$$\rho = \frac{D'}{D''} = \frac{\text{element spacing of the narrow aperture interferometer}}{\text{element spacing of the wide aperture interferometer}}$$

$\epsilon_B$  = error bound magnitude (say  $30^\circ$ )

$\phi'_{12}$  = phase difference measured in degrees with respect to the narrow aperture ( $D \leq \lambda / 2$ ) interferometer, between elements 1 and 2.

$\phi''_{12}$  = phase difference measured in degrees with respect to the wide aperture ( $D > \lambda / 2$ ) interferometer, between elements 1 and 2.

and similarly for  $\phi'_{13}$  and  $\phi''_{13}$  with elements 1 and 3.

## APPENDIX J

### PHASE TRANSIENTS IN DOUBLE-TUNED FILTERS

Papoulis\* shows that the response of a double-tuned filter to a carrier of unit amplitude  $\cos \omega_0 t$  modulated by the unit step function is given by:

$$g(t) = a(t) \sin \omega_0 t + e(t) \quad (J-1)$$

where

$$a(t) = \frac{k\omega_0}{4} \left[ \frac{1}{\alpha^2 + \beta^2} + \frac{1}{\beta \sqrt{\alpha^2 + \beta^2}} -\alpha t \sin (\beta t - \tan^{-1} \frac{\beta}{\alpha}) \right] \quad (J-2)$$

and

$$e(t) \approx -\frac{k}{8\beta} e^{-\alpha t} \sin \beta t \cos \omega_0 t \quad (J-3)$$

with

$$t \geq 0$$

The four poles of the filter, (viz.,  $-\alpha_1 \pm j\beta_1$  and  $-\alpha_2 \pm j\beta_2$ ) are such that subject to  $\alpha_1 = \alpha_2 = \alpha$ ,  $\alpha \ll \beta_1$ , and  $\beta_1 - \beta_2 \ll \beta_1$  its frequency response is symmetrical about its center (angular) frequency:

$$\omega_0 = \frac{\beta_1 + \beta_2}{2} \quad (J-4)$$

Simplifying further to  $\beta_1 = \beta_2 = \beta$  satisfies the above conditions and gives meaning to  $\beta$  in J-2 and J-3.

Substituting from J-2 and J-3 in J-1 and allowing for a phase epoch  $\theta$  of the excitation  $\cos \omega_0 t$  results in a response of the form:

$$g(t) = h(t) \sin [\omega_0 t + \theta - \phi(t, \theta)] \quad (J-5)$$

\*A. Papoulis, "The Fourier Integral and Its Applications", McGraw-Hill, 1962.



in which  $h(t)$  is a time varying envelope modulating function, and  $\phi(t, \theta)$  is a phase transient term given by:

$$\phi(t, \theta) = \tan^{-1} \left( \frac{\gamma^2 \sin \theta + \frac{e^{-\alpha t}}{2\beta\omega} \sin \beta t}{\gamma^2 \cos \theta + \frac{\gamma}{\beta} e^{-\alpha t} \sin (\beta t - \tan^{-1} \frac{\beta}{\alpha})} \right) \quad (J-6)$$

where

$$\gamma = \frac{1}{\alpha^2 + \beta^2}$$

For the two channel system, we are interested in the phase difference transient between the channels diminished by the steady-state displacement  $\theta$ : that is, in:

$$\Delta\phi = \phi(t, \theta) - \phi(t, 0) - \theta \quad (J-7)$$

and require that  $\Delta\phi$  decays to an acceptably small value prior to initiating the phase measuring process.

In computing  $\Delta\phi$  as a function of  $t$  and  $\theta$ , with the latter taken over a full cycle of 0 to  $2\pi$  radians, values of  $\alpha$ ,  $\beta$ , and  $\omega_0$  were selected appropriate to two IF filters of 20 MHz center frequency, 5 MHz bandwidth, and resonant circuit damping factors of 0.05 in one case and 0.1 in the other. Numerical results obtained for  $\Delta\phi$  using a computer program on the time sharing terminal were reduced and plotted in Figures 3-44 and 3-45 of the report text.

## APPENDIX K

### SWEPT BEARING ERROR DUE TO INTERCHANNEL PHASE IMBALANCE WHEN EMPLOYING THE CROSSED-AXIS INTERFEROMETER

The apparent direction-of-arrival angle (DOA) measured with a crossed-axis interferometer, wherein the axes are arranged orthogonally in the reference plane, is given by:

$$\alpha = \tan^{-1} \left( \frac{\phi_2 + \psi}{\phi_1 + \psi} \right) \quad (\text{K-1})$$

in which

$$\phi_1 = \frac{2\pi D}{\lambda} \sin \theta \quad (\text{K-2})$$

$$\phi_2 = \frac{2\pi D}{\lambda} \cos \theta \quad (\text{K-3})$$

where;

$\phi_1$  = phase angle between antenna elements lying in the reference axis

$\phi_2$  = phase angle between antenna elements lying in the orthogonal axis

$\theta$  = True DOA

D = Spacing between the pairs of antenna elements on each axis

$\lambda$  = wavelength

$\psi$  = phase imbalance between the two channels of the phasemeter employed to determine  $\phi_1$  and  $\phi_2$

NOTE:  $\psi$  is expressed as a positive or negative angle with respect to the phase in the reference channel, under the condition:  $|\psi| \leq \pi$ .

Writing

$$r = \frac{2\pi D}{\lambda}, \text{ (K-1) becomes:}$$

$$\delta = \tan^{-1} \left( \frac{r \sin \theta + \psi}{r \cos \theta + \psi} \right) \quad (\text{K-4})$$

To determine the effect of  $\psi$  on a small change ( $\delta\theta$ ) in  $\theta$ , corresponding to a swept bearing we have:

$$\delta\alpha \cong \frac{\partial\alpha}{\partial\theta} \delta\theta \quad (\text{K-5})$$

Hence the error in swept bearing is:

$$\begin{aligned} \epsilon &= \delta\alpha - \delta\theta \\ &\cong \delta\theta \left( \frac{\partial\alpha}{\partial\theta} - 1 \right) \end{aligned}$$

from which the fractional error is given by:

$$\epsilon_f = \frac{\epsilon}{\delta\theta} \cong \frac{\partial\alpha}{\partial\theta} - 1 \quad (\text{K-6})$$

Differentiating (K-4), after rewriting it in direct trigonometric form, gives:

$$\frac{\partial\alpha}{\partial\theta} = \frac{r^2 + r\psi(\sin\theta + \cos\theta)}{r^2 + 2r\psi(\sin\theta + \cos\theta) + 2\psi^2} \quad (\text{K-7})$$

From (K-6) and (K-7)

$$|\epsilon_f| = \frac{\psi [r(\sin\theta + \cos\theta) + 2\psi]}{r^2 + 2r\psi(\sin\theta + \cos\theta) + 2\psi^2} \quad (\text{K-8})$$

Clearly  $|\epsilon_f|$  is a minimum, i.e., zero, when  $\psi = 0$ . To find its maximum value ( $|\epsilon_f|_{\max}$ ) solve for  $\psi$  when  $\frac{\partial |\epsilon_f|}{\partial \theta} = 0$  corresponding to:

$$\begin{aligned} [r^2 + 2r\psi(\sin\theta + \cos\theta) + 2\psi^2]r(\cos\theta - \sin\theta) = \\ [r(\sin\theta + \cos\theta) + 2\psi]2r\psi(\cos\theta - \sin\theta) \end{aligned}$$

from which:

$$\psi_m = \frac{r}{\sqrt{2}} \quad (K-9)$$

where  $\psi_m$  is the value of  $\psi$  at which  $|\epsilon_f|_{\max}$  occurs.

Substituting from (K-9) for  $\psi$  in (K-8) produces:

$$\begin{aligned} |\epsilon_f|_{\max} &= \frac{r}{\sqrt{2}} \frac{[r(\sin\theta + \cos\theta) + r\sqrt{2}]}{2r^2 + r^2 \cdot 2(\sin\theta + \cos\theta)} \\ &\cong \frac{1}{2} \end{aligned}$$

That is, a maximum error in swept bearing of 50% is possible, regardless of  $\theta$ .



AD-A049 767

RCA ELECTROMAGNETIC AND AVIATION SYSTEMS DIV VAN NUY--ETC F/G 1/2  
BEARING STUDY PROGRAM. (U)

APR 74 E JELLINEK, W KRAM, M LEVINSEN

N62269-73-C-0906

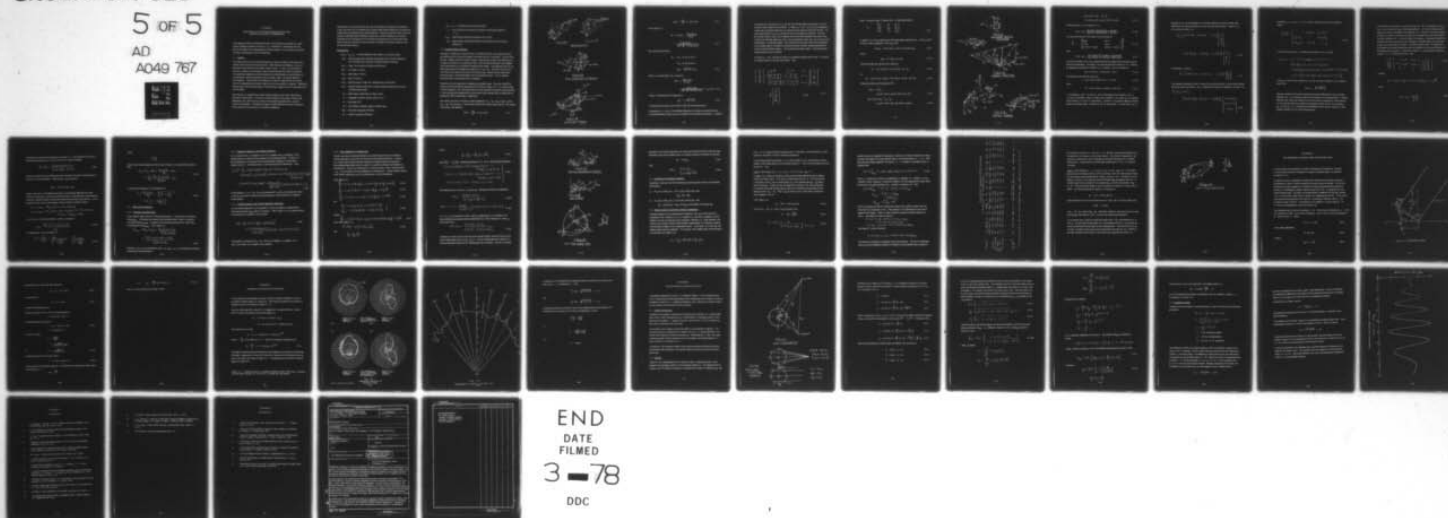
UNCLASSIFIED

RCA-EASD-TP-2146

NL

5 OF 5

AD  
A049 767



END  
DATE  
FILMED  
3-78  
DDC

## APPENDIX L

### DERIVATION OF ALGORITHM FOR MISS DISTANCE AND HORIZONTAL BEARING DETERMINATION

This Appendix provides the detailed derivation of the equations comprising the computational algorithm presented in Section 3.4.2. Additionally, consideration has been given to the effect of not compensating for attitude changes, so as to justify the inclusion of attitude compensation in the miss algorithm.

#### L.1 Abstract

The conflict plane of two aircraft approaching one another is defined as the plane of the relative range and relative velocity vectors. Miss distance is the distance, in the conflict plane, taken normal to the relative velocity vector. As such, the miss distance vector is, in general, not horizontal, but has both horizontal and vertical components. A computational algorithm is derived herein for the determination of miss distance and its components, utilizing sequential relative bearing, range, and altitude difference measurements. The horizontal miss distance may then be compared with a threshold value and an appropriate horizontal maneuver may be commanded, if required. Additionally, bearing angle in the horizontal plane can be determined, taking account of (measured) pitch and roll angles.

Miss distance, as computed from swept bearing, depends on the actual angle between successive range vectors. To obtain an accurate measure of this angle, attitude angle differences (yaw, pitch and roll), taken at the successive sampling times, must be measured and inputted. The effects of neglect of these differences has been considered in this analysis, and are shown to be relatively significant.

Expressions for hazard predictors other than miss distance components are presented, to show how these may be computed from bearing/range/altitude difference measurements. These evaluators include time-to-closest approach, minimum horizontal range, separation distance at specified altitude difference penetration, and time difference and vertical separation at the crossing point of the horizontal projections of the aircraft flight paths. These alternative evaluators could conceivably be utilized in horizontal maneuver logic for decision and command.

Nomenclature:

$\Delta h(t_1) = h_B - h_S =$  altitude difference with respect to own altitude (feet)

$\beta(t_1) =$  bearing angle; angle in antenna ground plane from aircraft longitudinal axis to projection of range line; measured positive clockwise

$R(t_1) =$  range, own aircraft to intruder aircraft (feet)

$\psi(t_1) =$  yaw angle, at time  $t_1$

$P(t_1) =$  pitch angle, at time  $t_1$

$r(t_1) =$  angle, at time  $t_1$

$E(t_1) =$  elevation angle of range line, determined in vertical plane

$\epsilon(t_1) =$  elevation angle of range line, in plane containing range line and normal to antenna ground plane

$\delta_{12} =$  angle between range lines at times  $t_1$  and  $t_2$

$V_R =$  magnitude of relative velocity vector (f.p.s.)

$\gamma_v =$  path angle of  $\bar{V}_R$

$M =$  miss distance; shortest range to intruder (feet)

$M_H =$  horizontal component of  $\bar{M}$  (feet)

$M_v =$  vertical component of  $\bar{M}$  (feet)

$\Delta t_{12} = t_2 - t_1$ , estimation time interval (seconds)

$t_1$  = time at which  $\beta_1$  is estimated (mid-point of track pulse sequence);

$i = 1, 2$

$\delta_{12H}$  = angle between horizontal projections of  $R_1$  and  $R_2$

$\theta_s$  = angle between horizontal projections of range line and aircraft longitudinal axis

## L.2 Horizontal Miss Component

In general, if either one or both aircraft, in a conflict situation, are maneuvering; then the relative path of the one with respect to the other will be a curved path. The true miss distance, defined as shortest relative range, is found along a normal to the relative path. If range is measured at two consecutive times, then the normal distances to the tangents of the relative path may be defined as projected miss values. The projected miss may be either decreasing or increasing (See Figures L-1a and L-1b). The miss value to be derived will be that based on the chord of the relative path, between the two range lines, and hence gives a value intermediate to the two projected misses. If  $\bar{V}_r$  is constant, determined miss and projected miss are identical.

The plane of the two range lines is defined as the conflict plane. The miss vector  $\bar{M}$  is normal to the line joining the end points of  $\bar{R}_1$  and  $\bar{R}_2$  (see Figure L-2). If a vertical plane is drawn through  $\bar{V}_r$ , and a horizontal plane is drawn through the protected aircraft position S, then vertical miss component  $M_v$  and horizontal miss component  $M_H$  are defined as the components of  $\bar{M}$  in these planes, respectively.

The intruder aircraft B is located at altitude difference  $\Delta h_1 = (h_B - h_S)_1$  at time  $t_1$  and at  $\Delta h_2 = (h_B - h_S)_2$  at time  $t_2$ . The elevation angles of the relative range vectors, with respect to horizontal, are defined by

$$\sin E_1 = \frac{\Delta h_1}{R_1}; \quad 0 \leq |E_1| \leq 90^\circ \quad (L-1)$$



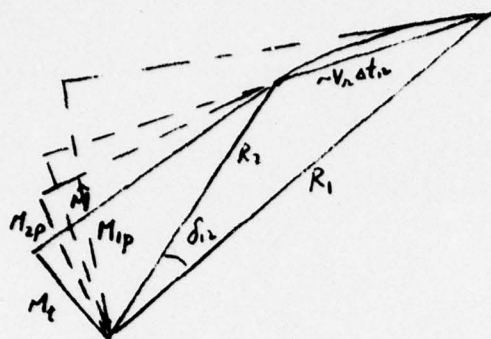


FIG. L-1a

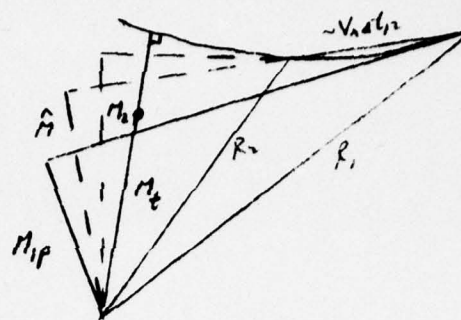


FIG. L-1b

PROJECTED MISS

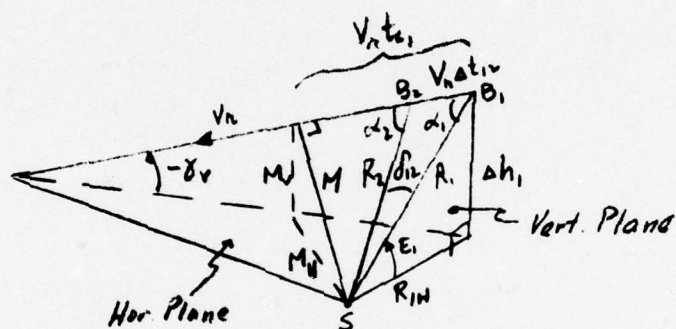


FIG. L-2

THREE-DIMENSIONAL MISS GEOMETRY

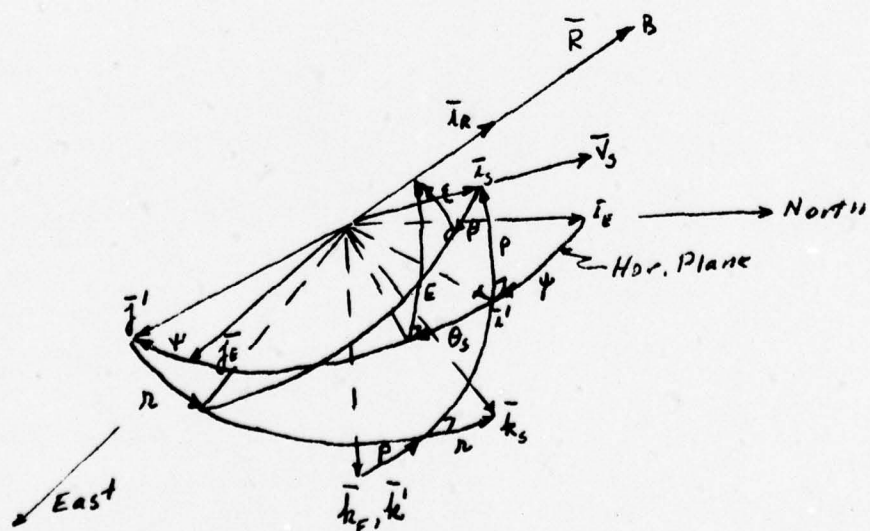


FIG. L-3

ATTITUDE ANGLES

$$\sin E_2 = \frac{\Delta h_2}{R_2} ; 0 \leq |E_2| \leq 90^\circ \quad (\text{L-2})$$

From Figure L-2,

$$\begin{aligned} M &= R_1 \sin \alpha_1 = \frac{R_1 R_2 \sin \delta_{12}}{V_r \Delta t_{12}} \\ &= \frac{R_1 R_2 \sin \delta_{12}}{\sqrt{R_1^2 + R_2^2 - 2 R_1 R_2 \cos \delta_{12}}} \end{aligned} \quad (\text{L-3})$$

The vertical component is

$$\begin{aligned} M_v &= \Delta h_1 + R_1 \cos \alpha_1 \sin \gamma_v \\ &= \Delta h_2 + R_2 \cos \alpha_2 \sin \gamma_v \\ &= \Delta h_2 + \sqrt{R_2^2 - M^2} \sin \gamma_v \end{aligned} \quad (\text{L-4})$$

where  $\gamma_v$ , the path angle of  $\bar{V}_r$ , is given by

$$\begin{aligned} \sin \gamma_v &= \frac{(\Delta h_2 - \Delta h_1)}{V_r \Delta t_{12}} \\ &= \frac{(\Delta h_2 - \Delta h_1)}{\sqrt{R_1^2 + R_2^2 - 2 R_1 R_2 \cos \delta_{12}}} ; 0 \leq |\gamma_v| \leq 90^\circ \end{aligned} \quad (\text{L-5})$$

Finally, the horizontal miss component is

$$M_H = \pm \sqrt{M^2 - M_v^2} \quad (\text{L-6})$$

(A discussion of the sign to be ascribed to  $M_H$  will be presented later.)

In Equations L-3, -4 and -5, the altitude differences and ranges are obtained directly by measurements; the angle  $\delta_{12}$  must be deduced from bearing measurements. In general,

the aircraft body axis system  $\bar{i}_S, \bar{j}_S, \bar{k}_S$  will have attitude angles with respect to a local vertical system centered at the aircraft. In Figure L-3, let  $\bar{i}_E, \bar{j}_E, \bar{k}_E$  be the topographic system with  $\bar{i}_E$  directed northward,  $\bar{j}_E$  eastward and  $\bar{k}_E$  along the downward vertical. The Euler angle sequence  $\psi$  (yaw),  $p$  (pitch) and roll ( $r$ ) are defined as indicated. Note that the aircraft velocity vector ( $\bar{V}_S$ ) is aligned with the aircraft longitudinal axis only if angle of attack and side-slip angles are zero or can be neglected; in that case, yaw is synonymous with heading, as ordinarily defined. The orientation of the range vector  $\bar{i}_R$  is determined by the bearing angle  $\beta$ , measured in the pitch-roll plane (actually antenna ground-plane) and the vertical elevation angle  $E$ . The cross-plane elevation angle  $\epsilon$ , and the horizontal bearing angle  $\theta_S$  must be deduced.

To obtain  $\delta_{12}$ ,  $\epsilon$ ,  $\theta_S$ , use must be made of a coordinate transformation matrix,  $D$ , relating the vertical system to the body axis system. Thus

$$\begin{bmatrix} \bar{i}_S \\ \bar{j}_S \\ \bar{k}_S \end{bmatrix} = \begin{bmatrix} c\psi & s\psi & -sp \\ s\psi & c\psi & sp \\ -c\psi & s\psi & cp \end{bmatrix} \begin{bmatrix} \bar{i}_E \\ \bar{j}_E \\ \bar{k}_E \end{bmatrix} \quad (L-7)$$

$$= \hat{D} \begin{bmatrix} \bar{i}_E \\ \bar{j}_E \\ \bar{k}_E \end{bmatrix}$$



(Note: C denotes cosine, S denotes sine). In shorthand notation,

$$\widehat{D} = \begin{bmatrix} d_{11} & d_{12} & d_{13} \\ d_{21} & d_{22} & d_{23} \\ d_{31} & d_{32} & d_{33} \end{bmatrix} \quad (L-8)$$

In Figure L-4, let  $\delta_{12H}$  represent the horizontal angle projection of  $\delta_{12}$ . Thus  $\delta_{12}$  could be found, albeit ambiguously, from  $\delta_{12H}$ , since

$$\cos \delta_{12} = \sin E_1 \sin E_2 + \cos E_1 \cos E_2 \cos \delta_{12H} \quad (L-9)$$

where

$$\delta_{12H} = (\psi + \theta_S)_2 - (\psi + \theta_S)_1 \quad (L-10)$$

The line-of-sight unit vector can be written as

$$\bar{i}_R = \cos \epsilon \cos \beta \bar{i}_S + \cos \epsilon \sin \beta \bar{j}_S - \sin \epsilon \bar{k}_S \quad (L-11)$$

or

$$\bar{i}_R = \cos E \cos (\psi + \theta_S) \bar{i}_E + \cos E \sin (\psi + \theta_S) \bar{j}_E - \sin E \bar{k}_E \quad (L-12)$$

Taking dot products and making use of  $\widehat{D}$ ,

$$\begin{aligned} -\sin E &= \bar{i}_R \cdot \bar{k}_E \\ &= d_{13} \cos \epsilon \cos \beta + d_{23} \cos \epsilon \sin \beta - d_{33} \sin \epsilon \end{aligned} \quad (L-13)$$

$$\begin{aligned} \cos E \sin (\psi + \theta_S) &= \bar{i}_R \cdot \bar{j}_E \\ &= d_{12} \cos \epsilon \cos \beta + d_{22} \cos \epsilon \sin \beta - d_{32} \sin \epsilon \end{aligned} \quad (L-14)$$



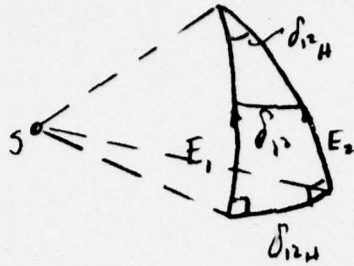


FIG. L-4  
HORIZONTAL BEARING  
DIFFERENCE

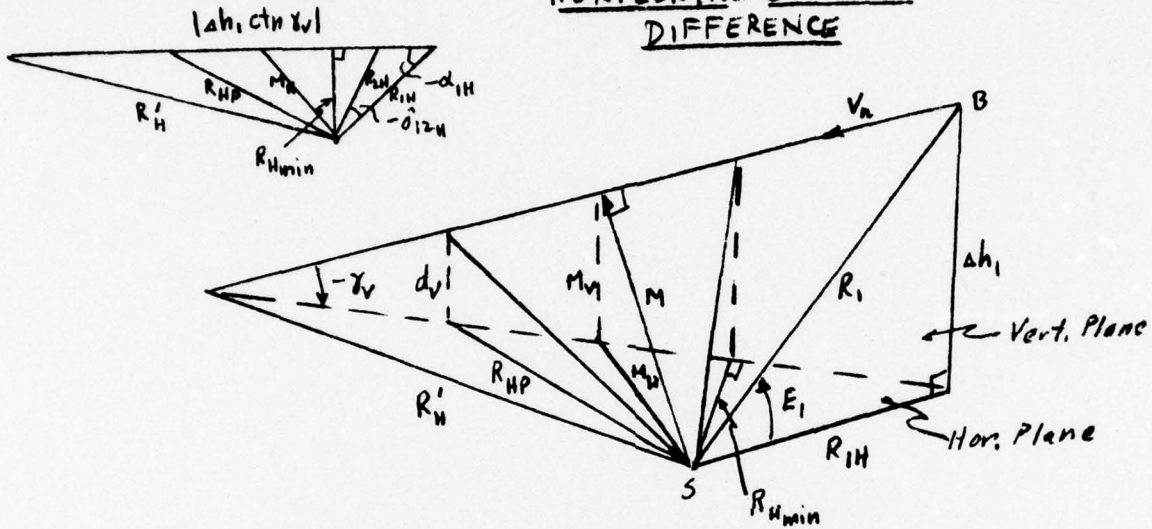


FIG. L-5  
HAZARD PREDICTORS

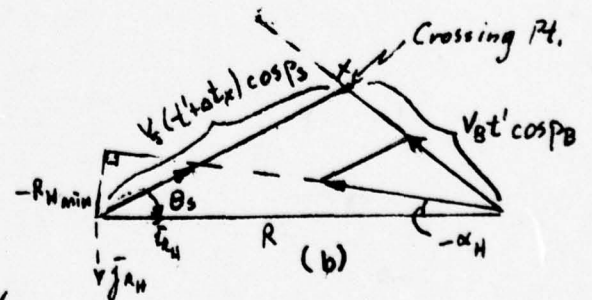
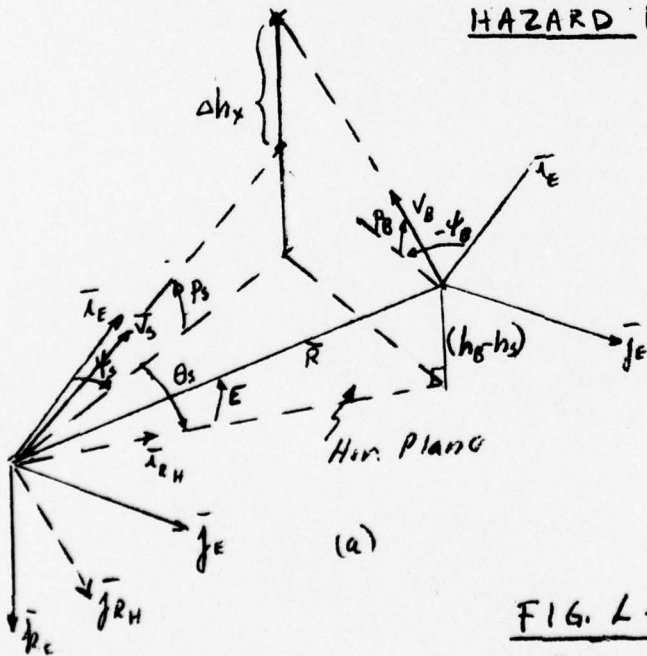


FIG. L-6  
CONFLICT GEOMETRY

$$\begin{aligned}\cos E \cos (\psi + \theta_S) &= \bar{i}_R \cdot \bar{i}_E \\ &= d_{11} \cos \epsilon \cos \beta + d_{21} \cos \epsilon \sin \beta - d_{31} \sin \epsilon\end{aligned}\quad (L-15)$$

Dividing Equation L-14 by Equation L-15,

$$\tan (\psi + \theta_S) = \frac{(d_{12} \cos \beta + d_{22} \sin \beta) \cos \epsilon - d_{32} \sin \epsilon}{(d_{11} \cos \beta + d_{21} \sin \beta) \cos \epsilon - d_{31} \sin \epsilon} \quad (L-16)$$

For small pitch and roll, the matrix D can be written as

$$\widehat{D} \approx \begin{bmatrix} \cos \psi & \sin \psi & -p \\ -\sin \psi & \cos \psi & r \\ (p \cos \psi + r \sin \psi) & (p \sin \psi - r \cos \psi) & 1 \end{bmatrix} \quad (L-17)$$

Then

$$\tan (\psi + \theta_S) \approx \frac{\cos \epsilon \sin (\psi + \beta) - (p \sin \psi - r \cos \psi) \sin \epsilon}{\cos \epsilon \cos (\psi + \beta) - (p \cos \psi + r \sin \psi) \sin \epsilon} \quad (L-18)$$

in which the quadrant of  $(\psi + \theta_S)$  is determined from the signs of the numerator and denominator expressions. The angle  $\epsilon$  can be determined from Equation L-13. Utilizing the approximate elements in Equation L-17, Equation L-13 can be written as

$$\sin \epsilon + (p \cos \beta - r \sin \beta) \cos \epsilon = \sin E \quad (L-19)$$

The solution to this equation is given by

$$\epsilon = \sin^{-1} [\sin E \cos \theta] - \theta; \quad 0 \leq |\epsilon| \leq 90^\circ \quad (L-20)$$

where

$$\theta = \tan^{-1} [p \cos \beta - r \sin \beta]; \quad 0 \leq |\theta| \leq 90^\circ. \quad (L-21)$$

To recapitulate, with  $\epsilon$  (at times  $t_1$  and  $t_2$ ) determined from Equation L-20,  $\psi + \theta_S$  can be obtained, at the two times, from Equation L-18; thence  $\delta_{12}$  are obtained from Equation L-10 and L-9 respectively. Equation L-18 requires inputs of attitude angles and bearing angle, measured at the two time points. A more direct way of

obtaining  $\cos \delta_{12}$  can be developed, the resulting expression involving attitude angle differences only; hence providing for a more accurate determination. Equation L-11 can be written at time  $t_1$ , as

$$\begin{aligned} \bar{\lambda}_{R_1} &= \begin{bmatrix} \cos \epsilon_1 \cos \beta_1 & \cos \epsilon_1 \sin \beta_1 & -\sin \epsilon_1 \end{bmatrix} \begin{bmatrix} \bar{\lambda}_s \\ \bar{f}_s \\ \bar{h}_s \end{bmatrix} \\ &= \begin{bmatrix} \cos \epsilon_1 \cos \beta_1 & \cos \epsilon_1 \sin \beta_1 & -\sin \epsilon_1 \end{bmatrix} \bar{D}_1 \begin{bmatrix} \bar{\lambda}_E \\ \bar{f}_E \\ \bar{h}_E \end{bmatrix} \end{aligned} \quad (\text{L-22})$$

and similarly, at time  $t_2$ ,

$$\bar{\lambda}_{R_2} = \begin{bmatrix} \cos \epsilon_2 \cos \beta_2 & \cos \epsilon_2 \sin \beta_2 & -\sin \epsilon_2 \end{bmatrix} \bar{D}_2 \begin{bmatrix} \bar{\lambda}_E \\ \bar{f}_E \\ \bar{h}_E \end{bmatrix} \quad (\text{L-23})$$

(The change in orientation of the E system, due to aircraft velocity, can be safely ignored during the short time interval,  $\Delta t_{12}$ .) Taking the dot product of Equations L-22 and L-23,

$$\begin{aligned} \bar{\lambda}_{R_1} \cdot \bar{\lambda}_{R_2} &= \cos \delta_{12} \\ &= \begin{bmatrix} \cos \epsilon_1 \cos \beta_1 & \cos \epsilon_1 \sin \beta_1 & -\sin \epsilon_1 \end{bmatrix} \bar{D}_1 \bar{D}_2^T \begin{bmatrix} \cos \epsilon_2 \cos \beta_2 \\ \cos \epsilon_2 \sin \beta_2 \\ -\sin \epsilon_2 \end{bmatrix} \end{aligned} \quad (\text{L-24})$$

Assuming  $\psi_2 - \psi_1$ ,  $p_1$ ,  $p_2$ ,  $r_1$ ,  $r_2$  to be small, couplet products can be neglected, whence

$$\hat{D}_1 \hat{D}_2^T \approx \begin{bmatrix} 1 & -(\psi_2 - \psi_1) & (p_2 - p_1) \\ (\psi_2 - \psi_1) & 1 & -(\lambda_2 - \lambda_1) \\ -(p_2 - p_1) & (\lambda_2 - \lambda_1) & 1 \end{bmatrix} \quad (\text{L-25})$$

a skew-symmetric matrix. Utilizing this in Equation L-24, we obtain

$$\begin{aligned} \cos \delta_{12} = & \cos \epsilon_1 \cos \epsilon_2 \cos(\beta_2 - \beta_1) + \sin \epsilon_1 \sin \epsilon_2 \\ & - (\psi_2 - \psi_1) \cos \epsilon_1 \cos \epsilon_2 \sin(\beta_2 - \beta_1) \\ & + (p_2 - p_1) [\sin \epsilon_1 \cos \epsilon_2 \cos \beta_2 - \sin \epsilon_2 \cos \epsilon_1 \cos \beta_1] \\ & + (\lambda_2 - \lambda_1) [\sin \epsilon_2 \cos \epsilon_1 \sin \beta_1 - \sin \epsilon_1 \cos \epsilon_2 \sin \beta_2] \end{aligned} \quad (\text{L-26})$$

Taking  $\delta_{12}$  to have no sign ascribed to it,  $\sin \delta_{12}$ , for use in Equation L-3, is obtained simply from

$$\sin \delta_{12} = \sqrt{1 - \cos^2 \delta_{12}}$$

Note that, except for the terms involving pitch and roll differences, only the bearing difference ( $\beta_2 - \beta_1$ ) is needed and this can be supplied as an accurate quantity. Although functions of  $\beta_1$  and  $\beta_2$  are needed for the last two terms in Equation 26, these need not be very accurate since they multiply the necessarily small (in time  $\Delta t_{12}$ ) quantities ( $p_2 - p_1$ ) and ( $r_2 - r_1$ ). The pitch and roll difference terms cannot, however, be neglected all together as will be demonstrated later.



In accordance with convention,  $M_H$  takes the sign of  $\dot{\psi} + \dot{\theta}_S$ , or equivalently, of  $\delta_{12H}$ ; that is,  $M_H$  is positive if  $\delta_{12H}$  is increasing positively.  $(\psi + \theta_S)$  is obtainable unambiguously at the two time points, from Equation L-18. However, for maneuver logic,  $\theta_S$  itself may need to be extracted, and this can be obtained in a more direct fashion than from Equation L-18. (In the NRL logic, for example, a knowledge of whether the intruder is in the forward or rearward hemisphere is needed; hence, for such logic,  $\theta_S$  need not be determined accurately. In another proposed logic, the magnitude of the absolute line-of-sight turning rate must be increased, so that  $\theta_S$  would need to be determined more accurately.) Referring to Figure L-3, let an auxiliary coordinate system  $\bar{i}', \bar{j}', \bar{k}'$  be defined as shown. Thus

$$\begin{bmatrix} \bar{i}' \\ \bar{j}' \\ \bar{k}' \end{bmatrix} = \begin{bmatrix} \cos \psi & \sin \psi & 0 \\ -\sin \psi & \cos \psi & 0 \\ 0 & 0 & 1 \end{bmatrix} \begin{bmatrix} \bar{i}_E \\ \bar{j}_E \\ -\bar{k}_E \end{bmatrix} \quad (L-27)$$

Evidently,

$$\bar{i}_R = \cos E \cos \theta_S \bar{i}' + \cos E \sin \theta_S \bar{j}' - \sin E \bar{k}'$$

so that

$$\tan \theta_S = \frac{\bar{i}_R \cdot \bar{j}'}{\bar{i}_R \cdot \bar{i}'} \quad (L-28)$$

Substituting the expression for  $\bar{i}_R$  given by Equation L-11, and utilizing the matrices of direction cosines given by L-17 and L-27 into L-28, there is obtained

$$\tan \theta_s = \frac{\cos \epsilon \sin \beta + \lambda \sin \epsilon}{\cos \epsilon \cos \beta - \rho \sin \epsilon} \quad (\text{L-29})$$

wherein the quadrant of  $\theta_s$  is determined from the signs of numerator and denominator, since  $\cos \epsilon$  is always positive. Evidently then,  $\delta_{12H}$  is given by

$$\delta_{12H} = (\psi_2 - \psi_1) + (\theta_{s2} - \theta_{s1})$$

Finally, with ANTC-117 modified threat logic, if both altitude difference and range alarm have been given, the computed horizontal miss is compared with a miss threshold value  $M_T$ . Maneuver alerts or commands would be given if  $M_H$  is less than  $M_T$ . In one proposed scheme,  $M_T$  is made adaptive, being a function of relative velocity:

$$\text{At } \tau_2 \text{ alarm : } M_{T_2} (ft.) = 11,200 + 4.73 V_R$$

$$\begin{aligned} \text{At } \tau_1 \text{ alarm : } M_{T_1} (ft.) &= 1700 + 4.14 V_R, \text{ for } M_{T_1} > 3038 \text{ ft.} \\ &= 3038, \text{ if } (M_{T_1})_{comp} < 3038 \end{aligned}$$

$V_R$  is in f.p.s. in the above formulae, where  $V_R$  is given by

$$V_R = \frac{\sqrt{R_1^2 + R_2^2 - 2R_1R_2 \cos \delta_{12}}}{\Delta t_{12}} \quad (\text{L-30})$$

or alternatively, if  $\dot{R}$  is measured, by

$$V_R = \frac{-\dot{R}}{\cos \alpha} = \frac{-\dot{R}}{\sqrt{1 - \left(\frac{M}{R}\right)^2}} = \frac{R}{\tau \sqrt{1 - \left(\frac{M}{R}\right)^2}} \quad (\text{L-31})$$

where

$$\tau \triangleq \frac{\Delta}{-\dot{R}}$$

If true time-to-closest approach (time-to-go) is desired, say measured from point 2, then,

$$\begin{aligned} t_{c2} &= t_{c1} - \Delta t_{12} = \frac{R_1 \cos \alpha_1}{V_h} - \Delta t_{12} \\ &= \frac{R_1}{V_h} \frac{[R_1 - R_2 \cos \delta_{12}]}{(V_h \Delta t_{12})} - \Delta t_{12} \end{aligned} \quad (\text{L-32})$$

An alternative expression, if  $\dot{R}$  is measured, is

$$\begin{aligned} t_{c2} &= \frac{R_2 \cos \alpha_2}{V_h} = \frac{R}{V_h} \sqrt{1 - \left(\frac{M}{R_2}\right)^2} \\ &= \tau_2 \left[ 1 - \left(\frac{M}{R_2}\right)^2 \right] \end{aligned} \quad (\text{L-33})$$

### L.3 Other Threat Evaluators

#### L.3.1 Minimum Horizontal Range

Every relative range vector has a horizontal projection. Just as there is a minimum range  $R_{\min} = M$  between the protected and intruding aircraft, there is a minimum horizontal distance  $R_{H\min}$ . In general, the horizontal projection of  $M$ , namely  $M_H$ , is not identical with  $R_{H\min}$ . From Figure L-5,

$$\begin{aligned} R_{H\min} &= R_{1H} \sin \alpha_{1H} = \frac{R_{1H} R_{2H} \sin \delta_{12H}}{V_h \Delta t_{12} \cos \gamma_V} \\ &= \frac{R_1 R_2 \cos E_1 \cos E_2 \sin \delta_{12H}}{V_h \Delta t_{12} \cos \gamma_V} \end{aligned} \quad (\text{L-34})$$

wherein  $R_1$ ,  $R_2$ ,  $\Delta t_{12}$  are measured, and  $E_1$ ,  $E_2$ ,  $\delta_{12H}$ ,  $V_r$ ,  $\gamma_V$  are obtained by utilization of previously derived equations.

### L.3.2 Separation Distance at Own Altitude Penetration

If  $\Delta h_1$  is positive and  $\gamma_v$  is negative, or if  $\Delta h_1$  is negative and  $\gamma_v$  is positive, the intruding aircraft can attain the same altitude as the protected aircraft. In Figure L-5, this is indicated by the piercing of the horizontal plane containing S by the relative velocity vector  $\bar{V}_r$ . The distance from S to the piercing point is denoted  $R_H$ . Then:

$$\begin{aligned} (R'_{1H})^2 &= R_{1H}^2 + (\Delta h_1 \cot \gamma_v)^2 + 2 R_{1H} \Delta h_1 \cot \gamma_v \cos \alpha_H \\ &= (R_1 \cos E_1)^2 + (\Delta h_1 \cot \gamma_v)^2 + 2 R_1 \cos E_1 \cdot \Delta h_1 \cot \gamma_v \cdot \frac{[R_1 \cos E_1 - R_2 \cos E_2 \cos \delta_{12H}]}{V_h \Delta t_{12} \cos \gamma_v} \\ &= (R_1 \cos E_1)^2 + (\Delta h_1 \cot \gamma_v)^2 + \frac{2 R_1 \Delta h_1 \cos E_1}{(\Delta h_2 - \Delta h_1)} [R_1 \cos E_1 - R_2 \cos E_2 \cos \delta_{12H}] \end{aligned} \quad (L-35)$$

In this equation,  $R_1$ ,  $R_2$ ,  $\Delta h_1$ ,  $\Delta h_2$  are measured and  $E_1$  and  $E_2$  are derived from these.  $\gamma_v$  and  $\delta_{12H}$  are given by previously derived equations, and are functions of measured bearing angles.

### L.3.3 Horizontal Range at Safe Altitude Difference Penetration

If a safe altitude difference ( $d_v$ ) is specified, it would be necessary to determine the horizontal separation ( $R_{HP}$ ) when  $d_v$  is attained. From Figure L-5, in a manner similar to the derivation of Equation L-35, we obtain

$$\begin{aligned} R_{HP}^2 &= (R_1 \cos E_1)^2 + [(\Delta h_1 - d_v) \cot \gamma_v]^2 \\ &\quad + \frac{2 R_1 (\Delta h_1 - d_v) \cos E_1}{(\Delta h_2 - \Delta h_1)} [R_1 \cos E_1 - R_2 \cos E_2 \cos \delta_{12H}] \end{aligned} \quad (L-36)$$

This equation is valid only if  $d_v < \Delta h_1$ , when  $\Delta h_1$  is positive,  $\gamma_v$  negative, or if  $|d_v| < |\Delta h_1|$  when  $\Delta h_1$  is negative and  $\gamma_v$  positive.



### L.3.4 Time Difference to Crossing Point

Thus far only hazard evaluators defined by the conflict plane have been considered. Criteria presently in use by the FAA involve the actual spatial geometry. In Figure L-6, assume that the ground speed of aircraft B is greater than that of aircraft S. The projected flight paths cross at the point X, aircraft B arriving over this point before aircraft S. That is, if B takes time  $t'$  to arrive at point X, then A will take time  $t' + \Delta t_x$ .  $\Delta t_x$  is denoted as the time difference to crossing point. Another useful evaluator is the vertical separation ( $\Delta h_x$ ) of the flight paths, at the crossing point.

From Figure L-6,

$$\frac{\bar{R}}{R} = \cos E \cos(\psi_s + \theta_s) \bar{l}_E + \cos E \sin(\psi_s + \theta_s) \bar{j}_E - \sin E \bar{k}_E \quad (L-37)$$

$$\frac{\bar{V}_s}{V_s} = \cos p_s \cos \psi_s \bar{l}_E + \cos p_s \sin \psi_s \bar{j}_E - \sin p_s \bar{k}_E \quad (L-38)$$

$$\frac{\bar{V}_h}{V_h} = \cos \gamma_v (-\cos \alpha_H \bar{l}_{RH} + \sin \alpha_H \bar{j}_{RH}) - \sin \gamma_v \bar{k}_E. \quad (L-39)$$

But

$$\left. \begin{aligned} \bar{l}_{RH} &= \cos(\psi_s + \theta_s) \bar{l}_E + \sin(\psi_s + \theta_s) \bar{j}_E \\ \bar{j}_{RH} &= -\sin(\psi_s + \theta_s) \bar{l}_E + \cos(\psi_s + \theta_s) \bar{j}_E \end{aligned} \right\} \quad (L-40)$$

whence

$$\frac{\bar{V}_h}{V_h} = -\cos \gamma_v \cos(\psi_s + \theta_s - \alpha_H) \bar{l}_E - \cos \gamma_v \sin(\psi_s + \theta_s - \alpha_H) \bar{j}_E - \sin \gamma_v \bar{k}_E \quad (L-41)$$

Now, from Figure L-6,

$$\bar{R} + \bar{V}_B t' = V_s (t' + \Delta t_x) + \Delta h_x \quad (L-42)$$

But

$$\bar{V}_B = \bar{V}_s + \bar{V}_h$$

so that

$$\overline{R} + \overline{V}_H t' = \overline{V}_S \Delta t_x + \Delta \overline{h}_x \quad (\text{L-43})$$

where  $\overline{\Delta h}_x = -\Delta h_x \overline{k_E}$ . Substituting equations L-37, -38, 41 and equating components,

$$\left. \begin{aligned} R \cos E \cos(\psi_s + \theta_s) - V_H t' \cos \gamma_v \cos(\psi_s + \theta_s - \alpha_H) \\ = V_S \Delta t_x \cos p_s \cos \psi_s \\ R \cos E \sin(\psi_s + \theta_s) - V_H t' \cos \gamma_v \sin(\psi_s + \theta_s - \alpha_H) \\ = V_S \Delta t_x \cos p_s \sin \psi_s \\ R \sin E + V_H t' \sin \gamma_v = V_S \Delta t_x \sin p_s + \Delta h_x \end{aligned} \right\} \quad (\text{L-44})$$

The unknowns in set L-44 are  $t'$ ,  $\Delta t_x$  and  $\Delta h_x$ . Solving for the latter two quantities,

$$\Delta t_x = \frac{-R \cos E \sin \alpha_H}{V_S \cos p_s \sin(\theta_s - \alpha_H)} \quad (\text{L-45})$$

$$\Delta h_x = R \sin E + \frac{R \cos E}{\sin(\theta_s - \alpha_H)} [\sin \theta_s \tan \gamma_v + \sin \alpha_H \tan p_s] \quad (\text{L-46})$$

$R$ ,  $E$ ,  $V_S$ ,  $P_s$  are measured at time  $t_1$  and  $\theta_s$  is determined at  $t_1$  by Equation L-29. Swept bearing measurements enable determination of  $\gamma_v$  from Equation L-5, and  $\alpha_{1H}$  can be found from

$$\tan \alpha_{1H} = \frac{R_2 \cos E_2 \sin \delta_{12H}}{R_1 \cos E_1 - R_2 \cos E_2 \cos \delta_{12H}} \quad (\text{L-47})$$

Equations L-45 and L-46 are valid only if the aircraft velocity vectors do not lie in the same vertical plane; that is, if  $\theta_s - \alpha_H \neq 0$ . For the vertical plane case (Figure L-7), vertical separation of paths at the crossing point has no meaning. However, a relevant

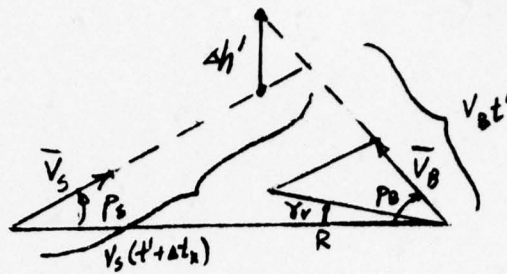


FIG. L-7

VERTICAL SEPARATION AT PASSING

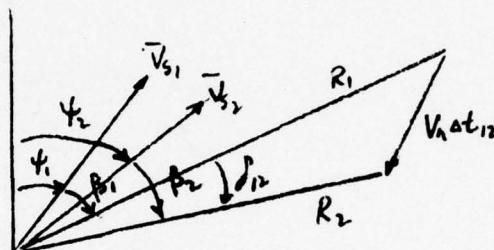


FIG. L-8

YAW EFFECT

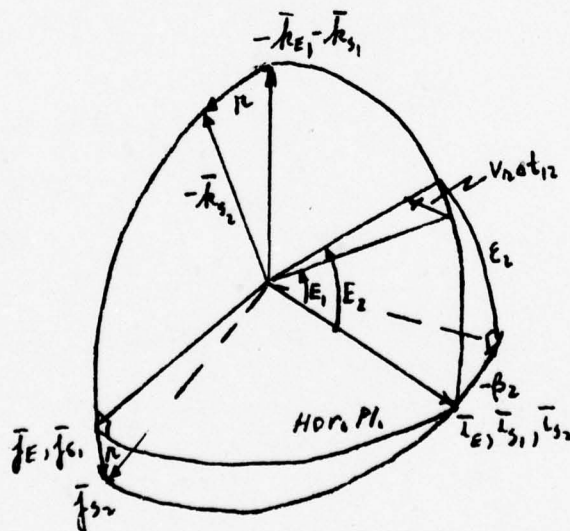


FIG. L-9

CASE 1 ROLL CHANGE ONLY

parameter is the vertical separation ( $\Delta h'$ ) when one aircraft is directly above the other. Derivations will not be provided herein, but results are given to complete the analysis:

$$\Delta h' = R \tan \gamma_v \quad (L-48)$$

Also,

$$\Delta t_x = \frac{R \sin \gamma_v}{V_s \sin (\psi_s + \gamma_v)} \quad (L-49)$$

#### L.4 Comparison of Horizontal Evaluators

Preliminary analysis of the three dimensional conflict geometry leads to the following observations:

- 1) If  $\gamma_v$  pos. and  $M_v$  pos., or if  $\gamma_v$  neg. and  $M_v$  neg.; then

$$R_{Hp} > R_H' > M_H$$

- 2) If  $\gamma_v$  pos. and  $M_v$  neg., or if  $\gamma_v$  neg. and  $M_v$  pos.; then

$$R_H' > M_H \text{ and } R_H' > R_{Hp}, \text{ but } R_{Hp} \text{ can be greater or less than } M_H$$

#### L.5 Effect of Neglect of Roll/Pitch Attitude Compensation

If attitude changes are not accounted for in Equation L-26, there will be errors of computation in  $M$ , Equation L-3, in  $\gamma_v$ , Equation L-5, and in  $M_v$ , Equation L-4; thus leading to an error in horizontal miss component, Equation L-6. Since Equation L-26 would be much simpler without attitude change compensations, it is relevant to inquire into the effect of neglect of the compensation terms. At the outset, it is clear that yaw attitude change cannot be neglected. For example, if the conflict plane were horizontal, we would have (See Figure L-8);

$$\delta_{12} = \delta_{12_H} = (\psi_2 - \psi_1) + (\beta_2 - \beta_1)$$



Thus, a 3° yaw change during the sampling time (~ 5 seconds), if not accounted for, would produce an equivalent 3° error in bearing measurement.

In the ensuing numerical examples,  $\psi_2 - \psi_1$  will be taken as zero, and the effects of pitch change or roll change neglect can be assessed separately. Also,  $\bar{V}_r$  will be taken horizontal, so that  $\Delta h_1 = \Delta h_2$ .

Case 1: Roll Change Only:  $P_1 = P_2 = 0$ ;  $r_1 = 0$ ,  $r_2 = 3^\circ$ ;  $\theta_{s1} = \theta_{s2} = 0$ :

In Figure L-9, assume for simplicity that  $\bar{i}_s$  (own aircraft longitudinal axis) is aligned with  $\bar{i}_E$ , the North vector.  $\bar{V}_r$  is in the  $-\bar{i}_E$  direction so that  $\beta_1 = 0$ . If the aircraft has a roll angle at time  $t_2$ , then a bearing angle,  $\beta_2$ , in the ground plane ( $\bar{i}_{s2} - \bar{j}_{s2}$  plane) will be measured. If pitch and roll are neglected in Equation L-29, this is equivalent to taking the horizontal bearing angle  $\theta_s$  equal to the measured bearing angle  $\beta$ ; introducing an error  $\Delta\theta_s = \beta_2$ . That is,  $\theta_{s2}$  is taken to have a value when it should have been computed to be zero.

From Figure L-9,

$$\beta_2 = \tan^{-1} [-\tan E_2 \sin r_2] \quad (L-50)$$

Also, if  $\Delta h_1 = \Delta h_2$ ,  $R_1$ , and  $V_r \Delta t_{12}$  are given, then

$$E_1 = \sin^{-1} \left[ \frac{\Delta h_1}{R_1} \right] \quad (L-51)$$

$$E_2 = \tan^{-1} \left[ \frac{\Delta h_2}{R_1 \cos E_1 - V_r \Delta t_{12}} \right]; \text{ for } r_v = 0 \quad (L-52)$$

If pitch and roll are neglected in computing  $\epsilon$  (Equation L-19) this is tantamount to taking elevation with respect to the ground plane equal to vertical elevation (i.e.,  $\epsilon \approx E$ ). With pitch and roll changes neglected, and with  $\psi_2 - \psi_1 = 0$ , Equation L-26 would provide, in simplest form:

$$\cos \delta_{12} \Big]_{app.} = \cos E_1 \cos E_2 \cos(\beta_2 - \beta_1) + \sin E_1 \sin E_2 \quad (L-53)$$

With  $\gamma_v = 0$ , there are no errors in computing  $M_v$  in Equation L-4. However,  $V_r \Delta t_{12}$  (Equation L-30),  $M$  (Equation L-3), and  $M_H$  (Equation L-6) have approximate values (hence errors) due to the approximation in  $\delta_{12}$ , as given by Equation L-53. Thus

$$[V_r \Delta t_{12}]_{app.}^2 = R_1^2 + R_2^2 - 2R_1 R_2 \cos \delta_{12} \Big]_{app.}$$

$$M_{app.} = \frac{R_1 R_2 \sin \delta_{12} \Big]_{app.}}{(V_r \Delta t_{12})_{app.}}$$

$$M_{H_{app.}} = \sqrt{M_{app.}^2 - M_v^2}$$

With  $\bar{V}_r$  horizontal and with the conflict plane (plane of  $\bar{R}_1$  and  $\bar{R}_2$ ) vertical, the true horizontal miss component is zero. Thus Equation L-56 represents the error due to neglect of roll change. Table L-1 lists numerical results for selected values of  $R_1$  and  $V_r$ . The range at  $\tau_2$  alarm is given by

$$R_1 (n.m.) = 1.8 + 40 V_r (n.m./sec.) \times \cos E_1$$

$$\approx 1.8 + 40 V_r (knots) / 3600$$

$$R_1 (ft.) = 1.8 \times 6076 + 40 V_r (knots) \times 6076 / 3600$$

The range at  $\tau_1$  alarm is given by

$$R_1 (ft.) \approx .25 \times 6076 + 25 V_r (knots) \times 6076 / 3600$$

The results are presumed to represent worst case situations. The error in horizontal miss may not be considered excessive in relation to miss threshold ( $M_T$ ), except for

TABLE L-1. Miss Error for Roll (or Pitch) Change

( $P_1 = P_2 = R_1 = 0$ ;  $R_2 = 3^\circ$  OR  $R_1 = R_2 = R = 0$ ;  $P_2 = 30^\circ$ )

| CONDITION         | $V_R$<br>(Knots) | $\Delta h = ah$<br>(feet) | $R_1$<br>(feet) | $R_2$<br>(feet) | $V_{at}$<br>(feet) | $E_1$<br>(deg's) | $E_2$<br>(deg's) | $\beta_1$<br>(deg's) | $\beta_2$<br>(deg's) | $\delta_{12}$<br>(deg's) | $\Delta \delta_{12}$<br>(deg's) | $\Delta E_{s_1}$<br>(deg's) | $\Delta M_H$<br>(feet) | $M_T$<br>(feet) |
|-------------------|------------------|---------------------------|-----------------|-----------------|--------------------|------------------|------------------|----------------------|----------------------|--------------------------|---------------------------------|-----------------------------|------------------------|-----------------|
| Low $V_R$         | 59.3             | 1000                      | 5099            | 4610            | 500                | 11.310           | 12.529           | 0                    | -666                 | 1.22                     | .163                            | 0                           | -666                   | 522             |
| $R_1 = .5$ n.mile | 100              | 600                       | 3097            | 2275            | 844                | 11.172           | 15.294           | 0                    | -820                 | 4.122                    | .077                            | 0                           | -820                   | 113             |
| T1 Alarm          | 315              | 600                       | 14810           | 12155           | 2658               | 2.322            | 2.830            | 0                    | -148                 | .508                     | .022                            | 0                           | -148                   | 178             |
| T2 Alarm          | 315              | 600                       | 32203           | 29545           | 2658               | 1.068            | 1.164            | 0                    | -1061                | .296                     | .035                            | 0                           | -1061                  | 554             |
| T2 Alarm          | 315              | 1000                      | 32203           | 29546           | 2658               | 1.780            | 1.940            | 0                    | -102                 | .160                     | .037                            | 0                           | -102                   | 722             |

$\Delta h = 3300^*$

|     |      |       |       |      |       |       |        |        |      |      |        |        |     |
|-----|------|-------|-------|------|-------|-------|--------|--------|------|------|--------|--------|-----|
| 315 | 3300 | 32203 | 29560 | 2658 | 5.882 | 6.410 | 87.982 | 88.119 | .528 | .018 | -1.881 | -2.018 | 855 |
|-----|------|-------|-------|------|-------|-------|--------|--------|------|------|--------|--------|-----|

\* This entry pertains to miss error at high pitch angle, with  $r_1 = r_2 = 0$ ;  $p_1 = 20^\circ$ ,  $p_2 = 17^\circ$

the low relative velocity ( $V_r = 100$  f.p.s.) run. However, the horizontal bearing error is significant at low range, or low relative velocity. With attitude compensation, and assuming an approximate linear relationship of horizontal bearing error to residual attitude error, an imprecision in attitude angle measurement of  $.3^\circ$  to  $.5^\circ$  should be acceptable.

Case 2: Pitch change only.  $r_1 = r_2 = 0$ ;  $p_1 = 0$ ,  $p_2 = 3^\circ$ ;  $\theta_{s1} = \theta_{s2} = 90^\circ$ . The conflict plane geometry is taken as before, with  $\bar{V}_r$  horizontal, but in the vertical plane through  $\bar{j}_E$ ; the aircraft is still aligned initially with  $\bar{i}_E$ , so that  $\beta_1 = 90^\circ$ . The effect of a pitch angle  $p_2$ , at time  $t_2$ , is to make the measured bearing angle  $\beta_2$  different from  $90^\circ$ . If the pitch angle is not accounted for in computing  $\theta_{s2}$ , an error is introduced,  $\Delta\theta_{s2} = \beta_2 - 90$ . Vertical elevation angles  $E_1$  and  $E_2$  are given by Equations L-51 and L-52, as before. The bearing angle  $\beta_2$  (See Figure L-10) is given by

$$\beta_2 = \tan^{-1} [\text{ctn } E_2 \csc P_2]$$

If  $\beta_2'$  represents the value in the previous case ( $3^\circ$  roll), and a  $3^\circ$  pitch is taken, then

$$\tan \beta_2 = -\text{ctn } \beta_2'$$

or  $\beta_2 = 90 + \beta_2'$ , whence  $\Delta\theta_{s2} = \beta_2'$ . Numerical results for  $\Delta\theta_{s2}$  and for  $M_H$  are therefore identical with those for Case 1, for the same conflict plane geometry.

As an extreme case, assume an initial pitch angle of  $20^\circ$ , with a perturbation of  $3^\circ$  at time  $t_2$ . The measured bearing angle at  $t_1$  is then different from  $90^\circ$ , so that there are errors in horizontal bearing angles at both sampling times. Although the error in  $\delta_{12}$  is small, the effect at long range and with substantial true miss ( $M_t = M_v = 3300$  feet) provides a sizeable value of error in horizontal miss component (see Table L-1).





L-24

## APPENDIX M

### TWO-DIMENSIONAL BEARING SITING ERROR DERIVATION

It is the purpose of this appendix to provide a derivation of the expression ( Equation 3.4-15) for phase lag due to reception of an indirect (reflected) signal, as described in Section 3.5.3.1.

In Figure M-1, point A represents an antenna stub viewed in the horizontal (wing) plane and situated on a line PP' which is parallel to the pitch axis of the aircraft. An arriving wavefront of the direct signal has a horizontal (or near horizontal) direction denoted by the line  $S_1A$ , subtending an angle  $\theta_1$  with the normal AN to PP'.  $\theta_1$  represents the true relative bearing angle. The path of an indirect signal is typified by the line  $S_2B$ , parallel to  $S_1A$ , and the line BA which meet at a point B on a reflecting surface RR'. R also designates the point of intersection of RR' with PP', occurring at a distance  $l$  from A. RR' subtends an angle  $\alpha$  with PP'. The direction BA is incident on A with an angle  $\theta_2$ . AC is a line drawn perpendicular to  $S_2B$  and hence to  $S_1A$ .

The expressions for  $\theta_2$  and for the distance  $S = CB + BA$  in terms of the known  $\theta_1$ ,  $\alpha$ , (M-1) and  $l$  will first be found. By the laws of reflection,  $\angle RBA = \angle R'BC$ , which are designated  $\beta$ . Also let  $\angle LAB = \gamma$ . Then:

$$\alpha + \beta + \gamma = 180^\circ \quad (M-2)$$

and by angle supplements

$$\theta_1 + \theta_2 = 2\beta \quad (M-3)$$

Further:

$$\theta_2 + \gamma = 90^\circ \quad (M-4)$$

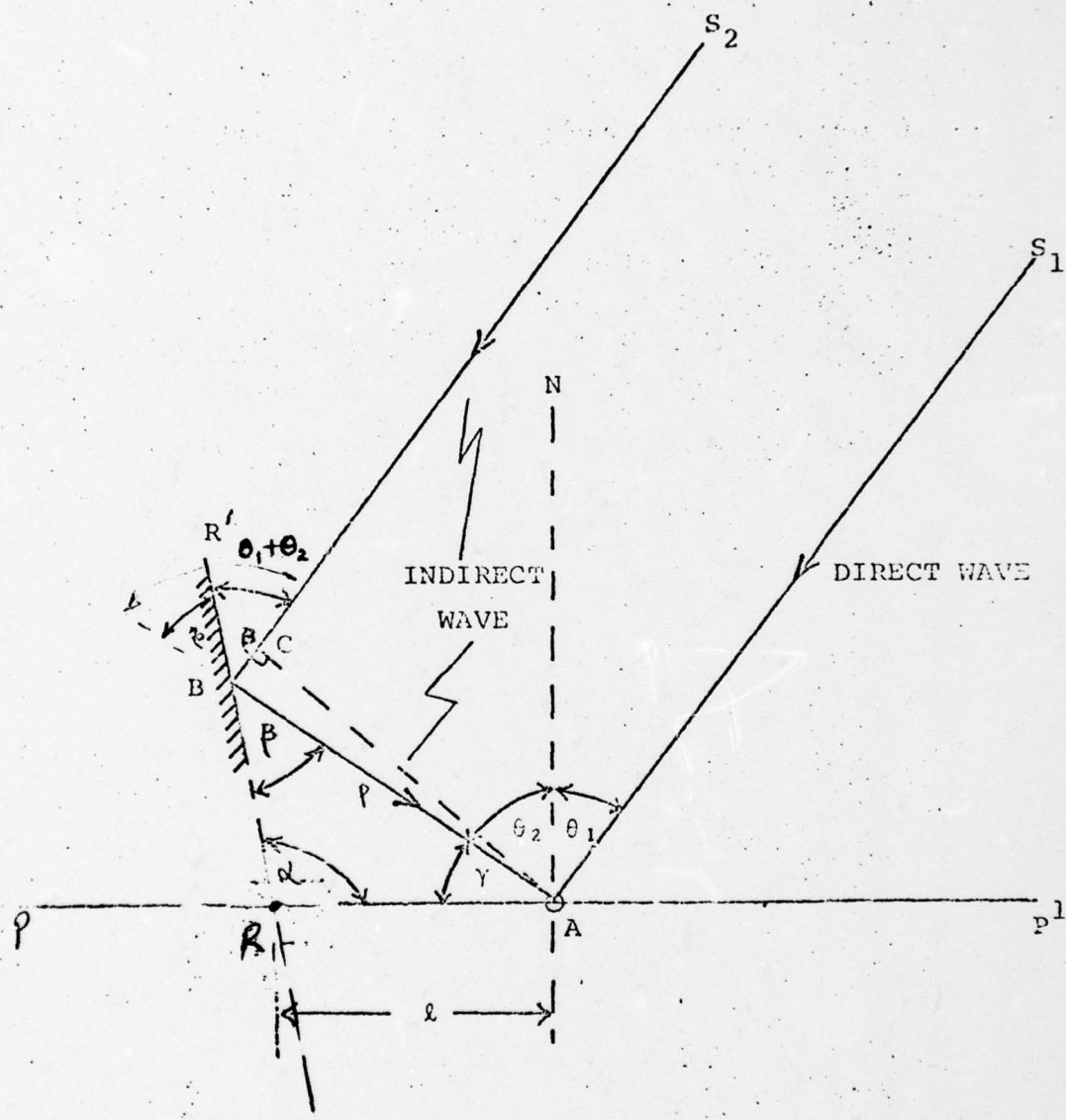


Fig. M-1. Interference Model

Eliminating  $\beta$  and  $\gamma$  from these equations gives

$$\theta_2 = \theta_1 + 2\alpha - 180^\circ \quad (\text{M-5})$$

$\beta$  is expressed by

$$\beta = \theta_1 + \alpha - 90^\circ \quad (\text{M-6})$$

as found on eliminating  $\theta_2$  and  $\gamma$ .

Writing the distance  $AB = p$ , (M-1) can be expressed as:

$$s = p \cos (180^\circ - 2\beta) + p$$

and substituting for  $\beta$  from (M-6)

$$s = p [1 + \cos 2(\theta_1 + \alpha)] \quad (\text{M-7})$$

$$s = 2p \cos^2 (\theta_1 + \alpha)$$

By the law of sines:

$$\begin{aligned} p &= \iota \frac{\sin \alpha}{\sin \beta} \\ &= \iota \frac{\sin \alpha}{\sin (\theta_1 + \alpha - 90^\circ)} \end{aligned}$$

or

$$p = -\iota \frac{\sin \alpha}{\cos (\theta_1 + \alpha)} \quad (\text{M-8})$$

Eliminating  $p$  from (M-7) and (M-8) gives

$$s = 2 \iota \sin \alpha \cos (\theta_1 + \alpha) \quad (\text{M-9})$$

Hence the phase of the indirect signal at A, as referred to the phase of the direct signal arriving there, is:

$$\psi_{12} = \frac{2\pi s}{\lambda}$$



$$\text{i.e.,} \quad \psi_{12} = -\frac{4\pi l}{\lambda} \sin \alpha \cos (\theta_1 + \alpha) \quad (\text{M-10})$$

Where  $\lambda$  is the wavelength of the signal carrier.

## APPENDIX N

### ESTIMATION OF REFLECTOR PARAMETER

It is the purpose of this Appendix to derive a value for reflection coefficient, based on the antenna radiation pattern of a Boeing 707. This value was utilized in the quantitative multipath analysis as presented in Section 3.5.3.1.

Using the model depicted by Figure M-1 in Appendix M, the signal induced in a single stub by the direct and indirect waves acting together is

$$\begin{aligned} e_S &= E_1 \cos \omega t + E_2 \cos (\omega t + \psi_{12}) \\ &= (E_1 + E_2 \cos \psi_{12}) \cos \omega t - (E_2 \sin \psi_{12}) \sin \omega t \end{aligned}$$

The amplitude of  $e_S$  is thus:

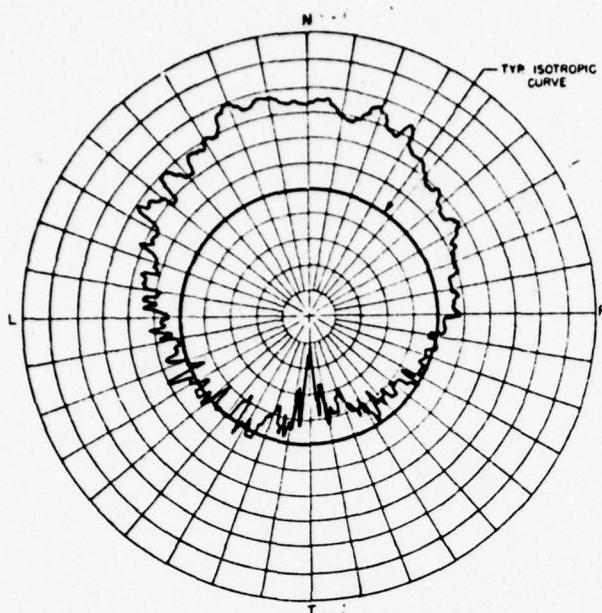
$$E_S = E_1 [(1 + \rho \cos \psi_{12})^2 + (\rho \sin \psi_{12})^2]^{1/2}$$

where  $\rho = \frac{E_2}{E_1}$ , as in Section 3.5.2.1.3. Hence the normalized amplitude  $E'_S$  is:

$$E'_S = \frac{E_S}{E_1} = (1 + 2 \rho \cos \psi_{12} + \rho^2)^{1/2} \quad (N-1)$$

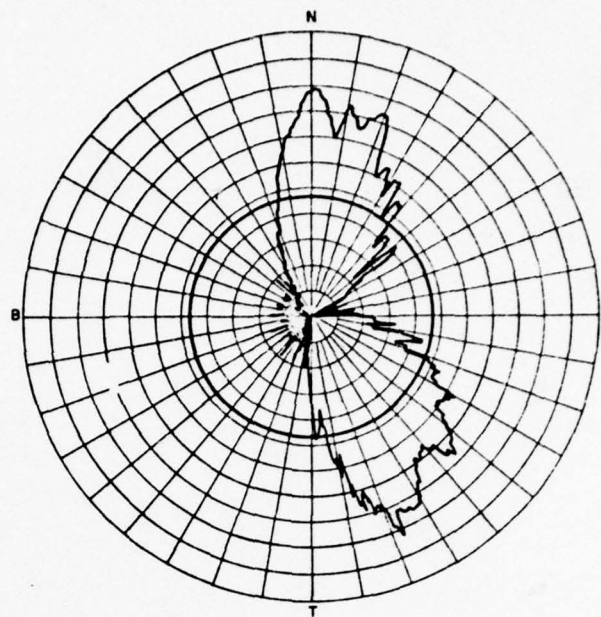
The angular separation between successive maxima depends on the relative bearing angle. This effect is apparent for a sector  $\pm 30^\circ$  about the N (nose) axis of the antenna pattern as shown in the upper left corner of Figure N-1\*. An enlargement for the sector of interest appears in Figure N-2.

\*Shear, W. G. "Elements of the ATA Collision Avoidance System" IEEE Trans. Aerospace and Electronic Systems, Vol. AE 5-4, No. 2, March 1968, pp 395-404.



VARIABLE ANGLE  $\theta(v)$   $\theta(1)$   $0^\circ$   
 CONSTANT ANGLE  $\theta(1)$   $0^\circ$   
 POLARIZATION  $E_\theta(1)$   $E_\theta(v)$   
 $\theta(1)$  HORIZONTAL ANGLE  
 $\theta(v)$  VERTICAL ANGLE  
 CURVE PLOTTED IN VOLTAGE

Fig. 5.

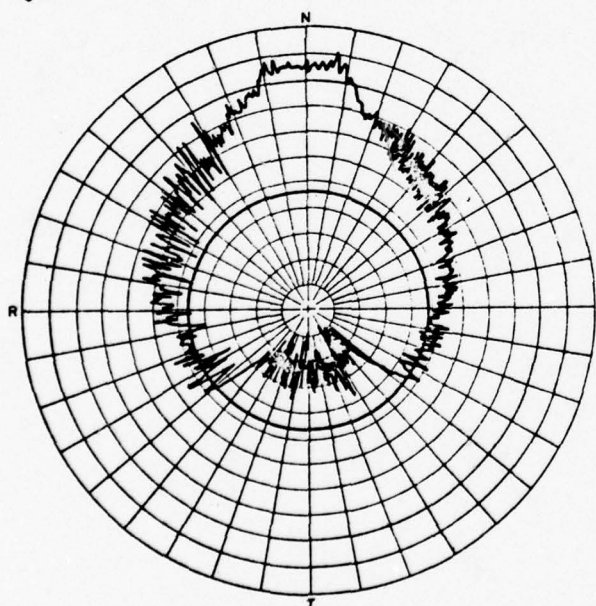


PLANE TYPE 707  
 ANTENNA TYPE L-BAND STUB  
 ANTENNA LOCATION STA. 303-TOP  
 FREQUENCY FULL SCALE 1,000 MC MODEL 25KMC  
 MODEL SURFACE CU

VARIABLE ANGLE  $\theta(1)$   $\theta(v)$   
 CONSTANT ANGLE  $\theta(1)$   $0^\circ$   
 POLARIZATION  $E_\theta(1)$   $E_\theta(v)$   
 $\theta(1)$  HORIZONTAL ANGLE  
 $\theta(v)$  VERTICAL ANGLE  
 CURVE PLOTTED IN VOLTAGE

Fig. 7.

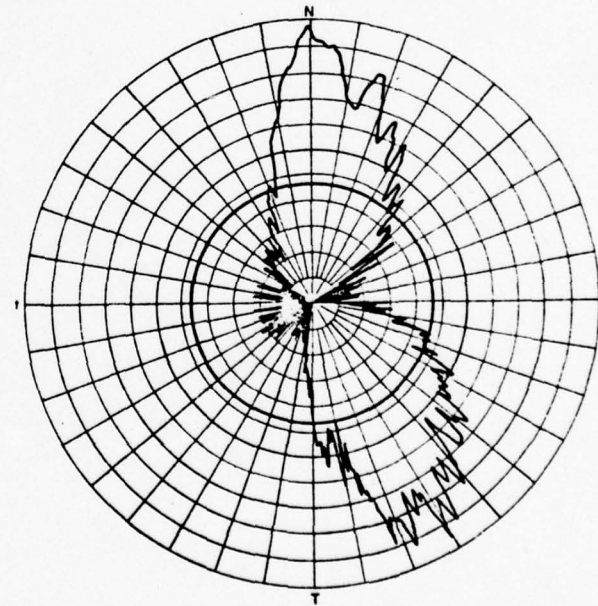
Fig. 6.



VARIABLE ANGLE  $\theta(v)$   $\theta(1)$   $0^\circ$   
 CONSTANT ANGLE  $\theta(1)$   $0^\circ$   
 POLARIZATION  $E_\theta(1)$   $E_\theta(v)$   
 $\theta(1)$  HORIZONTAL ANGLE  
 $\theta(v)$  VERTICAL ANGLE  
 CURVE PLOTTED IN VOLTAGE

PLANE TYPE 707  
 ANTENNA TYPE QUARTER-WAVE STUB  
 ANTENNA LOCATION STA. 247.7 BOTTOM  
 FREQUENCY FULL SCALE 1 KMC MODEL 25KMC  
 MODEL SURFACE COPPER  
 REMARKS LANDING GEAR RETRACTED

Fig. 8.



VARIABLE ANGLE  $\theta(1)$   $\theta(v)$   
 CONSTANT ANGLE  $\theta(1)$   $0^\circ$   
 POLARIZATION  $E_\theta(1)$   $E_\theta(v)$   
 $\theta(1)$  HORIZONTAL ANGLE  
 $\theta(v)$  VERTICAL ANGLE  
 CURVE PLOTTED IN VOLTAGE

# Fig. N-1 Radiation Patterns of Antenna Stubs

SHEAR: ATA COLLISION AVOIDANCE SYSTEM

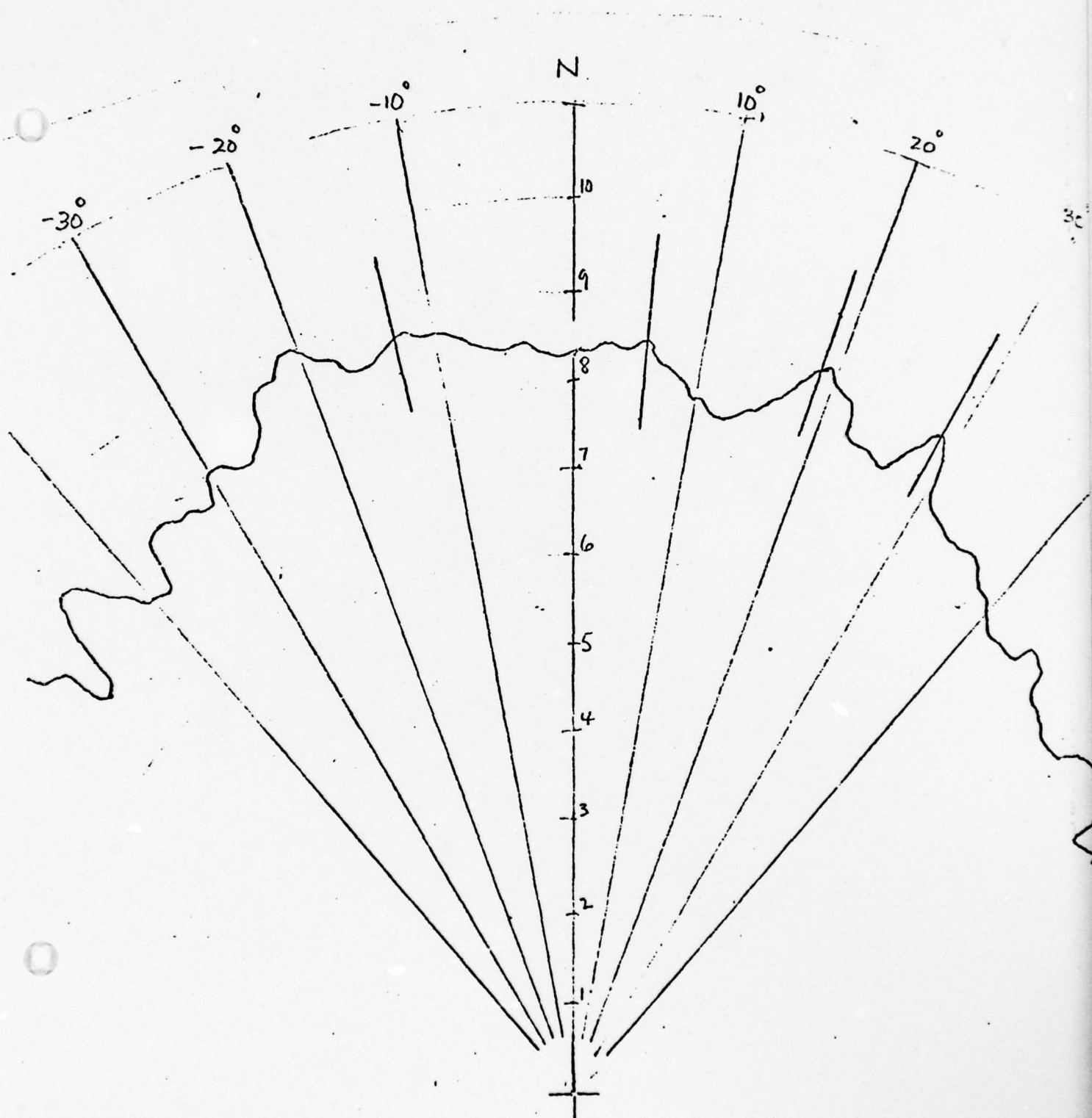


Fig. N-2  
Enlargement of Figure 5 of Fig. N-1  
N-3



An estimate of  $\rho$  is obtained from contiguous maxima and minima of  $E'_S$ , which occur when  $\cos \psi_{12} = \pm 1$  in Equation N-1. Thus

$$E'_S \text{ max} = \sqrt{1 + 2\rho + \rho^2} = 1 + \rho$$

and

$$E'_S \text{ min} = \sqrt{1 - 2\rho + \rho^2} = 1 - \rho$$

Successive minimum and maximum values of the antenna pattern in the region of  $20^\circ$  clockwise from the N axis are 7.75 and 8.60 respectively, so that

$$\frac{1 - \rho}{1 + \rho} = \frac{7.75}{8.60}$$

or

$$\rho = \frac{8.60 - 7.75}{8.60 + 7.75}$$

i.e.,

$$\rho = 0.0513$$

## APPENDIX O

### ANALYTIC MODEL OF MULTIPATH TEST

This appendix supplements Section 4.5.4 (Multipath Effects). It is the purpose herein to use a mathematical model representing the test configuration and to employ the analytic techniques of Section 3.5.2.1 (Ripple and Multipath Error Analysis) to ascertain whether analytic results and tests results can be correlated.

#### O.1 Abstract and Summary

Equations were developed to determine the deviation from linearity (i.e., bearing angle error) when a mode 4 ring antenna array is illuminated by an isotropic emitter, simulating the test condition. A computer run gave a bias error of  $.3^\circ$  and it is shown that this value is confirmed by the test result.

The equations were modified to include the effect of an introduced 5% reflector. The maximum peak error obtained from a computer run was  $1.9^\circ$ , again confirmed by test results when allowance is made for hybrid error. Subtracting the  $.3^\circ$  bias, this result correlates closely with the maximum peak (over frequency and bearing angle) of  $1.4^\circ$  given in Table 3-8 of Section 3.5.2.1.

In conclusion, the quantitative results of this analysis correlate well with test results, and therefore afford credence to the analytic results of the error analysis for the far field model.

#### O.2 Analysis

Figure O-1 is a representation of a 16 element, mode 4, ring antenna array, in the presence of an isotropic emitter E and an isotropic reflector R. The distance from the emitter to the  $j^{\text{th}}$  element is denoted  $d_j$ , the distance from emitter to reflector  $d_{ER}$ , and

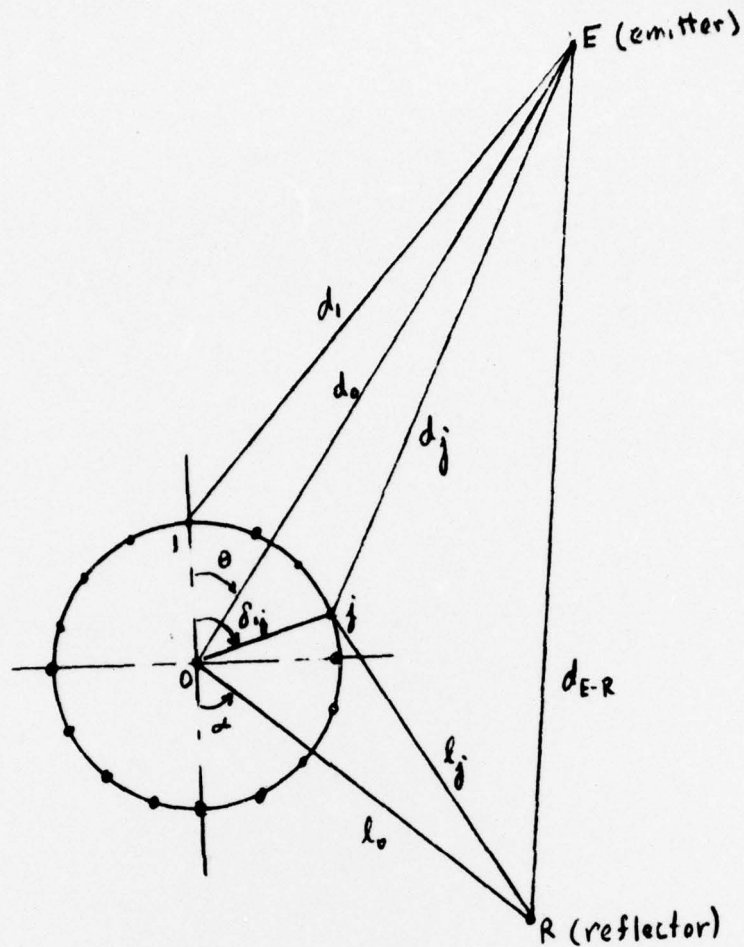
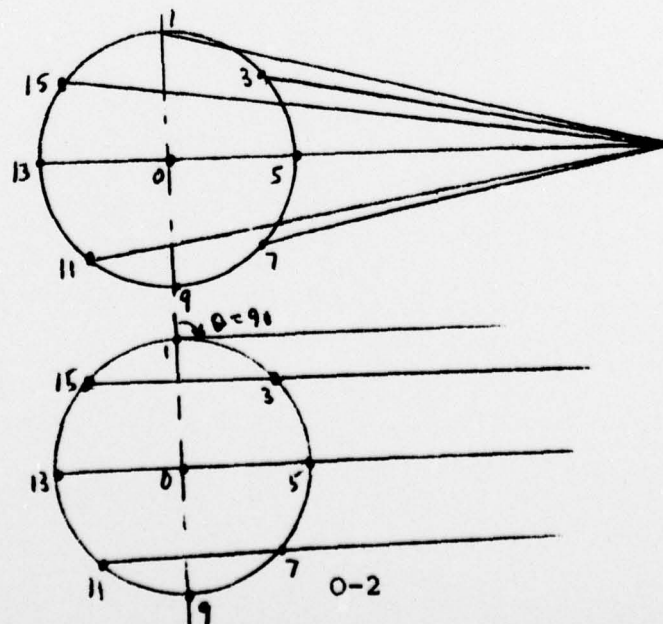


FIG 0-1  
TEST CONFIGURATION



$$\begin{aligned} d_1 - d_3 &\neq -(d_1 - d_{13}) \\ d_1 - d_5 &\neq -(d_1 - d_{15}) \\ d_1 - d_7 &\neq -(d_1 - d_{11}) \end{aligned}$$

$$z_{1,3} = -z_{1,15}$$

$$z_{1,5} = -z_{1,13}$$

$$z_{1,7} = -z_{1,11}$$

FIG 0-2  
NEAR-FIELD  
VS FAR-FIELD  
EMISSION

the distance from reflector to  $j^{\text{th}}$  element  $\iota_j$ . For the signals received at the antenna element as direct waves from the emitter, we have (similar to Equations 3.5-3, 3.5-4, 3.5-8 of Section 3.5.2.1):

$$\iota_1' = E_1 \cos \omega t \quad (\text{O-1})$$

$$\iota_0' = E_1 \cos \left[ \omega t - \frac{2\pi}{\lambda} (d_0 - d_1) \right] \quad (\text{O-2})$$

$$\iota_j' = E_1 \cos \left[ \omega t + \frac{2\pi}{\lambda} (d_1 - d_j) - \frac{\pi(j-1)}{2} \right] . \quad (\text{O-3})$$

Similar to Equations 3.5-22, 3.5-24, 3.5-27, we have for the signals received as reflected waves, and delayed in transmission to common port ( $j^{\text{th}} = 2$  to  $j^{\text{th}} = 16$  elements only),

$$\iota_1'' = \rho E_1 \cos \left[ \omega t - \frac{2\pi}{\lambda} S_1 \right] \quad (\text{O-4})$$

$$\iota_0'' = \rho E_1 \cos \left[ \omega t - \frac{2\pi}{\lambda} (d_0 - d_1) - \frac{2\pi}{\lambda} S_0 \right] \quad (\text{O-5})$$

$$\iota_j'' = \rho E_1 \cos \left[ \omega t + \frac{2\pi}{\lambda} (d_1 - d_j) - \frac{\pi(j-1)}{2} - \frac{2\pi}{\lambda} S_j \right] \quad (\text{O-6})$$

where the path differences between direct and indirect rays are given by

$$S_1 = d_{E-R} + \iota_1 - d_1 \quad (\text{O-7})$$

$$S_0 = d_{E-R} + \iota_0 - d_0 \quad (\text{O-8})$$

$$S_j = d_{E-R} + \iota_j - d_j \quad (\text{O-9})$$



Let  $\alpha$  be an angle specifying the orientation of the 0-R line of the reflector with respect to the 0-1 axis of the antenna array. The orientation of the 0-E line with respect to the 0-1 axis is the direction-of-arrival angle (i.e., bearing angle with respect to 0-1 axis), and is denoted  $\theta$ . Any element ( $j$ ) is located at  $\delta_{1j}$  from the 0-1 axis. With the radius ( $r$ ) of the array given, and with the emitter located at  $d_0$  distance from the central element 0, and the reflector located at  $l_0$  distance from 0; the distances  $d_{E-R}$ ,  $d_j$  (including  $d_1$ ) and  $l_j$  are given by

$$d_{E-R} = \sqrt{d_0^2 + l_0^2 + 2d_0l_0 \cos(\theta + \alpha)} \quad (O-10)$$

$$d_j = \sqrt{d_0^2 + r^2 - 2rd_0 \cos(\delta_{1j} - \theta)} ; j=1 \text{ to } 16 \quad (O-11)$$

$$l_j = \sqrt{l_0^2 + r^2 + 2rl_0 \cos(\delta_{1j} + \alpha)} \quad (O-12)$$

The phase angle of the summed signal, both direct and indirect, from all of the outer antenna elements is  $\Phi_{IND} + \omega t$ , defined by Equation 3.4-25, and  $\Phi_{IND}$  is given by Equation 3.5-26:

$$\Phi_{IND} = \tan^{-1} \left[ \frac{S_1 + \rho(S_2 - \sin \psi_1)}{1 + S_3 + \rho(S_4 + \cos \psi_1)} \right] \quad (3.5-26)$$

where, as before,

$$S_1 = \sum_{j=2}^{16} \sin(a_j + b_j)$$

$$S_2 = \sum_{j=2}^{16} \sin(a_j + b_j - \psi_j)$$

$$S_3 = \sum_{j=2}^{16} \cos(a_j + b_j)$$

$$S_4 = \sum_{j=2}^{16} \cos(a_j + b_j - \psi_j)$$

and where (all in radians)

$$a_j = \frac{2\pi}{\lambda} z_{1j} = \frac{2\pi}{\lambda} (d_1 - d_j) ; j = 2 \text{ to } 16$$

$$b_j = -\frac{\pi}{2} (j-1) ; j = 2 \text{ to } 16$$

$$\psi_j = \frac{2\pi}{\lambda} s_j ; j = 2 \text{ to } 16$$

$$\psi_0 = \frac{2\pi}{\lambda} s_0$$

$\rho$  is a reflection coefficient for the cone R. The quadrant of  $\Phi_{\text{IND}}$  is obtained as before:

$$0 \leq \Phi \leq \pi, \text{ for } 0 \leq \theta \leq 45^\circ ; -\frac{\pi}{2} \leq \Phi \leq \frac{\pi}{2}, \text{ for } 45^\circ \leq \theta \leq 90^\circ.$$

Finally, similar to Equation 3.5-30, the indicated bearing angle is  $A_{\text{IND}}/4$ , where

$$A_{\text{IND}} = 2\pi - \left[ \Phi_{\text{IND}} + \mu_0 + \frac{2\pi}{\lambda} (d_0 - d_1) \right] \quad (\text{O-13})$$

and where

$$\mu_0 = \tan^{-1} \left[ \frac{\rho \sin \psi_0}{1 + \rho \cos \psi_0} \right] \quad (\text{O-14})$$

$$-\frac{\pi}{2} \leq \mu_0 \leq \frac{\pi}{2}.$$

The total error, due to both nonlinearity and multipath effects, is

$$d\theta^\circ = 57.2958 \frac{A_{IND}}{4} - \theta^\circ$$

It is to be observed that the effect of nonlinearity alone is obtained by setting  $\rho = 0$  in Equations 3.5-26 and P-14.

### O.3 Quantitative Results

Computer runs were made for a nominal frequency of 1607.5 MHz and with the following parameters:

$$l_0 = 36''; d_0 = 360''; \alpha = 90^\circ$$

$$\lambda = \frac{3 \times 10^{10}}{1607.5 \times 10^6} \times \frac{1}{2.54} = 7.347''$$

$$r = \frac{2\lambda}{\pi} = 4.677''$$

$$\rho = 0 \text{ for nonlinearity effects}$$

$$\rho = .056 \text{ for multipath effects}$$

$$\theta = 0^\circ \text{ to } 90^\circ, \text{ in } .5^\circ \text{ increments}$$

The nonlinearity results (no multipath reflector) shows an essentially constant error value of  $.32^\circ$ , in contrast to the low valued oscillatory nature of the error displayed in Table 3-4, for the far field. The difference in results is due to the near field effect. For example, for the far field and for  $\theta = 90^\circ$  (Figure O-2) there are cancelling effects so that  $\Phi = 0$ . For the near field,  $d_1 - d_3 \neq d_{15} - d_1$ , etc. Note in particular that  $d_0 - d_1 \neq 0$ , as is the case with the far field. Making a comparison with Figure 4-10, in Section 4.5.4, the lower curve (no cone) appears to have a negative bias of

$$-1.1 + \left( \frac{1.1 + .4}{2} \right) = -.35^\circ$$

the same in magnitude as the analytic result. More significantly, in view of resolution and interpolation difficulties in the plotting and data reduction process used in obtaining Figure 4-10, the upper curve (with cone) can be interpreted as follows:

A positive bias is evident, equal to

$$1.9 - \left( \frac{1.9 + .3}{2} \right) = .8^\circ$$

Subtracting the presumed hybrid error of  $.5^\circ$  gives the expected  $.3^\circ$  bias due to near field nonlinearity.

The multipath error is shown, Figure O-3, and includes the nonlinear bias error. Thus, selecting the maximum at  $\theta = 42.5^\circ$  and minimum at  $\theta = 50.5^\circ$ , there is a bias of

$$1.9 - \left( \frac{1.9 + 1.24}{2} \right) = .33^\circ$$

Comparing the peak error of Figure O-3 with the peak value of the upper curve (test result) in Figure 4-10, and reducing the latter by the hybrid error, results in 2.45-.50, or  $1.95^\circ$ , which is in good agreement with the analytic result.

A rerun for nonlinearity was conducted with a ten-fold increase of the distance of the emitter to the antenna array. The nonlinear error was reduced to 1/10 the previous value, i.e., to  $.03^\circ$ . This lends credence to the very small nonlinearity evidenced in Table 3-4, for the far field emission.



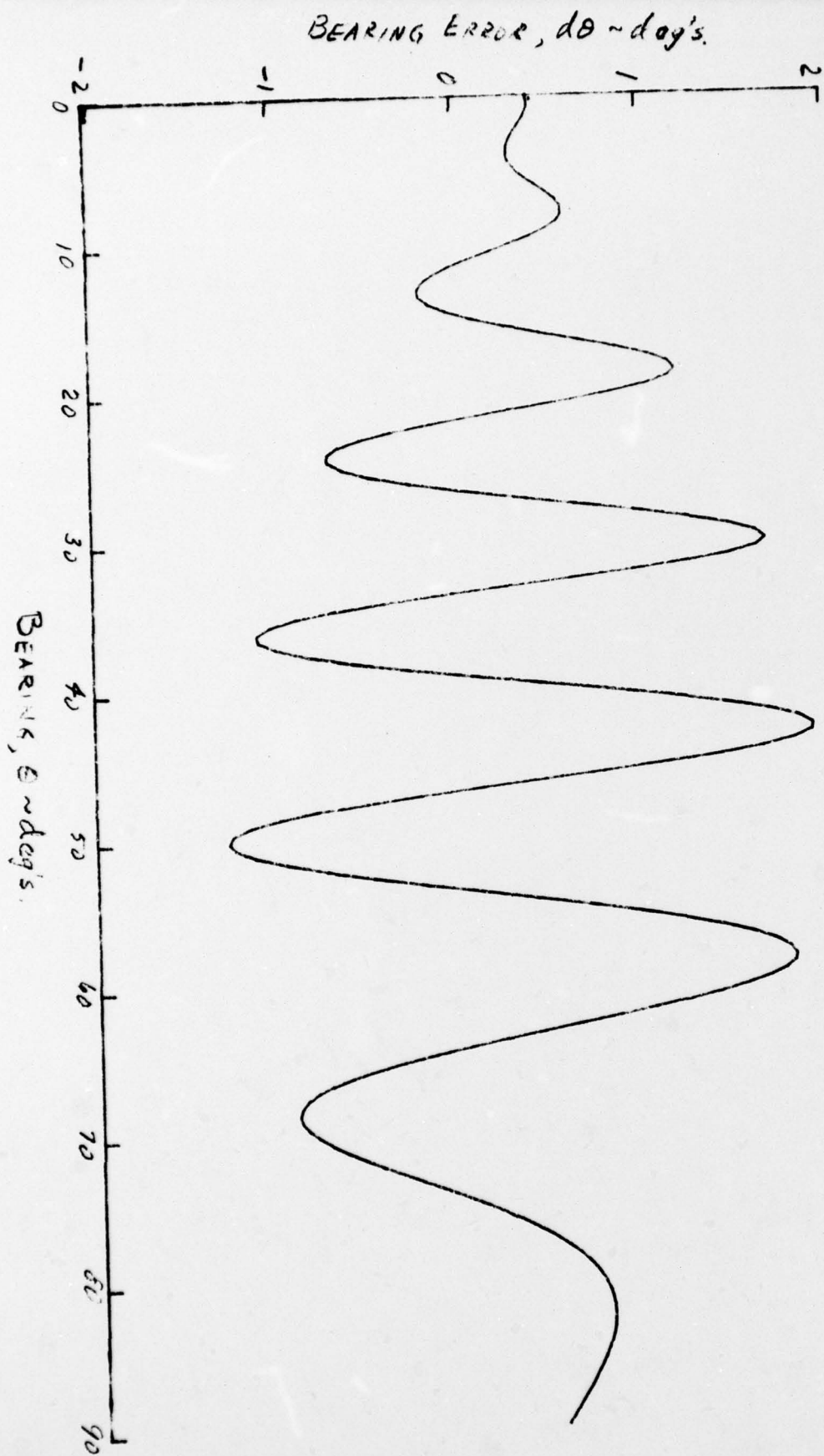


Figure O-3. Multipath Error (Test Simulation)

## APPENDIX P

### REFERENCES

1. J. Breckman, "SECANT - An Anti-Collision System for Airplanes"; RCA Status Report, April 30, 1970, p. 4-20.
2. O. M. Woodward, "A Mode Analysis of Quasi-Isotropic Antennas"; RCA Review, March 1965, p. 42ff.
3. H. Falk, "Computer Hardware/Software"; IEEE Spectrum, January 1974, pp. 39-42.
4. "Handbook of Electronic Measurements"; Ed. by M. Wind, Interscience Publishers, Vol. 2, Ch. VII.
5. "Phase Difference Navigation Satellite Study"; Interim Scientific Report, NASA Contract No. NAS-12-509, RCA Report, June 1967.
6. M. Kayton, "Avionics Navigation Systems"; Wiley 1969, p. 501ff.
7. "A Mode Analysis of Quasi-Isotropic Antennas"; O. M. Woodward, RCA Review, March 1965, p. 42.
8. "Radiation from Ring Quasi-Arrays"; H. L. Knudsen, I.R.E. Trans. Antennas and Propagation, July 1956, p. 452.
9. "A Radial-Waveguide Antenna and Multiple Amplifier System for Electronic Scanning"; C. P. Clasen, J. B. Rankin, and O. M. Woodward, Jr., RCA Review, September 1961, p. 543.
10. "AN/MRD-5 Direction Finder"; RCA Laboratories Technical Report PTR-34C prepared by O. M. Woodward, Jr., June 15, 1950.
11. "Antenna Engineering Handbook"; Henry Jasik, Editor, Mc Graw-Hill Book Co., Inc., New York, page 3-23.
12. M. Skolnik, "Radar Handbook"; Mc Graw-Hill, 1970, pp. 28-17 and 18.
13. "Measuring Phase with the 5360A Computing Counter"; Hewlett-Packard Co., Application Note 120-2.

14. M. Skolnik, "Radar Handbook"; Mc Graw-Hill, 1970. p. 5-37ff.
15. J. H. Kuck etal, "Studies of IF Solid State Limiters Designed for Minimization of Phase Changes"; APL Report CF-3069, 19 February 1964, AD622488.
16. D. K. Barton, "Radar System Analysis"; Prentice-Hall 1964, Table 15.1, p. 489.
17. Air Transport Association Specification ANTC 117.

## APPENDIX Q

### BIBLIOGRAPHY

- 1) "Aircraft Anti-Collision System Design and Evaluation"; E. J. Koepke, January 17, 1972.
- 2) "Theory of Aircraft Collision Avoidance System Design and Evaluation"; (p. 55-59), E. J. Koepke, May 1971.
- 3) "Basis for Acceptable Probability of Missed Alarm Due to Measurement Errors in Secant"; Internal memo, W. Kram, October 29, 1971.
- 4) "Parametric Curves for Secant Miss Distance Error"; Internal memo, W. Kram, October 18, 1971.
- 5) "CAS Warning Time and False Alarm Rates for Co-Altitude Encounters"; Internal memo, E. Jellinek, October 11, 1971.
- 6) "False and Missed Alarms in Secant"; Unpublished memo, W. Kram.
- 7) "Aircraft Distributions in Traffic Model"; Internal memo, W. Kram, July 19, 1973.
- 8) "Statistical Summary of the 1982 Los Angeles Basin Standard Traffic Model", Vols. I and II, Mitre Corporation, April 1973.



Unclassified

Security Classification

## DOCUMENT CONTROL DATA - R &amp; D

(Security classification of title, body of abstract and indexing annotation must be entered when the overall report is classified)

|   |  |   |                       |
|---|--|---|-----------------------|
| 1. ORIGINATING ACTIVITY (Corporate author)<br>RCA/Government and Commercial Systems<br>Electromagnetic & Aviation Systems Division<br>Van Nuys, California 91409  |  | 2a. REPORT SECURITY CLASSIFICATION<br>Unclassified                                  |                       |
|   |  | 2b. GROUP<br>N/A  |                       |
| 3. REPORT TITLE<br>Bearing Study Program  |  |   |                       |
| 4. DESCRIPTIVE NOTES (Type of report and inclusive dates)<br>Final Report   |  |   |                       |
| 5. AUTHOR(S) (First name, middle initial, last name)<br>Ernest Jellinek, Walter Kram, M. Levinson, O. M. Woodward, Bernard Case   |  |   |                       |
| 6. REPORT DATE<br>April, 1974   |  | 7a. TOTAL NO. OF PAGES<br>427   | 7b. NO. OF REFS<br>17 |
| 8a. CONTRACT OR GRANT NO.<br>N62269-73-C-0906   |  | 9a. ORIGINATOR'S REPORT NUMBER(S)<br>TP2146   |                       |
| b. PROJECT NO.<br>N/A   |  | 9b. OTHER REPORT NO(S) (Any other numbers that may be assigned this report)         |                       |
| 10. DISTRIBUTION STATEMENT<br>Distributing this document is unlimited   |  | DISTRIBUTION STATEMENT A<br>Approved for public release;<br>Distribution Unlimited  |                       |
| 11. SUPPLEMENTARY NOTES   |  | 12. SPONSORING MILITARY ACTIVITY<br>Naval Air Development Center<br>Warminster, Pa. |                       |
| 13. ABSTRACT<br>A study was conducted to assess the feasibility and define the system accuracy and equipment required to add a bearing measurement subsystem to the SECANT Collision Avoidance System (CAS). The results indicate the feasibility of achieving the accuracy required to serve useful functions. Equipment configurations required for Proximity Warning Indicator and CAS applications were evolved and are presented in detail in this study.<br><br>A design approach was developed and trade-off and accuracy analyses are presented. The approach utilizes a ring array antenna consisting of vertical monopoles interconnected by strip-line. It has a high accuracy outer ring of 16 monopoles, an inner ring of 4 monopoles for resolving ambiguities, and a central reference monopole. The array receives the signals transmitted by any of the equipment types in the SECANT family, and the relative bearing is determined by measuring the phase difference between the signals in the reference monopole and in the rings. Random errors are minimized by integration of the high pulse rate, frequency hopped signals. Predicted overall error is 1 degree, one sigma with a bias component of 0.8 degree and a random component of 0.5 degree.<br><br>An antenna array was constructed and tests in an anechoic chamber confirmed the validity of the design approach. Receiver and data processing configuration approaches were also developed for Proximity Warning Indicator and Collision Avoidance System applications. The general approach is also applicable to other system applications such as navigation, and electronic warfare. |  |   |                       |

DD FORM 1 NOV 65 1473

Unclassified

Security Classification

405740

JOB

Unclassified

Security Classification

| 14. | KEY WORDS  | LINK A |    | LINK B |    | LINK C |    |
|-----|--|--------|----|--------|----|--------|----|
|     |  | ROLE   | WT | ROLE   | WT | ROLE   | WT |
|     | Bearing Measurement<br>Air Traffic Control<br>Collision Avoidance Systems<br>Proximity Warning Indicator<br>Aircraft Equipment |        |    |        |    |        |    |

Unclassified

Security Classification